

**Identification and Characterization of New Genes Associated with Hearing
Loss**

Dissertation

der Mathematisch-Naturwissenschaftlichen Fakultät
der Eberhard Karls Universität Tübingen
zur Erlangung des Grades eines
Doktors der Naturwissenschaften
(Dr. rer. nat.)

vorgelegt von
Aboufazi Rad
aus Sabzevar, Iran

Tübingen

2024

Gedruckt mit Genehmigung der Mathematisch-Naturwissenschaftlichen Fakultät der Eberhard Karls Universität Tübingen.

Tag der mündlichen Qualifikation: 24.06.2024

Dekan: Prof. Dr. Thilo Stehle

1. Berichterstatter: Prof. Dr. med Olaf Rieß
2. Berichterstatter: Prof. Dr. Bernd Wissinger

1 Contents

1	List of figures and tables	5
2	Abbreviations	6
3	Summary	9
4	Zusammenfassung	10
5	List of publications	11
5.1	Publications	11
5.2	Poster presentations	12
5.3	Contribution to the publications as a first author	12
5.3.1	Aberrant <i>COL11A1</i> splicing causes prelingual autosomal dominant non-syndromic HL in the DFNA37 locus.	12
5.3.2	Identification of three novel homozygous variants in <i>COL9A3</i> causing autosomal recessive Stickler syndrome.	13
5.3.3	Expanding the spectrum of phenotypes for <i>MPDZ</i> : report of four unrelated families and review of the literature	13
6	Introduction	16
6.1	The global burden of HL	16
6.2	Etiologies of HL	16
6.3	Audiometric and clinical aspects of HL	17
6.3.1	Classifications of HL	17
6.3.2	Onset of HL	17
6.3.3	Severity of HL	18
6.4	Assessment of the auditory system	19
6.4.1	Audiometry	19
6.4.2	Objective measures	21
6.4.3	Conduction tests	22
6.4.4	Tympanometry	22
6.4.5	Vestibular function	22
6.5	Non-syndromic HL	22
6.6	Syndromic HL	26
6.6.1	Usher syndrome	26
6.6.2	Pendred syndrome	26
6.6.3	Jervell and Lange-Nielsen syndrome	26
6.6.4	Stickler syndrome	27
6.6.5	Waardenburg syndrome	27
6.6.6	Neurofibromatosis type 2	27

6.6.7 Treacher Collins syndrome.....	28
6.6.8 Branchio-oto-renal.....	28
6.6.9 Alport syndrome.....	28
6.6.10 Norrie syndrome.....	28
6.6.11 Otopalatodigital syndrome.....	28
6.7 American College of Medical Genetics and Genomics (ACMG) guideline for the evaluation and diagnosis of HL.....	29
6.8 Pedigree analysis and family history.....	29
6.9 Patient recruitment.....	30
6.10 Stage-wise testing for the identification and characterization of variants.....	30
6.10.1 GJB2 pre-screening.....	30
6.10.2 Genome-wide SNP array analysis.....	31
6.10.3 ES.....	31
6.10.4 GS.....	31
6.11 Functional studies.....	32
6.12 In-silico tools for predicting the impact of variants on splicing.....	32
6.13 Objectives and outcomes of doctoral research.....	34
7 Results and discussion (Summary and discussion of published results).....	35
7.1 Novel Loss-of-Function Variants in CDC14A are Associated with Recessive Sensorineural HL in Iranian and Pakistani Patients (Attachment 1).....	35
7.2 The Many Faces of DFNB9: Relating OTOF Variants to Hearing Impairment (Attachment 2).....	35
7.3 Aberrant COL11A1 splicing causes prelingual autosomal dominant non-syndromic HL in the DFNA37 locus (Attachment 3).....	37
7.4 Expanding the phenotype of PIGS-associated early onset epileptic developmental encephalopathy (Attachment 4).....	39
7.5 A biallelic variant in CLRN2 causes non-syndromic HL in humans (Attachment 5)	40
7.6 Bi-allelic variants in IPO8 cause a connective tissue disorder associated with cardiovascular defects, skeletal abnormalities, and immune dysregulation (Attachment 6).....	41
7.7 Unraveling the genetic complexities of combined retinal dystrophy and hearing impairment (Attachment 7).....	42
7.8 Biallelic variants in KARS1 are associated with neurodevelopmental disorders and HL recapitulated by the knockout zebrafish (Attachment 8).....	43
7.9 Bi-allelic variants in SPATA5L1 lead to intellectual disability, spastic-dystonic cerebral palsy, epilepsy, and HL (Attachment 9).....	44
7.10 Identification of three novel homozygous variants in COL9A3 causing autosomal recessive Stickler syndrome (Attachment 10).....	45

7.11 Unraveling haplotype errors in the DFNA33 locus (Attachment 11)	46
7.12 Expanding the spectrum of phenotypes for MPDZ: report of four unrelated families and review of the literature (Attachment 12)	46
7.13 Conclusion and Outlook	47
8 Acknowledgements	49
9 References	50
10 Appendix	55
10.1 Attachment 1	55
10.2 Attachment 2	70
10.3 Attachment 3	92
10.4 Attachment 4	99
10.5 Attachment 5	107
10.6 Attachment 6	125
10.7 Attachment 7	138
10.8 Attachment 8	158
10.9 Attachment 9	170
10.10 Attachment 10	182
10.11 Attachment 11	192
10.12 Attachment 12	200

1 List of figures and tables

Figure 1 Global overview of environmental and genetic contributions to congenital HL	17
Figure 2 Four categories for audiogram shape for individuals with hearing impairment.	21
Figure 3 Framework of approaches to the clinical evaluation and etiologic diagnosis of HL	30
Figure 4 A splicing variant visualized in Alamut tool.....	33
Figure 5 ESEfinder and RESCUE-ESE analyses for the variant in <i>CLRN2</i>	34
Figure 6 Audiogram from three patients with biallelic <i>COL9A3</i> variants	45
Table 1 Collaborative publication declarations.....	14
Table 2 Lay description of thresholds and severities in pure tone audiometry	18
Table 3 Non-syndromic HL gene list	23
Table 4 PIGS genetic findings in five families	39

2 Abbreviations

A	Adenine
ABR	Auditory brainstem response
<i>ACTG1</i>	Actin, gamma-1; MIM: *102560
<i>ADGRV1</i>	Adhesion G protein-coupled receptor V1; MIM: *602851
bp	Base pair
<i>BDP1</i>	B-double prime 1, subunit of RNA polymerase III transcription initiation factor IIIb; MIM: *607012
<i>CDH23</i>	Cadherin 23; MIM: *605516
cDNA	Complementary DNA
<i>CEACAM16</i>	Carcinoembryonic antigen-related cell adhesion molecule 16; MIM: *614591
<i>CHD7</i>	Chromodomain helicase DNA-binding protein 7; MIM: *608892
Chr	Chromosome
<i>CIB2</i>	Calcium and integrin binding family member 2; MIM: *605564
<i>CLDN14</i>	Claudin 14; MIM: *605608
<i>CLRN2</i>	Clarin 2; MIM: *618988
CNV	Copy number variation
<i>COL9A1</i>	Collagen, type IX, alpha-1; MIM: *120210
<i>COL9A2</i>	Collagen, type IX, alpha-2; MIM: *120260
<i>COL9A3</i>	Collagen type IX alpha 3 chain; MIM: *120270
<i>COL11A1</i>	Collagen, type XI, alpha-1; MIM: *120280
dB	Decibels
<i>DCDC2</i>	Doublecortin domain-containing protein 2; MIM: *605755
DFN	Deafness locus annotation (DeaFNess); also represents non-syndromic X-linked deafness locus annotation
DFNA	Autosomal dominant non-syndromic deafness
DFNB	Autosomal recessive non-syndromic deafness
DNA	Deoxyribonucleic acid
DVD	Deafness Variation Database
ECG	Electrocardiogram
ES	Exome sequencing
<i>ESRRB</i>	Estrogen-related receptor, beta; MIM: *602167
<i>ESPN</i>	Espin; MIM: *606351
ESTs	Expressed sequence tags
GS	Genome sequencing
G	Guanine
<i>GAB1</i>	Grb2-associated binding protein 1; MIM: *604439
<i>GAS2</i>	Growth arrest-specific 2
gDNA	Genomic DNA
<i>GJB2</i>	Gap junction protein, beta-2; MIM: *121011
<i>GIPC3</i>	GIPC PDZ domain-containing family, member 3; MIM *608792

<i>GPSM2</i>	G protein signalling modulator 2; MIM: *609245
<i>GRXCR1</i>	Glutaredoxin, cysteine-rich, 1; MIM: *613283
HI	Haploinsufficient/haploinsufficiency
HL	Hearing loss
<i>HGF</i>	Hepatocyte growth factor; MIM: *142409
<i>LHFPL5</i>	LHFPL tetraspan subfamily, member 5; MIM: *609427
ID	Intellectual disability
<i>ILDR1</i>	Immunoglobulin-like domain-containing receptor 1; MIM: *609739
<i>KARS</i>	Lysyl-tRNA synthetase; MIM: *601421
kb	Kilobase pair
kHz	Kilohertz
LOH	Loss of heterozygosity
LOF	Loss of function
<i>LOXHD1</i>	Lipoxygenase homology domain-containing 1; MIM: *613072
LR-PCR	Long-range polymerase chain reaction
MAF	Minor allele frequency
<i>MARVELD2</i>	MARVEL domain-containing protein 2; MIM: *610572
Mb	Megabase pair
MIM	Online Mendelian Inheritance in Man
mL	Milliliter
MLPA	Multiplex ligation-dependent probe amplification
mRNA	Messenger ribonucleic acid
<i>MYH4</i>	Myosin, heavy chain 4, skeletal muscle; MIM: *160742
<i>MYH9</i>	Myosin, heavy chain 9, non-muscle; MIM: *160775
<i>MYO3A</i>	Myosin IIIA; MIM: *606808
<i>MYO6</i>	Myosin VI; MIM: *600970
<i>MYO7A</i>	Myosin VIIA; MIM: *276903
<i>MYO15A</i>	Myosin XVA; MIM: *602666
NGS	Next generation sequencing
nt	Nucleotide
<i>OTOA</i>	Otoancorin; MIM: *607038
<i>OTOF</i>	Otoferlin; MIM: *603681
<i>OTOG</i>	Otogelin; MIM: *604487
<i>PCDH15</i>	Protocadherin 15; MIM: *605514
PCR	Polymerase chain reaction
<i>PNPT1</i>	Polyribonucleotide nucleotidyltransferase 1; MIM: *610316
<i>PJKK</i>	Pejvakin; MIM: *610219
<i>PTPRQ</i>	Protein-tyrosine phosphatase, receptor-type, Q; MIM: *603317
<i>PDZD7</i>	PDZ domain-containing 7; MIM: *612971
<i>RDX</i>	Radixin; MIM: *179410
qPCR	Quantitative polymerase chain reaction
<i>S1PR2</i>	Sphingosine-1-phosphate receptor 2; MIM: *605111
<i>SLC26A4</i>	Solute carrier family 26, member 4; MIM: *605646
<i>SLC26A5</i>	Solute carrier family 26, member 5; MIM: *604943

<i>SLC22A4</i>	Solute carrier family 22 (organic cation transporter), member 4; MIM: *604190
<i>SNP</i>	Single nucleotide polymorphism
<i>SNV</i>	Single nucleotide variant
<i>STRC</i>	Stereocilin; MIM: *606440
<i>SYNE4</i>	Spectrin repeat-containing nuclear envelope protein 4; MIM: *615535
<i>TBC1D24</i>	TBC1 domain family, member 24; MIM: *613577
<i>TECTA</i>	Tectorin, alpha; MIM: *602574
<i>TMC1</i>	Transmembrane channel-like protein 1; MIM: *606706
<i>TMIE</i>	Transmembrane inner ear-expressed gene; MIM: *607237
<i>TMPRSS3</i>	Transmembrane protease, serine 3, MIM: *605511
<i>TPRN</i>	Taperin; MIM: *613354
<i>TRIOBP</i>	Trio- and F-actin-binding protein; MIM: *609761
<i>USH1C</i>	Usher syndrome 1C/Harmonin; MIM: *605242
<i>USH2A</i>	Usher syndrome 2A; MIM: *608400
<i>USH3A</i>	Usher syndrome 3A/Clarin 1; MIM: *606397
<i>WHO</i>	World Health Organization
<i>WHRN</i>	Whirlin; MIM: *607928

3 Summary

In humans, hereditary hearing loss (HL) is a frequently occurring disorder with genetic heterogeneity. The incidence of sensorineural HL is 1 to 2 per 1000 at birth, and it is estimated that this disorder can be linked to as many as 1000 different genes. The main aim of this thesis is to identify novel genes and clarify clinical heterogeneity related to HL. The cohort for the thesis was mainly collected from Iran, with some families also from Germany. Using exome sequencing, genome sequencing, and functional *in vitro* tests, including splicing assays for a variety of genes, we detected and established diagnoses in about 74% of our patients. Interestingly, I was involved in the identification of a novel gene: *CLRN2*, which causes non-syndromic sensorineural HL. This thesis also confirmed gene-disease evidence for two genes, *COL11A1* and *COL9A3*, causing non-syndromic HL and Stickler syndrome type 6, respectively. In another part of this thesis, the phenotype related to *MPDZ* was expanded and its role was consolidated in human HL. Additionally, I contributed to functional validation of selected variants identified in *PIGS* and *IPO8* that are associated with variable syndromic HL. Furthermore, I was also involved in a project that established that *KARS1* causes syndromic HL with variable phenotypes, but HL is the main phenotype in all patients. In summary, the results of this thesis added several genes to molecular genetic diagnostic panels, as well as the literature and are highly recommended for re-analysis in unsolved cases with HL.

4 Zusammenfassung

Beim Menschen ist erblicher Hörverlust (HL) eine häufig auftretende Erkrankung mit genetischer Heterogenität. Die Inzidenz von sensorineurales HL liegt bei 1 bis 2 pro 1.000 Personen bei der Geburt, und es wird geschätzt, dass diese Störung mit bis zu 1.000 verschiedenen Genen in Verbindung gebracht werden kann. Das Hauptziel dieser Arbeit besteht darin, neue Gene zu identifizieren und die klinische Heterogenität im Zusammenhang mit HL zu klären. Die Kohorte für die Arbeit wurde hauptsächlich aus dem Iran zusammengestellt, einige Familien kamen auch aus Deutschland. Mithilfe von Exomsequenzierung, Genomsequenzierung und funktionellen In-vitro-Tests, einschließlich Splicing-Assays für eine Vielzahl von Genen, konnten wir bei etwa 74 Prozent unserer Patienten Diagnosen erkennen und stellen. Interessanterweise war ich an der Identifizierung eines neuen Gens beteiligt: *CLRN2*, das nicht-syndromalen sensorineuralen HL verursacht. Diese Arbeit bestätigte auch den Nachweis einer Generkrankung für zwei Gene, *COL11A1* und *COL9A3*, die nicht-syndromales HL bzw. Stickler-Syndrom Typ 6 verursachen. In einem anderen Teil dieser Arbeit wird der Phänotyp im Zusammenhang mit *MPDZ* erweitert und seine Rolle bei menschlichem HL gefestigt. Darüber hinaus habe ich zur funktionellen Validierung ausgewählter Varianten beigetragen, die in *PIGS* und *IPO8* identifiziert wurden und mit variablem syndromalem HL assoziiert sind. Darüber hinaus war ich auch an einem Projekt beteiligt, das feststellte, dass *KARS1* syndromales HL mit variablen Phänotypen verursacht, wobei HL bei allen Patienten der Hauptphänotyp ist. Zusammenfassend lässt sich sagen, dass die Ergebnisse dieser Arbeit mehrere Gene in molekulargenetische Diagnostik-Panels sowie in die Literatur eingebracht haben und für eine erneute Analyse in ungelösten Fällen mit HL dringend empfohlen werden.

5 List of publications

5.1 Publications

1. Julia Doll, Susanne Kolb, Linda Schnapp, **Aboufazi Rad**, Franz Rüschen-dorf, Imran Khan, et al. Novel Loss-of-Function Variants in *CDC14A* are Associated with Recessive Sensorineural HL in Iranian and Pakistani Patients. *Int J Mol Sci*. 2020;21(1).
2. Barbara Vona, **Aboufazi Rad**, Ellen Reisinger. The Many Faces of DFNB9: Relating *OTOF* Variants to Hearing Impairment. *Genes (Basel)*. 2020;11(12).
3. **Aboufazi Rad**, Thore Schade-Mann, Philipp Gamerdinger, Grigoriy A. Yanus, Björn Schulte, Marcus Müller, et al. Aberrant *COL11A1* splicing causes prelingual autosomal dominant non-syndromic HL in the DFNA37 locus. *Hum Mutat*. 2021;42(1):25-30.
4. Stephanie Efthymiou, Marina Dutra-Clarke, Reza Maroofian, Rauan Kaiyrzhanov, Marcello Scala, Javeria Reza Alvi, et al. Expanding the phenotype of *PIGS*-associated early onset epileptic developmental encephalopathy. *Epilepsia*. 2021;62(2):e35-e41.
5. Barbara Vona, Neda Mazaheri, Sheng-Jia Lin, Lucy A. Dunbar, Reza Maroofian, Hela Azaiez, et al. A biallelic variant in *CLRN2* causes non-syndromic HL in humans. *Hum Genet*. 2021;140(6):915-31.
6. Alban Ziegler, Re´mi Duclaux-Loras, Ce´line Revenu, Fabienne Charbit-Henrion, Bernadette Begue, Karine Duroure, et al. Bi-allelic variants in *IPO8* cause a connective tissue disorder associated with cardiovascular defects, skeletal abnormalities, and immune dysregulation. *Am J Hum Genet*. 2021;108(6):1126-37.
7. Paulina Bahena, Narsis Daftarian, Reza Maroofian, Paola Linares, Daniel Villalobos, Mehraban Mirrahimi, **Aboufazi Rad**, et al. Unraveling the genetic complexities of combined retinal dystrophy and hearing impairment. *Hum Genet*. 2022;141(3-4):785-803.
8. Sheng-Jia Lin, Barbara Vona, Patricia G. Barbalho, Rauan Kaiyrzhanov, Reza Maroofian, Cassidy Petree, et al. Biallelic variants in *KARS1* are associated with neurodevelopmental disorders and HL recapitulated by the knockout zebrafish. *Genet Med*. 2021;23(10):1933-43.
9. Elodie M. Richard, Somayeh Bakhtiari, Ashley P.L. Marsh, Rauan Kaiyrzhanov, Matias Wagner, Sheetal Shetty, et al. Bi-allelic variants in *SPATA5L1* lead to intellectual disability, spastic-dystonic cerebral palsy, epilepsy, and HL. *Am J Hum Genet*. 2021;108(10):2006-16.

10. **Aboufazi Rad**, Maryam Najafi, Fatemeh Suri, Soheila Abedini, Stephen Loum, Ehsan Ghayoor Karimiani, et al. Identification of three novel homozygous variants in *COL9A3* causing autosomal recessive Stickler syndrome. *Orphanet J Rare Dis.* 2022;17(1):97.
11. Barbara Vona, Sabrina Regele, **Aboufazi Rad**, Nicola Strenzke, Justin A. Pater, Katrin Neumann, et al. Unraveling haplotype errors in the DFNA33 locus. *Front Genet.* 2023;14:1214736.
12. **Aboufazi Rad**, Oliver Bartsch, Somayeh Bakhtiari, Changlian Zhu, Yiran Xu, Fabíola P Monteiro, et al. Expanding the spectrum of phenotypes for *MPDZ*: report of four unrelated families and review of the literature, accepted in *Clin Genet.* 2024.

5.2 Poster presentations

1. **Aboufazi Rad**, Maryam Najafi, Fatemeh Suri, Stephen Loum, Ehsan Ghayoor Karimiani, David Murphy, Mohammad Doosti, et al. Biallelic pathogenic variants in *COL9A3* confirm autosomal recessive stickler syndrome, *Eur J Hum Genet.* 30 (SUPPL 1), 139-139.
2. **Aboufazi Rad**, Reza Maroofian, Neda Mazaheri, Jaap Oostrik, Stephen Loum, Hubert Löwenheim, et al. Characterizing a large Iranian cohort of non-syndromic HL families using molecular inversion probe and exome sequencing, *Eur J Hum Genet.* 28 (SUPPL 1), 200-201.

5.3 Contribution to the publications as a first author

The declaration of collaboration in all publications is documented in Table 1. However, in this section, I provided detailed descriptions of the collaboration in two publications, and one submitted manuscript for which I served as the first author.

5.3.1 Aberrant *COL11A1* splicing causes prelingual autosomal dominant non-syndromic HL in the DFNA37 locus.

The study was conceptualized by Dr. Barbara Vona. The segregation analysis in Family 1 was done by Dr. Barbara Vona, while I performed segregation analysis in Family 2. The splicing assay to assess aberrant splicing of the variant in Family 1 was done by Dr. Barbara Vona, while I performed a splicing assay for the variant in Family 2. After observing multiple bands in the final RT-PCR result, I established TA cloning and analysed this experiment, which was performed in our lab for the first time. The multi-gene panel data of both families was provided by Dr. Saskia Biskup and Dr. Björn Schulte. The clinical information was aggregated by Dr. Thore Schade-Mann, Philipp Gamerdinger, Dr. Marcus Müller, Prof. Hubert Löwenheim, and Dr. Anke Tropitzsch. Following the splicing assay results, the r. and p. positions of both variants were

verified by Dr. Grigoriy A. Yanus and Dr. Evgeny N. Imyanitov. I prepared the complete first draft of the manuscript. It was revised by Dr. Barbara Vona and reviewed by all authors.

5.3.2 Identification of three novel homozygous variants in *COL9A3* causing autosomal recessive Stickler syndrome.

The original idea was jointly conceptualized by Dr. Barbara Vona, Dr. Miriam Schmidts and myself. I analyzed the exome sequencing (ES) data for all three index cases from three unrelated families and then segregated the identified variants in all available family members using Sanger sequencing. I performed detailed literature-review and collected all reported variants in this gene. Family 1 was referred by Dr. Ehsan Ghayoor Karimiani and his colleagues; Dr. Maryam Najafi, Mrs. Soheila Abedini and Dr. Mohammad Doosti provided detailed clinical information about this family. Families 2 and 3 were referred by Dr. Fatemeh Suri and her colleagues, Dr. Narsis Daftarian, Dr. Afrooz Moghaddasi, Dr. Hamid Ahmadi, Dr. Hamideh Sabbaghi, Dr. Mohsen Rajati, and Dr. Narges Hashemi. Mr. Stephen Loum helped with segregation analysis. Dr. David Murphy performed the bioinformatics analysis and annotation of ES data. I prepared the complete first draft of the manuscript and it was revised by Dr. Barbara Vona, Dr. Miriam Schmidts and reviewed by all authors.

5.3.3 Expanding the spectrum of phenotypes for *MPDZ*: report of four unrelated families and review of the literature

The study was conceptualized by Dr. Barbara Vona. The minigene assay of the splicing variant in Family 1 was done by myself. The ES, segregation study and collecting clinical information from Family 1 was done by Dr. Oliver Bartsch. The ES, segregation study and collecting clinical information from Family 2 was done by Dr. Fabíola P Monteiro and Dr. Fernando Kok. The ES, segregation study and collecting clinical information from Family 2 was done by Dr. Somayeh Bakhtiari, Dr. Changlian Zhu, Dr. Yiran Xu and Prof. Michael C Kruer. The genome sequencing (GS) and collecting clinical information from Family 4 was done by Dr. Anneke T. Vulto-van Silfhout. The analysis of data from knockout murine model was done by Dr. Michael R Bowl. The literature review was done by me and Dr. Barbara Vona. I prepared the complete first draft of the manuscript. It was revised by Dr. Barbara Vona and reviewed by all authors.



Table 1 Collaborative publication declarations

Nr.	Accepted publication yes/no	List of authors	Position of candidate in list of authors	Scientific ideas by the candidate (%)	Data generation by the candidate (%)	Analysis and Interpretation by the candidate (%)	Paper writing done by the candidate (%)
1	Yes	Julia Doll, Susanne Kolb, Linda Schnapp, Aboufazi Rad , Franz Rüschemdorf, Imran Khan, Abolfazl Adli, Atefeh Hasanzadeh, Daniel Liedtke, Sabine Knaup, Michaela AH Hofrichter, Tobias Müller, Marcus Dittrich, Il-Keun Kong, Hyung-Goo Kim, Thomas Haaf and Barbara Vona	4	20	20	20	5
2	Yes	Barbara Vona, Aboufazi Rad , and Ellen Reisinger	2	40	40	40	20
3	Yes	Aboufazi Rad , Thore Schade-Mann, Philipp Gamberdinger, Grigoriy A. Yanus, Björn Schulte, Marcus Müller, Evgeny N. Imyanitov, Saskia Biskup, Hubert Löwenheim, Anke Tropitzsch, and Barbara Vona	1	20	80	60	100
4	Yes	Stephanie Efthymiou, Marina Dutra-Clarke, Reza Maroofian, Rauan Kaiyrzhanov, Marcello Scala, Javeria Reza Alvi, Tipu Sultan, Marilena Christoforou, Thi Tuyet Mai Nguyen, Kshitij Mankad, Barbara Vona, Aboufazi Rad , Pasquale Striano, Vincenzo Salpietro, Maria J. Guillen Sacoto, Maha S. Zaki, Joseph G. Gleeson, Philippe M. Campeau, Bianca E. Russell, and Henry Houlden	12	10	20	10	5
5	Yes	Barbara Vona, Neda Mazaheri, Sheng-Jia Lin, Lucy A. Dunbar, Reza Maroofian, Hela Azalez, Kevin T. Booth, Sandrine Vitry, Aboufazi Rad , Franz Rüschemdorf, Pratishtha Varshney, Ben Fowler, Christian Beetz, Kumar N. Alagramam, David Murphy, Gholamreza Shariati, Alireza Sedaghat, Henry Houlden, Cassidy Petree, Shruthi VijayKumar, Richard J. H. Smith, Thomas Haaf, Aziz ElAmraoui, Michael R. Bow, Gaurav K. Varshney, and Hamid Galehdari	9	10	10	10	10
6	Yes	Alban Ziegler, Re'mi Duclaux-Loras, Céline Revenu, Fabienne Charbit-Henrion, Bernadette Begue, Karine Duroure, Linda Grimaud, Anne Laure Guihot, Valérie Desquirit-Dumas, Mohammed Zarhrate, Nicolas Cagnard, Emmanuel Mas, Anne Breton, Thomas Edouard, Clarisse Billon, Michael Frank, Estelle Colin, Guy Lenaers, Daniel Henrion, Stanislas Lyonnet, Laurence Faivre, Yves Alembik, Anaïs Philippe, Bruno Moulin, Eyal Reinstein, Shay Tzur, Ruben Attali, George McGillivray, Susan M. White, Lyndon Gallacher, Kerstin Kutsche, Pauline Schneeberger, Katta M. Girisha, Shalini S. Nayak, Lynn Pais, Reza Maroofian, Aboufazi Rad , Barbara Vona, Ehsan Ghayoor Karimiani, Caroline Lekszas, Thomas Haaf, Ludovic Martin, Frank Ruemmele, Dominique Bonneau, Nadine Cerf-Bensussan, Filippo Del Bene, and Marianna Parlato	37	2.5	2.5	2.5	2.5
7	Yes	Paulina Bahena, Narsis Daftarian, Reza Maroofian, Paola Linares, Daniel Villalobos, Mehraban Mirrahimi, Aboufazi Rad , Julia Doll, Michaela A. H. Hofrichter, Asuman Koparir, Tabea Röder, Seungbin Han, Hamideh Sabbaghi, Hamid Ahmadi, Hassan Behboud, Cristina VillanuevaMendoza, Vianney Cortés-Gonzalez, Rocio Zamora-Ortiz, Susanne Kohl, Laura Kuehlewein, Hossein Darvish, Elham Alehabib, Maria de la Luz Arenas-Sordo, Fatemeh Suri, Barbara Vona, and Thomas Haaf	7	10	10	10	5
8	Yes	Sheng-Jia Lin, Barbara Vona, Patricia G. Barbalho, Rauan Kaiyrzhanov, Reza Maroofian, Cassidy Petree, Mariasavina Severino, Valentina Stanley, Pratishtha Varshney, Paulina Bahena, Fatema Alzahrani, Amal Alhashem, Alistair T. Pagnamenta, Gudrun Aubertin, Juvianee I. Estrada-Veras, Héctor Adrián Díaz Hernández, Neda Mazaheri, Andrea Oza, Jenny Thies, Deborah L. Renaud, Sanmati Dugad, Jennifer McEvoy, Tipu Sultan, Lynn S. Pais, Brahim Tabarki,	27	2.5	2.5	2.5	2.5



		Daniel Villalobos-Ramirez, Aboufazi Rad , Genomics England Research Consortium, Hamid Galehdari, Farah Ashrafzadeh, Afsaneh Sahebzamani, Kolsoum Saeidi, Erin Torti, Houda Z. Elloumi, Sara Mora, Timothy B. Palculict, Hui Yang, Jonathan D. Wren, Ben Fowler, Manali Joshi, Martine Behra, Shawn M. Burgess, Swapan K. Nath, Michael G. Hanna, Margaret Kenna, J. Lawrence Merritt II, Henry Houlden, Ehsan Ghayoor Karimiani, Maha S. Zaki, Thomas Haaf, Fowzan S. Alkuraya, Joseph G. Gleeson, and Gaurav K. Varshney					
9	Yes	Elodie M. Richard, Somayeh Bakhtari, Ashley P.L. Marsh, Rauan Kaiyrzhanov, Matias Wagner, Sheetal Shetty, Alex Pagnozzi, Sandra M. Nordlie, Brandon S. Guida, Patricia Cornejo, Helen Magee, James Liu, Bethany Y. Norton, Richard I. Webster, Lisa Worgan, Hakon Hakonarson, Jiankang Li, Yiran Guo, Mahim Jain, Alyssa Blesson, Lance H. Rodan, Mary-Alice Abbott, Anne Comi, Julie S. Cohen, Bader Alhaddad, Thomas Meitinger, Dominic Lenz, Andreas Ziegler, Urania Kotzaeridou, Theresa Brunet, Anna Chassevent, Constance Smith-Hicks, Joseph Ekstein, Tzvi Weiden, Andreas Hahn, Nazira Zharkinbekova, Peter Turmpenny, Arianna Tucci, Melissa Yelton, Rita Horvath, Serdal Gungor, Semra Hiz, Yavuz Oktay, Hanns Lochmuller, Marcella Zollino, Manuela Morleo, Giuseppe Marangi, Vincenzo Nigro, Annalaura Torella, Michele Pinelli, Simona Amenta, Ralf A. Husain, Benita Grossmann, Marion Rapp, Claudia Steen, Iris Marquardt, Mona Grimme, Ute Grasshoff, G. Christoph Korenke, Marta Owczarek-Lipska, John Neidhardt, Francesca Clementina Radio, Cecilia Mancini, Dianela Judith Claps Sepulveda, Kirsty McWalter, Amber Begtrup, Amy Crunk, Maria J. Guillen Sacoto, Richard Person, Rhonda E. Schnur, Maria Margherita Mancardi, Florian Kreuder, Pasquale Striano, Federico Zara, Wendy K. Chung, Warren A. Marks, Clare L. van Eyk, Dani L. Webber, Mark A. Corbett, Kelly Harper, Jesia G. Berry, Alastair H. MacLennan, Jozef Gecz, Marco Tartaglia, Vincenzo Salpietro, John Christodoulou, Jan Kaslin, Sergio Padilla-Lopez, Kaya Bilguvar, Alexander Munchau, Zubair M. Ahmed, Robert B. Hufnagel, Michael C. Fahey, Reza Maroofian, Henry Houlden, Heinrich Sticht, Shrikant M. Mane, Aboufazi Rad , Barbara Vona, Sheng Chih Jin, Tobias B. Haack, Christine Makowski, Yoel Hirsch, Saima Riazuddin, and Michael C. Krueger	99	2.5	2.5	2.5	2.5
10	Yes	Aboufazi Rad , Maryam Najafi, Fatemeh Suri, Soheila Abedini, Stephen Loum, Ehsan Ghayoor Karimiani, Narsis Dattarian, David Murphy, Mohammad Doosti, Afroz Moghaddasi, Hamid Ahmadi, Hamideh Sabbaghi, Mohsen Rajati, Narges Hashemi, Barbara Vona, and Miriam Schmidts	1	50	100	100	100
11	Yes	Barbara Vona, Sabrina Regele, Aboufazi Rad , Nicola Strenzke, Justin A. Pater, Katrin Neumann, Marc Sturm, Tobias B. Haack, and Antoinette G. Am Zehnhoff-Dinnesen	3	25	50	50	25
12	Yes	Aboufazi Rad , Oliver Bartsch, Somayeh Bakhtari, Changlian Zhu, Yiran Xu, Fabiola P. Monteiro, Fernando Kok Anneke T. Vulto-van Silfhout, Michael C. Krueger, Michael R Bowl, Barbara Vona	1	50	80	60	100

I confirm that the above-stated is correct.

Aboufazi Rad
Date, Signature of the candidate

I certify that the above-stated is correct.

Date, Signature of the doctoral committee or at least of one of the supervisor

6 Introduction

6.1 The global burden of HL

HL is a significant global health issue that affects millions of people worldwide (1). In 2019, it was estimated to affect 1.57 billion people (2), or roughly 20.3% of the global population. Of these, 1.17 billion (1.12–1.22) people had mild HL (74.3% [71.8–76.8]) and 12.65 million (10.34–15.48) individuals had complete HL (2). Projections for 2050 estimate at least 700 million people will have moderate to complete HL (3). The burden of HL is not limited to the individuals experiencing it; it also has far-reaching consequences for their families, communities, and society as a whole (2). HL can lead to communication difficulties, social isolation, reduced educational, employment opportunities, and decreased quality of life (4). The causes of HL are diverse and can be attributed to various factors. These include genetic predisposition, complications during pregnancy or childbirth, certain infectious diseases such as meningitis or measles, chronic ear infections, exposure to excessive noise levels (both occupational and recreational), and the use of certain medications (5).

The impact of HL on different populations varies across regions and income levels. Low- and middle-income countries tend to have higher rates of HL due to limited access to healthcare services for prevention, early detection, and treatment. Additionally, these countries often lack resources for rehabilitation services such as hearing aids or cochlear (the inner ear's sensory organ responsible for hearing) implants. The burden of HL extends beyond health implications; it also carries significant economic costs. The World Health Organization estimates that unaddressed HL results in an annual global cost of around \$750 billion due to lost productivity and healthcare expenditures (6).

6.2 Etiologies of HL

HL can be caused by a variety of factors, ranging from genetic conditions to environmental exposures. Understanding the etiologies of HL is crucial for diagnosis, treatment, and prevention. The genetic contribution is about 50% of cases with HL, including both non-syndromic and syndromic forms and the rest is likely caused by environmental contributors, shown in Figure 1 (7). Some of the environmental factors that can cause HL include congenital infections (8), ototoxic medications (9), noise exposure (10, 11), age-related changes (12), trauma (13), autoimmune disorders (14), and tumours (15).

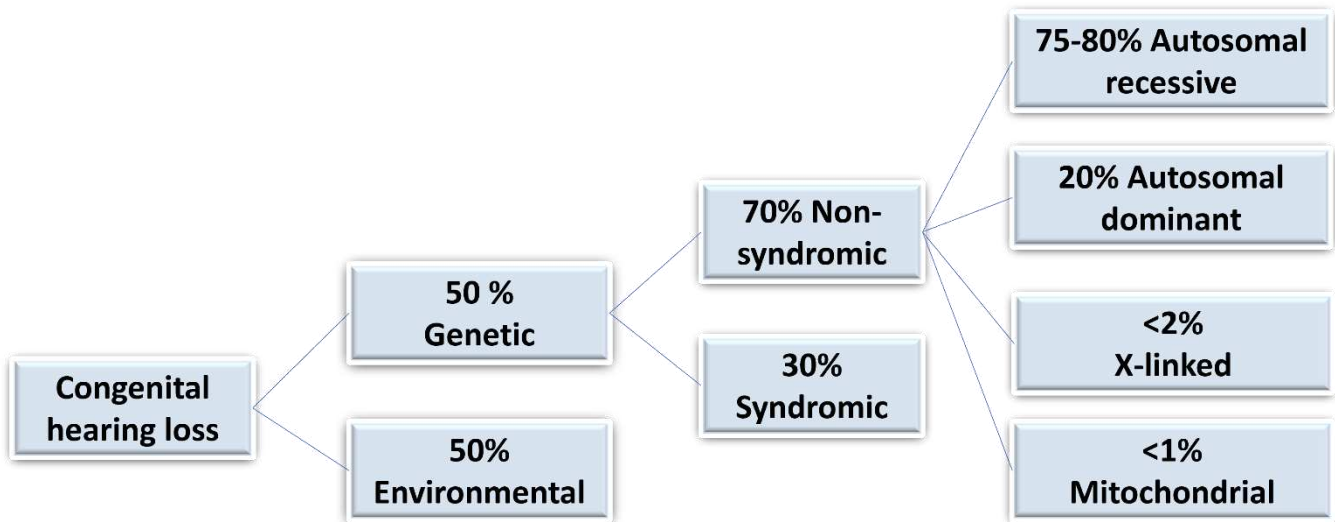


Figure 1 Global overview of environmental and genetic contributions to congenital HL

6.3 Audiometric and clinical aspects of HL

HL can be characterized by different aspects including type, onset, severity, and affected frequencies.

6.3.1 Classifications of HL

The classification of HL includes four types: conductive, sensorineural, mixed and central auditory dysfunction.

Conductive HL is due to abnormalities of the external ear or/and middle ear that prevent the transfer of sounds from the outer to inner ear, making it difficult to hear soft sounds while louder sounds may be muffled. Depending on the severity and the root cause, it can be treated partially or fully by surgical intervention or pharmaceuticals (16). Sensorineural HL is due to defects in the hair cells in the inner ear, the vestibulocochlear nerve or in the central nervous system (17). This type accounts for about 90% of reported HL (18). Mixed HL is a combination of two above types. Central auditory dysfunction or central auditory processing disorder is a rare and poorly understood type of HL which impacts the central auditory nervous system. Patients with this type have normal outer, middle and inner ear anatomy with maintained function; however, they have problems in the neural processing of the auditory stimuli (19). This disease is primarily a condition that affects children and is highly prevalent in patients with learning difficulties like dyslexia, attention deficit disorder, and autism spectrum disorder (20). It can affect adults at different ages with a variety of etiologies such as cerebrovascular disease, malignancy, and neurotoxicity (21).

6.3.2 Onset of HL

The onset of HL is categorized to five classes including: congenital, prelingual, postlingual, adult and presbycusis.

Congenital HL presents at birth and should be diagnosed by three months of age (22). Prelingual HL occurs before the completion of speech and language development (23). If HL occurs later in life, it is referred to as postlingual. Postlingual HL starts after speech and language development (24). Adult-onset HL is highly prevalent and can have gradual or sudden onset. Presbycusis, or age-related HL, typically occurs after middle age. This type is a progressive and irreversible bilateral sensorineural HL, and it results from degeneration of the cochlea or other structures in inner ear and auditory system. Presbycusis impacts a quarter of the world population and is increasing in prevalence due to the growing number of people exposed to noise in industrial regions of the world (25).

6.3.3 Severity of HL

The severity of HL can be measured in two ways: how loud the sound needs to be for hearing and which frequencies are harder for a person to hear (26).

The loudness of sound is measured in decibels (dB). To understand in simple examples, the following are common sounds with their corresponding approximate dB: Breathing: 10 dB; normal speaking volume with someone: 40-60 dB; lawnmower: 90 dB; rock concert: 120 dB; and gunshot: 140 dB. Prolonged exposure to sounds higher than 85 dB can damage hearing.

The second way to characterize hearing is through involved frequencies that are measured in Hertz (Hz). The most important frequency range for conversation is 250 Hz to 8000 Hz; therefore, this range is used for hearing measurements as well. The frequency level can be shown in three different categories including low: less than 500 Hz, medium: between 500 to 2000 Hz and high: more than 2000 Hz. Based on Table 2, the degree of HL can be categorized in six main types (2).

Table 2 Lay description of thresholds and severities in pure tone audiometry

Severity	Lay description	Decibel range
Normal	Normal hearing	0–19 dB
Mild	Has great difficulty hearing and understanding another person talking in a noisy place (e.g., on an urban street)	20–34 dB
Moderate	Is unable to hear and understand another person talking in a noisy place (e.g., on an urban street), and has difficulty hearing another person talking even in a quiet place or on the telephone	35–49 dB
Moderately severe	Has difficulty hearing normal conversation and can only start to hear sounds that are as loud as or louder than heavy traffic	50–64 dB

Severe	Is unable to hear and understand another person talking, even in a quiet place, and unable to take part in a telephone conversation; difficulties with communicating and relating to others sometimes cause emotional effects (e.g., worry or depression)	65–79 dB
Profound	Is unable to hear and understand another person talking, even in a quiet place, is unable to take part in a telephone conversation, and has great difficulty hearing anything in any other situation; difficulties with communicating and relating to others often cause worry, depression, and loneliness	80–94 dB
Complete	Cannot hear at all in any situation, including even the loudest sounds, and cannot communicate verbally or use a telephone; difficulties with communicating and relating to others often cause worry, depression, or loneliness	95+ dB

6.4 Assessment of the auditory system

The method of assessment of hearing depends on the individual's age and neurologic status (i.e., ability to respond to queries from the audiologist).

6.4.1 Audiometry

Several types of audiometry are used in clinical practice. The selection of the type that is used is based on the individual's age or ability to respond to queries from the audiologist. Visual response audiometry is appropriate for children less than 2.5 years. Conditioned play audiometry is effective for children between 2.5-5 years. In conventional audiometry (known as pure-tone audiometry), the suggested age is more than 5 years (27).

The gold standard of hearing measurement is the pure-tone audiogram. The audiogram illustrates the minimum levels (in dB hearing level, as per ANSI S3.6-1996) at which a listener can detect pure-tone signals. These signals are measured at octave intervals within a frequency range of 250-8000 Hz for both ears. This range includes the entire spectrum of speech sounds. As a result, the mean of the pure-tone detection thresholds aligns with the average threshold for speech (28).

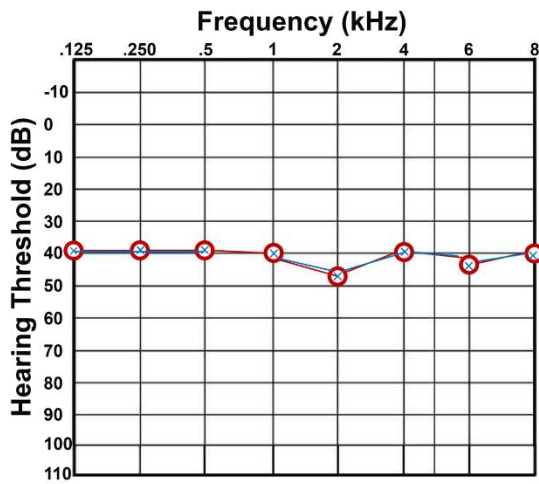
6.4.1.1 Configuration or shape of audio profile

The pattern of HL across frequencies is crucial in determining the underlying causes of hearing impairment and guiding treatment options, such as hearing aids or cochlear implants. Audiologists use audiograms, which graphically represent a person's hearing thresholds at various frequencies, to diagnose and classify the pattern and the degree of HL accurately. If the audiogram is drawn in colours, red is for thresholds detected by the right ear, and blue shows thresholds detected by the left ear (29).

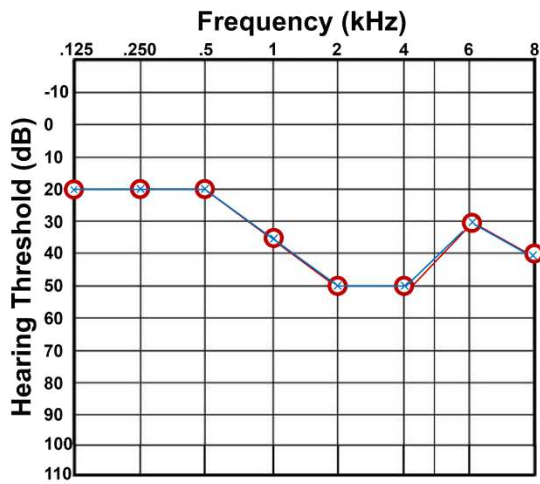
The following are also the explanation of common patterns of audiogram (30):

A person with normal hearing has no significant HL across the entire frequency range, typically from 125 Hz to 8,000 Hz. Their hearing threshold levels are within the normal range for their age group. The first pattern of HL is pantonal, or flat, HL shown as a flat audiogram with a uniform degree of HL across all frequencies. It means that the hearing thresholds are similar for low, mid, and high frequencies. Flat HL is often not varying more than 20 dB among the frequencies. The second pattern is sloping HL, where the degree of HL increases as the frequency gets higher. For example, a person might have relatively mild HL in the lower frequencies (bass sounds) but a more significant loss in the higher frequencies (treble sounds). This pattern is common in age-related HL (presbycusis). The third pattern is U-shaped (Cookie-Bite) HL, and it resembles a U shape on the audiogram. It indicates that a person has better hearing in the low and high frequencies but a dip in the mid-frequency range. U-shaped HL can be associated with genetic factors or specific medical conditions. The fourth pattern is rising HL where the degree of HL is better in the high frequencies and worse in the low frequencies. It can be caused by genetic factors or specific medical conditions like enlarged vestibular aqueduct syndrome (EVAS).

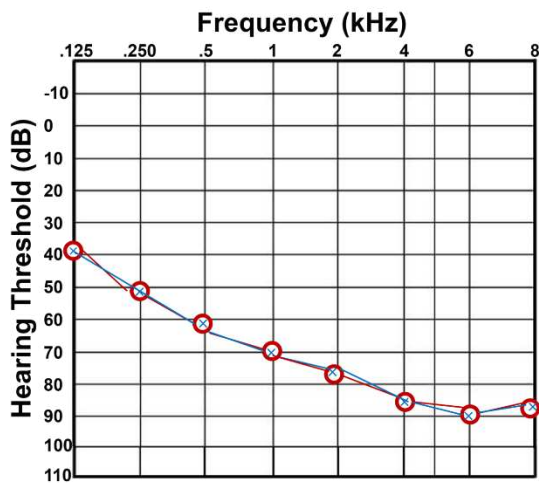
In Figure 2, four different categories are demonstrated with degree of severity of the audiograms for hearing impairment. In this figure, the Y-axis represents the 'Hearing Threshold' in decibels (dB) and measures the minimum sound intensity needed for a specific sound frequency to be heard. Lower dB values represent softer sounds, while higher dB values represent louder sounds. The X-axis shows the frequencies (measured in Hertz, Hz), and it means that a person's ability to hear can differ for low-pitched (low-frequency) and high-pitched (high-frequency) sounds. The "red circle" means unmasked air conduction thresholds in the right ear and "blue X" means unmasked air conduction in the left ear.



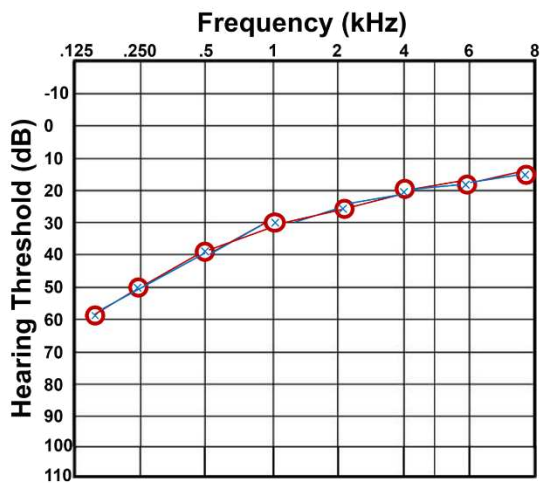
Flat, moderate bilateral HL



U-shaped, mild to moderate bilateral HL



Sloping, moderate to profound bilateral HL



Rising, severe to mild bilateral HL

Figure 2 Four categories for audiogram shape for individuals with hearing impairment.

6.4.2 Objective measures

Objective measures do not require participation of the individual and are typically used in young children or individuals who are unable to participate in other types of audiometric testing requiring active responses. Below are two methods used in clinical practice:

6.4.2.1 Auditory brainstem response (ABR)

Also called Brainstem Auditory Evoked Response (BAER) or Brainstem Evoked Response Audiometry (BERA), this diagnostic test is used to evaluate the auditory pathway's functionality, from the inner ear (cochlea) to the brainstem. The primary purpose of the ABR test is to assess a person's hearing, especially in cases where traditional behavioral audiometry (pure-tone audiometry) may not be feasible or reliable. It is often used for newborn hearing screening, assessing hearing in infants and young children, and diagnosing auditory disorders (31).

6.4.2.2 Otoacoustic Emissions (OAE)

OAE testing is a non-invasive diagnostic test used to assess the functionality of the cochlea (specifically the function of the hair cells). OAE testing measures the emission of sound waves generated by the cochlea in response to auditory stimuli (32).

6.4.3 Conduction tests

Conduction tests are used to distinguish between middle ear dysfunction (conductive HL) and inner ear dysfunction (sensorineural HL) by comparing sound conduction through air and bone. Air conduction tests measure responses to auditory stimuli presented through the external auditory canal, while bone conduction tests measure responses transmitted through the temporal bone (27).

6.4.4 Tympanometry

Tympanometry is a routine audiometric evaluation that assesses the function of the tympanic membrane and middle ear, aiming to differentiate conductive HL from sensorineural HL (27).

6.4.5 Vestibular function

Vestibular assessment evaluates the peripheral vestibular system's integrity. This testing assesses the inner ear's ability to maintain balance and coordinate vestibular-ocular pathways crucial for head position maintenance in space. Imbalance, dizziness, and vertigo are common among individuals with HL due to the shared physiology and developmental origin of the cochlea (responsible for hearing) and the vestibular organs (sacculle, utricle, and semicircular canals) (27).

6.5 Non-syndromic HL

Non-syndromic HL occurs without any other symptoms, and it accounts for approximately 70% of genetic HL cases at birth (Figure 1).

As the search for novel genes is on-going, the exact number of genes causing the HL is not yet possible to determine. Based on Hereditary HL database and last updated evidence, there are 148 genes associated with non-syndromic HL (33). Twelve genes (shown by a star in Table 3) can be inherited in both autosomal recessive and dominant patterns. It is estimated that autosomal dominant HL (represented by DFNA) comprises 20%, autosomal recessive HL (represented by DFNB) characterizes 75-80%, X-linked (DFN) constitutes 2%, and deleterious variants in the mitochondria represent 1% of all non-syndromic HL (7). Among the common HL-associated genes in diverse populations, *GJB2* is the most well-known, and for many years, this gene was routinely screened in HL diagnostics before parallel sequencing methods emerged. *GJB2* encodes connexin 26 with a main role to form functional gap-junction protein (34). During auditory function, connexin 26 maintains K⁺ homeostasis through traversing gap junctions (35). *SLC26A4* is also one of the most common genes in various genetic ancestries around the world.

This gene encodes pendrin that is mainly expressed in the inner ear, thyroid and kidney (36). Pendrin has 12 predicted transmembrane domains and is related to the solute carrier 26 family. This protein, as a transmembrane anion exchanger, has a role in exchanging chloride, bicarbonate (37), formate (38), and iodide (39). It has been demonstrated that disrupted pendrin function in the ear changes pH via HCO₃-transport and increases oxidative stress (40).

The genes comprising the molecular epidemiology of HL vary based on population. In Pakistan, five common genes including *GJB2*, *HGF*, *MYO7A*, *SLC26A4*, and *TMC1* together explain 57% of profound deafness (41). In the Chinese population, the most commonly involved genes are *GJB2*, *SLC26A4*, and *MT-RNR1* (42, 43). In the Iranian population, after first excluding *GJB2* in probands, over half of all diagnoses are attributable to variants in five genes: *SLC26A4*, *MYO15A*, *MYO7A*, *CDH23*, and *PCDH15* (44).

Several genes associated with non-syndromic HL are also associated with syndromic conditions. *GIPC3* is responsible for progressive sensorineural HL that can be associated with audiogenic seizures. *STRC* causes deafness-infertility syndrome in males when deleted in conjunction with *CATSPER2* (45). Variants in *CDC14A* cause deafness-infertility in males. *GPSM2* was initially associated with non-syndromic HL but later determined to cause Chudley-McCullough syndrome (46, 47).

For some genes, only few cases have been reported and the disease relationships are noted with question marks in OMIM, for instance *COL4A6* and *CLRN2*. Hence, in addition to exploring novel genes, I systematically examined our database for discoveries that enhance the existing literature. Notably, this thesis contributed to work that led to the publication of the second report associating *COL11A1* with non-syndromic autosomal dominant HL. Previous gene-disease associations of *COL11A1* are well established for autosomal dominant Marshall syndrome (48), autosomal dominant or recessive Stickler syndrome (49), and as well as autosomal recessive fibrochondrogenesis (50). These syndromes have phenotype-overlap including an auditory phenotype with mild-to-moderate HL and outer ear malformation. Booth *et al.* 2019 identified an extensive family with autosomal dominant inheritance pattern with a novel splice-site variant in *COL11A1* (51). The current work consolidates that splicing variants in *COL11A1* cause non-syndromic autosomal dominant HL in two unrelated families with several affected family members.

Table 3 Non-syndromic HL gene list

Nr.	Locus (OMIM)	Gene (OMIM)	Key Reference (PubMed)	Locus (OMIM)	Gene (OMIM)	Key Reference (PubMed)
1	DFNB1A	<i>GJB2</i>	Kelsell et al., 1997	DFNA1	<i>DIAPH1</i>	Lynch et al., 1997
2	DFNB2	<i>MYO7A</i>	Liu et al., 1997; Weil et al., 1997	DFNA2A	<i>KCNQ4</i>	Kubisch et al., 1999

3	DFNB3	<i>MYO15A</i>	Wang et al., 1998	DFNA2B	<i>GJB3</i>	Xia et al., 1998
4	DFNB4	<i>SLC26A4</i>	Li et al., 1998	DFNA2C	<i>IFNLR1</i>	Gao et al., 2017
5	DFNB6	<i>TMIE</i>	Naz et al., 2002	DFNA3A	<i>GJB2*</i>	Kelsell et al., 1997
6	DFNB7/11	<i>TMC1</i>	Kurima et al., 2002	DFNA3B	<i>GJB6</i>	Grifa et al., 1999
7	DFNB8/10	<i>TMPRSS3</i>	Scott et al., 2001	DFNA4A	<i>MYH14</i>	Donaudy et al., 2004
8	DFNB9	<i>OTOF</i>	Yasunaga et al., 1999	DFNA4B	<i>CEACAM16*</i>	Zheng et al., 2011
9	DFNB15/72/95	<i>GIPC3</i>	Ain et al., 2007; Rehman et al., 2011; Charizopoulou et al., 2011	DFNA5	<i>GSDME</i>	Van Laer et al., 1998
10	DFNB16	<i>STRC</i>	Verpy et al., 2001	DFNA6/14/38	<i>WFS1</i>	Bespalova et al., 2001; Young et al., 2001
11	DFNB18	<i>USH1C</i>	Ouyang et al., 2002; Ahmed et al., 2002	DFNA7	<i>LMX1A*</i>	Wesdorp et al., 2018
12	DFNB18B	<i>OTOG</i>	Schraders et al., 2012	DFNA8/12	<i>TECTA*</i>	Verhoeven et al., 1998
13	DFNB21	<i>TECTA</i>	Mustapha et al., 1999	DFNA9	<i>COCH</i>	Robertson et al., 1998
14	DFNB22	<i>OTOA</i>	Zwaenepoel et al., 2002	DFNA10	<i>EYA4</i>	Wayne et al., 2001
15	DFNB23	<i>PCDH15</i>	Ahmed et al., 2003	DFNA11	<i>MYO7A*</i>	Liu et al., 1997
16	DFNB24	<i>RDX</i>	Khan et al., 2007	DFNA13	<i>COL11A2*</i>	McGuirt et al., 1999
17	DFNB25	<i>GRXCR1</i>	Schraders et al., 2010	DFNA15	<i>POU4F3</i>	Vahava et al., 1998
18		<i>GAS2</i>	Chen et al., 2021	DFNA17	<i>MYH9</i>	Lalwani et al., 2000
19	DFNB26	<i>GAB1</i>	Yousaf et al., 2018	DFNA20/26	<i>ACTG1</i>	Zhu et al., 2003; van Wijk et al., 2003
20	DFNB28	<i>TRIOBP</i>	Shahin et al., 2006; Riazuddin et al., 2006	DFNA22	<i>MYO6*</i>	Melchionda et al., 2001
21	DFNB29	<i>CLDN14</i>	Wilcox et al., 2001	DFNA23	<i>SIX1</i>	Mosrati et al., 2011
22	DFNB30	<i>MYO3A</i>	Walsh et al., 2002	DFNA25	<i>SLC17A8</i>	Ruel et al., 2008
23	DFNB31	<i>WHRN</i>	Mburu et al., 2003	DFNA27	<i>REST</i>	Nakano et al., 2018
24	DFNB32/105	<i>CDC14A</i>	Delmaghani et al., 2016; Imtiaz et al., 2017	DFNA28	<i>GRHL2</i>	Peters et al., 2002
25	DFNB35	<i>ESRRB</i>	Collin et al., 2008	DFNA34	<i>NLRP3</i>	Nakanishi et al., 2017
26	DFNB36	<i>ESPN</i>	Naz et al., 2004	DFNA36	<i>TMC1*</i>	Kurima et al., 2002
27	DFNB37	<i>MYO6</i>	Ahmed et al., 2003	DFNA37	<i>COL11A1</i>	Booth et al., 2018
28	DFNB39	<i>HGF</i>	Schultz et al., 2009	DFNA40	<i>CRYM</i>	Abe et al., 2003
29	DFNB42	<i>ILDR1</i>	Borck et al., 2011	DFNA41	<i>P2RX2</i>	Yan et al., 2013
30	DFNB44	<i>ADCY1</i>	Santos-Cortez et al., 2014	DFNA44	<i>CCDC50</i>	Modamio-Hoybjor et al., 2007
31	DFNB48	<i>CIB2</i>	Riazuddin et al., 2012	DFNA50	<i>MIRN96</i>	Mencia et al., 2009
32	DFNB49	<i>MARVELD2</i>	Riazuddin et al., 2006	DFNA51	<i>TJP2</i>	Walsh et al., 2010
33	DFNB49	<i>BDP1</i>	Giroto et al., 2013	DFNA56	<i>TNC</i>	Zhao et al., 2013
34	DFNB53	<i>COL11A2</i>	Chen et al., 2005	DFNA64	<i>SMAC/DIABLO</i>	Cheng et al., 2011
35	DFNB57	<i>PDZD7</i>	Booth et al., 2015	DFNA65	<i>TBC1D24*</i>	Azaiez et al., 2014; Zhang et al., 2014
36	DFNB59	<i>PJVK</i>	Delmaghani et al., 2006	DFNA66	<i>CD164</i>	Nyegaard et al., 2015
37	DFNB60	<i>SLC22A4</i>	Ben Said et al., 2016	DFNA67	<i>OSBPL2</i>	Xing et al., 2014; Thoenes et al., 2015
38	DFNB61	<i>SLC26A5</i>	Liu et al., 2003	DFNA68	<i>HOMER2</i>	Azaiez et al., 2015

39	DFNB63	<i>LRTOMT/COMT2</i>	Ahmed et al., 2008; Du et al., 2008	DFNA69	<i>KITLG</i>	Zazo Seco et al., 2015
40	DFNB66	<i>DCDC2</i>	Grati et al., 2015	DFNA70	<i>MCM2</i>	Gao et al., 2015
41	DFNB66/67	<i>LHFPL5</i>	Tlili et al., 2005; Shabbir et al., 2006; Kalay et al., 2006	DFNA73	<i>PTPRQ*</i>	Eisenberger et al., 2017
42	DFNB68	<i>S1PR2</i>	Santos-Cortez et al., 2016	DFNA71	<i>DMXL2</i>	Chen et al., 2016
43	DFNB70	<i>PNPT1</i>	von Ameln et al., 2012	DFNA90	<i>MYO3A*</i>	Grati et al., 2016
44	DFNB73	<i>BSND</i>	Riazuddin et al., 2009	DFNA74	<i>PDE1C</i>	Wang et al., 2018
45	DFNB74	<i>MSRB3</i>	Waryah et al., 2009; Ahmed et al., 2011	DFNA75	<i>TRRAP</i>	Xia et al., 2019
46	DFNB76	<i>SYNE4</i>	Horn et al., 2013	DFNA76	<i>PLS1</i>	Morgan et al., 2019
47	DFNB77	<i>LOXHD1</i>	Grillet et al., 2009	DFNA82	<i>ATP2B2</i>	Smits et al., 2019
48	DFNB79	<i>TPRN</i>	Rehman et al., 2010; Li et al., 2010	DFNA79	<i>SCD5</i>	Lu et al., 2020
49	DFNB82	<i>GPSM2</i>	Walsh et al., 2010	DFNA78	<i>SLC12A2</i>	Mutai et al., 2020
50	DFNB84	<i>PTPRQ</i>	Schraders et al., 2010	DFNA83	<i>MAP1B</i>	Cui et al., 2020
51	DFNB84	<i>OTOGL</i>	Yariz et al., 2012	DFNA21	<i>RIPOR2*/FAM65B</i>	de Bruijn et al., 2020
52	DFNB86	<i>TBC1D24</i>	Rehman et al., 2014	DFNA84/ AUNA2	<i>ATP11A</i>	Pater et al., 2022/ Chepurwar et al., 2023
53	DFNB88	<i>ELMOD3</i>	Jaworek et al., 2013	DFNX1*	<i>PRPS1</i>	Liu et al., 2010
54	DFNB89	<i>KARS1</i>	Santos-Cortez et al., 2013	DFNX2	<i>POU3F4</i>	De Kok et al., 1995
55	DFNB91	<i>SERPINB6</i>	Sirmaci et al., 2010	DFNX4	<i>SMPX</i>	Schraders et al., 2011; Huebner et al., 2011
56	DFNB93	<i>CABP2</i>	Schrauwen et al., 2012	DFNX5	<i>AIFM1</i>	Zong et al., 2015
57	DFNB94	<i>NARS2</i>	Simon et al., 2015	DFNX6	<i>COL4A6</i>	Rost et al., 2014
58	DFNB97	<i>MET</i>	Mujtaba et al., 2015			
59	DFNB98	<i>TSPEAR</i>	Delmaghani et al., 2012			
60	DFNB99	<i>TMEM132E</i>	Li et al., 2015			
61	DFNB100	<i>PIIP5K2</i>	Yousaf et al., 2018			
62	DFNB101	<i>GRXCR2</i>	Imtiaz et al., 2014			
63	DFNB102	<i>EPS8</i>	Behlouli et al., 2014			
64	DFNB103	<i>CLIC5</i>	Seco et al., 2014			
65	DFNB104	<i>FAM65B/RIPOR2</i>	Diaz-Horta et al., 2014			
66	DFNB105	see DFNB32				
67	DFNB106	<i>EPS8L2</i>	Dahmani et al., 2015			
68	DFNB108	<i>ROR1</i>	Diaz-Horta et al., 2016			
69	DFNB107	<i>WBP2</i>	Buniello et al., 2016			
70	DFNB109	<i>ESRP1</i>	Rohacek et al., 2017			
71	DFNB 111	<i>MPZL2</i>	Wesdorp et al., 2018			
72	DFNB113	<i>CEACAM16</i>	Booth et al., 2018			
73	DFNB114	<i>GRAP</i>	Li et al., 2019			
74	DFNB115	<i>SPNS2</i>	Ingham et al., 2019			
75	DFNB116	<i>CLDN9</i>	Sineni et al., 2019			
76	DFNB117	<i>CLRN2</i>	Vona et al., 2021			
77	DFNB119	<i>SPATA5L1</i>	Richard EM et al., 2021			

Note: The current list of non-syndromic HL loci with causative genes was obtained from the Hereditary HL Homepage and OMIM.

6.6 Syndromic HL

The term syndromic HL is applied when a patient experiences HL along with other medical abnormalities. About 20% of children with genetic HL exhibit additional associated symptoms. This section outlines the assessment and treatment of syndromic sensorineural HL and emphasizes the importance of the interprofessional team in enhancing care for affected patients. Similar to non-syndromic HL, it is categorized based on mode of inheritance that includes autosomal recessive, autosomal dominant, X-linked and mitochondrial. Syndromes exhibiting a recessive inheritance pattern include Usher, Pendred and Jervell and Lange-Nielsen syndrome; syndromes with an autosomal dominant inheritance pattern include Stickler syndrome, Waardenburg syndrome, neurofibromatosis type 2, Treacher Collins syndrome, and branchio-oto-renal syndrome (Melnick-Fraser syndrome); and syndromes with an X-linked inheritance pattern include Alport, Norrie, and otopalatodigital syndrome.

In the following sections, the major syndromes associated with different patterns of inheritance are briefly described.

6.6.1 Usher syndrome

Usher syndrome is the most common type of syndromic HL. Usher syndrome is predominantly characterized as concomitant deafness and blindness with variable vestibular dysfunction and has four clinical sub-types. Type 1 causes profound sensorineural HL with absent vestibular function and retinitis pigmentosa (RP), which initially causes night-blindness and loss of peripheral (side) vision due to the progressive degeneration of cells in the retina. Type 2 causes moderate HL and RP with normal vestibular function. Type 3 results in progressive HL with variable vestibular function and RP. Type 4 is characterized by late onset of RP and usually late-onset of progressive sensorineural HL without vestibular involvement (52, 53). So far, the following genes are associated with these four types of Usher syndromes: *CDH23*, *CIB2*, *ADGRV1*, *MYO7A*, *PCDH15*, *PDZD7*, *USH1G*, *USH1C*, *USH2A*, *CLRN1*, and *ARSG* (52, 54-57).

6.6.2 Pendred syndrome

Pendred syndrome is associated with abnormal iodine metabolism and is caused by biallelic pathogenic variants in *SLC26A4*. Patients with this syndrome typically develop euthyroid goiter around the age of 8 years, along with bilateral moderate to severe high-frequency sensorineural HL with some residual low-frequency hearing. The most frequent inner ear abnormality seen in Pendred syndrome is an enlarged vestibular aqueduct, which is a connection between the inner ear's vestibule and the brain (58).

6.6.3 Jervell and Lange-Nielsen syndrome

Jervell and Lange-Nielsen syndrome is associated with profound sensorineural HL and cardiac arrhythmias caused by prolongation of the QT interval. This syndrome is associated with two genes: *KCNE1* or *KCNQ1*; 90% are caused by *KCNQ1* variants. Patients with this syndrome commonly exhibit abnormalities in both the inner ear and cardiac muscle due to biallelic pathogenic variants. Electrocardiogram (ECG) results in these individuals demonstrate enlarged T waves and a prolonged QT interval. Syncope is the typical manifestation observed in these patients (59).

6.6.4 Stickler syndrome

Stickler syndrome is inherited in both autosomal recessive and dominant manners, but most of the genes for this syndrome are associated with a dominant inheritance pattern. This thesis highlights Stickler type 6 as associated with rare biallelic variants in *COL9A3*. Stickler syndrome is characterized by cleft palate, micrognathia, myopia, retinal detachment, cataracts, and marfanoid habitus. The other sub-types of this syndrome are due to variants in *COL2A1* (Stickler type 1), *COL11A1* (Stickler type 2), *COL11A2* (Stickler type 3), *COL9A1* (Stickler type 4), and *COL9A2* (Stickler type 5) (60).

6.6.5 Waardenburg syndrome

Waardenburg syndrome is the most common form of autosomal dominant sensorineural HL, associated with 3% of childhood HL. This syndrome consists of HL (bilateral, unilateral, or asymmetric), pigmentary anomalies, and craniofacial features. The pigmentary anomalies include a white forelock, very pale blue eyes or different coloured eyes (such as one blue and one brown), premature greying of hair, and vitiligo. The craniofacial features include widely spaced medial canthi, a broad nasal root, and confluent eyebrows. There are four sub-types of Waardenburg syndrome. Type 1 is characterized by heterochromia iridis, a white forelock, patchy hypopigmentation, and widely spaced medial canthi. Congenital sensorineural HL is present in 20% of these patients. Type 2 patients do not have widely spaced medial canthi, distinguishing them from type 1. Up to 50% of these patients will have sensorineural HL. Type 3 includes the features of type 1 as well as microcephaly, skeletal abnormalities, and mental retardation. Type 4 is similar to type 2 but also includes Hirschsprung's disease, a gastrointestinal malformation. The following genes account for the different sub-types of this syndrome: *EDN3*, *EDNRB*, *MITF*, *PAX3*, *SNAI2*, and *SOX10* (58).

6.6.6 Neurofibromatosis type 2

Neurofibromatosis type 2 is caused by pathogenic variants in *NF2* leading to alterations in the merlin protein. This condition is characterized by bilateral vestibular schwannomas, cafe-au-lait spots, and subcapsular cataracts. Bilateral vestibular schwannomas are found in approximately

95% of individuals with this condition, but typically do not cause symptoms until early adulthood (61).

6.6.7 Treacher Collins syndrome

Treacher Collins syndrome, also known as mandibulofacial dysostosis, is characterized by facial malformations such as underdeveloped cheekbones, slanted eye openings, incomplete lower eyelids, underdeveloped jaw, abnormal external ear or ear canal, misaligned teeth, and a cleft palate. Around 30% of patients experience conductive HL, but sensorineural HL or vestibular dysfunction can also be present. Ossicular malformations are commonly observed. The most common causal gene is *TCOF1*, encoding the treacle protein (62).

6.6.8 Branchio-oto-renal

Branchio-oto-renal also known as Melnick-Fraser syndrome is present in approximately 2% of children with congenital HL. This syndrome is characterized by the presence of ear pits/tags, branchial cleft sinuses, and renal involvement ranging from minor dysplasia to complete agenesis. To date, three genes are established causing this syndrome including *EYA1*, *SIX5* and *SIX1*. Forty percent of these patients exhibit cochlear dysplasia, while 75% experience a significant HL. The type of HL can vary, with some patients having either conductive or sensorineural HL, and others having a mixed HL (58).

6.6.9 Alport syndrome

Alport syndrome causes lesions in the basement membrane collagen of the kidney and inner ear, leading to renal failure and progressive sensorineural HL. Pathogenic variants in *COL4A5* (X-linked), *COL4A4* (autosomal recessive) and *COL4A3* (autosomal dominant and recessive) are responsible for this syndrome.

6.6.10 Norrie syndrome

Norrie syndrome is an X-linked disorder characterized by ocular symptoms, progressive sensorineural HL, and intellectual disability. All patients are either born blind or they lose vision in the first years of life and have progressive sensorineural HL in the first or second decades of life (63). The onset of other phenotypes like seizure can also occur at a young age (64). This disease is caused by mutation in *NDP*, which encodes norrin.

6.6.11 Otopalatodigital syndrome

Otopalatodigital syndrome is associated with craniofacial deformities, hypertelorism, flattened midface, small nose, and cleft palate and includes: otopalatodigital syndrome type 1 (OPD1), otopalatodigital syndrome type 2 (OPD2), frontometaphyseal dysplasia type 1 (FMD1), Melnick-Needles syndrome (MNS), and terminal osseous dysplasia with pigmentary skin defects (TODPD). These patients also have short stature and abnormalities in their toes and fingers such

as varying lengths and spaces between digits. They also experience conductive HL due to ossicular abnormalities. The molecular genetic diagnosis of this syndrome is identification of pathogenic variants in the X-linked gene, *FLNA* (65).

6.7 American College of Medical Genetics and Genomics (ACMG) guideline for the evaluation and diagnosis of HL

The ACMG published the first practice guideline for the clinical evaluation and etiologic diagnosis of HL in 2014 (66). An updated algorithm for the evaluation of clinical and diagnostic of HL was recently published (67). This updated framework outlines the process for evaluating and diagnosing HL, incorporating genetic counselling and testing. The process begins with the clinical confirmation of HL. If additional findings are revealed during the evaluation, pre-test genetic counselling is conducted, followed by a standard clinical evaluation to identify genetic syndromes with genetic testing as indicated. Genetic testing could include single gene tests, multi-gene panels, chromosome analysis, or microarray depending on clinical findings. If a syndromic diagnosis is made according to these genetic tests, the process diverges based on whether HL is common in the syndrome. If it is, post-test genetic counselling initiates familial testing as needed. If HL is not common in the syndrome, a comprehensive HL gene panel is performed and if negative based on panel, ES or GS may be considered. If no additional findings are revealed during the initial evaluation, a comprehensive HL gene panel is directly administered. Positive results indicating pathogenic variant(s) that explain HL also lead to post-test genetic counselling and familial testing as indicated. Negative results lead to considering CMV testing on newborn screening blood-spot and re-evaluating periodically or considering research testing.

We also followed this approach and additionally screened a prevalent gene implicated in HL, *GJB2*, in our patient cohort due to its high frequency of pathogenic variants and low cost of screening by Sanger sequencing. Below is an introduction about the main steps of this approach that we performed in our cohort.

6.8 Pedigree analysis and family history

As HL can be caused by a variety of etiologies and exhibits diverse possible modes of inheritance, family history and pedigree analysis are essential steps to understanding the possible genetic contribution to HL and method for molecular genetic diagnosis. For many genes, intrafamilial variability, variable expressivity and incomplete penetrance are described. Drawing an informative pedigree requires that the information from at least three generations be collected. The information in pedigrees provides hints about the mode of inheritance, how to interpret variants of uncertain significance and prioritize segregation studies after identification of the

primary finding as diagnostics. For example, if an identified variant is of uncertain significance, and we know, based on the pedigree, that there are additional affected and unaffected individual(s) in the family, it is recommended to perform Sanger sequencing to segregate the variant in the family members. These segregation results help clarify the variant of uncertain significance by either adding more strength for its probable pathogenicity or supporting its exclusion as in the case of discordant segregation. Family history is also helpful to evaluate the genetic finding. For instance, if a variant arises *de novo*, it means the disease is most likely sporadic in the family unless there is a germline mosaic variant.

6.9 Patient recruitment

The patient cohort included 166 index patients from Iran and Germany with various forms of hearing impairment. The inclusion criteria were flexible to include patients with all types of suspected hereditary non-syndromic and syndromic HL (sensorineural, conductive, or mixed) with variable degrees from mild to profound. The age of onset and age of last measurement were important in our documentation process. Suspected hearing loss due to an environmental cause led to study exclusion (Figure 3).

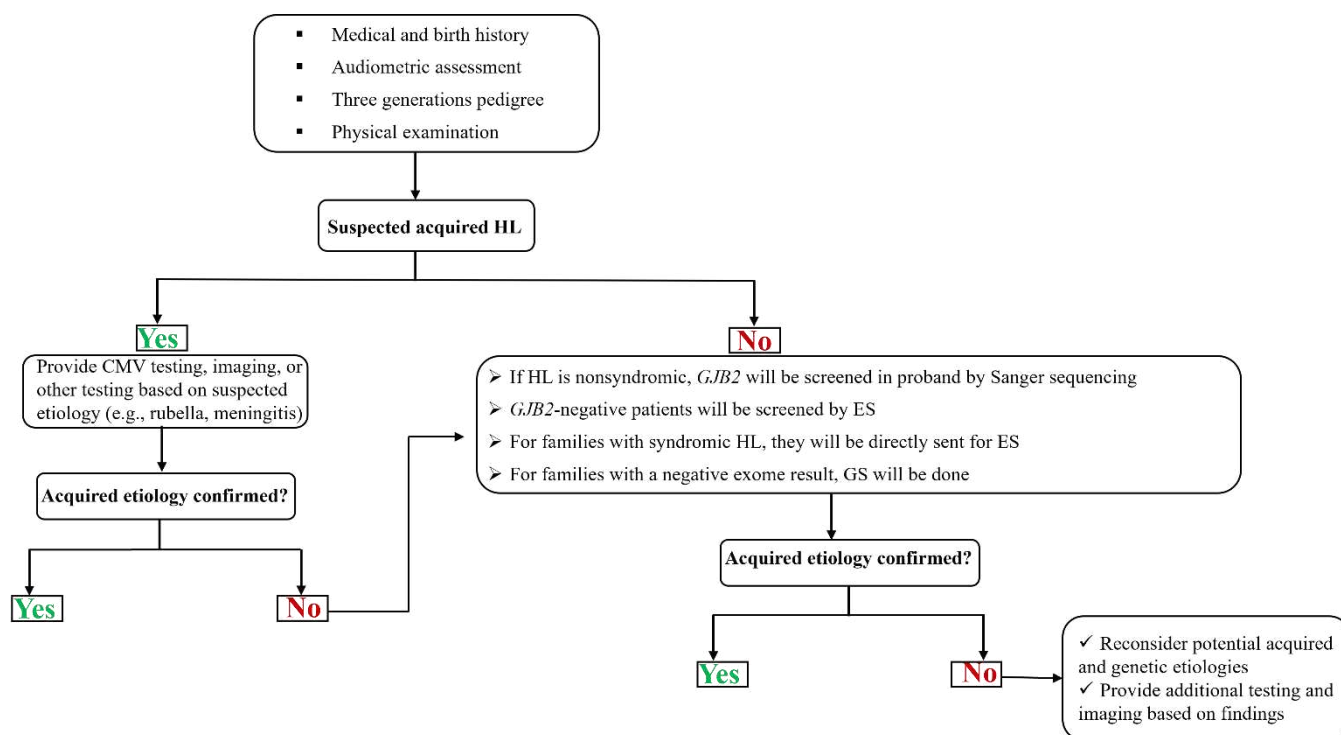


Figure 3 Framework of approaches to the clinical evaluation and etiologic diagnosis of HL

6.10 Stage-wise testing for the identification and characterization of variants

Based on ACMG guideline for the evaluation and diagnosis of HL and following study inclusion and exclusion criteria, the following steps were performed.

6.10.1 GJB2 pre-screening

GJB2 is the most common cause of congenital non-syndromic HL (68, 69). The first *GJB2* variant implicated in autosomal recessive non-syndromic HL was reported in 1997, and since then over 300 pathogenic variants have been identified worldwide (see the Connexin-deafness website: <http://davinci.crg.es/deafness/> and Deafness Variation Database (DVD): <https://deafnessvariationdatabase.org/>). In the US, *GJB2* variants are estimated to be responsible for about 15-20% of deafness cases (70), while in Asian countries like Japan, they account for 12.5% of cases (71). The most common pathogenic variant in the European population is c.35delG p.Gly12fs*2, while in individuals with Asian genetic ancestry, the most prevalent pathogenic variants are c.235delC p.Leu79Cysfs*3 and c.109G>A p.Val37Ile (72). As *GJB2* is a relatively small gene with two exons, it is possible to evaluate the coding region by Sanger sequencing using two primer pairs. All the index patients in the cohort with a suspected non-syndromic HL were screened using Sanger sequencing for *GJB2* variants.

6.10.2 Genome-wide SNP array analysis

Genome-wide SNP arrays identify heterozygous or homozygous SNP genotypes in the genome and support copy number variation (CNV) analysis to detect chromosomal abnormalities. There are two types of probes in this method for detection of SNP genotypes or CNVs. Besides microdeletion/microduplication detection, loss of heterozygosity (LOH), mosaicism, and uniparental disomy (UPD) can be detected. In this thesis, SNP array data was mainly used for homozygosity mapping and CNV analysis that was performed using homozygosity mapper (73), and GenomeStudio, respectively.

6.10.3 ES

The human genome has 3 billion nucleotides from four bases (A, T, C, and G). Only 1.5-2% of the genome is comprised of exons (Expressed regiON) that are translated into protein. ES is designed to sequence this part of the genome, with a diagnostic rate of roughly 45-50% (74). ES not only covers all exons, but it can also detect canonical and noncanonical splice sites. The main pitfall of ES includes lack of coverage of deep intronic variants, as well as limitations in coverage uniformity and the detection of duplications and repeat expansion variants, which all can be covered by GS.

6.10.4 GS

Over the last decade, the price of next generation sequencing (NGS) has significantly decreased, allowing for GS as the preferred method for molecular genetic diagnostic testing. This method provides the sequence of the entire genome and can allow for the identification of all types of variants including single nucleotides variants (SNVs), CNVs and structural variants (SVs). By developing and updating the bioinformatics pipeline (DRAGEN), repeat expansion variants can

also be detected. However, limitations remain with respect to the identification of complex rearrangements, as well as imprinting and methylation disorders, which can alternatively be detected by long-read sequencing or whole-genome bisulfite sequencing, respectively.

6.11 Functional studies

Functional studies aim to investigate how target genes contribute to biological processes, such as protein interactions, signalling pathways, gene expression regulation, and cellular functions. The scope of this project characterized variants identified in novel genes. One recurring variant type included splicing variants that were functionally characterized using *in vitro* splicing assay (minigene assay).

6.12 *In-silico* tools for predicting the impact of variants on splicing

In-silico splice prediction tools, such as those included in Alamut Visual Plus v.1.4, have been developed to predict variants that may impact pre-mRNA splicing. The following splicing tools were used to predict the probability of aberrant splicing for target variant: SpliceSiteFinder-like, MaxEntScan, GeneSplicer, and NNSplice (Figure 4).

SpliceSiteFinder-like is based on position weight matrices computed from a set of human exon/intron junctions for donor and acceptor sites. The tool calculates a score, which is the probability of observing a sequence given the motif model (matrix). This allows it to predict potential splice sites within a DNA sequence, providing valuable insights into the splicing process (75). MaxEntScan uses the 'Maximum Entropy Principle' to account for both adjacent and non-adjacent dependencies between positions. This approach generalizes most previous probabilistic models of sequence motifs, such as weight matrix models and inhomogeneous Markov models. MaxEntScan provides a score for potential splice sites within a DNA sequence, aiding in the prediction and analysis of splice-altering single nucleotide variants (76). GeneSplicer is a computational method used for predicting splice sites in genomic DNA of various eukaryotes. It has been trained and tested successfully on several organisms, including *Plasmodium falciparum* (malaria), *Arabidopsis thaliana*, human, *Drosophila*, and rice which aids in understanding of gene structure and function (77). NNSplice is an *in-silico* tool used for predicting splice sites in genomic DNA sequences. It uses a neural network-based approach to identify the 5' and 3' splice sites, which are crucial for pre-mRNA splicing. By accurately predicting these splice sites, NNSplice aids in the understanding of gene structure and function and can help identify variants that may disrupt normal splicing (78).



Figure 4 A splicing variant visualized in Alamut tool

This figure illustrates four panels. The top two panels represent the 5' and 3' regions for the reference sequence (wild-type), while two lower panels correspond to the variant (mutated). Each tool demonstrates scores represented as bars at variant positions. The scoring scale varies for each tool: a score of zero predicts that splicing does not occur at that position, whereas a high score suggests a high probability of splicing.

Besides four abovementioned tools, two other tools predict regulatory elements including ESEfinder and RESCUE-ESE. The figure 5 depicts these predictions, using the *CLRN2* variant (c.494C>A) as an example (79).

ESEfinder is a computational tool used to predict the impact of regulatory variants within genomic regions. These variants can alter regulatory elements such as enhancers, transcription factor binding sites, and DNA methylation regions. ESEfinder annotates these variants using information from large-scale projects that discover regulatory elements in different tissues and organisms. It predicts their effects, including potential pathogenicity, using rule-based and machine learning approaches (80). RESCUE-ESE is a hybrid computational/experimental tool designed to predict the impact of regulatory variants within exonic regions. Specifically, it focuses on exonic splicing enhancers (ESEs)—short oligonucleotide sequences that enhance pre-mRNA splicing when present in exons (81).

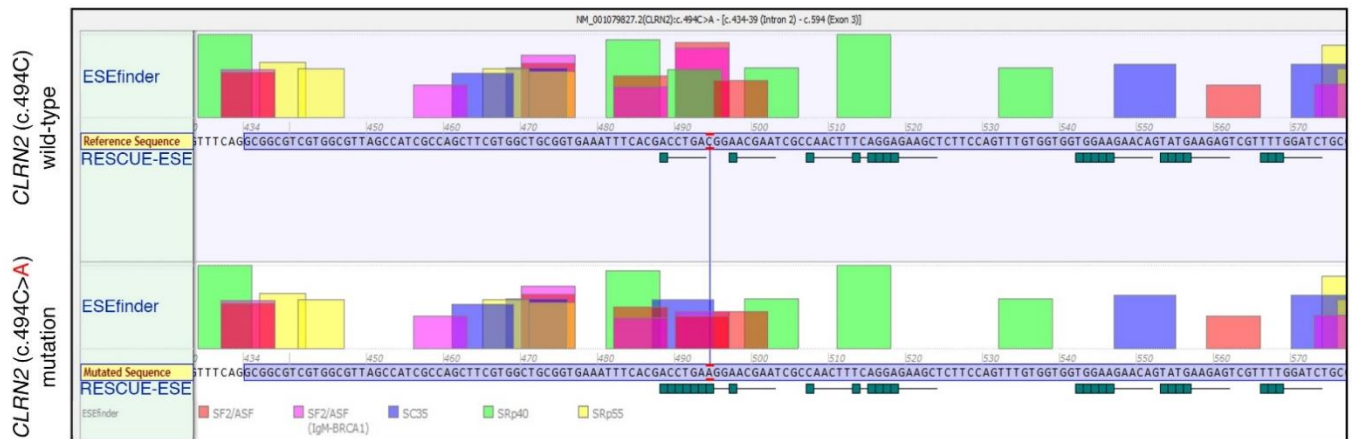


Figure 5 ESEfinder and RESCUE-ESE analyses for the variant in CLRN2

Using ESEfinder and RESCUE-ESE, the splicing sequence patterns were explored in both the wild-type (upper panel) and mutated (lower panel) human sequences at position c.494. The nucleotide at c.494 is highlighted in red. Above each sequence, ESE hits are indicated. Additionally, the green boxes below the nucleotide at c.494 corresponds to RESCUE-ESE hexamers. Notably, the c.494C>A variant is predicted to introduce an ESE hexamer, as evidenced by the string of green boxes in the lower sub-panel.

6.13 Objectives and outcomes of doctoral research

The present work is embedded in a larger collaborative cohort study of Iranian and German families with syndromic and non-syndromic HL. The aim is to establish the role of potential novel genes and allelic disorders of known genes. After excluding patients achieving a diagnosis through identification of likely causal variants in *GJB2*, ES was performed to identify variants for expanded exome-wide analysis. In five families with several affected siblings who remained undiagnosed after ES, we performed GS to attempt to identify novel genes or deep intronic variants. For segregation analysis, we performed Sanger sequencing in available DNA from family members. Additionally, minigene assays were performed for selected variants with predicted impact on splicing. In this study, allelic disorders of two genes were confirmed. First, the gene-disease association between *COL11A1* and non-syndromic HL was strengthened by including two unrelated families with established novel variants impacting splicing. Second, the association of biallelic variants in *COL9A3* as causal for Stickler syndrome type 6 was investigated in three unrelated families harbouring novel variants. Moreover, the discovery of novel variants in *MPDZ* further expanded the spectrum of phenotypes associated with *MPDZ*-related disorders. Additionally, this work solidified the role of *MPDZ* in HL by presenting a family with three affected individuals and analysing available phenotyping data in a mouse model. My work also contributed to establishing *CLRN2* as a novel autosomal recessive non-syndromic HL gene (DFNB117). Collaborating in a significant study, I was also involved in establishing the role of *SPATA5L1* in both syndromic and non-syndromic (DFNB119) HL. Furthermore, novel variants

in *CDC14A*, *ADGRV1*, *IPO8*, *PIGS*, and *KARS1* were confirmed through *in vitro* functional study (minigene assay). The minigene findings contribute valuable insights into the functional impact of these variants.

7 Results and discussion (Summary and discussion of published results)

7.1 Novel Loss-of-Function Variants in *CDC14A* are Associated with Recessive Sensorineural HL in Iranian and Pakistani Patients (Attachment 1)

Cell Division Cycle 14A (*CDC14A*) is associated with DFNB32, as well as hearing impairment and infertile male syndrome. This gene is located on chromosome 1p21.2 and is essential for centrosome separation and productive cytokinesis during cell division (82). In addition to being present in the kinocilia of hair cells, this gene is also found in the basal bodies and sound-transducing stereocilia of the mouse inner ear (83). Mice with a homozygous variant in *Cdc14a* experienced postnatal degeneration of hair cells, although their kinocilia remained normal in length. Additionally, these mice exhibited degeneration of seminiferous tubules and defects in spermiation, leading to infertility in males (84). Before this study, only nine genetic variants have been published related to HL, of which, five also associated with male infertility. Biallelic variants in this gene cause varying degrees of HL severity from moderate to profound. In this study, ES and gene mapping approaches were performed in two unrelated families (family 1, Iranian and family 2, Pakistani), uncovering a homozygous splicing variant (c.1421+2T>C p.?) abolished the donor splice site in intron 14 in family 1 and a homozygous frameshift variant (c.1041dupC p.Ser348Glnfs*2) in family 2. Both variants were submitted to LOVD V3.0 under the accession IDs 00269609 and 00269610. Segregation analyses were performed in available family members of both families. Functional *in vitro* splicing study (minigene assay) of the variant in family 1 (c.1421+2T>C p.?) was performed, and it showed that the variant activates a cryptic splice site in the exonic region. In order to determine if the variant in family 2 (c.1041dupC) causes nonsense-mediated mRNA decay (NMD) of *CDC14A*, the relative expression of *CDC14A* mRNA was measured. The introduction of a premature termination codon immediately after p.348 would result in the truncation of 44% of the amino acid residues in full length *CDC14A*. The infertility did not analyse in patients due to limitations. This study was published in the International Journal of Molecular Sciences. In this study, I collected clinical information for the Iranian family.

7.2 The Many Faces of DFNB9: Relating *OTOF* Variants to Hearing Impairment (Attachment 2)

OTOF encodes otoferlin, a critical protein at the synapse of auditory sensory cells, the inner hair cells (IHCs). In the absence of otoferlin, IHC signal transmission fails due to impaired release of

synaptic vesicles at the IHC synapse. Biallelic pathogenic variants in this gene cause autosomal recessive profound deafness (DFNB9). All pathogenic and likely pathogenic variants reported in literature or clinical database entries were collected (Leiden Open Variation Database v3.0 (LOVD v3), the DVD, ClinVar, and the Human Gene Mutation Database (HGMD)). This included 84 missense, 44 frameshift, 43 nonsense, 36 splice site, 7 in-frame duplications or deletions, 3 CNVs, as well as 1 stop loss and regulatory variant each. Additionally, we reviewed the broad phenotypic spectrum reported in patients with variants in *OTOF* that includes milder HL, as well as progressive and temperature-sensitive HL. By the end of preparation of our publication, 220 pathogenic and likely pathogenic variants in *OTOF* were reviewed and curated.

Studies in *Otof*-knock-out mouse models revealed that in the absence of otoferlin from IHCs, very few neurotransmitter-filled synaptic vesicles fuse with the plasma membrane (85). Thus, acoustic stimuli still generate receptor potentials in the IHCs (and OHCs), but this information is not passed to the auditory pathway. *In vitro* studies indicating that otoferlin can interact with neuronal SNARE proteins contributed to the hypothesis that otoferlin acts as a synaptotagmin-like Ca^{2+} sensor for exocytosis (86). However, later studies revealed that such neuronal SNAREs are expressed at only very low levels in IHCs and are absent from IHC synapses (87). Instead, the mechanism of vesicle fusion might rely on a unique molecular mechanism in IHCs (88). Later studies in a mouse line with the mutation of a presumed Ca^{2+} -binding site revealed a slight delay and slowing down of Ca^{2+} -triggered exocytosis, which would be in line with a Ca^{2+} -dependent acceleration of exocytosis and was interpreted as a Ca^{2+} sensor function for otoferlin in exocytosis and vesicle replenishment (89). However, the Ca^{2+} -binding capability of the site targeted in this study is still under debate. Mouse model studies also showed that in a reduction of otoferlin protein, IHC synapses are constantly deficient of fusion-competent synaptic vesicles. Consequently, no ABRs can be recorded in these animals (90).

Otoferlin isoforms

OTOF has long and short isoforms with alternative splicing of exons 6, 31 and 47. With respect to a potential functional role of the short isoforms, a review of pathogenic and likely pathogenic variants has shown no indication that variants only affecting the long, but not short, isoforms would cause a milder phenotype. This confirms that the long isoform is critically required for normal hearing function (91). There are two long isoforms for *OTOF*: isoform (a) was detected from brain cDNA extraction with the last codon in exon 47 but an alternative splice isoform (e) skips exon 47, instead using exon 48 to encode the C-terminus. Pathogenic and likely pathogenic variants in exon 48 confirmed that this exon is critical for the human cochlea.

Founder variants in *OTOF*

In Japanese patients with auditory neuropathy/synaptopathy, biallelic *OTOF* variants were uncovered in 56% of cases that included the identification of a founder variant c.5816G>A p.Arg1939Gln (92). The c.2485C>T p.Gln829* founder variant was identified in 87% of patients diagnosed with auditory neuropathy/synaptopathy in the Spanish population (93). Another founder variant c.5098G>C p.Glu1700Gln was identified in Taiwanese patients with progressive, moderate-to-profound HL. This variant was found to be present in 23% of a selected patient cohort consisting of 22 individuals with auditory neuropathy/synaptopathy (94).

Temperature-Sensitive Auditory Synaptopathy

There are nine variants in the *OTOF* gene that have been reported to cause temperature-dependent HL: c.1544T>C p.Ile515Thr, c.1621G>A p.Gly541Ser, c.4819C>T p.Arg1607Trp, c.3239G>C p.Arg1080Pro, c.2093G>C p.Arg698Thr, c.5410_5412delGAG p.Glu1804del, c.4981G>A p.Glu1661Lys, c.2383delC p.Leu795Serfs*5 and c.2975_2978del p.Gln994Valfs*6. At elevated temperature, patch clamp recordings revealed a decrease in exocytosis when cells were heated from near-physiological (35–37°C) to elevated temperatures (38.5–40°C). The wild-type protein is able to refold in higher temperatures. Potentially, any slight destabilization of this highly flexible protein might decrease the chance of re-folding after heat exposure, such that more protein is degraded at a slightly elevated body temperature, thereby exacerbating the hearing disturbance.

Current and Future Therapies for DFNB9

Diagnosing deafness caused by biallelic variants of *OTOF* or auditory neuropathies/synaptopathies of other origins is not reliably possible with OAE screening. However, in most countries, OAE assessment is the preferred method for screening in the first year of life, which may result in deafness not being diagnosed during this critical period, leading to missed opportunities for cochlear implantation. Therefore, it is recommended that newborn hearing screening protocols include ABRs, or a combination of OAEs and ABRs, to support early diagnosis. In this review, we introduced the currently favored gene therapeutic approach involves replacing the defective gene by transducing IHCs with correct cDNA by means of recombinant adeno-associated viruses (AAVs), reviewed in (95). Two separate trials have since shown promising results for this gene (96, 97). In this review, I collected all published variants, curated them and illustrated in Figure 2 of this paper.

7.3 Aberrant *COL11A1* splicing causes prelingual autosomal dominant non-syndromic HL in the DFNA37 locus (Attachment 3)

Collagen type XI alpha-1 chain (*COL11A1*) is associated with autosomal dominant Marshall syndrome (MRSHS) and autosomal dominant or recessive Stickler syndrome type 2, as well as

autosomal recessive fibrochondrogenesis (FBCG1). Each of these syndromes has a phenotypic overlap that includes skeletal abnormalities and dysmorphic features, as well as variable cleft palate, ocular, and auditory phenotypes that can include mild-to-moderate HL and outer ear malformations. Very recently, this gene has been associated with autosomal dominant non-syndromic HL (51). In our study, two non-consanguineous families with two separate splicing variants in *COL11A1* were identified that were re-evaluated in light of the new gene-disease association. After checking detailed clinical information by our colleagues, the first index was a 37-year-old proband, presenting stable, down-sloping, moderate-to-severe, high-frequency sensorineural HL, as well as hypothyroidism and diabetes. The speech discrimination with regard to monosyllables was 70% and 50% at 65-dB hearing level on the right side and 80% at 65 dB hearing level on the left side when evaluated at 34 and 37 years of age, respectively. He has worn hearing aids since age 6 years. His daughter was diagnosed with severe HL at the age of two years. All syndromic features including myopia, retinal detachment, midface hypoplasia, submucous cleft palate, and arthritis/joint pain have been excluded in both affected individuals. The second index of this study was a 31-year-old, female, presented moderate sensorineural HL in the mid- and high frequencies since early childhood. She did not have a severe form of HL that might be suggestive of progression. Her son was born at term after an unremarkable pregnancy and failed newborn hearing screening. The mother reported a cleft lip and palate, an occurrence not previously reported with Stickler syndrome type 2 and assumed to be due to other genetic or multifactorial causes. She reported no other abnormalities. Her son does not have any other symptoms except HL.

Two novel heterozygous variants in *COL11A1* were identified that each disrupt canonical splice sites: NM_080629.2:c.652-1G>C (ClinVar Accession: RCV000487702.2; LOVD Genomic Variant Accession: 0000686099) and NM_080629.2:c.4338+2T>C, arising *de novo*, (ClinVar Accession: RCV000585624.2; LOVD Genomic Variant Accession: 0000686100).

A minigene assay and TA cloning was performed for the c.652-1G>C genetic variant that identified two aberrant in-frame splice effects: r.652_663del p.Gly218_Gln221del and r.652_666del p.Gly218_Gln222del. For the second variant, c.4338+2T>C, the minigene assay showed three abnormally spliced amplicons including r.4338_4339ins4338+1_4338+4 p.Gly1447Alafs*12; r.4338_4339ins4338+1_4338+30 p.Gly1447Alafs*9 and r.4285_4338del p.Gly1429_Met1446del. In this study, I performed the minigene assay for the c.4338+2C genetic variant and confirmed the percentage of multiple bands in both minigene results by TA cloning.

Although the precise mechanism of *COL11A1*-associated hearing impairment has not been elucidated, disruption of *COL11A1* is consistently associated with HL, as demonstrated by about

84% of individuals diagnosed with MRSHS having HL, which supports the critical function of this protein in the auditory system (98). It also demonstrated that the source of *COL11A1* mRNA is in the tectorial membrane and suggested its mutation affects normal cochlear function (99). Moreover, the pleiotropy exhibited by this gene, like other genes that are associated with syndromic and non-syndromic HL, remains to be fully characterized. In summary, this work characterized two novel splice altering variants associated with DFNA37, providing confirmatory evidence of *COL11A1* as a bona fide autosomal dominant non-syndromic HL gene. It is recommended that *COL11A1* be included in the routine diagnostic testing of patients with both syndromic and non-syndromic forms of deafness.

7.4 Expanding the phenotype of *PIGS*-associated early onset epileptic developmental encephalopathy (Attachment 4)

Phosphatidylinositol glycan class S (*PIGS*) encodes a GPI-AP, specifically a subunit of the GPI transamidase complex that catalyses the attachment of preformed GPI to proteins containing a C-terminal GPI attachment signal. Biallelic pathogenic variants in *PIGS* have been reported for developmental and epileptic encephalopathy type 95 (DEE95). The phenotype for patients with DEE95 included severe global developmental delay, seizures, hypotonia, weakness, ataxia, and dysmorphic facial features, but also multiple joint contractures (consistent with fetal akinesia) in two fetuses. In this study, six patients with biallelic variants in *PIGS* were reported. All patients showed the previous reported phenotypes. Several patients also showed evidence of other phenotypes such as renal malformation (1/6, 17%), visual impairment (3/6, 50%), severe HL (2/6, 33%), and acquired arthrogryposis (2/6, 33%).

Table 4 PIGS genetic findings in five families

Family number	Variant c. and p. positions (NM_033198.4)	Zygosity	Comment
Family 1 and 2	c.174G>C p.Gln58His	Homozygous	The <i>in vitro</i> functional study was confirmed its impact on splicing
Family 3	c.1070G>A p.Gly357Asp	Homozygous	within a 10-Mb block of homozygosity
Family 4	c.986C>G p.Pro329Arg	Homozygous	Two affected, one deceased
Family 5	c.1141_1164dup24 p.Asp381_Val388dup and c.734G>A p.Trp245*	Compound heterozygous	Confirmed the trans status in parents

My contribution to this study focused on a minigene assay to assess aberrant splicing for the c.174G>C variant. It was designed to capture a 508-bp amplicon including exons 2 and 3, as well

as a 369-bp amplicon with only exon 3. The amplicon with the homozygous c.174G>C variant revealed only exon 3 (369 bp), indicating a skipping of exon 2 that was Sanger sequence confirmed. This out-of-frame deletion of exon 2 (r.35_174del) would result in a premature stop codon p.Glu12Alafs*31.

This study also introduced *PIGS* as a causal for syndromic HL. Furthermore, the significance of screening *PIGS* for infantile epilepsy is emphasized by our data. This can aid in the better understanding of new *PIGS* variants with the assistance of biochemical findings and flow cytometry analysis. Additionally, *PIGS* is not included in most commonly used epilepsy gene panels, indicating that it may be a more common cause of early infantile epilepsy than previously thought. With the expansion of epilepsy genetic testing and increased accessibility of ES, it is expected that more patients will be diagnosed in the future.

7.5 A biallelic variant in *CLRN2* causes non-syndromic HL in humans (Attachment 5)

The main aim of this thesis was to identify novel genes in HL and expand the phenotypes caused by known genes or clarify the clinical heterogeneity.

In the *CLRN2*-project, a diverse array of methodologies were employed, including genotyping, gene mapping, CNV analysis, ES data analyses, PCR and Sanger sequencing, CRISPR/Cas9-mediated inactivation of this gene in mice and zebrafish, and a minigene assay. These combined approaches were instrumental in elucidating the role of *CLRN2*, a novel gene, in the context of HL. A homozygous missense variant (c.494C>A p.Thr165Lys (NM_001079827.2)) in an Iranian family with three affected and 11 unaffected individuals was identified. Based on self-reporting of family, the earliest reported clinical diagnosis of HL in affected individuals was between 2 and 3 years of age. Newborn hearing screening was not routinely performed when the affected individuals were born, so it cannot be confirmed hearing was normal at birth.

The *in-silico* prediction via ESEs suggested that this variant impacts splicing. Therefore, *in vitro* functional assays (minigene assays) were performed in three different cell lines (HEK293, COS-7 and ARPE-19 cells), with all three experiments showing the same result, with the c.494C>A variant yielding two bands; one ~ 650 bp band matching the expected normally spliced exon, and a second abnormal band that was approximately ~ 1360 bp. Sequencing of these amplicons validated normal splicing including the c.494A variant and also revealed a retained intron 2 in the aberrantly spliced transcript. The retention of intron 2 results in a new reading frame that introduces a stop codon 26 amino acids after the native exon 2 splice site (p.Gly146Lysfs*26). Therefore, our data showed that the *CLRN2* c.494C>A variant probably affects protein function

in two ways: (1) as a missense variant (p.Thr165Lys) producing a mutant full length protein and (2) as a splice variant leading to intron retention.

In order to explore the crucial function of clarin 2 in the inner ear, zebrafish *clrn2* mutant phenotype and *Clrn2*^{del629/del629} mutant mice were produced that did not possess a functional protein. Analysis of *Clrn2*^{del629/del629} mice using ABR measurements demonstrated elevated hearing thresholds when compared to their *Clrn2*^{+/+} littermate controls at postnatal day 21 (mean click threshold of 87 dB SPL \pm 7 s.d. and 24 dB SPL \pm 6 s.d., respectively).

Altogether, this is the first time that *CLRN2* has been implicated as a gene responsible for deafness in humans, which has been confirmed through animal studies. Further investigation of families with *CLRN2* biallelic variants will be crucial in understanding the clinical characteristics of this type of HL. The experiments with zebrafish and mice have established that defective clarin 2 protein in hair cells is likely the cause of HL, as it is necessary for the proper organization and maintenance of mechanosensitive hair bundles. In this study, I performed TA cloning to clarify the percentage of different products after minigene assay.

7.6 Bi-allelic variants in *IPO8* cause a connective tissue disorder associated with cardiovascular defects, skeletal abnormalities, and immune dysregulation (Attachment 6)

Importin 8 (*IPO8*) has 25 exons that encode a 1,037 amino acid protein with the b-importin N-terminal domain (22–102 aa) and a CSE1-like domain (202–441 aa) containing a RanGTPase-binding motif characteristic of B-importins. I collaborated in a study that identified 11 novel variants in 12 individuals, with seven as homozygotes and four as compound heterozygotes in *IPO8* (GenBank: NM_006390.3). Out of the seven homozygous variants, four were likely LOF variants including three nonsense and one frameshift (c.2407C>T p.Arg803*, c.82C>T p.Gln28*, and c.2129C>G p.Ser710*, and c.728delC p.Pro243Leufs*27). One of the homozygous variants was a splicing variant (c.2695+3_2695+7delAAAGT) and two were missense variants (c.262G>A p.Asp88Asn and c.2500C>T p.Arg834Trp). The compound heterozygous variants were frameshift variants leading to a premature stop codon (c.2279delT p.Leu760ProfsTer10 and c.1538delC p.Pro513Leufs*13) *in trans* with a splicing (c.2900-1G>A p.?) and a missense variant (c.2245T>C p.Cys749Arg), respectively. Both, c.2695+3_2695+7delAAAGT and c.2900-1G>A variants were predicted to impact splicing according to SpliceAI. My contribution to this work involved analysis of the c.2695+3_2695+7delAAAGT variant using a minigene assay. The results demonstrated skipping of exon 22 and activation of a cryptic splicing site.

In summary, 12 individuals from nine families with bi-allelic LOF variants in *IPO8* were identified who presented with a syndromic association characterized by cardio-vascular anomalies, joint

hyperlaxity, and various degrees of dysmorphic features and developmental delay as well as immune dysregulation. One of the patients had severe language delay (first words spoken at the age of 6 years) contributed to by moderate to severe bilateral conductive HL. This study introduced that pathogenic variants in *IPO8* can cause conductive HL and this gene is associated with syndromic HL.

7.7 Unraveling the genetic complexities of combined retinal dystrophy and hearing impairment (Attachment 7)

Analysis of a deaf–blind cohort of 59 families was performed. This study includes the analysis of seven Mexican and 52 Iranian probands with combined retinal degeneration and hearing impairment (without intellectual disability). The clinical assessment encompassed ophthalmological examinations and a HL questionnaire. In this cohort, Usher syndrome, was primarily attributed to biallelic variants in *MYO7A* (USH1B in 16 probands), *USH2A* (17 probands), and *ADGRV1* (USH2C in 7 probands), and it was diagnosed in 44 out of 59 (75%) unrelated probands. Among the probands, 9 out of 59 (15%) exhibited other genetic conditions characterized by dual sensory impairment. These included Alström syndrome (observed in 3 patients), cone-rod dystrophy and HL 1 (seen in 2 probands), and Heimler syndrome (presented in 1 patient). Additionally, unexpected findings included individual probands with Scheie syndrome, coenzyme Q10 deficiency, and pseudoxanthoma elasticum. Two (3%) probands were partially solved and only three (5%) remained undiagnosed and the overall diagnostic yield of ES in this cohort was 92%. *In vitro* functional study (minigene assay) was performed for variants identified in two genes. I performed minigene assay for two variants to establish their impact on splicing (*ADGRV1* c.9623+3A>C and *PDSS2* c.702+1G>A splice variants). The minigene assay of the *ADGRV1* variant identified that the main donor splice site was not used and instead two cryptic donor splice sites in exon 44 were used, yielding an in-frame deletion r.9495_9623del p.Tyr3166_Arg3208del, frameshift deletion r.9530_9623del p.Gly3177Glufs*5, and partially caused skipping of exon 44 r.9448_9623del p.Ala3150Serfs*11. The minigene assay for the *PDSS2* variant detected that this variant causes skipping of exon 4, leading to an in-frame deletion r.631_702del p.Val211_Lys234del.

In summary, the findings from this study unveiled novel variants that contribute to the enrichment of existing scientific literature. It suggested that patients with dual sensory loss as the primary symptoms may suffer from various syndromes that include both hearing and vision impairment, not only limited to Usher syndrome, and can include mild symptoms or the absence of additional symptoms defining the syndrome. In many instances of monogenic disorders, the genotype does not accurately predict the phenotype. Variants found in patients with highly variable phenotypic

manifestations can also be present in seemingly healthy individuals, highlighting the importance of variable expressivity and reduced penetrance.

7.8 Biallelic variants in *KARS1* are associated with neurodevelopmental disorders and HL recapitulated by the knockout zebrafish (Attachment 8)

Aminoacyl-tRNA synthetases (ARS) are a class of enzymes that charge tRNAs with their cognate amino acids. *KARS1* (Lysyl-tRNA Synthetase 1) is one of the bifunctional ARS enzymes. In this study 10 new and four known biallelic missense variants in 22 affected individuals from 16 unrelated families were reported. Although *KARS1* was previously associated with non-syndromic HL, in this report, all patients presented syndromic HL: All cases uniformly expressed neurological symptoms (22/22, 100%), frequently involving sensorineural HL (20/21, 95%), seizures (13/22, 59%), hypotonia (9/22, 41%), cerebellar ataxia (7/22, 32%), spasticity (8/22, 36%), strabismus (6/20, 30%) and nystagmus (4/20, 20%), and acquired joint contractures (4/22, 18%). HL was severe-to-profound in 16/21 cases (76%), and 5/10 (50%) of them had cochlear implants. Other variable neurological features included visual impairment/optic atrophy (7/20, 35%), quadriplegia (3/22, 14%), dystonia and tremor (2/22, 9%), neuropathy (1/10, 10%), neurophysiologically confirmed skeletal myopathy (2/22, 9%), generalized muscle atrophy (2/22, 9%), and incontinence (4/22, 18%).

Based on this report, inter- and intrafamilial phenotypic variability was noticed among individuals with the same variants in the present *KARS1* cohort. For instance, three affected siblings in family 11 (see the attachment 8 in appendix section) each harboured a homozygous *KARS1* (c.379T>C p.Phe127Leu) variant, and although they shared common symptoms such as developmental delay, infantile-onset profound HL, dysmorphic facial features, spasticity, and varying degree of joint contractures, several important symptoms were expressed only by one of them. This included regression, epilepsy, optic atrophy, failure to thrive, and hyperactivity.

An animal model (zebrafish disease model) was generated and phenotype to attempt to recapitulate the patients' symptoms. In the brain of 5-day-old larvae, *kars1^{-/-}* mutants exhibited a vacuolated spongiosis appearance with reduced cell density and disorganized segment boundaries compared to their wild-type siblings, as revealed by histological analysis. Additionally, the mutants showed a significant reduction in eye volume and complete loss of retinal layer organization, strongly indicating impaired vision. Furthermore, staining showed a marked decrease in the number of neuronal cells in both the brain and retina of the *kars1^{-/-}* mutants compared to controls. Abnormal motor neuron morphology was also observed, including shrinkage of motor neuron axon projections and reduction of terminal axonal branching in the

mutants, further suggesting a significant alteration of locomotor function in these animals. Additionally behavioural testing showed hearing impairment in these models.

Further investigations by this project identified that loss of *kars1* leads to upregulation of p53, tissue-specific apoptosis, and downregulation of neurodevelopmental related genes, recapitulating key tissue-specific disease phenotypes of patients. Inhibition of p53 rescued several defects of *kars1*^{-/-} knockouts.

Overall, this study expands on the range of symptoms associated with *KARS1* variants, including autism/hyperactivity. Several dysmorphic facial features were noted that have rarely been reported in previous studies, with 11 out of 52 individuals showing these features. These findings also provide further evidence for skeletal myopathy, which has previously been reported in only one case. The significance of hypertrophic cardiomyopathy is highlighted, as it has been reported in a few cases and is also present in our study. Additionally, this work suggests that cerebellar ataxia may be a more frequent feature of *KARS1*-associated phenotypes than previously thought, as it was present in 32% of this cohort compared to only 10% in previous reports. Overall, this analysis shows that *KARS1* variants primarily affect neurological and neurosensory functions and are associated with facial dysmorphism, similar to other aminoacyl-tRNA synthetase disorders. In this study, I performed a minigene assay for select variant predicted to cause aberrant splicing. The minigene assay showed the variant behaves as wildtype, therefore the variant excluded from study and was not mentioned in the publication.

7.9 Bi-allelic variants in *SPATA5L1* lead to intellectual disability, spastic-dystonic cerebral palsy, epilepsy, and HL (Attachment 9)

A substantial cohort of individuals with *SPATA5L1* variants was assembled, revealing, for the first time, that biallelic pathogenic variants in this gene are associated with both non-syndromic and syndromic HL. Twenty-eight unique variants were identified with 25 compound heterozygous and 3 were homozygous.

In 25 patients with syndromic HL, 22 patients had movement disorder, 18 of them had abnormal MRI, 16 of patients had hypotonia and visual impairment, 13 of them had epilepsy and 11 of these patients had microcephaly.

In 22 patients with non-syndromic HL, all were of Ashkenazi Jewish decent, and in all, the missense variant (c.1398T>G p.Ile466Met), was identified in compound heterozygosity with various other pathogenic alleles, suggesting a hypomorphic founder allele, resulting in a partial rather than complete loss-of-protein function. My contribution to this study explored expression of *SPATA5L1* in the mouse inner ear. *SPATA5L1* is expressed at low levels in hair cells (inner and outer) as well as supporting cells (pillar and Deiter cells) in adult mice.

7.10 Identification of three novel homozygous variants in *COL9A3* causing autosomal recessive Stickler syndrome (Attachment 10)

COL9A3 serves as a good example of a gene that exhibits clinical heterogeneity. Previous studies have shown heterozygous variants in *COL9A3* as causing multiple epiphyseal dysplasia type 3. It also has been shown that heterozygous *COL9A3* variants have been identified as causing peripheral vitreoretinal degeneration and retinal detachment. Collagen IX proteins, encoded by *COL9A1*, *COL9A2*, and *COL9A3*, together form fibril heterotrimer-associated collagens. *COL9A1* and *COL9A2*, are causally associated with autosomal recessive Stickler type 4 and type 5, respectively. Through aggregating three unrelated families with deleterious biallelic variants in *COL9A3*, we confirmed its association with Stickler syndrome type 6.

By performing ES in three families, three LOF variants: (c.107_116del p.Pro36Argfs*49, rs1470627424) in exon 2, (c.1204C>T p.Arg402*, rs989413835) in exon 23, and (c.355delC p.Leu119Serfs*9) in exon 7 were identified. We gathered detailed clinical information and measurements from our patients compared to previous publications and confirmed that short stature and cleft palate were not observed in this sub-type of Stickler syndrome. Interestingly, the degree of hearing loss is variable for this syndrome, ranging from moderate to profound (Figure 6), for details see the attachment 10 in the appendix section.

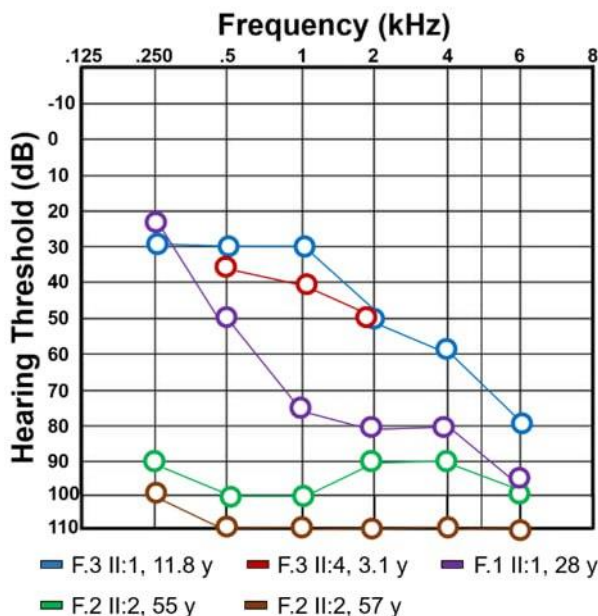


Figure 6 Audiogram from three patients with biallelic *COL9A3* variants

Before this study, four unrelated families were reported with homozygous LOF variants in this gene with overlapping phenotype (100-103). The current study confirmed that variants in homozygous status cause recessive Stickler syndrome, therefore designating it as Stickler

syndrome type 6. OMIM's gene-phenotype curation of this gene was updated following publication to include Stickler syndrome type 6.

In summary, this report consolidates that homozygous LOF variants in *COL9A3* cause Stickler syndrome type 6. It was mainly demonstrated that high myopia and moderate-severe HL to be consistent features amongst all cases while skeletal findings seem more variable.

7.11 Unraveling haplotype errors in the DFNA33 locus (Attachment 11)

The original family that mapped the DFNA33 locus in 2009 was analysed using GS (104). However, the causal gene and a priority question in the field remained unidentified. As recently, it was demonstrated that *ATP11A* is responsible for autosomal dominant non-syndromic HL (DFNA84) (105), this gene was an obvious candidate gene potentially causing HL in the original family. Therefore, we performed GS in a member of the original family to determine if the DFNA33 locus may also be assigned to *ATP11A*.

After GS and analysis, we identified a deep intronic variant in *ATP11A* intron 8 (chr13:113421269C>G (GRCh37), ENST00000375630: c.725 + 737C>T p.?) that was predicted via *in-silico* tools to activate exonic splice enhancers. A minigene assay showed that this intronic variant does not change the normal splicing process; therefore, the variant was classified as likely benign (PM2_Supporting, BP4_Supporting, and BS3_Strong; -4 points (likely benign point range: -6 to -1)) (106). After conducting short-read GS, this study determined that *ATP11A* is not the gene responsible for the DFNA33 locus. In this study, I performed the minigene assay for the deep intronic variant.

7.12 Expanding the spectrum of phenotypes for *MPDZ*: report of four unrelated families and review of the literature (Attachment 12)

MPDZ, also known as MUPP1, encodes the multiple PDZ domain crumbs cell polarity complex component. This protein stands as the largest among PDZ (PSD95/DLG1/ZO1) domain-containing proteins, with 13 PDZ domains. The *MPDZ* gene-disease relationship with biallelic variants currently extends to congenital hydrocephalus type 2 with or without brain or eye abnormalities. However, the literature presents a continuously evolving and complex phenotypic landscape. Several studies have demonstrated that variants in *MPDZ* have additional features, including vision impairment, hearing impairment, cardiac abnormalities, controllable seizure, mild intellectual disability, lung hypoplasia, malrotation of the gut, and multicystic dysplastic kidney. In this study, four more families were introduced with variable phenotypes. Family 1 has three affected siblings with a compound heterozygous variant and two living affected siblings who have an overlapping phenotype with hydrocephalus, mild intellectual disability, delayed speech

development, and congenital HL (mild to moderate sensorineural HL). The LOF variant (c.3508C>T p.Arg1170*) in this family was entered in ClinVar but the second variant (c.5231+1G>A p.?) was a novel splicing variant. I performed a minigene assay on this variant and the result of this assay confirmed aberrant splicing and cryptic splice sites were used in the transfected cell line by this variant. The c.5231+1G>A variant indicates this donor splice site is skipped and instead, either usage of two cryptic splice sites or skipping of exon 38 occurred. The first cryptic splice site (TGGT) in exon 38 causes a frameshift variant: g.13121740_13121746del, r.5227_5231+2del p.Asn1745Tyrfs*36. The second cryptic splice site in this exon, TTGT, causes an inframe deletion: g.13121739_13121749del, c.5223_5231+2del p.Gly1742_Arg1744del. The skipping of exon 38 causes another frameshift variant: g.13121741_13121934del, c.5041_5231+3del p.Asn1681Lysfs*38. In this study, two patients (the index patients in families 2 and 3) had spasticity that was not described in previous studies to date. The detected missense variants (c.4993G>A p.Ala1665Thr, c.5362G>C p.Val1788Leu, c.5701G>C p.Ala1901Pro) were classified as variants of uncertain significance. The auditory electrophysiology data from a knockout murine model (*Mpdz^{em1(IMPC)}/em1(IMPC)*) generated by the International Mouse Phenotyping Consortium (IMPC) demonstrated severe hearing impairment. Aside from describing four families with biallelic *MPDZ* variants, a comprehensive review of the literature identified nine studies with 18 index patients that were reported to date. The systematic review analysis in this study summarized that hydrocephalus, vision impairment, macrocephaly, hearing impairment, and cardiovascular were the main clinical features described in patients with biallelic variants in this gene. The other phenotypes are intellectual disability, seizure, frontal bossing, skeletal anomalies, hypotonia, and spasticity. This study not only expands the *MPDZ*-related phenotype by highlighting hearing impairment and spasticity, but also emphasizes that missense variants in this gene might be disease causing and suggests further functional validation of the pathogenicity of missense variants in this gene.

7.13 Conclusion and Outlook

As NGS technology continues to advance and become more accessible for the analysis of increasing numbers of cases, it is now possible to rapidly discover unknown genes related to different rare diseases. One of the most common sensory disorders is HL, which is estimated to include nearly 1000 genes. The primary objective of this project was to identify novel HL associated genes or known genes causing unrecognized allelic disorders. Several genes involved in HL that exhibit allelic disorders or variable severity of phenotype were established during this thesis. These findings are crucial for diagnostic labs to include for accelerating diagnoses. During the completion of this thesis, the role of *COL11A1* was confirmed in non-

syndromic HL through the *in vitro* functional characterization of two novel splice variants. While multiple epiphyseal dysplasia-3 is a well-established disease caused by heterozygous pathogenic variants in *COL9A3*, few studies have demonstrated the role of homozygous pathogenic variants in Stickler syndrome. Here, we introduced three unrelated families with LOF variants in *COL9A3*, designating it as causal for Stickler syndrome, type 6 due to biallelic deleterious variants. Another project expanded the spectrum of *MPDZ*, confirming its role in HL through introducing a new family with three affected individuals with compound heterozygous variants. Additionally, I was involved in characterization of two novel genes: *CLRN2*, causing non-syndromic HL (DFNB117) and *SPATA5L1*, causing both syndromic and non-syndromic (DFNB119) HL. Further case series are necessary to consolidate the role of *CLRN2* in HL as only one other report has very recently been published following the original gene discovery study (107). Regarding *SPATA5L1*, only a specific variant in a particular population has been shown to cause non-syndromic HL; however, further investigation is required to confirm whether this may be true of other variants.

After primarily using ES for diagnosis in our cohort, approximately 26% of individuals remained unresolved. We will regularly reannotate and reanalyze these cases based on updated evidence and tools. Every method has its limitations; for example, ES cannot accurately detect deep intronic variants. All variants detected in our cohort were SNVs, but variants in CNVs/SVs should be considered which may not be easily detected by ES, especially duplications. Therefore, we will need to focus on these two types of variants.

We have identified a potential novel gene associated with HL that is at an early stage of characterization. Besides functional studies, *in vitro* and animal models, we require further human cases. Consequently, we continuously monitor new cases by searching in different diagnosis labs and using specific tools like GeneMatcher.

8 Acknowledgements

I would like to express my sincere gratitude to Dr. Barbara Vona for her invaluable guidance and support throughout the process of writing my thesis. Her expertise, insightful feedback, and encouragement have been instrumental in shaping my research and improving the quality of my work. I am truly grateful for her time, patience, and dedication to helping me achieve my academic goals. Thank you for being an exceptional mentor and for providing me with the necessary tools to succeed.

I would also like to acknowledge Prof. Olaf Rieß and Prof. Bernd Wissinger for their careful supervision.

I would like to extend my heartfelt gratitude to the families and patients who participated in my thesis research. Your willingness to share your experiences and insights has been invaluable in advancing our understanding of the topic at hand. Your contribution has not only helped me fulfill my academic requirements but also has the potential to benefit others in similar situations.

I would like to express my deepest appreciation to my wife, Maryam Najafi, for her unwavering support and understanding throughout the entire process of completing my thesis. Her constant encouragement, patience, and love have been my source of strength and motivation. She has been my sounding board, my editor, and my cheerleader, always there to lend a helping hand whenever I needed it. Without her unwavering support, I would not have been able to complete this project. I am truly grateful for her presence in my life and for being my partner in this journey. Thank you for everything, my love.

9 References

1. . Available from: <https://www.who.int/publications/i/item/addressing-the-rising-prevalence-of-hearing-loss>.
2. Hearing loss prevalence and years lived with disability, 1990-2019: findings from the Global Burden of Disease Study 2019. *Lancet*. 2021;397(10278):996-1009.
3. loss W-Dah. [Available from: <https://www.who.int/news-room/fact-sheets/detail/deafness-and-hearing-loss>].
4. McDaid D, Park AL, Chadha S. Estimating the global costs of hearing loss. *Int J Audiol*. 2021;60(3):162-70.
5. Korver AM, Smith RJ, Van Camp G, Schleiss MR, Bitner-Glindzicz MA, Lustig LR, et al. Congenital hearing loss. *Nat Rev Dis Primers*. 2017;3:16094.
6. Deafness and hearing loss 2023 [Available from: <https://www.who.int/news-room/fact-sheets/detail/deafness-and-hearing-loss>].
7. Sheffield AM, Smith RJH. The Epidemiology of Deafness. *Cold Spring Harb Perspect Med*. 2019;9(9).
8. Andronaco DW. Congenital Cytomegalovirus and Hearing Loss. *J Obstet Gynecol Neonatal Nurs*. 2020;49(3):293-304.
9. Lindeborg MM, Jung DH, Chan DK, Mitnick CD. Prevention and management of hearing loss in patients receiving ototoxic medications. *Bull World Health Organ*. 2022;100(12):789-96a.
10. Wouters NL, Kaanen CI, den Ouden PJ, Schilthuis H, Böhringer S, Sorgdrager B, et al. Noise Exposure and Hearing Loss among Brewery Workers in Lagos, Nigeria. *Int J Environ Res Public Health*. 2020;17(8).
11. Noise and hearing loss. *Consens Statement*. 1990;8(1):1-24.
12. Bowl MR, Dawson SJ. Age-Related Hearing Loss. *Cold Spring Harb Perspect Med*. 2019;9(8).
13. Øhre B, Uthus MP, von Tetzchner S, Falkum E. Traumatization in Deaf and Hard-of-Hearing Adult Psychiatric Outpatients. *J Deaf Stud Deaf Educ*. 2015;20(3):296-308.
14. Mancini P, Atturo F, Di Mario A, Portanova G, Ralli M, De Virgilio A, et al. Hearing loss in autoimmune disorders: Prevalence and therapeutic options. *Autoimmun Rev*. 2018;17(7):644-52.
15. Totten DJ, Manzoor NF, Perkins EL, Cass ND, Bennett ML, Haynes DS. Management of vestibular dysfunction and hearing loss in intralabyrinthine schwannomas. *Am J Otolaryngol*. 2021;42(4):102984.
16. Collins A, Beswick R, Driscoll C, Kei J. Conductive hearing loss in newborns: Hearing profile, risk factors, and occasions of service. *Int J Pediatr Otorhinolaryngol*. 2023;171:111630.
17. Tanna RJ, Lin JW, De Jesus O. Sensorineural Hearing Loss. *StatPearls*. Treasure Island (FL): StatPearls Publishing Copyright © 2023, StatPearls Publishing LLC.; 2023.
18. Hopkins K. Deafness in cochlear and auditory nerve disorders. *Handb Clin Neurol*. 2015;129:479-94.
19. Heine C, Slone M. Case studies of adults with central auditory processing disorder: Shifting the spotlight! *SAGE Open Med Case Rep*. 2019;7:2050313x18823461.
20. Moore DR, Rosen S, Bamiou DE, Campbell NG, Sirimanna T. Evolving concepts of developmental auditory processing disorder (APD): a British Society of Audiology APD special interest group 'white paper'. *Int J Audiol*. 2013;52(1):3-13.
21. Aristidou IL, Hohman MH. Central Auditory Processing Disorder. *StatPearls*. Treasure Island (FL): StatPearls Publishing Copyright © 2023, StatPearls Publishing LLC.; 2023.
22. Chen MM, Oghalai JS. Diagnosis and Management of Congenital Sensorineural Hearing Loss. *Curr Treat Options Pediatr*. 2016;2(3):256-65.
23. Jallu AS, Hussain T, Hamid WU, Pampori RA. Prelingual Deafness: An Overview of Treatment Outcome. *Indian J Otolaryngol Head Neck Surg*. 2019;71(Suppl 2):1078-89.
24. Waldstein RS. Effects of postlingual deafness on speech production: implications for the role of auditory feedback. *J Acoust Soc Am*. 1990;88(5):2099-114.
25. Humes LE, Dubno JR, Gordon-Salant S, Lister JJ, Cacace AT, Cruickshanks KJ, et al. Central presbycusis: a review and evaluation of the evidence. *J Am Acad Audiol*. 2012;23(8):635-66.

26. Olusanya BO, Davis AC, Hoffman HJ. Hearing loss grades and the International classification of functioning, disability and health. *Bull World Health Organ.* 2019;97(10):725-8.
27. Shearer AE, Hildebrand MS, Schaefer AM, Smith RJH. Genetic Hearing Loss Overview. In: Adam MP, Feldman J, Mirzaa GM, Pagon RA, Wallace SE, Bean LJH, et al., editors. *GeneReviews*(®). Seattle (WA): University of Washington, Seattle Copyright © 1993-2024, University of Washington, Seattle. *GeneReviews* is a registered trademark of the University of Washington, Seattle. All rights reserved.; 1993.
28. Fletcher H. A method of calculating hearing loss for speech from an audiogram. *Acta Otolaryngol Suppl.* 1950;90:26-37.
29. Salmon MK, Brant J, Hohman MH, Leibowitz D. Audiogram Interpretation. *StatPearls.* Treasure Island (FL): StatPearls Publishing Copyright © 2023, StatPearls Publishing LLC.; 2023.
30. Pittman AL, Stelmachowicz PG. Hearing loss in children and adults: audiometric configuration, asymmetry, and progression. *Ear Hear.* 2003;24(3):198-205.
31. Slinger YS. Auditory brain stem response for objective measures of hearing. *Ear Hear.* 1993;14(1):23-30.
32. Young A, Ng M. Otoacoustic Emissions. *StatPearls.* Treasure Island (FL): StatPearls Publishing Copyright © 2023, StatPearls Publishing LLC.; 2023.
33. Hereditary Hearing Loss [Available from: <https://hereditaryhearingloss.org/>].
34. Bruzzone R, White TW, Paul DL. Connections with connexins: the molecular basis of direct intercellular signaling. *Eur J Biochem.* 1996;238(1):1-27.
35. Kikuchi T, Kimura RS, Paul DL, Adams JC. Gap junctions in the rat cochlea: immunohistochemical and ultrastructural analysis. *Anat Embryol (Berl).* 1995;191(2):101-18.
36. Everett LA, Glaser B, Beck JC, Idol JR, Buchs A, Heyman M, et al. Pendred syndrome is caused by mutations in a putative sulphate transporter gene (PDS). *Nat Genet.* 1997;17(4):411-22.
37. Scott DA, Wang R, Kreman TM, Andrews M, McDonald JM, Bishop JR, et al. Functional differences of the PDS gene product are associated with phenotypic variation in patients with Pendred syndrome and non-syndromic hearing loss (DFNB4). *Hum Mol Genet.* 2000;9(11):1709-15.
38. Scott DA, Karniski LP. Human pendrin expressed in *Xenopus laevis* oocytes mediates chloride/formate exchange. *Am J Physiol Cell Physiol.* 2000;278(1):C207-11.
39. Scott DA, Wang R, Kreman TM, Sheffield VC, Karniski LP. The Pendred syndrome gene encodes a chloride-iodide transport protein. *Nat Genet.* 1999;21(4):440-3.
40. Wangemann P, Itza EM, Albrecht B, Wu T, Jabba SV, Maganti RJ, et al. Loss of KCNJ10 protein expression abolishes endocochlear potential and causes deafness in Pendred syndrome mouse model. *BMC Med.* 2004;2:30.
41. Naz S. Molecular genetic landscape of hereditary hearing loss in Pakistan. *Human Genetics.* 2022;141(3):633-48.
42. Fang Y, Gu M, Wang C, Suo F, Wang G, Xia Y. GJB2 as Well as SLC26A4 Gene Mutations are Prominent Causes for Congenital Deafness. *Cell Biochem Biophys.* 2015;73(1):41-4.
43. Xiang YB, Tang SH, Li HZ, Xu CY, Chen C, Xu YZ, et al. Mutation analysis of common deafness-causing genes among 506 patients with nonsyndromic hearing loss from Wenzhou city, China. *Int J Pediatr Otorhinolaryngol.* 2019;122:185-90.
44. Sloan-Heggen CM, Babanejad M, Beheshtian M, Simpson AC, Booth KT, Ardalani F, et al. Characterising the spectrum of autosomal recessive hereditary hearing loss in Iran. *J Med Genet.* 2015;52(12):823-9.
45. Zhang Y, Malekpour M, Al-Madani N, Kahrizi K, Zanganeh M, Lohr NJ, et al. Sensorineural deafness and male infertility: a contiguous gene deletion syndrome. *J Med Genet.* 2007;44(4):233-40.
46. Diaz-Horta O, Sirmaci A, Doherty D, Nance W, Arnos K, Pandya A, et al. GPSM2 mutations in Chudley-McCullough syndrome. *Am J Med Genet A.* 2012;158a(11):2972-3.
47. Doherty D, Chudley AE, Coghlan G, Ishak GE, Innes AM, Lemire EG, et al. GSPM2 mutations cause the brain malformations and hearing loss in Chudley-McCullough syndrome. *Am J Hum Genet.* 2012;90(6):1088-93.
48. Ala-Kokko L, Shanske AL. Mosaicism in Marshall syndrome. *Am J Med Genet A.* 2009;149a(6):1327-30.
49. Poulson AV, Hooymans JM, Richards AJ, Bearcroft P, Murthy R, Baguley DM, et al. Clinical features of type 2 Stickler syndrome. *J Med Genet.* 2004;41(8):e107.
50. Tompson SW, Bacino CA, Safina NP, Bober MB, Proud VK, Funari T, et al. Fibrochondrogenesis results from mutations in the COL11A1 type XI collagen gene. *Am J Hum Genet.* 2010;87(5):708-12.

51. Booth KT, Askew JW, Talebizadeh Z, Huygen PLM, Eudy J, Kenyon J, et al. Splice-altering variant in COL11A1 as a cause of nonsyndromic hearing loss DFNA37. *Genet Med.* 2019;21(4):948-54.
52. Khateb S, Kowalewski B, Bedoni N, Damme M, Pollack N, Saada A, et al. A homozygous founder missense variant in arylsulfatase G abolishes its enzymatic activity causing atypical Usher syndrome in humans. *Genet Med.* 2018;20(9):1004-12.
53. Velde HM, Reurink J, Held S, Li CHZ, Yzer S, Oostrik J, et al. Usher syndrome type IV: clinically and molecularly confirmed by novel ARSG variants. *Hum Genet.* 2022;141(11):1723-38.
54. Bayazit YA, Yilmaz M. An overview of hereditary hearing loss. *ORL J Otorhinolaryngol Relat Spec.* 2006;68(2):57-63.
55. Bolz H, von Brederlow B, Ramírez A, Bryda EC, Kutsche K, Nothwang HG, et al. Mutation of CDH23, encoding a new member of the cadherin gene family, causes Usher syndrome type 1D. *Nat Genet.* 2001;27(1):108-12.
56. Ebermann I, Wiesen MH, Zrenner E, Lopez I, Pigeon R, Kohl S, et al. GPR98 mutations cause Usher syndrome type 2 in males. *J Med Genet.* 2009;46(4):277-80.
57. Puffenberger EG, Jinks RN, Sougnez C, Cibulskis K, Willert RA, Achilly NP, et al. Genetic mapping and exome sequencing identify variants associated with five novel diseases. *PLoS One.* 2012;7(1):e28936.
58. Huang BY, Zdanski C, Castillo M. Pediatric sensorineural hearing loss, part 2: syndromic and acquired causes. *AJNR Am J Neuroradiol.* 2012;33(3):399-406.
59. Hedley PL, Jørgensen P, Schlamowitz S, Wangari R, Moolman-Smook J, Brink PA, et al. The genetic basis of long QT and short QT syndromes: a mutation update. *Hum Mutat.* 2009;30(11):1486-511.
60. Acke FRE, De Leenheer EMR. Hearing Loss in Stickler Syndrome: An Update. *Genes (Basel).* 2022;13(9).
61. Halliday D, Parry A, Evans DG. Neurofibromatosis type 2 and related disorders. *Curr Opin Oncol.* 2019;31(6):562-7.
62. Marszałek-Kruk BA, Wójcicki P, Dowgierd K, Śmigiel R. Treacher Collins Syndrome: Genetics, Clinical Features and Management. *Genes (Basel).* 2021;12(9).
63. Bryant D, Pauzuolyte V, Ingham NJ, Patel A, Pagarkar W, Anderson LA, et al. The timing of auditory sensory deficits in Norrie disease has implications for therapeutic intervention. *JCI Insight.* 2022;7(3).
64. Sowden JC, Kros CJ, Sirimanna T, Pagarkar W, Oluonye N, Henderson RH. Impact of sight and hearing loss in patients with Norrie disease: advantages of Dual Sensory clinics in patient care. *BMJ Paediatr Open.* 2020;4(1):e000781.
65. Robertson S. X-Linked Otopalatodigital Spectrum Disorders. In: Adam MP, Feldman J, Mirzaa GM, Pagon RA, Wallace SE, Bean LJH, et al., editors. *GeneReviews*®. Seattle (WA): University of Washington, Seattle Copyright © 1993-2024, University of Washington, Seattle. GeneReviews is a registered trademark of the University of Washington, Seattle. All rights reserved.; 1993.
66. Alford RL, Arnos KS, Fox M, Lin JW, Palmer CG, Pandya A, et al. American College of Medical Genetics and Genomics guideline for the clinical evaluation and etiologic diagnosis of hearing loss. *Genet Med.* 2014;16(4):347-55.
67. Li MM, Tayoun AA, DiStefano M, Pandya A, Rehm HL, Robin NH, et al. Clinical evaluation and etiologic diagnosis of hearing loss: A clinical practice resource of the American College of Medical Genetics and Genomics (ACMG). *Genet Med.* 2022;24(7):1392-406.
68. Zelante L, Gasparini P, Estivill X, Melchionda S, D'Agruma L, Govea N, et al. Connexin26 mutations associated with the most common form of non-syndromic neurosensory autosomal recessive deafness (DFNB1) in Mediterraneans. *Hum Mol Genet.* 1997;6(9):1605-9.
69. Smith RJ, Bale JF, Jr., White KR. Sensorineural hearing loss in children. *Lancet.* 2005;365(9462):879-90.
70. Morton CC, Nance WE. Newborn hearing screening--a silent revolution. *N Engl J Med.* 2006;354(20):2151-64.
71. Usami S, Nishio SY, Nagano M, Abe S, Yamaguchi T. Simultaneous screening of multiple mutations by invader assay improves molecular diagnosis of hereditary hearing loss: a multicenter study. *PLoS One.* 2012;7(2):e31276.
72. Ohtsuka A, Yuge I, Kimura S, Namba A, Abe S, Van Laer L, et al. GJB2 deafness gene shows a specific spectrum of mutations in Japan, including a frequent founder mutation. *Hum Genet.* 2003;112(4):329-33.
73. homozygosity mapper [Available from: <https://www.homozygositymapper.org/>].

74. Shickh S, Mighton C, Uleryk E, Pechlivanoglou P, Bombard Y. The clinical utility of exome and genome sequencing across clinical indications: a systematic review. *Hum Genet.* 2021;140(10):1403-16.
75. Wang R, Wang Z, Wang J, Li S. SpliceFinder: ab initio prediction of splice sites using convolutional neural network. *BMC Bioinformatics.* 2019;20(Suppl 23):652.
76. Shamsani J, Kazakoff SH, Armean IM, McLaren W, Parsons MT, Thompson BA, et al. A plugin for the Ensembl Variant Effect Predictor that uses MaxEntScan to predict variant spliceogenicity. *Bioinformatics.* 2018;35(13):2315-7.
77. Pertea M, Lin X, Salzberg SL. GeneSplicer: a new computational method for splice site prediction. *Nucleic Acids Research.* 2001;29(5):1185-90.
78. Reese MG, Eeckman FH, Kulp D, Haussler D. Improved splice site detection in Genie. *J Comput Biol.* 1997;4(3):311-23.
79. Vona B, Mazaheri N, Lin SJ, Dunbar LA, Maroofian R, Azaiez H, et al. A biallelic variant in CLRN2 causes non-syndromic hearing loss in humans. *Hum Genet.* 2021;140(6):915-31.
80. Cartegni L, Wang J, Zhu Z, Zhang MQ, Krainer AR. ESEfinder: a web resource to identify exonic splicing enhancers. *Nucleic Acids Research.* 2003;31(13):3568-71.
81. Fairbrother WG, Yeo GW, Yeh R, Goldstein P, Mawson M, Sharp PA, et al. RESCUE-ESE identifies candidate exonic splicing enhancers in vertebrate exons. *Nucleic Acids Research.* 2004;32(suppl_2):W187-W90.
82. Stegmeier F, Amon A. Closing mitosis: the functions of the Cdc14 phosphatase and its regulation. *Annu Rev Genet.* 2004;38:203-32.
83. Delmaghani S, Aghaie A, Bouyacoub Y, El Hachmi H, Bonnet C, Riahi Z, et al. Mutations in CDC14A, Encoding a Protein Phosphatase Involved in Hair Cell Ciliogenesis, Cause Autosomal-Recessive Severe to Profound Deafness. *Am J Hum Genet.* 2016;98(6):1266-70.
84. Imtiaz A, Belyantseva IA, Beirl AJ, Fenollar-Ferrer C, Bashir R, Bukhari I, et al. CDC14A phosphatase is essential for hearing and male fertility in mouse and human. *Hum Mol Genet.* 2018;27(5):780-98.
85. Pangrsic T, Lasarow L, Reuter K, Takago H, Schwander M, Riedel D, et al. Hearing requires otoferlin-dependent efficient replenishment of synaptic vesicles in hair cells. *Nat Neurosci.* 2010;13(7):869-76.
86. Beurg M, Michalski N, Safieddine S, Bouleau Y, Schneggenburger R, Chapman ER, et al. Control of exocytosis by synaptotagmins and otoferlin in auditory hair cells. *J Neurosci.* 2010;30(40):13281-90.
87. Nouvian R, Neef J, Bulankina AV, Reisinger E, Pangršič T, Frank T, et al. Exocytosis at the hair cell ribbon synapse apparently operates without neuronal SNARE proteins. *Nat Neurosci.* 2011;14(4):411-3.
88. Pangršič T, Reisinger E, Moser T. Otoferlin: a multi-C2 domain protein essential for hearing. *Trends Neurosci.* 2012;35(11):671-80.
89. Michalski N, Goutman JD, Auclair SM, Boutet de Monvel J, Tertrais M, Emptoz A, et al. Otoferlin acts as a Ca(2+) sensor for vesicle fusion and vesicle pool replenishment at auditory hair cell ribbon synapses. *Elife.* 2017;6.
90. Schwander M, Sczaniecka A, Grillet N, Bailey JS, Avenarius M, Najmabadi H, et al. A forward genetics screen in mice identifies recessive deafness traits and reveals that pejvakin is essential for outer hair cell function. *J Neurosci.* 2007;27(9):2163-75.
91. Yasunaga S, Grati M, Chardenoux S, Smith TN, Friedman TB, Lalwani AK, et al. OTOF encodes multiple long and short isoforms: genetic evidence that the long ones underlie recessive deafness DFNB9. *Am J Hum Genet.* 2000;67(3):591-600.
92. Matsunaga T, Mutai H, Kunishima S, Namba K, Morimoto N, Shinjo Y, et al. A prevalent founder mutation and genotype-phenotype correlations of OTOF in Japanese patients with auditory neuropathy. *Clin Genet.* 2012;82(5):425-32.
93. Rodríguez-Ballesteros M, Reynoso R, Olarte M, Villamar M, Morera C, Santarelli R, et al. A multicenter study on the prevalence and spectrum of mutations in the otoferlin gene (OTOF) in subjects with nonsyndromic hearing impairment and auditory neuropathy. *Hum Mutat.* 2008;29(6):823-31.
94. Chiu YH, Wu CC, Lu YC, Chen PJ, Lee WY, Liu AY, et al. Mutations in the OTOF gene in Taiwanese patients with auditory neuropathy. *Audiol Neurootol.* 2010;15(6):364-74.
95. Reisinger E. Dual-AAV delivery of large gene sequences to the inner ear. *Hear Res.* 2020;394:107857.
96. Qi J, Tan F, Zhang L, Lu L, Zhang S, Zhai Y, et al. AAV-Mediated Gene Therapy Restores Hearing in Patients with DFNB9 Deafness. *Adv Sci (Weinh).* 2024:e2306788.
97. Lv J, Wang H, Cheng X, Chen Y, Wang D, Zhang L, et al. AAV1-hOTOF gene therapy for autosomal recessive deafness 9: a single-arm trial. *Lancet.* 2024.

98. Bacciu A, Di Lella F, Iaccarino I, Pasanisi E, Fava G, Vincenti V, et al. Audiologic Manifestations of Marshall Syndrome. *Otol Neurotol*. 2018;39(8):e691-e8.
99. Shpargel KB, Makishima T, Griffith AJ. Col11a1 and Col11a2 mRNA expression in the developing mouse cochlea: implications for the correlation of hearing loss phenotype with mutant type XI collagen genotype. *Acta Otolaryngol*. 2004;124(3):242-8.
100. Faletra F, D'Adamo AP, Bruno I, Athanasakis E, Biskup S, Esposito L, et al. Autosomal recessive Stickler syndrome due to a loss of function mutation in the COL9A3 gene. *Am J Med Genet A*. 2014;164a(1):42-7.
101. Hanson-Kahn A, Li B, Cohn DH, Nickerson DA, Bamshad MJ, Hudgins L. Autosomal recessive Stickler syndrome resulting from a COL9A3 mutation. *Am J Med Genet A*. 2018;176(12):2887-91.
102. Nixon TRW, Alexander P, Richards A, McNinch A, Bearcroft PWP, Cobben J, et al. Homozygous Type IX collagen variants (COL9A1, COL9A2, and COL9A3) causing recessive Stickler syndrome-Expanding the phenotype. *Am J Med Genet A*. 2019;179(8):1498-506.
103. Markova T, Sparber P, Borovikov A, Nagornova T, Dadali E. Clinical and genetic characterization of autosomal recessive stickler syndrome caused by novel compound heterozygous mutations in the COL9A3 gene. *Mol Genet Genomic Med*. 2021;9(3):e1620.
104. Bönsch D, Schmidt CM, Scheer P, Bohlender J, Neumann C, Am Zehnhoff-Dinnesen A, et al. [A new gene locus for an autosomal-dominant non-syndromic hearing impairment (DFNA 33) is situated on chromosome 13q34-qter]. *Hno*. 2009;57(4):371-6.
105. Pater JA, Penney C, O'Rielly DD, Griffin A, Kamal L, Brownstein Z, et al. Autosomal dominant non-syndromic hearing loss maps to DFNA33 (13q34) and co-segregates with splice and frameshift variants in ATP11A, a phospholipid flippase gene. *Hum Genet*. 2022;141(3-4):431-44.
106. Richards S, Aziz N, Bale S, Bick D, Das S, Gastier-Foster J, et al. Standards and guidelines for the interpretation of sequence variants: a joint consensus recommendation of the American College of Medical Genetics and Genomics and the Association for Molecular Pathology. *Genet Med*. 2015;17(5):405-24.
107. Mendia C, Peineau T, Zamani M, Felgerolle C, Yahiaoui N, Christophersen N, et al. Clarin-2 gene supplementation durably preserves hearing in a model of progressive hearing loss. *Mol Ther*. 2024.

10 Appendix

10.1 Attachment 1

Novel Loss-of-Function Variants in CDC14A are Associated with Recessive Sensorineural HL in Iranian and Pakistani Patients



Article

Novel Loss-of-Function Variants in *CDC14A* are Associated with Recessive Sensorineural Hearing Loss in Iranian and Pakistani Patients

Julia Doll ¹, Susanne Kolb ¹, Linda Schnapp ¹, Abolfazl Rad ^{2,3} , Franz Rüschemdorf ⁴, Imran Khan ⁵, Abolfazl Adli ², Atefeh Hasanzadeh ², Daniel Liedtke ¹ , Sabine Knaup ¹, Michaela AH Hofrichter ¹, Tobias Müller ⁶, Marcus Dittrich ^{1,6}, Il-Keun Kong ⁷ , Hyung-Goo Kim ⁸, Thomas Haaf ¹ and Barbara Vona ^{1,3,*}

- ¹ Institute of Human Genetics, Julius Maximilians University, 97074 Würzburg, Germany; julia.doll@uni-wuerzburg.de (J.D.); susi_kolb@yahoo.de (S.K.); schnapp-linda@web.de (L.S.); liedtke@biozentrum.uni-wuerzburg.de (D.L.); sabine.knaup@uni-wuerzburg.de (S.K.); michaela.hofrichter@uni-wuerzburg.de (M.A.H.); marcus.dittrich@biozentrum.uni-wuerzburg.de (M.D.); thomas.haaf@uni-wuerzburg.de (T.H.)
 - ² Cellular and Molecular Research Center, Sabzevar University of Medical Sciences, Sabzevar 009851, Iran; rad6790@yahoo.com (A.R.); abolfazl_adli@yahoo.com (A.A.); atefeh.hasanzadeh5@gmail.com (A.H.)
 - ³ Tübingen Hearing Research Centre, Department of Otorhinolaryngology, Head and Neck Surgery, Eberhard Karls University, 72076 Tübingen, Germany
 - ⁴ Max Delbrück Center for Molecular Medicine in the Helmholtz Association, 13125 Berlin, Germany; fruesch@mdc-berlin.de
 - ⁵ Department of Chemistry, Bacha Khan University, Charsadda, Khyber Pakhtunkhwa 24420, Pakistan; imrangnu@gmail.com
 - ⁶ Institute of Bioinformatics, Julius Maximilians University, 97074 Würzburg, Germany; tobias.mueller@uni-wuerzburg.de
 - ⁷ Department of Animal Science, Division of Applied Life Science (BK21plus), Institute of Agriculture and Life Science, Gyeongsang National University, Jinju 52828, Korea; ikong7900@gmail.com
 - ⁸ Neurological Disorders Research Center, Qatar Biomedical Research Institute, Hamad Bin Khalifa University, Doha 34110, Qatar; hkim@hbku.edu.qa
- * Correspondence: barbara.vona@uni-tuebingen.de; Tel.: +49-7071-29-88154

Received: 12 December 2019; Accepted: 31 December 2019; Published: 2 January 2020



Abstract: *CDC14A* encodes the Cell Division Cycle 14A protein and has been associated with autosomal recessive non-syndromic hearing loss (DFNB32), as well as hearing impairment and infertile male syndrome (HIIMS) since 2016. To date, only nine variants have been associated in patients whose initial symptoms included moderate-to-profound hearing impairment. Exome analysis of Iranian and Pakistani probands who both showed bilateral, sensorineural hearing loss revealed a novel splice site variant (c.1421+2T>C, p.?) that disrupts the splice donor site and a novel frameshift variant (c.1041dup, p.Ser348Glnfs*2) in the gene *CDC14A*, respectively. To evaluate the pathogenicity of both loss-of-function variants, we analyzed the effects of both variants on the RNA-level. The splice variant was characterized using a minigene assay. Altered expression levels due to the c.1041dup variant were assessed using RT-qPCR. In summary, cDNA analysis confirmed that the c.1421+2T>C variant activates a cryptic splice site, resulting in a truncated transcript (c.1414_1421del, p.Val472Leufs*20) and the c.1041dup variant results in a defective transcript that is likely degraded by nonsense-mediated mRNA decay. The present study functionally characterizes two variants and provides further confirmatory evidence that *CDC14A* is associated with a rare form of hereditary hearing loss.

Keywords: *CDC14A*; DFNB32; autosomal recessive hearing loss; exome sequencing; splicing; frameshift; non-sense mediated mRNA decay

1. Introduction

Hearing loss (HL) is a highly heterogeneous disorder and belongs to one of the most common sensory disorders in humans with a prevalence of 1–2 in 1000 newborns. Approximately 120 genes responsible for non-syndromic HL have been identified so far [1,2]. Since 2016, the gene *CDC14A* (OMIM: *603504, ENSG00000079335) has been associated with autosomal recessive non-syndromic deafness-32 (DFNB32, OMIM: #608653) [3]. Two years later, it was recognized as causing hearing impairment and infertile male syndrome (HIIMS) [4]. *CDC14A* is located on chromosome 1p21.2 and encodes an evolutionarily conserved protein tyrosine phosphatase (Cell Division Cycle 14A) that is important for centrosome separation and productive cytokinesis during cell division [5]. It is present in the kinocilia of hair cells, as well as basal bodies and sound-transducing stereocilia of the mouse inner ear [3]. Homozygous *Cdc14a* mutant mice showed postnatal degeneration of hair cells but normal length kinocilia. Additionally, degeneration of seminiferous tubules and spermiation defects resulted in infertile male mice [4]. Alternative splicing of *CDC14A* yields six different transcripts, with the largest protein encoding 623 amino acids [3]. To date, only nine homozygous genetic variants in 10 different families with a Middle Eastern background have been associated with hearing impairment (Table 1). Five of these variants with one additional presumed variant also caused male infertility [3,4]. Patients with biallelic *CDC14A* variants present variable degrees of HL that range from moderate to profound in severity [4].

Exome sequencing and gene mapping approaches revealed a homozygous splice variant in a 22.5 Mb homozygous interval on chromosome 1 in two hearing impaired patients from an Iranian family (family 1). Additionally, a homozygous frameshift variant in a 13.6 Mb homozygous interval on chromosome 1 was identified in two Pakistani patients (family 2). Both families had a consanguineous background and both genetic variants were novel. We subsequently evaluated the functional effects of the two variants by assessing aberrant splicing and abnormal gene expression. Our findings widen the spectrum of clinically relevant *CDC14A* mutations that are associated with hearing impairment and reinforce its role within the auditory system.

Table 1. Summary of previously described and newly identified families with homozygous variants in CDC14A.

Family ID	Variant	Sex	HL Onset	HL Severity	Male Infertility	Ethnicity	Reference
HLRB11	c.376delT	Male	Congenital	moderate-to-profound, progressive	Yes	Pakistani	Imtiaz et al. [4]
	p.Tyr126Ilefs*64	Female					
HLAI24	c.417C>G	Male	Congenital	moderate-to-profound, progressive	Yes	Pakistani	Imtiaz et al. [4]
	p.Tyr139Ter	Female					
FT1	c.935G>A	Male	Congenital	moderate-to-severe, progressive	n.a.	Tunisian	Imtiaz et al. [4]
	p.Arg312Gln	Female					
HPK1	c.839-3C>G	Male	Congenital	moderate-to-profound, progressive	Yes	Pakistani	Imtiaz et al. [4]
MORL1	p.?	Male	Congenital	severe-to-profound, progressive	Yes	Iranian	Imtiaz et al. [4]
	c.934C>G	Female					
PKDF539	p.Arg312Gly	Male	Congenital	severe-to-profound, progressive	Yes	Pakistani	Imtiaz et al. [4]
	c.959A>C	Female					
Mauritanian family	p.Chr320Pro	Male	Congenital	Profound	No	Mauritanian	Delmaghani et al. [3]
	c.1015C>T	Female					
PKSN10	p.Arg339Ter	Male	Congenital	moderate-to-profound, progressive	No	Pakistani	Imtiaz et al. [4]
	c.1033C>T	Female					
MORL2	p.Arg345Ter	Male	Congenital	moderate-to-profound	No	Iranian	Imtiaz et al. [4]
	c.1126C>T	Female					
Iranian family	p.Arg376Ter	Male	Congenital	severe-to-profound	No	Iranian	Delmaghani et al. [3]
	c.1126C>T	Female					
Family 1	p.Arg376Ter	Female	Congenital	severe-to-profound	No	Iranian	Present study
	c.1421+2T>C	Male					
Family 2	p.Val472Leufs*20	Female	Congenital	Profound	n.a.	Pakistani	Present study
	c.1041dup	Male					
	p.Ser348Glnfs*2	Female					

Abbreviations: n.a., not available.

2. Results

2.1. Clinical Presentation

All patients reported congenital, bilateral, sensorineural HL (Figure 1). The affected individuals in family 1 reported severe-to-profound HL (II.2 (asymmetrical HL, age 43), II.8; Figure 1a,c), whereas the affected individuals in family 2 (II.1 (age 29), II.2 (age 27)) showed profound HL (Figure 1b,d). A diagnosis of clinical HL of the older sibling in family 2 (II.2) was secured at 1 year of age after his mother recognized signs of hearing impairment. However, HL was suspected since birth and was the case with his younger sibling. Furthermore, the HL in the proband of family 1 can be described as non-progressive. Information about progression is unavailable from the affected individuals in family 2. There were no complaints of vestibular dysfunction or tinnitus in the affected individuals of family 2. The ophthalmic examination of family 1 was normal apart from mild refractive error. In addition to HL, the affected individuals in family 2 (II.1, II.2) suffer from compound myopic astigmatism. Both affected individuals in family 2 (II.1, II.2) are unmarried and have no children.

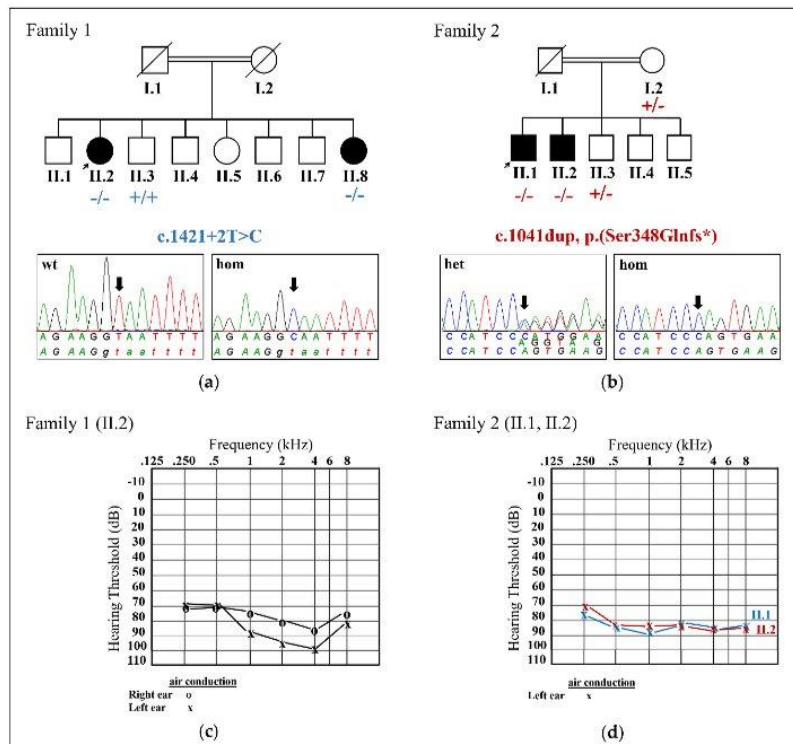


Figure 1. Pedigree, segregation of the *CDC14A* variants in families 1 and 2 and pure-tone audiometry. (a,b) An Iranian ((a) family 1) and Pakistani family ((b) family 2) with a consanguineous background, each showing two affected individuals ((a), II.2, II.8; (b) II.1, II.2) who are shown in black symbols. Unaffected parents and siblings are shown in white symbols. The probands are marked with arrows. The mutated allele is marked with a “-”. The wild type allele is displayed with a “+”. Sanger sequence chromatograms of the *CDC14A* c.1421+2T>C variant in wild type (WT; (a), left) and homozygous ((a), right) orientation and the *CDC14A* c.1041dup variant in heterozygous ((b), left) and homozygous ((b), right) orientation. (c,d) Audiograms showing pure-tone air conduction thresholds of II.2 ((c), family 1) and II.1, II.2 ((d), family 2). Air conduction thresholds for right and left ears are represented with circles and crosses, respectively. Abbreviations: het, heterozygous; hom, homozygous; wt, wild type.

2.2. Identification of Two Novel *CDC14A* Variants

Exome sequencing and bioinformatics analysis of 174 HL-associated genes (Supplementary Table S1) ensued using the genomic DNA of the probands of each family. The proband from family 1 (II.2) revealed a homozygous *CDC14A* (NCBI Reference Sequence: NM_033312.2) splice variant c.1421+2T>C that abolished the donor splice site in intron 14 out of 15 encoded exons and was consistent with segregation analysis within family 1 (Figure 1a). Both affected individuals II.2 and II.8 were homozygous for the c.1421+2T>C variant, while an unaffected brother (II.3) was wild type (WT). A homozygous frameshift variant c.1041dup (p.Ser348Glnfs*) in exon 11 out of 15 exons was detected in the proband from family 2 (II.1) after exome sequencing and bioinformatics analysis, which also co-segregated within family 2 (Figure 1b). The affected individuals II.1 and II.2 were homozygous for the c.1041dup, while the mother (I.2) and unaffected brother (II.3) were heterozygous. Both variants were absent from all applied population databases. All other variants that were identified by bioinformatics analysis of the in silico gene panel were prioritized as benign or could not explain the HL phenotype. Bioinformatic screening of the gene *CDC14A* in our in-house exome database that includes approximately 330 individuals with HL did not reveal additional potentially pathogenic variants. Copy number variations were excluded in the 174 HL-associated genes.

Homozygosity mapping disclosed a 22.5 Mb (chr1: 89,845,926-112,389,040; all subsequent coordinates reported in GRCh37) homozygous interval on chromosome 1 including the *CDC14A* gene (coordinates chr1: 100,810,598-100,985,833) in the Iranian proband (II.2, family 1). The Pakistani family 2 was genotyped with a genome-wide SNP array and homozygosity mapping, identical by descent (IBD), with linkage analysis revealed 15 regions reaching the maximal logarithm of the odds (LOD) score of 1.927. The longest region (chr1: 88,430,037-102,069,696) of 13.6 Mb spans the *CDC14A* gene.

According to four out of five in silico prediction tools (MaxEntScan, NNSplice, GeneSplicer and Human Splicing Finder; Alamut visual, version 2.10), the homozygous c.1421+2T>C variant is predicted to disrupt the exon 14 to intron 14/15 splice donor site (Figure 2d). That loss would likely mediate exon skipping or the use of an alternative cryptic splice site nearby. The duplication c.1041dup (p.Ser348Glnfs*2) in family 2 leads to a frameshift and the incorporation of a premature stop codon two triplicate bp positions downstream.

2.3. Functional Characterization of the Splice Variant c.1421+2T>C

The effect of the splice variant (c.1421+2T>C) in intron 14 was subjected to testing using a minigene assay that included cloning of exon 14, as well as the 5' and 3' flanking intronic sequences into an exon trapping vector (Figure 2a). PCR amplification and Sanger sequencing of WT and mutant cDNA revealed two products of different sizes (Figure 2b,c) that is the result of a truncation of eight nucleotides (GTAAGAAG) in the mutated sequence (372 bp) compared to the WT control (380 bp) due to activation of a cryptic splice site in exon 14 (Figure 2d). The 257 bp sequence in the empty vector control appeared as expected. The eight nucleotide deletion leads to a frameshift c.1414_1421del, p.Val472Leufs*20 (NM_033312.2) and the incorporation of a premature stop codon 20 triplicate bp positions downstream (Figure 2e). Assuming that a protein is translated, it is expected that the full protein would be truncated by approximately 21%.

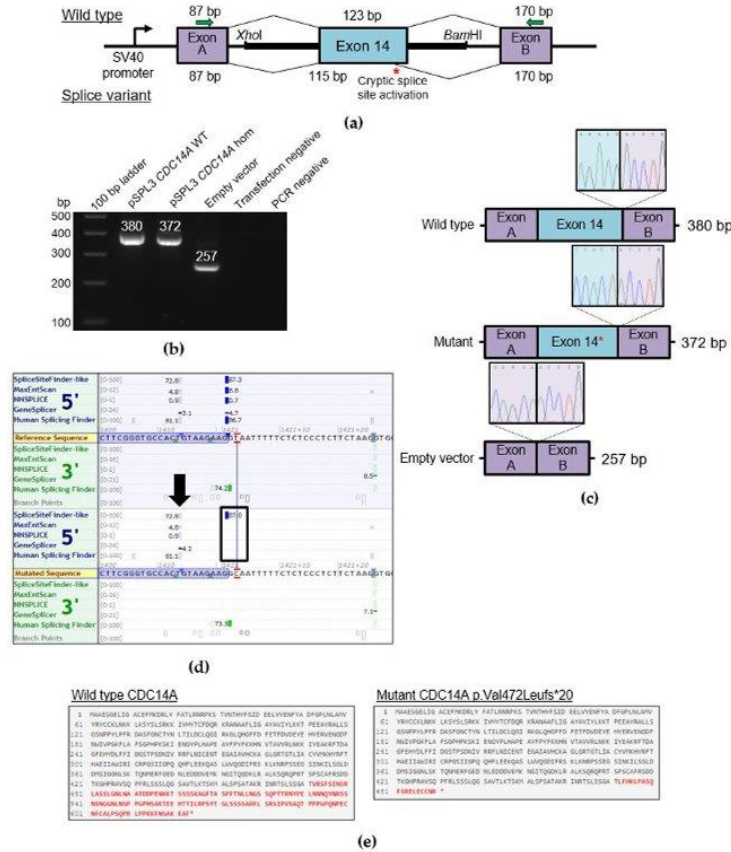


Figure 2. Characterization of the *CDC14A* c.1421+2T>C exchange via a minigene assay. **(a)** A schematic of the pSPL3 exon trapping vector with cloned *CDC14A* exon 14 (blue) and flanking sequence containing *XhoI* and *BamHI* restriction sites that was directly amplified from proband and wild type genomic DNA. Exons A and B (purple) originate from the vector. A schematic of the resulting splice products is shown, with the wild type splicing profile (top) and splice variant sequence that activates a cryptic splice site (bottom, red asterisk). The PCR primers that were used to amplify the Exon A splice donor region (SD6) and Exon B splice acceptor region (SA2) are depicted by green arrows. **(b)** Electrophoretic visualization of cDNA RT-PCR products amplified from constructs after transfection into HEK293T cells. Amplicons were resolved on a 1% agarose gel. Wild type splicing (lane: pSPL3 *CDC14A* WT) yields a 380 bp product that constitutes the Exon A, exon 14 and Exon B amplified regions. The homozygous mutant amplicon (lane: pSPL3 *CDC14A* hom) shows a band around 380 bp that, when sequenced, indicates a cryptic splice site activation. The empty vector shows the expected 257 bp product. **(c)** Sequencing electropherograms of the exon 14 5' splice site boundaries for the RT-PCR products for wild type (top), mutant showing cryptic splice site activation (middle) and empty vector (bottom). **(d)** In silico splice prediction tools for the c.1421+2T>C exchange that is marked with red lines visualized with Alamut visual (2.10). The upper panel shows the reference sequence splice scores and the lower panel shows the splice scores for the c.1421+2T>C exchange with multiple in silico prediction tools estimating the loss of the native exon 14 5' donor splice site that is due to the variant (shown with a black box). In the mutant panel, the splice scores of an adjacent cryptic 5' donor site are either unchanged or strengthened and marked with a black arrow. **(e)** Effect of the splice variant on the protein, comparing wild type (top) and the truncated (bottom) protein resulting from the aberrantly spliced product (visualized with Mutalyzer). The amino acid residues marked in red are those that are altered due to the variant.

2.4. Quantification of Relative Expression Levels for CDC14A

To investigate whether the premature termination codon (PTC) induced by the c.1041dup (p.Ser348Glnfs*2) variant triggers nonsense-mediated mRNA decay (NMD) of CDC14A in family 2, we quantified relative CDC14A mRNA expression. RT-qPCR was performed utilizing whole blood of homozygous (II.2) and heterozygous (I.2) individuals with two different primer pairs targeting a region at the anterior part of the gene (exon 2–3, NM_033312.2) and a region posterior to the frameshift variant in exon 11 (exon 11–12, NM_033312.2). The RT-qPCR analysis showed that the relative expression levels of CDC14A were significantly reduced by approximately 99% relative expression for both targeted regions for the homozygous individual (II.2) relative to WT controls. We could observe a difference of 17%–34% (exon 2–3) and approximately 57% (exon 11–12) relative expression for the heterozygous individual I.2 when compared relative to WT controls (Figure 3a). In principle, the introduction of a PTC directly after p.348 would truncate 44% of the amino acid residues in full length CDC14A (Figure 3b).

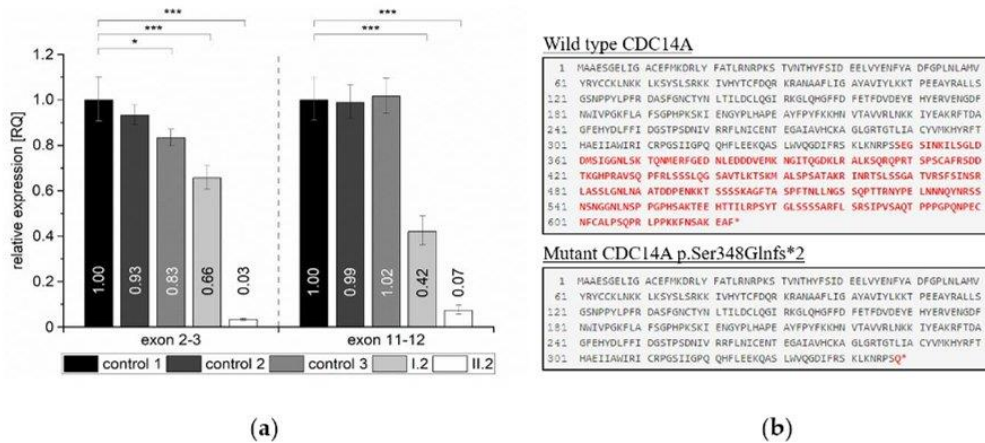


Figure 3. Quantification of the RT-qPCR relative expression values for the CDC14A c.1041dup variant in homozygous, heterozygous and wild type control individuals. (a) Relative expression levels are shown for exon 2–3 ($F_{(4, 10)} = 150.69$) and exon 11–12 ($F_{(4, 10)} = 112.84$) for the normalized reference samples (wt controls 1, 2 and 3), and both tested individuals in family 2 (I.2, heterozygous for c.1041dup and II.2, homozygous for c.1041dup). $N = 3$ for each group. Values are represented as means and error bars extend to the respective minimal and maximal values. To improve readability, significant differences are only indicated for pairwise comparisons to the normalized reference sample (wt control 1). See Supplementary Table S2 for extended information. * $p < 0.05$ and *** $p < 0.001$. (b) Effect of the c.1041dup variant on the protein, comparing wild type (top) and the truncated (bottom) protein resulting from the aberrantly spliced product (visualized with Mutalyzer). The amino acid residues marked in red are those that are altered due to the variant.

Both variants have been submitted to LOVD v 3.0 under the accession IDs 00269609 and 00269610.

3. Discussion

The CDC14A gene encodes a protein that is a member of the highly conserved dual specificity protein-tyrosine phosphatase family existing in a wide range of organisms from yeast to human [6]. Their ability to dephosphorylate serine, threonine, as well as tyrosine residues of different proteins is required for the regulation of essential signaling pathways and biological processes such as protein–protein interactions, cell-cycle progression or apoptosis [7]. The encoded protein CDC14A is thought to be involved in the conservation of hair cells in mice and is essential both for normal hearing and male fertility in humans according to nine previously described mutations [3,4]. Furthermore,

in mice, CDC14A appears to be advantageous for perinatal survival [4]. The paralogue CDC14B may compensate for the loss of some CDC14A functions in vivo, but does not compensate for male infertility and hearing impairment with loss of CDC14A [4].

Interestingly, there is a noticeable accumulation of pathogenic variants that are responsible for a distinct hearing impaired phenotype in exon 11 (NM_033312.2) and variants that are responsible for HIIMS in exon 10, containing the core dual-specificity phosphatase domain (DSPc/PTPc; Figure 4). Patients who have thus far been identified with C-terminal truncating variants have moderate-to-profound hearing impairment and males with apparently normal fertility, whereas patients with truncating variants in exons encoding two protein domains (exon 10 encodes part of the DSPc/PTPc domain and exons 5 and 6 encode the dual-specificity phosphatase domain (DSPn)) have HIIMS that includes moderate-to-profound hearing impairment (Figure 4, Table 1). It is thought that transcripts with truncating mutations in exon 11 probably avoid NMD since a short isoform containing only 11 exons (NM_003672) also exists compared to the longest isoform (NM_0033312.2) that has 15 exons [4].

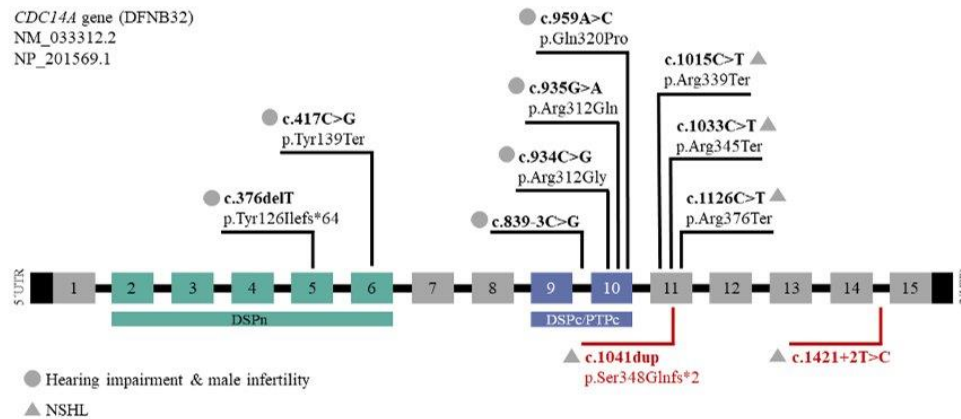


Figure 4. Summary of all variants in the gene *CDC14A* (NM_033312.2, NP_201569.1) that is composed of 15 exons. The dual-specificity phosphatase domain (DSPn) and the core dual-specificity phosphatase domain (DSPc/PTPc) are represented in green and blue bars, respectively. Indicated are the nine previously described mutations (above) and the two newly identified variants in the affected individuals from family 1 and 2 (red, below). The two different phenotypes are indicated with a circle (hearing impairment and male infertility) or triangle (NSHL).

The congenital, sensorineural HL phenotype in our patients that ranged from severe-to-profound in the Iranian family (family 1) and profound in the Pakistani family (family 2) can be compared to already presented HL patients with mutations in *CDC14A* that showed prelingual severe-to-profound deafness (Table 1) [3]. Most of the families with autosomal recessive non-syndromic hearing loss (ARNSHL) come from the ‘consanguinity belt’ that includes regions of North Africa, the Middle East and India and uncovered unique signatures of variants in the past [8]. All previously described variants in *CDC14A* were found in families originating from this specific region such as Pakistan, Iran, Tunisia and Mauritania and show a comparable ethnicity as the two families (Iranian and Pakistani) presented in this study.

In contrast to some of the already described HIIMS patients that showed signs of progressive moderate-to-profound HL [4], progression was unreported in our families. Since both affected individuals in family 1 are female and the unmarried status of both affected males in family 2, we cannot exclude that the newly identified *CDC14A* variants would also cause male infertility.

The process of RNA splicing is an essential post-transcriptional mechanism ensuring the correct junction of neighboring exons by the removal of intermediate intronic sequences through the

spliceosome complex [9]. Sequence variants in regions critical for correct splicing can consequently lead to exon-skipping or the activation of cryptic splice sites and are responsible for a variety of different diseases [10]. Cryptic splice sites are normally repressed by stronger splice sites that are located nearby, competing for selection by the splicing machinery [11]. One possible consequence of the splice variant c.1421+2T>C in family 1 that is located in intron 14 was exon skipping of exon 14 due to a disruption and consequently weakening of the splice donor site. We verified the activation of an alternative cryptic splice site located eight base pairs upstream within exon 14 (Figure 2d) that results in a frameshift and a truncated protein (p.Val472Leufs*20; Figure 2e) instead of exon skipping and postulate that this variant is responsible for the hearing impaired phenotype within this family.

The vital process of eukaryotic gene expression such as transcription, translation and degradation of mRNA and proteins is essential to ensure a functional gene product [12]. There are several different pathways that are involved in the decay of defectively transcribed gene products most often starting with poly(A) shortening by the Ccr4-Not deadenylase complex followed by either 5' end decapping (Dcp1/2) and Xrn1 mediated decay [13] or 3' end exonucleolytic decay mediated by an exosome [14]. Frameshift or nonsense mutations are often responsible for NMD, a crucial process that prevents the production of truncated or potentially toxic dominant-negative proteins [15]. The c.1041dup frameshift variant in family 2 is responsible for the incorporation of a premature stop-codon likely resulting in a truncated transcript. If translated, over >40% of the transcript would be missing that is likely degraded by NMD. We could confirm significantly decreased relative *CDC14A* expression levels for both the unaffected heterozygous and the affected homozygous individual including both the anterior and the posterior part of the mRNA transcript (Figure 3a). Since we only investigated total mRNA levels isolated from whole blood, targeting distinct transcripts of the *CDC14A* gene, we cannot rule out the possibility of compensatory mechanisms such as upregulation of different gene transcripts in other human tissues [16]. Nevertheless, we have experimentally shown that the truncated *CDC14A* product by the c.1041dup frameshift variant is likely targeted by the mechanism of NMD resulting in insufficient levels of functional transcript for the homozygous proband (Figure 3).

Both variants are anticipated to produce a loss-of-function, either through possible truncated protein from the c.1421+2T>C variant, or NMD that is anticipated to occur as a result of the c.1041dup variant.

In order to distinguish between a regular stop codon and a PTC, the NMD machinery recognizes the position of the PTC within newly produced mRNAs. If the PTC is located at least 50–55 nucleotides upstream of the 3'-most exon–exon junction, degradation by the NMD machinery is likely induced to avoid unfavorable transcripts [17]. Since the PTC of the *CDC14A* frameshift variant c.1041dup is located in exon 11 and is followed by a 3' exon–exon junction more than 55 nucleotides downstream, NMD is likely triggered. Our results showing reduced relative expression levels for *CDC14A* in patients also confirmed this hypothesis. The PTC that originates from the aberrantly spliced transcript (p.Val472Leufs*20) due to the c.1421+2T>C variant is located in the last exon (exon 15) of *CDC14A*. Since there is no 3' exon–exon junction further downstream of the PTC, a transcript is likely produced to subsequently escape the NMD machinery.

4. Materials and Methods

4.1. Patient Recruitment and Clinical Assessment

Informed written consent was obtained from the families. This study was performed under the tenets of the Declaration of Helsinki and was approved by the Ethics Commission of the University of Würzburg (46/15, approval date: 31 March 2015).

We recruited an Iranian (family 1) and Pakistani (family 2) family who both showed a history of parental consanguinity for a total of four affected individuals, as well as unaffected parents and siblings (Figure 1a,b). The affected individuals (family 1: II.2, II.8; family 2: II.1, II.2) underwent audiological assessment and were tested by pure-tone audiometry adhering to recommendations described in

Mazzoli et al. (2003) [18]. Ophthalmic examination of the proband in family 1, as well as both affected individuals from family 2 was performed.

4.2. Exome Sequencing

Genomic DNA (gDNA) from the two affected individuals was extracted from whole blood. Diagnostic screening of *GJB2*, the most frequently implicated gene in non-syndromic hearing loss, excluded putative pathogenic variants. gDNA of the probands were exome sequenced. Exome library preparation was performed with the TruSeq Exome Enrichment (family 1) and the Nextera Rapid Capture Exome (family 2) kits (Illumina, San Diego, CA, USA) according to manufacturer's instructions and paired-end sequenced (2 × 76 bp) with the NextSeq500 sequencer (Illumina, San Diego, CA, USA). A v2 high output reagent kit (Illumina) was used and the data were aligned to the human reference genome GRCh37 (hg19).

4.3. In Silico Variant Analysis

Data analysis was performed with GensearchNGS software (PhenoSystems SA, Wallonia, Belgium) and an in-house bioinformatics pipeline. Variant filtering was done with a minor allele frequency <0.01 and alternate allele present at >20%. The pipeline data were analyzed based on the GATK toolkit [19] and BWA based read alignment to the human genome (hg19) following GATK best practice recommendations [20,21]. Quality filtering was performed based on the VQSLOD score. Data from the Greater Middle East Variome Project [22], the Iranome Database [23] and gnomAD [24] were used for population-specific filtering. Variant analysis was done with the use of PolyPhen-2 [25], SIFT [26] and MutationTaster [27], as well as variant information annotated in the Deafness Variation Database (DVD) [28]. Exome CNV analysis was performed using the eXome Hidden MarkovModel (XHMM, version 1.0) approach [29]. Splice-site variants were classified on the basis of in-silico splice predictors such as SpliceSiteFinder-like [30], MaxEntScan [31], NNSPLICE [32], Genesplicer [33] and Human Splicing Finder [34]. Homozygosity mapping was done and visualized with HomozygosityMapper [35]. Mutalyzer was used to assess the effect of the variants on the protein in silico [36].

4.4. Gene Mapping Approaches

The exome data of the proband from family 1 was subjected to homozygosity mapping that was performed using HomozygosityMapper [35]. The gDNA from individuals (I.2, II.1, II.2, II.3) from family 2 were subjected to genome-wide genotyping using the Infinium HumanCore-24 v1.0 Bead Chip (Illumina) using manufacturer's protocols.

Data conversion to linkage format files and quality control (QC) was managed with ALOHOMORA software [37]. Up to 258,000 biallelic SNPs after QC were used for linkage analysis with Merlin [38]. Linkage analysis was done with a recessive genetic model with complete penetrance, a rare disease allele frequency of 0.001 and a pedigree with a consanguinity loop (cousin marriage of parents I.1 and I.2). As genetic coordinates, we used the physical position (1 cM \Leftrightarrow 1 Mb, hg19). Linkage regions where the LOD score reached the maximal value of 1.927 for this family, indicate homozygous (autozygous) stretches for the two affected individuals (II.1 and II.2) and where the unaffected brother (II.3) is not homozygous. Linkage analysis was repeated with a linkage disequilibrium (LD) reduced marker set to verify that LOD score peaks are not inflated by LD.

Genomic coordinates are reported using the GRCh37 human genome assembly.

4.5. Validation of The *CDC14A* Variants and Segregation Analysis

Validation of the *CDC14A* frameshift and splice variants was carried out by Sanger sequencing from PCR-amplified gDNA from the probands and available family members using standard cycling conditions and primers (F: 5'-TCCGCAAAGATTAAGTTCATCCC-3' and R: 5'-TCTGGATCACACTAAGCCAGC-3') to validate the c.1421+2T>C and (F:

5'-CTGAGGACTTCAGCAGTCAA-3' and R: 5'-AACTTGGTACTCGTGGCATC-3') c.1041dup variants (Metabion, Martinsried, Germany). Primers were designed with Primer3 [39]. The amplicons were sequenced with an ABI 3130xl 16-capillary sequencer (Life Technologies, Carlsbad, CA, USA) and the data were analyzed with Gensearch 4.3 software (PhenoSystems SA, Wallonia, Belgium).

4.6. Minigene Assay

To test the in silico splice predictions, an in vitro splicing assay was carried out using a modified protocol from Tompson and Young [40]. Briefly, wild-type and mutant *CDC14A* exon 14 (123 bp) were directly PCR amplified from a control individual and the proband with specific primers containing an additional *XhoI* and *BamHI* restriction site (forward primer with *XhoI* restriction site: 5'-aattctcgagCCGCTGCTGTCATCACTATTA-3' and reverse primer with *BamHI* restriction site: 5'-attggtaccACCATTCCCTCCACAACCTT-3'). The PCR reaction amplified the entire exon 14 sequence plus an additional 133 bp (5') and 193 bp (3') from the flanking intronic regions. After PCR amplification, PCR clean-up, restriction enzyme digestion of the PCR fragments and pSPL3 exon trapping vector was performed prior to cloning of exon A and exon B fragments into the linearized pSPL3-vector and DH5 α competent cells (NEB 5-alpha, New England Biolabs, Ipswich, MA, USA). The WT and mutant-containing vector sequences were Sanger sequenced.

Vectors containing either homozygous or WT sequence were transfected into HEK 293T cells (ATCC) at a density of 2×10^5 cells per mL. Of the respective pSPL3 vector 2 μ g was transiently transfected using 6 μ L of FuGENE 6 Transfection Reagent (Promega, Madison, WI, USA). An empty vector and negative transfection reactions were included as controls. The transfected cells were harvested 24 h after transfection for RNA extraction. Total RNA was prepared using miRNAeasy Mini Kit (Qiagen, Venlo, Netherlands). Approximately 1 μ g of RNA was reverse transcribed using a High Capacity RNA-to-cDNA Kit (Applied Biosystems, Waltham, MA, USA) following the manufacturer's protocols. The cDNA was PCR amplified using vector-specific SD6 forward (5'-TCTGAGTCACCTGGACAACC-3') and reverse SA2 (5'-ATCTCAGTGGTATTTGTGAGC-3') primers. The amplified fragments were visualized on a 1% agarose gel and subsequently Sanger sequenced.

4.7. Expression Analysis Using Reverse Transcription Quantitative Real-Time PCR (RT-qPCR)

To examine altered expression levels in *CDC14A* due to the loss-of-function variant in family 2, total RNA was extracted from whole blood of probands I.2 and II.2 (family 2) using PAXgene Blood RNA Kit (Qiagen) according to manufacturer's instructions. cDNA was synthesized using High Capacity RNA-to-cDNA Kit (Applied Biosystems). We performed RT-qPCR using a ViiA7 Real-Time PCR System (Thermo Fisher Scientific, Waltham, MA, USA). Each sample and primer pair was analyzed in triplicates on a single qPCR plate using HOT FIRE Pol Eva Green Mix Plus (Solis BioDyne, Tartu, Estonia). Relative expression levels were calculated using the QuantStudio Real-Time PCS Software v1.3 by $\Delta\Delta C_t$ method. Control samples were either used as reference samples or for relative expression comparison. Combined cT values of housekeeping genes *GAPDH*, *IPO8* and *HPRT1* were used for endogenous cDNA controls. Used primer pairs are listed in Table 2.

Table 2. Primer sequences for RT-qPCR.

Exon	5'-3' Primer Sequence (Forward)	5'-3' Primer Sequence (Reverse)
<i>CDC14A</i> Ex2_3	CCCACTATTTCTCCATCGATGA	GTACACCATTGCCAAGTTCAG
<i>CDC14A</i> Ex11_12	TGGCCTAGATGATATGTCTATTG	CTTCTAAGTTATCCTCTCCAAATC
<i>GAPDH</i>	TGCACCACCAACTGCTTAGC	GGCATGGACTGTGGTCATGAG
<i>IPO8</i>	CGAGCTAGATCTTGCTGGGT	CGCTAATTCAACGGCATTCTT
<i>HPRT1</i>	TGACACTGGCAAACAATGCA	GGTCCTTTTACCAGCAAGCT

4.8. Statistical Data Collection

The results of RT-qPCR are represented as relative quantification (RQ) means. Statistical analysis was performed using OriginPro 2018G. Normality (Shapiro–Wilk) and equality of variances (Levene's) were calculated and a one-way ANOVA with Bonferroni correction for multiple comparisons was subsequently conducted. A *p*-value of less than 0.05 is considered statistically significant.

Supplementary Materials: Supplementary materials can be found at <http://www.mdpi.com/1422-0067/21/1/311/s1>.

Author Contributions: Conceptualization, T.H., B.V.; Manuscript drafting, J.D., T.H., B.V.; Ascertained families and obtained clinical data, A.A., H.-G.K., A.H., A.R., I.K.; Supervision, T.H., B.V., I.-K.K.; Exome sequencing and segregation analysis, J.D., M.A.H., S.K. (Susanne Kolb), L.S., B.V.; Homozygosity mapping, J.D.; Linkage analysis, F.R.; Bioinformatics support, T.M., M.D.; Minigene analysis, B.V.; RT-qPCR analysis, J.D., D.L., S.K. (Sabine Knaup). All authors participated in final review and editing of the manuscript. All authors have read and agreed to the published version of the manuscript.

Funding: This research was supported by Intramural Funding (fortune) at the University of Tübingen (2545-1-0 to B.V.)

Acknowledgments: The authors would like to express their sincere gratitude to the families for their participation in this study. We would also like to thank Larissa Haertle at the Department of Internal Medicine, Würzburg, Indrajit Nanda at the Institute of Human Genetics, Würzburg and Dennis Segebarth at the Institute of Clinical Neurobiology, Würzburg for their expert advice. We thank Stuart W. Tompson at the University of Wisconsin-Madison for sharing the pSPL3 vector.

Conflicts of Interest: The authors declare no conflict of interest.

Abbreviations

ARNSHL	Autosomal Recessive Non-Syndromic Hearing Loss
CDC14A	Cell Division Cycle 14A
DFNB32	Deafness B32
DSPc/PTPc	Dual-specificity phosphatase domain
DSPn	Dual-specificity phosphatase domain
GJB2	Gap Junction Protein Beta 2
HIIMS	Hearing Impairment and Infertile Male Syndrome
HL	Hearing Loss
LD	Linkage Disequilibrium
LOD	Logarithm of the Odds
NMD	Nonsense-Mediated mRNA Decay
PTC	Premature Termination Codon
QC	Quality Control
RT-qPCR	Reverse Transcription Quantitative Real-Time Polymerase Chain Reaction
RQ	Relative Quantification
SNP	Single Nucleotide Polymorphism
WT	Wild Type

References

1. Vona, B.; Nanda, I.; Hofrichter, M.A.; Shehata-Dieler, W.; Haaf, T. Non-syndromic hearing loss gene identification: A brief history and glimpse into the future. *Mol. Cell. Probes* **2015**, *29*, 260–270. [CrossRef]
2. Van Camp, G.; Smith, R.J.H. Hereditary Hearing Loss Homepage. Available online: <https://hereditaryhearingloss.org/> (accessed on 10 December 2019).
3. Delmaghani, S.; Aghaie, A.; Bouyacoub, Y.; El Hachmi, H.; Bonnet, C.; Riahi, Z.; Chardenoux, S.; Perfettini, I.; Hardelin, J.P.; Houmeida, A.; et al. Mutations in CDC14A, Encoding a Protein Phosphatase Involved in Hair Cell Ciliogenesis, Cause Autosomal-Recessive Severe to Profound Deafness. *Am. J. Hum. Genet.* **2016**, *98*, 1266–1270. [CrossRef] [PubMed]
4. Intiaz, A.; Belyantseva, I.A.; Beirl, A.J.; Fenollar-Ferrer, C.; Bashir, R.; Bukhari, I.; Bouzid, A.; Shaukat, U.; Azaiez, H.; Booth, K.T.; et al. CDC14A phosphatase is essential for hearing and male fertility in mouse and human. *Hum. Mol. Genet.* **2018**, *27*, 780–798. [CrossRef]
5. Stegmeier, F.; Amon, A. Closing mitosis: The functions of the Cdc14 phosphatase and its regulation. *Annu. Rev. Genet.* **2004**, *38*, 203–232. [CrossRef] [PubMed]

6. Mociaro, A.; Schiebel, E. Cdc14: A highly conserved family of phosphatases with non-conserved functions? *J. Cell Sci.* **2010**, *123*, 2867–2876. [[CrossRef](#)] [[PubMed](#)]
7. Patterson, K.L.; Brummer, T.; O'Brien, P.M.; Daly, R.J. Dual-specificity phosphatases: Critical regulators with diverse cellular targets. *Biochem. J.* **2009**, *418*, 475–489. [[CrossRef](#)]
8. Hilgert, N.; Smith, R.J.; Van Camp, G. Forty-six genes causing nonsyndromic hearing impairment: Which ones should be analyzed in DNA diagnostics? *Mutat. Res.* **2009**, *681*, 189–196. [[CrossRef](#)]
9. Wang, G.S.; Cooper, T.A. Splicing in disease: Disruption of the splicing code and the decoding machinery. *Nat. Rev. Genet.* **2007**, *8*, 749–761. [[CrossRef](#)]
10. Lopez-Bigas, N.; Audit, B.; Ouzounis, C.; Parra, G.; Guigo, R. Are splicing mutations the most frequent cause of hereditary disease? *FEBS Lett.* **2005**, *579*, 1900–1903. [[CrossRef](#)]
11. Kapustin, Y.; Chan, E.; Sarkar, R.; Wong, F.; Vorechovsky, I.; Winston, R.M.; Tatusova, T.; Dibb, N.J. Cryptic splice sites and split genes. *Nucleic Acids Res.* **2011**, *39*, 5837–5844. [[CrossRef](#)]
12. Balagopal, V.; Fluch, L.; Nissan, T. Ways and means of eukaryotic mRNA decay. *Biochim. Biophys. Acta* **2012**, *1819*, 593–603. [[CrossRef](#)] [[PubMed](#)]
13. Jinek, M.; Coyle, S.M.; Doudna, J.A. Coupled 5' nucleotide recognition and processivity in Xrn1-mediated mRNA decay. *Mol. Cell* **2011**, *41*, 600–608. [[CrossRef](#)] [[PubMed](#)]
14. Meola, N.; Domanski, M.; Karadoulama, E.; Chen, Y.; Gentil, C.; Pultz, D.; Vitting-Seerup, K.; Lykke-Andersen, S.; Andersen, J.S.; Sandelin, A.; et al. Identification of a Nuclear Exosome Decay Pathway for Processed Transcripts. *Mol. Cell* **2016**, *64*, 520–533. [[CrossRef](#)]
15. Kurosaki, T.; Popp, M.W.; Maquat, L.E. Quality and quantity control of gene expression by nonsense-mediated mRNA decay. *Nat. Rev. Mol. Cell Biol.* **2019**, *20*, 406–420. [[CrossRef](#)] [[PubMed](#)]
16. El-Brolosy, M.A.; Stainier, D.Y.R. Genetic compensation: A phenomenon in search of mechanisms. *PLoS Genet.* **2017**, *13*, e1006780. [[CrossRef](#)]
17. Maquat, L.E. Nonsense-mediated mRNA decay: Splicing, translation and mRNP dynamics. *Nat. Rev. Mol. Cell Biol.* **2004**, *5*, 89–99. [[CrossRef](#)]
18. Mazzoli, M.G.; Van Camp, G.U.; Newton, V.; Giarbini, N.; Declau, F.; Parving, A. Recommendations for the description of genetic and audiological data for families with nonsyndromic hereditary hearing impairment. *Audiol. Med.* **2003**, *1*, 148–150. [[CrossRef](#)]
19. McKenna, A.; Hanna, M.; Banks, E.; Sivachenko, A.; Cibulskis, K.; Kernytzky, A.; Garimella, K.; Altshuler, D.; Gabriel, S.; Daly, M.; et al. The Genome Analysis Toolkit: A MapReduce framework for analyzing next-generation DNA sequencing data. *Genome Res.* **2010**, *20*, 1297–1303. [[CrossRef](#)]
20. DePristo, M.A.; Banks, E.; Poplin, R.; Garimella, K.V.; Maguire, J.R.; Hartl, C.; Philippakis, A.A.; del Angel, G.; Rivas, M.A.; Hanna, M.; et al. A framework for variation discovery and genotyping using next-generation DNA sequencing data. *Nat. Genet.* **2011**, *43*, 491–498. [[CrossRef](#)]
21. Li, H.; Durbin, R. Fast and accurate long-read alignment with Burrows-Wheeler transform. *Bioinformatics* **2010**, *26*, 589–595. [[CrossRef](#)]
22. Scott, E.M.; Halees, A.; Itan, Y.; Spencer, E.G.; He, Y.; Azab, M.A.; Gabriel, S.B.; Belkadi, A.; Boisson, B.; Abel, L.; et al. Characterization of Greater Middle Eastern genetic variation for enhanced disease gene discovery. *Nat. Genet.* **2016**, *48*, 1071–1076. [[CrossRef](#)] [[PubMed](#)]
23. Fattahi, Z.; Beheshtian, M.; Mohseni, M.; Poustchi, H.; Sellars, E.; Nezhadi, S.H.; Amini, A.; Arzhanghi, S.; Jalalvand, K.; Jamali, P.; et al. Iranome: A catalog of genomic variations in the Iranian population. *Hum. Mutat.* **2019**, *40*, 1968–1984. [[CrossRef](#)] [[PubMed](#)]
24. Karczewski, K.J.; Francioli, L.C.; Tiao, G.; Cummings, B.B.; Alfoldi, J.; Wang, Q.; Collins, R.L.; Laricchia, K.M.; Ganna, A.; Birnbaum, D.P.; et al. Variation across 141,456 human exomes and genomes reveals the spectrum of loss-of-function intolerance across human protein-coding genes. *bioRxiv* **2019**. [[CrossRef](#)]
25. Adzhubei, I.A.; Schmidt, S.; Peshkin, L.; Ramensky, V.E.; Gerasimova, A.; Bork, P.; Kondrashov, A.S.; Sunyaev, S.R. A method and server for predicting damaging missense mutations. *Nat. Methods* **2010**, *7*, 248–249. [[CrossRef](#)] [[PubMed](#)]
26. Ng, P.C.; Henikoff, S. Predicting deleterious amino acid substitutions. *Genome Res.* **2001**, *11*, 863–874. [[CrossRef](#)]
27. Schwarz, J.M.; Cooper, D.N.; Schuelke, M.; Seelow, D. MutationTaster2: Mutation prediction for the deep-sequencing age. *Nat. Methods* **2014**, *11*, 361–362. [[CrossRef](#)]

28. Azaiez, H.; Booth, K.T.; Ephraim, S.S.; Crone, B.; Black-Ziegelbein, E.A.; Marini, R.J.; Shearer, A.E.; Sloan-Heggen, C.M.; Kolbe, D.; Casavant, T.; et al. Genomic Landscape and Mutational Signatures of Deafness-Associated Genes. *Am. J. Hum. Genet.* **2018**, *103*, 484–497. [[CrossRef](#)]
29. Fromer, M.; Purcell, S.M. Using XHMM Software to Detect Copy Number Variation in Whole-Exome Sequencing Data. *Curr. Protoc. Hum. Genet.* **2014**, *81*, 7–23. [[CrossRef](#)]
30. Shapiro, M.B.; Senapathy, P. RNA splice junctions of different classes of eukaryotes: Sequence statistics and functional implications in gene expression. *Nucleic Acids Res.* **1987**, *15*, 7155–7174. [[CrossRef](#)]
31. Yeo, G.; Burge, C.B. Maximum entropy modeling of short sequence motifs with applications to RNA splicing signals. *J. Comput. Biol.* **2004**, *11*, 377–394. [[CrossRef](#)]
32. Reese, M.G.; Eeckman, F.H.; Kulp, D.; Haussler, D. Improved splice site detection in Genie. *J. Comput. Biol.* **1997**, *4*, 311–323. [[CrossRef](#)] [[PubMed](#)]
33. Pertea, M.; Lin, X.; Salzberg, S.L. GeneSplicer: A new computational method for splice site prediction. *Nucleic Acids Res.* **2001**, *29*, 1185–1190. [[CrossRef](#)] [[PubMed](#)]
34. Desmet, F.O.; Hamroun, D.; Lalande, M.; Collod-Beroud, G.; Claustres, M.; Beroud, C. Human Splicing Finder: An online bioinformatics tool to predict splicing signals. *Nucleic Acids Res.* **2009**, *37*, e67. [[CrossRef](#)] [[PubMed](#)]
35. Seelow, D.; Schuelke, M.; Hildebrandt, F.; Nurnberg, P. HomozygosityMapper—An interactive approach to homozygosity mapping. *Nucleic Acids Res.* **2009**, *37*, W593–W599. [[CrossRef](#)]
36. Wildeman, M.; van Ophuizen, E.; den Dunnen, J.T.; Taschner, P.E. Improving sequence variant descriptions in mutation databases and literature using the Mutalyzer sequence variation nomenclature checker. *Hum. Mutat.* **2008**, *29*, 6–13. [[CrossRef](#)]
37. Ruschendorf, F.; Nurnberg, P. ALOHOMORA: A tool for linkage analysis using 10K SNP array data. *Bioinformatics* **2005**, *21*, 2123–2125. [[CrossRef](#)]
38. Abecasis, G.R.; Cherny, S.S.; Cookson, W.O.; Cardon, L.R. Merlin—rapid analysis of dense genetic maps using sparse gene flow trees. *Nat. Genet.* **2002**, *30*, 97–101. [[CrossRef](#)]
39. Untergasser, A.; Cutcutache, I.; Koressaar, T.; Ye, J.; Faircloth, B.C.; Remm, M.; Rozen, S.G. Primer3—New capabilities and interfaces. *Nucleic Acids Res.* **2012**, *40*, e115. [[CrossRef](#)]
40. Tompson, S.W.; Young, T.L. Assaying the Effects of Splice Site Variants by Exon Trapping in a Mammalian Cell Line. *Bio Protoc* **2017**, *7*. [[CrossRef](#)]



© 2020 by the authors. Licensee MDPI, Basel, Switzerland. This article is an open access article distributed under the terms and conditions of the Creative Commons Attribution (CC BY) license (<http://creativecommons.org/licenses/by/4.0/>).

10.2 Attachment 2

The Many Faces of DFNB9: Relating OTOF Variants to Hearing Impairment

Review

The Many Faces of DFNB9: Relating *OTOF* Variants to Hearing Impairment

Barbara Vona , Aboufazel Rad  and Ellen Reisinger * 

Tübingen Hearing Research Centre, Department of Otolaryngology, Head & Neck Surgery, University of Tübingen Medical Center, 72076 Tübingen, Germany; barbara.vona@uni-tuebingen.de (B.V.); Aboufazel.rad@uni-tuebingen.de (A.R.)

* Correspondence: ellen.reisinger@uni-tuebingen.de; Tel.: +49-7071-29-88184

Received: 3 November 2020; Accepted: 25 November 2020; Published: 26 November 2020



Abstract: The *OTOF* gene encodes otoferlin, a critical protein at the synapse of auditory sensory cells, the inner hair cells (IHCs). In the absence of otoferlin, signal transmission of IHCs fails due to impaired release of synaptic vesicles at the IHC synapse. Biallelic pathogenic and likely pathogenic variants in *OTOF* predominantly cause autosomal recessive profound prelingual deafness, DFNB9. Due to the isolated defect of synaptic transmission and initially preserved otoacoustic emissions (OAEs), the clinical characteristics have been termed “auditory synaptopathy”. We review the broad phenotypic spectrum reported in patients with variants in *OTOF* that includes milder hearing loss, as well as progressive and temperature-sensitive hearing loss. We highlight several challenges that must be addressed for rapid clinical and genetic diagnosis. Importantly, we call for changes in newborn hearing screening protocols, since OAE tests fail to diagnose deafness in this case. Continued research appears to be needed to complete otoferlin isoform expression characterization to enhance genetic diagnostics. This timely review is meant to sensitize the field to clinical characteristics of DFNB9 and current limitations in preparation for clinical trials for *OTOF* gene therapies that are projected to start in 2021.

Keywords: DFNB9; otoferlin; sensorineural hearing loss; auditory synaptopathy/neuropathy; temperature-sensitive auditory neuropathy; progressive hearing loss

1. Introduction

Sensorineural hearing loss is one of the most common sensory deficits in humans, affecting one to two per 1000 newborns in developed countries [1]. Over the past 25 years since the discovery of the first deafness gene, more than 120 genes have been causally associated with non-syndromic hearing loss (<https://hereditaryhearingloss.org/>) and over 6000 disease-causing variants have been identified [2]. As most variants implicated in hearing loss are small insertions/deletions (indels) or single nucleotide variants [2], high-throughput sequencing is a well-suited method to rapidly allow for a deeper understanding of the spectrum of variants involved in deafness and their consequences on the auditory phenotype.

Using a candidate gene approach, the DFNB9 locus (OMIM: 601071) was mapped to chromosome 2p23.1 in 1996 by studying a genetically isolated family from Lebanon [3]. Three years later, the gene *OTOF* (OMIM: 603681), encoding a transmembrane (TM) protein called otoferlin, was mapped to the DFNB9 locus and identified as causing prelingual autosomal recessive, non-syndromic deafness [4]. Biallelic pathogenic variants in *OTOF* cause auditory synaptopathy due to deficient pre-synaptic neurotransmitter release at the ribbon synapse of the inner hair cells (IHCs) [5].

Since its initial identification, about 220 pathogenic and likely pathogenic variants in *OTOF* have been identified. In addition to an expanded understanding of the types of variants in otoferlin that

cause deafness, the structure and function of otoferlin have been extensively characterized through functional studies that have greatly informed experimental therapies. This review covers the challenges of clinically diagnosing *OTOF*-associated hearing impairment, the spectrum of phenotypes that have been observed in patients with *OTOF* variants and a current review of genotype-phenotype correlations.

1.1. Mouse Studies Reveal Insights into Otoferlin Function

Otoferlin is distributed throughout the cytoplasm and plasma membrane of IHCs with the exception of the most apical part that forms the cuticular plate and tight junctions with neighboring cells (Figure 1). In addition, type I vestibular hair cells and immature outer hair cells (OHCs) express otoferlin, yet the physiological function for this expression in the mature inner ear is still unclear [6,7]. Although the mRNA of otoferlin can be isolated from several tissues including the brain, clear immunohistochemical proof of otoferlin protein expression outside hair cells is missing. Studies in *Otof*-knock-out mouse models revealed that, in the absence of otoferlin from IHCs, very few neurotransmitter-filled synaptic vesicles fuse with the plasma membrane [5,8]. Thus, acoustic stimuli still generate receptor potentials in the IHCs (and OHCs), but this information is not passed to the auditory pathway. In vitro studies indicating that otoferlin can interact with neuronal SNARE proteins contributed to the hypothesis that otoferlin acts as a synaptotagmin-like Ca^{2+} sensor for exocytosis [5,9]. However, later studies revealed that such neuronal SNAREs are expressed at only very low levels in IHCs and are absent from IHC synapses [10]. Instead, the mechanism of vesicle fusion might rely on a unique molecular mechanism in IHCs [11]. Later studies in a mouse line with the mutation of a presumed Ca^{2+} -binding site revealed a slight delay and slowing down of Ca^{2+} -triggered exocytosis, which would be in line with a Ca^{2+} -dependent acceleration of exocytosis and was interpreted as a Ca^{2+} sensor function for otoferlin in exocytosis and vesicle replenishment [12]. However, the Ca^{2+} -binding capability of the site targeted in this study is still under debate (see Section 5).

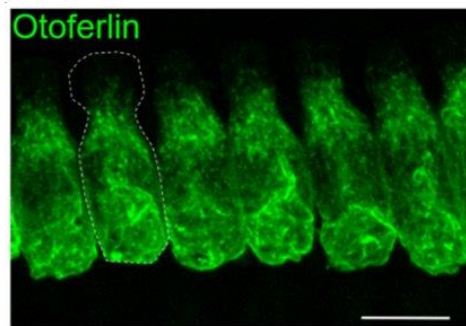


Figure 1. Expression of otoferlin in a row of inner hair cells (IHCs). Maximum projection of optical confocal sections, scale bar: 10 μm (modified from [13]). The dotted white line marks the cell boundary.

Notably, mouse models with reduced levels of otoferlin revealed additional functions for the protein at the synapse: In these models, Ca^{2+} -triggered vesicle fusion still occurred, which allowed for the observation of synaptic processes that are closely linked to exocytosis. In this way, it was uncovered that the rate with which synaptic vesicles are regenerated, supplied to the active zones of the synapses, and rendered competent for Ca^{2+} -triggered fusion depends on the quantity of otoferlin in the basolateral plasma membrane of IHCs [8,13]. A reduction to ~3% of otoferlin protein levels in the plasma membrane in the *pachanga* mouse model still enabled IHCs to release transmitter in response to short (<10 ms) stimuli, but strongly impaired the synaptic transmission for longer stimuli [8,13]. This was attributed to a defect in accomplishing vesicles competent for fusion—also termed “priming” or “vesicle replenishment to the readily releasable pool of vesicles”. As a result, in a living organism, such IHC synapses are constantly deficient of fusion-competent synaptic vesicles. Consequently, no auditory

brainstem responses (ABRs) can be recorded in these animals [8,14], as this requires the synchronous action potential firing in the auditory pathway for hundreds of stimulus repetitions.

A milder reduction to 35% of wild-type otoferlin levels in the plasma membrane of a mouse model for the human p.Ile515Thr substitution halved the rate of vesicle replenishment compared to normal hearing controls [13]. This only mildly affected the auditory threshold but impaired the ability to detect changes on top of sustained stimuli. In this mouse line, stimulation of exocytosis resulted in enlarged synaptic vesicles. Together with the finding of otoferlin immunoreactivity on endosomal vesicular structures, it was concluded that otoferlin is involved in the reformation of synaptic vesicles from bulk endosomes [13]. This is in agreement with the finding that otoferlin interacts with the clathrin adaptor protein AP2 [15,16]. Presumably, otoferlin is retrieved from the plasma membrane mostly by bulk endocytosis. On the large endosomal structures, clathrin-coated pits appear, supposedly forming novel synaptic vesicles [13,16]. In conclusion, the proper function of the synapse being able to faithfully transmit highly fluctuating acoustic stimuli to the auditory pathway requires a high expression and proper localization of otoferlin. In contrast, low otoferlin levels allow for the transmission of acoustic signals as long as individual synapses are only sparsely activated.

1.2. Otoferlin Isoforms

The structural diversity of *OTOF* has been expanded since its identification to include long and short isoforms that make use of distinctive transcription and translational start sites, as well as alternative splicing of exons 6, 31, and 47. The short and long isoforms range from 28 exons spanning 21 kb [4] to 48 exons across 90 kb [17], respectively. In total, two long and three short isoforms have been identified in humans. Long isoforms are characterized by the presence of six (or seven) C₂ domains and a C-terminal transmembrane (TM) domain, whereas the short isoforms are comprised of only the final three C₂ domains and the TM domain [17]. C₂ domains are globular domains composed of antiparallel β -sheets, which are known for Ca²⁺ and phospholipid binding. In humans, the short isoforms are comprised of isoform b (NP_004793) and d (NP_919304), each with 1230 amino acids and isoform c (NP_919303), with 1307 amino acids, employing an alternate starting exon, compared to the long isoforms a (NP_919224) and e (NP_001274418), which both encode 1997 amino acids.

With respect to a potential functional role of the short isoforms, a review of pathogenic and likely pathogenic variants has shown no indication that variants only affecting the long, but not short, isoforms would cause a milder phenotype. This confirms that the long isoform is critically required for normal hearing function [17].

The two long isoforms of otoferlin can be distinguished by virtue of tissue mRNA expression and subtle differences in exon usage at the 3' end of the gene. Isoform a was identified from brain cDNA libraries with a termination codon in exon 47 [17]. An alternative splice isoform has been identified in the human cochlea that exclusively uses exon 48 to encode the C-terminus (isoform e, [18]), but lacks exon 47, a finding that was consistent with the mouse [17]. Moreover, pathogenic variants in exon 48, but not exon 47, indicate that the isoform that skips exon 47 and makes use of the termination codon in exon 48 seems to be the predominant isoform in the human cochlea [18–20].

Limitations in obtaining mRNA from human IHCs has presented a major bottleneck in profiling and quantifying the relative fractions of all otoferlin isoforms. According to Yasunaga et al. [17], an alternative splice acceptor site in exon 31 may be employed, eliminating 20 amino acids from the longest variant. This alternative splicing was predicted for the short isoform b and seems to be the predominant variant in mouse inner ear tissue [13]. In the presence of this 20 amino acid “RXR” motif, the p.Ile515Thr substitution caused a retraction of mouse otoferlin from the plasma membrane, which was not the case for the p.Ile515Thr-protein lacking the RXR motif. The authors of this study speculated that the phenotype found in patients with the p.Ile515Thr substitution would be best explained if the human cochlea expresses a mixture of both splice variants [13]. Furthermore, transcript analyses suggest the presence of so far undetected exons (described in Section 3.4 below). Despite these uncertainties, we recommend that human *OTOF* sequence analysis utilizes the reference sequence for variant e,

NM_001287489, encoding the 1997 amino acid protein, NP_001274418. Furthermore, we propose that *OTOF* variants from human molecular genetic diagnostic laboratories that are deposited in clinical variant repositories be adjusted to this reference sequence.

2. Hallmarks of Audiometric Testing in DFNB9 Patients

Since its discovery, *OTOF*-associated hearing loss in humans has presented several challenges, making the selection of clinical diagnostic protocols an essential undertaking for an early diagnosis. Based on the finding that *OTOF* variants disrupt presynaptic function in IHCs rather than neuronal function, a change in terminology from “auditory neuropathy” to “auditory synaptopathy” has been adopted to more precisely describe this. A lesion to the neural pathway that transmits signals from the cochlea to the brain is clinically characterized by an absence of ABRs and the presence of otoacoustic emissions (OAEs). The testing of OAEs indicates proper functioning of cochlear amplification by the OHCs. As OHCs and IHCs employ the same protein machinery for mechanotransduction at their stereocilia bundle, any malfunction of this can be excluded if OAEs are present. Similarly, both hair cell types depend on proper endolymph composition and endocochlear potential as the driving force; a functional deficiency which would be detectable in altered OAE recordings. However, patients with *OTOF* variants lose OHC function, occasionally within the first year, and in about one-third of cases in the second year of life, with only few individuals displaying OAEs in early adulthood [20–22]. Therefore, individuals without OAEs should be considered for genetic testing that includes *OTOF*.

As is true for all forms of auditory neuropathy or synaptopathy, newborn hearing screening that tests for OAEs, e.g., with distortion product otoacoustic emissions (DPOAEs) or transient evoked otoacoustic emissions (TEOAEs), fail to detect a hearing disorder in most cases, as OAEs are initially present. Passing OAE tests despite profound deafness can be misleading and, in the worst-case scenario, prevent parents and pediatricians from pursuing a more complete audiological diagnostic testing. ABRs in patients with synaptopathies are typically absent, even for high sound pressure levels, making them well-suited for the detection of profound deafness. Moreover, even mild forms of hearing loss result in abnormal ABRs in case of DFNB9 (see below). However, as ABR testing is a more time-consuming procedure, this is not routinely applied in newborn hearing screening protocols, delaying the diagnosis of a baby with congenital auditory synaptopathy by months or even years until it is recognized and confirmed. In children with *OTOF* variants, behavioral audiometry, with or without visual reinforcement, can indicate severe to profound hearing loss across all frequencies. While some patients display residual hearing in the low-frequency region (with thresholds of ~75 dB hearing level (HL) for 250 Hz; e.g., [23]), pure tone audiograms may be flat, or bowl-shaped, but in all such cases, average thresholds are above 90 dB HL.

A reliable diagnosis of even mild forms of hearing loss caused by *OTOF* variants is of relevance, especially for young children whose speech acquisition may become strongly impaired. Moreover, a precise diagnosis will also help later in life to specify impairments of speech comprehension, which, for example, may explain why following multiple speakers is much more exhausting for DFNB9 listeners than for normal hearing listeners. Despite pure tone audiograms being only mildly or moderately affected in such cases, ABRs are mostly abnormal, indicating higher thresholds than expected from psychophysical testing. ABR waves I to III are hardly detectable and waves IV and V are delayed [24]. Speech comprehension testing should be performed both in silence and in background noise, the latter of which is typically strongly affected.

A more specific test for this type of synaptopathy would be to quantify the time required for synaptic regeneration. This could be done by gap detection tests, i.e., silent gaps of different length in broadband noise. Intact IHC synapses accurately detect the onset of the white noise after a gap as short as 2–4 ms in humans, at least after some training [25]. This depends on the ability of the IHC synapse to reliably induce a precisely timed postsynaptic action potential at the onset of the white noise after the silent interval, which will require readily releasable synaptic vesicles. Although this has not been systematically tested in patients with mild forms of DFNB9, we expect that silent gaps will need

to be substantially longer to be detected by the probands [26]. On average, animal models with the p.Ile515Thr mutation required 17 ms silence (interpolated value, [13]) to detect the gap, whereas normal hearing mice can perceive gaps as short as 1–2 ms [27].

The combination OAE recordings and ABR or pure tone audiometry are, in principle, sufficient to diagnose hearing impairment due to *OTOF* mutations. Other tests do not provide additional information as, for example, even at high sound pressure levels (SPLs), no auditory reflexes can be elicited, which confirms the absence of auditory evoked signal transmission indicated by absent signals in ABRs. In only a few cases, transtympanic electrocochleography (ECoChG), with a recording electrode placed at the promontory wall, will be of use for diagnoses. However, since it requires local anesthesia of the tympanic membrane and is rather invasive, it is questionable if this justifies the limited additional information. ECoChG is employed to record the summing potential (SP), cochlear microphonics and compound action potentials (CAPs). Cochlear microphonics originate from functional OHCs such that this recording would be redundant to OAE tests, although amplitudes of cochlear microphonics can be highly variable [23,28].

Recording the SP in response to click stimuli may add novel information in particular cases when OAEs are absent, but might be hard to interpret. Since the SP derives from the depolarization of inner and outer hair cells [29], the depolarization of the IHCs may still result in a small but measurable SP even if OHCs are degenerated. This can help to distinguish from forms of hearing loss involving the stereocilia and/or the mechanotransduction channels, since, in this case, no depolarization of hair cells occurs.

CAPs that record the first action potential in the auditory pathway are absent in some DFNB9 patients, while others exhibit a prolonged CAP with reduced amplitude, at least for single click stimuli [23]. Repetitions of click stimuli with short interstimulus intervals of 2.9 ms abolish CAP responses. Findings from a detailed assessment of pre- and postsynaptic function in the *pachanga* mouse model (p.Asp1772Gly) can likely explain this observation: The IHCs in this animal model display intact synaptic signal transmission for short (<10 ms) interspaced stimuli, given that the interstimulus intervals allow for sufficient recovery [8]. Under repetitive stimulation, as in ABR recordings, the strong defect in vesicle replenishment abolishes reliable signal transmission. In single auditory nerve fiber recordings, the first spike was found to be highly variable in timing and was, on average, delayed, which is likely to reflect the prolonged CAP response. The spike rate in *pachanga* mice reached up to 200 spikes/second (compared to >400 spikes/second in wild-type mice), but only when stimuli were presented once every two seconds (0.5 Hz stimulus frequency) [8]. Increasing the stimulus frequency to 10 Hz strongly diminished neural responses (<10 spikes/second) except for the very first trials. Therefore, we infer that the CAP signals for isolated click stimuli in DFNB9 patients indeed originate from an auditory evoked neural response and are prolonged due to the increased first spike latency. Presenting repetitive click stimuli to these patients—a second stimulus after 15 ms and subsequent ones at 33 Hz—strongly reduced or even abolished these CAP responses, which might be the direct equivalent to the diminished neural spiking found in the mouse models. The reason for this is that the replenishment of synaptic vesicles is strongly slowed down when the amount of otoferlin at the IHC plasma membrane is reduced [8,13]. Thus, long silent intervals are required to regenerate the first auditory synapse to enable another cycle of auditory evoked synaptic transmission.

However, why is the CAP response absent in some DFNB9 patients, or prolonged and with a small amplitude in others? This question arose in a study that analyzed CAP responses in patients with various types of variants in the *OTOF* gene. Two frameshift variants were associated with absent CAPs in two patients [23]. Individuals with biallelic premature stop variants exhibited the largest CAP response in this study, while the amplitude of the CAP was intermediate in patients with one frameshift and one premature stop variant. While frameshift variants cause termination of the amino acid chain in all cases, stop codon read-through can occasionally occur with an efficiency of up to 3–4% (reviewed in [30]). As only 3% of the otoferlin protein is localized at the plasma membrane in *pachanga* mice, it is tempting to speculate that an *OTOF* gene with premature stop codons described in this study

may have undergone partial natural stop codon read-through, inducing residual synaptic function of an order of magnitude as in *pachanga* mice.

3. Molecular Epidemiology of *OTOF*-Associated Hearing Loss

3.1. Summary of Variants Identified in *Otoferlin*

By virtue of being one of the first deafness genes identified, *OTOF* has been tested in molecular genetic diagnostic settings for over two decades, allowing an estimate of the global burden of *OTOF*-associated hearing loss. There are presently 219 genetic changes that are classified as pathogenic or likely pathogenic according to the literature or clinical database entries (Leiden Open Variation Database v3.0 (LOVD v3), the Deafness Variation Database (DVD), ClinVar, and the Human Gene Mutation Database (HGMD)) (Table S1). This includes 84 missense, 44 frameshift, 43 nonsense, 36 splice site, 7 in-frame duplications or deletions, 3 copy number variations, as well as 1 stop loss and regulatory variant each (Figures 2 and 3, Table S1).

3.2. Population-Based Diagnostic Rates of *Otoferlin*

The prevalence of *OTOF*-associated hearing loss varies according to population background. For example, *OTOF* variants account for approximately 5% of genetic diagnoses in the Turkish population [31], and 3.1% of diagnoses in the Pakistani population [32]. A common founder variant (p.Gln829*) was identified in 3% of Spanish cohorts [21,33]. In other populations, *OTOF* has been identified as a cause of hearing impairment in 3.1% of Taiwanese [34], 2.4% (primarily) European-American [35], 2–3% of Pakistani [18,32], 1.9% of French [36] and 1.7% of Japanese [37] patients who were not pre-selected on the basis of auditory neuropathy/synaptopathy. In Iranian patients, a study that included 38 consanguineous patients identified only one family with a homozygous frameshift variant (c.1981dupG, p.Asp661Glyfs*2) and suggested *OTOF* is not a major contributor to hearing loss in the Iranian population [38].

3.3. Diagnostic Rates of *Otoferlin* in Patients with Auditory Neuropathy/Synaptopathy

Auditory synaptopathy with prelingual onset has been identified in patients with genetic aberrations in a small subset of genes (*PJVK*, *OPA1*, and *DIAPH3* (AUNA1 locus)), and a limited number of suspected cases in a few other genes such as *GJB2* [39–44], although the *GJB2* cases are controversially discussed [45]. The unique phenotypic presentation of DFNB9 makes a targeted selection for *OTOF* screening in patients for genetic testing rather successful. As exemplified by a study that included Japanese patients with auditory neuropathy/synaptopathy, biallelic *OTOF* variants were uncovered in 56% of cases that included the identification of a founder variant (p.Arg1939Gln) [46]. The p.Gln829* founder variant was identified in 87% of patients diagnosed with auditory neuropathy/synaptopathy in the Spanish population [21]. Another founder variant (p.Glu1700Gln) in Taiwanese patients with progressive, moderate-to-profound hearing loss was identified that diagnosed 23% of a selected patient cohort of 22 individuals with auditory neuropathy/synaptopathy [47]. A study that screened the *OTOF* gene in 37 Chinese patients with congenital auditory neuropathy/synaptopathy had a diagnostic yield of 41.2% [48]. On the contrary, a study that involved the screening of 73 Chinese Han patients with auditory neuropathy/synaptopathy resolved only 5.5% of patients and uncovered a temperature-sensitive variant, which was lower than anticipated and demonstrates a high diagnostic variability [49].

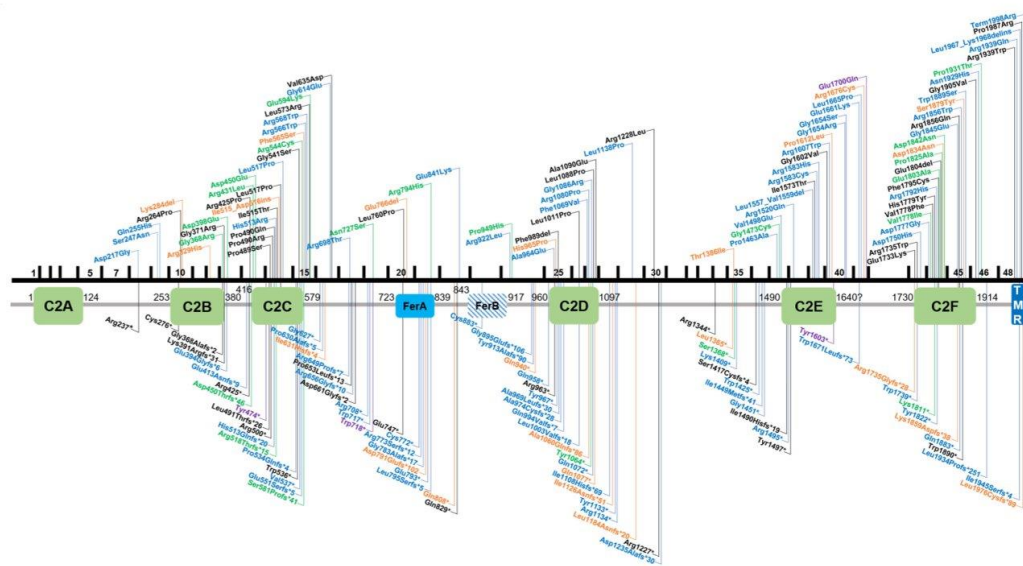


Figure 2. Overview of OTOF variants that are classified as pathogenic/likely pathogenic in the databases ClinVar, Leiden Open Variation Database v3.0 (LOVD v3), the Deafness Variation Database (DVD) or Human Gene Mutation Database (HGMD). Variants in the upper part of the figure are non-truncating, variants below are truncating. Black text indicates homozygous variants, blue and green text represents compound heterozygous and heterozygous variants, respectively. Orange text show variants that are reported in databases without a publication reference with undetermined zygosity. Purple text indicates two different variants on the cDNA level that cause the same protein-level change. Variants are annotated according to NM_001274489.1, encoding NP_001274418.1, or isoform e.

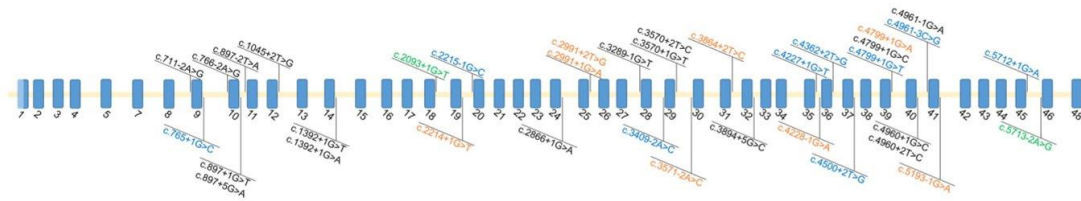


Figure 3. Overview of OTOF splice variants according to ClinVar, Leiden Open Variation Database v3.0 (LOVD v3), the Deafness Variation Database (DVD) or the Human Gene Mutation Database (HGMD). Black text indicates homozygous variants, blue and green text represents compound heterozygous and heterozygous variants, respectively. Orange text shows variants that are reported in databases without a publication reference with undetermined zygosity. Variants are annotated according to NM_001287489.1, encoding NP_001274418.1, or isoform e.

3.4. Missing Variants

The diagnostic yield of patients with audiological hallmarks of DFNB9 suggests multifaceted deficits in general isoform and variant knowledge, as well as possible technical limitations. Beyond the possibility of additional genes harboring causally associated variants that evoke the same clinical features, there are several reasons explaining why patients with auditory synaptopathy due to biallelic variants in *OTOF* remain undiagnosed after molecular genetic screening. Such reasons include possible limitations stemming from methodology (e.g., sequencing coverage gaps), missed copy number variations that either fall below the detection resolution of commonly used microarrays in genetic diagnostics or missed due to uneven high-throughput sequencing coverage, especially in the case of exome sequencing, or deep intronic variants that are not captured in targeted enrichment approaches. Furthermore, variant interpretation bottlenecks that could also be due to incorrect transcript usage in variant annotation, current limitations in knowledge about the pathogenicity of rare variants and lack of opportunity for segregation testing in families that can complicate outcomes for definitive statements about variant pathogenicity. Another hypothesis points to variants occurring in currently unannotated exons.

Sequence analysis is primarily focused on exonic regions and relies on the complete understanding of gene isoform structure (i.e., exon annotation). The cochlea is encased in one of the hardest bones of the body, making it one of the least accessible tissues for transcriptome studies. However, many microarray and RNA-seq-based studies using the human and rodent whole cochlea have ensued since the early 2000s [50,51]. Though challenging, single-cell isolation of the inner ear and long read single-cell RNA-seq have recently been performed in mice at several developmental time points [52] to reveal cell-type defining genes and pathways. Long-read sequencing and isoform analysis has identified unappreciated splicing heterogeneity and expression of cell-specific isoforms with unannotated exons [52]. A recent study marked a crucial gap in this understanding in many well-studied genes, such as *Otof*, by mapping a novel non-coding exon 6b and suggesting an in-frame exon 10b (Figure 4). Extending this finding by annotating novel *OTOF* exons in humans could yield significant implications for undiagnosed patients who would otherwise fit the characteristic DFNB9 phenotypic spectrum.

4. Genotype-Phenotype Correlations in DFNB9 Patients

The uniformity of available clinical and genetic information about the current set of identified variants is highly variable. For example, reported variant zygosity (i.e., homozygous versus compound heterozygous) and the extent of audiological characterization and recorded onset in patients are highly heterogeneous. Most variants lack recorded audiological information. Generally, biallelic *OTOF* variants cause congenital or early onset ($n = 114$) hearing impairment. Few variants have been identified with progressive hearing loss ($n = 3$). Seven variants have been linked to temperature-sensitive hearing loss, five of which are located within C₂ domains. While premature stop and frameshift variants typically cause profound prelingual deafness, non-truncating variants can cause a highly variable phenotype. Depending on the localization and the physico-chemical properties of the substituted (or deleted) amino acid residues, variants can severely affect protein stability and contribute to protein degradation. In some cases, the deterioration of protein folding is less severe, leaving some endogenous otoferlin at the plasma membrane that may vary with age and body temperature. This typically results in mildly to moderately elevated thresholds in pure tone audiograms but severely impaired speech comprehension. Notably, patients with point mutations and residual otoferlin expression report perceiving a fading out of a tone burst presented with constant intensity [23,53]. These characteristics of hearing impairment seem to be true for both types of moderate auditory synaptopathy that include the temperature-sensitive and progressive variants.

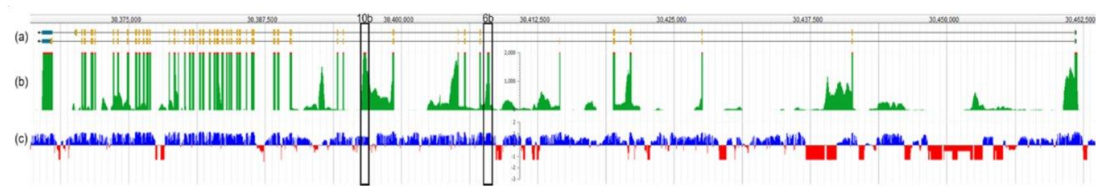


Figure 4. Overview of the *Otof* transcript structure based on single-cell RNA-seq data from mouse IHCs. (a) Transcript structure of *Otof*, with exon 1 on the right side of the figure. Exons are depicted as gold bars. Ensembl transcripts *Otof-201* (upper isoform, encoding 1997 amino acids) and *Otof-202* (lower isoform, encoding 1992 amino acids) are shown. (b) The read depth of each exon is shown in green, with the highest covered regions showing in red. Note that maximum read peaks (red) correspond with exons shown in (a) if they are expressed in the IHC. (c) Mammalian conservation track for *Otof*. Conserved sequences are shown in blue and those not conserved are shown in red. The predicted novel exons 6b and 10b are marked with black boxes. This figure was generated by querying morlscrnaseq.org using the “Transcript Structure Browser” tool [52].

4.1. Temperature-Sensitive Auditory Synaptopathy

Temperature-sensitive auditory synaptopathy has been reported by parents observing profound deafness as soon as their children are febrile. Mirroring daytime changes in body temperature, fluctuations in speech comprehension have been described, which was least affected in the early morning and progressed throughout the day to a point where vocal communication is hardly possible [24]. Even a slight increase in body temperature from 36.5 to 36.8 °C in the course of a day seems to attenuate auditory perception. However, in addition to increased body temperature, acoustic exposure is likely higher during the daytime than at night, which may aggravate hearing impairment due to defective synaptic regeneration. Potentially, both body temperature and increased sound stimulation compound to impair speech comprehension during daytime.

When measured in febrile conditions, both an elevation in pure tone thresholds and zero speech comprehension can confirm the diagnosis of temperature-sensitive auditory synaptopathy. The first variant discovered causing temperature-sensitive auditory synaptopathy, p.Ile515Thr [54], has been extensively studied in a mouse model [13]. At normal body temperature, the hearing phenotype of these mice mirrored what is observed in the affected human siblings. When afebrile, they have tremendous difficulties understanding speech in background noise despite having almost normal pure tone audiograms. In the mouse models, ABR thresholds were mildly elevated, 10 dB SPL for click stimuli and ~20 dB SPL across tone burst frequencies at the age of 3–4 weeks. When the same mice were tested again at the age of 8 and 25 weeks, ABR thresholds increased to an average of 80 dB SPL for tone bursts and to 50 (8 weeks) to ~75 dB SPL (25 weeks) for click stimuli. In parallel, ABR wave amplitudes were strongly diminished. In contrast, behavioral tests and auditory nerve fiber recordings revealed only mild threshold shifts in these mice at that age. This correlates well in patients with impaired ABR despite only mild threshold elevations in psychophysical tests. In mice, single auditory nerve fiber recordings were employed to assess the effect of the presynaptic impairment on action potential generation. In agreement with the presynaptic deficiency in replenishing vesicles, the spike rate in the auditory nerve decreased with longer acoustic stimuli or with upscaling of the stimulus frequency, representing a correlate of the auditory fatigue observed in humans. Moreover, the timing of the first spike after sound onset was of greater variability compared to normal hearing controls. In addition, the phase locking to amplitude modulated tones was strongly impaired. If this timely precision of spiking is lower, click sounds or consonants will become blurred. With respect to human hearing, these deficits most likely explain difficulties in speech comprehension and the abolishment of the latter in background noise. At elevated temperature, patch clamp recordings revealed a decrease in exocytosis when cells were heated from near-physiological (35–37 °C) to elevated temperatures (38.5–40 °C). This was especially obvious for wild-type IHCs, indicating that even the wild-type otoferlin protein is very sensitive to elevated temperature and may unfold rather quickly [13]. However, the wild-type protein seemed to be capable of re-folding, as it gained back initial exocytosis when temperature was lowered to <29 °C. In contrast, the IHCs in the p.Ile515Thr model showed impaired recovery, suggesting that the destabilization of the substitution in the C₂C domain reduces the likelihood of proper refolding. This interpretation would be in concordance with the observation that patients regain hearing a few hours after temperature-induced deafening, which would be consistent with the time required for *de novo* synthesis of sufficient quantities of otoferlin.

A similar phenotype to the p.Ile515Thr variant was described in humans with the p.Gly541Ser variant, which also localizes to the C₂C domain of otoferlin [24,46]. In addition, temperature-sensitive auditory neuropathy has been described for the p.Arg1607Trp variant in the C₂E domain [24,49] and for an individual with compound heterozygosity for the p.Gly614Glu and p.Arg1080Pro substitutions, the latter of which resides in the C₂D domain [55]. Remarkably, patients with the p.Arg1607Trp substitution in homozygosity or compound heterozygosity reported hearing loss that ameliorated with increasing age [24]. An in-frame deletion, p.Glu1804del in the C₂F domain, was also attributed to temperature-dependent hearing loss [56]. Notably, no other genes apart from *OTOF* have been associated with temperature-sensitive forms of hearing loss and all cases presenting a similar

phenotype in the literature have disclosed pathogenic *OTOF* variants, regardless of population background. All described substitutions seem to cause only slight destabilizations of one C₂ domain. However, since mutations in different otoferlin C₂ domains cause a similar phenotype, we consider it unlikely that each of the substitutions causes heat-sensitivity of the protein. Rather, as shown in Strenzke et al. [13], even the native otoferlin protein is considerably temperature sensitive at 38.5–40 °C. Potentially, any slight destabilization of this highly flexible protein might decrease the chance of re-folding after heat exposure, such that more protein is degraded at a slightly elevated body temperature, thereby exacerbating the hearing disturbance.

4.2. Progressive Hearing Impairment

Progressive forms of *OTOF* hearing impairment have been described for three variants: p.Ile1573Thr, p.Glu1700Gln and p.Ter1998Argext30Ter [46,47,57]. In all cases, the hearing impairment onset was prelingual, but the severity ranged from mild to profound at onset, even for individuals with the same variant.

The homozygous p.Glu1700Gln substitution was identified in several Taiwanese families [47]. In patients from three families, hearing loss was initially mild and became moderate to severe within a few years. In two other families, affected individuals were identified with severe or profound hearing impairment already at the first hearing assessment at the age of two and one years of age, respectively. The reason for hearing loss progression and variability of the onset severity is currently unknown since the linker region between the C₂E and the C₂F domains, in which this substitution lies, has not been studied so far.

A homozygous p.Ile1573Thr substitution was identified in a child with parental consanguinity, in whom hearing deterioration correlated with age [57]. This substitution in the 6th β-strand of the C₂E domain likely reduces the stability of protein folding. The four children of this family were found to have mild (9 years of age), moderate (11 y, 13 y) or severe hearing loss (17 y). All children displayed OAEs. Absence of ABR waves in the 9-year-old child (the only one tested) is in concordance with the severe abnormality described for all DFNB9 patients, even those with only mildly elevated hearing thresholds. A follow-up of the progression of hearing impairment of this family has not been performed so far.

A stop loss variant p.Ter1998Argext30Ter associated with progressive hearing impairment was found in compound heterozygosity with the p.Arg1939Gln substitution [46]. Since the latter causes profound hearing loss in homozygosity, the early onset, moderate hearing loss, with a steeply sloping audiogram in one ear and a gently sloping audiogram in the other, is presumably due to the elongation of the C-terminus. The C-terminal TM domain (amino acids 1964–1984), as well as the 13 amino acids more downstream, are highly sensitive to substitutions (see Section 5.)

In summary, progression of hearing impairment was typically observed over the course of a few months or years, such that affected individuals reached profound deafness in the second decade of life. Presumably due to the residual otoferlin function, OAEs remained preserved in these intermediate forms of hearing impairment; thus, affected individuals may be candidates for gene therapies even in adulthood.

5. Localization and Presumed Effects of Single Amino Acid Substitutions in Otoferlin

Many of the non-truncating variants affect the C₂, FerA and TM domains, meriting a broader discussion about domain functions and deteriorating effects due to substitutions. C₂ domains are globular domains comprised of eight antiparallel β-strands, many of which bind phospholipids and Ca²⁺. Since the Ca²⁺-binding site is localized in the structure to five specific aspartate residues in two top loops, the Ca²⁺-binding ability can be reasonably predicted from the sequence. With respect to the C₂A domain, the structure of the rat protein, which is 91% identical and 96% similar to the human otoferlin C₂A domain, has been solved with X-ray crystallography [58]. Since only one aspartate is

present in the two top loops at respective positions, the C₂A domain was predicted not to bind Ca²⁺, which was confirmed experimentally [58–60].

Different from substitutions in the other otoferlin C₂ domains, neither amino acid replacements in the β-strands nor in the loops of the C₂A domain cause malfunction of the protein. The reasons for this might be first, that the C₂A domain folds much more stably than the other C₂ domains. Crystallization from heterologous expression has been successful for the C₂A domain. However, despite laborious efforts from several research groups, this has not been the case for other C₂ domains so far, presumably because higher protein dynamics prevent the forming of crystals. Notably, the same seems to be true for the myoferlin and dysferlin C₂ domains, of which only the structures of the C₂A domains could be resolved to date [61]. Whether the high flexibility of the ferlin C₂B–C₂F domains is a biological defect or a feature relevant for proper function remains to be determined. The second reason why substitutions may be tolerated well in the C₂A domain is that this domain does not bind Ca²⁺ or phospholipids [58–60] and thus might be not directly involved in the process of Ca²⁺-triggered vesicle fusion or Ca²⁺-dependent vesicle replenishment.

Prediction of Ca²⁺-binding sites or the location of pathogenic substitutions in the other C₂ domains is rather challenging due to the low sequence similarity of the otoferlin C₂B to C₂F domains to C₂ domains with known structure. Automatic domain annotation algorithms such as SMART (EMBL, Heidelberg, Germany) [62] do not predict the extent of these domains reliably. We therefore employed Phyre2 to predict the structures of these domains, which is based on homology modelling and makes use of all structures in the protein data bank (PDB) database [63] (Figure 5). Within the predicted structures, we mapped the substitutions causing profound deafness (shaded in orange), and substitutions causing milder forms of hearing loss (shaded yellow/red; Figure 5). With the exception of the 7th and 8th β-strand of the C₂E domain and the 7th β-strand of the C₂F domain, all β-strands could be localized in the predictions. The first top loop connecting β-strands 1 and 2 and the third top loop between β-strand 5 and 6 comprise five aspartate residues (blue fonts) that coordinate one to three Ca²⁺ ions. Consistent with experimental data revealing that the C₂A domain does not bind Ca²⁺, its first top loop misses the motif containing the first aspartate, and, in the third top loop, the three aspartate sites are replaced by neutral or positively charged amino acids. Similarly, the C₂B domain comprises only one aspartate residue in the top loops, indicating that this C₂ domain cannot bind Ca²⁺. Consistent with this prediction, one lab found no Ca²⁺ binding for the C₂B domain using microscale thermophoresis assays [59]; however, other labs did find indications of Ca²⁺ binding with other tests (e.g., [60]).

The same is true for the C₂C domains, for which some labs found Ca²⁺ and phospholipid binding, while one other lab found that this domain binds Ca²⁺ only after including a phosphomimetic mutation in the first top loop (replacing the blue shaded threonine in the first loop by a glutamate, since this threonine is a site for activity-dependent CaMKIIδ phosphorylation [59]). The actual structure prediction reveals a very long top loop 1, even slightly longer than the one on the PKCα C₂ domain, comprising a predicted (otoferlin C₂C) and a confirmed (PKCα) α-helical region. The PKCα C₂ domain does bind phospholipids, but not Ca²⁺. For the otoferlin C₂C domain, one aspartate resides in the first top loop and two aspartates to a short top loop three, allowing no clear prediction whether this domain can bind Ca²⁺. We presume that the Ca²⁺ binding of this domain likely depends on posttranslational modifications such as phosphorylation and the direct domain environment, which could be phospholipid membranes, interacting proteins, or both. In a mouse model in which two aspartate residues in the C₂C domain were replaced by alanine residues, exocytosis appeared to be slightly slowed [12]. This finding would be consistent with such a context-dependent Ca²⁺-binding ability of this domain, but also with interfered phospholipid binding due to altered domain folding.

The C₂D and C₂E domains exhibit the five canonical aspartate residues at respective positions in the top loops, and experimental data confirm that both domains bind Ca²⁺ and phospholipids [60]. Nevertheless, for the C₂E domain, the precise localization of the last two β-strands could not be predicted with the algorithm and the current dataset of structures. Since a growing number of structures is solved and deposited in databases, future structure predictions might result in a reasonable model of

the position of the two β -strands. Pathogenic single amino acid substitutions in these domains typically lie within β -strands (Figure 5), likely destabilizing the structure of the domains. The effect is nicely demonstrated in an ENU-mutagenesis induced mouse line, *deaf5Jcs*, with a p.Ile318Asn substitution in the 5th β -strand of the C₂B domain (indicated with green shading in Figure 5). Immunohistochemical analyses of mouse IHCs revealed almost complete absence of the protein, despite mRNA transcripts were present [64], most likely because misfolding of one domain leads to proteasomal degradation of the mutated protein.

```

A_1  --MALLIHLKTVSE--LRGR-----GRIAKVTFRG---QSFYSRVLE--NCEDVADFDETFRWPVASSI
B_251 PMDYQVSIITVIEARQLVG-----LNMDPVVGVVEVD---DKYITSMKRESTNCPYYNEYFVDFHVSVDVM
C_414 RQWARFYVKIYRAEGLPRMNTSLMANVKKAFIGENKDLVDPVVQVFFAG---QKGTSTVQKSSYPLWNEQVVFDTLFPF
D_498 QAFQLRSMYQ--ARSL-----FAAUSGLSDPFARVFIN---QSQCTEVLNETLCPDWDQMVFDNLELYGEAHELK
E_1488 DPINVLVRVYVVRATDLH-----PAQINGKADPYLAIKLGK---TDIRDKENYISKQLNPVFGKSPDIEASF
F_1728 KPKKYELRVIIWNTDEVVL-----EDDQFTTGEKSSDIFVRGWLKGGQEDKQDTDVIYHSLTGEQGNFNRVLEPFDYLAASEEKIVISKKEQMFSDWDETEY

A_57  DRNEMLEIQVFNYSKVFNSKLIQTFRMVLQKVVEE-----SHVEVTDLTIDDNNAI-----IKTSLCQVEVRYQATDGT-----124
B_313 FDKLIKSVIHSKNLLRSGTLVGSFKMDVGTVYSQ-----PEHQFHHKWAISLDPDD-----ISSGLKQVVKCDVAVVKGKD-----384
C_491 LCK-RMKVQIRDSKVN-NDVAIGTHFDLIRKISNDGDKGFLPTLGPWVNMYSSTRNYTLTLDHQQDLEGLGEGVSEARALLIGAVEIVDTSNP-----583
D_1027 DPPPILVIEIYDQDSMGKADFMGRTFAKPLVKMADEAYCPRPFPQLEYQIY--RGNAT-----ADLLAFAPELLQIGPAG-----1101
E_1552 PMESMLTVAVIWDLVGTDDLGETKIDLENRFY-----SKHRATCGIAQTYSTHYNIWEDPMKPSQILTRLCKDQKVDGPHFGPPG-----1634
F_1823 KPEARLTQIWDADHFSADDFLGAIELDLNRFPFGAKTAKQCTMEMATGEVDVPLVLSIFPKQKRVKGNWPLLARNENDEFELTKVVEAELHLLTAE--1918

```

Figure 5. Alignment of otoferlin C₂ domains A to F with β -strands in brown fonts and α -helices in green fonts. The structure of the C₂A domain was resolved by X-ray crystallography ([58], PDB accession code 3L9B, www.rcsb.org). The structures of the other C₂ domains were modelled by means of Phyre2 [63]. The two last β -strands of the C₂E domain and the 7th β -strand of the C₂F domain could not be reliably predicted due to low sequence homology. In case the modelling of the β -strands is rather uncertain, amino acids are depicted in purple font. The aspartate residues that coordinate Ca²⁺ are depicted in blue fonts, in case several aspartates or glutamates could potentially play a role for Ca²⁺ co-ordination in dark blue fonts. Pathogenic variants leading to profound deafness are shaded in orange. Those causing moderate hearing loss are shaded in yellow, and if the hearing loss appears to be temperature sensitive, in red. Shading in green indicates mutations in deaf mouse models, *deaf5Jcs* in the C₂B domain and *pachanga* in the C₂F domain [14,64]. Threonine or serine residues that were found to be phosphorylated by CaMKII δ are shaded in blue [59]. Few pathogenic variants affect the CaMKII consensus phosphorylation site, which is RXXS or RXXT.

Structure predictions have hinted to a seventh C₂ domain, termed C₂de, between the C₂D and the C₂E domains that spans amino acids 1143–1220 according to the *Pfam* algorithm. Due to the low sequence similarity and the rather short length of this predicted domain, it is currently unclear if this region folds as a C₂ domain at all. One frameshift and three splice site mutations have been found in this potential domain, but so far no non-truncating pathogenic variant (Table S1).

The C₂F domain seems to be the most unconventional and most susceptible to alterations ultimately leading to protein malfunction. There are presently 18 reported pathogenic/likely pathogenic variants mapping to this domain.

The first top loop comprises eight negatively charged amino acid residues that could potentially contribute to Ca²⁺ co-ordination. Three aspartate residues reside in the canonical positions of the third top loop. Substitution of one of the aspartates in the first top loop (p.Asp1750His) and two in the third top loop (p.Asp1834Asn and p.Asp1842Asn) are each pathogenic. Accordingly, Ca²⁺ co-ordination seems plausible and has experimentally been confirmed [59,60], despite the fact that the precise folding of the first loop is unable to be predicted. Since these Asp>Asn substitutions in the third loop do not change the hydrophobicity, we presume that the Ca²⁺ affinity is strongly reduced by these substitutions, indicating that Ca²⁺ binding to the C₂F domain is essential for proper function.

Different from the other otoferlin C₂ domains, where only two amino acids form the bottom loop between β -strands 2 and 3, the loop in the C₂F domain is predicted to be longer and consists of hydrophobic tryptophane residues flanked by positively charged side chains. This loop comprises the p.Asp1772Gly mutation found in *pachanga* mice which strongly reduced plasma membrane association of otoferlin [8,13,14]. This indicates that this loop structure, also found in other ferlin C₂F

domains [65], seems to be crucial for a partial insertion into phospholipid membranes. Despite homology modelling with alignments with different structures leaving some uncertainty about the beginning of the subsequent β -strand, the consensus prediction of this β -strand includes the position of three consecutive amino acids whose substitutions cause profound hearing loss (p.Asp1777Gly, p.Val1778Ile, p.Val1778Phe, p.His1779Tyr). Moreover, these three amino acids reside just before a CaMKII δ phosphorylation site, S1782, and might interfere with the binding of the CaMKII δ and thus phosphorylation [59]. The subsequent bottom loop comprises two glutamate residues. The deletion of one (p.Glu1804del) causes temperature-sensitive auditory neuropathy, presumably because the shortening of this loop destabilizes the domain. Thus, it seems as if the C₂F domain is especially sensitive to point mutations and that Ca²⁺ and phospholipid binding are crucial for proper protein function.

The function of the FerA domain for synaptic transmission is presently less clear. Small-angle X-ray scattering and in vitro experiments indicated that this domain is comprised of four α -helices, which are connected by a dynamic linker region [66]. The FerA domain binds to phospholipid membranes that is enhanced by Ca²⁺. Four non-truncating substitutions have been identified in the FerA domain so far, but three of those could not be linked to a phenotype (heterozygous, or no reference). The fourth homozygous substitution found in a Taiwanese family alters the second helix (p.Leu760Pro). This suggests that misfolding of the FerA domain is not tolerated, indicating a role for the FerA domain for synaptic transmission that requires further studies.

Substitutions of amino acids in the TM domain cause variable severities of hearing loss. The homozygous p.Pro1987Arg substitution causes early onset, severe to profound hearing impairment, in this specific case, with a bowl-shaped audiogram [19] (Table S1). A three base pair deletion (p.Leu1967_Lys1968delinsGln) at the TM domain caused early onset, mild hearing loss, similar to the p.Ter1998Argext30Ter [46]. This is likely due to the mechanism by which this tail-anchored structure is inserted into the membrane. Once translation of the amino acid chain has been completed, the C-terminal amino acids bind to the chaperone TRC40 and this complex is targeted to the TRC40 receptors WRB and CAML, which insert the C-terminus into the phospholipid membrane [67,68]. These mutations likely interfere with this tail insertion mechanism, thereby reducing the amount of otoferlin at the plasma membrane, leading to a moderate hearing impairment. In contrast, variants truncating the amino acid chain behind the C₂F domain and before the TM domain, such as p.Gln1883Ter or the c.5833delA deletion (p.Ile1945Serfs*4), cause profound deafness, indicating that the TM domain is essential for protein function [48].

6. Current and Future Therapies for DFNB9

The established therapy for individuals with severe to profound hearing loss due to otoferlin deficiency is currently cochlear implantation. Since this prosthetic bridges the first auditory synapse, which is the only part of the auditory pathway involved in DFNB9, patients benefit well from these devices and gain good or even excellent speech understanding. However, the most sensitive period for developing the capability to understand spoken language is within the first two years of life. It is, therefore, critical to implant patients as early as possible. This requires an early diagnosis, but most children with severe to profound hearing loss due to variants in *OTOF* pass newborn hearing testing because, in most countries, the assessment of OAEs is the method of choice for screening. These children are typically diagnosed at a later stage after parents report a severe delay in speech development. Knowing that deafness, either due to biallelic variants in *OTOF* or auditory neuropathies/synaptopathies of other etiologies, cannot be reliably diagnosed with OAE screenings, but could be aided with currently available therapies, requires switching newborn hearing screenings to routine ABR testing. This is not only of importance with respect to cochlear implantation, which will yield much better outcomes if implanted earlier, but also with respect to a gene therapy, which is currently under development.

The currently favored gene therapeutic approach involves replacing the defective gene by transducing IHCs with correct cDNA by means of recombinant adeno-associated viruses (AAVs,

reviewed in [69]). These viral vectors have a series of beneficial features: they are non-pathogenic, they evoke the least inflammatory response, they do not integrate into the genome under most conditions, and the choice of their surface protein allows the vector to target different cell types. The main disadvantage is that they can transport only up to 4.9 kb of foreign DNA, which needs to be subcloned between two AAV gene sequences called inverted terminal repeats (ITRs) of 145 bp each. The 6 kb cDNA length encoding otoferlin has successfully been transduced into IHCs by dual-AAV-approaches, where the cDNA is split to two AAV genomes [70,71]. The latter form head-to-tail multimers in the nuclei of target cells, thereby assembling the split cDNA. By means of splice donor and splice acceptor sites, the ITRs are excised, and the otoferlin mRNA transcribed from dual-AAVs has been demonstrated as being correct [70]. Studies in *Otof^{-/-}* mice have revealed that such dual-AAV strategies successfully and persistently restored hearing [70,71]. At least three companies have prepared for clinical trials with dual-AAV approaches, the first intending to start in 2021 (Akouos, Boston, MA, USA; Decibel Therapeutics, Boston, MA, USA; Sensorion, Montpellier, France). This causal therapy is expected to result in more natural hearing compared to cochlear implants, overcoming limitations such as poor perception of vocal emotions, poor frequency discrimination, or poor speech comprehension in background noise, just to name a few. DFNB9 is predestined for a gene therapy, as all cells develop normally and are in place at birth. However, OHCs degenerate within a few years after birth, as discussed above. For cochlear implantation, the loss of OHCs is not of relevance; however, gene therapy will only yield good outcomes with intact OHC-driven cochlear amplification. Hence, a gene therapy for profoundly deaf DFNB9 patients will need to be applied ideally within the first year of life, both to have OHCs still present and to be within the sensitive time window for language acquisition.

Especially with respect to the envisioned gene therapy, the use of hearing aids for rehabilitation of severe to profound hearing impairment should be critically evaluated. While power hearing aids have successfully induced behavioral responses in DFNB9 children with severe to profound deafness [23], we have to assume that the use of hearing aids is unlikely to assure proper speech comprehension. Studies from animal models indicate that challenging the synapse with a higher rate of acoustic stimuli or more intense stimuli will cause a faster depletion of synaptic transmission. This reduces the capability of the synapse to encode modulations of the input. Moreover, it presumably lowers the timely precision of spiking in the auditory nerve, and thus might blur auditory cues required for speech comprehension.

In addition to being questionable for language acquisition, the use of power hearing aids might accelerate the loss of OHCs, as proposed from observations in retrospective studies [22,72,73]. Whether and potentially why OHCs are more susceptible to noise trauma in DFNB9 patients compared to normal hearing individuals still awaits experimental proof and basic research in animal models. Is the expression of otoferlin in immature OHCs or unknown genetic modifiers related to the loss of DPOAEs (as proposed by [22]) or rather the lack of OHC suppression by efferent inhibition? In intact cochleae, OHCs mechanically amplify the motion of the basilar membrane, which increases the sensitivity of gentle sounds by several orders of magnitude, i.e., they lower hearing thresholds by 50–60 dB SPL. For high SPLs, inhibitory innervation from efferent fibers originating from the medial olivocochlear (MOC) system hyperpolarizes OHCs and thereby suppresses this mechanical amplification. Activation of the MOC efferents occurs through activity in the auditory pathway, which is strongly reduced or missing in absence of otoferlin. Thus, even during exposure to intense sounds, we hypothesize that OHCs do not perceive any inhibitory neurotransmission in DFNB9 patients, as is the case for normal hearing individuals. Chronically high levels of OHC activation, such as, for example, in noise trauma experiments, have been associated with cell death, potentially involving oxidative stress. Thus, power hearing aids should be prescribed and used with caution, potentially only for specialized auditory trainings and not for full day usage.

7. Outlook and Conclusions

A timely clinical and molecular genetic diagnosis of *OTOF* hearing impairment should be made as early as possible. Ideally, a clinical diagnosis should occur within the first few days of life if already apparent at birth, with rapid molecular genetic diagnostic results thereafter. Therefore, changes in newborn hearing screening protocols from OAEs to ABRs, or a combination of the two will support an early diagnosis. This will become increasingly important as promising gene therapies emerge. The structure of otoferlin, particularly of the C₂E and C₂F domains, is provisionally incomplete based on structural modelling. The possibility of an incomplete overall structure is supported by the identification of novel exons in mouse IHC transcriptome data. Therefore, we recommend genetic re-testing of undiagnosed individuals, especially those with auditory neuropathy/synaptopathy to profit from advances in basic knowledge of isoform structure, as well as improvements in sequencing technologies, bioinformatics approaches, and variant interpretation. Diagnostic laboratories critically rely on annotation of variants to the correct transcript in databases such as LOVD, DVD, ClinVar, and HGMD. In many instances in current versions of these databases, the transcript that is used is incorrect. Therefore, careful attention must be exercised by medical geneticists to report variants with the correct transcript until this can be revised.

Supplementary Materials: The following are available online at <http://www.mdpi.com/2073-4425/11/12/1411/s1>. Table S1: Overview of pathogenic/likely pathogenic *OTOF* variants from literature and database review.

Author Contributions: Conceptualization, E.R.; data curation, B.V., A.R., E.R.; writing, E.R., B.V.; construction of figures, B.V., A.R., E.R. All authors have read and agreed to the published version of the manuscript.

Funding: This research was supported by Intramural Funding (fortune) at the University of Tübingen (2545-1-0 to B.V.) and the Ministry of Science, Research and Art Baden-Württemberg (to B.V.). The German Research Foundation (DFG) supports E.R. by the Heisenberg-Program (RE 3174/2-1) and a grant (RE 3174/3-1). We acknowledge support by Open Access Publishing Fund of University of Tübingen.

Acknowledgments: We thank Hanan Al-Moyed for the graph in Figure 1, and Youssef Adel for critically reading the manuscript.

Conflicts of Interest: A.R. and B.V. declare no conflict of interest. E.R. is co-inventor on a patent for dual-AAV vectors to restore hearing. The University Medical Center Göttingen has licensed the rights to these parts of the patent exclusively to Akouos Inc. (Boston, MA, USA). The company had no role in the design of the study; in the collection, analyses, or interpretation of data; in the writing of the manuscript, or in the decision to publish the results.

References

1. Morton, C.C.; Nance, W.E. Newborn Hearing Screening—A Silent Revolution. *N. Engl. J. Med.* **2006**, *354*, 2151–2164. [[CrossRef](#)] [[PubMed](#)]
2. Azaiez, H.; Booth, K.T.; Ephraim, S.S.; Crone, B.; Black-Ziegelbein, E.A.; Marini, R.J.; Shearer, A.E.; Sloan-Heggen, C.M.; Kolbe, D.; Casavant, T.; et al. Genomic Landscape and Mutational Signatures of Deafness-Associated Genes. *Am. J. Hum. Genet.* **2018**, *103*, 484–497. [[CrossRef](#)] [[PubMed](#)]
3. Chaib, H.; Place, C.; Salem, N.; Chardenoux, S.; Vincent, C.; Weissenbach, J.; El-Zir, E.; Loiselet, J.; Petit, C. A gene responsible for a sensorineural nonsyndromic recessive deafness maps to chromosome 2p22-23. *Hum. Mol. Genet.* **1996**, *5*, 155–158. [[CrossRef](#)]
4. Yasunaga, S.; Grati, M.; Cohen-Salmon, M.; El-Amraoui, A.; Mustapha, M.; Salem, N.; El-Zir, E.; Loiselet, J.; Petit, C. A mutation in *OTOF*, encoding otoferlin, a FER-1-like protein, causes DFNB9, a nonsyndromic form of deafness. *Nat. Genet.* **1999**, *21*, 363–369. [[CrossRef](#)] [[PubMed](#)]
5. Roux, I.; Safieddine, S.; Nouvian, R.; Grati, M.; Simmler, M.-C.; Bahloul, A.; Perfettini, I.; Le Gall, M.; Rostaing, P.; Hamard, G.; et al. Otoferlin, defective in a human deafness form, is essential for exocytosis at the auditory ribbon synapse. *Cell* **2006**, *127*, 277–289. [[CrossRef](#)] [[PubMed](#)]
6. Dulon, D.; Safieddine, S.; Jones, S.M.; Petit, C. Otoferlin Is Critical for a Highly Sensitive and Linear Calcium-Dependent Exocytosis at Vestibular Hair Cell Ribbon Synapses. *J. Neurosci.* **2009**, *29*, 10474–10487. [[CrossRef](#)]

7. Beurg, M.; Safieddine, S.; Roux, I.; Bouleau, Y.; Petit, C.; Dulon, D. Calcium- and otoferlin-dependent exocytosis by immature outer hair cells. *J. Neurosci. Off. J. Soc. Neurosci.* **2008**, *28*, 1798–1803. [[CrossRef](#)]
8. Pangrsic, T.; Lasarow, L.; Reuter, K.; Takago, H.; Schwander, M.; Riedel, D.; Frank, T.; Tarantino, L.M.; Bailey, J.S.; Strenzke, N.; et al. Hearing requires otoferlin-dependent efficient replenishment of synaptic vesicles in hair cells. *Nat. Neurosci.* **2010**, *13*, 869–876. [[CrossRef](#)]
9. Beurg, M.; Michalski, N.; Safieddine, S.; Bouleau, Y.; Schneggenburger, R.; Chapman, E.R.; Petit, C.; Dulon, D. Control of exocytosis by synaptotagmins and otoferlin in auditory hair cells. *J. Neurosci. Off. J. Soc. Neurosci.* **2010**, *30*, 13281–13290. [[CrossRef](#)]
10. Nouvian, R.; Neef, J.; Bulankina, A.V.; Reisinger, E.; Pangršič, T.; Frank, T.; Sikorra, S.; Brose, N.; Binz, T.; Moser, T. Exocytosis at the hair cell ribbon synapse apparently operates without neuronal SNARE proteins. *Nat. Neurosci.* **2011**, *14*, 411–413. [[CrossRef](#)] [[PubMed](#)]
11. Pangršič, T.; Reisinger, E.; Moser, T. Otoferlin: A multi-C2 domain protein essential for hearing. *Trends Neurosci.* **2012**, *35*, 671–680. [[CrossRef](#)] [[PubMed](#)]
12. Michalski, N.A.; Goutman, J.D.; Auclair, S.M.; De Monvel, J.B.; Tertrais, M.; Emptoz, A.; Parrin, A.; Nouaille, S.; Guillon, M.; Sachse, M.; et al. Otoferlin acts as a Ca²⁺ sensor for vesicle fusion and vesicle pool replenishment at auditory hair cell ribbon synapses. *eLife* **2017**, *6*, e31013. [[CrossRef](#)] [[PubMed](#)]
13. Strenzke, N.; Chakrabarti, R.; Al-Moyed, H.; Müller, A.; Hoch, G.; Pangrsic, T.; Yamanbaeva, G.; Lenz, C.; Pan, K.-T.; Auge, E.; et al. Hair cell synaptic dysfunction, auditory fatigue and thermal sensitivity in otoferlin Ile515Thr mutants. *EMBO J.* **2016**, *35*, e201694564. [[CrossRef](#)] [[PubMed](#)]
14. Schwander, M.; Sczaniecka, A.; Grillet, N.; Bailey, J.S.; Avenarius, M.; Najmabadi, H.; Steffy, B.M.; Federe, G.C.; Lagler, E.A.; Banan, R.; et al. A Forward Genetics Screen in Mice Identifies Recessive Deafness Traits and Reveals That Pejvakin Is Essential for Outer Hair Cell Function. *J. Neurosci.* **2007**, *27*, 2163–2175. [[CrossRef](#)]
15. Duncker, S.V.; Franz, C.; Kuhn, S.; Schulte, U.; Campanelli, D.; Brandt, N.; Hirt, B.; Fakler, B.; Blin, N.; Ruth, P.; et al. Otoferlin Couples to Clathrin-Mediated Endocytosis in Mature Cochlear Inner Hair Cells. *J. Neurosci.* **2013**, *33*, 9508–9519. [[CrossRef](#)]
16. Jung, S.; Maritzen, T.; Wichmann, C.; Jing, Z.; Neef, A.; Revelo, N.H.; Al-Moyed, H.; Meese, S.; Wojcik, S.M.; Panou, I.; et al. Disruption of adaptor protein 2 μ (AP-2 μ) in cochlear hair cells impairs vesicle reloading of synaptic release sites and hearing. *EMBO J.* **2015**, *34*, 2686–2702. [[CrossRef](#)]
17. Yasunaga, S.; Grati, M.; Chardenoux, S.; Smith, T.N.; Friedman, T.B.; Lalwani, A.K.; Wilcox, E.R.; Petit, C. OTOF Encodes Multiple Long and Short Isoforms: Genetic Evidence That the Long Ones Underlie Recessive Deafness DFNB9. *Am. J. Hum. Genet.* **2000**, *67*, 591–600. [[CrossRef](#)]
18. Choi, B.Y.; Ahmed, Z.M.; Riazuddin, S.; Bhinder, M.A.; Shahzad, M.; Husnain, T.; Riazuddin, S.; Griffith, A.J.; Friedman, T.B. Identities and frequencies of mutations of the otoferlin gene (OTOF) causing DFNB9 deafness in Pakistan. *Clin. Genet.* **2009**, *75*, 237–243. [[CrossRef](#)]
19. Varga, R.; Kelley, P.M.; Keats, B.J.; Starr, A.; Leal, S.M.; Cohn, E.; Kimberling, W.J. Non-syndromic recessive auditory neuropathy is the result of mutations in the otoferlin (OTOF) gene. *J. Med. Genet.* **2003**, *40*, 45–50. [[CrossRef](#)]
20. Rodríguez-Ballesteros, M.; del Castillo, F.J.; Martín, Y.; Moreno-Pelayo, M.A.; Morera, C.; Prieto, F.; Marco, J.; Morant, A.; Gallo-Terán, J.; Morales-Angulo, C.; et al. Auditory neuropathy in patients carrying mutations in the otoferlin gene (OTOF). *Hum. Mutat.* **2003**, *22*, 451–456. [[CrossRef](#)]
21. Rodríguez-Ballesteros, M.; Reynoso, R.; Olarte, M.; Villamar, M.; Morera, C.; Santarelli, R.; Arslan, E.; Medá, C.; Curet, C.; Völter, C.; et al. A multicenter study on the prevalence and spectrum of mutations in the otoferlin gene (OTOF) in subjects with nonsyndromic hearing impairment and auditory neuropathy. *Hum. Mutat.* **2008**, *29*, 823–831. [[CrossRef](#)] [[PubMed](#)]
22. Kitao, K.; Mutai, H.; Namba, K.; Morimoto, N.; Nakano, A.; Arimoto, Y.; Sugiuchi, T.; Masuda, S.; Okamoto, Y.; Morita, N.; et al. Deterioration in Distortion Product Otoacoustic Emissions in Auditory Neuropathy Patients With Distinct Clinical and Genetic Backgrounds. *Ear Hear.* **2019**, *40*, 184–191. [[CrossRef](#)] [[PubMed](#)]
23. Santarelli, R.; Del Castillo, I.; Cama, E.; Scimemi, P.; Starr, A. Audibility, speech perception and processing of temporal cues in ribbon synaptic disorders due to OTOF mutations. *Hear. Res.* **2015**, *330*, 200–212. [[CrossRef](#)] [[PubMed](#)]
24. Zhang, Q.; Lan, L.; Shi, W.; Yu, L.; Xie, L.-Y.; Xiong, F.; Zhao, C.; Li, N.; Yin, Z.; Zong, L.; et al. Temperature sensitive auditory neuropathy. *Hear. Res.* **2016**, *335*, 53–63. [[CrossRef](#)]

25. Mishra, S.K.; Panda, M.R. Rapid auditory learning of temporal gap detection. *J. Acoust. Soc. Am.* **2016**, *140*, EL50. [[CrossRef](#)]
26. Michalewski, H.J.; Starr, A.; Nguyen, T.T.; Kong, Y.Y.; Zeng, F.G. Auditory temporal processes in normal-hearing individuals and in patients with auditory neuropathy. *Clin. Neurophysiol.* **2005**, *116*, 669–680. [[CrossRef](#)]
27. Radziwon, K.E.; June, K.M.; Stolzberg, D.J.; Xu-Friedman, M.A.; Salvi, R.J.; Dent, M.L. Behaviorally measured audiograms and gap detection thresholds in CBA/CaJ mice. *J. Comp. Physiol. A* **2009**, *195*, 961–969. [[CrossRef](#)]
28. Santarelli, R.; Del Castillo, I.; Rodríguez-Ballesteros, M.; Scimemi, P.; Cama, E.; Arslan, E.; Starr, A. Abnormal cochlear potentials from deaf patients with mutations in the otoferlin gene. *J. Assoc. Res. Otolaryngol. JARO* **2009**, *10*, 545–556. [[CrossRef](#)]
29. Pappa, A.K.; Hutson, K.A.; Scott, W.C.; Wilson, J.D.; Fox, K.E.; Masood, M.M.; Giardina, C.K.; Pulver, S.H.; Grana, G.D.; Askew, C.; et al. Hair cell and neural contributions to the cochlear summing potential. *J. Neurophysiol.* **2019**, *121*, 2163–2180. [[CrossRef](#)]
30. Dabrowski, M.; Bukowy-Bieryllo, Z.; Zietkiewicz, E. Translational readthrough potential of natural termination codons in eucaryotes—The impact of RNA sequence. *RNA Biol.* **2015**, *12*, 950–958. [[CrossRef](#)]
31. Duman, D.; Sirmaci, A.; Cengiz, F.B.; Ozdag, H.; Tekin, M. Screening of 38 genes identifies mutations in 62% of families with nonsyndromic deafness in Turkey. *Genet. Test. Mol. Biomark.* **2011**, *15*, 29–33. [[CrossRef](#)] [[PubMed](#)]
32. Richard, E.M.; Santos-Cortez, R.L.P.; Faridi, R.; Rehman, A.U.; Lee, K.; Shahzad, M.; Acharya, A.; Khan, A.A.; Imtiaz, A.; Chakchouk, I.; et al. Global genetic insight contributed by consanguineous Pakistani families segregating hearing loss. *Hum. Mutat.* **2019**, *40*, 53–72. [[CrossRef](#)] [[PubMed](#)]
33. Migliosi, V.; Modamio-Hoybjor, S.; Moreno-Pelayo, M.A.; Rodriguez-Ballesteros, M.; Villamar, M.; Telleria, D.; Menendez, I.; Moreno, F.; Del Castillo, I. Q829X, a novel mutation in the gene encoding otoferlin (OTOF), is frequently found in Spanish patients with prelingual non-syndromic hearing loss. *J. Med. Genet.* **2002**, *39*, 502. [[CrossRef](#)] [[PubMed](#)]
34. Wu, C.-C.; Tsai, C.-Y.; Lin, Y.-H.; Chen, P.-Y.; Lin, P.-H.; Cheng, Y.-F.; Wu, C.-M.; Lin, Y.-H.; Lee, C.-Y.; Erdenechuluun, J.; et al. Genetic Epidemiology and Clinical Features of Hereditary Hearing Impairment in the Taiwanese Population. *Genes* **2019**, *10*, 772. [[CrossRef](#)] [[PubMed](#)]
35. Sloan-Heggen, C.M.; Bierer, A.O.; Shearer, A.E.; Kolbe, D.L.; Nishimura, C.J.; Frees, K.L.; Ephraim, S.S.; Shibata, S.B.; Booth, K.T.; Campbell, C.A.; et al. Comprehensive genetic testing in the clinical evaluation of 1119 patients with hearing loss. *Hum. Genet.* **2016**, *135*, 441–450. [[CrossRef](#)]
36. Baux, D.; Vaché, C.; Blanchet, C.; Willems, M.; Baudoin, C.; Moclyn, M.; Faugère, V.; Touraine, R.; Isidor, B.; Dupin-Deguine, D.; et al. Combined genetic approaches yield a 48% diagnostic rate in a large cohort of French hearing-impaired patients. *Sci. Rep.* **2017**, *7*, 16783. [[CrossRef](#)]
37. Iwasa, Y.-I.; Nishio, S.-Y.; Sugaya, A.; Kataoka, Y.; Kanda, Y.; Taniguchi, M.; Nagai, K.; Naito, Y.; Ikezono, T.; Horie, R.; et al. OTOF mutation analysis with massively parallel DNA sequencing in 2,265 Japanese sensorineural hearing loss patients. *PLoS ONE* **2019**, *14*, e0215932. [[CrossRef](#)]
38. Mahdieh, N.; Shirkavand, A.; Rabbani, B.; Tekin, M.; Akbari, B.; Akbari, M.T.; Zeinali, S. Screening of OTOF mutations in Iran: A novel mutation and review. *Int. J. Pediatr. Otorhinolaryngol.* **2012**, *76*, 1610–1615. [[CrossRef](#)]
39. Delmaghani, S.; del Castillo, F.J.; Michel, V.; Leibovici, M.; Aghaie, A.; Ron, U.; Van Laer, L.; Ben-Tal, N.; Van Camp, G.; Weil, D.; et al. Mutations in the gene encoding pejvakin, a newly identified protein of the afferent auditory pathway, cause DFNB59 auditory neuropathy. *Nat. Genet.* **2006**, *38*, 770–778. [[CrossRef](#)]
40. Amati-Bonneau, P.; Guichet, A.; Olichon, A.; Chevrollier, A.; Viala, F.; Miot, S.; Ayuso, C.; Odent, S.; Arrouet, C.; Verny, C.; et al. OPA1 R445H mutation in optic atrophy associated with sensorineural deafness. *Ann. Neurol.* **2005**, *58*, 958–963. [[CrossRef](#)]
41. Starr, A.; Isaacson, B.; Michalewski, H.J.; Zeng, F.-G.; Kong, Y.-Y.; Beale, P.; Paulson, G.W.; Keats, B.J.B.; Lesperance, M.M. A Dominantly Inherited Progressive Deafness Affecting Distal Auditory Nerve and Hair Cells. *J. Assoc. Res. Otolaryngol.* **2004**, *5*, 411–426. [[CrossRef](#)] [[PubMed](#)]
42. Kim, T.B.; Isaacson, B.; Sivakumaran, T.A.; Starr, A.; Keats, B.J.B.; Lesperance, M.M. A gene responsible for autosomal dominant auditory neuropathy (AUNA1) maps to 13q14–21. *J. Med. Genet.* **2004**, *41*, 872. [[CrossRef](#)] [[PubMed](#)]

43. Cheng, X.; Li, L.; Brashears, S.; Morlet, T.; Ng, S.S.; Berlin, C.; Hood, L.; Keats, B. Connexin 26 variants and auditory neuropathy/dys-synchrony among children in schools for the deaf. *Am. J. Med. Genet. Part A* **2005**, *139A*, 13–18. [[CrossRef](#)] [[PubMed](#)]
44. Santarelli, R.; Cama, E.; Scimemi, P.; Monte, E.D.; Genovese, E.; Arslan, E. Audiological and electrocochleography findings in hearing-impaired children with connexin 26 mutations and otoacoustic emissions. *Eur. Arch. Oto-Rhino-Laryngol.* **2008**, *265*, 43–51. [[CrossRef](#)]
45. Del Castillo, F.J.; Del Castillo, I. Genetics of isolated auditory neuropathies. *Front. Biosci.* **2012**, *17*, 1251–1265. [[CrossRef](#)]
46. Matsunaga, T.; Mutai, H.; Kunishima, S.; Namba, K.; Morimoto, N.; Shinjo, Y.; Arimoto, Y.; Kataoka, Y.; Shintani, T.; Morita, N.; et al. A prevalent founder mutation and genotype-phenotype correlations of OTOF in Japanese patients with auditory neuropathy. *Clin. Genet.* **2012**, *82*, 425–432. [[CrossRef](#)]
47. Chiu, Y.-H.; Wu, C.-C.; Lu, Y.-C.; Chen, P.-J.; Lee, W.-Y.; Liu, A.Y.-Z.; Hsu, C.-J. Mutations in the OTOF gene in Taiwanese patients with auditory neuropathy. *Audiol. Neurootol.* **2010**, *15*, 364–374. [[CrossRef](#)]
48. Zhang, Q.-J.; Han, B.; Lan, L.; Zong, L.; Shi, W.; Wang, H.-Y.; Xie, L.-Y.; Wang, H.; Zhao, C.; Zhang, C.; et al. High frequency of OTOF mutations in Chinese infants with congenital auditory neuropathy spectrum disorder. *Clin. Genet.* **2016**, *90*, 238–246. [[CrossRef](#)]
49. Wang, D.-Y.; Wang, Y.-C.; Weil, D.; Zhao, Y.-L.; Rao, S.-Q.; Zong, L.; Ji, Y.-B.; Liu, Q.; Li, J.-Q.; Yang, H.-M.; et al. Screening mutations of OTOF gene in Chinese patients with auditory neuropathy, including a familial case of temperature-sensitive auditory neuropathy. *BMC Med. Genet.* **2010**, *11*, 79. [[CrossRef](#)]
50. Cho, Y.; Gong, T.-W.L.; Stöver, T.; Lomax, M.I.; Altschuler, R.A. Gene expression profiles of the rat cochlea, cochlear nucleus, and inferior colliculus. *J. Assoc. Res. Otolaryngol. JARO* **2002**, *3*, 54–67. [[CrossRef](#)]
51. Cai, T.; Jen, H.-I.; Kang, H.; Klisch, T.J.; Zoghbi, H.Y.; Groves, A.K. Characterization of the transcriptome of nascent hair cells and identification of direct targets of the Atoh1 transcription factor. *J. Neurosci. Off. J. Soc. Neurosci.* **2015**, *35*, 5870–5883. [[CrossRef](#)] [[PubMed](#)]
52. Ranum, P.T.; Goodwin, A.T.; Yoshimura, H.; Kolbe, D.L.; Walls, W.D.; Koh, J.-Y.; He, D.Z.Z.; Smith, R.J.H. Insights into the Biology of Hearing and Deafness Revealed by Single-Cell RNA Sequencing. *Cell Rep.* **2019**, *26*, 3160–3171.e3. [[CrossRef](#)] [[PubMed](#)]
53. Wynne, D.P.; Zeng, F.-G.; Bhatt, S.; Michalewski, H.J.; Dimitrijevic, A.; Starr, A. Loudness adaptation accompanying ribbon synapse and auditory nerve disorders. *Brain J. Neurol.* **2013**, *136*, 1626–1638. [[CrossRef](#)]
54. Varga, R.; Avenarius, M.R.; Kelley, P.M.; Keats, B.J.; Berlin, C.L.; Hood, L.J.; Morlet, T.G.; Brashears, S.M.; Starr, A.; Cohn, E.S.; et al. OTOF mutations revealed by genetic analysis of hearing loss families including a potential temperature sensitive auditory neuropathy allele. *J. Med. Genet.* **2006**, *43*, 576–581. [[CrossRef](#)]
55. Romanos, J.; Kimura, L.; Fávero, M.L.; Izarra, F.A.R.; Auricchio, M.T.B.D.M.; Batissoco, A.C.; Lezirovitz, K.; Abreu-Silva, R.S.; Mingroni-Netto, R.C. Novel OTOF mutations in Brazilian patients with auditory neuropathy. *J. Hum. Genet.* **2009**, *54*, 382–385. [[CrossRef](#)] [[PubMed](#)]
56. Marlin, S.; Feldmann, D.; Nguyen, Y.; Rouillon, I.; Loundon, N.; Jonard, L.; Bonnet, C.; Couderc, R.; Garabedian, E.N.; Petit, C.; et al. Temperature-sensitive auditory neuropathy associated with an otoferlin mutation: Deafening fever! *Biochem. Biophys. Res. Commun.* **2010**, *394*, 737–742. [[CrossRef](#)] [[PubMed](#)]
57. Yildirim-Baylan, M.; Bademci, G.; Duman, D.; Ozturkmen-Akay, H.; Tokgoz-Yilmaz, S.; Tekin, M. Evidence for genotype-phenotype correlation for OTOF mutations. *Int. J. Pediatr. Otorhinolaryngol.* **2014**, *78*, 950–953. [[CrossRef](#)]
58. Helfmann, S.; Neumann, P.; Tittmann, K.; Moser, T.; Ficner, R.; Reisinger, E. The crystal structure of the C₂A domain of otoferlin reveals an unconventional top loop region. *J. Mol. Biol.* **2011**, *406*, 479–490. [[CrossRef](#)]
59. Meese, S.; Cepeda, A.P.; Gahlen, F.; Adams, C.M.; Ficner, R.; Ricci, A.J.; Heller, S.; Reisinger, E.; Herget, M. Activity-Dependent Phosphorylation by CaMKII δ Alters the Ca²⁺Affinity of the Multi-C₂-Domain Protein Otoferlin. *Front. Synaptic Neurosci.* **2017**, *9*, 13. [[CrossRef](#)]
60. Padmanarayana, M.; Hams, N.; Speight, L.C.; Petersson, E.J.; Mehl, R.A.; Johnson, C.P. Characterization of the lipid binding properties of Otoferlin reveals specific interactions between PI(4,5)P₂ and the C₂C and C₂F domains. *Biochemistry* **2014**, *53*, 5023–5033. [[CrossRef](#)]
61. Harsini, F.M.; Bui, A.A.; Rice, A.M.; Chebrolov, S.; Fuson, K.L.; Turtoi, A.; Bradberry, M.; Chapman, E.R.; Sutton, R.B. Structural Basis for the Distinct Membrane Binding Activity of the Homologous C₂A Domains of Myoferlin and Dysferlin. *J. Mol. Biol.* **2019**, *431*, 2112–2126. [[CrossRef](#)] [[PubMed](#)]

62. Letunic, I.; Bork, P. 20 years of the SMART protein domain annotation resource. *Nucleic Acids Res.* **2018**, *46*, D493–D496. [[CrossRef](#)] [[PubMed](#)]
63. Kelley, L.A.; Mezulis, S.; Yates, C.M.; Wass, M.N.; Sternberg, M.J.E. The Phyre2 web portal for protein modeling, prediction and analysis. *Nat. Protoc.* **2015**, *10*, 845–858. [[CrossRef](#)] [[PubMed](#)]
64. Longo-Guess, C.; Gagnon, L.H.; Bergstrom, D.E.; Johnson, K.R. A missense mutation in the conserved C2B domain of otoferlin causes deafness in a new mouse model of DFN9. *Hear. Res.* **2007**, *234*, 21–28. [[CrossRef](#)] [[PubMed](#)]
65. Jiménez, J.L.; Bashir, R. In silico functional and structural characterisation of ferlin proteins by mapping disease-causing mutations and evolutionary information onto three-dimensional models of their C2 domains. *J. Neurol. Sci.* **2007**, *260*, 114–123. [[CrossRef](#)]
66. Harsini, F.M.; Chebrou, S.; Fuson, K.L.; White, M.A.; Rice, A.M.; Sutton, R.B. FerA is a Membrane-Associating Four-Helix Bundle Domain in the Ferlin Family of Membrane-Fusion Proteins. *Sci. Rep.* **2018**, *8*, 10949. [[CrossRef](#)]
67. Vilardi, F.; Stephan, M.; Clancy, A.; Janshoff, A.; Schwappach, B. WRB and CAML are necessary and sufficient to mediate tail-anchored protein targeting to the ER membrane. *PLoS ONE* **2014**, *9*, e85033. [[CrossRef](#)]
68. Vogl, C.; Panou, I.; Yamanbaeva, G.; Wichmann, C.; Mangosing, S.J.; Vilardi, F.; Indzhukulian, A.A.; Pangršič, T.; Santarelli, R.; Rodriguez-Ballesteros, M.; et al. Tryptophan-rich basic protein (WRB) mediates insertion of the tail-anchored protein otoferlin and is required for hair cell exocytosis and hearing. *EMBO J.* **2016**, *35*, 2536–2552. [[CrossRef](#)]
69. Reisinger, E. Dual-AAV delivery of large gene sequences to the inner ear. *Hear. Res.* **2019**, *394*, 107857. [[CrossRef](#)]
70. Al-Moyed, H.; Cepeda, A.P.; Jung, S.; Moser, T.; Kügler, S.; Reisinger, E. A dual-AAV approach restores fast exocytosis and partially rescues auditory function in deaf otoferlin knock-out mice. *EMBO Mol. Med.* **2019**, *11*, e9396. [[CrossRef](#)]
71. Akil, O.; Dyka, F.; Calvet, C.; Emptoz, A.; Lahlou, G.; Nouaille, S.; De Monvel, J.B.; Hardelin, J.-P.; Hauswirth, W.W.; Avan, P.; et al. Dual AAV-mediated gene therapy restores hearing in a DFN9 mouse model. *Proc. Natl. Acad. Sci. USA* **2019**, *116*, 4496–4501. [[CrossRef](#)] [[PubMed](#)]
72. Starr, A.; Picton, T.W.; Sininger, Y.; Hood, L.J.; Berlin, C.I. Auditory neuropathy. *Brain* **1996**, *119*, 741–754. [[CrossRef](#)] [[PubMed](#)]
73. Rouillon, I.; Marcolla, A.; Roux, I.; Marlin, S.; Feldmann, D.; Couderc, R.; Jonard, L.; Petit, C.; Denoyelle, F.; Garabédian, E.N.; et al. Results of cochlear implantation in two children with mutations in the OTOF gene. *Int. J. Pediatr. Otorhinolaryngol.* **2006**, *70*, 689–696. [[CrossRef](#)] [[PubMed](#)]

Publisher's Note: MDPI stays neutral with regard to jurisdictional claims in published maps and institutional affiliations.



© 2020 by the authors. Licensee MDPI, Basel, Switzerland. This article is an open access article distributed under the terms and conditions of the Creative Commons Attribution (CC BY) license (<http://creativecommons.org/licenses/by/4.0/>).

10.3 Attachment 3

Aberrant COL11A1 splicing causes prelingual autosomal dominant non-syndromic HL in the DFNA37 locus

Aberrant *COL11A1* splicing causes prelingual autosomal dominant nonsyndromic hearing loss in the DFNA37 locus

Aboufazi Rad¹  | Thore Schade-Mann¹ | Philipp Gamerding¹ |
Grigoriy A. Yanus^{2,3}  | Björn Schulte⁴ | Marcus Müller¹  |
Evgeny N. Imyanitov^{2,3,5} | Saskia Biskup⁴ | Hubert Löwenheim¹  |
Anke Tropitzsch¹ | Barbara Vona¹ 

¹Department of Otolaryngology-Head & Neck Surgery, Tübingen Hearing Research Centre, Eberhard Karls University Tübingen, Tübingen, Germany

²Department of Medical Genetics, Saint Petersburg State Pediatric Medical University, Saint Petersburg, Russia

³Department of Tumor Growth Biology, N. N. Petrov Institute of Oncology, Saint Petersburg, Russia

⁴CeGaT GmbH and Praxis für Humangenetik Tübingen, Tübingen, Germany

⁵Department of Oncology, I. I. Mechnikov North-Western Medical University, Saint Petersburg, Russia

Correspondence

Barbara Vona, Department of Otolaryngology-Head & Neck Surgery, Tübingen Hearing Research Centre, Eberhard Karls University Tübingen, Elfriede-Aulhorn-Str. 5, 72076 Tübingen, Germany.
Email: barbara.vona@uni-tuebingen.de

Funding information

Ministerium für Wissenschaft, Forschung und Kunst Baden-Württemberg, Grant/Award Number: RISC; Eberhard Karls Universität Tübingen, Grant/Award Number: Intramural Funding (fortune) (2545-1-0)

Abstract

Alpha-chain collagen molecules encoded by genes that include *COL11A1* are essential for skeletal, ocular, and auditory function. *COL11A1* variants have been reported in syndromes involving these organ systems. However, a description of the complete clinical spectrum is lacking, as evidenced by a recent association of autosomal dominant nonsyndromic hearing loss due to a splice-altering variant in *COL11A1*, mapping the DFNA37 locus. Here, we describe two German families presenting prelingual autosomal dominant nonsyndromic hearing loss with novel *COL11A1* heterozygous splice-altering variants (c.652-1G>C and c.4338+2T>C) that were molecularly characterized. Interestingly, the c.652-1G>C variant affects the same intron 4 canonical splice site originally reported in the DFNA37 family (c.652-2A>C) but elicits a different splicing outcome. Furthermore, the c.4338+2T>C variant originated de novo. We provide clinical and molecular genetic evidence to unambiguously confirm that *COL11A1* splice-altering variants cause DFNA37 hearing loss and affirm that *COL11A1* be included in the genetic testing of patients with nonsyndromic deafness.

KEYWORDS

autosomal dominant hearing loss, *COL11A1*, DFNA37, nonsyndromic hearing loss, splice-site altering variant

Hereditary hearing loss is a clinically and genetically heterogeneous disorder. Autosomal dominant nonsyndromic hearing loss (ADNSHL) is present in roughly 20% of hearing-impaired individuals. More than 20% of genes exhibit pleiotropy, whereby variants in a single gene can be associated with syndromic or nonsyndromic hearing loss and

can follow an autosomal dominant or recessive inheritance pattern (Vona et al., 2020).

The gene *COL11A1* (collagen type XI alpha-1 chain; MIM #120280) is associated with autosomal dominant Marshall syndrome (MRSHS) and autosomal dominant or recessive Stickler syndrome

This is an open access article under the terms of the Creative Commons Attribution License, which permits use, distribution and reproduction in any medium, provided the original work is properly cited.

© 2020 The Authors. *Human Mutation* published by Wiley Periodicals LLC

type II (STL2), as well as autosomal recessive fibrochondrogenesis (FBCG1). Each of these syndromes has a phenotypic overlap that includes skeletal abnormalities and dysmorphic features, as well as variable cleft palate, ocular, and auditory phenotypes that can include mild-to-moderate hearing loss and outer ear malformations. Recently, the gene *COL11A1* has been associated with ADNSHL (DFNA37; MIM #618533) through the genetic analysis of a large European-American family presenting a novel splice-site altering variant (Booth et al., 2019).

Written informed consent was obtained from participants (Approval of the University of Tübingen Ethics Commission; Nos.: 016/2014BO1 and 197/2019BO1). Medical history excluded acquired forms of hearing loss. The 37-year-old proband in Family 1 (III:3) (Figure 1a), presents stable, down-sloping, moderate-to-severe, high-frequency sensorineural hearing loss (Figure 1c), as well as hypothyroidism and diabetes. The speech discrimination with regard to monosyllables was 70% and 50% at 65-dB hearing level (HL) on the right side and 80% and 80% at 65 dB(HL) on the left side when evaluated at 34 and 37 years of age, respectively. Regarding the speech recognition threshold (SRT), the proband achieved a score of 35- and 32.5-dB hearing loss ("a1 value") on the right and 27- and 30-dB hearing loss on the left ear at 34 and 37 years of age, respectively. He has worn hearing aids since age 6 years. His daughter (Family 1, IV:1) is currently 6.9 years old and was born after an unremarkable pregnancy and delivery. She failed newborn hearing screening but passed follow-up testing. At the age of 2 years, she was diagnosed with severe hearing loss and has used hearing aids since

diagnosis. Serial audiometry has revealed stable, moderate-to-severe, high-frequency sensorineural hearing loss (Figure 1c). Her monosyllable discrimination was 75% and 65% at 65 dB(HL) on the right and 65% and 100% at 65 dB(HL) on the left side at 4.8 and 6.9 years, respectively. SRT was 27 and 30 dB hearing loss on the right, 25 and 27.5 dB hearing loss on the left at 4.8 and 6.9 years, respectively. Syndromic features including myopia, retinal detachment, midface hypoplasia, submucous cleft palate, and arthritis/joint pain have been excluded in both affected individuals in Family 1 (III:3 and IV:1). The 31-year-old proband (III:3) in Family 2 (Figure 1b) presented moderate sensorineural hearing loss in the mid- and high-frequencies since early childhood (Figure 1d) and she has worn hearing aids since age 27 years. Her pure-tone audiograms showed nearly identical thresholds taken 5 months apart at the age of 28 years (data not shown). She does not have a severe form of hearing loss that might be suggestive of progression. Her monosyllable recognition was 80% at 65 dB(HL) (SRT 20-dB hearing loss) on the right ear and 75 dB(HL) (SRT 25-dB hearing loss) on the left ear. She had a normal tympanogram and otoscopy exam. Two of her grandparents wear hearing aids. Her parents underwent pure-tone audiometry testing and had normal thresholds. Her son (Family 2, IV:1; Figure 1b) was born at term after an unremarkable pregnancy and failed newborn hearing screening. Evoked response audiometry showed mild hearing loss (Figure 1d). Transient evoked otoacoustic emissions were bilaterally absent. Distortion product otoacoustic emissions were absent on the right side and partially evocable on the left side. At the last evaluation at the age of 3.5 years, he had mild

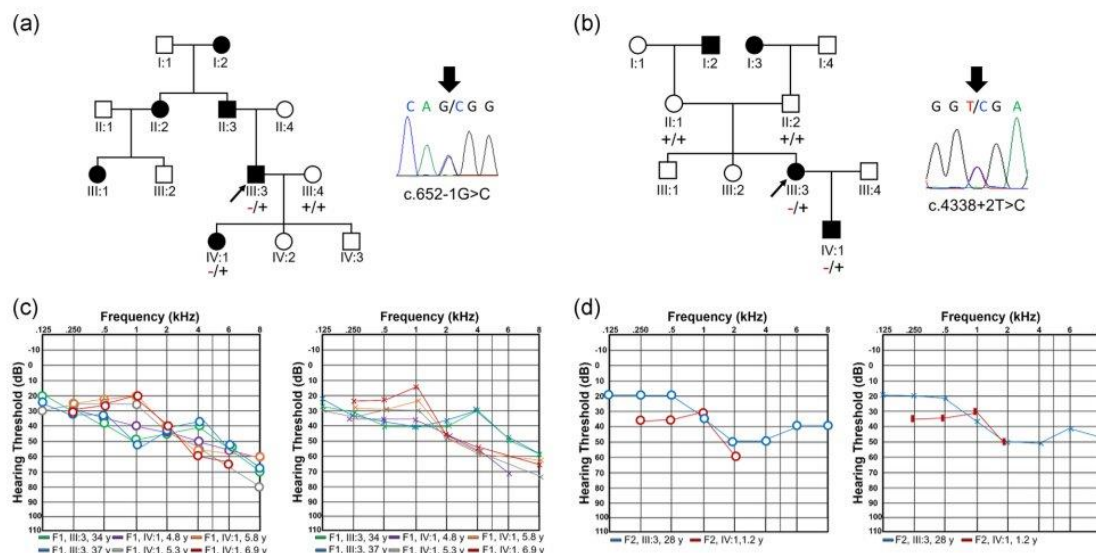


FIGURE 1 Pedigree and Sanger sequencing result in (a) Family 1 and (b) Family 2 showing segregation of the c.652-1G>C and c.4338+2T>C variants, respectively. Mutant alleles are represented with "-" and the reference allele is shown with "+." Sanger electropherograms of the variant are shown to the right of each pedigree. Audiometry of right and left ears from (c) individuals III:3 and IV:1 in Family 1 and (d) individual III:3 in Family 2, represented as pure-tone air-conduction thresholds, as well as evoked response audiometry from individual IV:1 in Family 2 (d). Thresholds are shown with circles and crosses/vertical rectangles, for right and left ears, respectively

bilateral sensorineural hearing loss and no other abnormalities. He was too young to undergo speech audiometry. The mother (Family 2, III:3) reported a cleft lip and palate, an occurrence not previously reported with *STL2* and assumed to be due to other genetic or multifactorial causes. She reported no other abnormalities. Submucous cleft palate in her son (Family 2, IV:1) has been ruled out. Ophthalmic examination excluded amblyopia, strabismus, and phoria and confirmed normal vision. Affected individuals in both families do not report otorrhea, otalgia, tinnitus, or vertigo. Bone conduction thresholds from individuals III:3 and IV:1 in Family 1 and III:3 in Family 2 confirm sensorineural hearing loss (Figure S1).

Blood samples were collected from affected (III:3 and IV:1 of Family 1, as well as III:3 and IV:1 of Family 2) and unaffected (III:4 from Family 1 and II:1 and II:2 from Family 2) individuals in two unrelated German families (Figure 1a,b). The genomic DNAs from individuals III:3 and IV:1 in Family 1 and III:3 in Family 2 were subjected to a custom-designed high-throughput sequencing panel that included 164 hearing loss genes (HiSeq4000; Illumina Inc.). Duplication/deletion analysis of *GJB6*, *WFS1*, and *POU3F4* was carried out using MLPA (P163-D1-V16; MRC Holland).

Two novel heterozygous variants in *COL11A1* were identified that each disrupt canonical splice sites: NM_080629.2:c.652-1G>C (ClinVar Accession: RCV000487702.2; LOVD Genomic Variant Accession: 0000686099) in Family 1 and NM_080629.2:c.4338+2T>C (ClinVar Accession: RCV000585624.2; LOVD Genomic Variant Accession: 0000686100) in Family 2 in introns 4 and 57, respectively (Table S1). The c.652-1G>C variant in Family 1 segregated in two generations (Figure 1a), while the c.4338+2T>C variant was suspected de novo origin in the proband and transmitted to her hearing-impaired son (Figure 1b). Paternity testing of the mother was not possible to perform for definitive confirmation of the de novo status. An in vitro splicing assay was carried out as previously described (Doll et al., 2020; Tompson & Young, 2017) using amplified genomic DNA of the probands (Family 1 III:3: 1835-bp amplified genomic DNA length and Family 2 IV:1: 803-bp amplified genomic DNA length) and a normal hearing control. The c.652-1C variant impacts splicing through the loss of an acceptor site and activation of two cryptic splice acceptor sites in exon 5 that cause in-frame deletions (Figure 2a–c). TA cloning, followed by reverse-transcription polymerase chain reaction and Sanger sequencing of complementary DNA (cDNA) amplicons with the patient variant showed that 67% (28 out of 42 analyzed clones) of the amplicons utilized the first cryptic splice site (r.652_663del, p.(Gly218_Gln221del)) and 33% (14 out of 42 analyzed clones) of the amplicons used the second cryptic acceptor site (r.652_666del, p.(Gly218_Gln222del); Figure 2b and Table S2). The c.4338+2C variant leads to three abnormally spliced amplicons that include the activation of two cryptic splice donor sites in intron 57 (r.4338_4339ins4338+1_4338+4, p.(Gly1447Alafs*12); r.4338_4339ins4338+1_4338+30, p.(Gly1447Alafs*9)) and the skipping of exon 57 (r.4285_4338del, p.(Gly1429_Met1446del); Figure 2d–f). TA cloning and follow-up testing as described above of cDNA amplicons with the patient variant indicated that 87% (40 out of 46 analyzed clones) of the amplicons showed evidence of a skipped

exon 57, 6.5% (3 out of 46 analyzed clones) used the first cryptic donor site (r.4338_4339ins4338+1_4338+4) and 6.5% (3 out of 46 analyzed clones) used the second cryptic donor site (r.4338_4339ins4338+1_4338+30) (Figure 2e and Table S2).

More than 60 different variants including frameshift, splicing, missense, in-frame, and even two synonymous variants have been classified as pathogenic in *COL11A1* and reported in MRSHS, *STL2*, and FBCG1 (deafnessvariationdatabase.org; Azaiez et al., 2018); however, only one molecularly characterized splice-altering variant has been associated with ADNSHL (Booth et al., 2019). In line with this study, our findings confirm *COL11A1* splice-altering variants as causally implicated in DFNA37. Interestingly, the c.652-1G>C variant in Family 1 resides in the same canonical splice site as the c.652-2A>C variant previously reported by Booth et al. (2019) that associated *COL11A1* with ADNSHL. The c.652-2A>C variant created a leaky acceptor splice site that produced a normally spliced transcript in addition to a transcript with exon 5 skipping. It was suggested that the variant may result in the loss of key N-terminal propeptide regulatory sequences of *COL11A1*. In vitro testing of the c.4338+2T>C variant in intron 57 disclosed skipping of exon 57 and the use of two cryptic donor sites with an in-frame and out-of-frame consequence. Considering the clinical presentation of our patients with the molecular characterization of splice variants that revealed multiple in-frame mutant transcripts, we hypothesize that these in-frame variants may lead to a milder phenotype (DFNA37) due to partial residual function of the protein (i.e., noncomplete loss-of-function alleles), whereas those with more severe phenotypes may be due to frameshift, truncating loss-of-function alleles, and missense variants which induce splice altering effects or substitution of glycine in a repeat Gly-Xaa-Yaa region. Interestingly, one additional variant was recently described in a Czech family (NM_080629.2:c.1560delC) with ADNSHL. The variant was described as a splice-altering variant but a splicing assay was not performed and in silico tools did not predict a splicing effect (Čopíková et al., 2020). Functional characterization of this variant will be important for a refined genotype–phenotype correlation due to variants in *COL11A1*.

The family described by Booth et al. (2019) demonstrated bilateral, postlingual, slowly progressive, and mild-to-moderate sensorineural hearing loss without any other symptoms. Consistent with this report, the two families manifested bilateral sensorineural hearing loss without other symptoms. The thresholds from individuals III:1 and IV:1 in Family 1 were both either normal or indicate a mild hearing loss in low frequencies and were sloping to a moderate-to-severe hearing loss in high frequencies (Figure 1c). Importantly, the hearing loss in the affected individuals in Family 1 is stable and at last measurement, there was no evidence of progression to a severe hearing loss in Family 2 individual III:3. The thresholds from the individual III:3 in Family 2 were normal to 1 kHz, then increased to show moderate hearing loss until 4 kHz and slightly increased at 6 and 8 kHz (Figure 1d). Newborn hearing screening of individuals IV:1 in both families confirmed one individual with congenital onset (Family 2, IV:1), which is the first reported congenital onset with *COL11A1*-associated ADNSHL and

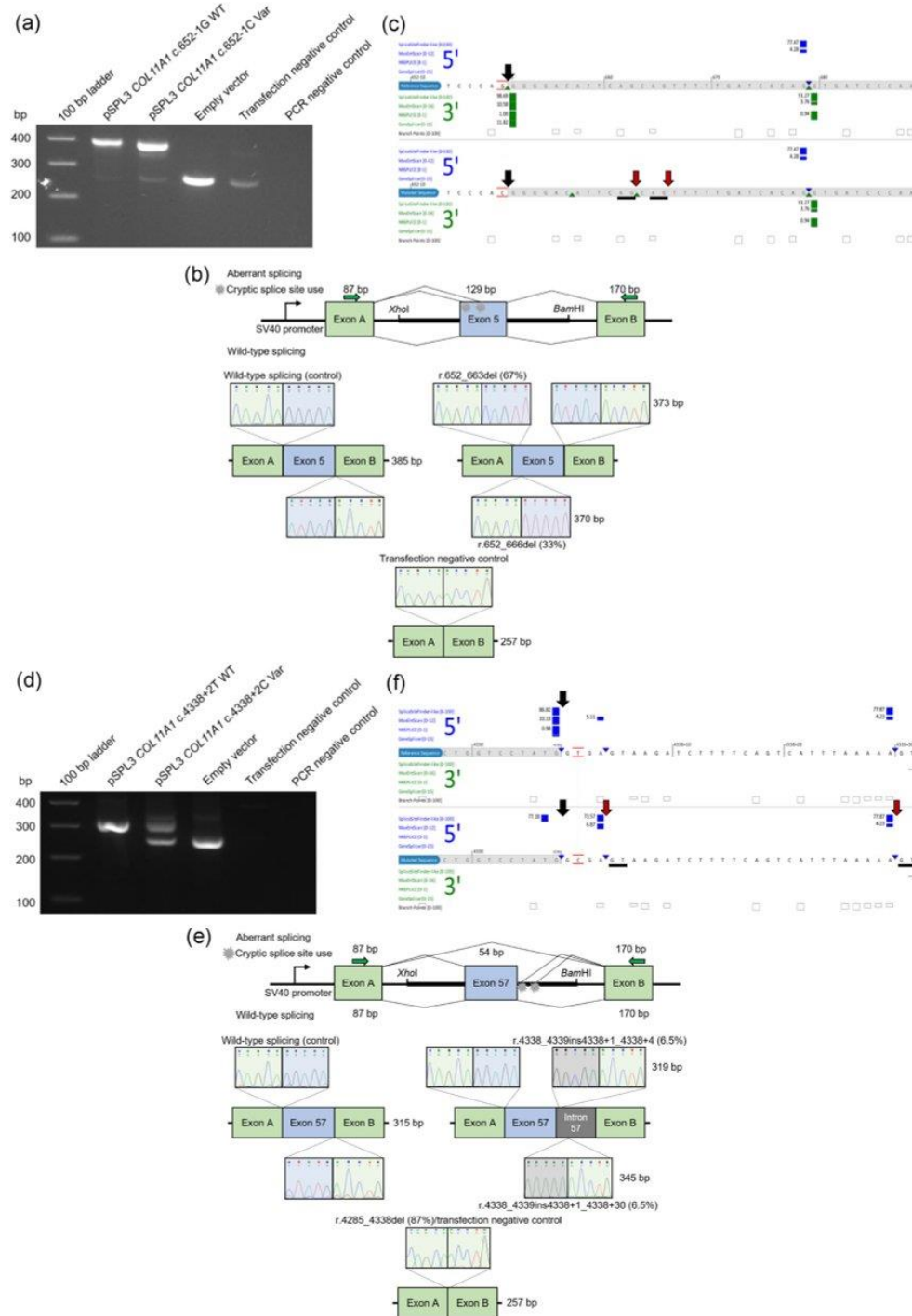


FIGURE 2 (See caption on next page)

also demonstrates that variants in this gene can cause prelingual deafness, as documented in all affected individuals in this study.

Although the precise mechanism of *COL11A1*-associated hearing impairment has not been elucidated, disruption of *COL11A1* is consistently associated with hearing loss, as demonstrated by about 84% of individuals diagnosed with MRSHS having hearing loss, which supports the critical function of this protein in the auditory system (Bacciu et al., 2018). It also demonstrated that the source of *COL11A1* mRNA is in the tectorial membrane and suggested its mutation affects normal cochlear function (Shpargel et al., 2004). Moreover, the pleiotropy exhibited by this gene, like other genes that are associated with syndromic and nonsyndromic hearing loss, remains to be fully characterized.

In summary, we report on and characterize two novel splice-altering variants associated with DFNA37, providing confirmatory evidence of *COL11A1* as a bona fide ADNSHL gene. We recommend *COL11A1* be included in the routine diagnostic testing of patients with both syndromic and nonsyndromic forms of deafness.

ACKNOWLEDGMENTS

The authors thank the families for their participation in this study. We thank Stuart W. Tompson at the University of Wisconsin-Madison for sharing the pSPL3 vector. This study was supported by Intramural Funding (fortune) at the University of Tübingen (2545-1-0 to Barbara Vona), the Ministry of Science, Research and Art Baden-Württemberg (to Barbara Vona). Open access funding enabled and organized by Projekt DEAL.

CONFLICT OF INTERESTS

Saskia Biskup is an owner of CeGaT. The remaining authors declare that there are no conflict of interests.

AUTHOR CONTRIBUTIONS

Björn Schulte, Saskia Biskup, and Barbara Vona generated, analyzed, and validated high-throughput sequencing data sets and variant segregation results. Aboufazel Rad, Björn Schulte, Saskia Biskup, and

Barbara Vona submitted variants to clinical databases. Aboufazel Rad and Barbara Vona provided functional experiments and wrote the first manuscript draft. Grigoriy A. Yanus and Evgeny N. Imyanov validated splicing nomenclature, performed the literature review, and curated genetics data. Thore Schade-Mann, Philipp Garmendinger, Marcus Müller, Hubert Löwenheim, and Anke Tropitzsch recruited the families, and curated and interpreted clinical data. Thore Schade-Mann performed clinical re-examination. Anke Tropitzsch, Hubert Löwenheim, and Barbara Vona conceived the study. All authors approved the final version of the manuscript.

DATA AVAILABILITY STATEMENT

The data that support the findings of this study are available upon request from the corresponding author. The genetic data are not publicly available due to data privacy or ethical restrictions. *COL11A1* variants were submitted to ClinVar (<https://www.ncbi.nlm.nih.gov/clinvar/?term=COL11A1>) with accession IDs RCV000487702.2 (NM_080629.2:c.652-1G>C) and RCV000585624.2 (NM_080629.2:c.4338+2T>C). Additionally, they were deposited in LOVD v.3.0 (<https://databases.lovd.nl/shared/genes/COL11A1>) under genomic variant accession nos. 0000686099 (NM_080629.2:c.652-1G>C) and 0000686100 (NM_080629.2:c.4338+2T>C).

LIST OF WEB RESOURCES AND URLS

ClinVar: <https://www.ncbi.nlm.nih.gov/clinvar/>
Deafness Variation: databases.lovd.nl/3.0/home
LOVD v.3.: <https://www.lovd.nl/3.0/home>
OMIM: <https://www.omim.org/clinvar>

ORCID

Aboufazel Rad  <http://orcid.org/0000-0001-8627-8828>
Grigoriy A. Yanus  <http://orcid.org/0000-0002-9844-4536>
Marcus Müller  <http://orcid.org/0000-0001-5881-7708>
Hubert Löwenheim  <http://orcid.org/0000-0001-8200-8804>
Barbara Vona  <http://orcid.org/0000-0002-6719-3447>

FIGURE 2 (a) Gel electrophoresis of the reverse-transcription polymerase chain reaction (RT-PCR) from the wild-type control, the c.652-1C variant, and empty pSPL3 vector amplicons, as well as transfection-negative and PCR-negative controls. (b) The vector construct of the *in vitro* splice assay illustrates the wild-type or mutant amplicons inserted between exons A and B of the pSPL3 vector with a splicing schematic of the c.652-1C variant (upper) and wild-type allele (lower). The wild-type (upper left sequencing panel) shows expected splicing. The c.652-1C variant activates two cryptic acceptor splice sites (r.652_663del and r.652_666del) in exon 5 (upper right sequencing panels). The empty vector control (lower sequencing panel) performed as expected. (c) *In silico* splice predictions of the wild-type (top, red G) and c.652-1G>C (bottom, red C) marked with black arrows. Cryptic splice acceptor sites that are activated due to the variant are underlined and marked with red arrows and validated with an *in vitro* splice assay and TA cloning. (d) Gel electrophoresis of the RT-PCR from the wild-type control, the c.4338+2C variant, and empty pSPL3 vector amplicons. The transfection and PCR-negative controls performed as expected. (e) The vector construct of the *in vitro* splice assay illustrates the wild-type or mutant amplicons inserted between exons A and B of the pSPL3 vector with a splicing schematic of three splice products (r.4338_4339ins4338+1_4338+4, r.4338_4339ins4338+1_4338+30, and r.4285_4338del) due to the c.4338+2C variant (upper) and wild-type allele (lower). The wild-type (upper left sequencing panel) shows the expected splicing. The c.4338+2C variant activates two cryptic acceptor splice sites in intron 57 (upper right sequencing panels) and evokes skipping of exon 57 (lower sequencing panel) that was the same sequence as the empty vector control (lower sequencing panel). (f) *In silico* splice predictions of the wild-type (top, red T) and c.4338+2T>C (bottom, red C) marked with black arrows. Cryptic splice donor sites that are activated due to the variant are underlined and marked with red arrows and validated with an *in vitro* splice assay and TA cloning. Var, variant; WT, wild type

REFERENCES

- Azaiez, H., Booth, K. T., Ephraim, S. S., Crone, B., Black-Ziegelbein, E. A., Marini, R. J., Shearer, A. E., Sloan-Heggen, C. M., Kolbe, D., Casavant, T., Schnieders, M. J., Nishimura, C., Braun, T., & Smith, R. J. H. (2018). Genomic landscape and mutational signatures of deafness-associated genes. *American Journal of Human Genetics*, 103(4), 484–497. <https://doi.org/10.1016/j.ajhg.2018.08.006>
- Bacciu, A., Di Lella, F., Iaccarino, I., Pasanisi, E., Fava, G., Vincenti, V., & Falcioni, M. (2018). Audiologic manifestations of Marshall syndrome. *Otology & Neurotology*, 39(8), e691–e698.
- Booth, K. T., Askew, J. W., Talebizadeh, Z., Huygen, P. L. M., Eudy, J., Kenyon, J., Hoover, D., Hildebrand, M. S., Smith, K. R., Bahlo, M., Kimberling, W. J., Smith, R. J. H., Azaiez, H., & Smith, S. D. (2019). Splice-altering variant in COL11A1 as a cause of nonsyndromic hearing loss DFNA37. *Genetics in Medicine*, 21(4), 948–954. <https://doi.org/10.1038/s41436-018-0285-0>
- Čopíková, J., Paděrová, J., Románková, V., Havlovcová, M., Balaščíková, M., Zelinová, M., Vejvalková, Š., Simandlová, M., Štěpánková, J., Hořínová, V., Kantorová, E., Křečková, G., Pospíšilová, J., Boday, A., Meszarosová, A. U., Turnovec, M., Votýpka, P., Lišková, P., & Pourová, R. K. (2020). Expanding the phenotype spectrum associated with pathogenic variants in the COL2A1 and COL11A1 genes. *Annals of Human Genetics*, 84(5), 380–392. <https://doi.org/10.1111/ahg.12386>
- Doll, J., Kolb, S., Schnapp, L., Rad, A., Rüschenhoff, F., Khan, I., Adli, A., Hasanzadeh, A., Liedtke, D., Knaup, S., Hofrichter, M. A., Müller, T., Dittrich, M., Kong, I. K., Kim, H. G., Haaf, T., & Vona, B. (2020). Novel loss-of-function variants in CDC14A are associated with recessive sensorineural hearing loss in Iranian and Pakistani patients. *International Journal of Molecular Sciences*, 21(1), 311. <https://doi.org/10.3390/ijms21010311>
- Shpargel, K. B., Makishima, T., & Griffith, A. J. (2004). Col11a1 and Col11a2 mRNA expression in the developing mouse cochlea: Implications for the correlation of hearing loss phenotype with mutant type XI collagen genotype. *Acta Oto-Laryngologica*, 124(3), 242–248.
- Tompson, S. W., & Young, T. L. (2017). Assaying the effects of splice site variants by exon trapping in a mammalian cell line. *Bio-protocol*, 7(10), e2281.
- Vona, B., Doll, J., Hofrichter, M. A., Haaf, T., & Varshney, G. K. (2020). Small fish, big prospects: Using zebrafish to unravel the mechanisms of hereditary hearing loss [published online ahead of print February 6, 2020]. *Hearing Research*, 107906.

SUPPORTING INFORMATION

Additional Supporting Information may be found online in the supporting information tab for this article.

How to cite this article: Rad A, Schade-Mann T, Gamerdinger P, et al. Aberrant COL11A1 splicing causes prelingual autosomal dominant nonsyndromic hearing loss in the DFNA37 locus. *Human Mutation*. 2021;42:25–30. <https://doi.org/10.1002/humu.24136>

10.4 Attachment 4

Expanding the phenotype of PIGS-associated early onset epileptic developmental encephalopathy

BRIEF COMMUNICATION

Expanding the phenotype of *PIGS*-associated early onset epileptic developmental encephalopathy

Stephanie Efthymiou¹  | Marina Dutra-Clarke² | Reza Maroofian¹ |
Rauan Kaiyrzhanov¹ | Marcello Scala^{3,4} | Javeria Reza Alvi⁵ | Tipu Sultan⁵ |
Marilena Christoforou¹ | Thi Tuyet Mai Nguyen⁶ | Kshitij Mankad⁷ | Barbara Vona⁸  |
Aboufazel Rad⁸ | Pasquale Striano^{3,4}  | Vincenzo Salpietro^{3,4} | Maria J. Guillen Sacoto⁹ |
Maha S. Zaki¹⁰ | Joseph G. Gleeson¹¹ | Philippe M. Campeau⁶ | Bianca E. Russell² |
Henry Houlden¹

¹Department of Neuromuscular Disorders, UCL Queen Square Institute of Neurology, University College London, London, UK

²Department of Pediatrics, Division of Genetics, University of California, Los Angeles, Los Angeles, CA, USA

³Pediatric Neurology and Muscular Diseases Unit, IRCCS Giannina Gaslini Institute, Genoa, Italy

⁴Department of Neurosciences, Rehabilitation, Ophthalmology, Genetics, Maternal and Child Health, University of Genoa, Genoa, Italy

⁵Department of Pediatric Neurology, Institute of Child Health, Children's Hospital Lahore, Lahore, Pakistan

⁶Research Center, Saint Justine University Hospital Center, University of Montreal, Montreal, QC, Canada

⁷Department of Neuroradiology, Great Ormond Street Hospital for Children, London, UK

⁸Department of Otolaryngology-Head and Neck Surgery, Tübingen Hearing Research Center, Eberhard Karls University, Tübingen, Germany

⁹GeneDx, Gaithersburg, MA, USA

¹⁰Clinical Genetics Department, Human Genetics and Genome Research Division, National Research Center, Cairo, Egypt

¹¹Department of Neuroscience, Rady Children's Institute for Genomic Medicine, Howard Hughes Medical Institute, University of California, San Diego, San Diego, CA, USA

Correspondence

Henry Houlden, UCL Queen Square
Institute of Neurology, Queen Square,
London WC1N 3BG, UK.
Email: h.houlden@ucl.ac.uk

Funding information

Medical Research Council, Grant/Award
Number: G0601943, MR/S005021/1 and
MR/S01165X/1

Abstract

The phosphatidylinositol glycan anchor biosynthesis class S protein (*PIGS*) gene has recently been implicated in a novel congenital disorder of glycosylation resulting in autosomal recessive inherited glycosylphosphatidylinositol-anchored protein (GPI-AP) deficiency. Previous studies described seven patients with biallelic variants in the *PIGS* gene, of whom two presented with fetal akinesia and five with global developmental delay and epileptic developmental encephalopathy. We present the molecular and clinical characteristics of six additional individuals from five families with unreported variants in *PIGS*. All individuals presented with hypotonia, severe global developmental delay, microcephaly, intractable early infantile epilepsy, and structural brain abnormalities. Additional findings include vision impairment, hearing loss, renal malformation, and hypotonic facial appearances with minor dysmorphic features but without a distinctive facial gestalt. Four

Stephanie Efthymiou and Marina Dutra-Clarke are shared first authors and contributed equally to the work.

This is an open access article under the terms of the Creative Commons Attribution License, which permits use, distribution and reproduction in any medium, provided the original work is properly cited.

© 2021 The Authors. *Epilepsia* published by Wiley Periodicals LLC on behalf of International League Against Epilepsy

individuals died due to neurologic complications. GPI anchoring studies performed on one individual revealed a significant decrease in GPI-APs. We confirm that biallelic variants in *PIGS* cause vitamin pyridoxine-responsive epilepsy due to inherited GPI deficiency and expand the genotype and phenotype of *PIGS*-related disorder. Further delineation of the molecular spectrum of *PIGS*-related disorders would improve management, help develop treatments, and encourage the expansion of diagnostic genetic testing to include this gene as a potential cause of neurodevelopmental disorders and epilepsy.

KEYWORDS

congenital disorders of glycosylation, epilepsy, epileptic encephalopathy, exome sequencing, inherited GPI deficiency, neurodevelopmental disorders, phosphatidylinositol glycan class S, *PIGS*

1 | INTRODUCTION

Congenital disorders of glycosylation (CDGs) are a rapidly growing heterogeneous group of genetic conditions. Inherited glycosylphosphatidylinositol-anchored protein (GPI-AP) deficiencies (IGDs) are a subset of CDGs that account for 0.15% of all neurodevelopmental disorders.¹ In many cases, IGDs result from the failure of the GPI anchor to regulate APs on the external cell surface. This has consequences for early human neurogenesis and neurodevelopment.^{2–5} To date, 17 known IGDs lead to a wide range of symptoms, including variable intellectual disabilities and developmental impairment, seizures, hypotonia, weakness, ataxia, congenital malformations, and dysmorphic facial features. There are more than 150 human GPI-APs, which often play a role in synaptic function, development of the central nervous system (CNS), and plasticity; defects in several of these proteins have been implicated in various neurological disorders.²

Developmental and epileptic encephalopathies include a range of severe epilepsies in which intractable seizures are accompanied by impairment of motor and cognitive functions.⁶ Recently, many cases of IGD have been found among individuals with intellectual disability and intractable seizures. Early infantile epileptic encephalopathy-55 (EIEE; Mendelian Inheritance in Man [MIM] #617599), a severe form of epilepsy with frequent tonic seizures or spasms beginning in infancy, and developmental delay or regression, has been linked to several genes important for GPI biosynthesis and attachment. For example, *PIGB*, *PIGQ*, *PIGP*, and *PGAPI* have all been linked to novel autosomal recessive IGDs^{7–9}; *PIGA* is an X-linked recessive disorder.¹⁰

Phosphatidylinositol glycan class S (*PIGS*; MIM #610271) encodes a GPI-AP, specifically a subunit of the GPI transamidase complex that catalyzes the attachment of preformed GPI to proteins containing a C-terminal GPI attachment

signal. Biallelic variants in *PIGS* have recently been implicated in human diseases, with the observation of seven individuals affected with EIEE.^{11,12} Phenotypes included severe global developmental delay, seizures, hypotonia, weakness, ataxia, and dysmorphic facial features, but also multiple joint contractures (consistent with fetal akinesia) in two fetuses. All seven individuals showed a GPI-AP deficiency profile. Notably, one individual showed a reduction in seizure frequency with pyridoxine (100 mg per day).

We describe six individuals (from five unrelated families) carrying biallelic variants in *PIGS* and presenting with hypotonia, severe global developmental delay, infantile onset (intractable) seizures, and different CNS anomalies identified on brain imaging. Two patients in this cohort are responsive to pyridoxine. This study provides additional evidence for *PIGS* as an emerging gene associated with autosomal recessive EIEE and describe the clinical characteristics, prognosis, and treatment outcomes, to improve patient care.

2 | MATERIALS AND METHODS

2.1 | Human participants

The study was approved by the ethics institutional review board of University College London and additional local ethics committees of the participating centers (see also Supplementary Data S1). Informed consent was obtained from all families.

2.2 | Exome and Sanger sequencing

Biallelic variants in the *PIGS* gene were identified by exome sequencing (ES) as previously described.^{13,14} All variants are listed using canonical transcript NM_033198.4.

2.3 | Computational and in vitro splice analysis

Computational analysis of the c.174G>C variant was performed as previously described.¹⁵ To assess the predicted splicing impact of the c.174G>C (p.Gln58His) variant in Patients 1 and 2, an in vitro splicing assay was performed with minor modifications.¹⁶

2.4 | Flow cytometry analyses

Fluorescence-activated cell sorting analysis to assess for reduction in cell-surface expression of GPI-APs was done for Patient 6 and performed as previously described.¹⁵

3 | RESULTS

3.1 | Clinical findings

We identified six novel patients from five families with biallelic variants in the *PIGS* gene found by trio ES. Parental consanguinity was reported in four of the five families, all of whom had homozygous variants in *PIGS*. The clinical features of the affected individuals are summarized in Table S1 and are described further in Supplementary Data S1. All individuals presented with severe global developmental delay, intractable early infantile onset seizures, and absent speech. Patients 2, 3, and 5 died from complications of recurrent respiratory infections. Intractable seizures requiring multiple antiepileptic drugs (AEDs) were noted in all patients. The electroencephalographic (EEG) features in our cohort were variable, influenced by the age of the patients and the effect of the specific variant; however, all subjects showed EEG recording indicative of a severe developmental epileptic encephalopathy, that is, pseudohypsarrhythmia with runs of high amplitude and slow waves predominant over posterior regions associated with multifocal epileptic abnormalities within a diffusely slowed high amplitude during wakefulness and sleep or within a burst-suppression pattern. All of the individuals in this cohort had abnormal findings on brain magnetic resonance imaging, including atrophy of the frontal and anterior temporal lobes, with or without generalized brain atrophy. Frontal atrophy led to the development of bilateral subdural hygromas in one patient (Patient 5). We noted hypoplasia of the pons in four patients. One individual with severe pontine hypoplasia had large thalami and massa intermedia. All six affected individuals had microcephaly (−3 SD). Behavioral anomalies in two siblings (Patients 4 and 5) included autistic features and excessive laughing/crying. Other variable features include renal malformation

(1/6, 17%), visual impairment (3/6, 50%), severe hearing loss (2/6, 33%), and acquired arthrogryposis (2/6, 33%). Facial dysmorphism was observed in most of the affected individuals (Figure 1B), mainly consisting of coarse features such as thick arched eyebrows, almond-shaped palpebral fissures, depressed nasal bridge, and deep philtrum. Brachytelephalangy was also observed in three subjects (Patients 1–3), although in one of them (Patient 1) there was no evident epiphyseal or metaphyseal abnormality upon skeletal survey. Alkaline phosphatase levels (normal value = 0–281 U/L) were normal in Patient 2 (206 U/L) and mildly elevated in Patient 4 (445 U/L). This finding was not available for other affected individuals.

Although seizure management with AEDs is challenging, Patients 1 and 6 improved with pyridoxine (15 mg/kg/day) and folinic acid (1 mg/kg/day). Patient 1 reported decrease in seizure frequency, and Patient 6 reported improved developmental progress.

3.2 | Genetic findings

ES in the probands of Families 1 and 2 revealed a novel homozygous variant in exon 2 of *PIGS*, c.174G>C (p.Gln58His), predicted to affect RNA splicing. The variant segregated with the disease in both families (Figure 1A) and was located within a 14-Mb region of homozygosity. The variant was absent in publicly available population databases, including gnomAD, Exome Sequencing Project, GME Variome, and Iranome, as well as in more than 14,000 in-house exomes. In Family 3, a novel homozygous missense variant c.1070G>A (p.Gly357Asp) within a 10-Mb block of homozygosity was detected. The variant occurs at a highly conserved amino acid residue (Figure 1E), has a Combined Annotation Dependent Depletion score of 27 and Genomic Evolutionary Rate Profiling (GERP) score of 5.49, and segregated with the disease in the family. A novel segregating homozygous missense variant c.986C>G, (p.Pro329Arg), altering a highly conserved amino acid (Figure 1E), was identified for Family 4 (GERP score = 5.37). Both p.Gly357Asp and p.Pro329Arg are predicted to have a deleterious impact on the resulting *PIGS* protein, based on in silico predictions (Table S2).

In Family 5, Patient 6 has two variants. One variant is a paternally inherited in-frame insertion of eight amino acids in a nonrepeat region, as c.1141_1164dup24 (p.Asp381_Val388dup) in exon 10. This variant has been previously reported in the literature in a male of Chinese descent with *PIGS*-related disorder and seen in gnomAD in a heterozygous carrier state in five individuals of East Asian ethnicity. The second variant is a maternally inherited nonsense variant c.734G>A (p.Trp245*) in exon 7. This variant has been seen in gnomAD but only in the heterozygous carrier

state in one individual of African ethnicity. Table S2 shows the allele frequency and American College of Medical Genetics and Genomics criteria-based assessment of these variants.

3.3 | Splicing analysis

Computational splice analysis of the c.174G>C variant predicted two possible effects that prompted RNA studies: (1) a decrease in the splice donor scores between 12.6% and 43.3% and (2) the abolishment of an exonic splicing enhancer motif (Figure S2). In vitro RNA analysis of the wild-type c.174G disclosed a 508-bp amplicon including exons 2 and 3, as

well as a 369-bp amplicon with only exon 3 (Figure 1F,G). This likely reflects alternative splicing (NM_033198.4/ENST00000308360.8 and ENST00000395346.6). The amplicon with the homozygous c.174G>C variant revealed only exon 3 (369 bp), indicating a skipping of exon 2 (Figure 1F,G) that was Sanger sequence confirmed (Figure 1H). This out-of-frame deletion of exon 2 (r.35_174del) would result in a premature stop codon (p.Glu12Alafs*31).

3.4 | Flow cytometric analysis

Individual 6 had significantly lower levels of CD16 and fluorescent aerolysin (FLAER) in granulocytes, the most sensitive

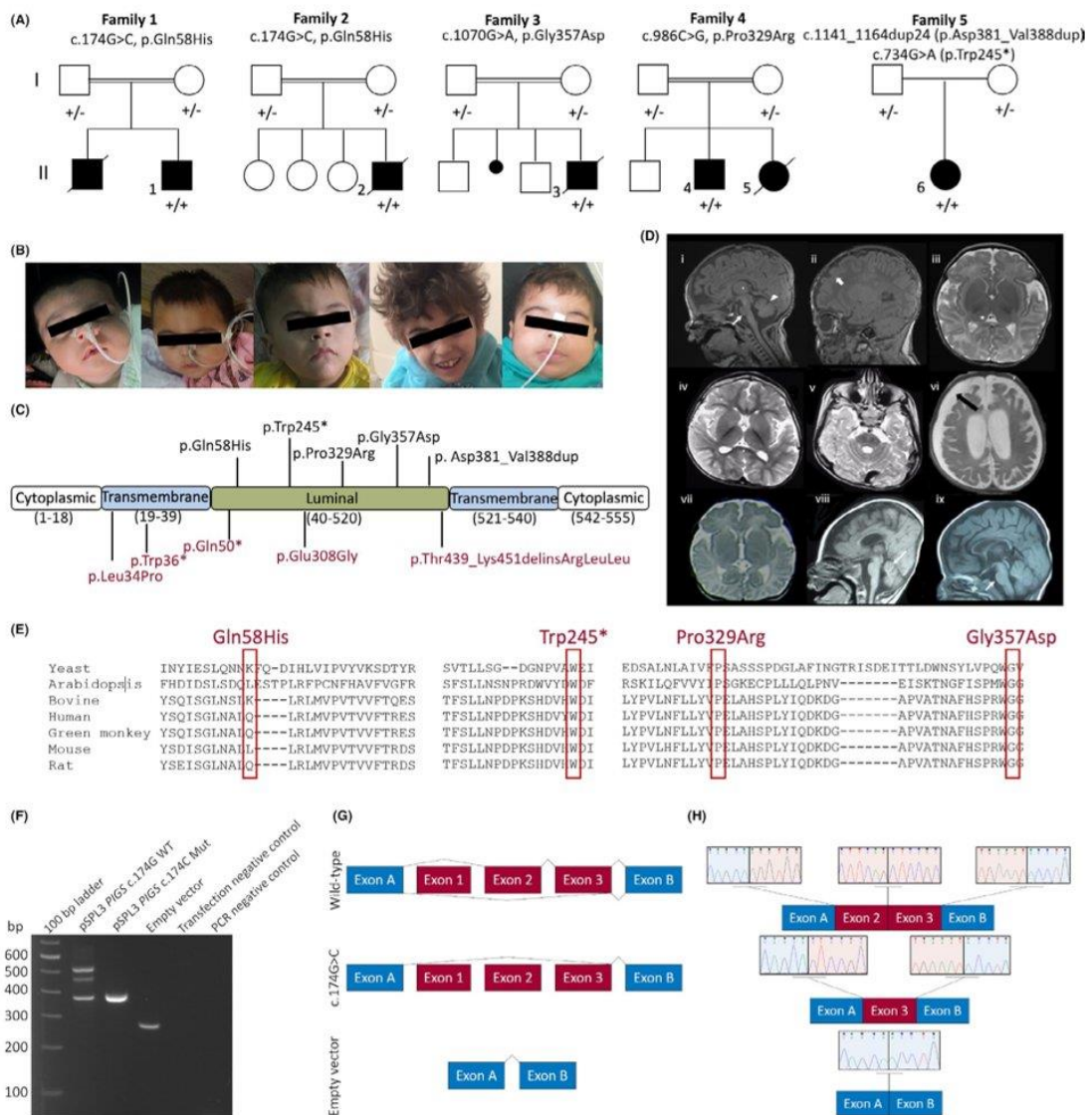


FIGURE 1 Clinico-genetic, radiological, and molecular findings of individuals in our cohort. (A) Pedigrees and segregation results (+ represents the variant) of the five families carrying biallelic *PIGS* variants. (B) Patients 1–5 show coarse facial features, including arched eyebrows, almond-shaped palpebral fissures, depressed nasal bridge, deep philtrum, and pointed chin. (C) A schematic representation of the *PIGS* protein showing the position of all *PIGS* variants identified, with previously reported variants in red. (D) Magnetic resonance imaging findings of (i–iii) Patient 6 at 5 weeks. Sagittal T-weighted image at the midline (i) shows small pons (arrow), early superior cerebellar vermal atrophy (arrowhead), and a large massa intermedia (star). Parasagittal T1-weighted image (ii) shows underdeveloped and undersulcated frontal lobes (arrow). Compare the sulcation in the anterior aspects with the posterior cerebral hemisphere. Axial T2-weighted image (iii) shows underpercularization due to underdevelopment of the frontal and anterior temporal lobes and large thalami (star). (iv, v) Patient 4 at 5 years. Axial T2-weighted images at the supratentorial (iv) and infratentorial (v) levels show generalized brain atrophy and delayed maturation of myelin. Note again the worse atrophy anteriorly in the frontotemporal regions. (vi) Patient 5 at 5 months. Axial T2-weighted image shows atrophy-related bilateral subdural hygromas (arrow). (vii) Patient 1 at 3.5 months. Axial T2-weighted image shows underpercularization bilaterally secondary to frontotemporal atrophy. Frontal dysgyria is also noted. (viii) Patient 2 at 34 weeks. Sagittal T1-weighted image shows microcephaly, with greater volume reduction in the frontal lobe, as well as early superior cerebellar vermal atrophy (arrow). (ix) Patient 3 at 14 months. Sagittal T1-weighted image shows a small pons and globally reduced cerebral white matter volume (worse anteriorly) associated with hypoplasia of the corpus callosum. (E) Interspecies alignment performed with Clustal Omega shows the complete conservation down to invertebrates of the amino acid residues affected by the substitutions. (F) RNA analysis of the *PIGS* c.174G>C variant. Gel electrophoresis of the reverse transcriptase polymerase chain reaction (PCR) wild-type (WT), mutant (Mut) c.174G>C variant, and empty pSPL3 vector amplicons. Transfection negative and PCR negative controls performed as expected. (G) Overview of the splicing of the wild-type (upper panel), patient (middle panel), and empty vector (lower panel) splicing. Note that although exon 1 was cloned into the vector, it was not spliced to exon A and exon 2, as it lacks a splice acceptor site. (H) Visualization of the exon junction sequence of the wild-type (upper panel), patient (middle panel), and empty vector (lower panel)

markers of inherited GPI deficiency (Figure 2). There was no decrease for CD55 and CD59 in granulocytes, but these are less sensitive markers of inherited GPI deficiency. There was also low CD14 in monocytes and low FLAER in lymphocytes (Figure S3). This is consistent with the previously reported case series that showed biallelic variants in *PIGS* lead to reduced amounts of GPI-AP at the cell surface.^{15,16} Due to the country of origin of the two patients still alive and the limited clinical facilities, we could not replicate the flow cytometric analysis in additional individuals.

4 | DISCUSSION

Our study expands the phenotypic and genotypic spectrum of *PIGS* variants, which have been previously associated with profound neurodevelopmental impairment, EIEE, and premature death. We expand the known population of seven individuals with biallelic pathogenic variants in *PIGS* reported so far by adding five novel patients. We report five variants, four of which were previously unreported; namely, one truncating, one in-frame duplication, and three missense variants. According to gnomAD constraint scores, *PIGS* is intolerant toward both missense variants ($Z = .7801$) and biallelic loss of function variants (probability of being loss-of-function intolerant = 0, pREC = .9943).

All patients had hypotonia, microcephaly, global developmental delay, absent speech, and infantile onset epilepsy. Brachytelephalangy was also observed in three patients. Although first reported in *PIGV*-related disorders,¹⁷ it is not present in all GPI deficiencies.¹¹ We also identified neuroimaging findings in our patients, consistent with previously published studies that described cerebellar and diffuse cortical

atrophy in individuals carrying biallelic *PIGS* variants.^{11,12} In this cohort, vision impairment, hearing loss, and behavioral abnormalities were also commonly observed. Taken together, biallelic (gene-disruptive) variants in *PIGS* are associated with an early infantile encephalopathy refractory to standard AEDs co-occurring with global developmental delay, severe hypotonia, and visual and hearing impairment.

Elevated alkaline phosphatase levels have been observed in other disorders of GPI anchor synthesis.⁷ In our cohort, only one of two tested patients showed mildly elevated alkaline phosphatase levels, supporting the evidence that increased alkaline phosphatase levels are not observed in all GPI deficiencies.¹¹

GPI-AP function is also implicated in vitamin B6 and folate transport, nucleotide metabolism, and lipid homeostasis. B6-dependent enzymes are involved in the metabolism of amino acids, neurotransmitters, molybdenum cofactor, and sphingolipids.¹⁸ Two of our patients were treated with pyridoxine and folinic acid, with some benefit in seizure control even before the genetic analysis; moreover, we could not measure the cerebrospinal fluid pyridoxal-5-phosphate levels primarily due to the limited testing ability of their referring hospitals. Although anecdotal, previous studies have also shown the effects of pyridoxine in other IGDs.¹⁹ Pyridoxine has been shown effective in various GPI deficiency disorders, although there is no clear evidence describing the effect of folinic acid. The ketogenic diet has also been previously reported to improve outcome in cases of *PIGA* deficiency and may be a consideration for individuals with *PIGS*-related disorder.²⁰

This study further reviewed the clinical features of *PIGS*-related disorders. Distinguishing *PIGS*-related disorders from other pediatric neurological syndromes will rely on

Cell surface GPI-APs of the granulocytes

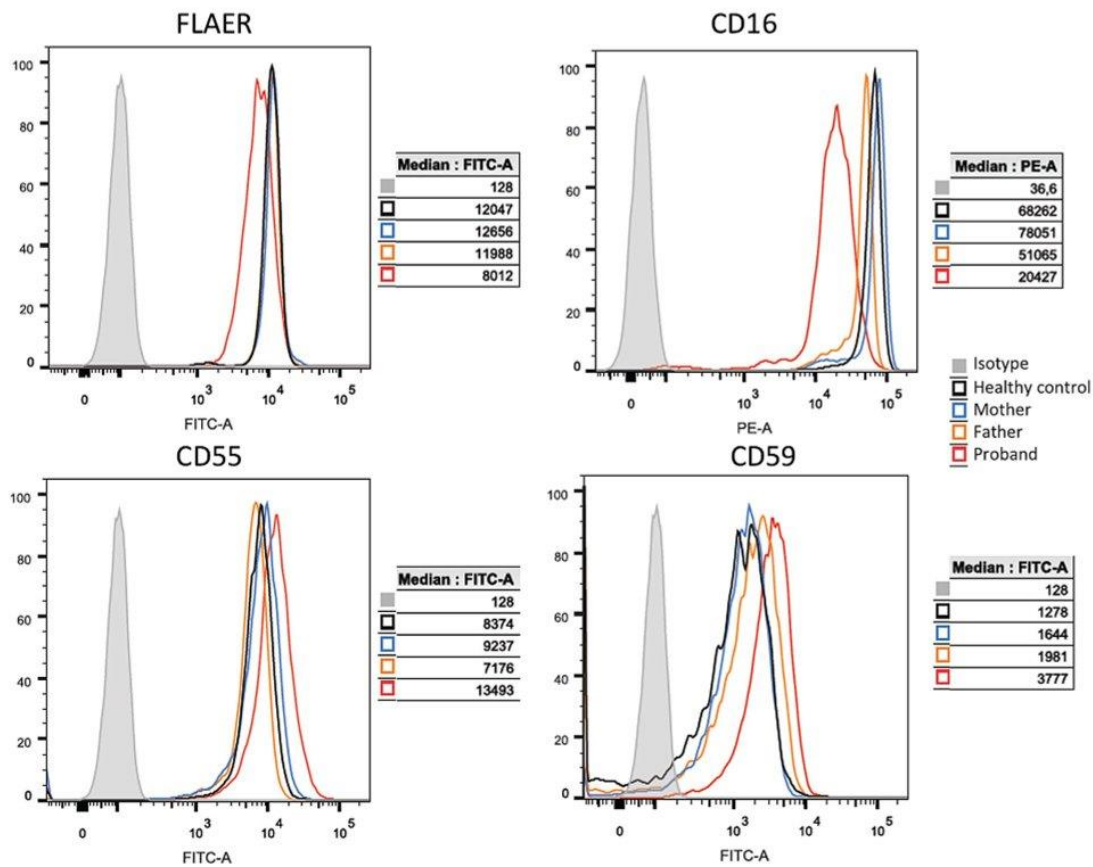


FIGURE 2 Impact of the *PIGS* variants on individual granulocyte cell-surface glycosylphosphatidylinositol-anchored protein (GPI-AP). Fluorescence-activated cell sorting (FACS) analysis on granulocytes indicated that individual red blood cells from Patient 6 of Family 5 had less signal of CD16, CD55, and CD59 than age-matched control cells, showing a reduced cell-surface expression. FLAER, fluorescent aerolysin; FITC, fluorescein isothiocyanate; PE, phycoerythrin

the combination of physical examination findings and identifying the phenotypic features resulting from disruption of *PIGS*. These include intractable epilepsy, severe developmental delay, hypotonia, and coarse faces. Our data further highlight the importance of including the screening of the *PIGS* gene in the case of infantile epilepsy and may serve for improved interpretation of new *PIGS* variants with the help of biochemical findings and flow cytometry analysis. Finally, *PIGS* is not found on most clinically utilized epilepsy gene panels, suggesting that it may be a more frequent cause of early infantile epilepsy than reported. As epilepsy genetic testing expands and ES becomes more available, more patients will likely be identified in the future.

ACKNOWLEDGMENTS

We are grateful to all patients and families whose participation in the study enabled the data collection and the analyses.

All families were collected as part of the SYNAPS Study Group collaboration funded by the Wellcome Trust and strategic award (Synaptopathies) funding (WT093205 MA and WT104033AIA). This research was conducted as part of the Queen Square Genomics group at University College London, supported by the National Institute for Health Research University College London Hospitals Biomedical Research Centre. P.S. and V.S. developed this work within the framework of the DINOGMI Department of Excellence of MIUR 2018-2022 (legge 232 del 2016). H.H. is funded by the Medical Research Council (MR/S01165X/1, MR/S005021/1, G0601943), the National Institute for Health Research University College London Hospitals Biomedical Research Centre, Rosetree Trust, Ataxia UK, MSA Trust, Brain Research UK, Sparks GOSH Charity, Muscular Dystrophy UK, Muscular Dystrophy Association (USA). B.V. is funded by Intramural Funding (Fortune) at the

University of Tübingen (2545-1-0) and the Ministry of Science, Research, and Art Baden-Württemberg.

CONFLICT OF INTEREST


M.J.G.S. is an employee of GeneDx. None of the other authors has any conflict of interest to disclose.

ETHICAL PUBLICATION STATEMENT

We confirm that we have read the Journal's position on issues involved in ethical publication and affirm that this report is consistent with those guidelines.

ORCID

Stephanie Efthymiou  <https://orcid.org/0000-0003-4900-9877>

Barbara Vona  <https://orcid.org/0000-0002-6719-3447>

Pasquale Striano  <https://orcid.org/0000-0002-6065-1476>

REFERENCES

- Pagnamenta AT, Murakami Y, Taylor JM, Anzilotti C, Howard MF, Miller V, et al. Analysis of exome data for 4293 trios suggests GPI-anchor biogenesis defects are a rare cause of developmental disorders. *Eur J Hum Genet.* 2017;25(6):669–79.
- Kinoshita T, Fujita M. Biosynthesis of GPI-anchored proteins: special emphasis on GPI lipid remodeling. *J Lipid Res.* 2016;57(1):6–24.
- Nozaki M, Ohishi K, Yamada N, Kinoshita T, Nagy A, Takeda J. Developmental abnormalities of glycosylphosphatidylinositol-anchor-deficient embryos revealed by Cre/loxP system. *Lab Invest.* 1999;79(3):293–9.
- Alfieri JA, Martin AD, Takeda J, Kondoh G, Myles DG, Primakoff P. Infertility in female mice with an oocyte-specific knockout of GPI-anchored proteins. *J Cell Sci.* 2003;116(Pt 11):2149–55.
- Kondoh G, Tojo H, Nakatani Y, Komazawa N, Murata C, Yamagata K, et al. Angiotensin-converting enzyme is a GPI-anchored protein releasing factor crucial for fertilization. *Nat Med.* 2005;11(2):160–6.
- Scheffer IE, Liao J. Deciphering the concepts behind "epileptic encephalopathy" and "developmental and epileptic encephalopathy". *Eur J Paediatr Neurol.* 2020;24:11–4.
- Murakami Y, Nguyen TTM, Baratang N, Raju PK, Knaus A, Ellard S, et al. Mutations in PIGB cause an inherited GPI biosynthesis defect with an axonal neuropathy and metabolic abnormality in severe cases. *Am J Hum Genet.* 2019;105(2):384–94.
- Martin HC, Kim GE, Pagnamenta AT, Murakami Y, Carvill GL, Meyer E, et al. Clinical whole-genome sequencing in severe early-onset epilepsy reveals new genes and improves molecular diagnosis. *Hum Mol Genet.* 2014;23(12):3200–11.
- Johnstone DL, Nguyen TT, Murakami Y, Kernohan KD, Tetreault M, Goldsmith C, et al. Compound heterozygous mutations in the gene PIGP are associated with early infantile epileptic encephalopathy. *Hum Mol Genet.* 2017;26(9):1706–15.
- Johnston JJ, Gropman AL, Sapp JC, Teer JK, Martin JM, Liu CF, et al. The phenotype of a germline mutation in PIGA: the gene somatically mutated in paroxysmal nocturnal hemoglobinuria. *Am J Hum Genet.* 2012;90(2):295–300.
- Nguyen TTM, Murakami Y, Wigby KM, Baratang NV, Rousseau J, St-Denis A, et al. Mutations in PIGS, encoding a GPI transamidase, cause a neurological syndrome ranging from fetal akinesia to epileptic encephalopathy. *Am J Hum Genet.* 2018;103(4):602–11.
- Zhang L, Mao X, Long H, Xiao B, Luo Z, Xiao W, et al. Compound heterozygous PIGS variants associated with infantile spasm, global developmental delay, hearing loss, visual impairment, and hypotonia. *Front Genet.* 2020;11:564.
- Makrythanasis P, Maroofian R, Stray-Pedersen A, Musaev D, Zaki MS, Mahmoud IG, et al. Biallelic variants in KIF14 cause intellectual disability with microcephaly. *Eur J Hum Genet.* 2018;26(3):330–9.
- Guillen Sacoto MJ, Tchasovnikarova IA, Torti E, Forster C, Andrew EH, Anselm I, et al. De novo variants in the ATPase module of MORC2 cause a neurodevelopmental disorder with growth retardation and variable craniofacial dysmorphism. *Am J Hum Genet.* 2020;107(2):352–63.
- Vona B, Mazaheri N, Lin S-J, Dunbar LA, Maroofian R, Azaiez H, et al. Biallelic mutation of CLRN2 causes non-syndromic hearing loss in humans. *bioRxiv.* 2020. doi:<https://doi.org/10.1101/2020.07.29.222828>.
- Tompson SW, Young TL. Assaying the effects of splice site variants by exon trapping in a mammalian cell line. *Bio Protoc.* 2017;7(10):e2281.
- Horn D, Krawitz P, Mannhardt A, Korenke GC, Meinecke P. Hyperphosphatasia-mental retardation syndrome due to PIGV mutations: expanded clinical spectrum. *Am J Med Genet A.* 2011;155A(8):1917–22.
- Manea E. A step closer in defining glycosylphosphatidylinositol anchored proteins role in health and glycosylation disorders. *Mol Genet Metab Rep.* 2018;16:67–75.
- Kuki I, Takahashi Y, Okazaki S, Kawawaki H, Ehara E, Inoue N, et al. Vitamin B6-responsive epilepsy due to inherited GPI deficiency. *Neurology.* 2013;81(16):1467–9.
- Joshi C, Kolbe DL, Mansilla MA, Mason S, Smith RJ, Campbell CA. Ketogenic diet—a novel treatment for early epileptic encephalopathy due to PIGA deficiency. *Brain Dev.* 2016;38(9):848–51.

SUPPORTING INFORMATION

Additional supporting information may be found online in the Supporting Information section.

How to cite this article: Efthymiou S, Dutra-Clarke M, Maroofian R, et al. Expanding the phenotype of PIGS-associated early onset epileptic developmental encephalopathy. *Epilepsia.* 2021;62:e35–e41. <https://doi.org/10.1111/epi.16801>

10.5 Attachment 5

A biallelic variant in CLRN2 causes non-syndromic HL in humans



A biallelic variant in *CLRN2* causes non-syndromic hearing loss in humans

Barbara Vona^{1,2} · Neda Mazaheri³ · Sheng-Jia Lin⁴ · Lucy A. Dunbar⁵ · Reza Maroofian⁶ · Hela Azaiez⁷ · Kevin T. Booth^{7,8} · Sandrine Vitry⁹ · Aboufazel Rad² · Franz Rüschenhoff¹⁰ · Pratihtha Varshney⁴ · Ben Fowler¹¹ · Christian Beetz¹² · Kumar N. Alagramam^{13,14,15} · David Murphy⁶ · Gholamreza Shariati^{16,17} · Alireza Sedaghat¹⁸ · Henry Houlden⁶ · Cassidy Petree⁴ · Shruthi VijayKumar⁴ · Richard J. H. Smith⁷ · Thomas Haaf¹ · Aziz El-Amraoui⁹ · Michael R. Bowl^{5,19} · Gaurav K. Varshney⁴ · Hamid Galehdari³

Received: 25 September 2020 / Accepted: 31 December 2020 / Published online: 26 January 2021
© The Author(s) 2021

Abstract

Deafness, the most frequent sensory deficit in humans, is extremely heterogeneous with hundreds of genes involved. Clinical and genetic analyses of an extended consanguineous family with pre-lingual, moderate-to-profound autosomal recessive sensorineural hearing loss, allowed us to identify *CLRN2*, encoding a tetraspan protein, as a new deafness gene. Homozygosity mapping followed by exome sequencing identified a 14.96 Mb locus on chromosome 4p15.32p15.1 containing a likely pathogenic missense variant in *CLRN2* (c.494C > A, NM_001079827.2) segregating with the disease. Using in vitro RNA splicing analysis, we show that the *CLRN2* c.494C > A variant leads to two events: (1) the substitution of a highly conserved threonine (uncharged amino acid) to lysine (charged amino acid) at position 165, p.(Thr165Lys), and (2) aberrant splicing, with the retention of intron 2 resulting in a stop codon after 26 additional amino acids, p.(Gly146Lysfs*26). Expression studies and phenotyping of newly produced zebrafish and mouse models deficient for clarin 2 further confirm that clarin 2, expressed in the inner ear hair cells, is essential for normal organization and maintenance of the auditory hair bundles, and for hearing function. Together, our findings identify *CLRN2* as a new deafness gene, which will impact future diagnosis and treatment for deaf patients.

Introduction

The mammalian inner ear is an exquisite and highly complex organ, made up of the vestibule, the organ responsible for balance, and the cochlea, the sensory organ for hearing. The

auditory sensory cells of the inner ear are called the inner and outer hair cells that are responsible for transduction of sound wave-induced mechanical energy into neuronal signals (Gillespie and Müller 2009; Hudspeth 1997). The functional mechano-electrical transduction machinery involves intact formation and maintenance of a highly specialized and organized structure, the hair bundle. The hair bundle contains a few dozen F-actin-filled stereocilia, arranged in a highly interconnected and highly organized staircase-like pattern, which is critical for function (Kazmierczak et al. 2007). Knowledge of the mechanisms of formation, maintenance, and function of the transduction complex is limited (Cunningham and Müller 2019). In this regard, identification of novel genes that encode protein products essential for hearing is likely to improve our understanding of the physical, morphological and molecular properties of hair cells and associated mechanistic processes.

Hereditary hearing loss is one of the most common and genetically heterogeneous disorders in humans (Wright et al. 2018). Sensorineural hearing loss has an incidence of 1 to

Neda Mazaheri, Sheng-Jia Lin, Lucy A. Dunbar contributed equally.

Aziz El-Amraoui, Michael R. Bowl, Gaurav K. Varshney and Hamid Galehdari share senior authorship.

Supplementary Information The online version contains supplementary material available at <https://doi.org/10.1007/s00439-020-02254-z>.

✉ Barbara Vona
barbara.vona@uni-wuerzburg.de;
barbara.vona@uni-tuebingen.de

✉ Michael R. Bowl
m.bowl@har.mrc.ac.uk; m.bowl@ucl.ac.uk

Extended author information available on the last page of the article

2 per 1000 at birth (Morton and Nance 2006). It displays extraordinary phenotypic, genetic and allelic heterogeneity, with up to 1000 different genes potentially involved (Ingham et al. 2019). So far, about 120 genes and more than 6000 disease causing variants (Azaiez et al. 2018) have been identified as responsible for non-syndromic hearing loss in humans (see <http://hereditaryhearingloss.org/> and <http://deafnessvariationdatabase.org/>), and many more are yet to be discovered. Genetic factors predominate the etiological spectrum and most hereditary hearing loss appears to follow an autosomal recessive inheritance pattern (Smith et al. 2005). To date, approximately 80% of the known autosomal recessive deafness-associated genes have been originally identified by studying extended consanguineous families (Hofrichter et al. 2018). There are many forms of hearing loss that are clinically indistinguishable but caused by distinct genetic entities that are presently unknown. Identification of additional genes essential for auditory function, through the study of families exhibiting hereditary hearing loss, will not only help increase our understanding of the biology of hearing, but will also identify new molecular targets for therapeutic intervention.

Through the study of an extended consanguineous Iranian family, we have identified a *CLRN2* coding lesion as the likely cause of hearing loss in family members that are homozygous for the allele. We have established that clarin 2 likely plays a critical role in mechanotransducing stereocilia of the hair bundle in zebrafish and mouse. *CLRN2* belongs to the clarin (*CLRN*) family of proteins that are comprised of three orthologues named clarin 1, 2, and 3 that encode four-transmembrane domain proteins. Pathogenic variants in *CLRN1* (clarin 1) cause either non-syndromic retinitis pigmentosa (RP) (Khan et al. 2011) or Usher syndrome type 3A (USH3A), that is characterized by progressive hearing loss, RP and variable vestibular dysfunction (Adato et al. 2002; Joensuu et al. 2001; Ness et al. 2003; Plantinga et al. 2005). This study establishes clarin 2 as essential for inner ear function in zebrafish, mice and humans, with a loss-of-function allele leading to autosomal recessive non-syndromic sensorineural hearing loss (ARNSHL).

Materials and methods

Patient clinical and audiometry data

Written informed consent was provided from all participating individuals. This study has been approved by the Faculty of Medicine ethics commissions at the University of Würzburg (46/15) and Shahid Chamran University of Ahvaz (#EE/97.24.3 17654). A three generation Iranian family of Lurs ethnicity was ascertained as part of a large ethnically

diverse Iranian population rare disease study. Pure-tone audiograms and medical information were collected from participating members. Clinical examination excluded additional syndromic features.

Individuals IV-1, IV-6, and V-1 (Fig. 1) underwent complete ear, nose and throat examination, including binocular ear microscopy and external ear inspection. Routine pure-tone audiometry was performed according to current standards that measured hearing thresholds at frequencies 0.25, 0.5, 1, 2, 4, 6 and 8 kHz. Both air- and bone-conduction thresholds were determined. Severity of hearing loss was defined as previously described (Mazzoli et al. 2003). Individuals IV-1 and IV-6 underwent additional tympanometry and speech recognition threshold testing. Audiometry testing for individuals IV-1, IV-6, and V-1 was performed at ages 29, 44, and 20 years, respectively.

Genotyping, gene mapping, copy number variation and exome sequencing data analyses

Due to parental consanguinity and suspected autosomal recessive mode of inheritance, we assumed that the causal variant would be homozygous and identical by descent in affected individuals in the fourth generation of the family. Blood samples from 14 family members were obtained and genomic DNA was isolated from whole blood using standard procedures. DNA from affected (IV-1, IV-6, and IV-8) and unaffected (IV-2, IV-3, IV-4, and IV-5) individuals were genotyped using the Infinium Global Screening Array-24 v1.0 BeadChip (Illumina, San Diego, CA, USA) according to manufacturer's protocols. Copy number variation calling was performed using GenomeStudio v.2011.1 and cnvPartition 3.2.0 (Illumina).

From the 618,540 markers on the array, we filtered out InDels, MT- and Y-chromosomal SNPs, multi-allelic SNPs, SNPs with missing genotypes in more than one individual, and SNPs having a minor allele frequency (MAF) lower than 5% in gnomAD European individuals (NFE) resulting in 242,705 bi-allelic SNPs for quality control (QC) and Linkage analysis. Data conversion to Linkage format files and QC was managed with the ALOHOMORA software (Rüschendorf and Nürnberg 2005). The sex of individuals was estimated by counting heterozygous genotypes on the X-chromosome and compared to the given pedigree data. The relationships between family members were verified with the program Graphical Relationship Representation (GRR) (Abecasis et al. 2001). PedCheck (O'Connell and Weeks 1998) was used to detect Mendelian errors (ME) and SNPs with ME were removed from the data set. Unlikely genotypes, e.g., double recombinants, were identified with Merlin (Abecasis et al. 2002) and deleted in the individuals.

Linkage analysis was performed with Merlin (Abecasis et al. 2002) using an autosomal recessive mode of

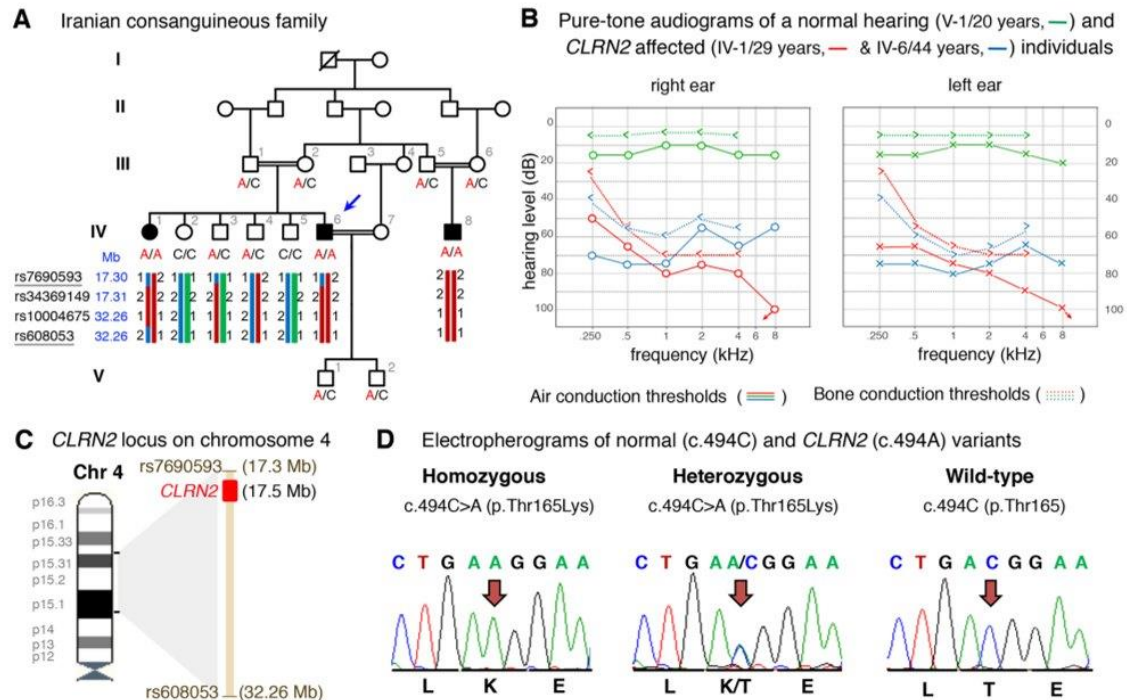


Fig. 1 Pedigree, audiological data, genetic data, and locus mapping. **a** The consanguineous family of Iranian origin with hearing loss and segregation of the *CLRN2* c.494C>A variant. Linked haplotypes harbouring the pathogenic variant coloured in red with meiotic recombination SNP markers underlined. SNP positions are annotated using the GRCh37 human genome assembly. **b** Pure-tone audiograms from affected individuals IV-1 (red) and IV-6 (blue), as well as an unaffected heterozygous individual V-1 (green). Air-conduction thresh-

olds in dB HL for the right and left ears are represented by circles and crosses, respectively. Bone-conduction thresholds are represented by < and > for right and left ears, respectively, and confirm a sensorineural hearing loss in the affected individuals. **c** Linkage mapping reveals a 14.96 Mb locus on chromosome 4 containing *CLRN2*. **d** Sequence electropherograms showing the homozygous, heterozygous and WT images of the *CLRN2* c.494C>A; pThr165Lys pathogenic variants

inheritance with complete penetrance and a mutant allele frequency of 0.001. To avoid the problem of Linkage Disequilibrium (LD) between markers, which can lead to inflated LOD scores, we created a less dense, LD-reduced marker set of 91,426 SNPs with a minimal distance of 10,000 bases between markers and a MAF > 0.15. The exact position of the LOD score regions, e.g., the recombination events, were identified with the full marker set of 242,705 SNPs.

Additionally, homozygosity mapping was performed using HomozygosityMapper to identify common homozygous intervals among the affected individuals (Seelow et al. 2009). Runs of homozygosity with a maximum threshold of 0.99 were checked after the exome-wide analysis was completed.

For exome sequencing, DNA samples from two affected individuals (IV-1 and IV-6) were used. The data from individual IV-6 were analyzed exome-wide and data from individual IV-1 were used for determination of allele sharing. Exome capture using genomic DNA was performed using

the SureSelect Target Enrichment v6 (Agilent) kit following manufacturer's recommendations. The libraries were sequenced with a HiSeq4000 (Illumina). Data analysis was performed using the Burrows–Wheeler Alignment (BWA) tool for read mapping to the human reference genome GRCh37 (hg19), Picard for duplicate removal, GATK for local re-alignment, base recalibration, variant calling, and variant annotation, and SnpEff for variant annotation. Variant filtering was based on: coverage > 10X, Phred quality score ≥ 30 , and MAF ≤ 0.005 as reported in 1000 Genomes Project and EVS6500. Variants were filtered based on coding effect (non-synonymous, synonymous, indels, and splice site variants), and artifact-prone genes (*HLAs*, *MAGEs*, *MUCs*, *NBPFs*, *ORs*, *PRAMEs*) were excluded. ACMG guidelines were used for variant interpretation (Oza et al. 2018). Visualization was performed using the Integrative Genomics Viewer. Analysis of homozygous and compound heterozygous variants between the two sequenced affected individuals (IV-6 and IV-1) followed. We analyzed missense

variants using a combination of criteria that scored conservation using GERP++ and PhyloP, and deleterious or pathogenic scores in Combined Annotation Dependent Depletion (CADD) (Kircher et al. 2014), LRT (Chun and Fay 2009), MutationTaster (Schwarz et al. 2014), PolyPhen-2 (Adzhubei et al. 2010), and SIFT (Ng and Henikoff 2001). Missense variants were excluded when three out of five in silico pathogenicity prediction tools yielded a benign score. Manual MAF analysis used gnomAD (Lek et al. 2016), GME (Scott et al. 2016) and Iranome (Fattahi et al. 2019). Potential effects on splicing were assessed using ESEfinder (Cartegni et al. 2003) and RESCUE-ESE (Fairbrother et al. 2004).

Segregation, sequence and in vitro splicing analyses of the *CLRN2* c.494C > A likely pathogenic variant

To confirm segregation of the *CLRN2* c.494C > A; p.(Thr165Lys) (NM_001079827.2) homozygous variant, Sanger sequencing was completed in all 14 family members using the following primers (*CLRN2* Ex3 F: 5'-AAATGC CACCTCTTACAGAGTTGC-3' and *CLRN2* Ex3 R: 5'-ACC GTGGCCTCTTCGATTTTGGTC-3') and standard PCR and sequencing parameters.

To document residue conservation, CLRN1 (UniProt: P58418) and CLRN2 (UniProt: A0PK11) were aligned and visualized in Jalview (Waterhouse et al. 2009) with an overview of the pathogenic and likely pathogenic missense and nonsense *CLRN1* variants retrieved from the Deafness Variation Database v 8.2 (Azaiez et al. 2018).

In addition, secondary protein structure prediction of human CLRN2 (NP_001073296.1) that included the wild-type (WT) and mutated amino acid residues was performed using I-TASSER (Yang et al. 2015).

To assess the splicing effect of the c.494C > A variant, in vitro splicing assays, also called mini-genes, were carried out as described (Booth et al. 2018a, b). WT *CLRN2* exon 3 (266 bp) plus 183 and 51 nucleotides from intron 2 and the 3'UTR were PCR amplified with gene-specific primers containing *Sall* or *SacII* restriction enzyme sites, respectively. After PCR amplification, clean up, and restriction enzyme digestion, the PCR fragment was ligated into the pET01 Exontrap vector (MoBiTec) and the sequence was confirmed. Variants were then introduced into the WT sequence using QuikChange Lightning Site-Directed Mutagenesis (Agilent) according to the manufacturer's protocols via overlapping primers containing the alteration. The WT and mutant mini-genes were sequence confirmed.

WT or mutant mini-genes were transfected in triplicates into COS-7 and ARPE-19 cells using TransIT-LT1 Transfection Reagent (Mirus). Cells were harvested 36 h after transfection and total RNA was extracted using Quick-RNA MiniPrep Plus kit (ZYMO Research). cDNA was transcribed

using 750 ng of isolated RNA SuperScript™ III Reverse Transcriptase (ThermoFisher Scientific) using a primer specific to the 3' native exon of the pET01 vector according to manufacturer's protocol. PCR amplification followed using primers specific to the 5' and 3' native exons of the pET01 vector, and products were visualized on a 1.5% agarose gel. As a negative control, rs117875715 (chr4(GRCh37):g.17,528,480G > A), a benign polymorphism, was used to test and validate the designed mini-gene assay.

Concurrently, the mini-gene splice assay experiment was conducted in a double-blind manner as previously described (Lekszas et al. 2020). Genomic DNAs of an affected homozygous (IV-6) and WT individual (IV-5) were amplified using a forward primer with a *XhoI* restriction site (*CLRN2* Ex3 *XhoI* F: 5'-aattctcagTTGCAGTGAGCTGAG ATGGT-3') and a reverse primer with a *BamHI* restriction site (*CLRN2* Ex3 *BamHI* R: 5'-attggtaccGCCTTGCGAAGT TGTTACTG-3'). The 886 bp amplicon included the entire exon 3 sequence plus additional flanking 320 bp (5') and 306 bp (3') sequence that was ligated into a multiple cloning site between native exons A and B in the linearized pSPL3b exon-trapping vector. The vector was transformed into DH5 α competent cells and plated overnight. All mutant mini-genes were Sanger sequence confirmed.

Homozygous and WT mini-genes were transfected in triplicate into HEK 293 T cells cultured in FCS-free medium in 6 well culture plates with a density of 2×10^5 cells per mL. The mini-genes in the pSPL3b vector were transiently transfected using 6 μ l of FuGENE 6 Transfection Reagent (Roche) with 2 μ g of vector. An empty vector and HEK 293 T cells were included as controls. The transfected cells were harvested 24–48 h post-transfection. Total RNA was prepared using the miRNAeasy Mini Kit (Qiagen). Approximately, 1 μ g of RNA was reverse transcribed using a High Capacity RNA-to-cDNA Kit (Applied Biosystems) following manufacturer's protocols. The cDNA was used for PCR amplification using a vector specific SD6 forward (5'-TCT GAGTCACCTGGACAACC-3') and a terminal *CLRN2* exon 3 reverse cDNA primer (5'-CAAGATATCCTCAGCTGT GACC-3'). The resulting amplified fragments were visualized on a 1.5% agarose gel. cDNA amplicons were Sanger sequenced. cDNA amplicons from the homozygous individual were cloned following standard protocols for the TA cloning (dual promoter with pCRII) kit (Invitrogen).

CRISPR/Cas9-mediated inactivation of *clrn2* in zebrafish

Zebrafish (*Danio rerio*) were raised and maintained in an AALAC accredited facility at the Oklahoma Medical Research Foundation (OMRF) under standard conditions. Zebrafish embryos/larvae were maintained in embryo medium with 0.00002% methylene blue and raised at 28 °C.

All animal experiments were performed as per protocol (17-01) and approved by the Institutional Animal Care Committee of OMRF (IACUC). All zebrafish handling, embryo care, and microinjections were performed as previously described (Westerfield 2000). WT zebrafish strain NHGRI-1 was used for all experiments (LaFave et al. 2014). The zebrafish embryonic staging was determined by morphological features according to (Kimmel et al. 1995).

To produce zebrafish *clrn2* crispants, the sgRNA target sequences were selected from the UCSC genome browser tracks generated by the Burgess lab. Five independent targets were chosen and sgRNAs were synthesized by in vitro transcription as described earlier (Varshney et al. 2016). sgRNAs and Cas9 protein complex were used to generate indels. A 6 μ L mixture containing 2 μ L of 40 μ M Spy Cas9 NLS protein (New England Biolabs, MA, USA), 200 ng each of five sgRNAs (in 2 μ L) and 2 μ L of 1 M potassium chloride was injected into one-cell-stage WT embryos. Injection volumes were calibrated to 1.4 nL per injection. Insertion/deletion (indel) variants were detected by amplifying the target region by PCR and Sanger sequencing as described earlier (Varshney et al. 2016). The sequencing data were analyzed by Inference of CRISPR Edits (ICE) v2 CRISPR analysis tool. The sgRNA target sequences and PCR primer sequences are listed in Supplementary Table S1.

Zebrafish RNA extraction and quantitative reverse transcription PCR (RT-qPCR)

Total RNA at different developmental stages, adult tissues, and CRISPR/Cas9 injected larvae were extracted using the TRIzol Reagent (Thermo Fisher Scientific, CA, USA) and purified by RNA clean and concentrator-5 kit (Zymo Research, CA, USA) according to the manufacturer's instructions. RNA concentration was measured by DeNovix DS-11 spectrophotometer (DeNovix Inc., USA). The cDNA was synthesized by iScript RT Supermix (Bio-Rad, USA), and was used as a template for performing the RT-qPCR with SYBR Green Supermix (Thermo Fisher Scientific, CA, USA) and the Light Cycler® 96 System (Roche, CA, USA). All RT-qPCR reactions were carried out using three biological and technical replicates. The housekeeping gene *18S* was used as a reference gene.

All RT-qPCR primer pairs were designed across exon-exon junctions using NCBI Primer-BLAST program (Supplementary Table S1). PCR cycling conditions were used as per manufacturer instructions. All reactions were carried out using three biological and technical replicates. The housekeeping gene *18S* was used as a reference gene. Amplification specificity was assessed by dissociation curve analysis. The cycle threshold values (Ct) data were imported into Microsoft Excel for the relative gene expression analysis. Quantification was based on $2^{(-\Delta\Delta CT)}$ method (Livak and

Schmittgen 2001), and using 18 h post fertilization (hpf) for *clarin 2* temporal expression, muscle for *clarin 2* in different tissue expression and the corresponding age-matched control for *clarin 2* CRISPR injected F₀ larvae as normalization control.

Distribution of *clrn2*, phalloidin staining and behavioral analysis in zebrafish

To determine *clrn2* expression, we used in situ hybridization on larvae and inner ear-containing cryosections. The full-length coding sequence of zebrafish *clarin 2* (NM_001114690.1) was PCR amplified from WT zebrafish cDNA using primer pairs with *Bam*HI and *Xho*I restriction sites cloned into the pCS2+ vector (a kind gift from Dr. Dave Turner, University of Michigan). After restriction digestion, the resulting clones were sequenced and used as templates for riboprobe synthesis. The digoxigenin-UTP-labeled riboprobes were synthesized according to the manufacturer's instructions (Millipore Sigma, MO, USA). Briefly, the *clarin 2* and the *pvalb9* plasmids (Horizon Discovery) were linearized by *Bam*HI and *Not*I restriction enzymes, respectively. The linearized plasmid was purified and used as template for in vitro transcription using T7 RNA polymerase to synthesize anti-sense probes. The sense probe was made using *Xba*I linearized *clarin 2* plasmid and SP6 RNA polymerase.

Whole-mount in situ hybridization (WISH) on 3 and 5 dpf zebrafish embryos/larvae was performed following the procedures as described by Thisse et al. with minor modifications (Thisse and Thisse 2008). Age-matched zebrafish embryos were randomly collected by breeding WT zebrafish pairs. The embryos were treated with 0.003% phenylthiourea (PTU) (Millipore Sigma, MO, USA) in embryo medium at 1 day post-fertilization (dpf) until the desired stages reached to reduce the pigment formation that will facilitate color visualization during in situ hybridization. Embryos/larvae were then fixed with 4% (V/V) paraformaldehyde in phosphate-buffered saline (PBS) at 3 and 5 dpf. An additional bleaching step was carried out after fixation by incubating the embryos at room temperature in a 3% hydrogen peroxide and 0.5% potassium hydroxide solution. The permeabilization of 3 dpf embryos and 5 dpf larvae was performed using 2 μ g/mL proteinase K for 12 and 18 min, respectively. Color development was conducted using the BM-Purple alkaline phosphatase substrate (Millipore Sigma, MO, USA).

For preparation of cryo-sectioned samples after WISH, the 5 dpf larvae were soaked in 25, 30% (V/V) sucrose/PBS and optimum cutting temperature (OCT) each for at least 2 days, and embedded in OCT, then Cryotome sectioned at a 10- μ m thickness.

For phalloidin staining of the zebrafish inner ear, 5 dpf larvae were euthanized with tricaine and fixed in 4% (V/V) paraformaldehyde (PFA) at 5 dpf, fixed embryos were

washed by PBSTx (1% PBS, 0.2% triton X-100) and incubated in 2% triton X-100 in PBS at room temperature for overnight with agitation until the otoliths were completely dissolved. The larvae were sequentially washed in PBSTx and incubated with Alexa Fluor 488 Phalloidin (1:50) (Thermo Fisher Scientific, CA, USA) in PBSTw (1% PBS, 0.1% Tween-20) at room temperature for 4 h. The samples were washed in PBSTx after staining and mounted laterally in 75% glycerol on slides. Images were acquired with a Zeiss LSM-710 Confocal microscope.

To perform the acoustic evoked behavioral response (AEBR) test, 6 dpf larvae were placed in a 48-well plate with 200 μ L embryo water and placed in a Zebrabox (View-Point Life Sciences) and embryos were adapted in the dark for 15–30 min (until spontaneous movements were less frequent). The embryos were subjected to a 100 ms, 1 kHz pure tone at 100% target power every 20 s for 4 min (12 stimuli) in the dark. The Zebrabox recorded the animals using infrared light and measured the activity as pixel changes over time. The burst threshold was set at 50 pixels, the freeze threshold set at 10 pixels, and sensitivity was set at 20 pixels. Movement over the 50 pixel burst threshold within the 2 s after stimulus was considered an evoked response. Responses were excluded if the larvae had spontaneous movement within the 2 s before the stimulus. All responses for a larva were excluded if they had spontaneous movement before 6 or more of the stimuli. The response rate was calculated by how many times an embryo had an evoked response out of the total number of stimuli and converted to a percentage.

Production and phenotyping of clarin 2 deficient mutant in mice

The *Clnr2*^{del629} mutant line was generated on a C57BL/6N background by the Molecular and Cellular Biology group at the Mary Lyon Centre (MLC), MRC Harwell Institute, using CRISPR/Cas9 genome editing (Dunbar et al. 2019). The mice were housed and maintained under specific pathogen-free conditions in individually ventilated cages, with environmental conditions as outlined in the Home Office Code of Practice. Animals were housed with littermates until weaned, and then housed with mice of the same sex and of similar ages, which was often their littermates. Both male and female animals were used for all experiments. Animal procedures at the MRC Harwell Institute were licenced by the Home Office under the Animals (Scientific Procedures) Act 1986, UK and additionally approved by the Institutional Animal Welfare and Ethical Review Body (AWERB). The *Clnr1*^{-/-} mice (*Clnr1*^{tm1.2Ugpa}, MGI: 6099052) used for comparative scanning electron microscopy analyses were previously described (Dulon et al. 2018).

To screen mice for auditory phenotypes and investigate auditory function, Auditory Brainstem Response (ABR)

tests (measured using a click stimulus and frequency-specific tone-burst stimuli (at 8, 16 and 32 kHz) and Distortion Product Oto-Acoustic Emission (DPOAE) tests (measured using frequency-specific tone-burst stimuli from 8 to 32 kHz with the TDT RZ6 System 3 hardware and BioSig RZ software (Tucker Davis Technology, Alachua, FL, USA)) were performed as described in Dunbar et al., 2019. For scanning electron microscopy imaging, fixed inner ear samples were processed by the osmium tetroxide/thiocarbohydrazide (OTOTO) method, as previously described (Dulon et al. 2018; Dunbar et al. 2019). Samples were visualized with a JSM-6010LV Scanning Electron Microscope (JEOL). Micrographs were pseudo-coloured in Adobe Photoshop.

Statistical analysis

To compare the *clnr2* mRNA expression in zebrafish, data are presented as mean values \pm standard deviation (SD). Statistical analysis was performed using GraphPad Prism version 8.4 (GraphPad Software, San Diego, CA, USA). The significance level was set to 0.05. The *p* value was determined using a two-tailed unpaired Student's *t*-test for RT-qPCR of *clnr2* mRNA expression, and a two-tailed unpaired nonparametric Mann–Whitney *U* test for AEBR analysis. The statistical significance is represented in the figures as ****p* < 0.001.

To assess ABR thresholds and DPOAE responses in the *Clnr2*^{del629} mice, one-way ANOVA statistical tests were used. Each frequency was tested for statistical significance separately. A threshold of *p* > 0.05 was used to determine if differences were statistically significant. Statistical significance is represented in the figure as follows: ****p* < 0.001. All data shown are mean \pm SD, and all statistical analyses was performed in GraphPad Prism.

Results

Identification of CLRN2 as a novel deafness gene in a consanguineous Iranian family exhibiting autosomal recessive non-syndromic sensorineural hearing loss

A three generation Iranian family of Lurs ethnicity was ascertained as part of a large ethnically diverse Iranian population rare disease study (Fig. 1a). Three individuals that included the proband (IV-6), his sibling (IV-1), and a cousin (IV-8), born from consanguineous marriages, have reported moderate-to-profound bilateral non-syndromic sensorineural hearing loss (Fig. 1b). The age of onset for these three individuals was between 2 and 3 years of age. Pure-tone air- and bone-conduction audiometry thresholds (Fig. 1b) show evidence of intrafamilial variability. Individual IV-1

has a down sloping audiogram, with bilateral moderate-to-profound deafness. Individual IV-6 presented a moderate-to-severe hearing loss with slightly better hearing at higher frequencies. Both individuals showed normal (type A) tympanograms bilaterally. Speech recognition thresholds for individual IV-1 were 80 and 75 dB at 84 and 88% for right and left ears, respectively, and a most comfortable level of 95 dB. Speech recognition thresholds for individual IV-6 were 75 and 80 dB, each at 84%, for right and left ears, respectively. Patients have normal neuromotor, speech and language development, and did not show signs of impaired balance. No other abnormalities, including potential vision deficit, were present in the affected individuals, who were last evaluated at the age of 29 (IV-1), 44 (IV-6), and 25 (IV-8) years. For comparison, pure-tone audiometry was also recorded from a family member (V-1), with no reported history of hearing deficits.

To identify the underlying genetic lesion, genome-wide linkage analysis identified one single significant maximum LOD score of 3.8 on chromosome 4 (Supplementary Fig. S1a–b). Linkage analysis and haplotyping with the dense marker set showed the adjacent markers rs7690593 and rs608053 (GRCh37/hg19, chr4: 17,298,007–32,261,222 bp, hg19). The homozygous region spans 14.96 Mb and overlaps with the *CLRN2* gene position (Fig. 1c). As a second independent method, we applied homozygosity mapping in the extended family to identify a 15.2 Mb locus on chromosome 4p15.32p15.1 (GRCh37/hg19, chr4:17,298,445–32,495,165), defined by the SNPs rs7692897 and rs17081424 (Supplementary Fig. S1c, Supplementary Table S2) that mirror the linkage results. This locus contains 30 genes, none of which are presently associated with deafness in humans (Supplementary Table S2). This approach also revealed four much smaller homozygous intervals on chromosomes 2p21 (137.3 kb), 3p22.2 (262.5 kb), 13q13.1 (90.7 kb), and 17q21.31 (292.6 kb) (Supplementary Fig. S1c, Supplementary Table S2) that do not contain known deafness-associated genes (Supplementary Table S2). Pathogenic copy number variations were excluded. Next, we undertook exome sequencing of affected individual IV-6 (arrow, Fig. 1a). This generated 56,387,543 mappable reads, with 75.5% on-target reads. The mean depth was 57.3-fold, with 97.3% of regions with a tenfold read depth. Analysis of the exome data of individual IV-6 excluded any candidate pathogenic variants in known deafness-associated genes (Doll et al. 2020) prompting an exome-wide analysis followed by filtering and re-analysis of variants in homozygous intervals (Supplementary Table S3). Further, close inspection of the exome sequencing data revealed complete sequencing coverage of genes in the homozygous intervals (Supplementary Table S4). Variant filtering detected a single homozygous missense variant in *CLRN2* c.494C > A, (p.(Thr165Lys)) (NM_001079827.2) in the linked and

homozygous interval on chromosome 4 (Supplementary Fig. S1a–c). This variant was shared with individual IV-1 and segregated in the extended family comprising a total of 14 individuals (Fig. 1a, d) and was the only remaining variant in the locus fulfilling variant filtering criteria. Only individuals homozygous for the *CLRN2* c.494C > A variant exhibit hearing loss confirming the recessive nature of the allele (Fig. 1a). This variant fulfills ACMG criteria for classification as likely pathogenic (PM2_Moderate, PP1_Strong, PP3_Supporting).

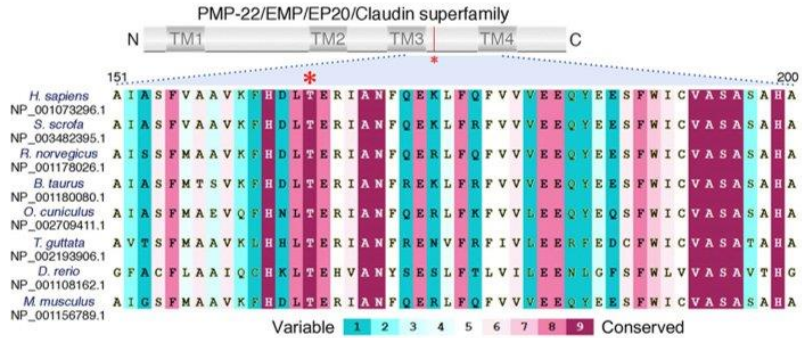
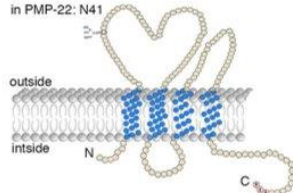
The *CLRN2* c.494C > A leads to a likely pathogenic missense substitution and aberrant splicing

The c.494C > A variant on chromosome 4p15.32 is unanimously predicted to be deleterious and disease causing by in silico tools (Supplementary Table S5). The c.494C > A variant in *CLRN2* replaces a polar uncharged amino acid (threonine) with a positively charged amino acid (lysine) in clarin 2, (p.(Thr165Lys)) (Creixell et al. 2012). This variant, as well as homozygous loss-of-function alleles, are absent in population frequency databases. This suggests *CLRN2* is intolerant to biallelic loss-of-function. Our in-house collection of 89,041 additional exomes/genomes, including a multiethnic cohort of 842 exomes from probands with autosomal recessive hearing loss, identified four individuals from three families of Iranian, Turkish, and Emirati ethnicities, who carried the *CLRN2* c.494C > A variant (allele frequency 2.24×10^{-5}). An Iranian hearing impaired individual was included among the carriers.

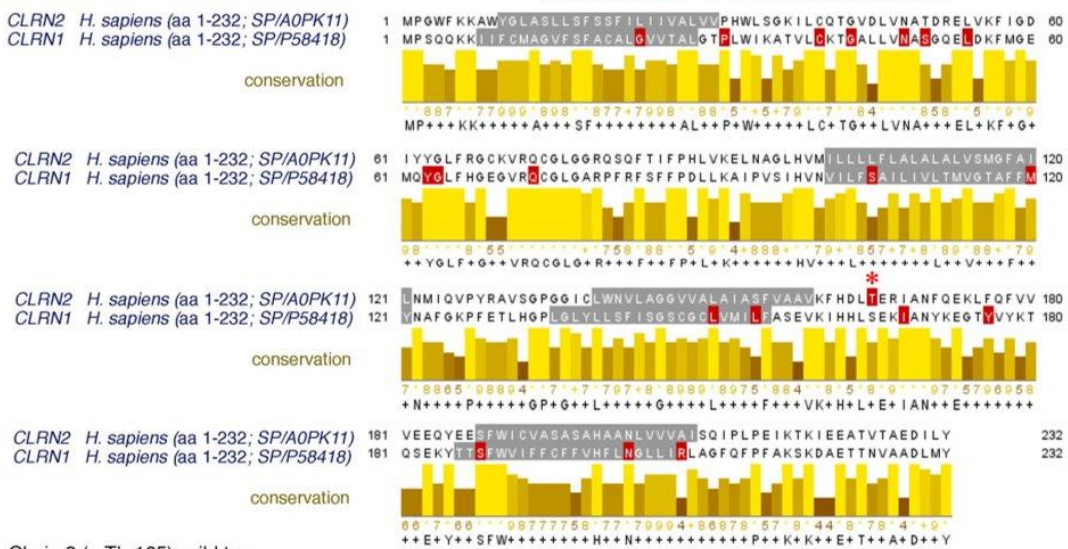
The c.494C > A variant involves the exchange of a novel polar threonine (Thr) residue to a basic lysine (Lys) amino acid that affects a highly conserved amino acid in the alpha-helix of the PMP-22/EMP/MP20/Claudin superfamily domain (Fig. 2a–c). Among clarin proteins, clarin 2 and clarin 1 show 34.9% identity with 81 identical and 91 similar amino acids (using UniProt (UniProt Consortium 2018), Fig. 2b). The outcome of *CLRN1* pathogenic or likely pathogenic missense variants, as well as nonsense variants (queried from the Deafness Variation Database v8.2 (Azaiez et al. 2018)) are marked in red (Fig. 2b) along with the clarin 2 p.(Thr165Lys) amino acid substitution (Fig. 2b, asterisk). Interestingly, nine out of the 19 clarin 1 amino acid mutated residues are identical in clarin 2. Three clarin 1 amino acid substitutions (p.(Leu163Pro), p.(Leu167Trp), and p.(Ile181Asn), NP_001182723.1) align in close proximity to the clarin 2 p.(Thr165Lys). Furthermore, clarin 1 p.Leu163Pro (Fields et al. 2002) and p.Ile181Asn (García-García et al. 2012), that are both reported in USH3A, are p.Leu150 and p.Ile168 in clarin 2. Most importantly, the threonine residue at position 165 (Thr165) *CLRN2* is conserved across species and the corresponding amino acid in clarin 1 is a serine residue (Fig. 2a–b), a scenario often

A The tetraspan-like clarin proteins

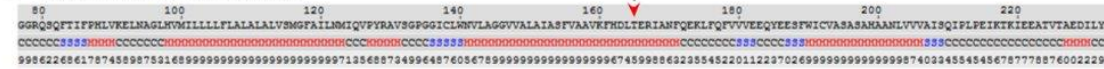
Glycosylation at asparagine:
 in Clarin 1 and Clarin 2: N48
 in Clarin 3: N83
 in PMP-22: N41



B



C Clarin 2 (p.Thr165): wild type



Mutant Clarin 2 (p.Thr165Lys): normally spliced variant



Fig. 2 Conservation of the p.Thr165 residue, and clarin 1/clarin 2 alignment. **a** Overview of clarin 2 protein and modular structure of the PMP-22/EMP/EP20/Claudin superfamily, with amino acid residue coordinates and position of the p.(Thr165Lys) substitution shown (upper panel). An alignment of the amino acid sequences from the segment of clarin 2 (represented by dashed lines) from vertebrate species shows the Thr165 position (asterisk) is well conserved among vertebrates. **b** Alignment of clarin 2 (UniProtKB: A0PK11, upper alignment) and clarin 1 (UniProtKB: P58418, lower align-

ment) amino acid residues. Transmembrane domains are marked in grey, conservation is shown in yellow, and consensus sequences are shown below for the 232 amino acid proteins. Missense and nonsense variants in clarin 1 (Deafness Variation Database v8.2) and clarin 2 (present study, asterisk) are marked in red. **c** The predicted secondary structure of human clarin 2 (NP_001073296.1) wild-type (Thr165) and mutated (Thr165Lys) protein. H represents alpha-helix, S represents beta-strand and C represents coil

associated with conserved phosphorylation site residue, here by serine/threonine protein kinases (Creixell et al. 2012).

In addition to causing an amino acid missense substitution, computational analysis also predicts that the c.494C > A variant will create an exonic splicing enhancer

(ESE) motif, modifying the ESE hexameric sequence landscape of exon 3, which could interfere with the normal processing of *CLRN2* mRNA (Figs. S2a–b; ESEfinder and RESCUE-ESE, Human Splicing Finder) (Cartegni et al. 2003; Desmet et al. 2009; Fairbrother et al. 2004). To investigate

the effect of the c.494C>A variant on *CLRN2* splicing, we used mini-gene assays using two different exon-trapping vectors and three different cell lines, Cos-7, ARPE-19, and HEK 293 T. The mini-gene contained the 3' end of intron 2, all of exon 3 (with and without the *CLRN2* variant), and ~50 bp of the 3' UTR (Fig. 3a) and was transfected into COS-7 and ARPE-19 cells. As a negative *CLRN2* control, we used the rs117875715 SNP, a common polymorphism, with a global MAF of ~1.25% and >100 homozygous alleles reported in

gnomAD (Lek et al. 2016) (<http://gnomad.broadinstitute.org/variant/4-17528480-G-A>) that is 20 nucleotides away from c.494C>A. Given its frequency, rs117875715 is predicted to be benign for hearing loss. Of note, this polymorphism is absent in the proband and family members reported here. Since exon 3 is the last exon of *CLRN2*, we designed our PCR primers to exclude the human poly-A signal and used the poly-A signal native to the pET01 vector. As expected for WT *CLRN2* (c.494C), we detected the splicing of the 5'

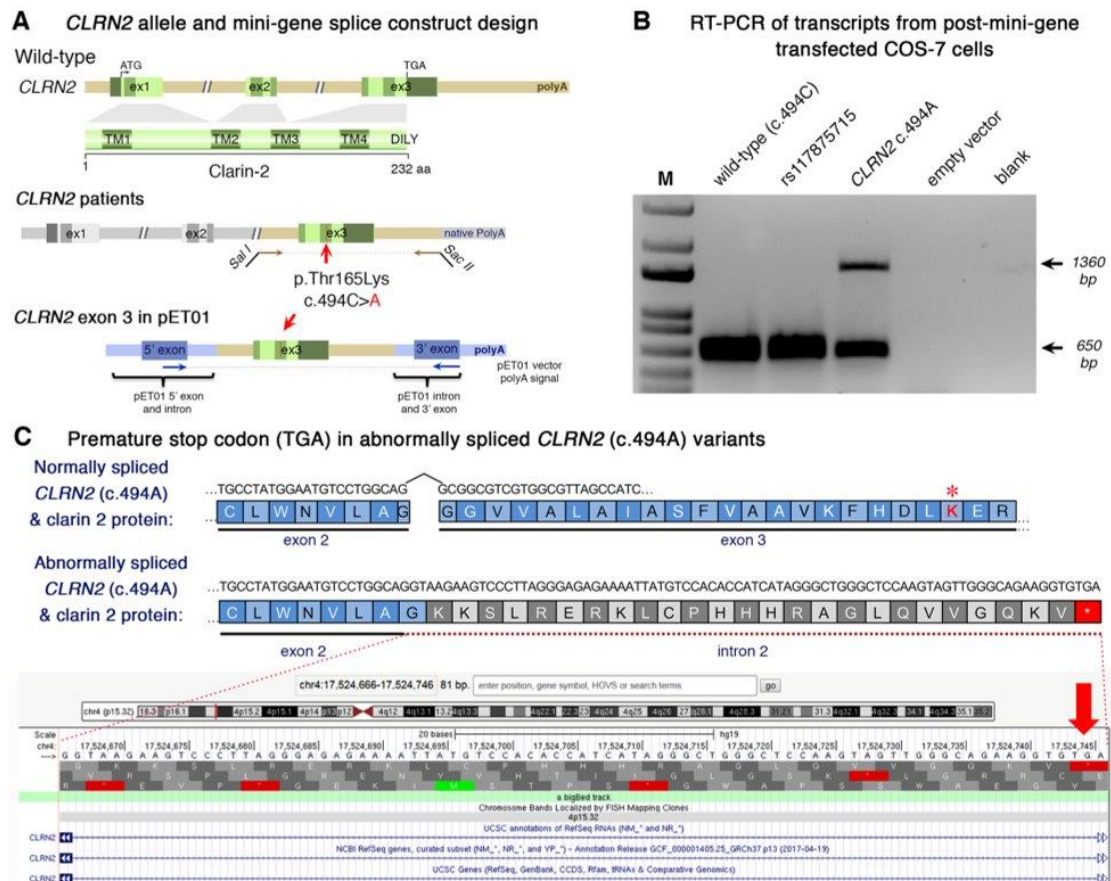


Fig. 3 Analysis of the *CLRN2* c.494C>A variant on splicing. **a** Schematic illustration of the mini-gene splice construct design. Genomic representation of *CLRN2*, including the position of the missense variant c.494C>A (arrow) on exon 3 with 3' UTR (green), and the 5' UTR, as well as exons 1 and 2 (grey) (upper panel). Regions captured by mini-gene PCR primers are represented in brown. Schematic illustration of the mini-gene splice construct including exon 3 and its flanking sequence (green) cloned into multiple cloning sites (*SacI* and *SacII* sites) of pET01 backbone vector (lower panel). Blue boxes represent native exons of the pET01 vector. **b** RT-PCR of transcripts from post-mini-gene transfected COS-7 cells. Amplicons derived from the transcripts of WT (*CLRN2*), a benign *CLRN2* polymor-

phism (rs117875715, chr4(GRCh37):g.17,528,480G>A), the *CLRN2* c.494C>A variant and a negative control, were visualized on a 1.5% agarose gel. The SNP, rs117875715, was used to test and validate the designed WT and mutant mini-gene assay. The ~650 bp amplicon was associated with the WT and validation control rs117875715. The amplicon derived from the *CLRN2* c.494C>A transcripts showed two bands: a 650 bp band and a larger ~1360 bp band, indicating retention of intron separating the donor site of the 5' exon and the acceptor site of *CLRN2* exon 3. **c** Retention of intron in *CLRN2* c.494C>A mini-gene results in a stop codon (TGA) after *CLRN2* exon 2

native pET01 exon only to exon 3 of *CLRN2* (Fig. 3a–b). The same normal splicing was obtained in all cell types transfected with *CLRN2* containing the control (rs117875715) variant (Fig. 3b). However, the c.494C>A variant yielded two bands; one ~650 bp band matching the expected normally spliced exon, and a second abnormal band that was approximately ~1360 bp (Fig. 3b). Sequencing of these amplicons validated normal splicing including the c.494A variant and also revealed a retained intron 2 in the aberrantly spliced transcript (Supplementary Fig. S3c). The retention of intron 2 results in a new reading frame that introduces a stop codon 26 amino acids after the native exon 2 splice site (p.(Gly146Lysfs*26)) (Fig. 3c). These results were replicated using the pSPL3b vector and HEK 293 T cells (Supplementary Fig. S3a–c), confirming the c.494C>A induced normal and aberrant splicing, independent of the cell type context. Following TA-cloning of cDNA amplicons from the homozygous individual (from Supplementary Fig. S3b), 23 of 26 amplicons (88.5%) showed normal splicing, and 3 of 26 amplicons (11.5%) showed a retained intron.

The mini-gene splicing assays and sequence analyses clearly show that the c.494C>A affects a highly conserved and key residue in clarin 2 sequence, while also creating aberrant mRNA splicing in vivo likely leading to a truncated protein. Altogether, this further confirms that variants in *CLRN2* can lead to sensorineural hearing loss.

***Clrn2*, a hair cell expressed gene key to hearing also in zebrafish and mice**

To further study the role of clarin 2 in the inner ear, we investigated its expression and analyzed potential impact of *Clrn2* loss-of-function in two other species, zebrafish and mice.

***clrn2* in zebrafish**

Taking advantage of larva transparency, we used zebrafish as a model to investigate the *clarin 2* expression during early embryonic development. The RT-qPCR at different developmental stages revealed that *clrn2* mRNA was first detected at 18 hpf (Fig. 4a), a stage when the otic placode begins to form the otic vesicle in zebrafish (this stage is similar to mouse embryonic day 9 (E9), a stage of otic placode formation) (Kopecky et al. 2012; Whitfield et al. 2002). *clrn2* mRNA expression increased (twofold at 72 and 96 hpf compared to 18 hpf) and was maintained at later stages, up to 120 hpf (Fig. 4a). Comparative analyses of *clrn2* mRNA expression in different adult tissues of zebrafish revealed a significant enrichment in utricle, saccule and lagena of the inner ear (Fig. 4b). Our data are in agreement with RNA expression data from the Genotype-Tissue Expression (GTEx) project, wherein *CLRN2* mRNA in humans is enriched in the nervous

system, testis, kidney, salivary gland, and lung. *CLRN1* has a similar expression profile in humans.

To determine *clrn2* cellular expression, we used WISH in the inner ear of 3 and 5 dpf embryos (Fig. 4c–d). Unlike the *clrn2* sense probe, the anti-sense *clrn2* revealed strong expression in the otic vesicle, similar to the expression of anti-sense *pvalb9*, used as a marker of hair cells (Fig. 4c). Histological examination of 5 dpf embryos further confirmed that *clrn2* expression is more specifically, restricted to hair cells, and is not expressed in the supporting cells of the inner ear (Fig. 4d).

To elucidate the function of *clrn2* in zebrafish, we used CRISPR/Cas9 to generate loss-of-function alleles. To maximize the knockout efficiency, we used five sgRNAs targeting the first and second exon of *clrn2* gene (Supplementary Fig. S4). Injected embryos (crispants) were sequenced and, as expected, a mix of alleles in the form of deletions ranging from 4 to 73 bp, as well as insertions spanning +1 to +11 bp were observed. The majority of the variants were frameshift that would most likely create a premature stop codon in the protein (Supplementary Fig. S4). The RT-qPCR analyses on injected embryos showed that *clrn2* crispants have a significantly reduced amount of *clrn2* mRNA (Fig. 4e), suggesting nonsense mediated decay, leading to disrupted clarin 2 protein function.

To test acoustic responses, we performed the AEBR analysis. The *clrn2* crispants showed significantly reduced response after sound stimulation (Fig. 4f) compared to the control animals, indicating a hearing loss phenotype. Considering *clrn2* expression in hair cells (Fig. 4d), we investigated the architecture of their mechanosensory hair cell bundles, which are important for hearing and balance function in zebrafish. Interestingly, fluorescent phalloidin staining of the hair bundles of the inner ear in *clrn2* crispants ($n=10$) showed disrupted hair bundle structure and fewer hair cells compared to the WT controls (arrowheads in Fig. 4g). This defective phenotype, suggesting a critical role in hair bundle structures, is similar to the hair bundles in zebrafish *clrn1* knockouts (Gopal et al. 2015), the *orbiter* mutants (defective in *protocadherin 15* (*pcdh15*), a gene associated with human Usher syndrome 1F) (Seiler et al. 2005) and *ush1c* morphants and *ush1c* mutants (Phillips et al. 2011).

***Clrn2* in mice**

To further assess the requirement of clarin 2 for auditory function in mammals, and assess further its role in auditory hair bundles, we extended our analyses to mouse. Consistent with expression data in zebrafish (Fig. 4a, c–d), single cell RNA-seq data available to visualize on the gEAR portal (umgear.org) show that in the mouse cochlear epithelium at postnatal day 1 (P1) and P7, *Clrn2* transcripts are almost exclusively detectable only in inner and outer

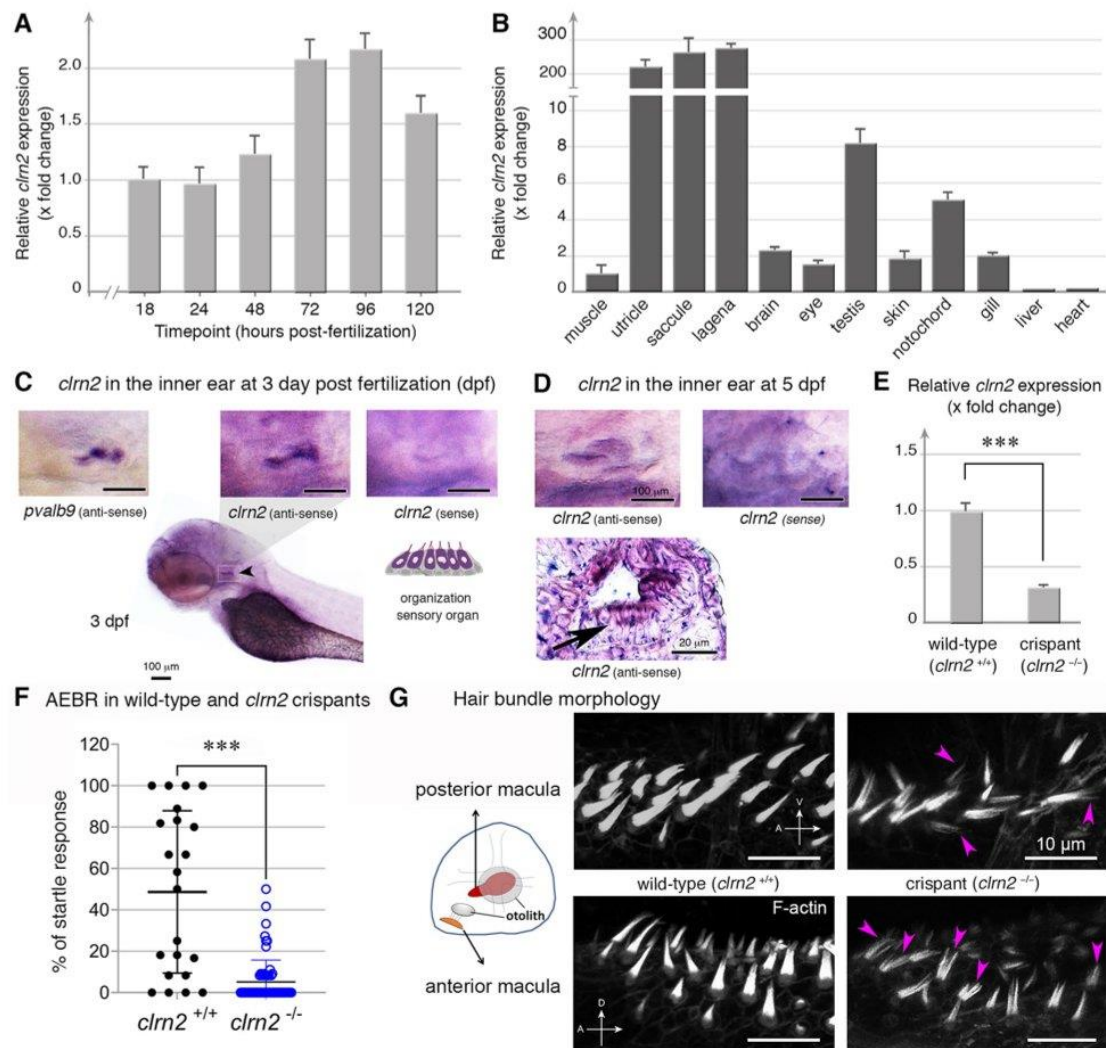


Fig. 4 Clarin 2 is required for the inner ear function in zebrafish. **a** RT-qPCR of *clrn2* mRNA expression from 1 to 120 hpf of WT embryos/larvae. *clrn2* mRNA expression can be detected starting from 18 hpf and then increased throughout development. Data shown are mean \pm SD and compared to 18 hpf. **b** RT-qPCR of *clrn2* mRNA expression in different adult tissues. Data shown are mean \pm SD and compared to muscle. **c–d** Whole-mount in situ hybridization (WISH) using antisense *clrn2* probe reveals the inner ear expression of *clrn2* mRNA (relative dark purple color, black arrowhead) at 3 (c) and 5 (d) dpf embryos. Sense *clrn2* probe was used as negative control and relative light purple color is considered as background. *clrn2* mRNA was consistently expressed in hair cells within inner ear macula (c–d) with lined and arrayed structure. A known hair cell marker *pvalb9* was used as an indicator for hair cells in the inner ear of 3

dpf embryos (c). Cryosection was performed after *clrn2* WISH at 5 dpf to confirm the small patch of signal on the macula is from hair cells rather than supporting cells (d, black arrow lower panel). Scale bar = 100 μ m, except lower panel in D (20 μ m). **e** RT-qPCR of *clrn2* mRNA expression level was decreased 70% in *clrn2* crispants compared to uninjected larvae, indicating *clrn2* was successfully knocked out ($p = 2.06E-06$). Data shown are mean \pm SD. $***p < 0.001$, two-tailed unpaired Student's *t* test. **f** Acoustically evoked behavioral responses (AEBR) in *clrn2* wild type and crispants reveal significant reduction of sound induced responses. **g** Phalloidin staining on *clrn2* crispants show that the hair cells in the inner ear anterior and posterior maculae display splayed, thin and split structures (purple arrowheads). A, anterior to the left. D, dorsal to the top. V, ventral to the top. Scale bar = 10 μ m

hair cell populations (Kolla et al. 2020) (see also Supplementary Fig. S5). We utilized a CRISPR/Cas9-engineered *Clrn2* mouse mutant, in which exon 2 has been deleted (*Clrn2^{del629}*) (Fig. 5a). While this deletion leaves exon 3 in-frame with exon 1, exon 2 encodes two of the transmembrane domains present in the tetraspan clarin 2 protein (lower panels Fig. 5a), and is therefore expected to severely affect protein function. In a preliminary work focused on *clarinet* mice, which display a nonsense *Clrn2* mutation, p.(Trp4*), we showed that addition of the *Clrn2^{del629}* allele

into the *clarinet* background, *Clrn2^{clarinet/del629}*, was unable to complement the *clarinet* allele causing hearing loss in these mice, indicating *Clrn2^{del629}* is also a loss-of-function allele (Dunbar et al. 2019). Here, we provide the first morpho-functional characterization of *Clrn2^{del629/del629}* mice, which, unlike the previously reported *clarinet* mice, are congenic on the C57BL/6N background, and measured ABRs in P21 (± 1 day) mice in response to click and tone-burst stimuli.

Analysis of ABR thresholds, which is the lowest sound stimulus required to elicit measurable activity in the auditory

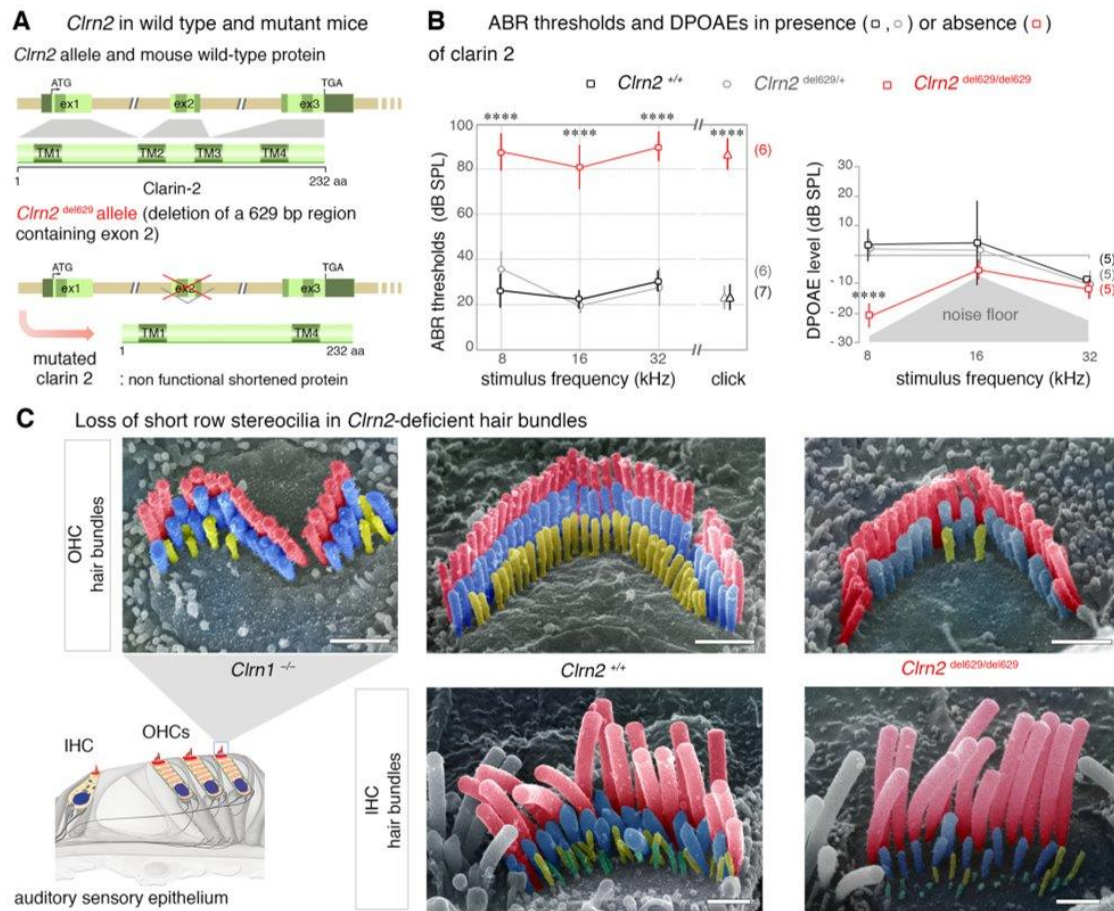


Fig. 5 Clarin 2 is required for hearing function in mouse. **a** The genomic structure of mouse *Clrn2* (ENSMUST00000053250), and domains of the encoded tetraspan-like glycoprotein (232 amino acids). The positions of the transmembrane (TM) domains (dark green) and the structures of the WT *Clrn2* and *Clrn2^{del629}* alleles are indicated. Deletion of exon 2 leads to a shortened clarin 2 lacking the two central transmembrane domains. **b** ABR threshold measurements at P21 (± 1 day) show that *Clrn2^{del629/del629}* mice (red) exhibit a severe-to-profound hearing loss affecting all frequencies tested, with thresholds at 80 dB SPL and beyond. Age-matched *Clrn2^{+/+}* (black) and *Clrn2^{del629/+}* (grey) controls display thresholds within the expected range (15–40 dB SPL). Averaged DPOAE

responses at P28 (± 1 day), showing significantly reduced responses in *Clrn2^{del629/del629}* mice. Data shown are mean \pm SD. $**p < 0.001$, one-way ANOVA. **c** Pseudo-colored scanning electron micrographs illustrate the three full rows, tallest (red), middle (blue) and short (yellow), of P28 (± 1 day) stereocilia in IHC and OHC hair bundles. Unlike the fragmented hair bundle in *Clrn1^{-/-}* mice, lack of clarin 2 does not affect the shape of IHC or OHC hair bundles. However, all the short row stereocilia have completely or partially regressed in the absence of either clarin protein. Scale bar = 1 μ m

nerve, showed that homozygous (*Cln2*^{del629/del629}) mice display very elevated thresholds (> 80 decibel sound pressure level (dB SPL)) at all frequencies tested: 8, 16 and 32 kHz (Fig. 5b). Whereas, *Cln2*^{del629/+} mice exhibit thresholds comparable with those of WT (*Cln2*^{+/+}) littermates (< 40 dB SPL), demonstrating the absence of a heterozygous auditory phenotype (Fig. 5b).

To further assess cochlear function, DPOAEs were measured in P28 (± 1 day) *Cln2*^{del629/del629} mice. Compared to their *Cln2*^{+/+} and *Cln2*^{del629/+} littermates, *Cln2*^{del629/del629} mice have reduced DPOAEs (Fig. 5b) suggesting impaired outer hair cell (OHC) function.

To investigate stereocilia bundle morphology in *Cln2*^{del629/del629} mice, we used scanning electron microscopy to examine the cochlear sensory epithelia. At P28 (± 1 day), the inner and outer hair cell stereocilia bundles of *Cln2* mutant mice display the expected U- and V-shape, respectively, which contrasts with the grossly misshapen OHC bundles found in *Cln1* mutant mice (Fig. 5c). However, while the patterning of the bundles appears normal in *Cln2*^{del629/del629} mice the heights of their middle and short row stereocilia are visibly more variable compared with those of *Cln2*^{+/+} littermates, and many of the short row ‘mechanotransducing’ stereocilia are missing (Fig. 5c).

Together, our findings establish that clarin 2 is key to hearing function in zebrafish and mouse, supporting that this protein has an evolutionary conserved role in the maintenance of hair bundle architecture in fish and mammals.

Discussion

We identify *CLRN2* as a novel deafness gene in human and zebrafish and describe a new deafness-causing allele in mice. Genetic study using gene mapping and exome sequencing of an extended Iranian family with multiple consanguineous marriages identified a pathogenic variant, c.494C>A in exon 2 of *CLRN2* segregating with pre-lingual ARNSHL. Due to restricted expression of *CLRN2* in accessible tissues such as blood or saliva, we performed in vitro splice analysis. The c.494C>A variant results in a missense and splicing defect in clarin 2. By producing mutant zebrafish and mice lacking clarin 2, we demonstrated the key role the protein plays to ensure normal structural and functional integrity of the hair bundle, the sound- and motion-receptive structure of inner ear hair cells.

The clarin gene family also includes the *CLRN1* gene. Pathogenic variants in *CLRN1* have been linked to variable clinical outcomes, ranging from non-syndromic RP (Khan et al. 2011) to USH3A characterized by variable and progressive post-lingual hearing loss, RP, and variable vestibular responses (Plantinga et al. 2005). Several cases of later onset HL and/or RP, as late as the sixth decade of life, have

been reported for USH3A patients (Ness et al. 2003). Clinical examination of affected individuals in this family, at the age of 25 (IV-8), 29 (IV-1), and 44 (IV-6) years of age, excluded the presence of additional syndromic features showing that homozygosity for the c.494C>A variant causes non-syndromic hearing loss, ranging from moderate-severe (IV-6) to profound (IV-1) deafness. In regard to the observed progressivity of the hearing impairment in *clarinet* mice (Dunbar et al. 2019), the earliest reported clinical diagnosis of hearing loss of the *CLRN2* affected individuals in the family we present is between 2 and 3 years of age. Newborn hearing screening was not routinely performed when the affected individuals were born, so we cannot confirm hearing was normal at birth. In light of absent serial audiograms, we cannot report if the hearing loss experienced in these patients is progressive, as is observed in the mouse model (Dunbar et al. 2019). So far, we could not identify, through our current network, additional families with *CLRN2* variants. Featuring *CLRN2* as a new human deafness gene, future genetic screenings of hearing impaired families worldwide will probably unveil additional *CLRN2* families and provide important clues about associated clinical phenotype progression and severity.

Our data showed that the *CLRN2* c.494C>A variant probably affects protein function in two ways: (1) as a missense variant (p.(Thr165Lys)) producing a mutant full length protein and (2) as a splice variant leading to intron retention (Fig. 3b, and Supplementary Fig. S3b–c) expected to cause a premature stop codon 26 amino acids into intron 2 (p.(Gly146Lysfs*26)).

In normally spliced *CLRN2* transcripts, the c.494C>A variant affects an amino acid that is highly conserved among PMP-22/EMP/EP20/Claudin superfamily proteins. Two potential mechanisms could synergistically contribute to the disruptive effect of the missense variant. *First*, the replacement of threonine with lysine, an amino acid with a positively charged ‘bulky’ side chain (lysine), may affect protein folding (Creixell et al. 2012) and transport to the plasma membrane. Membrane proteins sort to the plasma membrane via the conventional secretory pathway associated with ER-to-Golgi complex (Viotti 2016). Misfolded membrane proteins are typically retained in the endoplasmic reticulum (ER) and degraded by the ER-associated degradation pathway (Kincaid and Cooper 2007; Sano and Reed 2013). It is possible that a small fraction of the misfolded clarin 2 p.(Thr165Lys) could reach the plasma membrane via the unconventional secretory pathway, similar to that reported for clarin 1 p.(Asn48Lys) (p.(N48K)) (Gopal et al. 2019). The unconventional secretory pathway is induced by the ER-associated misfolded or unfolded protein response (Kinseth et al. 2007; Schröder and Kaufman 2005). However, the mutant clarin 2 reaching the surface may be functionally inactive. *Second*, evolutionarily conserved threonine residues are also conserved protein phosphorylation

sites. Phosphorylation adds a negative charge to the side chain of the amino acid and it serves as an important post-translational mechanism for regulation of protein function (Pearlman et al. 2011). Loss of threonine at position 165 would potentially prevent functional activation of clarin 2. As our attempts to discriminate impact of the amino acid substitution in a human cell line yielded no conclusive results (KNA, unpublished data), additional experiments in an in vivo context are essential to test these hypotheses and unravel the true pathogenic mechanism associated with the p.(Thr165Lys) missense variant.

With respect to the aberrantly spliced *CLRN2* transcripts, variants that disrupt splicing machinery signals are recognized as significant contributors to human genetic diseases (Xiong et al. 2015), with variants shown to impact accurate recognition and removal of intronic sequences from pre-mRNA (Fairbrother et al. 2004). ESE sequences are cis-acting elements primarily recognized by the SR family proteins that function by recruiting core splicing machinery components to splice sites or by acting antagonistically against nearby silencing elements (Fairbrother et al. 2004; Graveley 2000; Kan and Green 1999). ESEs are often associated with introns that contain weak splicing signals, but they can also reside in exons and impact the splicing process. Using mini-gene assays in human cell lines, we could show that the *CLRN2* variant-induced aberrant splicing amounts to 10–15%, but its occurrence and rate in a biological context remains to be established. We, however, expect that the partial (only 3 out of 4 TM domains) and truncated (lack of C-terminal region) protein resulting from aberrant splicing due to *CLRN2* c.494C>A variant is non-functional. Indeed, the integrity of all 4 TM domains seems to be necessary for a functional clarin tetraspan protein. This is supported by our data in *Clrn2*^{del629/del629} mice where transcripts lacking exon 2 do exist, but if translated would result in a predicted protein lacking the two central transmembrane domains. The severe hearing loss observed in these *Clrn2*^{del629/del629} mice clearly indicate that such partial clarin protein is insufficient to ensure normal hearing.

Repeated attempts to detect endogenous clarin 2 in the inner ear, under various conditions of fixation and antigen-retrieval at different postnatal stages were unsuccessful. We therefore used in situ hybridization in zebrafish and in silico analyses in mouse to confirm predominant expression of *Clrn2* in the sensory hair cells. To examine further the key role of clarin 2 in the inner ear, we generated zebrafish and mice lacking a functional protein. ABR measurements in *Clrn2*^{del629/del629} mice revealed an early-onset hearing loss with elevated hearing thresholds compared with their *Clrn2*^{+/+} littermate controls (mean click threshold 87 dB SPL \pm 7 s.d. and 24 dB SPL \pm 6 s.d., respectively). These data are consistent with early-onset hearing loss observed in another loss-of-function *Clrn2* mutant (*Clrn2*^{clarinet}), which harbors an early truncating nonsense variant (p.Trp4*)

(Dunbar et al. 2019). However, comparison with the previously reported *Clrn2*^{clarinet} P21 ABR data suggests that the extent of hearing loss in age-matched *Clrn2*^{del629} mice is more severe and less variable, which is most evident in the click ABR measures (80 \pm 15 dB SPL and 87 \pm 7 dB SPL, respectively). This difference could be due to strain effect, with the *Clrn2*^{clarinet} mice being on a C57BL/6J background and the *Clrn2*^{del629} mice being on the related but distinct, C57BL/6N (Simon et al. 2013). Interestingly, startle response measurements in *clrn2* zebrafish crispants also reveal significant reduction in sound-induced responses. This, together with the severe-to-profound hearing loss already exhibited at P21 and the reduced DPOAEs in both *Clrn2*^{del629/del629} and in *Clrn2*^{clarinet/clarinet} mice (Dunbar et al. 2019) points to gene defects likely affecting both inner hair cells (IHCs) and OHCs. This is further supported by scanning electron microscopy data showing loss of shortest row stereocilia in both the cochlear IHCs and OHCs. Phalloidin staining of *clrn2* crispants also confirms hair bundle abnormalities in zebrafish. The loss of the mechanotransducing stereocilia, here the short stereocilia row in *Clrn2*^{del629/del629} and in *Clrn2*^{clarinet/clarinet} mice is similar to that observed in hair cells defective for components of the mechano-electrical transduction machinery. Electrophysiological recordings in OHCs of clarinet mice did indeed show that lack of clarin 2 causes significant reduction in hair cell mechano-electrical transduction activity (Dunbar et al. 2019). However, whether the loss of short row stereocilia is a downstream consequence of defective MET activity or due to yet unknown structural changes in the stereocilia remains to be established.

In conclusion, we demonstrate the c.494C>A variant affects exon 3 splicing efficiency. We showed, for the first time, that *CLRN2* is a deafness-causing gene in humans. A variant causes hearing loss in humans, replicated by animal studies. Additional reports of families segregating *CLRN2* biallelic variants will be crucial to refine and dissect the clinical course and characteristics of hearing loss due to this gene. Together, our studies in zebrafish and mice establish that hearing loss is probably due to defective protein in the hair cells, where the presence of clarin 2 is essential for normal organization and maintenance of the mechanosensitive hair bundles.

Acknowledgements We would like to extend our gratitude to the family for their participation. We thank Dr. Caroline Lekszas, Dr. Daniel Liedtke, and Dr. Indrajit Nanda from the Institute of Human Genetics at the University of Würzburg for their technical expertise. This work was supported by Intramural Funding (fortune) at the University of Tübingen (2545-1-0 to B.V.), the Ministry of Science, Research and Art Baden-Württemberg (to B.V.), the Medical Research Council (MC_UP_1503/2 to M.R.B.), ANR light4deaf (ANR-15-RHUS-0001), HearInNoise (ANR-17-CE16-0017), LHW-stiftung (to A.E.), and a grant from NIH/COBRE GM103636 (Project 3); the Presbyterian

Health Foundation (PHF) Grant to G.K.V. This study was funded in part by NIDCDs R01s DC002842 and DC012049 to R.J.S and T32 GM007748 to K.T.B. L.A.D is a Medical Research Council DPhil student (1774724).

Author contributions BV, HA, KTB, and AR conducted in vitro studies. SJL, LAD, SV, PV, CP, SVK, AE and MRB conducted in vivo studies. BF performed histology. BV, NM, RM, HA, KTB and HG performed genomic studies. NM, AS, GS, and HG identified patients, collected and analyzed clinical data, provided the biological specimens. RM, HA, KTB, FR, CB, DM, and HH conducted database analyses and data sharing. BV, RM, HA, KTB, KNA, RJHS, TH, AE, MRB and GKV wrote the manuscript. BV, HA, TH, RJHS, AE, MRB, GKV and HG supervised and conceived the study.

Funding Open Access funding enabled and organized by Projekt DEAL. This work was supported by Intramural Funding (fortune) at the University of Tübingen (2545-1-0 to BV), the Ministry of Science, Research and Art Baden-Württemberg (to BV), the Medical Research Council (MC_UP_1503/2 to MRB), ANR light4deaf (ANR-15-RHUS-0001), HearInNoise (ANR-17-CE16-0017), LHW-stiftung (to AE), and a grant from NIH/COBRE GM103636 (Project 3); the Presbyterian Health Foundation (PHF) Grant to GKV. This study was funded in part by NIDCDs R01s DC002842 and DC012049 to RJS and T32 GM007748 to KTB. LAD is a Medical Research Council DPhil student (1774724).

Data availability All data needed to evaluate the conclusions in the paper are present in the paper and/or the Supplementary Materials. Additional data related to this paper may be requested from the authors.

Compliance with ethical standards

Conflicts of interest CB is an employee of Centogene AG (Rostock, Germany).

Ethical approval Human studies were approved by the Faculty of Medicine ethics commissions at the University of Würzburg (46/15) and Shahid Chamran University of Ahvaz (#EE/97.24.3 17654). All zebrafish experiments were performed as per protocol (17-01) and approved by the Institutional Animal Care Committee of Oklahoma Medical Research Foundation (OMRF) (IACUC). Mouse studies at the MRC Harwell Institute were licenced by the Home Office under the Animals (Scientific Procedures) Act 1986, UK and additionally approved by the Institutional Animal Welfare and Ethical Review Body (AWERB).

Informed consent to participate Written informed consent was obtained from all participants.

Informed consent for publication Consent for publication was obtained from all participants.

Open Access This article is licensed under a Creative Commons Attribution 4.0 International License, which permits use, sharing, adaptation, distribution and reproduction in any medium or format, as long as you give appropriate credit to the original author(s) and the source, provide a link to the Creative Commons licence, and indicate if changes were made. The images or other third party material in this article are included in the article's Creative Commons licence, unless indicated otherwise in a credit line to the material. If material is not included in the article's Creative Commons licence and your intended use is not permitted by statutory regulation or exceeds the permitted use, you will

need to obtain permission directly from the copyright holder. To view a copy of this licence, visit <http://creativecommons.org/licenses/by/4.0/>.

References

- Abecasis GR, Cherny SS, Cookson WO, Cardon LR (2001) GRR: graphical representation of relationship errors. *Bioinformatics* 17:742–743. <https://doi.org/10.1093/bioinformatics/17.8.742>
- Abecasis GR, Cherny SS, Cookson WO, Cardon LR (2002) Merlin—rapid analysis of dense genetic maps using sparse gene flow trees. *Nat Genet* 30:97–101. <https://doi.org/10.1038/ng786>
- Adato A et al (2002) USH3A transcripts encode clarin-1, a four-transmembrane-domain protein with a possible role in sensory synapses. *Eur J Hum Genet* 10:339–350. <https://doi.org/10.1038/sj.ejhg.5200831>
- Adzhubei IA et al (2010) A method and server for predicting damaging missense mutations. *Nat Methods* 7:248–249
- Azaiez H et al (2018) Genomic landscape and mutational signatures of deafness-associated genes. *Am J Hum Genet* 103:484–497. <https://doi.org/10.1016/j.ajhg.2018.08.006>
- Booth KT et al (2018a) Exonic mutations and exon skipping: Lessons learned from DFNA5. *Hum Mutat* 39:433–440. <https://doi.org/10.1002/humu.23384>
- Booth KT, Kahrizi K, Najmabadi H, Azaiez H, Smith RJ (2018b) Old gene, new phenotype: splice-altering variants in CEACAM16 cause recessive non-syndromic hearing impairment. *J Med Genet* 55:555–560. <https://doi.org/10.1136/jmedgenet-2018-105349>
- Cartegni L, Wang J, Zhu Z, Zhang MQ, Krainer AR (2003) ESEfinder: a web resource to identify exonic splicing enhancers. *Nucleic Acids Res* 31:3568–3571
- Chun S, Fay JC (2009) Identification of deleterious mutations within three human genomes. *Genome Res* 19:1553–1561. <https://doi.org/10.1101/gr.092619.109>
- Creixell P, Schoof EM, Tan CS, Linding R (2012) Mutational properties of amino acid residues: implications for evolvability of phosphorylatable residues. *Philos Trans R Soc Lond B Biol Sci* 367:2584–2593. <https://doi.org/10.1098/rstb.2012.0076>
- Cunningham CL, Müller U (2019) Molecular structure of the hair cell mechano-electrical transduction complex. *Cold Spring Harb Perspect Med* 9:a033167
- Desmet FO, Hamroun D, Lalonde M, Collod-Beroud G, Claustres M, Beroud C (2009) Human splicing finder: an online bioinformatics tool to predict splicing signals. *Nucleic Acids Res* 37:e67. <https://doi.org/10.1093/nar/gkp215>
- Doll J et al (2020) A novel missense variant in MYO3A is associated with autosomal dominant high-frequency hearing loss in a German family. *Mol Genet Genomic Med*. <https://doi.org/10.1002/mgg3.1343>
- Dulon D et al (2018) Clarin-1 gene transfer rescues auditory synaptopathy in model of Usher syndrome. *J Clin Invest* 128:3382–3401. <https://doi.org/10.1172/JCI94351>
- Dunbar LA et al (2019) Clarin-2 is essential for hearing by maintaining stereocilia integrity and function. *EMBO Mol Med* 11:e10288
- Fairbrother WG, Yeo GW, Yeh R, Goldstein P, Mawson M, Sharp PA, Burge CB (2004) RESCUE-ESE identifies candidate exonic splicing enhancers in vertebrate exons. *Nucleic Acids Res* 32:W187–190. <https://doi.org/10.1093/nar/gkh393>
- Fattahi Z et al (2019) Iranome: a catalogue of genomic variations in the Iranian population. *Hum Mutat*. <https://doi.org/10.1002/humu.23880>
- Fields RR et al (2002) Usher syndrome type III: revised genomic structure of the USH3 gene and identification of novel mutations. *Am J Hum Genet* 71:607–617. <https://doi.org/10.1086/342098>

- García-García G et al (2012) Two novel disease-causing mutations in the CLRN1 gene in patients with Usher syndrome type 3. *Mol Vis* 18:3070–3078
- Gillespie PG, Müller U (2009) Mechanotransduction by hair cells: models, molecules, and mechanisms. *Cell* 139:33–44. <https://doi.org/10.1016/j.cell.2009.09.010>
- Gopal SR et al (2015) Zebrafish models for the mechanosensory hair cell dysfunction in usher syndrome 3 reveal that clarin-1 is an essential hair bundle protein. *J Neurosci* 35:10188–10201. <https://doi.org/10.1523/Jneurosci.1096-15.2015>
- Gopal SR, Lee YT, Stepanyan R, McDermott BM Jr, Agramam KN (2019) Unconventional secretory pathway activation restores hair cell mechanotransduction in an USH3A model. *Proc Natl Acad Sci U S A* 116:11000–11009. <https://doi.org/10.1073/pnas.1817500116>
- Graveley BR (2000) Sorting out the complexity of SR protein functions. *RNA* 6:1197–1211
- Hofrichter MAH et al (2018) The conserved pArg108 residue in S1PR2 (DFNB68) is fundamental for proper hearing: evidence from a consanguineous Iranian family. *BMC Med Genet* 19:81. <https://doi.org/10.1186/s12881-018-0598-5>
- Hudspeth AJ (1997) How hearing happens. *Neuron* 19:947–950
- Ingham NJ et al (2019) Mouse screen reveals multiple new genes underlying mouse and human hearing loss. *PLoS Biol* 17:e3000194. <https://doi.org/10.1371/journal.pbio.3000194>
- Joensuu T et al (2001) Mutations in a novel gene with transmembrane domains underlie Usher syndrome type 3. *Am J Hum Genet* 69:673–684. <https://doi.org/10.1086/323610>
- Kan JLC, Green MR (1999) Pre-mRNA splicing of IgM exons M1 and M2 is directed by a juxtaposed splicing enhancer and inhibitor. *Gene Dev* 13:462–471
- Kazmierczak P, Sakaguchi H, Tokita J, Wilson-Kubalek EM, Milligan RA, Muller U, Kachar B (2007) Cadherin 23 and protocadherin 15 interact to form tip-link filaments in sensory hair cells. *Nature* 449:87–91. <https://doi.org/10.1038/nature06091>
- Khan MI et al (2011) CLRN1 mutations cause nonsyndromic retinitis pigmentosa. *Ophthalmology* 118:1444–1448. <https://doi.org/10.1016/j.ophtha.2010.10.047>
- Kimmel CB, Ballard WW, Kimmel SR, Ullmann B, Schilling TF (1995) Stages of embryonic development of the zebrafish. *Dev Dyn* 203:253–310. <https://doi.org/10.1002/aja.1002030302>
- Kincaid MM, Cooper AA (2007) Misfolded proteins traffic from the endoplasmic reticulum (ER) due to ER export signals. *Mol Biol Cell* 18:455–463. <https://doi.org/10.1091/mbc.E06-08-0696>
- Kinseth MA, Anjard C, Fuller D, Guizzunti G, Loomis WF, Malhotra V (2007) The golgi-associated protein GRASP is required for unconventional protein secretion during development. *Cell* 130:524–534. <https://doi.org/10.1016/j.cell.2007.06.029>
- Kircher M, Witten DM, Jain P, O’Roak BJ, Cooper GM, Shendure J (2014) A general framework for estimating the relative pathogenicity of human genetic variants. *Nat Genet* 46:310–315. <https://doi.org/10.1038/ng.2892>
- Kolla L et al (2020) Characterization of the development of the mouse cochlear epithelium at the single cell level. *Nat Commun*. <https://doi.org/10.1038/s41467-020-16113-y>
- Koepcke B, Johnson S, Schmitz H, Santi P, Fritsch B (2012) Scanning thin-sheet laser imaging microscopy elucidates details on mouse ear development. *Dev Dyn* 241:465–480. <https://doi.org/10.1002/dvdy.23736>
- LaFave MC, Varshney GK, Vemulapalli M, Mullikin JC, Burgess SM (2014) A defined zebrafish line for high-throughput genetics and genomics: NHGRI-1. *Genetics* 198:167–170. <https://doi.org/10.1534/genetics.114.166769>
- Lek M et al (2016) Analysis of protein-coding genetic variation in 60,706 humans. *Nature* 536:285–291. <https://doi.org/10.1038/nature19057>
- Lekszas C et al (2020) Biallelic TANGO1 mutations cause a novel syndromal disease due to hampered cellular collagen secretion. *Elife* 9:e51319
- Livak KJ, Schmittgen TD (2001) Analysis of relative gene expression data using real-time quantitative PCR and the 2(T)(-Delta Delta C) method. *Methods* 25:402–408. <https://doi.org/10.1006/meth.2001.1262>
- Mazzoli M, Van Camp G, Newton V, Giarbini N, Declau F, Parving A (2003) Recommendations for the description of genetic and audiological data for families with nonsyndromic hereditary hearing impairment. *Audiol Med* 1:148–150
- Morton CC, Nance WE (2006) Newborn hearing screening—a silent revolution. *N Engl J Med* 354:2151–2164. <https://doi.org/10.1056/NEJMra050700>
- Ness SL et al (2003) Genetic homogeneity and phenotypic variability among Ashkenazi Jews with Usher syndrome type III. *J Med Genet* 40:767–772
- Ng PC, Henikoff S (2001) Predicting deleterious amino acid substitutions. *Genome Res* 11:863–874. <https://doi.org/10.1101/gr.176601>
- O’Connell JR, Weeks DE (1998) PedCheck: a program for identification of genotype incompatibilities in linkage analysis. *Am J Hum Genet* 63:259–266. <https://doi.org/10.1086/301904>
- Oza AM et al (2018) Expert specification of the ACMG/AMP variant interpretation guidelines for genetic hearing loss. *Hum Mutat* 39:1593–1613. <https://doi.org/10.1002/humu.23630>
- Pearlman SM, Serber Z, Ferrell JE Jr (2011) A mechanism for the evolution of phosphorylation sites. *Cell* 147:934–946. <https://doi.org/10.1016/j.cell.2011.08.052>
- Phillips JB et al (2011) Harmonin (Ush1c) is required in zebrafish Müller glial cells for photoreceptor synaptic development and function. *Dis Model Mech* 4:786–800
- Plantinga RF, Kleemola L, Huygen PL, Joensuu T, Sankila EM, Penning RJ, Cremers CW (2005) Serial audiometry and speech recognition findings in Finnish Usher syndrome type III patients. *Audiol Neurootol* 10:79–89. <https://doi.org/10.1159/000083363>
- Rüschendorf F, Nürnberg P (2005) ALOHOMORA: a tool for linkage analysis using 10K SNP array data. *Bioinformatics* 21:2123–2125. <https://doi.org/10.1093/bioinformatics/bti264>
- Sano R, Reed JC (2013) ER stress-induced cell death mechanisms. *Biochim Biophys Acta* 1833:3460–3470. <https://doi.org/10.1016/j.bbamcr.2013.06.028>
- Schröder M, Kaufman RJ (2005) The mammalian unfolded protein response. *Annu Rev Biochem* 74:739–789. <https://doi.org/10.1146/annurev.biochem.73.011303.074134>
- Schwarz JM, Cooper DN, Schuelke M, Seelow D (2014) MutationTaster2: mutation prediction for the deep-sequencing age. *Nat Methods* 11:361–362. <https://doi.org/10.1038/nmeth.2890>
- Scott EM et al (2016) Characterization of Greater Middle Eastern genetic variation for enhanced disease gene discovery. *Nat Genet* 48:1071–1076. <https://doi.org/10.1038/ng.3592>
- Seelow D, Schuelke M, Hildebrandt F, Nürnberg P (2009) HomozygosityMapper—an interactive approach to homozygosity mapping. *Nucleic Acids Res* 37:W593–W599. <https://doi.org/10.1093/nar/gkp369>
- Seiler C, Finger-Baier KC, Rinner O, Makhankov YV, Schwarz H, Neuhauss SC, Nicolson T (2005) Duplicated genes with split functions: independent roles of protocadherin15 orthologues in zebrafish hearing and vision. *Development* 132:615–623. <https://doi.org/10.1242/dev.01591>
- Simon MM et al (2013) A comparative phenotypic and genomic analysis of C57BL/6J and C57BL/6N mouse strains. *Genome Biol* 14:R82. <https://doi.org/10.1186/gb-2013-14-7-r82>
- Smith RJ, Bale JF Jr, White KR (2005) Sensorineural hearing loss in children. *Lancet* 365:879–890. [https://doi.org/10.1016/S0140-6736\(05\)1047-3](https://doi.org/10.1016/S0140-6736(05)1047-3)

- Thisse C, Thisse B (2008) High-resolution in situ hybridization to whole-mount zebrafish embryos. *Nat Protoc* 3:59–69. <https://doi.org/10.1038/nprot.2007.514>
- UniProt Consortium T (2018) UniProt: the universal protein knowledgebase. *Nucleic Acids Res* 46:2699. <https://doi.org/10.1093/nar/gky092>
- Varshney GK et al (2016) A high-throughput functional genomics workflow based on CRISPR/Cas9-mediated targeted mutagenesis in zebrafish. *Nat Protoc* 11:2357–2375. <https://doi.org/10.1038/nprot.2016.141>
- Viotti C (2016) ER to golgi-dependent protein secretion: the conventional pathway. *Methods Mol Biol* 1459:3–29. https://doi.org/10.1007/978-1-4939-3804-9_1
- Waterhouse AM, Procter JB, Martin DM, Clamp M, Barton GJ (2009) Jalview Version 2—a multiple sequence alignment editor and analysis workbench. *Bioinformatics* 25:1189–1191. <https://doi.org/10.1093/bioinformatics/btp033>
- Westerfield M (2000) The zebrafish book. A guide for the laboratory use of zebrafish (*Danio rerio*). 4th edn. University of Oregon Press, Eugene, Oregon, USA
- Whitfield TT, Riley BB, Chiang MY, Phillips B (2002) Development of the zebrafish inner ear. *Dev Dyn* 223:427–458
- Wright CF, FitzPatrick DR, Firth HV (2018) Paediatric genomics: diagnosing rare disease in children. *Nat Rev Genet* 19:253–268
- Xiong HY et al (2015) RNA splicing. The human splicing code reveals new insights into the genetic determinants of disease. *Science* 347:125806
- Yang J, Yan R, Roy A, Xu D, Poisson J, Zhang Y (2015) The I-TASSER Suite: protein structure and function prediction. *Nat Methods* 12:7–8. <https://doi.org/10.1038/nmeth.3213>

Publisher's Note Springer Nature remains neutral with regard to jurisdictional claims in published maps and institutional affiliations.

Authors and Affiliations

Barbara Vona^{1,2} · Neda Mazaheri³ · Sheng-Jia Lin⁴ · Lucy A. Dunbar⁵ · Reza Maroofian⁶ · Hela Azaiez⁷ · Kevin T. Booth^{7,8} · Sandrine Vitry⁹ · Aboufazel Rad² · Franz Rüschemdorf¹⁰ · Pratishtha Varshney⁴ · Ben Fowler¹¹ · Christian Beetz¹² · Kumar N. Alagramam^{13,14,15} · David Murphy⁶ · Gholamreza Shariati^{16,17} · Alireza Sedaghat¹⁸ · Henry Houlden⁶ · Cassidy Petree⁴ · Shruthi VijayKumar⁴ · Richard J. H. Smith⁷ · Thomas Haaf¹ · Aziz El-Amraoui⁹ · Michael R. Bowl^{15,19} · Gaurav K. Varshney⁴ · Hamid Galehdari³

¹ Institute of Human Genetics, Julius Maximilians University Würzburg, Würzburg, Germany

² Department of Otolaryngology—Head and Neck Surgery, Tübingen Hearing Research Centre, Eberhard Karls University Tübingen, Tübingen, Germany

³ Department of Genetics, Faculty of Science, Shahid Chamran University of Ahvaz, Ahvaz, Iran

⁴ Genes & Human Disease Research Program, Oklahoma Medical Research Foundation, Oklahoma City, OK, USA

⁵ Mammalian Genetics Unit, MRC Harwell Institute, Harwell Campus, Didcot OX11 0RD, UK

⁶ Department of Neuromuscular Disorders, UCL Queen Square Institute of Neurology, London WC1N 3BG, UK

⁷ Molecular Otolaryngology and Renal Research Laboratories, Department of Otolaryngology and Interdisciplinary Graduate Program in Molecular Medicine, Carver College of Medicine, University of Iowa, Iowa City, IA, USA

⁸ Department of Neurobiology, Harvard Medical School, Boston, MA, USA

⁹ Unit Progressive Sensory Disorders, Pathophysiology and Therapy Institut Pasteur, Institut de L'Audition, INSERM-UMRS1120, Sorbonne Université, 63 rue de Charenton, 75012 Paris, France

¹⁰ Max Delbrück Center for Molecular Medicine in the Helmholtz Association, 13125 Berlin, Germany

¹¹ Imaging & Histology Core, Oklahoma Medical Research Foundation, Oklahoma City, OK, USA

¹² Centogene AG, Rostock, Germany

¹³ Department of Otolaryngology, School of Medicine, University Hospitals Cleveland Medical Center, Case Western Reserve University, 11100 Euclid Avenue, Cleveland, OH 44106, USA

¹⁴ Department of Neurosciences, Case Western Reserve University, 11100 Euclid Avenue, Cleveland, OH 44106, USA

¹⁵ Department of Genetics and Genomic Sciences, Case Western Reserve University, Cleveland, OH 44106, USA

¹⁶ Department of Medical Genetics, Faculty of Medicine, Ahvaz Jundishapur, University of Medical Sciences, Ahvaz, Iran

¹⁷ Narges Medical Genetics and Prenatal Diagnostics Laboratory, East Mihan Ave, Kianpars, Ahvaz, Iran

¹⁸ Diabetes Research Center, Health Research Institute, Ahvaz Jundishapur University of Medical Sciences, Ahvaz, Iran

¹⁹ UCL Ear Institute, University College London, 332 Gray's Inn Road, London WC1X 8EE, UK

10.6 Attachment 6

Bi-allelic variants in IPO8 cause a connective tissue disorder associated with cardiovascular defects, skeletal abnormalities, and immune dysregulation

REPORT

Bi-allelic variants in *IPO8* cause a connective tissue disorder associated with cardiovascular defects, skeletal abnormalities, and immune dysregulation

Alban Ziegler,^{1,2,33} Rémi Duclaux-Loras,^{3,33} Céline Revenu,^{4,5,33} Fabienne Charbit-Henrion,^{3,6,7} Bernadette Begue,³ Karine Duroure,^{4,5} Linda Grimaud,² Anne Laure Guihot,² Valérie Desquière-Dumas,^{1,2} Mohammed Zarhrate,⁸ Nicolas Cagnard,⁹ Emmanuel Mas,^{10,11} Anne Breton,^{10,11} Thomas Edouard,¹² Clarisse Billon,¹³ Michael Frank,¹³ Estelle Colin,¹ Guy Lenaers,² Daniel Henrion,² Stanislas Lyonnet,^{14,15} Laurence Faivre,¹⁶ Yves Alembik,¹⁷ Anaïs Philippe,¹⁷ Bruno Moulin,¹⁸ Eyal Reinstein,^{19,20} Shay Tzur,²¹ Ruben Attali,²¹ George McGillivray,²² Susan M. White,²² Lyndon Gallacher,^{22,23} Kerstin Kutsche,²⁴ Pauline Schneeberger,²⁴ Katta M. Girisha,²⁵ Shalini S. Nayak,²⁵ Lynn Pais,²⁶ Reza Maroofian,²⁷ Aboufazel Rad,²⁸ Barbara Vona,^{28,29} Ehsan Ghayoor Karimiani,^{30,31} Caroline Lekszas,²⁹ Thomas Haaf,²⁹ Ludovic Martin,^{2,32} Frank Ruummele,^{3,6} Dominique Bonneau,^{1,2} Nadine Cerf-Bensusan,³ Filippo Del Bene,^{4,5,*} and Marianna Parlato^{3,*}

Summary

Dysregulated transforming growth factor TGF- β signaling underlies the pathogenesis of genetic disorders affecting the connective tissue such as Loeys-Dietz syndrome. Here, we report 12 individuals with bi-allelic loss-of-function variants in *IPO8* who presented with a syndromic association characterized by cardio-vascular anomalies, joint hyperlaxity, and various degree of dysmorphic features and developmental delay as well as immune dysregulation; the individuals were from nine unrelated families. Importin 8 belongs to the karyopherin family of nuclear transport receptors and was previously shown to mediate TGF- β -dependent SMADs trafficking to the nucleus *in vitro*. The important *in vivo* role of *IPO8* in pSMAD nuclear translocation was demonstrated by CRISPR/Cas9-mediated inactivation in zebrafish. Consistent with *IPO8*'s role in BMP/TGF- β signaling, *ipo8*^{-/-} zebrafish presented mild to severe dorso-ventral patterning defects during early embryonic development. Moreover, *ipo8*^{-/-} zebrafish displayed severe cardiovascular and skeletal defects that mirrored the human phenotype. Our work thus provides evidence that *IPO8* plays a critical and non-redundant role in TGF- β signaling during development and reinforces the existing link between TGF- β signaling and connective tissue defects.

¹Department of Biochemistry and Molecular Biology, CHU d'Angers, 49000 Angers, France; ²University of Angers, MitoVasc, UMR CNRS 6015, INSERM 1083, 49933 Angers, France; ³Université de Paris, Imagine Institute, Laboratory of Intestinal Immunity, INSERM, UMR1163, 75015 Paris, France; ⁴Sorbonne Université, INSERM, CNRS, Institut de la Vision, 17 Rue Moreau, 75012 Paris, France; ⁵Institut Curie, PSL Research University, INSERM U934, CNRS UMR3215, 75005 Paris, France; ⁶Department of Pediatric Gastroenterology, Assistance Publique-Hôpitaux de Paris, Hôpital Necker-Enfants Malades, 75015 Paris, France; ⁷Department of Molecular Genetics, Assistance Publique-Hôpitaux de Paris, Hôpital Necker-Enfants Malades, 75015 Paris, France; ⁸Genomics Core Facility, Institut Imagine-Structure Federative de Recherche Necker, INSERM U1163 et INSERM US24/CNRS UMS3633, Paris Descartes Sorbonne Paris Cité University, 75015 Paris, France; ⁹Bioinformatics Core Facility, INSERM-UMR 1163, Imagine Institute, 75015 Paris, France; ¹⁰IRSD, Université de Toulouse, INSERM, INRA, ENVT, UPS, Toulouse 31300, France; ¹¹Centre de Référence des Maladies Rares Digestives, and Pediatric Clinical Research Unit, Toulouse Clinical Investigation Center INSERM U1436, Hôpital des Enfants, CHU de Toulouse, Toulouse 31300, France; ¹²Reference Centre for Marfan Syndrome and Reference Centre on Rare Bone Diseases, Pediatric Clinical Research Unit, Children's Hospital, Toulouse University Hospital, RESTORE, INSERM UMR1301, 31300 Toulouse, France; ¹³Centre de Génétique, Centre de Référence des Maladies Vasculaires Rares, Assistance Publique-Hôpitaux de Paris, Hôpital Européen Georges Pompidou, 75015 Paris, France; ¹⁴Université de Paris, Imagine Institute, Laboratory of Embryology and Genetics of Malformations, INSERM UMR 1163, 75015 Paris, France; ¹⁵Fédération de Génétique, Hôpital Necker-Enfants Malades, Assistance Publique Hôpitaux de Paris, 75015 Paris, France; ¹⁶Centre de Référence Anomalies du Développement et Syndromes Malformatifs, FHU TRANSLAD, Hôpital d'Enfants, CHU Dijon, 21000 Dijon, France; ¹⁷Département de Génétique Médicale, CHU de Haute-pierre, 67200 Strasbourg, France; ¹⁸Nephrology and Transplantation Department, Nouvel Hôpital Civil, Hôpitaux Universitaires de Strasbourg, 67200 Strasbourg, France; ¹⁹Medical Genetics Institute, Meir Medical Center, Kfar-Saba 4428164, Israel; ²⁰Sackler Faculty of Medicine, Tel Aviv University, Tel Aviv 6997801, Israel; ²¹Genomic Research Department, Emedgene Technologies, 67443 Tel Aviv, Israel; ²²Victorian Clinical Genetics Services, Murdoch Children's Research Institute, Parkville 3052, Melbourne, VIC, Australia; ²³Department of Paediatrics, The University of Melbourne, 3010 Parkville, Melbourne, VIC, Australia; ²⁴Institute of Human Genetics, University Medical Center Hamburg-Eppendorf, 20246 Hamburg, Germany; ²⁵Department of Medical Genetics, Kasturba Medical College, Manipal, Manipal Academy of Higher Education, Manipal 576104, India; ²⁶Broad Center for Mendelian Genomics, Program in Medical and Population Genetics, Broad Institute of Massachusetts Institute of Technology and Harvard, Cambridge, MA 02142, USA; ²⁷Department of Neuromuscular Disorders, Queen Square Institute of Neurology, University College London, WC1N 3BG London, UK; ²⁸Department of Otolaryngology-Head & Neck Surgery, Tübingen Hearing Research Centre, Eberhard Karls University of Tübingen, 72076 Tübingen, Germany; ²⁹Institute of Human Genetics, Julius Maximilians University Würzburg, 97074 Würzburg, Germany; ³⁰Molecular and Clinical Sciences Institute, St. George's, University of London, Cranmer Terrace London, SW17 0RE London, UK; ³¹Innovative Medical Research Center, Mashhad Branch, Islamic Azad University, Mashhad 9133736351, Iran; ³²Department of Dermatology, CHU d'Angers, 49000 Angers, France

³³These authors contributed equally to this work

*Correspondence: filippo.del-bene@inserm.fr (F.D.B.), marianna.parlato@inserm.fr (M.P.)

<https://doi.org/10.1016/j.ajhg.2021.04.020>

© 2021 The Authors. This is an open access article under the CC BY-NC-ND license (<http://creativecommons.org/licenses/by-nc-nd/4.0/>).



First isolated as a RanGTP-binding protein, importin 8 encoded by *IPO8* (MIM: 605600) was then identified as a member of the β -karyopherin family, the largest group of nuclear transport receptors.^{1,2} Accordingly, *in vitro* studies have implicated importin 8 in cytoplasm-to-nucleus shuttling of a broad spectrum of cargos, including the signal recognition particle protein SRP19,³ Argonaute-microRNAs complexes,^{4,5} the c-Jun protein,⁶ the NF- κ B p65 subunit,⁷ the eukaryotic translation initiation factor eIF4E,⁸ and a set of receptor-activated mothers against decapentaplegic homolog (SMAD) transcription factors⁹ that play a critical role downstream of the large family of tumor growth factor β (TGF- β) and bone morphogenetic protein (BMP) cytokines. In contrast, *in vivo* data on *IPO8* functions are lacking except for a report in *Drosophila* showing that Msk, the ortholog of mammalian importins 7 and 8 (which share 60% homology), mediates nuclear accumulation of phosphorylated MAD downstream of decapentaplegic, the homolog of mammalian BMP.¹⁰ Msk inactivation was embryonically lethal, suggesting its key role in *Drosophila* development, but no link was clearly established with impairment of BMP signaling.¹⁰

Strikingly, the TGF- β /BMP cytokine family exerts pleiotropic functions during embryonic development, tissue homeostasis, and tissue repair as well as within the immune system.¹¹ Accordingly, dysregulation of TGF- β signaling is the cause of severe congenital disorders characterized by developmental defects with or without impaired immune regulation.¹² This is notably the case of Loey-Dietz syndrome (LDS), which is caused by heterozygous loss-of-function (LOF) variants in *TGFBR1* (MIM: 190181), *TGFBR2* (MIM: 190182), *TGFBR3* (MIM: 190220) or *TGFBR4* (MIM: 190230), and *SMAD2* (MIM: 601366) or *SMAD3* (MIM: 603109);¹³ of Shprintzen-Goldberg syndrome (SGS), which results from heterozygous variants in *SKI* (MIM: 182212), a negative regulator of the TGF- β signaling pathway;¹⁴ and of Marfan syndrome (MFS) (MIM: 154700) caused by variants in *FBN1* (MIM: 134797), encoding fibrillin-1, the main component of extracellular matrix microfibrils that, in turn, scaffolds latent TGF- β . Thus, individuals with LDS, SGS, and MFS display systemic connective tissue disorders of variable expressivity, which notably affect the vascular tree and the skeleton, causing life-threatening arterial aneurysms, dysmorphic features, pectus deformity, scoliosis, and joint hyperlaxity.^{14,15} In keeping with the immunoregulatory functions of TGF- β ,^{16,17} developmental defects of LDS have been associated with increased frequency of allergic manifestations¹⁸ and a 10-fold increase in the risk of inflammatory bowel diseases (IBDs).¹⁹ More recently, bi-allelic LOF variants in *TGFBI* (MIM: 190180) were identified as the cause of a severe syndrome combining very early-onset IBD and encephalopathy.²⁰

Here, we report 12 individuals with bi-allelic pathogenic *IPO8* variants who displayed a complex syndrome reminiscent of LDS and SGS that variably combined cardiovascular, neurologic, skeletal and immunologic abnormalities

along with dysmorphic features; the individuals are from nine unrelated families (Table 1, Figures 1 and S1). Affected individuals were recruited through an international collaborative effort facilitated by Genematcher.²¹ All procedures were performed in accordance with the Helsinki Declaration and were approved by the ethics committees and the institutional review boards from each center. Sequencing (targeted/whole-exome sequencing and Sanger sequencing) was performed after obtaining informed written consent from all affected individuals or their legal guardians. Table 1 summarizes the main phenotypic features in the cohort. Seven individuals showed early-onset (before the age of 1 year for the youngest) dilatation of the ascending aorta. Individuals 1 and 2 (I-1 and I-2), the two oldest siblings (59 and 53 years old at the time of the first assessment, respectively) had diffuse arterial frailty with multiple aneurysms affecting the abdominal aorta, iliac, coronary, and renal arteries and, in I-1, the thoracic aorta (Figure 1A). Arterial tortuosity similar to that observed in LDS²² was noted in four individuals. Recurrent spontaneous pneumothorax was noted in I-1 and I-2. Pulmonary emphysema was present in I-1 (Figure 1B) as well as in two younger individuals (I-5 and I-6). Facial dysmorphism was observed in ten individuals (Figure 1C, Table 1), while I-11 had joint hyperlaxity complicated by multiple joint dislocations. All displayed skeletal features, including scoliosis (n = 9), pectus excavatum or carinatum (n = 6), arachnodactyly (n = 6), or pes planus or talipes equinovarus (n = 6) (Figures 1D–1F and S1). Eight individuals developed myopia complicated by retinal detachment for two of them and by early-onset cataract for two others, but none of them had lens dislocation. In line with a generalized connective tissue disorder, skin hyperextensibility and/or hernia were observed in 11 individuals (Figure 1G). Delayed motor milestone presumably consecutive to joint instability was observed in seven individuals; four of them also had mild (I-5, I-6, and I-8) or severe (I-7) intellectual disability. Predisposition to allergic or inflammatory diseases, which was previously documented in LDS,^{18,19} was evidenced in six individuals (I-5, I-6, I-7, I-8, I-10, and I-12), some of whom also displayed immunological parameters consistent with impaired TGF- β signaling, including hyperIgE, hyperIgG, hypoIgA, and hypereosinophilia.

As detailed in Table 2, 11 variants were identified in the 12 individuals: seven as homozygous and four as compound heterozygous in *IPO8* (GenBank: NM_006390.3). This gene (25 exons, 24 introns) encodes a 1,037 amino acid protein with the β -importin N-terminal domain (22–102 aa) and a CSE1-like domain (202–441 aa) containing a RanGTPase-binding motif characteristic of β -importins (Figures 2A and 2B). Segregation of the variant within each family was analyzed by Sanger sequencing (Figure S2) whenever DNA was available (n = 8). They were all exceedingly rare (MAF < 0.01%), and only three were found in the gnomAD at a heterozygous state (Table 2).

Table 1. Clinical features of individuals carrying *IP08* variants

	Family 1		Family 2		Family 3		Family 4		Family 5		Family 6		Family 7		Family 8		Family 9		Total
Individual	I-1	I-2	I-3	I-4	I-5	I-6	I-7	I-8	I-9	I-10	I-11	I-12	I-13	I-14	I-15	I-16	I-17	I-18	–
Sex	M	F	M	M	F	M	M	M	F	F	M	F	F	F	M	F	F	F	–
Age at last examination	62 years	62 years	1 year 8 months	2 years 2 months	16 years	15 years	9 years 6 months	13 years	22 years	33 years	7 years 6 months	26 years	–	–	–	–	–	–	–
Vascular abnormalities																			
Dilatation of the ascending aorta	yes	yes	yes	no	yes	yes	yes	yes	yes	yes	yes	yes	yes	yes	yes	yes	yes	yes	11/12
Other abnormal great vessels	dilated and calcified iliac arteries, AAA	calcified coronary arteries, AAA, dilated iliac arteries	no	no	carotid artery tortuosity	carotid artery tortuosity	no	no	carotid artery tortuosity	no	no	internal carotid tortuosity and ectasia	no	no	no	no	no	no	6/12
Heart malformation	MVP	no	ASD, left atrium and ventricle mild dilatation	no	ASD, VSD	no	N/A	N/A	ASD	ASD, VSD	MVP	no	no	no	no	no	no	no	6/10
Ocular abnormalities																			
Myopia	severe	severe	no	no	severe	no	no	severe	severe	mild	severe	severe	no	no	no	no	no	no	8/12
Retinal detachment	yes	yes	no	no	no	no	no	no	no	no	no	no	no	no	no	no	no	no	2/12
Dysmorphic features																			
Proptosis	no	no	yes	no	no	yes	yes	no	yes	yes	yes	yes	yes	yes	yes	yes	yes	yes	7/12
Micrognathia	no	no	yes	yes	yes	yes	yes	no	yes	no	no	yes	no	no	no	no	no	no	7/12
Hypertelorism	no	no	yes	yes	yes	yes	yes	no	no	no	no	yes	no	no	no	no	no	no	6/12
Frontal bossing	no	no	yes	no	yes	yes	no	no	no	no	no	no	no	no	no	no	no	no	3/12
Ptosis	no	no	yes	no	no	no	yes	no	no	no	yes	no	no	no	yes	no	no	no	3/12
Abnormal palate	no	no	cleft uvula	no	no	no	no	no	no	no	no	cleft uvula	no	no	no	no	no	no	2/12
Skeletal abnormalities																			
Hyperlaxity	yes	yes	yes	yes	yes	yes	yes	yes	yes	yes	yes	no	yes	yes	no	yes	yes	yes	11/12
Recurrent joint dislocations	yes	yes	yes	no	no	no	yes	no	yes	yes	no	yes	yes	yes	no	yes	yes	yes	7/12
Pectus	no	no	carinatum	carinatum	excavatum	excavatum	no	no	excavatum	no	no	carinatum	no	no	no	no	no	no	6/12
Scoliosis	yes	yes	no	no	yes	yes	yes	yes	yes	yes	yes	yes	yes	yes	yes	yes	yes	yes	9/12
Arachnodactyly	no	no	yes	yes	yes	yes	no	no	yes	no	no	yes	no	no	yes	no	no	no	6/12

(Continued on next page)

Table 1. Continued																			
	Family 1		Family 2		Family 3		Family 4		Family 5		Family 6		Family 7		Family 8		Family 9		Total
Feet malposition	no	no	yes	yes	no	no	no	yes	yes	yes	yes	yes	yes	yes	yes	no	no	no	6/12
Connective tissue abnormalities																			
Skin hyperextensibility	no	no	yes	yes	yes	yes	no	yes	no	yes	no	yes	yes	yes	yes	yes	yes	yes	8/12
Hernia	umbilical hernia	spigelian and umbilical hernia	inguinal, umbilical, diaphragmatic hernia	umbilical hernia	umbilical and inguinal hernia	umbilical and inguinal hernia	umbilical and inguinal hernia	umbilical and inguinal hernia	umbilical hernia	no	umbilical and abdominal hernia	umbilical hernia	umbilical and abdominal hernia	umbilical and abdominal hernia	umbilical and abdominal hernia	umbilical and abdominal hernia	umbilical and abdominal hernia	umbilical and abdominal hernia	11/12
Developmental delay/intellectual disability	no	no	yes	yes	yes	yes	yes	yes	yes	no	no	yes	yes	yes	yes	no	no	no	7/12
Immunological abnormalities																			
HyperIgE	N/A	N/A	N/A	N/A	yes	yes	N/A	yes	N/A	N/A	N/A	N/A	N/A	N/A	N/A	N/A	N/A	N/A	3/3
HyperIgG	N/A	N/A	N/A	N/A	yes	yes	N/A	yes	N/A	N/A	N/A	N/A	N/A	N/A	N/A	N/A	N/A	N/A	3/3
HypolgA	N/A	N/A	N/A	N/A	yes	yes	N/A	yes	N/A	N/A	N/A	N/A	N/A	no	N/A	N/A	N/A	N/A	3/4
Hypereosinophilia mild	N/A	N/A	N/A	N/A	yes	yes	N/A	yes	N/A	N/A	N/A	N/A	N/A	no	N/A	N/A	N/A	N/A	4/5
Intestinal inflammation	no	no	no	no	severe colitis	celiac disease/gastritis	no	dysimmune gastroenterocolitis	no	no	no	no	no	chronic gastritis and duodenitis	no	no	no	celiac disease	5/12
Allergic symptoms	no	no	no	no	asthma, eczema	asthma, eczema	asthma	eczema, rhinoconjunctivitis	no	no	no	asthma	no	no	no	no	no	drug allergies	6/12
Urogenital/kidney anomalies	large cortical cyst	ischemic nephropathy	ureterohydronephrosis	no	pyelo-ureteral duplication	no	N/A	ureterohydronephrosis	no	no	no	no	no	hydronephrosis	no	no	no	hydronephrosis	6/11

AAA, ascending aortic aneurysm; ASD, atrial septal defect; MVP, mitral valve prolapse; VSD, ventricular septal defect; N/A, not available. Severe myopia was defined as of -6.00 diopters or greater.



Figure 1. Clinical features of affected individuals

- (A) CT scan showing dilated aortic root and thoracic aorta (TA), calcified asymmetric large femoral arteries (FA), calcified and dilated abdominal aorta (AA), and large renal cyst (white star) in individual 1.
 (B) CT scan showing emphysema of the apex of the left lung in individual 1.
 (C) Proptosis, micrognathia, and hypertelorism in individuals 3, 4, and 10.
 (D) X-ray showing scoliosis in individuals 1 and 7.
 (E) Arachnodactyly in individuals 3 and 7.
 (F) Hyperlaxity of small and large joints in individuals 10 and 7.
 (G) Pes planus and talipes equinovarus in individuals 10 and 3, respectively.
 (H) Skin hyperextensibility in individuals 4, 7, and 10 and umbilical hernia in individual 5.

Out of the seven homozygous variants, four were likely LOF variants (three nonsense, c.2407C>T [p.Arg803*], c.82C>T [p.Gln28*], and c.2129C>G [p.Ser710*], and one frameshift c.728delC [p.Pro243Leufs*27]), one was a splicing variant (c.2695+3_2695+7delAAAGT), and two were missense (c.262G>A [p.Asp88Asn] and c.2500C>T [p.Arg834Trp]). The compound heterozygous variants were frameshift variants leading to a premature stop codon (c.2279delT [p.Leu760ProfsTer10] and c.1538delC [p.Pro513Leufs*13]) in *trans* with a splicing (c.2900-1G>A) and a missense variant (c.2245T>C [p.Cys749Arg]), respectively. Both, c.2695+3_2695+7delAAAGT and c.2900-1G>A variants were predicted to impact the splicing according to SpliceAI.²³ Although the lack of available biospecimens or DNA from I-10 (family 7) prevented assess-

ment of the splicing variant C.2900-1 G>A, analysis of the c.2695+3_2695+7delAAAGT variant by minigene assay demonstrated that it resulted in exon 22 skipping and activation of a cryptic splicing site (Figure S3). The IPO8 missense variants, namely p.Asp88Asn, p.Cys749Arg, and p.Arg834Trp, affected highly conserved residues among IPO8 orthologs and were predicted to be damaging by several *in silico* tools, including CADD score (Figure 2B).

The impact of variants on protein level was evaluated by immunoblot analysis of protein lysates from primary cells, either fibroblasts or Epstein-Barr virus-immortalized B cell lines (EBV-B cells). A striking reduction of IPO8 level was observed in the four individuals who could be tested, including I-2 and I-9, who carried homozygous missense variants (Figure 2C). The overlap of clinical features

Table 2. Characteristics of IPO8 variants identified by next-generation sequencing in affected individuals

Individual	Chromosome position (Hg19-GRCh37) chr12	cDNA change (GenBank: NM_006390.3)	Amino acid change	SIFT	PolyPhen	DANN	CADD	Mutation Taster	Allele frequency gnomAD
1–2	g.30837296C>T	c.262G>A	p.Asp88Asn	damaging	probably damaging	0.9989	25.3	disease causing	not observed
3–4	g.30792531G>A	c.2407C>T	p.Arg803*	N/A	N/A	0.9979	36	disease causing	3.98E–6, no homozygotes
5–6	g.30848500G>A	c.82C>T	p.Gln28*	N/A	N/A	0.9984	39	disease causing	not observed
7	g.30789909_30789913del	c.2695+3_2695+7delAAAGT	N/A	N/A	N/A	N/A	22.8	disease causing	not observed
8	g.30816479del	c.1538delC	p.Pro513Leufs* 13	N/A	N/A	N/A	33	disease causing	not observed
	g.30802094A>G	c.2245T>C	p.Cys749Arg	damaging	probably damaging	0.9978	28.4	disease causing	not observed
9	g.30790111G>A	c.2500C>T	p.Arg834Trp	damaging	probably damaging	0.9993	32	disease causing	4.03E–6, no homozygotes
10	g.30784946C>T	c.2900–1G>A	N/A	N/A	N/A	0.9935	34	disease causing	not observed
	g.30792659del	c.2279delT	p.Leu760Profs* 10	N/A	N/A	N/A	33	disease causing	1.06E–5, no homozygotes
11	g.30829433del	c.728del	p.Pro243Leufs* 27	N/A	N/A	N/A	33	disease causing	not observed
12	g.30805169G>C	c.2129C>G	p.Ser710*	N/A	N/A	0.9962	38	disease causing	not observed

between all the affected individuals and the rarity or absence of the identified *IPO8* variants in population databases, including LOF variants and three missense variants impairing protein level and/or with predicted damaging effect on protein function, strongly supported *IPO8* deficiency as disease causing in all the 12 individuals.

We next assessed how *ipo8* disruption might affect development by using a zebrafish model and focused attention on early dorso-ventral patterning defects that are a telltale sign of altered TGF- β /BMP signaling, as well as on skeletal and cardiovascular defects that were the main clinical hallmarks in the cohort. The zebrafish genome encodes one single *ipo8* ortholog with 72% identity and 85% similarity with human *IPO8*. *IPO8* mutants were generated via CRISPR/Cas9 genome editing and two RNA guides simultaneously. The selected fish line carried both one insertion and two deletions (indels) in exon 4 that overall resulted in alternative translation from amino acid 125 and introduction of an early stop codon after amino acid 136 (Figure 3A). Zygotic mutants derived from the incross of two heterozygous parents (*ipo8*^{div1/+} or simply *ipo8*^{+/-}) did not develop any obvious phenotype and could be grown to adulthood, a result in keeping with the fact that maternal factors stored as mRNAs and proteins in the egg can compensate for zygotic loss of function during embryonic stages of zebrafish.^{24,25} In order to obtain maternal-zygotic mutants (MZ *ipo8*^{-/-}, here referred to simply as *ipo8*^{-/-}) that lacked wild-type (WT) *ipo8* provided in the egg by the mother, we incrossed homozygous *ipo8* zygotic mutant adults. Their homozygous

WT siblings were incrossed as controls. At 10 h post fertilization (hpf) (bud stage), *ipo8*^{-/-} MZ embryos appeared ovoid rather than round (Figure 3B). Moreover, during the following early somite stages, their tail bud failed to extend around the yolk but extended off prematurely, generating elongated, pear-shaped embryos (86% of 36 embryos from 3 clutches). These early morphological changes correlated with increased death rate that varied between 20% to 100% of the embryos per clutch. As development proceeded, a range of tail elongation defects became apparent, from embryos displaying an entirely normal or only partially absent ventral tail fin to embryos with a strongly twisted body axis resembling a snail shell-like trunk (Figure 3C). In addition, at 3 days post fertilization (dpf), most embryos (81% of 83 larvae from 6 clutches) developed heart edemas (as highlighted by arrows in Figure 3C). Morphological changes were strongly pronounced in the tail region, while anterior parts appeared comparatively normal with well-developed eyes and visible midbrain-hindbrain boundaries. These features are typical of dorsalized zebrafish mutants that result from mutations affecting the specification of ventral regions.²⁶ To quantify the dorsalization phenotypic spectrum of the *ipo8*^{-/-} mutants, we evaluated each analyzed clutch at 24 hpf and divided the phenotypes into five severity classes as previously described.²⁶ A normal phenotype was observed in 96.5% of WT embryos but only 4.5% of *ipo8*^{-/-} embryos, which displayed a whole spectrum of dorsalization phenotypes (Figures 3D and 3E).

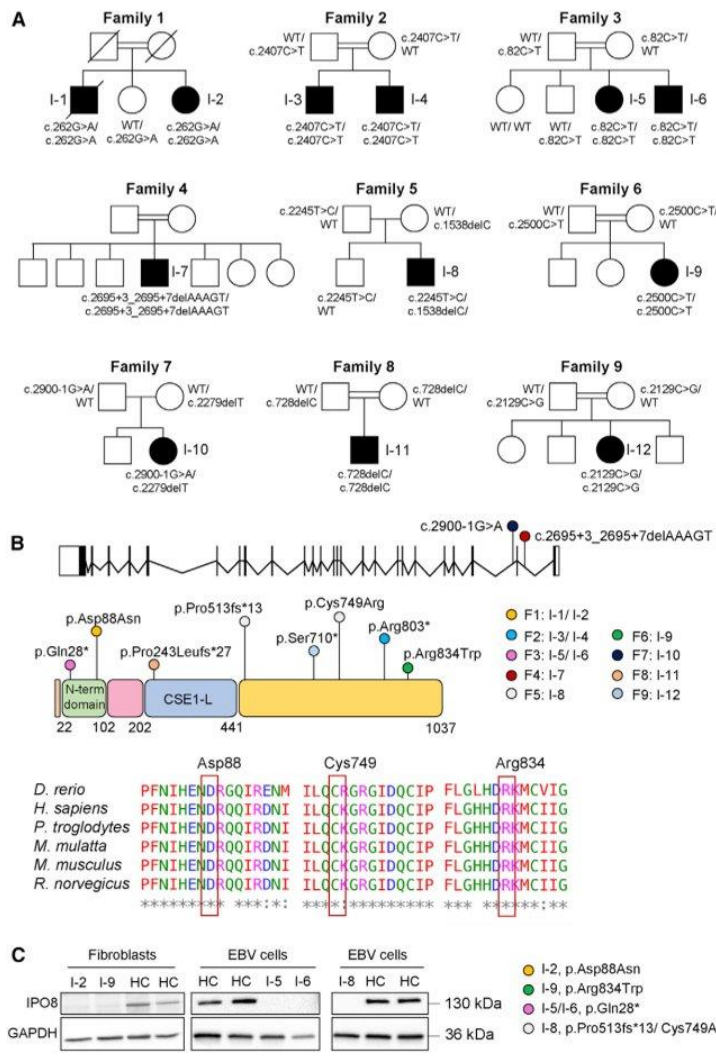


Figure 2. Molecular features of identified variants

(A) Pedigrees of families 1–9. (B) Schematic representation of *IPO8* gene (25 exons, 24 introns) and importin 8 protein (1,037 amino acids), which features the importin N-terminal domain and the CSE1-like domain, containing tandem HEAT repeats and a RanGTP-binding motif. *IPO8* variants identified in this study as well as their location are shown. Protein sequence alignments of *IPO8* orthologs are provided for each affected residue. (C) Importin 8 expression in fibroblasts or EBV cells derived from individuals 2, 5, 6, 8, and 9. GAPDH served as loading control.

the transcription factor *sox9a*, a marker of chondrogenic precursor development (Figure S4D). Shorter trabeculae of the neurocranium were observed in mutant embryos by 2 dpf. In the tail region, *sox9a* expression was strongly reduced or appeared in irregular patches along the spinal cord axis, consistent with defects in vertebrae formation. Heart and vessel morphologies were analyzed after crossing the *ipo8* mutant line with a transgenic line expressing a reporter fluorescently labeling blood vessels in living embryos (*Tg(kdrl:Hsa.HRAS-mCherry)*). Analysis at 2 dpf revealed severe defects in heart chamber formation and atrial and ventricular chambers were less or not delimited in *ipo8*^{-/-} mutants (Figure 4A). *Ipo8*^{-/-} mutants also exhibited arterio-venous malformations in the head and over 70% of mutant embryos in 5 independent clutches showed abnormal arterio-venous con-

nections in the dorsal midline junction and poorly differentiated central arteries that appeared irregular, thin, and poorly lumenized (Figure 4B). By 3 dpf, various severe cardiovascular defects were observed in mutant embryos, including heart edema and, in the subset of embryos with mild tail morphological defects (normal or C1 class in Figure 3D), various blood vessel patterning abnormalities that resulted in the absence of blood circulation or abnormal blood flow in the tail region (e.g., looping or clogging, Figure 4C). Putative defects in TGF- β /BMP signaling in the *ipo8*^{-/-} mutants were next investigated with an antibody specific for pSmad1/5/9. This antibody revealed the expected ventral to dorsal gradient of pSmad1/5/9 detected in WT gastrulating embryos with nuclear localization in the ventral part. In *ipo8*^{-/-} embryos, nuclear localization of

connections in the dorsal midline junction and poorly differentiated central arteries that appeared irregular, thin, and poorly lumenized (Figure 4B). By 3 dpf, various severe cardiovascular defects were observed in mutant embryos, including heart edema and, in the subset of embryos with mild tail morphological defects (normal or C1 class in Figure 3D), various blood vessel patterning abnormalities that resulted in the absence of blood circulation or abnormal blood flow in the tail region (e.g., looping or clogging, Figure 4C).

Putative defects in TGF- β /BMP signaling in the *ipo8*^{-/-} mutants were next investigated with an antibody specific for pSmad1/5/9. This antibody revealed the expected ventral to dorsal gradient of pSmad1/5/9 detected in WT gastrulating embryos with nuclear localization in the ventral part. In *ipo8*^{-/-} embryos, nuclear localization of

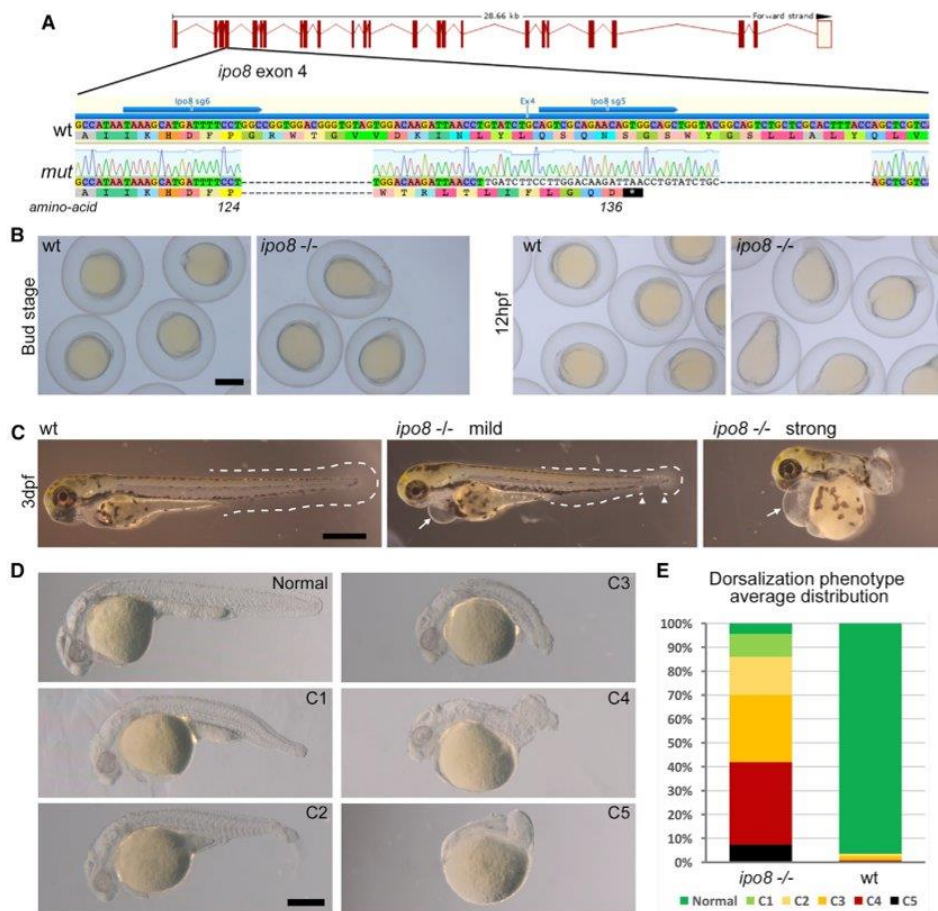


Figure 3. Zebrafish *ipo8* mutants show a range of dorsalization phenotypes

(A) Schematics of CRISPR/Cas9-mediated gene disruption at the *ipo8* genomic locus. The sgRNAs (sg5 and sg6, blue arrows) targeted exon 4. Compared to the wild-type (WT) sequence, the mutated allele from the founder fish (*mut*) displayed two deletions of 18 and 22 bases and an insertion of 34 bp generating a frameshift from amino acid 124 and a premature STOP codon after 136 amino acids. (B) Bright field pictures of bud (10 hpf) and early somite stages (12 hpf) embryos showing the elongating shape of the *ipo8*^{-/-} embryos compared to WT controls. Scale bar represents 500 μ m. (C) Bright field pictures of 3 dpf larvae presenting the variable penetrance of the *ipo8*^{-/-} phenotype (mild and strong) compared to WT controls. The tail fin is circled with dashed lines when visible. Gaps are highlighted by arrowheads. Arrows point at heart edema. Scale bar represents 200 μ m. (D) Nomarski pictures depicting the different classes of the dorsalization phenotype at 24 hpf as described in Mullins et al.²⁶ (from severe C5 to mild C1) in the *ipo8*^{-/-} mutants compared to the normal phenotype of a WT embryo. Scale bar represents 200 μ m. (E) Quantification of the distribution of the dorsalization classes in *ipo8*^{-/-} mutants (5 clutches, n = 903) compared to WT clutches (4 WT clutches, n = 503). Average values in *ipo8*^{-/-} mutants were 7.3% C5, 34.6% C4, 28.0% C3, 16.0% C2, 9.6% C1, and 4.5% normal, and average values in WT controls were 0% C5, 0.8% C4, 1.6% C3, 1.1% C2, 0% C1, and 96.5% normal.

pSmad was significantly reduced (Figures 5A and 5B). In contrast and in keeping with a defect in pSMAD translocation in *ipo8*^{-/-} embryos, the pSMAD signal was detected in the cytoplasm and at membranes, as shown by its colocalization with phalloidin at cell outlines.

To further demonstrate the role of *ipo8* in TGF- β /BMP signaling during development, we compared the transcriptomes of WT and *ipo8*^{-/-} embryos at two different time points during early embryogenesis (13 and 24 hpf) (Figure 5C). We chose these early developmental stages to

avoid secondary effects deriving from abnormalities developing later on. *Ipo8* itself, as expected, was significantly downregulated in *ipo8*^{-/-} fish (Figure S5A). Principal-component analysis (PCA) showed close clustering of biological replicates and a clear segregation of the *ipo8*^{-/-} samples from WT samples both at 13 and 24 hpf (Figure S5B). Genes differentially regulated between the *ipo8*^{-/-} and WT embryos (adjusted p value < 0.01) were analyzed by pathway enrichment analysis (Figure 5C). Strikingly, genes differentially regulated upon *ipo8*

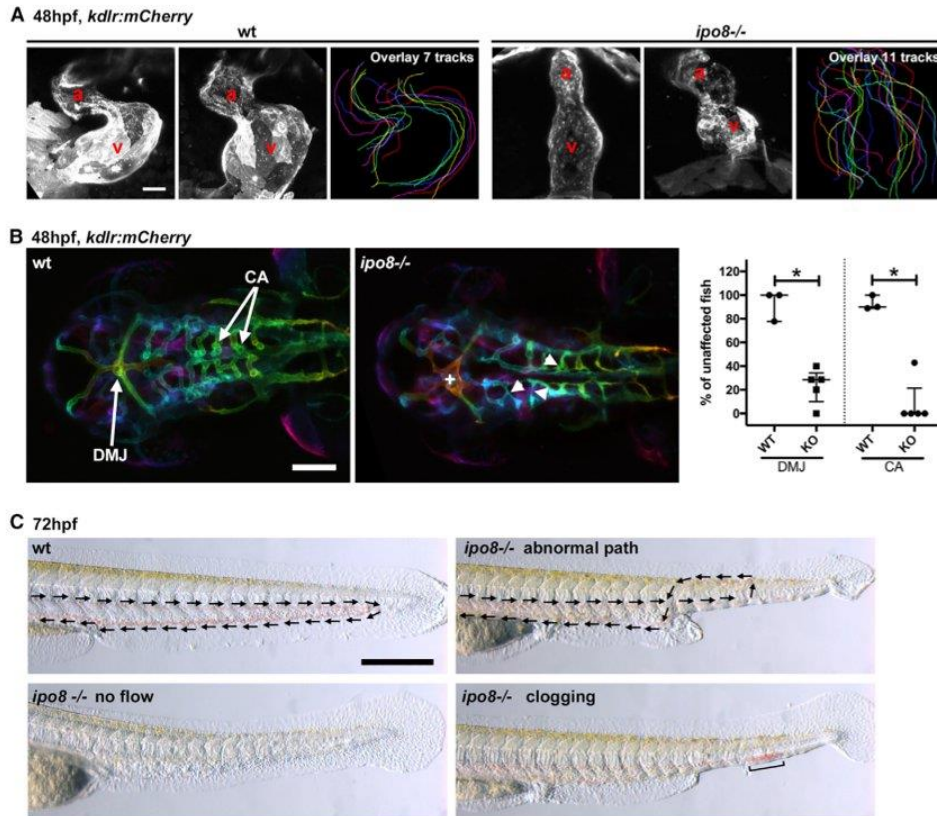


Figure 4. *Ipo8* deficiency causes cardiovascular defects in zebrafish

(A) Defects in heart chamber formation exemplified by two maximal projections of confocal Z stacks of the hearts of WT and *ipo8*^{-/-} 48 hpf embryos carrying the *kdr:mCherry* transgene to label endothelial cells. For each line, the third panel shows the overlays of the outlines of the 7 (WT) and 11 (*ipo8*^{-/-}) analyzed hearts. a, atrium; v, ventricle. Scale bar represents 30 μ m.

(B) Maximal projections of depth color-coded confocal Z stacks of the head vessels of WT and *ipo8*^{-/-} embryos at 48 hpf, and quantifications of the percentage of fish showing dorsal midline junction (DMJ) defects and central arteries (CA) differentiation defects. Twenty-three WT and 30 *ipo8*^{-/-} embryos from 3 and 5 clutches, respectively, were analyzed. Median and IQR are shown. p values were calculated by Mann Whitney test (*p < 0.05). +, abnormal DMJ; arrowheads, abnormal CA. Scale bar represents 100 μ m.

(C) Maximal projections of time-lapses of Nomarsky imaging of the tails of 3 dpf larvae highlighting absence of blood circulation (no flow) or defects in blood vessel patterning (abnormal path and clogging) in *ipo8*^{-/-} mutants. Arrows indicate flow direction. Scale bar represents 200 μ m.

depletion encoded multiple components of the TGF- β /BMP pathway as well as genes involved in angiotensin/angiogenesis pathways. Notably, expression of *smad7*, one of the direct transcriptional targets of the TGF- β /BMP pathway, was strongly decreased in *ipo8*^{-/-} embryos compared to WT at both 13 and 24 hpf, compatible with lack of translocation to the nucleus and, as a consequence, impaired downstream activation of SMAD-dependent transcription.

Overall, our zebrafish model demonstrates that importin 8 plays a critical role during the early stage of development by controlling pSmad nuclear translocation and downstream TGF- β /BMP-dependent transcription. Because homozygous *ipo8*^{-/-} embryos born from heterozygous parents were normal, and because the abnormal phenotype was observed only in MZ mutant embryos, it is likely

that Ipo8 is not essential after the initial embryogenesis occurs. This may be due to genetic compensation²⁹ or simply to Ipo8 function's being redundant with that of a paralog. We cannot, however, exclude subtler cellular/organ phenotypes that may occur later in development or in adult animals and have not been characterized in this study. Importantly, data in the zebrafish model support a causative role of IPO8 deficiency in the vascular and skeleton defects observed in all affected individuals. While our results indicate a role for Ipo8 via the nuclear translocation of phosphorylated SMAD proteins, future investigation remains necessary to define whether and how the role of IPO8 in the translocation of other putative cargoes³⁻⁷ (see above) may participate in the phenotypic features of IPO8 deficiency.

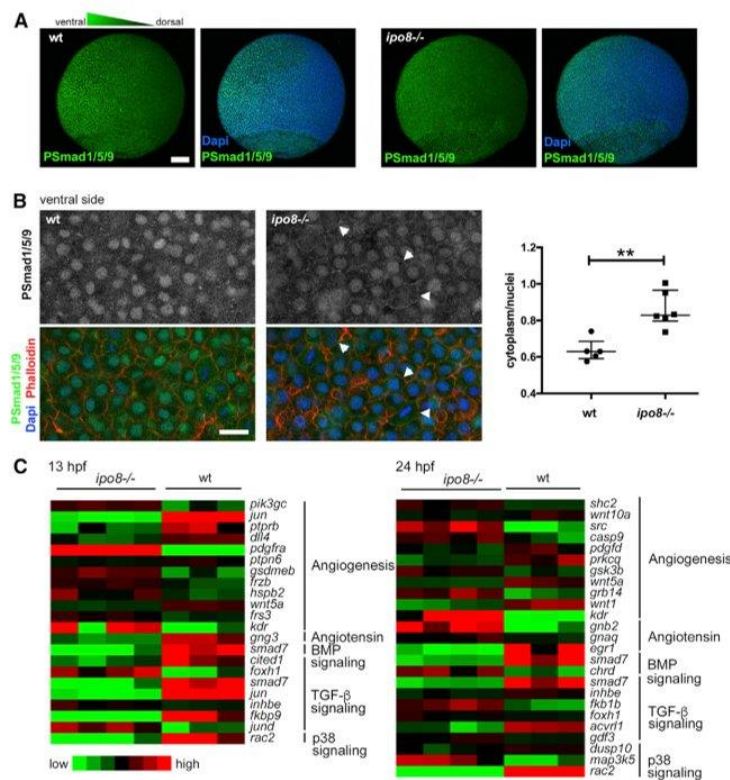


Figure 5. pSMAD nuclear translocation defects in *ipo8*^{-/-} embryos highlight impaired TGF-β/BMP signaling

(A) Maximal projections of confocal Z stacks of WT and *ipo8*^{-/-} embryos labeled for pSmad1/5/9 (green) and DAPI (blue) showing well-defined ventral to dorsal gradient of pSmad5 in WT gastrulating zebrafish embryos (left panel) but not in the *ipo8*^{-/-} embryos (right panel). Scale bar represents 100 μm.

(B) Confocal images of the ventral sides of WT and *ipo8*^{-/-} embryos labeled for pSmad1/5/9 (green), phalloidin (red), and DAPI (blue). Arrowheads highlight the membrane localization of the pSmad staining in the *ipo8*^{-/-} mutants. Scale bar represents 20 μm. Dot plots representative of three experiments show quantifications of the ratio of pSmad1/5/9 cytoplasmic signal over nuclear signal; 5 WT and 6 *ipo8*^{-/-} embryos were analyzed. Median and IQR are shown. p values were calculated by Mann Whitney test (**p < 0.01).

(C) Heatmaps of differentially expressed genes between WT and *ipo8*^{-/-} embryos at 13 and 24 hpf. Three to four biological replicates are shown per group. The top enriched gene ontology term for biological process is highlighted for each cluster.

In summary, we have identified *IPO8* deficiency as the cause of a previously uncharacterized syndrome that is inherited in an autosomal-recessive pattern. This syndrome is characterized by deregulation of TGF-β signaling pathway and overlaps clinically with other TGF-β signalopathies: MFS, LDS, and SGS as depicted in Figure S6 and Table S1. Common features observed in *IPO8* individuals and shared with LDS, MFS, and SGS include cardiovascular anomalies with notably strong predisposition for ascending aorta aneurysm and facial and skeletal anomalies (Table S1). Other less recurrent manifestations displayed by *IPO8*-deficient individuals were immune dysregulation and allergic diseases, which have also been reported in a subset of LDS-affected individuals,³⁰ and developmental delay that was observed in SGS.¹⁴ The accompanying article by Van Gucht et al.³¹ in this issue of *The American Journal of Human Genetics* reports largely overlapping developmental abnormalities in seven additional *IPO8*-deficient individuals.³¹ Their data showing that the loss of *ipo8* causes severe early-onset thoracic aortic aneurysm in a mouse model supports the causative role of the gene defect in the most severe manifestation of the disease and complements our demonstration that *IPO8* plays a crucial role in TGF-β-dependent organogenesis and in cardio-vascular development in the zebrafish

model. Overall, the identification of *IPO8* deficiency as cause of TGF-β signalopathy stresses the essential functions of this pathway in development, patterning, and homeostasis of the affected tissues.

Data and code availability

The *IPO8* variants were submitted to ClinVar (<https://www.ncbi.nlm.nih.gov/clinvar/>) (GenBank: NM_006390.3; accession numbers SCV001571677, SCV001571678, SCV001571679, SCV001571680, SCV001571681, SCV001571682, SCV001571683, SCV001571684, SCV001571685, SCV001571686, and SCV001571687). The WES datasets supporting this study have not been deposited in a public repository because of ethical restriction but are available from the corresponding author on request.

Supplemental information

Supplemental information can be found online at <https://doi.org/10.1016/j.ajhg.2021.04.020>.

Acknowledgments

We are grateful to the families who participated in this work. We thank Nicole Van Bergen, MCRI, for performing the confirmatory Sanger sequencing in individual 10. This work was supported by

the Agence Nationale de la Recherche under “Investissements d’avenir” program (ANR-10-IAHU-01), institutional grants from INSERM, the European grant ERC-2013-AdG-339407-IMMUNOBIOTA, and grants from Fondation Princesse Grace and “Fondation Maladies Rares” (to N.C.B.); by institutional grants from the CNRS and the University of Angers (to D.B.); by intramural funding (fortune) at the University of Tübingen (2545-1-0) and the Ministry of Science, Research and Art Baden-Württemberg (to B.V.); and by the Programme Investissements d’Avenir IHU FORESIGHT (ANR-18-IAHU-01) (to F.D.B.). C.R. was supported by an EU Horizon 2020 Marie Skłodowska-Curie Action fellowship (H2020-MSCA-IF-2014 #661527). K.M.G. and K.K. are jointly funded by the Indian Council of Medical Research (file no. 5/7/1508/2016 to K.M.G.) and the Federal Ministry of Education and Research (01DQ17003 to K.K.). Sequencing and analysis for individual 10 were provided by the Broad Institute of MIT and Harvard Center for Mendelian Genomics (Broad CMG) and was funded by the National Human Genome Research Institute, the National Eye Institute, and the National Heart, Lung, and Blood Institute grant UMI HG008900 and in part by National Human Genome Research Institute grant R01 HG009141. Funding for the UDP-Vic was provided by philanthropic donation and the Murdoch Children’s Research Institute. The research conducted at the Murdoch Children’s Research Institute was supported by the Victorian Government’s Operational Infrastructure Support Program, the Harbig Family Foundation, and The Royal Children’s Hospital Foundation.

Declaration of interests

The authors declare no competing interests.

Received: January 24, 2021

Accepted: April 23, 2021

Published: May 18, 2021

Web resources

CADD, <https://cadd.gs.washington.edu/>
 GenBank, <https://www.ncbi.nlm.nih.gov/genbank/>
 GeneMatcher, <https://genematcher.org/>
 gnomAD, <https://gnomad.broadinstitute.org/>
 Mutation Taster, <http://www.mutationtaster.org/>
 OMIM, <https://omim.org>
 PolyPhen2, <http://genetics.bwh.harvard.edu/pph2/>
 SIFT, <https://sift.bii.a-star.edu.sg/>

References

- Görlich, D., Dabrowski, M., Bischoff, F.R., Kutay, U., Bork, P., Hartmann, E., Prehn, S., and Izaurralde, E. (1997). A novel class of RanGTP binding proteins. *J. Cell Biol.* *138*, 65–80.
- Stewart, M. (2007). Molecular mechanism of the nuclear protein import cycle. *Nat. Rev. Mol. Cell Biol.* *8*, 195–208.
- Dean, K.A., von Ahlsen, O., Görlich, D., and Fried, H.M. (2001). Signal recognition particle protein 19 is imported into the nucleus by importin 8 (RanBP8) and transportin. *J. Cell Sci.* *114*, 3479–3485.
- Wei, Y., Li, L., Wang, D., Zhang, C.-Y., and Zen, K. (2014). Importin 8 regulates the transport of mature microRNAs into the cell nucleus. *J. Biol. Chem.* *289*, 10270–10275.
- Weinmann, L., Höck, J., Ivacevic, T., Ohrt, T., Mütze, J., Schwille, P., Kremmer, E., Benes, V., Urlaub, H., and Meister, G. (2009). Importin 8 is a gene silencing factor that targets argonaute proteins to distinct mRNAs. *Cell* *136*, 496–507.
- Schreck, I., Al-Rawi, M., Mingot, J.-M., Scholl, C., Diefenbacher, M.E., O’Donnell, P., Bohmann, D., and Weiss, C. (2011). c-Jun localizes to the nucleus independent of its phosphorylation by and interaction with JNK and vice versa promotes nuclear accumulation of JNK. *Biochem. Biophys. Res. Commun.* *407*, 735–740.
- Liang, P., Zhang, H., Wang, G., Li, S., Cong, S., Luo, Y., and Zhang, B. (2013). KPNB1, XPO7 and IPO8 mediate the translocation of NF- κ B/p65 into the nucleus. *Traffic* *14*, 1132–1143.
- Volpon, L., Culjkovic-Kraljacic, B., Osborne, M.J., Ramteke, A., Sun, Q., Niesman, A., Chook, Y.M., and Borden, K.L.B. (2016). Importin 8 mediates m7G cap-sensitive nuclear import of the eukaryotic translation initiation factor eIF4E. *Proc. Natl. Acad. Sci. USA* *113*, 5263–5268.
- Yao, X., Chen, X., Cottonham, C., and Xu, L. (2008). Preferential utilization of Imp7/8 in nuclear import of Smads. *J. Biol. Chem.* *283*, 22867–22874.
- Xu, L., Yao, X., Chen, X., Lu, P., Zhang, B., and Ip, Y.T. (2007). Msk is required for nuclear import of TGF- β /BMP-activated Smads. *J. Cell Biol.* *178*, 981–994.
- David, C.J., and Massagué, J. (2018). Contextual determinants of TGF β action in development, immunity and cancer. *Nat. Rev. Mol. Cell Biol.* *19*, 419–435.
- MacFarlane, E.G., Haupt, J., Dietz, H.C., and Shore, E.M. (2017). TGF- β Family Signaling in Connective Tissue and Skeletal Diseases. *Cold Spring Harb. Perspect. Biol.* *9*, a022269.
- Schepers, D., Tortora, G., Morisaki, H., MacCarrick, G., Lindsay, M., Liang, D., Mehta, S.G., Hague, J., Verhagen, J., van de Laar, I., et al. (2018). A mutation update on the LDS-associated genes TGF β 2/3 and SMAD2/3. *Hum. Mutat.* *39*, 621–634.
- Doyle, A.J., Doyle, J.J., Bessling, S.L., Maragh, S., Lindsay, M.E., Schepers, D., Gillis, E., Mortier, G., Homfray, T., Sauls, K., et al. (2012). Mutations in the TGF- β repressor SKI cause Shprintzen-Goldberg syndrome with aortic aneurysm. *Nat. Genet.* *44*, 1249–1254.
- Loeys, B.L., Chen, J., Neptune, E.R., Judge, D.P., Podowski, M., Holm, T., Meyers, J., Leitch, C.C., Katsanis, N., Sharifi, N., et al. (2005). A syndrome of altered cardiovascular, craniofacial, neurocognitive and skeletal development caused by mutations in TGFBR1 or TGFBR2. *Nat. Genet.* *37*, 275–281.
- Chen, W., and Ten Dijke, P. (2016). Immunoregulation by members of the TGF β superfamily. *Nat. Rev. Immunol.* *16*, 723–740.
- Kelly, A., Houston, S.A., Sherwood, E., Casulli, J., and Travis, M.A. (2017). Regulation of Innate and Adaptive Immunity by TGF β . *Adv. Immunol.* *134*, 137–233.
- Frischmeyer-Guerrero, P.A., Guerrero, A.L., Oswald, G., Chichester, K., Myers, L., Halushka, M.K., Oliva-Hemker, M., Wood, R.A., and Dietz, H.C. (2013). TGF β receptor mutations impose a strong predisposition for human allergic disease. *Sci. Transl. Med.* *5*, 195ra94.
- Guerrero, A.L., Frischmeyer-Guerrero, P.A., Huang, C., Wu, Y., Haritunians, T., McGovern, D.P.B., MacCarrick, G.L., Brant, S.R., and Dietz, H.C. (2016). Increased Prevalence of Inflammatory Bowel Disease in Patients with Mutations in Genes Encoding the Receptor Subunits for TGF β . *Inflamm. Bowel Dis.* *22*, 2058–2062.

20. Kotlarz, D., Marquardt, B., Barøy, T., Lee, W.S., Konnikova, L., Hollizeck, S., Magg, T., Lehle, A.S., Walz, C., Borggraefe, I., et al. (2018). Human TGF- β 1 deficiency causes severe inflammatory bowel disease and encephalopathy. *Nat. Genet.* *50*, 344–348.
21. Sobreira, N., Schiettecatte, F., Valle, D., and Hamosh, A. (2015). GeneMatcher: a matching tool for connecting investigators with an interest in the same gene. *Hum. Mutat.* *36*, 928–930.
22. Loeys, B.L., Schwarze, U., Holm, T., Callewaert, B.L., Thomas, G.H., Pannu, H., De Backer, J.F., Oswald, G.L., Symoens, S., Manouvrier, S., et al. (2006). Aneurysm syndromes caused by mutations in the TGF-beta receptor. *N. Engl. J. Med.* *355*, 788–798.
23. Jaganathan, K., Kyriazopoulou Panagiotopoulou, S., McRae, J.F., Darbandi, S.F., Knowles, D., Li, Y.I., Kosmicki, J.A., Arbe-laez, J., Cui, W., Schwartz, G.B., et al. (2019). Predicting Splicing from Primary Sequence with Deep Learning. *Cell* *176*, 535–548.e24.
24. Abrams, E.W., and Mullins, M.C. (2009). Early zebrafish development: it's in the maternal genes. *Curr. Opin. Genet. Dev.* *19*, 396–403.
25. Stainier, D.Y.R., Raz, E., Lawson, N.D., Ekker, S.C., Burdine, R.D., Eisen, J.S., Ingham, P.W., Schulte-Merker, S., Yelon, D., Weinstein, B.M., et al. (2017). Guidelines for morpholino use in zebrafish. *PLoS Genet.* *13*, e1007000.
26. Mullins, M.C., Hammerschmidt, M., Kane, D.A., Odenthal, J., Brand, M., van Eeden, F.J., Furutani-Seiki, M., Granato, M., Haffter, P., Heisenberg, C.P., et al. (1996). Genes establishing dorsoventral pattern formation in the zebrafish embryo: the ventral specifying genes. *Development* *123*, 81–93.
27. Tucker, J.A., Mintzer, K.A., and Mullins, M.C. (2008). The BMP signaling gradient patterns dorsoventral tissues in a temporally progressive manner along the anteroposterior axis. *Dev. Cell* *14*, 108–119.
28. Hammerschmidt, M., and Mullins, M.C. (2002). Dorsoventral patterning in the zebrafish: bone morphogenetic proteins and beyond. *Results Probl. Cell Differ.* *40*, 72–95.
29. Rossi, A., Kontarakis, Z., Gerri, C., Nolte, H., Höpfer, S., Krüger, M., and Stainier, D.Y.R. (2015). Genetic compensation induced by deleterious mutations but not gene knockdowns. *Nature* *524*, 230–233.
30. Cannnaerts, E., van de Beek, G., Verstraeten, A., Van Laer, L., and Loeys, B. (2015). TGF- β signalopathies as a paradigm for translational medicine. *Eur. J. Med. Genet.* *58*, 695–703.
31. Van Gucht, I., Meester, J.A.N., Bento, J.R., Bastiaansen, M., Bastianen, J., Luyckx, I., Van Den Heuvel, L., Neutel, C.H.G., Guns, P.J., Vermont, M., et al. (2021). A human importin- β -related disorder: Syndromic thoracic aortic aneurysm caused by bi-allelic loss-of-function variants in IPO8. *Am. J. Hum. Genet.* Published online May 18, 2021. <https://doi.org/10.1016/j.ajhg.2021.04.019>.

10.7 Attachment 7

Unraveling the genetic complexities of combined retinal dystrophy and hearing impairment



Unraveling the genetic complexities of combined retinal dystrophy and hearing impairment

Paulina Bahena¹ · Narsis Daftarian² · Reza Maroofian³ · Paola Linares⁴ · Daniel Villalobos⁵ · Mehraban Mirrahimi² · Aboufazel Rad⁶ · Julia Doll¹ · Michaela A. H. Hofrichter¹ · Asuman Koparir¹ · Tabea Röder¹ · Seungbin Han¹ · Hamideh Sabbaghi⁷ · Hamid Ahmadieh⁷ · Hassan Behboudi⁸ · Cristina Villanueva-Mendoza⁹ · Vianney Cortés-Gonzalez⁹ · Rocio Zamora-Ortiz¹⁰ · Susanne Kohl¹¹ · Laura Kuehlewein^{11,12} · Hossein Darvish¹³ · Elham Alehabib¹⁴ · Maria de la Luz Arenas-Sordo¹⁵ · Fatemeh Suri⁷ · Barbara Vona^{1,6} · Thomas Haaf¹

Received: 26 March 2021 / Accepted: 15 June 2021 / Published online: 20 June 2021
© The Author(s) 2021

Abstract

Usher syndrome, the most prevalent cause of combined hereditary vision and hearing impairment, is clinically and genetically heterogeneous. Moreover, several conditions with phenotypes overlapping Usher syndrome have been described. This makes the molecular diagnosis of hereditary deaf–blindness challenging. Here, we performed exome sequencing and analysis on 7 Mexican and 52 Iranian probands with combined retinal degeneration and hearing impairment (without intellectual disability). Clinical assessment involved ophthalmological examination and hearing loss questionnaire. Usher syndrome, most frequently due to biallelic variants in *MYO7A* (USH1B in 16 probands), *USH2A* (17 probands), and *ADGRV1* (USH2C in 7 probands), was diagnosed in 44 of 59 (75%) unrelated probands. Almost half of the identified variants were novel. Nine of 59 (15%) probands displayed other genetic entities with dual sensory impairment, including Alström syndrome (3 patients), cone-rod dystrophy and hearing loss 1 (2 probands), and Heimler syndrome (1 patient). Unexpected findings included one proband each with Scheie syndrome, coenzyme Q10 deficiency, and pseudoxanthoma elasticum. In four probands, including three Usher cases, dual sensory impairment was either modified/aggravated or caused by variants in distinct genes associated with retinal degeneration and/or hearing loss. The overall diagnostic yield of whole exome analysis in our deaf–blind cohort was 92%. Two (3%) probands were partially solved and only 3 (5%) remained without any molecular diagnosis. In many cases, the molecular diagnosis is important to guide genetic counseling, to support prognostic outcomes and decisions with currently available and evolving treatment modalities.

Introduction

Neuro-sensory deficits are among the most prevalent congenital disorders in humans. Impaired hearing and/or vision can negatively affect a person's communication abilities, cognitive functions, and social competencies. Both senses

work together and to some extent, one can help compensate for loss of the other. Therefore, deaf–blindness, including a wide range of hearing and vision levels (99% of patients have some residual hearing and/or vision capabilities), is more than the sum of hearing impairment (HI) and vision impairment (VI); it seriously impacts multiple areas of development. Children with dual sensory impairments have specific educational needs, requiring an interdisciplinary team of medical specialists and teachers (Dammeyer 2014).

Deaf–blindness may be acquired, e.g. by intrauterine infections (e.g. rubella, cytomegalovirus), premature birth, and cerebral palsy. However, in developed countries, the vast majority of congenital cases have a genetic basis. Usher syndrome (USH), a heterogeneous autosomal recessive disorder, accounts for approximately 50% of hereditary cases of combined deafness and blindness; it has an incidence of 1 in 6000–25,000 (Kimberling et al. 2010). In addition,

Fatemeh Suri, Barbara Vona and Thomas Haaf contributed equally to this work.

✉ Fatemeh Suri
fatemehsuri@gmail.com

✉ Barbara Vona
barbara.vona@uni-tuebingen.de

✉ Thomas Haaf
thomas.haaf@uni-wuerzburg.de

Extended author information available on the last page of the article

variants in USH genes account for up to 10% of children diagnosed with non-syndromic HI (Jouret et al. 2019). The most severe form, USH1, is characterized by congenital severe to profound deafness, vestibular dysfunction, and retinal degeneration in the first decade of life. USH1 can be caused by variants in at least five genes (*MYO7A*, *USH1C*, *CDH23*, *PCDH15*, and *USH1G*). The most common form is USH2, accounting for diagnoses in two-thirds of USH patients, that is characterized by moderate to severe congenital HI and retinitis pigmentosa (RP) in the second decade of life. USH2 results from mutations in at least three genes (*USH2A*, *ADGRV1*, and *WHRN*); mutations in *USH2A* are by far the most common cause accounting for 90% of USH2 cases (Bonnet et al. 2016). The mildest form, USH3, exhibits variable, usually progressive, HI and RP later in life and has been associated with variants in *CLRN1* (Hereditary Hearing Loss Homepage; <https://hereditaryhearingloss.org>; Retinal Information Network; <https://sph.uth.edu/retnet/disease.htm>).

Here, we performed whole exome analysis (WEA) of 59 unrelated, mainly consanguineous families with at least one proband clinically diagnosed with HI and retinal degeneration. Our study highlights the enormous molecular genetic heterogeneity of combined HI and VI and the need to analyze larger gene panels (for both diseases of the auditory and visual system) in addition to known or suspected USH genes.

Materials and methods

Patients

This study was approved by the ethics committees at the Medical Faculty of Würzburg University, Germany (approval number 46/15), the National Institute of Rehabilitation Luis Guillermo Ibarra (INR), Mexico (no. 12/13), and the Shahid Beheshti University of Medical Sciences, Tehran, Iran and was carried out following the ethical principles of the declaration of Helsinki. Written informed consent was obtained from all participating families prior to their inclusion in the study.

We recruited 59 unrelated probands with combined HI and retinal degeneration resulting in reduced vision and nyctalopia. None of the probands reportedly suffered from intellectual disability. Fifty-two Iranian index patients from consanguineous families were seen by ophthalmologists in different centers and were cataloged in the Iranian Inherited Retinal Disease Registry (NCT04131400) (Sabbaghi et al. 2020). Seven non-consanguineous Mexican probands were recruited by medical geneticists in the Asociación Para Evitar la Ceguera en México (APEC) and the National Institute of Rehabilitation (INR), Mexico City.

Medical, drug and familial histories were recorded. Ocular examinations (Supplementary Table 1) of all Iranian patients were performed at Labbafinejad Medical Center, affiliated with the Shahid Beheshti University of Medical Sciences. These included examination of the best corrected visual acuity (VA) using Snellen charts, slit lamp biomicroscopy of the anterior and posterior segments (using +90 lens), Goldmann tonometry, and color vision and visual field testing using a Humphrey Field Analyzer II, model 750 (Zeiss Humphrey Systems, Dublin, CA, USA). For patients with VA scores under 20/200, a semi-quantitative scale was used, including counting fingers at different distances, hand movements and light perception. In many cases, depending on the level of vision, standard full field electroretinography (ERG) was performed under photopic and scotopic conditions. Ocular imaging included color fundus photography (CFP), spectral domain optical coherence tomography (OCT) (6 mm scans centered from the fovea, using a Spectralis imaging platform, Heidelberg, Germany), and fundus autofluorescence (FAF) imaging (HRA, Heidelberg, Germany). Patients with apparent USH were classified with mild, moderate or severe cystoid macular edema (CME), using the grading system of Sliesoraityte et al. (2015). The following features were considered: subretinal fluid without clearly detectable cystic macular lesion (CML) boundaries, central macular thickness, largest diameter of CML, calculated mean of all detectable CMLs, total number of detectable CML, and retinal layers affected by CML.

HI was determined by anamnesis and by questionnaire. Audiograms were available from probands 1, 6, 8, 9, 12, 24, 25, 42, 44, 47, 52, 54, and 58 (Supplementary Table 1). Severity of HI was assessed by averaging pure-tone thresholds of the better hearing ear over 0.5, 1, 2, and 4 kHz. Averaged thresholds between 41–70 dB represent moderate, 71–95 dB severe, and > 95 dB profound HL. Interpretation of audiometry followed the recommendations of the GEN-DEAF study group (Mazzoli et al. 2003).

Sequence analysis and variant classification

Genomic DNAs of probands and available family members were extracted from whole blood samples using a standard salting out method and quantified using Qubit 2.0 (Life Technologies, Carlsbad, CA, USA). Exome capture was performed using the TruSeq Rapid Exome or Nextera DNA Exome (Illumina, San Diego, CA, USA) enrichment according to manufacturer's protocols. Libraries were paired-end sequenced (2 × 76 bp) with the v2 reagent kit (Illumina) on a NextSeq 500 (Illumina) sequencer. The generated sequences were de-multiplexed and mapped to the human genome reference (NCBI build 37/hg19 version) with Burrows Wheeler Aligner.

First, a targeted analysis of the following USH-associated genes was performed using GensearchNGS software (PhenoSystems SA, Wallonia, Belgium): *ABDH12* (OMIM 613599, NM_001042472.2), *ADGRV1* (OMIM 602851, NM_032119.3), *CDH23* (OMIM 605516, NM_022124.5), *CEP250* (OMIM 609689, NM_007186.5), *CLRN1* (OMIM 606397, NM_001195794.1), *MYO7A* (OMIM 276903, NM_000260.3), *PCDH15* (OMIM 605514, NM_001142763.1), *PDZD7* (OMIM 612971, NM_001195263.1), *USH1C* (OMIM 605242, NM_153676.3), *USH1G* (OMIM 607696, NM_173477.4), *USH2A* (OMIM 608400, NM_206933.2), and *WHRN* (OMIM 607928, NM_015404.3). In a second step, the whole exome was analyzed in patients without molecular USH diagnoses. A refuted USH1J gene, *CIB2* (Riazuddin et al. 2012; Booth et al. 2018), a questionable USH1M gene, *ESPN* (Ahmed et al. 2018), a refuted USH3B gene, *HARS* (Puffenberger et al. 2012; DiStefano et al. 2019), and a recently identified USH4 gene, *ARSG* (Peter et al. 2021), were not included in our original screen, but rather in exome-wide analysis.

Single nucleotide variants (SNVs) and small indels (< 15 bp) were analyzed using GensearchNGS, MutationDistiller (Hombach et al. 2019), and Moon Diploid (<http://www.diploid.com/moon>). Alternative alleles present at > 20% and a minor allele frequency (MAF) < 0.01 were used for variant filtering. Population-specific allele frequencies were assessed using gnomAD (Karczewski et al. 2020) and the Greater Middle Eastern (GME) variome (Scott et al. 2016). PolyPhen-2 (Adzhubei et al. 2010), MutationTaster (Ng and Henikoff 2001), and SIFT (Schwarz et al. 2014) were used to analyze pathogenicity of SNVs. Variants were queried in the Deafness Variation Database (DVD) (Azaiez et al. 2018), the Human Gene Mutation Database (HGMD) (Stenson et al. 2014), and the Leiden Open Variation Database (LOVD) (<https://www.lovd.nl>). Potential splicing effects of variants were classified by in silico prediction tools such as SpliceSiteFinder-like (Shapiro and Senapathy 1987), MaxEntScan (Yeo and Burge 2004), NNSPLICE (Reese et al. 1997), Genesplicer (Peretea et al. 2001), and Human Splicing Finder (Desmet et al. 2009). Variants were classified according to the recommendations of the American College of Medical Genetics and Genomics (ACMG) and the Association for Molecular Pathology (AMP) (Richards et al. 2015), as well as established recommendations for hereditary HI (Oza et al. 2018). Potentially disease-causing and compound heterozygous variants were validated by segregation analysis in the index patients and available family members using Sanger sequencing on an ABI 3130xl 16-capillary sequencer (Life Technologies). Primer sequences were designed using Primer 3 (<https://primer3.org>).

In probands with a single pathogenic *USH2A* variant (50, 51, and 57), partially solved (45 and 53), and unsolved

cases (55, 57, and 59), multiplex ligation-dependent probe amplification (MLPA) with the SALSA Probemix P361, P362, and P292 (MRC Holland, Amsterdam, The Netherlands) was used to exclude copy number variations (CNVs) in *USH2A* and *PCDH15*. In addition, these probands were screened by Sanger sequencing for deep intronic mutations (DIMs) in *USH2A* introns 27 (c.5573-843A>G), 40 (c.7595-2144A>G), 44 (c.8845+628C>T), 50 (c.9959-4159A>G), and 64 (c.14134-3169A>G) (Vache et al. 2012; Liquori et al. 2016; Baux et al. 2017). In some probands showing multi-locus variation (42, 43, 44, 45, and 58), the Infinium Global Screening Array-24 v1.0 BeadChip (Illumina, San Diego, CA, USA) was applied for genome-wide CNV screening.

In vitro splice assays

To evaluate the impact of the *ADGRV1* c.9623+3A>C and *PDSS2* c.702+1G>A splice variants, PCR amplification from patient and control genomic DNA ensued following a modified protocol (Tompson and Young 2017). For testing of the *ADGRV1* variant, amplification of a region including exon 44 (176 bp) with an additional 589 bp (5') and 340 bp (3') from the flanking intronic region was performed using primers containing *XhoI* and *BamHI* restriction sites (forward primer with a *XhoI* restriction site: 5'-aattctcgagTTTGCTGGTTCCTGAGCTTC-3' and reverse primer with a *BamHI* restriction site: 5'-attggatccTCATCACT TGGTTTGAGCAG-3'). Similarly, for testing of the *PDSS2* variant, amplification of a region containing exon 4 (71 bp) that included 390 bp (5') and 1380 bp (3') from the flanking intronic regions was performed (forward primer with a *XhoI* restriction site: 5'-aattctcgagTTGTAATTGCTCCCA GAATGG-3' and reverse primer with a *BamHI* restriction site: 5'-attggatccTGACTTCAAATCCCTGAGAGC-3'). Following PCR amplification and clean-up, restriction enzyme digestion of the PCR fragment and pSPL3 exon trapping vector was performed prior to ligation between exons A and B of the linearized pSPL3-vector. The vector was transformed into DH5 α competent cells (NEB 5-alpha, New England Biolabs, Frankfurt am Main, Germany), plated, and incubated overnight. The wild-type and mutant-containing vector sequences were Sanger sequence confirmed. Vectors containing mutant and wild-type sequence were transfected into HEK 293T cells (ATCC) at a density of 2×10^5 cells per milliliter. 1 μ g of the respective pSPL3 vectors were transiently transfected using 3 μ l of FuGENE 6 Transfection Reagent (Promega, Walldorf, Germany). An empty vector and transfection negative reactions were included as controls. The transfected cells were harvested 24 h after transfection. Total RNA was prepared using miRNAeasy Mini Kit (Qiagen, Hilden, Germany). Approximately 1 μ g of RNA was reverse transcribed using a High Capacity RNA-to-cDNA Kit (Applied Biosystems, Foster City, CA, USA)

following the manufacturer's protocols. The cDNA was PCR amplified using vector-specific SD6 forward (5'-TCT GAGTCACCTGGACAACC-3') and SA2 reverse (5'-ATC TCAGTGGTATTTGTGAGC-3') primers. The amplified fragments were visualized on a 2% agarose gel and Sanger sequenced. *ADGRV1* fragments were cloned using the TA cloning dual promoter with pCRII kit (Invitrogen, Karlsruhe, Germany) and subsequently Sanger sequenced.

Results

Clinical and molecular characterization of the analyzed cohort

Staged exome diagnostics was performed on 59 unrelated probands with co-occurring HI and VI (due to retinal dystrophy) and without apparent intellectual disability. Patient age at the time of recruitment ranged from 8 to 65 years with a mean age of 34 years. Clinical parameters are presented in Supplementary Table 1. The reported visual acuity ranged from 20/30 Snellen equivalent to no light perception. The most common symptom was nyctalopia accompanied by bilateral reduced vision. The most common ophthalmological findings included waxy pallor discs, retinal atrophy, mottling and diffuse bone spicule pigmentary changes, cataracts, and macular edema. With exception of proband 11, intraocular pressure of both eyes by Goldmann tonometry was normal. The majority (64%) of the probands presented

with prelingual HI, the rest with postlingual HI. If available, tympanograms showed normal middle ear function.

Forty-seven of the 52 (90%) cases from consanguineous Iranian families and all 7 cases from non-consanguineous Mexican families were solved. The overall diagnostic yield was 92% (54 of 59). A molecular diagnosis pointing to USH accounted for 44 of 59 (75%) and non-USH syndromes for 9 of 59 (15%) index probands. In three of the USH cases, additional variants in genes for non-syndromic HI (*OTOG*, *TECTA*) or *ABCA4*-related VI (Stargardt disease, cone-rod dystrophy, and RP) may modify/aggravate the phenotype (Fig. 1, left). In one of 59 (2%) probands, HI and VI were caused by variants in different genes. Two additional probands with a blended phenotype were partially solved.

Usher syndrome as the most common cause of dual sensory loss

Forty-four patients showed biallelic variants in known USH genes, approximately half of the variants being novel (Table 1; Fig. 1, right). Nineteen of these 44 patients suffered from USH1, 24 from USH2, and only one from USH3. The most frequently affected genes in our cohort were *MYO7A* (USH1B) in 16 patients and *USH2A* (USH2A) in 17 patients, followed by *ADGRV1* (USH2C) in 7 patients. Biallelic variants in *USH1C*, *CDH23* (USH1D), *USH1G*, and *CLRN1* (USH3A) were diagnosed in single patients each. It is noteworthy that although the vast majority of our USH probands were from consanguineous families, compound heterozygous variants

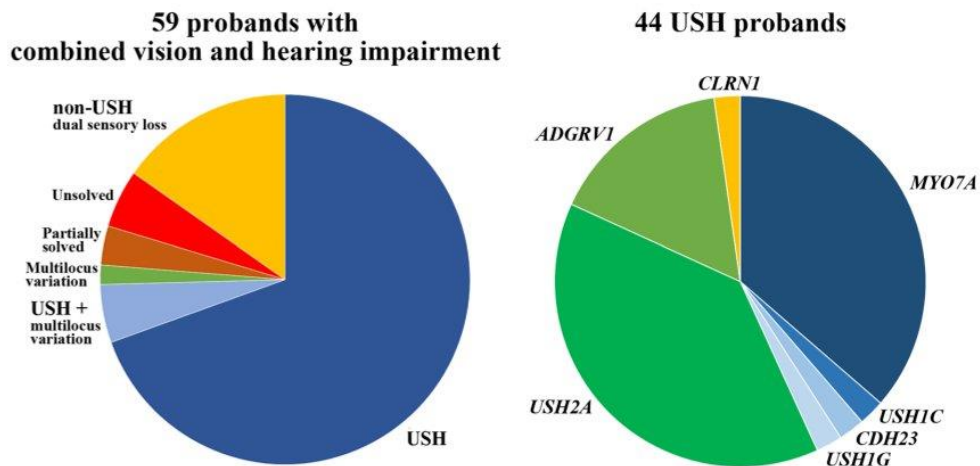


Fig. 1 The left diagram shows the diagnostic yield in 59 probands with combined vision and hearing impairment. As expected, USH was the most common diagnosis accounting for 75% of cases. Please note that three USH (+multi-locus variation) probands exhibited variants in additional genes for HI and VI. Different non-USH syn-

dromes with co-occurring HI and VI were found in 15% of cases. The right diagram represents the mutational spectrum in the 44 USH probands. Mutations in USH1 genes are marked in different shades of blue and in USH2 genes in green

Table 1 Biallelic variants and genotypes in USH genes

ID	Gene	Variant	Protein	Zygoty ^a	Classification	References	Phenotype
1	<i>MYO7A</i>	c.1969C>T	p.(Arg657Trp)	Hom	Pathogenic	Cremers et al. (2007)	USH1B
2	<i>MYO7A</i>	c.73G>A	p.(Gly25Arg)	Hom	Pathogenic	Watanabe et al. (2008)	USH1B
3	<i>MYO7A</i>	c.5617C>T	p.(Arg1873Trp)	Het	Pathogenic	Roux et al. (2006)	USH1B
	<i>MYO7A</i>	c.2904G>T	p.(Glu968Asp)	Het	Pathogenic	Bonnet et al. (2016)	
4	<i>MYO7A</i>	c.5573T>C	p.(Leu1858Pro)	Hom	Pathogenic	Bademci et al. (2016)	USH1B
5	<i>MYO7A</i>	c.397dup	p.(His133Profs*7)	Hom	Pathogenic	Bonnet et al. (2011)	USH1B
6	<i>MYO7A</i>	c.2282 + 1G>C	p.?	Het	Pathogenic	Novel	USH1B
	<i>MYO7A</i>	c.721C>T	p.(Arg241Cys)	Het	Pathogenic	Bharadwaj et al. (2000)	
7	<i>MYO7A</i>	c.397dup	p.(His133Profs*7)	Het	Pathogenic	Bonnet et al. (2011)	USH1B
	<i>MYO7A</i>	c.4513G>T	p.(Glu1505*)	Het	Pathogenic	Kooshavar et al. (2018)	
8	<i>MYO7A</i>	c.487G>A	p.(Gly163Arg)	Hom	Pathogenic	Roux et al. (2006)	USH1B
9	<i>MYO7A</i>	c.3564_3570delinsA	p.(Tyr1188*)	Hom	Pathogenic	Duzkale et al. (2013)	USH1B
10	<i>MYO7A</i>	c.6204dup	p.(Ile2069Tyrf*7)	Het	Pathogenic	Cremers et al. (2007)	USH1B
	<i>MYO7A</i>	c.3564_3570delinsA	p.(Tyr1188*)	Het	Pathogenic	Duzkale et al. (2013)	
11	<i>MYO7A</i>	c.722G>A	p.(Arg241His)	Het	Likely pathogenic	Bademci et al. (2016)	USH1B
	<i>MYO7A</i>	c.1388A>G	p.(Gln463Arg)	Het	Likely pathogenic	Novel	
12	<i>MYO7A</i>	c.75_82del	p.(Ala26Glu*13)	Hom	Pathogenic	Novel	USH1B
13	<i>MYO7A</i>	c.5510T>C	p.(Leu1837Pro)	Het	Likely pathogenic	Jiang et al. (2015)	USH1B
	<i>MYO7A</i>	c.487G>A	p.(Gly163Arg)	Het	Pathogenic	Sloan-Heggen et al. (2016)	
14	<i>MYO7A</i>	c.496del	p.(Glu166Argfs*5)	Het	Pathogenic	Riazuddin et al. (2008)	USH1B
	<i>MYO7A</i>	c.4117C>T	p.(Arg1373*)	Het	Pathogenic	Jaijo et al. (2006)	
15	<i>MYO7A</i>	c.6228_6232del	p.(Asp2076Glu*50)	Hom	Pathogenic	Novel	USH1B
16	<i>MYO7A</i>	c.2914C>T	p.(Arg972*)	Hom	Pathogenic	Riazuddin et al. (2008)	USH1B
18	<i>USH1C</i>	c.2191C>T	p.(Arg731Trp)	Het	Uncertain significance	Novel	USH1C
	<i>USH1C</i>	c.658C>G	p.(Arg220Gly)	Het	Uncertain significance	Novel	
41	<i>CDH23</i>	c.7921G>A	p.(Asp2641Asn)	Hom	Likely pathogenic	Novel	USH1D
17	<i>USH1G</i>	c.742C>T	p.(Gln248*)	Hom	Pathogenic	Bonnet et al. (2016)	USH1G
19	<i>USH2A</i>	c.4732C>T	p.(Arg1578Cys)	Hom	Likely pathogenic	Le Quesne Stabej et al. (2012)	USH2A
20	<i>USH2A</i>	c.236_239dup	p.(Gln81Tyrf*28)	Hom	Pathogenic	Khalailah et al. (2018)	USH2A
21	<i>USH2A</i>	c.1571C>T	p.(Ala524Val)	Het	Likely pathogenic	Novel	USH2A
	<i>USH2A</i>	c.4628-2A>T	p.?	Het	Pathogenic	Novel	
22	<i>USH2A</i>	c.11955G>C	p.(Trp3985Cys)	Hom	Likely pathogenic	Novel	USH2A
23	<i>USH2A</i>	c.12394del	p.(Leu4132Trpf*35)	Hom	Pathogenic	Sloan-Heggen et al. (2015)	USH2A
24	<i>USH2A</i>	c.11357del	p.(Pro3786Leufs*6)	Hom	Pathogenic	Novel	USH2A
25	<i>USH2A</i>	c.13510G>T	p.(Glu4504*)	Het	Pathogenic	Gao et al. (2021)	USH2A
	<i>USH2A</i>	c.13018G>C	p.(Gly4340Arg)	Het	Likely pathogenic	Bonnet et al. (2016)	
26	<i>USH2A</i>	c.12067-2A>G	p.?	Hom	Pathogenic	Auslender et al. (2008)	USH2A
27	<i>USH2A</i>	c.2512C>T	p.(Gln838*)	Het	Pathogenic	Novel	USH2A
	<i>USH2A</i>	c.2299del	p.(Glu767Serfs*21)	Het	Pathogenic	Eudy et al. (1998)	
28	<i>USH2A</i>	c.5251_5267del	p.(Gly1751Leufs*2)	Het	Pathogenic	Novel	USH2A
	<i>USH2A</i>	c.8141G>A	p.(Trp2714*)	Het	Pathogenic	Baux et al. (2014)	
29	<i>USH2A</i>	c.5521G>A	p.(Gly1841Arg)	Het	Likely pathogenic	Novel	USH2A
	<i>USH2A</i>	c.7915T>C	p.(Ser2639Pro)	Het	Likely pathogenic	Bonnet et al. (2016)	
30	<i>USH2A</i>	c.8497dup	p.(Ser2833Lysfs*2)	Hom	Pathogenic	Novel	USH2A
31	<i>USH2A</i>	c.12067-1G>C	p.?	Hom	Pathogenic	Novel	USH2A
32	<i>USH2A</i>	c.8682-1G>A	p.?	Het	Pathogenic	Novel	USH2A
	<i>USH2A</i>	c.2014C>T	p.(Gln672*)	Het	Pathogenic	Pierrache et al. (2016)	
42	<i>USH2A</i>	c.11389 + 3A>T	p.?	Hom	Pathogenic	Soens et al. (2017)	USH2A
	<i>OTOG</i>	c.7454del	p.(Arg2485His*77)	Hom	Pathogenic	Downie et al. (2020)	DFNB18B

Table 1 (continued)

ID	Gene	Variant	Protein	Zygosity ^a	Classification	References	Phenotype
	<i>PRPF31</i>	c.632G>A	p.(Arg211Gln)	Het	Uncertain significance	Novel	RP11, dominant
	<i>ROM1</i>	c.859C>T	p.(Arg287Trp)	Het	Uncertain significance	Novel	RP7, digenic
43	<i>USH2A</i>	c.5438C>A	p.(Ser1813*)	Het	Pathogenic	Novel	USH2A
	<i>USH2A</i>	c.7595-2144A>G	p.?(DIM)	Het	Pathogenic	Liquori et al. (2016)	
	<i>TECTA</i>	c.2572G>A	p.(Asp858Asn)	Het	Uncertain significance	Novel	DFNA8/12
58	<i>USH2A</i>	c.236_239dup	p.(Gln81Tyrfs*28)	Hom	Pathogenic	Khalailah et al. (2018)	USH2A
	<i>KCNQ1</i>	c.733_734del	p.(Gly245Argfs*39)	Het	Pathogenic	Amirian et al. (2018)	Long QT 1
33	<i>ADGRV1</i>	c.9623 + 3A>C ^b	p.?	Hom	Likely pathogenic	Novel	USH2C
34	<i>ADGRV1</i>	c.15736C>T	p.(Arg5246*)	Hom	Pathogenic	Oishi et al. (2014)	USH2C
35	<i>ADGRV1</i>	c.4231del	p.(Ala1411Profs*6)	Hom	Pathogenic	Novel	USH2C
36	<i>ADGRV1</i>	c.4231del	p.(Ala1411Profs*6)	Het	Pathogenic	Novel	USH2C
	<i>ADGRV1</i>	c.10088_10091del	p.(Val3363Aspfs*11)	Het	Pathogenic	Ebermann et al. (2009)	
38	<i>ADGRV1</i>	c.9512T>C	p.(Leu3171Ser)	Hom	Uncertain significance	Novel	USH2C
52	<i>ADGRV1</i>	c.2261T>C	p.(Val754Ala)	Het	Uncertain significance	Myers et al. (2018)	USH2C
	<i>ADGRV1</i>	c.10878A>C	p.(Lys3626Asn)	Het	Uncertain significance	Novel	
	<i>ABCA4</i>	c.4919G>A	p.(Arg1640Gln)	Hom	Pathogenic	Simonelli et al. (2000)	Stargardt 1
56	<i>ADGRV1</i>	c.5167C>G	p.(Pro1723Ala)	Het	Uncertain significance	Novel	USH2C
	<i>ADGRV1</i>	c.14939T>C	p.(Val4980Ala)	Het	Uncertain significance	Novel	
37	<i>CLRN1</i>	c.630del	p.(Phe210Leufs*5)	Hom	Pathogenic	Novel	USH3A
	<i>CLRN1</i>	c.625T>A	p.(Phe209Ile)	Hom	Uncertain significance	Novel	USH3A

^aHom = homozygous; Het = heterozygous

^bTesting with an in vitro splice assay showed a mixture of amplicons, r.9495_9623del p.(Tyr3166_Arg3208del), r.9530_9623del p.(Gly3177Glufs*5), and r.9448_9623del p.(Ala3150Serfs*11)

were found in 18 of 44 (41%) cases. Fundus examination, FAF, and OCT of selected patients with USH showed findings consistent with RP (Fig. 2). Using a grading system for CME (Sliesoraityte et al. 2015), moderate and severe cystic lesions were most prevalent among patients with USH1B and biallelic *MYO7A* variants (Supplementary Table 1). Bilateral pantonal profound sensorineural HI without vestibular dysfunction was the most common form of HI in the USH cohort (Supplementary Table 1).

Patient 33 displayed a homozygous likely pathogenic splice variant, *ADGRV1* c.9623 + 3A>C (Table 1). In vitro splice assays showed three bands after RT-PCR (Supplementary Fig. 1). TA cloning showed 54% of transcripts using a first cryptic splice site 129 nucleotides before the native exon 44 splice donor site, leading to an in-frame deletion, r.9495_9623del p.(Tyr3166_Arg3208del); 38% of transcripts where splicing involved the second cryptic splice donor site 94 nucleotides before the exon 44 native splice site, causing a frameshift, r.9530_9623del p.(Gly3177Glufs*5), and 8% of misspliced transcripts showed skipping of exon 44, r.9448_9623del p.(Ala3150Serfs*11), also resulting in a frameshift. The wild-type minigene showed two main bands comprised of an upper band containing the expected exon 44 sequence (433 bp) and a lower band showing a skipped exon 44 (257 bp) that maps to exon 1 of a shorter transcript

(ENST00000640464.1) lacking a splice acceptor site for splicing.

No pathogenic variants in *CIB2* (USH1J), *ESPN* (USH1M), *HARS* (USH3B), and *ARSG* (USH4) were found by WEA in the remaining 15 non-USH probands. Probands 50, 51, and 57 who exhibited single variants in *USH2A*, were analyzed by MLPA and Sanger sequencing to exclude CNVs and DIMs, which are not detectable by WEA. In addition to a novel pathogenic variant, c.5438C>A p.(Ser1813*), proband 43 was endowed with a well-known DIM, c.7595-2144A>G, in exon 40 (Table 1). Since her unaffected sister displayed only the pathogenic nonsense variant but not the DIM, this is consistent with the diagnosis USH2A in the index patient. Moreover, proband 43 (but not her unaffected sister) displayed a variant of uncertain significance (VUS) in *TECTA* (Table 1), which is associated with autosomal dominant deafness (DFNA8/12) and may contribute to her HI.

Proband 42, a 25-year-old female, with bilateral severe prelingual HI, bilateral reduced vision and nyctalopia starting at the age of 7 years, macular atrophy, diffuse retinal atrophy and pigmentary changes displayed a homozygous splice mutation, *USH2A* c.11389 + 3A>T (Table 1), which has been associated with retinal dystrophy and USH2A. An in vitro minigene assay has been reported, confirming truncation of 48 bp due to usage of a cryptic donor splice site

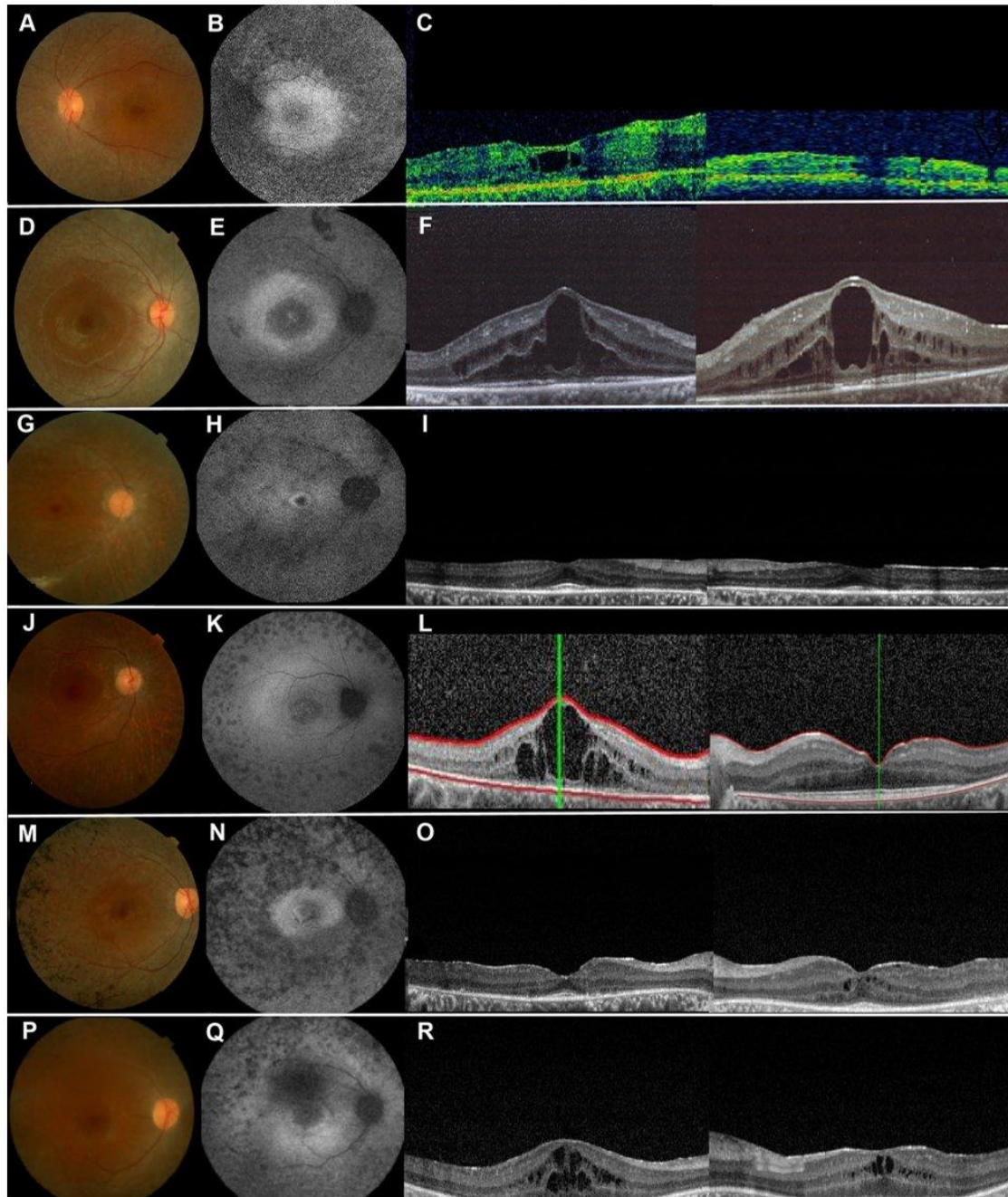


Fig. 2 Retinal phenotype of selected probands with co-occurring HI and VI due to USH entities consistent with retinitis pigmentosa. **A, D, G, J, M, P** Fundus photography (FP), **B, E, H, K, N, Q** fundus autofluorescence (FAF), and **C, F, I, L, O, R** optical coherence tomography (OCT) imaging of patients 1 (**A–C**) and 7 (**D–F**) with USH1B, patient 18 (**G–I**) with USH1C, patient 41 (**J–L**) with USH1D, patient 21 (**M–O**) with USH2A, and patient 37 (**P–R**) with USH3A. Note

retinal atrophy along the arcades in all patients, and bone spicules in patient 21 on FP imaging, decreased autofluorescence along the arcades, and increased and/or decreased autofluorescence centrally in all patients on FAF imaging, and macular pathology on OCT imaging in all patients, i.e. atrophy in patient 1, cystoid macular edema in patients 1, 7, 41, 21, and 37, and epiretinal membrane in patient 18

in exon 58 (Soens et al. 2017). In addition, proband 42 was endowed with a homozygous missense variant, c.7454del p.(Arg2485Hisfs*77) in *OTOG* (Table 1), which causes autosomal recessive deafness (DFNB18B; OMIM 614945) (Downie et al. 2020) and may aggravate the HI phenotype. Her father and two unaffected siblings were heterozygous for this variant. The VI of proband 42 may be modified by the heterozygous variant c.632G>A p.(Arg211Gln) in *PRPF31* (Table 1), which has been associated with RP11 (OMIM 600138) in a single sporadic RP case (Rose et al. 2016). Although the MAF of this variant is about 0.001, functional studies have associated incomplete penetrance and variable expressivity of RP11 with *PRPF31* mRNA levels (Rivolta et al. 2006; Rio Frio et al. 2009). Moreover, proband 42 displayed a heterozygous VUS, c.632G>A p.(Arg287Trp) in *ROM1* (Table 1), which can cause RP7 together with mutations in *PRPH2* (Kajiwara et al. 1994). In this example of digenic RP, *ROM1* is considered as a dominant modifier of *PRPH2* (Nadeau 2001).

Proband 52, a 48-year-old female with prelingual onset, bilateral, profound, steeply sloping high-frequency HI with type A tympanogram and bilateral reduced vision, nyctalopia, and photophobia starting at 5 years of age, showed two missense variants in *ADGRV1*, c.2261T>C p.(Val754Ala) and c.10878A>C p.(Lys3626Asn) (Table 1). Since two unaffected siblings were each heterozygous for either variant, the proband must be compound heterozygous, consistent with the diagnosis USH2C (Fig. 3B, C). The early onset and rapidly progressing vision loss (with light perception in the left eye and no light perception in the right eye), which is incompatible with USH2C, may be explained by an additional homozygous variant c.4919G>A p.(Arg1640Gln) in *ABCA4* (Table 1), which causes Stargardt disease (Simonelli et al. 2000). The most recent ocular examination revealed bilateral pseudophakic status, pale discs, atrophy and pigmentary changes in the macula, atrophy, bone spicules and pigment clumps in the retinal periphery (Fig. 3A). The variants segregated in a heterozygous state in two unaffected brothers (Fig. 3B, C).

In addition to a homozygous frameshift mutation in *USH2A*, c.236_239dup p.(Gln81Tyrfs*28), proband 58 presented with a medically actionable pathogenic variant, c.733_734del p.(Gly245Argfs*39) in *KCNQ1* (Table 1) (Amirian et al. 2018), which is associated with long QT syndrome 1 (OMIM 192500) and familial atrial fibrillation 3 (OMIM 607554).

Non-USH syndromes causing combined HI and retinal degeneration

Nine of 59 probands with combined HI and retinal degeneration displayed clinical entities different from USH (Table 2). These included well-known syndromes that should be

considered as part of the differential diagnosis of USH as well as unexpected inborn errors of metabolism. In many of the identified cases, the age-dependent manifestation of additional symptoms and the large clinical heterogeneity rendered a clinical diagnosis difficult or even impossible, hereby supporting the implementation of genetic testing.

It is noteworthy that three probands (47, 48, and 49) were endowed with different homozygous variants, c.6299C>A p.(Ser2100*), c.7471_7472del p.(Ser2491Thrfs*5), and c.11410C>T p.(Arg3804*), respectively, in *ALMS1*, causing Alström syndrome (OMIM 203800) (Table 2). This pleiotropic ciliopathy is associated with HI and VI, cardiomyopathy, endocrine, neurological, and hepatic symptoms (Rethanavelu et al. 2020). At the time of recruitment, our three Alström patients presented with photophobia, visual field constriction, posterior subcapsular cataracts, pigmentary retinopathy (Fig. 4A, B), and progressive sensorineural HI without vestibular dysfunction. Proband 47 suffered from bilateral severely reduced vision and bilateral profound steeply sloping high-frequency HI. Ophthalmological examinations revealed normal intraocular pressure, a pseudophakic status of the anterior segment, chalky white pale discs, severe macular atrophy (beaten bronze), diffuse bone spicule pigmentary changes, and mottling. At the time of examination, no clinical sign of cardiomyopathy was seen in our three Alström probands. Retrospectively, we learnt that proband 47 suffered from insulin-resistant diabetes and renal failure.

Two patients, 39 and 40, suffered from another ciliopathy, namely cone-rod dystrophy and hearing loss 1 (CRDHL1; OMIM 617236), due to homozygous or compound heterozygous variants in *CEP78*, respectively (Table 2). A possible founder mutation, c.515T>G p.(Ile172Arg) was identified. This variant has not been annotated in gnomAD, GME, LOVD, and HGMD. It was homozygous in a 32-year-old female (proband 39) who reported HI starting at the age of 5 years and bilateral reduced vision, photophobia and hemeralopia at 26 years. Clinical examination revealed pale discs, mild macular atrophy, diffuse retinal atrophy, and retinal pigment epithelium (RPE) mottling in both eyes (Fig. 4E–H). Kinetic and/or static visual field examination revealed a generalized depression with reduced mean deviation (−3.344 dB; $p < 0.01$) with a central 10–2 threshold, consistent with RP. The ERG showed severe reduced amplitude in scotopic, photopic, and flicker responses.

A novel homozygous missense VUS in *PEX26*, c.349C>A p.(Pro117Thr) (Table 2) was found in a 12-year-old female (proband 46) with bilateral reduced vision, nyctalopia, bilateral subcapsular cataract, diffuse retinal atrophy with diffuse pigmentary changes in both eyes (Fig. 4C, D), and severely reduced amplitudes in scotopic and photopic ERG. This variant segregated in a heterozygous state in unaffected family members who were available for testing.

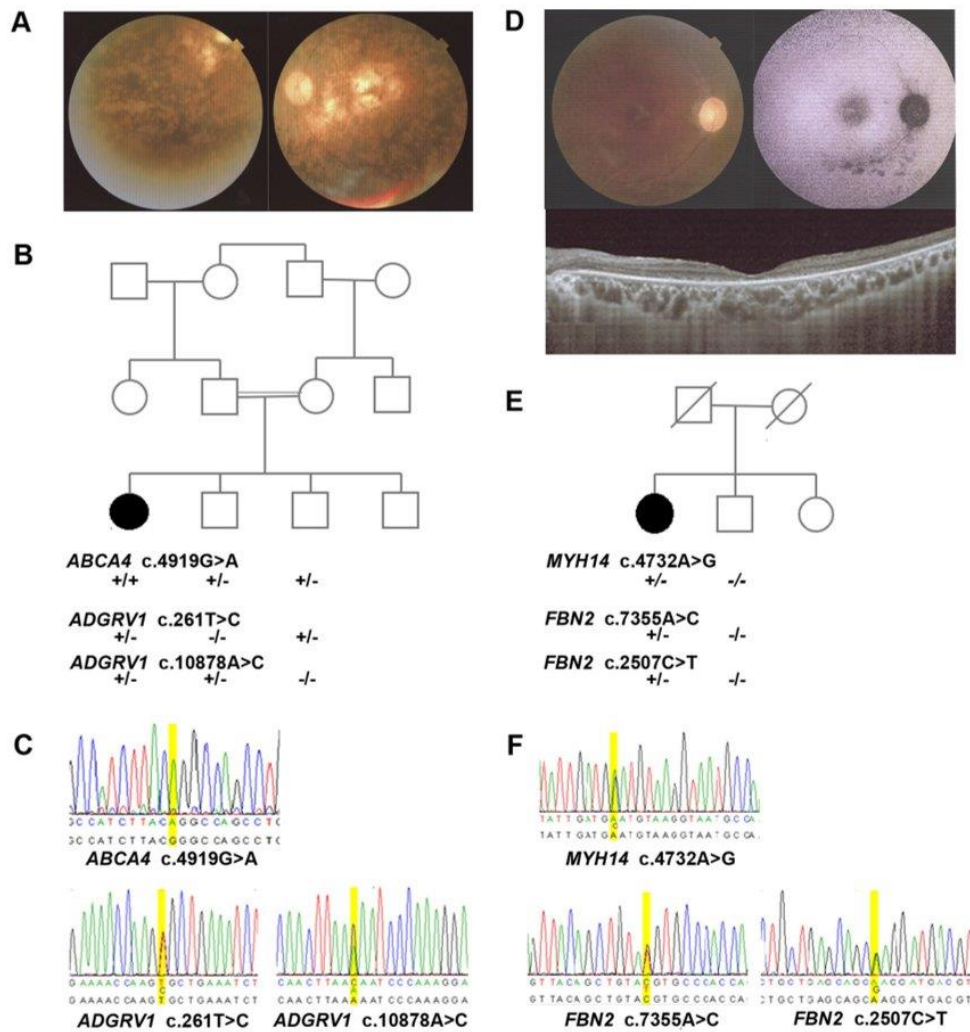


Fig. 3 Possible coincidence and genetic heterogeneity underlying combined HI and VI. **A** Fundus photography (FP) of proband 52 showing central retinal atrophy and pigment clumping in both eyes consistent with *ABCA4*-spectrum disease. **B, C** Pedigree and segregation analysis of disease-causing variants in *ABCA4* and *ADGRV1*. **D** FP, fundus autofluorescence (FAF) and optical coherence tomography

(OCT) imaging of proband 44 showing decreased autofluorescence along the inferior arcade and centrally on FAF imaging (right eye) and retinal atrophy on OCT imaging consistent with retinal dystrophy. **E, F** Pedigree and segregation analysis of variants in *MYH14* and *FBN2*. (+/+ variant present in homozygous state, ± variant present in heterozygous state, -/- wild type.)

Pathogenic variants in *PEX26* are associated with a wide spectrum of peroxisomal diseases, including Heimler syndrome, previously described in patients with concurrent HI and VI (Neuhaus et al. 2017). When the molecular diagnosis was communicated to the recruiting clinic, amelogenesis imperfecta in secondary teeth was retrospectively identified, which is in line with Heimler syndrome.

The homozygous likely pathogenic variant c.956C>T p.(Ala319Val) in *IDUA* in proband 50 (Table 2) has been

previously reported in patients with Scheie syndrome (OMIM 607016), a mild form of mucopolysaccharidosis type I (Beesley et al. 2001). The 65-year-old female patient presented with diffuse RPE mottling, CME, generalized depression in her visual field exam (Fig. 4I–L), and post-lingual HI. There were no other evident clinical findings indicative of Scheie syndrome.

The 29-year-old proband 51 with optic atrophy, retinal degeneration, and sensorineural HI was

Table 2 Non-Usher syndromes underlying combined hearing loss and retinal degeneration

ID	Gene	Variant	Protein	Zygoty ^a	Classification	References	Phenotype
39	<i>CEP78</i>	c.515T>G	p.(Ile172Arg)	Hom	Uncertain significance	Novel	Cone-rod dystrophy and hearing loss 1
40	<i>CEP78</i>	c.515T>G	p.(Ile172Arg)	Het	Uncertain significance	Novel	Cone-rod dystrophy and hearing loss 1
	<i>CEP78</i>	c.534del	p.(Lys179Argfs*10)	Het	Pathogenic	Namburi et al. (2016)	
46	<i>PEX26</i>	c.349C>A	p.(Pro117Thr)	Hom	Uncertain significance	Novel	Peroxisome biogenesis disorder IC
47	<i>ALMS1</i>	c.6299C>A	p.(Ser2100*)	Hom	Pathogenic	Novel	Alström syndrome
48	<i>ALMS1</i>	c.7471_7472del	p.(Ser2491Thrfs*5)	Hom	Pathogenic	Novel	Alström syndrome
49	<i>ALMS1</i>	c.11410C>T	p.(Arg3804*)	Hom	Pathogenic	Liu et al. (2017)	Alström syndrome
50	<i>IDUA</i>	c.956C>T	p.(Ala319Val)	Hom	Likely pathogenic	Beesley et al. (2001)	Scheie syndrome (MPS1-S)
	<i>USH2A</i>	c.3045C>G	p.(His1015Gln)	Het	Pathogenic	Pierrache et al. (2016)	
	<i>ADGRV1</i>	c.1563del	p.(Pro522Leufs*18)	Het	Pathogenic	Novel	
51	<i>PDSS2</i>	c.702+1G>A ^b	p.?	Het	Likely pathogenic	Novel	Coenzyme Q10 deficiency primary 3
	<i>PDSS2</i>	c.488G>A	p.(Arg163His)	Het	Uncertain significance	Novel	
	<i>USH2A</i>	c.174T>A	p.(Cys58*)	Het	Pathogenic	Novel	
54	<i>ABCC6</i>	c.1171A>G	p.(Arg391Gly)	Hom	Uncertain significance	Chassaing et al. (2004)	Pseudoxanthoma elasticum

^aHom = homozygous; Het = heterozygous

^bTesting with an in vitro splice assay showed exon skipping, r.631_702del p.(Val211_Lys234del)

compound heterozygous for a missense variant c.488G>A p.(Arg163His) and a splice site variant c.702+1G>A p.? in *PDSS2* (Table 2) that has been associated with coenzyme Q10 deficiency (OMIM 614652). Compound heterozygosity of the respective VUS and likely pathogenic splice variant was confirmed by segregation analysis in unaffected family members. In vitro splice testing of the *PDSS2* c.702+1G>A mutant allele indicated skipping of exon 4 (257 bp), leading to an in-frame deletion, r.631_702del p.(Val211_Lys234del). The wild-type amplicon included the correctly spliced complete exon 4 sequence, showing as a 328 bp band (Supplementary Fig. 1).

The homozygous variant c.1171A>G p.(Arg391Gly) in *ABCC6* (Table 2) has been previously associated with pseudoxanthoma elasticum (Chassaing et al. 2004). Proband 54, a 31-year-old female, presented with progressive visual impairment, optic disc drusen, beaten bronze macular atrophy, diffuse RPE mottling, choroidal neovascularization, and postlingual sensorineural HI.

Possible multi-locus genomic variation

Proband 44, a 42-year-old female, suffered from bilateral moderate high-frequency HI as well as late-manifesting (at the age of 38 years) severely reduced visual acuity, photophobia, nyctalopia, severe macular atrophy, diffuse pigmentary changes, and mottling with notable diminished central macular thickness (Fig. 3D). She displayed three

novel missense variants; one, c.4732A>G p.(Lys1578Glu) in *MYH14*, and two, c.7355A>C p.(Glu2452Ala) and c.2507C>T p.(Thr836Met) in *FBN2* (Table 3). Since the unaffected brother did not exhibit *FBN2* variants (Fig. 3E, F) and other family members were not available, we do not know whether both variants reside on the same or on different parental alleles. Rare dominant variants in *FBN2* have been described in relationship with early onset macular degeneration (OMIM 616118) but also age-related macular degeneration (Ratnapriya et al. 2014). Variants in *MYH14* cause autosomal dominant HI (DFNA4A; OMIM 600652).

Proband 45, a 40 year-old male, reported reduced vision and nyctalopia starting at 10 years of age and bilateral post-lingual HI. He displayed macular pathology with pigmentary changes and bone spicules in the retinal periphery. He comes from a large consanguineous family. There are multiple members with dual sensory impairment and one brother with isolated HI. Both the proband and his deaf-blind youngest sister were endowed with a missense variant c.659T>G p.(Phe220Cys) in *RHO* (Table 3), that has been previously reported in patients with RP4 (OMIM 13731) (Bunge et al. 1993). Since the variant was also present in the hearing-impaired brother, reduced penetrance and/or variable expressivity must be assumed and the evidence for this variant is limited. Functional studies of RP-linked rhodopsin mutations have yielded conflicting results (Mallory et al. 2018; Lewis et al. 2020). The molecular basis of the HI in this family remains unknown. As an incidental finding, the

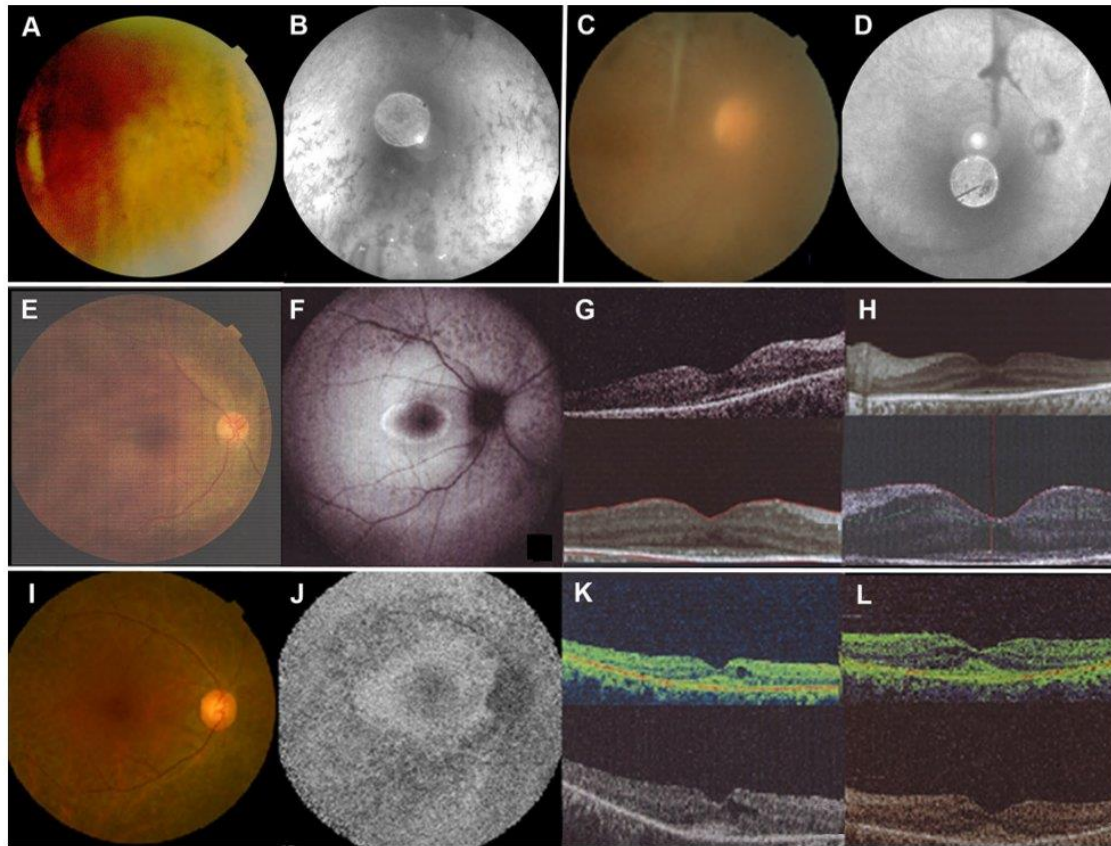


Fig. 4 Retinal phenotype of selected probands with co-occurring HI and VI due to non-USH syndromic entities. **A, B** Fundus photography (FP) and fundus autofluorescence (FAF) in proband 49 with Alström syndrome (*ALSM1*) showing bone spicules in the retinal periphery (right and left eye) consistent with retinitis pigmentosa (RP). **C, D** FP and FAF of proband 46 with Heimler syndrome (*PEX26*) showing optic atrophy and pigment clumping despite reduced image quality due to cataracts (both eyes) consistent with RP. **E–H** FP, FAF, and optical coherence tomography (OCT) imaging of

proband 39 with *CRDHL1* (*CEP78*) showing decreased autofluorescence along the arcades on FAF imaging (right eye) and atrophy of the outer retina outside the center on OCT imaging (both eyes) consistent with RP. **I–L** FP, FAF, and OCT of proband 50 with Scheie syndrome (*IDUA*) showing decreased autofluorescence along the arcades on FAF imaging (right eye) and atrophy of the outer retina outside the center and mild cystoid macular edema on OCT imaging (both eyes) consistent with RP

proband displayed a common pathogenic variant in *MEFV*, that has been associated with familial Mediterranean fever and Behcet's disease (Tasliyurt et al. 2013).

In proband 53, a 13-year-old girl, we identified a heterozygous variant, c.6462C>A p.(His2154Gln), in *PRPF8* (Table 3), which has been associated with RP13 (OMIM 600059), which is typically inherited as an autosomal dominant trait. In addition, she was endowed with a homozygous variant c.2551 + 8C>T in *CACN2D4* (Table 3), which has been associated with retinal cone

dystrophy 4 (OMIM 610478). Variants in both genes may contribute to VI within the first year of life. A segregating variant underlying the HI has not been identified.

Unsolved cases

In 3 of 59 probands (55, 57, and 59), we could not establish a molecular diagnosis for HI and/or VI. Interestingly, proband 57 exhibited a single pathogenic mutation, c.5388T>A p.(Cys1796*), in *USH2A* and proband 59 was heterozygous

Table 3 Possibly solved, partially solved, and unsolved cases showing multi-locus variation

ID	Gene	Variant	Protein	Zygosity ^a	Classification	References	Phenotype
44 ^b	<i>MYH14</i>	c.4732A>G	p.(Lys1578Glu)	Het	Uncertain significance	Novel	DFNA4A
	<i>FBN2</i>	c.7355A>C	p.(Glu2452Ala)	Het	Uncertain significance	Novel	Macular degeneration, early onset
	<i>FBN2</i>	c.2507C>T	p.(Thr836Met)	Het	Uncertain significance	Novel	
45 ^c	<i>RHO</i>	c.659T>G	p.(Phe220Cys)	Het	Likely Pathogenic	Bunge et al (1993)	Autos. dominant or recessive RP4
	<i>MEFV</i>	c.2040G>C	p.(Met680Ile)	Het	Pathogenic	Tasliyurt et al. (2013)	Familial Mediterranean fever
53 ^c	<i>PRPF8</i>	c.6462C>A	p.(His2154Gln)	Het	Uncertain significance	Novel	Autosomal dominant RP13
	<i>CACNA2D4</i>	c.2551+8C>T	p.?	Hom	Uncertain significance	Novel	Retinal cone dystrophy 4
57 ^d	<i>USH2A</i>	c.5388T>A	p.(Cys1796*)	Het	Pathogenic	Novel	
59 ^d	<i>MYO7A</i>	c.3750+7G>A	p.?	Het	Uncertain significance	ClinVar ID 43221	
	<i>CDH23</i>	c.5653C>T	p.(Arg1885Cys)	Het	Uncertain significance	ClinVar ID 522828	
	<i>G6PD</i>	c.1057C>T	p.(Pro353Ser)	Hemi	Pathogenic	Beutler et al. (1992)	Hemolytic anemia

^aHom = homozygous; Het = heterozygous; Hemi = hemizygous

^bThis case is considered as solved

^cThese cases are considered as partially solved, with variants explaining vision impairment

^dThese cases are considered as unsolved

for two VUS, c.3750+7G>A p.? in *MYO7A* and c.5653C>T p.(Arg1885Cys) in *CDH23* (Table 3). Proband 59, a 47-year-old male with prelingual HI and VI since birth, was also endowed with a pathogenic variant, c.1057C>T p.(Pro353Ser) in *G6PD* (Beutler et al. 1992), which is associated with X-linked hemolytic anemia (OMIM 300908) in hemizygous males. Hyperbilirubinemia due to G6PD deficiency can induce neurological damage (kernicterus) in neonates and children, which may clinically manifest as auditory neuropathy spectrum disorder (Boskabadi et al. 2018).

Discussion

As expected, most (44 of 59; 75%) of our deaf–blind patients were diagnosed with USH. Approximately half were USH1 and half USH2, with *MYO7A* (USH1B) and *USH2A* being the most prevalent genes. The relatively high proportion of *ADGRV1* (USH2C) (7 of 24; 29%) compared to *USH2A* (17 of 24; 71%) within the USH2 group may be explained by ethnicity of our cohort, mainly from Iran, which is an understudied population. In addition to USH, there is a wide variety of hereditary, non-hereditary and independent causes of HI and/or VI, which makes a correct diagnosis for clinicians and human geneticists challenging (Stiff et al. 2020).

Next generation sequencing (NGS) has greatly transformed the molecular diagnostics of both clinically and genetically highly heterogeneous neuro-sensory disorders, allowing rapid screening of large gene panels or the entire exome. Using WEA, we found genetic variants associated with combined HI and VI in 54 of 59 (92%) probands. Two

probands (3%) were partially solved and only three (5%) remained without a molecular diagnosis explaining their phenotype. This is consistent with recent NGS screens of patients with combined HI and VI, which have yielded diagnostic efficiencies > 90% (Bonnet et al. 2016; Neuhaus et al. 2017; Jouret et al. 2019). This unusually high solve rate for a heterogeneous Mendelian disorder argues in favor of the notion that most genes underlying dual sensory loss have been identified. Our study also shows the utility of OCT for monitoring RP patients. The presence of macular edema, macular hole, epiretinal membrane, etc. has prognostic value and therapeutic implications.

The vast majority of variants underlying USH in our deaf–blind cohort were classified as pathogenic (44 of 63; 70%) or likely pathogenic (11 of 63; 18%) and most of them were already known (36 of 63; 57%). In contrast, the majority of presumably disease-causing variants in non-USH probands were VUS (10 of 17; 59%) and/or novel (12 of 17; 71%). This is not unexpected, considering that USH is one of the most extensively studied neuro-sensory disorders and updated comprehensive information on USH genes is available in variant data bases. Compared to USH, the data situation of the genes identified in probands with non-USH syndromes and multi-locus variation is relatively poor. Therefore, segregation analyses were performed in the families of the index probands to validate or discard variants.

Non-Usher syndromes associated with combined hearing loss and retinal degeneration

Although USH is by far the most prevalent cause of deaf–blindness worldwide and also in our study, there are other syndromes that combine retinal dystrophy and HI with a number of additional symptoms. Five of our probands exhibited ciliopathies due to variants in *ALMS1* (Alström syndrome) and *CEP78* (CRDHL1). The absence of additional clinical symptoms in our three Alström patients may be explained by the variable and age-dependent expressivity of the phenotype. Only 17 and 19% of patients with Alström syndrome display intellectual disability and cardiomyopathy, respectively (Rethanavelu et al. 2020).

Heimler syndrome is a peroxisome disorder caused by biallelic variants in *PEX1*, *PEX6*, and *PEX26*. Proband 46 and several published cases with suspected USH presented biallelic mutations in *PEX1* and *PEX26* (Neuhaus et al. 2017; Diñeiro et al. 2020). The typical tooth (enamel) and nail abnormalities of Heimler syndrome were overlooked before molecular diagnosis. When assessed retrospectively, our proband presented mild amelogenesis imperfecta in secondary teeth.

Although it is known that patients with alpha-L-iduronidase deficiency (MPS1S or Scheie syndrome) can have HI and retinal degeneration, it was surprising that these were the cardinal symptoms leading to a molecular diagnosis (homozygous *IDUA* variant) in proband 50. This illustrates that mild phenotypic expression, in this case of a MPS1S, can complicate or delay diagnosis.

Another unexpected finding was compound heterozygosity of a likely pathogenic variant and a novel missense variant in *PDSS2* in proband 51. Coenzyme Q10 (CoQ₁₀) deficiency is characterized by highly variable multi-systemic manifestations, ranging from fatal neonatal encephalopathy with hypotonia to isolated steroid-resistant nephrotic syndrome. The establishment of this molecular diagnosis in one of our probands with HI and VI is especially relevant, since high-dose oral CoQ₁₀ supplementation can slow disease progression and even reverse some manifestations (Alcazar-Fabra et al. 2018).

Proband 54 was homozygous for a known variant in *ABCC6*, causing pseudoxanthoma elasticum (OMIM 264800). This systemic elastic tissue disorder progressively affects the skin, forming yellowish papules that coalesce to form plaques until the skin becomes loose and redundant. Ophthalmological findings include angioid streaks, reticular macular dystrophy and speckled appearance of the macula. The clinical diagnosis is typically made in the second or third decade of life, when the skin and retinal symptoms are evident. Although HI has not been associated with pseudoxanthoma elasticum, it has been reported in patients with

generalized arterial calcification of infancy (OMIM 624473), which is also caused by recessive variants in *ABCC6*.

Collectively, these results suggest that patients with dual sensory loss as the primary symptoms can suffer from a long list of syndromes (Stiff et al. 2020) that have HI and VI as part of their symptoms and with mild phenotypic expression or absence of additional symptoms that define the syndrome. In many monogenic disorders, the genotype is not predictive of the phenotype (Cooper et al. 2013). Variants that have been found in patients with highly variable phenotypic manifestations and apparently normal healthy individuals underscore the importance of variable expressivity and reduced penetrance.

Blended phenotypes

Large WEA studies revealed dual molecular diagnoses in a considerable number of patients (Yang et al. 2014; Balci et al. 2017; Posey et al. 2017). Therefore, it is not surprising that three of our Usher probands exhibited additional variants in genes causing HI (*OTOG*, *TECTA*) or VI (*ABCA4*). One non-USH proband exhibited variants in different genes underlying HI (*MYH14*) and retinal or macular degeneration (*FBN2*). In two probands, we found variants segregating with VI but no variants in deafness genes. Altogether, in 6 (10%) of 59 probands dual sensory loss may represent a blended phenotype of variants in different genes for HI and/or VI.

In this context, it is noteworthy that although the vast majority of our patients come from consanguineous families, 20 of 54 (37%) solved cases are due to compound heterozygous variants in recessive genes. In 5 of 6 probands with likely multi-locus variation, dominant variants contributed to the phenotype. This accumulation of heterozygous variants in deaf–blind families may be at least partially related to phenotypic mating structure among individuals with HI and/or VI.

Limitations

In probands with a single pathogenic *USH2A* variant (50, 51, and 57), partially solved (45 and 53), and unsolved cases (55, 57, and 59), CNVs and DIMs in *USH2A* were excluded by MLPA and Sanger sequencing. Similarly, CNVs in *PCDH15* were excluded by MLPA. In some probands (42, 43, 44, 45, and 58), genome-wide microarray screening revealed several CNVs; however, none were associated with HI and/or VI. Although we did not perform a comprehensive CNV analysis in all our probands, we can largely exclude a major contribution of CNVs to the etiopathogenesis of deaf–blindness in our cohort.

Despite diagnostic yields over 90%, some patients with dual sensory impairment remain without firm molecular

diagnosis. This may be due to not yet discovered genes or variants in non-coding (intronic and regulatory) sequences, undetected CNVs and structural variants (i.e. inversions), or unannotated exons of known genes. Indeed, two of three unsolved patients displayed single pathogenic variants in USH genes, arguing in favor of the notion that we may have missed the mutation in the second allele. Although switching molecular diagnostics from WEA to whole-genome sequencing and improvement of diagnostic algorithms may overcome some of these problems, our capacity for interpretation variants outside the exome is still very limited.

Benefits of improved molecular diagnostics

Many patients with neuro-sensory impairments benefit from an early molecular diagnosis, which may have important implications for disease management (i.e. tailoring optimum educational programs) and treatment (i.e. cochlear implantation, timely eye examinations and implementation of prophylactic or therapeutic measures to improve vision or slow the progression of retinal degeneration), prognosis (progressive or stable, development of additional symptoms), and family planning. Diagnosing syndromes in patients who are pre-symptomatic (for a given symptom) enables patients to consult respective specialists before symptoms manifest or progress. A variety of gene therapy approaches using adeno-associated viral vectors for gene delivery, antisense oligonucleotides or genome editing agents have already yielded promising results to prevent HI and retinal degeneration in murine USH models (Nagel-Wolfrum et al., 2014; Géléoc and El-Amraoui, 2020; Lentz et al. 2020), including clinical trials in patients related to mutations in exon 13 of *USH2A* (NCT03780257). Molecular diagnosis of the underlying defect is crucial to stratify patients for a growing number of successful ongoing clinical trials of ocular gene therapy, which represents a notable advancement to other inherited disorders (Cehajic-Kapetanovic et al. 2020).

Using state-of-the art clinical exome analysis, incidental or secondary findings unrelated to the primary reason for sequencing but of medical value for the proband, are identified in several percent of cases (Hart et al. 2019). The ACMG recommends returning highly penetrant pathogenic variants for a list of several dozen genes (Kalia et al. 2017; <https://www.ncbi.nlm.nih.gov/clinvar/docs/acmg/>). Important inclusion criteria are the possibility to confirm the associated phenotype, the availability of preventive measures and treatments, and that the mutation carriers can be asymptomatic for prolonged periods of time. Ideally, the patients should be alerted to this possibility before testing and have the chance to opt-out of receiving such unexpected findings. In this study we detected one medically actionable variant in *KCNQ1*, which is associated with long QT syndrome and

has immediate implications for patient management. In addition, we found a pathogenic variant in *MEFV* which is associated with familial Mediterranean fever and a hemizygous variant in *G6PD*, which is associated with X-linked hemolytic anemia. Although not included in the list of actionable genes, these variants were considered as medically relevant and returned to the affected probands/families. Thus, altogether three (5%) probands in our cohort displayed secondary findings.

Web resources

ClinVar, <https://www.ncbi.nlm.nih.gov/clinvar>.

Deafness Variation Database, <https://deafnessvariantdatabase.org>.

Hereditary Hearing Loss Homepage, <https://hereditaryhearingloss.org>.

Leiden Open Variation Database (LOVD), <https://www.lovd.nl>.

Moon Diploid, <https://www.diploid.com/moon>.

Mutation Distiller, <https://www.mutationdistiller.org>.

Primer 3, <https://primer3.org/>.

ACMG Recommendations for Reporting of Incidental Findings in Clinical Exome and Genome Sequencing, <https://www.ncbi.nlm.nih.gov/clinvar/docs/acmg/>.

Retinal Information Network, <https://sph.uth.edu/retnet/disease.htm>.

Supplementary Information The online version contains supplementary material available at <https://doi.org/10.1007/s00439-021-02303-1>.

Acknowledgements We appreciate the collaboration of the probands and their families in this study. This study was performed with the help of "The Iranian National Registry of Inherited Retinal Dystrophy (IRDReg)" (code number of IR.SBMU.ORC.REC.1396.15) and supported by the Deputy of Research and Technology at Shahid Beheshti University of Medical Sciences, Tehran, Iran (<http://dregistry.sbm.ac.ir>).

Author contributions PB, FS, BV, and TH designed the study. ND, RM, MM, HS, HA, HB, CVM, VCG, HD, EA, MAS, and FS recruited probands and provided clinical information. PB, PL, DV, AR, JD, MH, AK, TR, and SH performed the experiments. PB, SK, RZO, LK, FS, and BV analyzed the data. PB, BV, and TH wrote the manuscript. All authors read and approved the manuscript.

Funding Open Access funding enabled and organized by Projekt DEAL. This study was supported by Intramural Funding (fortune) at the University of Tübingen (2545-1-0 to BV) and the Ministry of Science, Research and Art Baden-Württemberg (to BV).

Availability of data and materials All data generated during this study are included in this article and supplementary information file. All variants have been entered into LOVD. Accession numbers are included in Supplementary Table 2.

Declarations

Conflict of interest The authors declare no conflict of interest.

Ethical approval This study was approved by the ethical review boards at the Medical Faculty of Würzburg University, Germany (approval number 46/15), the National Institute of Rehabilitation Luis Guillermo Ibarra (INR), Mexico (no. 12/13), and the Shahid Beheshti University of Medical Sciences, Tehran, Iran.

Consent to participate Consent for participation was received from the probands and their families.

Consent for publication Consent for publication was received from the probands and their families.

Animal experiments Not applicable as no animal experiments were performed.

Open Access This article is licensed under a Creative Commons Attribution 4.0 International License, which permits use, sharing, adaptation, distribution and reproduction in any medium or format, as long as you give appropriate credit to the original author(s) and the source, provide a link to the Creative Commons licence, and indicate if changes were made. The images or other third party material in this article are included in the article's Creative Commons licence, unless indicated otherwise in a credit line to the material. If material is not included in the article's Creative Commons licence and your intended use is not permitted by statutory regulation or exceeds the permitted use, you will need to obtain permission directly from the copyright holder. To view a copy of this licence, visit <http://creativecommons.org/licenses/by/4.0/>.

References

- Adzhubei IA, Schmidt S, Peshkin L, Ramensky VE, Gerasimova A, Bork P, Kondrashov AS, Sunyaev SR (2010) A method and server for predicting damaging missense mutations. *Nat Methods* 7:248–249
- Ahmed ZM, Jaworek TJ, Sarangdhar GN, Zheng L, Gul K, Khan SN, Friedman TB, Sisk RA, Bartles JR, Riazuddin S, Riazuddin S (2018) Inframe deletion of human *ESPN* is associated with deafness, vestibulopathy and vision impairment. *J Med Genet* 55:479–488
- Alcazar-Fabra M, Trevisson E, Brea-Calvo G (2018) Clinical syndromes associated with coenzyme Q10 deficiency. *Essays Biochem* 62:377–398
- Amirian A, Zafari Z, Dalili M, Saber S, Karimipour M, Dabbagh Bagheri S, Fazelifar AF, Zeinali S (2018) Detection of a new *KCNQ1* frameshift mutation associated with Jervell and Lange-Nielsen syndrome in 2 Iranian families. *J Arrhythm* 34:286–290
- Auslender N, Bandah D, Rizel L, Behar DM, Shohat M, Banin E, Allon-Shalev S, Sharony R, Sharon D, Ben-Yosef T (2008) Four *USH2A* founder mutations underlie the majority of Usher syndrome type 2 cases among non-Ashkenazi Jews. *Genet Test* 12:289–294
- Azaiez H, Booth KT, Ephraim SS, Crone B, Black-Ziegelbein EA, Marini RJ, Shearer AE, Sloan-Heggen CM, Kolbe D, Casavant T, Schnieders MJ, Nishimura C, Braun T, Smith RJH (2018) Genomic landscape and mutational signatures of deafness-associated genes. *Am J Hum Genet* 103:484–497
- Bademci G, Cengiz FB, Foster II J, Duman D, Sennaroglu L, Diaz-Horta O, Atik T, Kirazli T, Olgun L, Alper H, Menendez I, Loclar I, Sennaroglu G, Tokgoz-Yilmaz S, Guo S, Olgun Y, Mahdih N, Bonyadi M, Bozan N, Ayril A, Ozkinay F, Yildirim-Baylan M, Blanton SH, Tekin M (2016) Variations in multiple syndromic deafness genes mimic non-syndromic hearing loss. *Sci Rep* 6:31622
- Balci TB, Hartley T, Xi Y, Dymont DA, Beaulieu CL, Bernier FP, Dupuis L, Horvath GA, Mendoza-Londono R, Prasad C, Richer J, Yang XR, Armour CM, Bareke E, Fernandez BA, McMillan HJ, Lamont RE, Majewski J, Parboosingh JS, Prasad AN, Rupar CA, Schwartztruber J, Smith AC, Tétreault M, FORGE Canada Consortium, Care4Rare Canada Consortium, Innes AM, Boycott KM (2017) Debunking Occam's razor: diagnosing multiple genetic diseases in families by whole-exome sequencing. *Clin Genet* 92:281–289
- Baux D, Blanchet C, Hamel C, Meunier I, Larrieu L, Faugère V, Vaché C, Castorina P, Puech B, Bonneau D, Malcolm S, Claustres M, Roux AF (2014) Enrichment of LOVD-USH-bases with 152 *USH2A* genotypes defines an extensive mutational spectrum and highlights missense hotspots. *Hum Mutat* 35:1179–1186
- Baux D, Vaché C, Blanchet C, Willems M, Baudoin C, Moclyn M, Faugère V, Touraine R, Isidor B, Dupin-Deguine D, Nizon M, Vincent M, Mercier S, Calais C, Garcia-García G, Azher Z, Lambert L, Perdomo-Trujillo Y, Giuliano F, Claustres M, Koenig M, Mondain M, Roux AF (2017) Combined genetic approaches yield a 48% diagnostic rate in a large cohort of French hearing-impaired patients. *Sci Rep* 7:16783
- Beesley CE, Meaney CA, Greenland G, Adams V, Vellodi A, Young EP, Winchester BG (2001) Mutational analysis of 85 mucopolysaccharidosis type I families: frequency of known mutations, identification of 17 novel mutations and in vitro expression of missense mutations. *Hum Genet* 109:503–511
- Beutler E, Westwood B, Prchal JT, Vaca G, Bartsocas CS, Baronciani L (1992) New glucose-6-phosphate dehydrogenase mutations from various ethnic groups. *Blood* 80:255–256
- Bharadwaj AK, Kasztejna JP, Huq S, Berson EL, Dryja TP (2000) Evaluation of the myosin VIIA gene and visual function in patients with Usher syndrome type I. *Exp Eye Res* 71:173–181
- Bonnet C, Grati M, Marlin S, Levilliers J, Hardelin JP, Parodi M, Niasme-Grare M, Zelenika D, Délépine M, Feldmann D, Jonard L, El-Amraoui A, Weil D, Delobel B, Vincent C, Dollfus H, Eliot MM, David A, Calais C, Vigneron J, Montaut-Verient B, Bonneau D, Dubin J, Thauvin C, Duvillard A, Francannet C, Mom T, Lacombe D, Duriez F, Drouin-Garraud V, Thuillier-Obstoy MF, Sigaudy S, Frances AM, Collignon P, Challe G, Couderc R, Lathrop M, Sahel JA, Weissenbach J, Petit C, Denoyelle F (2011) Complete exon sequencing of all known Usher syndrome genes greatly improves molecular diagnosis. *Orphanet J Rare Dis* 6:21
- Bonnet C, Riahi Z, Chantot-Bastaraut S, Smaghe L, Letexier M, Marcaillou C, Lefèvre GM, Hardelin JP, El-Amraoui A, Singh-Estivalet A, Mohand-Saïd S, Kohl S, Kurtenbach A, Sliessoraityte I, Zobor D, Gherbi S, Testa F, Simonelli F, Banfi S, Fakin A, Glavač D, Jarc-Vidmar M, Zupan A, Battelino S, Martorell Sampol L, Claveria MA, Catala Mora J, Dad S, Möller LB, Rodriguez Jorge J, Hawlina M, Auricchio A, Sahel JA, Marlin S, Zrenner E, Audo I, Petit C (2016) An innovative strategy for the molecular diagnosis of Usher syndrome identifies causal biallelic mutations in 93% of European patients. *Eur J Hum Genet* 24:1730–1738
- Booth KT, Kahrizi K, Babanejad M, Daghighi H, Bademci G, Arzhanghi S, Zareabdollahi D, Duman D, El-Amraoui A, Tekin M, Najmabadi H, Azaiez H, Smith RJ (2018) Variants in *C12B* cause DFNB48 and not *USH1J*. *Clin Genet* 93:812–821
- Boskabadi H, Zakerihamidi M, Moradi A, Mehdi Bakhshae M (2018) Risk factors for sensorineural hearing loss in neonatal hyperbilirubinemia. *Iran J Otorhinolaryngol* 30:195–202

- Bunge S, Wedemann H, David D, Terwilliger DJ, van den Born LI, Aulehla-Scholz C, Samanns C, Horn M, Ott J, Schwinger E, Schinzel A, Denton MJ, Gal A (1993) Molecular analysis and genetic mapping of the rhodopsin gene in families with autosomal dominant retinitis pigmentosa. *Genomics* 17:230–233
- Cehajic-Kapetanovic J, Xue K, Martinez-Fernandez de la Camara C, Nanda A, Davies A, Wood LJ, Salvetti AP, Fischer MD, Aylward JW, Barnard AR, Jolly JK, Luo E, Lujan BJ, Ong T, Girach A, Black GCM, Gregori NZ, Davis JL, Rosa PR, Lotery AJ, Lam BL, Stanga PE, MacLaren RE (2020) Initial results from a first-in-human gene therapy trial on X-linked retinitis pigmentosa caused by mutations in RPGR. *Nat Med* 26:354–359
- Chassaing N, Martin L, Mazereeuw J, Barrié L, Nizard S, Bonafé JL, Calvas P, Hovnanian A (2004) Novel ABCC6 mutations in pseudo-xanthoma elasticum. *J Invest Dermatol* 122:608–613
- Cooper DN, Krawczak M, Polychronakos C, Tyler-Smith C, Kehrer-Sawatzki H (2013) Where genotype is not predictive of phenotype: towards an understanding of the molecular basis of reduced penetrance in human inherited disease. *Hum Genet* 132:1077–1130
- Cremers FP, Kimberling WJ, Külm M, de Brouwer AP, van Wijk E, te Brinke H, Cremers CW, Hoefsloot LH, Banfi S, Simonelli F, Fleischhauer JC, Berger W, Kelley PM, Haralambous E, Bitner-Glindzicz M, Webster AR, Saihan Z, de Baere E, Leroy BP, Silvestri G, McKay GJ, Koenekoop RK, Millan JM, Rosenberg T, Joensuu T, Sankila EM, Weil D, Weston MD, Wissinger B, Kremmer H (2007) Development of a genotyping microarray for Usher syndrome. *J Med Genet* 44:153–160
- Dammeyer J (2014) Deafblindness: a review of the literature. *Scand J Public Health* 42:554–562
- Desmet FO, Hamroun D, Lalande M, Colod-Béroud G, Claustres M, Béroud C (2009) Human splicing finder: an online bioinformatics tool to predict splicing signals. *Nucleic Acids Res* 37:e67
- Diñeiro M, Capín R, Cifuentes GA, Fernández-Vega B, Villota E, Otero A, Santiago A, Pruneda PC, Castillo D, Viejo-Díaz M, Hernando I, Durán NS, Álvarez R, Lago CG, Ordóñez GR, Fernández-Vega Á, Cabanillas R, Cadiñanos J (2020) Comprehensive genomic diagnosis of inherited retinal and optical nerve disorders reveals hidden syndromes and personalized therapeutic options. *Acta Ophthalmol* 98:1034–1048
- DiStefano MT, Hemphill SE, Oza AM, Siegert RK, Grant AR, Hughes MY, Cushman BJ, Azaiez H, Booth KT, Chapin A, Duzkale H, Matsunaga T, Shen J, Zhang W, Kenna M, Schimmenti LA, Tekin M, Rehm HL, Tayoun ANA, Amr SS, ClinGen Hearing Loss Clinical Domain Working Group (2019) ClinGen expert clinical validity curation of 164 hearing loss gene-disease pairs. *Genet Med* 21:2239–2247
- Downie L, Halliday J, Burt R, Lunke S, Lynch E, Martyn M, Poulakis Z, Gaff C, Sung V, Wake M, Hunter MF, Saunders K, Rose E, Lewis S, Jarmolowicz A, Phelan D, Rehm HL, Alliance MGH, Amor D (2020) Exome sequencing in infants with congenital hearing impairment: a population-based cohort study. *Eur J Hum Genet* 28:587–596
- Duzkale H, Shen J, McLaughlin H, Alfares A, Kelly MA, Pugh TJ, Funke BH, Rehm HL, Lebo MS (2013) A systematic approach to assessing the clinical significance of genetic variants. *Clin Genet* 84:453–463
- Ebermann I, Wiesen MH, Zrenner E, Lopez I, Pigeon R, Kohl S, Löwenheim H, Koenekoop RK, Bolz HJ (2009) GPR98 mutations cause Usher syndrome type 2 in males. *J Med Genet* 46:277–280
- Eudy JD, Weston MD, Yao S, Hoover DM, Rehm HL, Ma-Edmonds M, Yan D, Ahmad I, Cheng JJ, Ayuso C, Cremers C, Davenport S, Moller C, Talmadge CB, Beisel KW, Tamayo M, Morton CC, Swaroop A, Kimberling WJ, Sumegi J (1998) Mutation of a gene encoding a protein with extracellular matrix motifs in Usher syndrome type IIa. *Science* 280:1753–1757
- Gao FJ, Wang DD, Cheng F, Sun HX, Hu FY, Xu P, Li J, Liu W, Qi YH, Li W, Wang M, Zhang S, Xu GZ, Chang Q, Wu JH (2021) Prevalence and genetic–phenotypic characteristics of patients with USH2A mutations in a large cohort of Chinese patients with inherited retinal disease. *Br J Ophthalmol* 105:87–92
- Géléoc GGS, El-Amraoui A (2020) Disease mechanisms and gene therapy for Usher syndrome. *Hear Res* 394:107932
- Hart MR, Biesecker BB, Blout CL, Christensen KD, Amendola LM, Bergstrom KL, Biswas S, Bowling KM, Brothers KB, Conlin LK, Cooper GM, Dulik MC, East KM, Everett JN, Finnila CR, Ghazani AA, Gilmore MJ, Goddard KAB, Jarvik GP, Johnston JJ, Kauffman TL, Kelley WV, Krier JB, Lewis KL, McGuire AL, McMullen C, Ou J, Plon SE, Rehm HL, Richards CS, Romasko EJ, Miren Sagardia A, Spinner NB, Thompson ML, Turbitt E, Vassy JL, Wilfond BS, Veenstra DL, Berg JS, Green RC, Biesecker LG, Hindorf LA (2019) Secondary findings from clinical genomic sequencing: prevalence, patient perspectives, family history assessment, and health-care costs from a multisite study. *Genet Med* 21:1100–1110
- Hombach D, Schuelke M, Knierim E, Ehmke N, Schwarz JM, Fischer-Zirnsak B, Seelow D (2019) MutationDistiller: user-driven identification of pathogenic DNA variants. *Nucleic Acids Res* 47:W114–W120
- Jajjo T, Aller E, Oltra S, Beneyto M, Nájera C, Ayuso C, Baiget M, Carballo M, Antiñolo G, Valverde D, Moreno F, Vilela C, Perez-Garrigues H, Navea A, Millán JM (2006) Mutation profile of the MYO7A gene in Spanish patients with Usher syndrome type I. *Hum Mutat* 27:290–291
- Jiang L, Liang X, Li Y, Wang J, Zaneveld JE, Wang H, Xu S, Wang K, Wang B, Chen R, Sui R (2015) Comprehensive molecular diagnosis of 67 Chinese Usher syndrome probands: high rate of ethnicity specific mutations in Chinese USH patients. *Orphanet J Rare Dis* 10:110
- Jouret G, Poirsier C, Spodenkiewicz M, Jaquin C, Gouy E, Arndt C, Labrousse M, Gaillard D, Doco-Fenzy M, Lebre AS (2019) Genetics of Usher syndrome: new insights from a meta-analysis. *Otol Neurotol* 40:121–129
- Kajiwara K, Berson EL, Dryja TP (1994) Digenic retinitis pigmentosa due to mutations at the unlinked peripherin/RDS and ROM1 loci. *Science* 264:1604–1608
- Kalia SS, Adelman K, Bale SJ, Chung WK, Eng C, Evans JP, Herman GE, Hufnagel SB, Klein TE, Korf BR, McKelvey KD, Ormond KE, Richards CS, Vlangos CN, Watson M, Martin CL, Miller DT (2017) Recommendations for reporting of secondary findings in clinical exome and genome sequencing, 2016 update (ACMG SF v2.0): a policy statement of the American College of Medical Genetics and Genomics. *Genet Med* 19:249–255
- Karczewski KJ, Francioli LC, Tiao G, Cummings BB, Alfoldi J, Wang Q, Collins RL, Laricchia KM, Ganna A, Birnbaum DP, Gauthier LD, Brand H, Solomonson M, Watts NA, Rhodes D, Singer-Berk M, England EM, Seaby EG, Kosmicki JA, Walters RK, Tashman K, Farjoun Y, Banks E, Poterba T, Wang A, Seed C, Whiffin N, Chong JX, Samocha KE, Pierce-Hoffman E, Zappala Z, O'Donnell-Luria AH, Minikel EV, Weisburd B, Lek M, Ware JS, Vittal C, Armean IM, Bergelson L, Cibulskis K, Connolly KM, Covarrubias M, Donnelly S, Ferriera S, Gabriel S, Gentry J, Gupta N, Jeandet T, Kaplan D, Llanwarne C, Munshi R, Novod S, Petrillo N, Roazen D, Ruano-Rubio V, Saltzman A, Schleicher M, Soto J, Tibbetts K, Tolonen C, Wade G, Talkowski ME, Genome Aggregation Database Consortium, Neale BM, Daly MJ, MacArthur DG (2020) The mutational constraint spectrum quantified from variation in 141,456 humans. *Nature* 581:434–443
- Khalailah A, Abu-Diab A, Ben-Yosef T, Raas-Rothschild A, Lerer I, Alswaiti Y, Chowers I, Banin E, Sharon D, Khateb S (2018) The genetics of Usher syndrome in the Israeli and Palestinian populations. *Invest Ophthalmol vis Sci* 59:1095–1104

- Kimberling WJ, Hildebrand MS, Shearer AE, Jensen ML, Halder JA, Trzupek K, Cohn ES, Weleber RG, Stone EM, Smith RJ (2010) Frequency of Usher syndrome in two pediatric populations: implications for genetic screening of deaf and hard of hearing children. *Genet Med* 12:512–516
- Kooshavar D, Raziropour M, Movasat M, Keramatipour M (2018) Targeted next generation sequencing identified a novel mutation in MYO7A causing Usher syndrome type I in an Iranian consanguineous pedigree. *Int J Pediatr Otorhinolaryngol* 104:10–13
- Le Quesne SP, Saihan Z, Rangesh N, Steele-Stallard HB, Ambrose J, Coffey A, Emmerson J, Haralambous E, Hughes Y, Steel KP, Luxon LM, Webster AR, Bitner-Glindzic M (2012) Comprehensive sequence analysis of nine Usher syndrome genes in the UK National Collaborative Usher Study. *J Med Genet* 49:27–36
- Lentz JJ, Pan B, Ponnath A, Tran CM, Nist-Lund C, Galvin A, Goldberg H, Robillard KN, Jodelka FM, Farris HE, Huang J, Chen T, Zhu H, Zhou W, Rigo F, Hastings ML, Géléc GSG (2020) Direct delivery of antisense oligonucleotides to the middle and inner ear improves hearing and balance in Usher mice. *Mol Ther* 28:2662–2676
- Lewis TR, Shores CR, Cady MA, Hao Y, Arshavsky VY, Burns ME (2020) The F220C and F45L rhodopsin mutations identified in retinitis pigmentosa patients do not cause pathology in mice. *Sci Rep* 10:7538
- Liquori A, Vaché C, Baux D, Blanchet C, Hamel C, Malcolm S, Koenig M, Claustres M, Roux AF (2016) Whole USH2A gene sequencing identifies several new deep intronic mutations. *Hum Mutat* 37:184–193
- Liu L, Li H, Shi L (2017) Alström syndrome with novel ALMS mutations: a case report. *Exp Clin Endocrinol Diabetes Rep* 5:e10-13
- Mallory DP, Gutierrez E, Pinkevitch M, Klinginsmith C, Comar WD, Roushar FJ, Schleich JP, Smith AW, Jastrzebska B (2018) The retinitis pigmentosa-linked mutations in transmembrane helix 5 of rhodopsin disrupt cellular trafficking regardless of oligomerization state. *Biochemistry* 57:5188–5201
- Mazzoli M, van Camp G, Newton V, Giarbini N, Declau F, Parving A (2003) Recommendations for the description of genetic and audiological data for families with nonsyndromic hereditary hearing impairment. *Audiol Med* 1:148–150
- Myers KA, Nasioulas S, Boys A, McMahon JM, Slater H, Lockhart P, Sart DD, Scheffer IE (2018) ADGRV1 is implicated in myoclonic epilepsy. *Epilepsia* 59:381–388
- Nadeau JH (2001) Modifier genes in humans and mice. *Nat Rev Genet* 2:165–174
- Nagel-Wolfrum K, Baasov T, Wolfrum U (2014) Therapy strategies for Usher syndrome type 1C in the retina. *Adv Exp Med Biol* 801:741–747
- Namburi P, Ratnapriya R, Khateb S, Lazar CH, Kinarty Y, Obolensky A, Erdinest I, Marks-Ohana D, Pras E, Ben-Yosef T, Newman H, Gross M, Swaroop A, Banin E, Sharon D (2016) Bi-allelic truncating mutations in CEP78, encoding centrosomal protein 78, cause cone-rod degeneration with sensorineural hearing loss. *Am J Hum Genet* 99:777–784
- Neuhaus C, Eisenberger T, Decker C, Nagl S, Blank C, Pfister M, Kennerknecht I, Müller-Hofstede C, Charbel Issa P, Heller R, Beck B, Rüter K, Mitter D, Rohrschneider K, Steinhauer U, Korbacher HM, Huhle D, Elsayed SM, Taha HM, Baig SM, Stöhr H, Preising M, Markus S, Moeller F, Lorenz B, Nagel-Wolfrum K, Khan AO, Bolz HJ (2017) Next-generation sequencing reveals the mutational landscape of clinically diagnosed Usher syndrome: copy number variations, phenocopies, a predominant target for translational read-through, and PEX26 mutated in Heimler syndrome. *Mol Genet Genomic Med* 5:531–552
- Ng PC, Henikoff S (2001) Predicting deleterious amino acid substitutions. *Genome Res* 11:863–874
- Oishi M, Oishi A, Gotoh N, Ogino K, Higasa K, Iida K, Makiyama Y, Morooka S, Matsuda F, Yoshimura N (2014) Comprehensive molecular diagnosis of a large cohort of Japanese retinitis pigmentosa and Usher syndrome patients by next-generation sequencing. *Invest Ophthalmol Vis Sci* 55:7369–7735
- Oza AM, DiStefano MT, Hemphill SE, Cushman BJ, Grant AR, Siegrist RK, Shen J, Chapin A, Boczek NJ, Schimmenti LA, Murry JB, Hasadsri L, Nara K, Kenna M, Booth KT, Azaiez H, Griffith A, Avraham KB, Kremer H, Rehm HL, Amr SS, Abou Tayoun AN, ClinGen Hearing Loss Clinical Domain Working Group (2018) Expert specification of the ACMG/AMP variant interpretation guidelines for genetic hearing loss. *Hum Mutat* 39:1593–1613
- Pertea M, Lin X, Salzberg SL (2001) GeneSplicer: a new computational method for splice site prediction. *Nucleic Acids Res* 29:1185–1190
- Peter VG, Quinodoz M, Sadio S, Held S, Rodrigues M, Soares M, Sousa AB, Coutinho Santos L, Damme M, Rivolta C (2021) New clinical and molecular evidence linking mutations in ARSG to Usher syndrome type IV. *Hum Mutat* 42:261–271
- Pierrache LH, Hartel BP, van Wijk E, Meester-Smoor MA, Cremers FP, de Baere E, de Zaeytijd J, van Schooneveld MJ, Cremers CW, Dagnelie G, Hoyng CB, Bergen AA, Leroy BP, Pennings RJ, van den Born LI, Klaver CC (2016) Visual prognosis in USH2A-associated retinitis pigmentosa is worse for patients with Usher syndrome type IIa than for those with nonsyndromic retinitis pigmentosa. *Ophthalmology* 123:1151–1160
- Posey JE, Harel T, Liu P, Rosenfeld JA, James RA, Coban Akdemir ZH, Walkiewicz M, Bi W, Xiao R, Ding Y, Xia F, Beaudet AL, Muzny DM, Gibbs RA, Boerwinkle E, Eng CM, Sutton VR, Shaw CA, Plon SE, Yang Y, Lupski JR (2017) Resolution of disease phenotypes resulting from multilocus genomic variation. *N Engl J Med* 376:21–31
- Puffenberger EG, Jinks RN, Sougnez C, Cibulskis K, Willert RA, Achilly NP, Cassidy RP, Fiorentini CJ, Heiken KF, Lawrence JJ, Mahoney MH, Miller CJ, Nair DT, Politi KA, Worcester KN, Setton RA, Dipiazza R, Sherman EA, Eastman JT, Francklyn C, Robey-Bond S, Rider NL, Gabriel S, Morton DH, Strauss KA (2012) Genetic mapping and exome sequencing identify variants associated with five novel diseases. *PLoS ONE* 7:e28936
- Ratnapriya R, Zhan X, Fariss RN, Branham KE, Zipperer D, Chakarova CF, Sergeev YV, Campos MM, Othman M, Friedman JS, Maminishkis A, Waseem NH, Brooks M, Rajasimha HK, Edwards AO, Lotery A, Klein BE, Truitt BJ, Li B, Schaumberg DA, Morgan DJ, Morrison MA, Souied E, Tsironi EE, Grassmann F, Fishman GA, Silvestri G, Scholl HP, Kim IK, Ramke J, Tuo J, Merriam JE, Merriam JC, Park KH, Olson LM, Farrer LA, Johnson MP, Peachey NS, Lathrop M, Baron RV, Igo RP Jr, Klein R, Hagstrom SA, Kamatani Y, Martin TM, Jiang Y, Conley Y, Sahel JA, Zack DJ, Chan CC, Pericak-Vance MA, Jacobson SG, Gorin MB, Klein ML, Allikmets R, Iyengar SK, Weber BH, Haines JL, Léveillard T, Deangelis MM, Stambolian D, Weeks DE, Bhattacharya SS, Chew EY, Heckenlively JR, Abecasis GR, Swaroop A (2014) Rare and common variants in extracellular matrix gene fibrillin 2 (FBN2) are associated with macular degeneration. *Hum Mol Genet* 23:5827–5837
- Reese MG, Eeckman FH, Kulp D, Haussler D (1997) Improved splice site detection in Genie. *J Comput Biol* 4:311–323
- Rethanavelu K, Fung JLF, Chau JFT, Pei SLC, Chung CCY, Mak CCY, Luk HM, Chung BHY (2020) Phenotypic and mutational spectrum of 21 Chinese patients with Alström syndrome. *Am J Med Genet A* 182:279–288
- Riazuddin S, Nazli S, Ahmed ZM, Yang Y, Zulfiqar F, Shaikh RS, Zafar AU, Khan SN, Sabar F, Javid FT, Wilcox ER, Tsilou E, Boger ET, Sellers JR, Belyantseva IA, Riazuddin S, Friedman TB (2008) Mutation spectrum of MYO7A and evaluation of a

- novel nonsyndromic deafness DFNB2 allele with residual function. *Hum Mutat* 29:502–511
- Riazzuddin S, Belyantseva IA, Giese AP, Lee K, Indzhykuliaan AA, Nandamuri SP, Yousaf R, Sinha GP, Lee S, Terrell D, Hegde RS, Ali RA, Anwar S, Andrade-Elizondo PB, Sirmaci A, Parise LV, Basit S, Wali A, Ayub M, Ansar M, Ahmad W, Khan SN, Akram J, Tekin M, Riazzuddin S, Cook T, Buschbeck EK, Frolenkov GI, Leal SM, Friedman TB, Ahmed ZM (2012) Alterations of the CIB2 calcium- and integrin-binding protein cause Usher syndrome type 1J and nonsyndromic deafness DFNB48. *Nat Genet* 44:1265–1271
- Richards S, Aziz N, Bale S, Bick D, Das S, Gastier-Foster J, Grody WW, Hegde M, Lyon E, Spector E, Voelkerding K, Rehm HL, ACMG Laboratory Quality Assurance Committee (2015) Standards and guidelines for the interpretation of sequence variants: a joint consensus recommendation of the American College of Medical Genetics and Genomics and the Association for Molecular Pathology. *Genet Med* 17:405–424
- Rio Frio T, McGee TL, Wade NM, Iseli C, Beckmann JS, Berson EL, Rivolta C (2009) A single-base substitution within an intronic repetitive element causes dominant retinitis pigmentosa with reduced penetrance. *Hum Mutat* 30:1340–1347
- Rivolta C, McGee TL, Rio Frio T, Jensen RV, Berson EL, Dryja TP (2006) Variation in retinitis pigmentosa-11 (PRPF31 or RP11) gene expression between symptomatic and asymptomatic patients with dominant RP11 mutations. *Hum Mutat* 27:644–653
- Rose AM, Shah AZ, Venturini G, Krishna A, Chakravarti A, Rivolta C, Bhattacharya SS (2016) Transcriptional regulation of PRPF31 gene expression by MSR1 repeat elements causes incomplete penetrance in retinitis pigmentosa. *Sci Rep* 6:19450
- Roux AF, Faugère V, Le Guédard S, Pallares-Ruiz N, Vielle A, Chamberlain S, Marlin S, Hamel C, Gilbert B, Malcolm S, Claustres M, Collaboration FUS (2006) Survey of the frequency of USH1 gene mutations in a cohort of Usher patients shows the importance of cadherin 23 and protocadherin 15 genes and establishes a detection rate of above 90%. *J Med Genet* 43:763–768
- Sabbaghi H, Daftarian N, Suri F, Mirrahimi M, Madani S, Sheikhtaheri A, Khorrami F, Saviz P, Zarei Nejad M, Tivay A, Shahriari HA, Maleki A, Ahmadi SS, Sargazi M, Cremers FPM, Najafi M, Vona B, Haaf T, Bahena-Carbajal P, Moghadasi A, Naraghi H, Yaseri M, Kheiri B, Kalantarion M, Sabbaghi E, Salami M, Pazooki L, Zendedel K, Mojarab S, Ahmadi H (2020) The first inherited retinal disease registry in Iran: research protocol and results of a pilot study. *Arch Iran Med* 23:445–454
- Schwarz JM, Cooper DN, Schuelke M, Seelow D (2014) Mutation-Taster2: mutation prediction for the deep-sequencing age. *Nat Methods* 11:361–362
- Scott EM, Halees A, Itan Y, Spencer EG, He Y, Azab MA, Gabriel SB, Belkadi A, Boisson B, Abel L, Clark AG, Greater Middle East Variome Consortium, Alkuraya FS, Casanova JL, Gleeson JG (2016) Characterization of Greater Middle Eastern genetic variation for enhanced disease gene discovery. *Nat Genet* 48:1071–1076
- Shapiro MB, Senapathy P (1987) RNA splice junctions of different classes of eukaryotes: sequence statistics and functional implications in gene expression. *Nucleic Acids Res* 15:7155–7174
- Simonelli F, Testa F, de Crecchio G, Rinaldi E, Hutchinson A, Atkinson A, Dean M, D'Urso M, Allikmets R (2000) New ABCR mutations and clinical phenotype in Italian patients with Stargardt disease. *Invest Ophthalmol vis Sci* 41:892–897
- Sliesoraityte I, Peto T, Mohand-Said S, Sahel JA (2015) Novel grading system for quantification of cystic macular lesions in Usher syndrome. *Orphanet J Rare Dis* 10:157
- Sloan-Heggen CM, Babanejad M, Beheshtian M, Simpson AC, Booth KT, Ardalani F, Frees KL, Mohseni M, Mozafari R, Mehrjoo Z, Jamali L, Vaziri S, Akhtarkhavari T, Bazazzadegan N, Nikzat N, Arzhanghi S, Sabbagh F, Otukesh H, Seifati SM, Khodaei H, Taghdiri M, Meyer NC, Daneshi A, Farhadi M, Kahrizi K, Smith RJ, Azaiez H, Najmabadi H (2015) Characterising the spectrum of autosomal recessive hereditary hearing loss in Iran. *J Med Genet* 52:823–829
- Sloan-Heggen CM, Bierer AO, Shearer AE, Kolbe DL, Nishimura CJ, Frees KL, Ephraim SS, Shibata SB, Booth KT, Campbell CA, Ranum PT, Weaver AE, Black-Ziegelbein EA, Wang D, Azaiez H, Smith RJH (2016) Comprehensive genetic testing in the clinical evaluation of 1119 patients with hearing loss. *Hum Genet* 135:441–450
- Soens ZT, Branch J, Wu S, Yuan Z, Li Y, Li H, Wang K, Xu M, Rajan L, Motta FL, Simões RT, Lopez-Solache I, Ajlan R, Birch DG, Zhao P, Porto FB, Sallum J, Koenekoop RK, Sui R, Chen R (2017) Leveraging splice-affecting variant predictors and a mini-gene validation system to identify Mendelian disease-causing variants among exon-captured variants of uncertain significance. *Hum Mutat* 38:1521–1533
- Stenson PD, Mort M, Ball EV, Shaw K, Phillips A, Cooper DN (2014) The Human Gene Mutation Database: building a comprehensive mutation repository for clinical and molecular genetics, diagnostic testing and personalized genomic medicine. *Hum Genet* 133:1–9
- Stiff HA, Sloan-Heggen CM, Ko A, Pfeifer WL, Kolbe DL, Nishimura CJ, Frees KL, Booth KT, Wang D, Weaver AE, Azaiez H, Kamholz J, Smith RJH, Drack AV (2020) Is it Usher syndrome? Collaborative diagnosis and molecular genetics of patients with visual impairment and hearing loss. *Ophthalmic Genet* 41:151–158
- Tasliyurt T, Yigit S, Rustemoglu A, Gul U, Ates O (2013) Common MEFV gene mutations in Turkish patients with Behcet's disease. *Gene* 530:100–103
- Tompson SW, Young TL (2017) Assaying the effects of splice site variants by exon trapping in a mammalian cell line. *Bio Protoc* 7:e2281
- Vaché C, Besnard T, le Berre P, García-García G, Baux D, Larrieu L, Abadie C, Blanchet C, Bolz HJ, Millan J, Hamel C, Malcolm S, Claustres M, Roux AF (2012) Usher syndrome type 2 caused by activation of an USH2A pseudoexon: implications for diagnosis and therapy. *Hum Mutat* 33:104–108
- Watanabe S, Umeki N, Ikebe R, Ikebe M (2008) Impacts of Usher syndrome type IB mutations on human myosin VIIa motor function. *Biochemistry* 47:9505–9513
- Yang Y, Muzny DM, Xia F, Niu Z, Person R, Ding Y, Ward P, Braxton A, Wang M, Buhay C, Veeraraghavan N, Hawes A, Chiang T, Leduc M, Beuten J, Zhang J, He W, Scull J, Willis A, Landsverk M, Craigen WJ, Bekheirnia MR, Stray-Pedersen A, Liu P, Wen S, Alcaraz W, Cui H, Walkiewicz M, Reid J, Bainbridge M, Patel A, Boerwinkle E, Beaudet AL, Lupski JR, Plon SE, Gibbs RA (2014) Molecular findings among patients referred for clinical whole-exome sequencing. *JAMA* 312:1870–1879
- Yeo G, Burge CB (2004) Maximum entropy modeling of short sequence motifs with applications to RNA splicing signals. *J Comput Biol* 11:377–394

Publisher's Note Springer Nature remains neutral with regard to jurisdictional claims in published maps and institutional affiliations.

Authors and Affiliations

Paulina Bahena¹ · Narsis Daftarian² · Reza Maroofian³ · Paola Linares⁴ · Daniel Villalobos⁵ · Mehraban Mirrahimi² · Aboufazel Rad⁶ · Julia Doll¹ · Michaela A. H. Hofrichter¹ · Asuman Koparir¹ · Tabea Röder¹ · Seungbin Han¹ · Hamideh Sabbaghi⁷ · Hamid Ahmadi⁷ · Hassan Behboudi⁸ · Cristina Villanueva-Mendoza⁹ · Vianney Cortés-Gonzalez⁹ · Rocio Zamora-Ortiz¹⁰ · Susanne Kohl¹¹ · Laura Kuehlewein^{11,12} · Hossein Darvish¹³ · Elham Alehabib¹⁴ · Maria de la Luz Arenas-Sordo¹⁵ · Fatemeh Suri⁷ · Barbara Vona^{1,6} · Thomas Haaf¹ 

¹ Institute of Human Genetics, Julius Maximilians University Würzburg, 97074 Würzburg, Germany

² Ocular Tissue Engineering Research Center, Research Institute for Ophthalmology and Vision Science, Shahid Beheshti University of Medical Sciences, Tehran, Iran

³ Department of Neuromuscular Disorders, UCL Queen Square Institute of Neurology, London, UK

⁴ Universidad Nacional Autónoma de México, Mexico City, Mexico

⁵ Department of Bioinformatics, University of Würzburg, Würzburg, Germany

⁶ Department of Otolaryngology-Head and Neck Surgery, Tübingen Hearing Research Centre, Eberhard Karls University Tübingen, 72076 Tübingen, Germany

⁷ Ophthalmic Epidemiology Research Center, Research Institute for Ophthalmology and Vision Science, Shahid Beheshti University of Medical Sciences, No. 23, Paidarfard St., Boostan 9 St., Pasdaran Ave., Tehran 1666673111, Iran

⁸ Amirmomenin Hospital, Eye Research Center, Guilan University of Medical Sciences, Rasht, Iran

⁹ Genetics Department, Asociación Para Evitar la Ceguera en México (APEC), Mexico City, Mexico

¹⁰ Ophthalmic Department, Instituto de Seguridad y Servicios sociales de los Trabajadores del Estado, Hospital de Alta Especialidad, Puebla, Mexico

¹¹ Centre for Ophthalmology, Institute for Ophthalmic Research, Eberhard Karls University Tübingen, Tübingen, Germany

¹² University Eye Hospital, Centre for Ophthalmology, Eberhard Karls University Tübingen, Tübingen, Germany

¹³ Faculty of Medicine, Neuroscience Research Center, Golestan University of Medical Sciences, Gorgan, Iran

¹⁴ Student Research Committee, Department of Medical Genetics, School of Medicine, Shahid Beheshti University of Medical Sciences, Tehran, Iran

¹⁵ Department of Genetics, National Institute of Rehabilitation Luis Guillermo Ibarra (INR), Mexico City, Mexico

10.8 Attachment 8

Biallelic variants in KARS1 are associated with neurodevelopmental disorders and HL recapitulated by the knockout zebrafish



ARTICLE

Biallelic variants in *KARS1* are associated with neurodevelopmental disorders and hearing loss recapitulated by the knockout zebrafish

Sheng-Jia Lin^{1,38}, Barbara Vona^{2,3,38}, Patricia G. Barbalho^{1,38}, Rauan Kaiyrzhanov⁴, Reza Maroofian⁴, Cassidy Petree¹, Mariasavina Severino⁵, Valentina Stanley⁶, Prathishtha Varshney¹, Paulina Bahena³, Fatema Alzahrani⁷, Amal Alhashem⁸, Alistair T. Pagnamenta⁹, Gudrun Aubertin¹⁰, Juviane I. Estrada-Veras^{11,12,13}, Héctor Adrián Díaz Hernández¹⁴, Neda Mazaheri^{15,16}, Andrea Oza¹⁷, Jenny Thies¹⁸, Deborah L. Renaud¹⁹, Sanmati Dugad²⁰, Jennifer McEvoy⁶, Tipu Sultan²¹, Lynn S. Pais²², Brahim Tabarki⁸, Daniel Villalobos-Ramirez²³, Aboufazel Rad², Genomics England Research Consortium*, Hamid Galehdari¹⁴, Farah Ashrafzadeh²⁴, Afsaneh Sahebzamani²⁵, Kolsoum Saeidi²⁶, Erin Torti²⁷, Houda Z. Elloumi²⁷, Sara Mora²⁷, Timothy B. Palculict²⁷, Hui Yang²⁷, Jonathan D. Wren¹, Ben Fowler²⁸, Manali Joshi²⁰, Martine Behra²⁹, Shawn M. Burgess³⁰, Swapan K. Nath³¹, Michael G. Hanna⁴, Margaret Kenna¹⁷, J. Lawrence Merritt II³², Henry Houlden⁴, Ehsan Ghayoor Karimiani^{33,34}, Maha S. Zaki³⁵, Thomas Haaf³, Fozwan S. Alkuraya^{7,8}, Joseph G. Gleeson⁶ and Gaurav K. Varshney¹✉

PURPOSE: Pathogenic variants in Lysyl-tRNA synthetase 1 (*KARS1*) have increasingly been recognized as a cause of early-onset complex neurological phenotypes. To advance the timely diagnosis of *KARS1*-related disorders, we sought to delineate its phenotype and generate a disease model to understand its function in vivo.

METHODS: Through international collaboration, we identified 22 affected individuals from 16 unrelated families harboring biallelic likely pathogenic or pathogenic in *KARS1* variants. Sequencing approaches ranged from disease-specific panels to genome sequencing. We generated loss-of-function alleles in zebrafish.

RESULTS: We identify ten new and four known biallelic missense variants in *KARS1* presenting with a moderate-to-severe developmental delay, progressive neurological and neurosensory abnormalities, and variable white matter involvement. We describe novel *KARS1*-associated signs such as autism, hyperactive behavior, pontine hypoplasia, and cerebellar atrophy with prevalent vermian involvement. Loss of *kars1* leads to upregulation of p53, tissue-specific apoptosis, and downregulation of neurodevelopmental related genes, recapitulating key tissue-specific disease phenotypes of patients. Inhibition of p53 rescued several defects of *kars1*^{-/-} knockouts.

CONCLUSION: Our work delineates the clinical spectrum associated with *KARS1* defects and provides a novel animal model for *KARS1*-related human diseases revealing p53 signaling components as potential therapeutic targets.

Genetics in Medicine (2021) 23:1933–1943; <https://doi.org/10.1038/s41436-021-01239-1>

¹Genes & Human Disease Research Program, Oklahoma Medical Research Foundation, Oklahoma City, OK, USA. ²Department of Otolaryngology–Head & Neck Surgery, Tübingen Hearing Research Centre, Eberhard Karls University of Tübingen, Tübingen, Germany. ³Institute of Human Genetics, Julius Maximilians University Würzburg, Würzburg, Germany. ⁴Department of Neuromuscular Disorders, Queen Square Institute of Neurology, University College London, London, UK. ⁵Neuroradiology Unit, IRCCS Istituto Giannina Gaslini, Genoa, Italy. ⁶Department of Neurosciences, Rady Children’s Institute for Genomic Medicine, University of California San Diego, La Jolla, CA, USA. ⁷Department of Genetics, King Faisal Specialist Hospital and Research Center, Riyadh, Saudi Arabia. ⁸Department of Pediatrics, Prince Sultan Military Medical City, Riyadh, Saudi Arabia. ⁹NIHR Biomedical Research Centre, Wellcome Centre for Human Genetics, University of Oxford, Oxford, UK. ¹⁰Division of Medical Genetics, Department of Pathology and Lab Medicine, Island Health, Victoria General Hospital, Victoria, BC, Canada. ¹¹Henry M Jackson Foundation for the Advancement of Military Medicine, Bethesda, MD, USA. ¹²Pediatric Subspecialty Genetics Walter Reed National Military Medical Center, Bethesda, MD, USA. ¹³Murtha Cancer Center / Research Program, Department of Surgery, Uniformed Services University of the Health Sciences, Bethesda, MD, USA. ¹⁴Department of Gastrointestinal Endoscopy, National Institute of Medical Sciences and Nutrition Salvador Zubirán, Mexico City, Mexico. ¹⁵Department of Genetics, Faculty of Science, Shahid Chamran University of Ahvaz, Ahvaz, Iran. ¹⁶Narges Medical Genetics and Prenatal Diagnostics Laboratory, East Mihan Ave., Kianpars, Iran. ¹⁷Otolaryngology and Communication Enhancement, Boston Children’s Hospital, and Dept. of Otolaryngology, Harvard medical School, Boston, USA. ¹⁸Department of Biochemical Genetics, Seattle Children’s Hospital, Seattle, WA, USA. ¹⁹Departments of Neurology and Pediatrics, Mayo Clinic College of Medicine and Science, Rochester, MN, USA. ²⁰Bioinformatics Centre, S. P. Pune University, Pune, India. ²¹Department of Pediatric Neurology, Children’s Hospital and Institute of Child Health, Lahore, Pakistan. ²²Broad Center for Mendelian Genomics, Program in Medical and Population Genetics, Broad Institute of Massachusetts Institute of Technology and Harvard, Cambridge, MA, USA. ²³Department of Bioinformatics, Biocenter, University of Würzburg, Würzburg, Germany. ²⁴Department of Pediatric Diseases, Mashhad University of Medical Sciences, Mashhad, Iran. ²⁵Pediatric and Genetic Counselling Center, Kerman Welfare Organization, Kerman, Iran. ²⁶Neuroscience Research Center, Institute of Neuropharmacology, Kerman University of Medical Sciences, Kerman, Iran. ²⁷GeneDx, 207 Perry Parkway Gaithersburg, Gaithersburg, MD, USA. ²⁸Imaging core facility, Oklahoma Medical Research Foundation, Oklahoma City, OK, USA. ²⁹Department of Neurobiology, University of Puerto Rico, San Juan, PR, USA. ³⁰Translational & Functional Genomics Branch, National Human Genome Research Institute, NIH, Bethesda, MD, USA. ³¹Arthritis & Clinical Immunology Research Program, Oklahoma Medical Research Foundation, Oklahoma City, OK, USA. ³²Department of Pediatrics, Biochemical Genetics, University of Washington, Seattle, WA, USA. ³³Molecular and Clinical Sciences Institute, St. George’s, University of London, Cranmer Terrace London, London, UK. ³⁴Innovative Medical Research Center, Mashhad Branch, Islamic Azad University, Mashhad, Iran. ³⁵Clinical Genetics Department, Human Genetics and Genome Research Division, National Research Center, Cairo, Egypt. ³⁶These authors contributed equally: Sheng-Jia Lin, Barbara Vona, Patricia G. Barbalho. ³⁷A list of authors and their affiliations appears at the end of the paper. ³⁸email: gaurav-varshney@omrf.org

INTRODUCTION

Aminoacyl-tRNA synthetases (ARSs) are ubiquitously expressed and essential enzymes required for the aminoacylation of specific amino acids onto their cognate transfer RNAs (tRNAs). Biallelic variants in ARS genes have been shown to cause a variety of severe and early-onset human diseases [1]. These diseases appear with diverse clinical manifestations such as Charcot-Marie-Tooth disease [2], leukodystrophies [1, 3–5], cardiomyopathies [6], hearing loss, [7] and other central nervous system (CNS)-related pathologies [8–11]. ARS variants can lead to reduced aminoacylation activity, decreased translation accuracy, and defects in noncanonical processes [1], but the underlying mechanisms leading to pathology remain poorly understood [12]. As a result, there are no effective treatment strategies for these pathologies.

Of the 37 ARS genes in humans, 18 encode cytoplasmic enzymes, 17 encode mitochondrial enzymes, and 2 encode bifunctional enzymes; *KARS1* (lysyl-tRNA synthetase) is one of the bifunctional ARS enzymes. In humans, a single *KARS1* gene (MIM 601421) [13] encodes both the cytoplasmic and mitochondrial lysyl-tRNA synthetases, which are generated by alternative splicing. Biallelic variants in *KARS1* have been reported in patients with a broad spectrum of clinical manifestations including Charcot-Marie-Tooth [2], nonsyndromic hearing loss [14, 15], peripheral neuropathy [2], congenital visual impairment [16], progressive microcephaly [16], hypertrophic cardiomyopathy [17], leukoencephalopathies [15, 18, 19], leukodystrophy, [20] and severe neurological and neurosensory disease with optic neuropathy [21]. Twenty-eight pathogenic variants in 30 affected individuals from 25 families have been identified to date, following an autosomal recessive inheritance pattern.

Here, we report 10 new and 4 known biallelic missense variants in *KARS1* in 22 affected individuals from 16 unrelated families. Having included data from 30 previously published *KARS1* cases, we provide a cumulative and comprehensive phenotypic characterization of 52 affected individuals. A mouse knockout of *Kars1* is embryonic lethal and dies before organogenesis occurs [22]. Nevertheless, the function of *Kars1* in specific tissues *in vivo* remained unknown. Here, we generated loss-of-function alleles in zebrafish using CRISPR/Cas9 to understand the function of *kars1* *in vivo*.

MATERIALS AND METHODS

Genetic and phenotypic analysis

Blood samples were collected from all participants and genomic DNA was extracted using standard methods. Sequencing methods and genetic analysis summaries per individual sequenced in each family are summarized in Table S1. Clinical information was collected using standardized templates and completed by collaborating geneticists and clinicians. Brain magnetic resonance images (MRIs)/computed tomography (CT) images from all previously published reports and our cohort were systematically analyzed by a pediatric neuroradiologist. Detailed clinical methods are described in Supplementary information.

Zebrafish functional studies

Zebrafish (*Danio rerio*) were raised and maintained in an Association for Assessment and Accreditation of Laboratory Animal Care (AAALAC) accredited facility at the Oklahoma Medical Research Foundation (OMRF) under standard conditions, and all experiments were performed as per protocol 17-01 approved by the Institutional Animal Care Committee (IACUC) of OMRF. All zebrafish work was carried out in wild-type (WT) strain NHGRI-1. Detailed methods related to zebrafish work are described in Supplementary information.

Statistical analysis

Each experiment was repeated three times, and sample sizes are described in the Supplementary information. Data are presented as mean value \pm standard deviation (SD). Statistical analysis was performed using GraphPad

Prism version 8.4 (GraphPad Software, San Diego, CA, USA). In all analyses, the significance level was set to 0.05. The *p* value was determined as follows. The larval survival curve (Kaplan–Meier representation) was assessed using the log rank Mantel–Cox test. One-way analysis of variance (ANOVA) with Tukey's multiple comparisons test was used for eye and head size comparisons. Two-tailed unpaired Student's *t*-test with nonparametric Mann–Whitney test was used for hair cell and motor exon diameter calculation. Two-tailed unpaired Student's *t*-test was used for the comparison of gene expression levels between two groups, and Holm–Sidak multiple comparisons correction was used for multiple groups comparison. Two-tailed unpaired *t*-test with Welch's correction was used for the visual startle response (VSR) and auditory evoked behavior response (AEBR) analyses.

RESULTS

Patients with *KARS1* variants show multisystem abnormalities primarily involving the nervous system

We investigated 22 affected individuals from 16 unrelated families who harbored biallelic *KARS1* variants (Fig. 1a). Clinical summaries and variant details are presented in the Case Reports in Supplementary information, Table 1, Fig. 1c, and Tables S2 and S3. All patients underwent either exome, genome, or targeted gene sequencing and analyses, which excluded other functionally relevant variants compatible with Mendelian diseases, based on mode of inheritance and clinical presentation. Variants were Sanger sequence-confirmed (Fig. S1). We identified ten previously unpublished variants and four previously reported variants [18, 19, 21, 23, 24] as listed in Table 1, and Fig. S2. Each substitution affected a conserved amino acid, and all the variants are predicted to be deleterious (Supplementary information, Fig. S3).

Clinical description. The cohort mostly presented with a moderate-to-severe developmental delay, progressive neurological and neurosensory impairment, and white matter involvement, variably associated with developmental regression, intellectual disability, behavioral abnormalities, and additional extraneurological signs. The disease typically manifested during early childhood with developmental delay and/or hearing impairment. Developmental regression was reported in 7/22 cases (32%). Four cases died at the mean age of 13.9 years due to respiratory infection (2/4), sepsis (1/4), or postfebrile illness associated with severe deterioration (1/4). All parents were asymptomatic and did not exhibit neurological symptoms. Developmental delay was present in 86% of cases (19/22) followed by intellectual disability (15/21, 71%), speech delay (11/19, 58%), absent speech (11/20, 55%), failure to thrive (4/22, 18%), and behavioral abnormalities such as autism (3/21, 14%) and hyperactive behavior (6/21, 29%).

All cases uniformly expressed neurological symptoms (22/22, 100%), frequently involving sensorineural hearing loss (20/21, 95%), seizures (13/22, 59%), hypotonia (9/22, 41%), cerebellar ataxia (7/22, 32%), spasticity (8/22, 36%), strabismus (6/20, 30%) and nystagmus (4/20, 20%), and acquired joint contractures (4/22, 18%). Hearing loss was severe-to-profound in 16/21 cases (76%), and 5/10 (50%) of them had cochlear implants. Other variable neurological features included visual impairment/optic atrophy (7/20, 35%), quadriplegia (3/22, 14%), dystonia and tremor (2/22, 9%), neuropathy (1/10, 10%), neurophysiologically confirmed skeletal myopathy (2/22, 9%) (Video S1-2), generalized muscle atrophy (2/22, 9%), and incontinence (4/22, 18%). None of the cases expressed isolated hearing loss or sensory-motor neuropathy as the main clinical feature.

While not every case was uniformly examined, roughly half were clinically diagnosed with microcephaly (10/18, 56%). Interestingly, dysmorphic facial features were common in 67% (14/21) of the cohort and this included a high or narrow forehead, prominent nose, short philtrum, low-set ears, broad nasal bridge, thin upper lip, epicanthus, and telecanthus

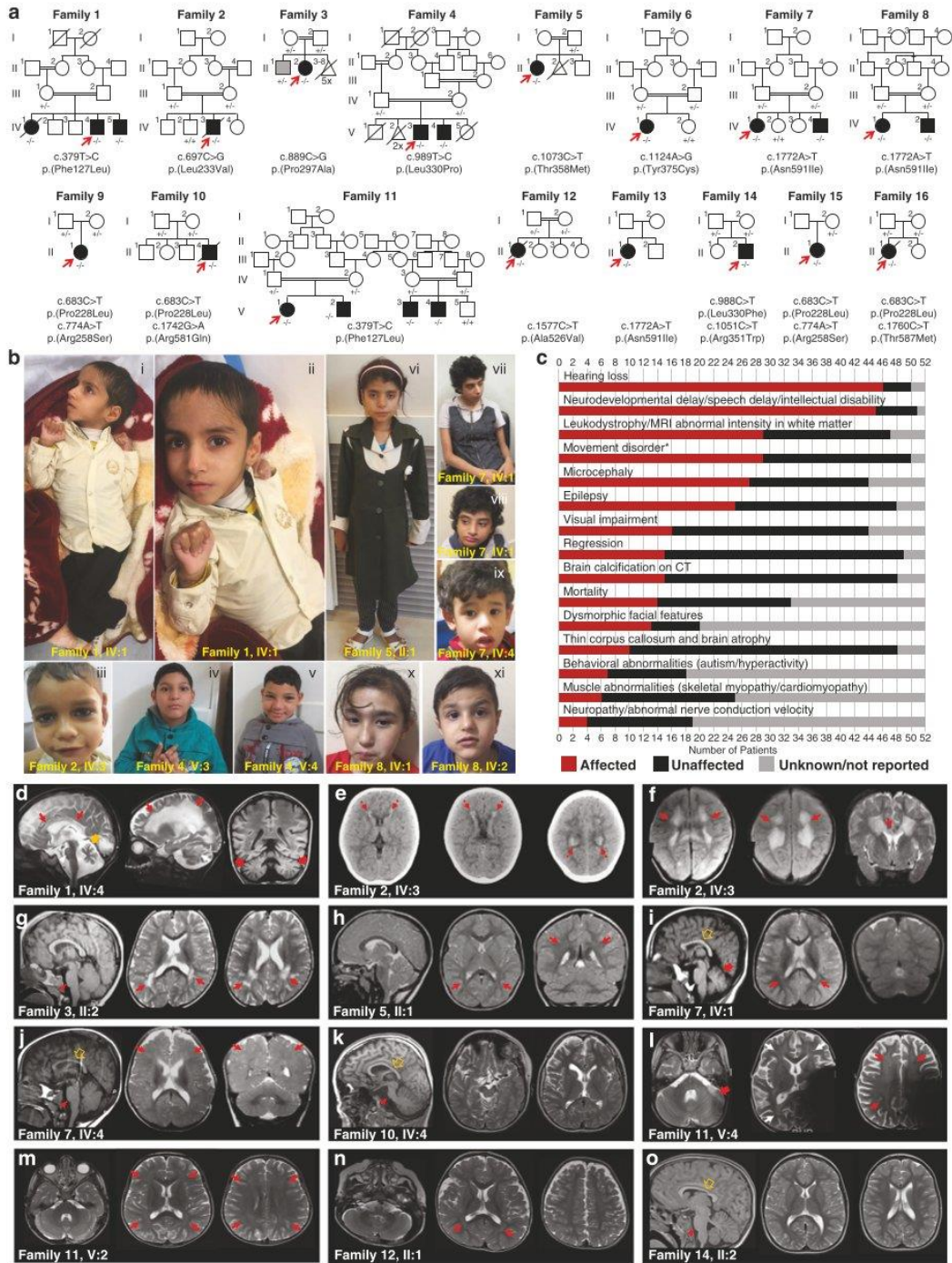


(Fig. 1b; Supplementary Case Report includes detailed descriptions). Other extraneurological signs included feeding difficulties (6/22, 27%), and neonatal vomiting with diarrhea (2/22, 11%). Single isolated cases displayed hypertrophic cardiomyopathy

(1/11, 9%), and neonatal vomiting with diarrhea (2/22, 11%). The case with hypertrophic cardiomyopathy did not have available levels of lactate and mitochondrial respiratory chain enzymes measured.

Fig. 1 Identification of pathogenic variants in *KARS1* in 16 families and clinical summary. (a) Pedigrees and segregation data for the 16 families included in this study. Affected and unaffected individuals are indicated by filled and open squares (males) and circles (females), respectively. Proband is marked with red arrows. Double lines indicate consanguinity. Genetic diagnoses were made in 22 individuals. (b) Clinical characteristics of patients with homozygous *KARS1* variants, including affected individuals from family 1 (IV:4) (i, ii), family 2 (IV:3) (iii), family 4 (V:3) (iv) and (V:4) (v), family 5 (II:1) (vi), family 7 (IV:1) (vii, viii) and IV:4 (ix), and family 8 (IV:1) (x) (IV:2) (xi). Frequent clinical features include: spasticity and contractures in the limbs with clenched hands (i, ii), high forehead (iv, v, vi, vii, x), prominent nose (i, ii, iv, v, vi, vii, viii), low-set ears (i, ii, iv, v, vii, viii, ix), and short philtrum (i, ii, iv, v, vi, vii, ix, x). (c) Phenotype summary of features associated with *KARS1* pathogenic variants. Asterisk denotes movement disorders that include ataxia, spasticity, quadriplegia, dystonia, or chorea/tremor. (d–o) Neuroimaging features associated with *KARS1* variants, with variable patterns of white matter (WM) involvement (red arrows), calcifications (red dotted arrows), pontine hypoplasia (red arrowheads), cerebellar atrophy (red thick arrows), enlargement of the cerebral cerebrospinal fluid (CSF) spaces, and corpus callosum hypoplasia (gold arrows).

Neuroimaging findings. Brain MRI studies were available for 21/22 (95%) individuals (with more than one examination in 2 cases), while head CT and spinal MRI were available for three and one subjects, respectively (Fig. 1d–o). White matter involvement was noted in 13/21 (61.9%) individuals. In 5/13 (38.4%) subjects, there were confluent T2 hyperintensities in the periventricular white matter, with prevalent involvement of parieto-occipital regions; one of these subjects studied at 53 years of age had a previous normal brain MRI (performed 8 years before). In 4/13 (23%) subjects, there was mild diffuse T2 hyperintensity of the supratentorial white matter, with sparing of the corpus callosum and U fibers; one of these individuals studied at 4 years of age had a previous normal brain MRI (performed 2 years before). Two subjects (2/13, 15.3%) presented diffuse leukodystrophy with corpus callosum involvement, sparing of the U fibers, and calcifications; in one of them the cerebellar white matter was also involved. Delayed myelination was noted in 2 other subjects (2/13, 15.3%). White matter volume loss with ventricular enlargement was present in 10/21 (47.6%) cases. Enlargement of the cerebral CSF spaces, mainly in the frontotemporal regions was observed in 9/21 (42.8%) individuals. Hypoplasia of the pons and corpus callosum was noted in 7/21 (33.3%) and 6/21 (28.5%) of cases, respectively. Cerebellar atrophy, with prevalent or isolated vermian involvement was noted in 5/21 (23.8%) of cases. Finally, in 4/21 (19%) subjects, the brain MRI was normal.

Genotype–phenotype correlation. Inter- and intrafamilial phenotypic variability was noticed among individuals with the same variants in the present *KARS1* cohort. For instance, three affected siblings in family 11 each harbored a homozygous *KARS1* c.379T>C (p.[Phe127Leu]) variant, and although they shared common symptoms such as developmental delay, infantile-onset profound hearing loss, dysmorphic facial features, spasticity, and varying degree of joint contractures, several important symptoms were expressed only by one of them. This included regression, epilepsy, optic atrophy, failure to thrive, and hyperactivity. The same *KARS1* variant was homozygous in the proband from family 1, who differed from family 11 by a preserved vision, cerebellar ataxia, classic leukodystrophy on MRI, and the basal ganglia calcification. Similarly, five affected members from three independent families were homozygous for the *KARS1* c.1772A>T (p.[Asn591Ile]) variant and they had variable intra- and interfamilial expression of epileptic seizures, cerebellar ataxia, intellectual disability, hypotonia, polyneuropathy, behavioral abnormalities, and impaired speech. Significant phenotypic variability was also noticed between families 9 and 15 harboring the similar compound heterozygous *KARS1* variants c.683C>T (p.[Pro228Leu]) and c.774A>T (p.[Arg258Ser]).

***kars1* zebrafish disease model using CRISPR/Cas9-mediated targeted mutagenesis.** Zebrafish has a single *kars1* gene (NCBI Gene ID: 280647) generating two transcript variants via alternative RNA splicing, confirmed by reverse transcription polymerase chain reaction (RT-PCR) from multiple developmental stages (Fig. S4, and Supplementary information). To unravel the function of

KARS1, we examined *kars1* messenger RNA (mRNA) expression in zebrafish embryonic development using whole-mount in situ hybridization (WISH). *kars1* mRNA was initially ubiquitously expressed but gradually became more prominent in the CNS, eye, inner ear, muscles, and digestive system (liver, intestine, and pancreas) (Fig. 2a–c, Supplementary information, and Fig. S5a–g). We generated *kars1* loss-of-function zebrafish mutant lines using CRISPR/Cas9 and identified three independent alleles *kars1*^{om1del7}, *kars1*^{om2del8}, and *kars1*^{om3del7} (Fig. S6a–d). Homozygous *kars1*^{−/−} animals showed morphological abnormalities starting at approximately 3 dpf including heart edema (black arrow), as well as smaller heads (blue line), eye (red line) and otic vesicle (red arrowhead) when compared to WT animals (Fig. 2d, e, and Fig. S7a–c). *Kars1* homozygous larvae also failed to inflate the swim bladder (black arrowhead) and showed abnormal trunk muscle fibers. We observed 100% mortality by 10 dpf for all three *kars1* homozygous mutant larvae, possibly because of the inability to feed (Fig. 2f and Fig. S7d). We quantified the eye and head axial length which were significantly reduced in *kars1*^{−/−} mutants compared to control animals (Fig. 2g, h). Additionally, the *kars1*^{−/−} larvae failed to respond to touch and displayed a loss of spatial orientation (Fig. S7e, f and Video S3). The side-laying position observed in *kars1*^{−/−} mutant larvae might reflect loss of vestibular function, severe muscle control failure, and/or absence of an inflated swim bladder, which all affect balance. Given the *kars1*^{−/−} mutants showed morphological defects in the eyes and ears, and failed to respond to touch, we further quantified their VSR and AEBR; *kars1*^{−/−} mutants showed completed loss of locomotor activity in response to light or acoustic startle (Fig. 2i, j). Overall, the tissue/organ-specific morphological defects in *kars1*^{−/−} mutants found in the eye, inner ear, and trunk muscles appeared to directly correlate with *kars1* mRNA expression patterns during embryo development, strongly suggesting these phenotypes and behaviors arose from *Kars1* loss of function.

To confirm the phenotypes of the *kars1*^{−/−} mutant animals arise from loss of *kars1* function, we performed mRNA rescue experiments by injecting either human WT *KARS1* or the zebrafish WT *kars1* mRNA. Coinjection of mRNAs encoding the mitochondrial and cytoplasmic isoforms into 1-cell stage showed reduced frequencies of heart edema (Fig. 2k) and significantly restored eye size in *kars1*^{−/−} mutants (Fig. 2l). Furthermore, microinjection of zebrafish *kars1* mRNA further rescued the startle responses compared to *kars1*^{−/−} mutant animals (Fig. 2m, n) suggesting mutant phenotypes are caused by *kars1* loss of function.

The *kars1* loss-of-function zebrafish model recapitulates patient symptoms. Histological analysis of the brain of 5-dpf larvae revealed a vacuolated spongios appearance with areas of reduced cell density and disorganized segment boundaries in *kars1*^{−/−} mutants compared to WT siblings (Fig. 3a–c). Moreover, eye volume was reduced and the retinal layer organization was completely lost in the *kars1*^{−/−} mutants compared to WT siblings (Fig. 3b) strongly suggesting impaired vision. Furthermore, the number of neuronal cells appeared strongly reduced in the brain and retina in *kars1*^{−/−} mutants compared to controls (Fig. 3a, b).

Table 1. Summary of molecular and key clinical findings.

	F1 IV1/F11 V11/ V21/V3V4	F2 IV3	F3 II.2	F4 V3/V4	F5 II.1	F6 IV.1	F7 IV1/IV4/F8 IV1/IV2/ F13 II.2	F9 III1/F10 III4/ F15 III1	F10 II.4	F12 II.1	F14 II.2	F16 II.1
Molecular genetics summary												
Chr16 g. position	g.75674175A>G	g.75669866G>C	g.75668181C>G	g.75668081A>G	g.75665680G>A	g.75665629T>C	g.75664747T>A	g.75669887G>A	g.75662304C>T	g.75663371G>A	g.75668082G>A	g.75665702G>A
KARS1 c. position	c.379T>C	c.69T>G	c.889C>G	c.989T>C	c.1073C>T	c.1124A>G	c.1772A>T	c.683C>T	c.1742G>A	c.1577C>T	c.988C>T	c.1051C>T
KARS1 p. position	F127L	L233V	P297A	L330P	T388M	Y375C	N591I	P228L	R581Q	A526V	L330F	R351W
phyloP	8.92	5.66	9.87	9.34	9.84	8.02	7.95	9.59	7.77	5.94	5.86	2.14
CADD	29.7	22.2	27.0	31	29.4	32	28.1	25.5	28.6	31	29.4	32
MT	DC	DC	DC	DC	DC	DC	DC	DC	DC	DC	DC	DC
PP2	PrD	B	PrD	PrD	PrD	PrD	PrD	PrD	PrD	PrD	PrD	PrD
SIFT	D	D	D	D	D	D	D	T	D	D	D	D
gnomAD MAF	0	3.98e-6	0	0	4.95e-5	3.98e-6	7.97e-6	1.415e-4	0	3.184e-5	0	7.070e-6
In-house MAF ^a	1/171,678	0/171,678	1/171,678	1/171,678	18/257,204	3/212,968	1/229,162	39/262,730	1/181,974	0/38,634	2/222,356	3/149,466
Clinical summary												
DD	+/+/+/+/+	+	-	+/+	-	+	+/+/+/+/+	+/+/+	+	+	+	+
ID	+/+/+/+/+/+	+	+/+	+/+	-	-	+/+/+/+/+	-/NA	-	+	+	+
Hearing loss	+/+/+/+/+/+	+	+/+	+/+	-	+	+/+/+/+/+	+/NA/+	NA	+	+	+
Regression	+/+/+/+/+	+	-	-	-	-	-/+/+/+	-/+/+	+	-	-	-
Seizures	+/+/+/+/+	+	-	+/+	-	-	-/+/+/+/+	+/+/+	+	+	+	-
Ataxia	+/+/+/+/+	-	+	-	-	+	+/+/+/+/+	+/+/+	-	-	+	-
Hypotonia	-/+/+/+/+	-	-	+/+	-	+	+/+/+/+/+	-/+/+	+	+	+	+
Spasticity	+/+/+/+/+/+	+	-	-	-	-	-/+/+/+/+	+/+/+	+	-	-	+
Visual impairment	-/+/+/+/+/+	-	NA	-	-	-	-/+/+/+/+	+/+/+	+	NA	+	+
Absent speech	-/+/NA/+/+	-	-	-	+	+	+/+/+/+/+	+/+/+	+	NA	-	+
Mortality	-/+/+/+	+	-	-	-	-	-/+/+/+	-/+/+	+	+	-	+
Dysmorphic facial features	+/+/+/+/+/+	+	-	+/+	+	-	+/+/+/+/+	-/NA	-	-	+	-
Behavioral abnormalities	-/+/+/+	-	-	-	-	-	+/+/+/+/+	-/NA	-	-	+	-
Leukodystrophy	+/+/+/+/+/+	+	+	-	-	NA	+/+/+/+/+	+/+/+	+	+	-	-

Genomic coordinates are listed according to GRCh37 genome build, transcript: NM_001130089.1, phyloP scale [-14.1; 6.4].
B benign, *D* deleterious, *DC* disease causing, *DD* developmental delay, *F* family, *ID* intellectual disability, *MAF* minor allele frequency, *MT* MutationTaster, *NA* not assessed, *PP2* PolyPhen-2, *PrD* probably damaging, *T* tolerated.
^aNo homozygous individuals were identified. The in-house database consists of aggregated multiethnic cohorts from study groups.

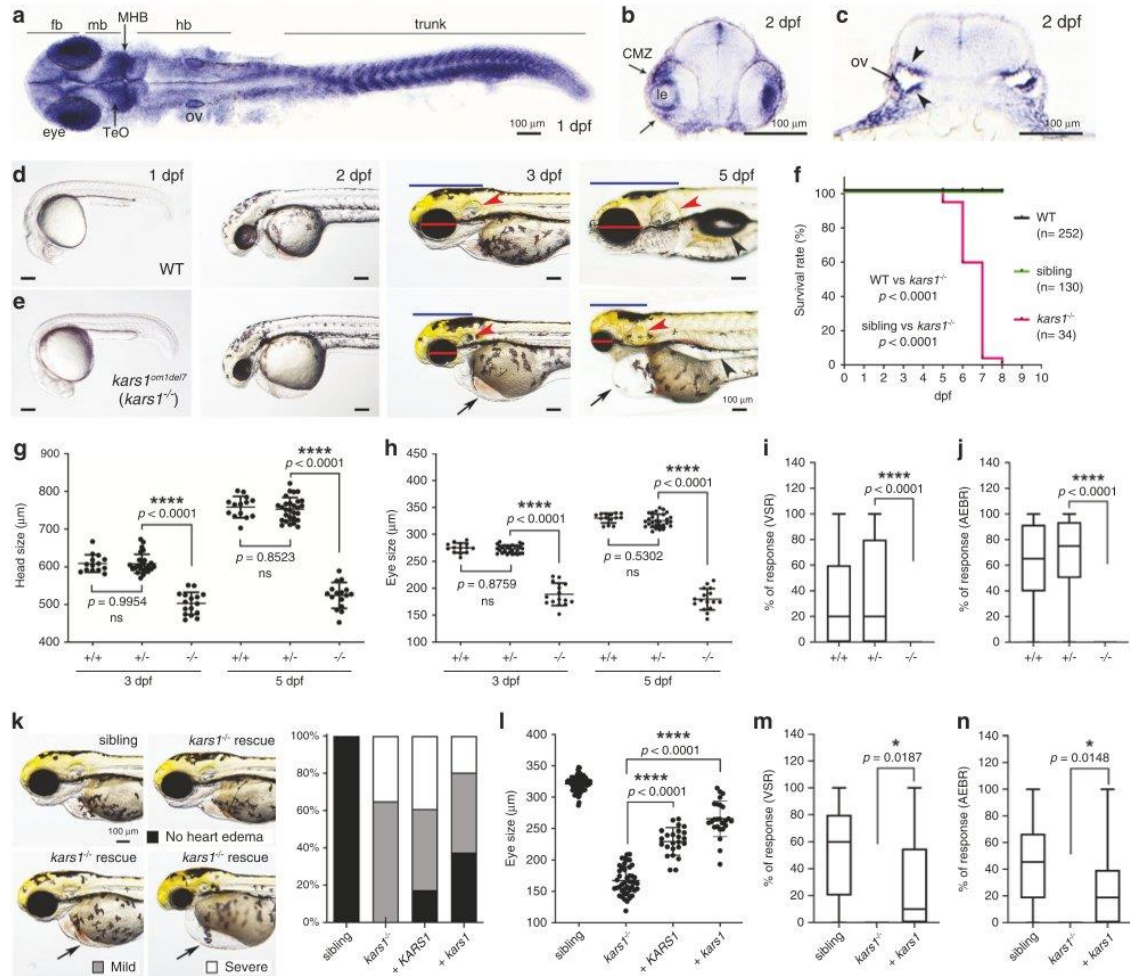


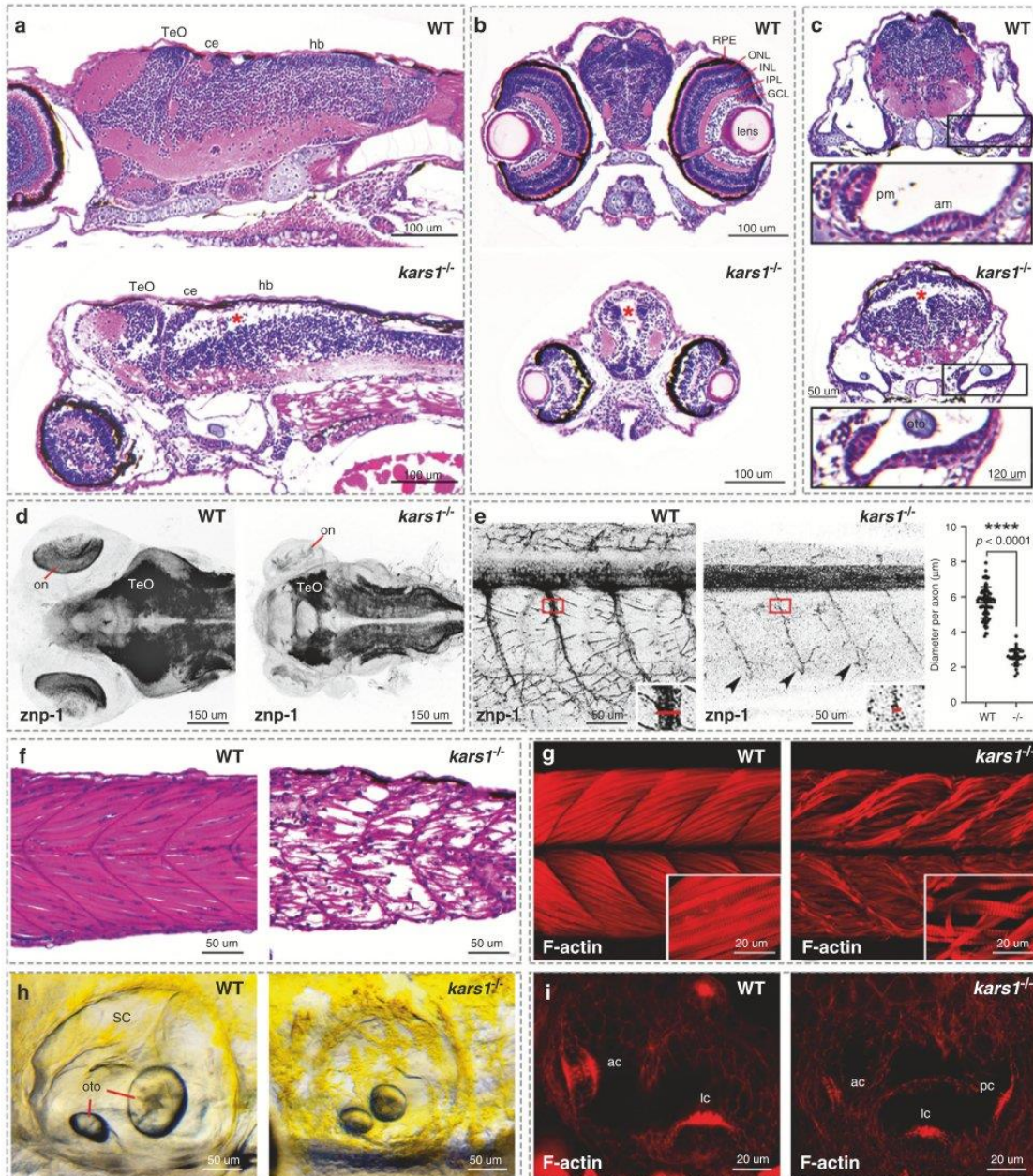
Fig. 2 Expression of *kars1* messenger RNA (mRNA) in embryos and *kars1* knockouts show gross morphological and behavioral defects. **(a)** *kars1* expression in 1 days postfertilization (dpf) embryo. Dorsal view. **(b,c)** The cross-section of 2 dpf embryo. CMZ ciliary marginal zone, fb forebrain, hb hindbrain, le lens, mb midbrain, MHB midbrain and hindbrain boundary, ov otic vesicle, TeO optic tectum. Black arrowheads indicating the otic vesicle epithelium of otic vesicles. **(d,e)** Representative images of wild-type (WT) and *kars1^{om1del7}* (*kars1^{-/-}*) from 1 dpf to 5 dpf. Lateral view, anterior to the left. Red lines: eye diameter. Blue lines: brain size. Red arrowheads: heart edema. Black arrowhead: swim bladder. **(f)** Kaplan–Meier survival curves. Time is shown in days. The log rank test was used for statistical analysis. **(g,h)** Quantification of eye and head size from *kars1^{+/-}* mutant in-cross at 3 and 5 dpf. **(i,j)** The visual startle response (VSR) and auditory evoked behavior response (AEBR) analyses of animals at 6 dpf from *kars1^{+/-}* mutant in-cross. **(k)** Representative images of *kars1^{-/-}* mutant rescue experiments and the quantification of heart edema phenotype. Animals were collected by defined heart edema categories at 3 dpf as shown in pictures and calculated in percentage of total animals. **(l)** Eye size quantification of mRNA rescue experiments at 5 dpf. **(m,n)** The VSR and AEBR analyses after RNA rescue at 6 dpf. *n* = number of animals. In **(g,h,l)**, each dot represents one animal and error bars are presented as mean \pm SD. One-way analysis of variance (ANOVA) with Tukey's multiple comparisons test: *****p* < 0.0001. In **(i,j,m,n)**, data are plotted by box and whiskers plot and error bars indicate values from minimum to the maximum. Two-tailed unpaired *t*-test with Welch's correction: ns, not significant *p* \geq 0.05, **p* < 0.05 and *****p* < 0.0001.

Immunohistochemical analysis of neuronal synapses revealed reduced staining in all brain and eye regions pointing to a significant reduction of synapses in *kars1^{-/-}* mutants (Fig. 3d), suggesting impaired neuronal transmission. Additionally, staining revealed abnormal motor neuron morphology, including shrinkage of motor neuron axon projections and reduction of terminal axonal branching in the mutants (Fig. 3e), further indicating strong alteration of locomotor function in those animals.

Individuals with biallelic *KARS1* pathogenic variants usually present with combined neuronal and muscular dysfunction.

Indeed, our WISH data revealed *kars1* mRNA expression in trunk muscles (Fig. 2a) and a loss of touch-evoked responses in the *kars1^{-/-}* mutants (Fig. S7e and Video S3). Phalloidin staining that labels actins showed weaker staining in the myotomes and presented misaligned and detached muscle fibers from the myotendinous junction (MTJ) (Fig. 3f, g) suggesting severe neuromuscular dysfunction leading to absence of coordinated locomotion.

Several individuals with *KARS1* variant alleles also display hearing disorders reminiscent of the inner ear defects observed



in *kars1*^{-/-} mutant larvae, such as perturbed sensory epithelia and loss of AEBR startle response. Morphological analysis of the mutants showed smaller otic vesicles and otoliths (Fig. 3h) and flattened sensory epithelia in both anterior and posterior maculae (Fig. 3c). The phalloidin staining in the inner ear showed strong reduction in the number of F-actin-rich stereocilia, which are crucial for the formation of hair cell bundles and thus for mechano-electrical transduction (Fig. 3i). Vital stain Yo-PRO-1 iodide, showed fewer hair cells in the zebrafish lateral line which are morphologically and functionally similar to those of the inner

ear [25] (Fig. S8a, b). Taken together, these findings suggest that *kars1* plays a crucial role in hair cell formation in zebrafish, reminiscent of hearing disorders found in a subset of individuals affected with *KARS1* variants.

Variants in *KARS1* have been shown to be associated with seizures (Table S2). Seizure activity positively correlates with the expression of *c-fos* (*fosab* in zebrafish), a marker for general neuronal activity. We used classical pro-chemoconvulsant drug pentylenetetrazol (PTZ) to induce seizure activity and elevated expression of *fosab* mRNA (Fig. S8c). Intriguingly, untreated

Fig. 3 The *kars1*^{-/-} larvae display neurological, muscle, and inner ear defects by histological analysis at 5 dpf. (a) Head region of wild-type (WT) and *kars1*^{-/-} mutant by sagittal section. Red asterisks indicate massive loss of cell density, as well as in (b) and (c). Anterior to the left and dorsal to the top. (b) Eye region of WT and *kars1*^{-/-} mutant by cross-section. Dorsal to the top. (c) Inner ear region of WT and *kars1*^{-/-} mutant by cross-section. Dorsal to the top. Lower panels were enlarged picture from black box. (d) Head region of WT and *kars1*^{-/-} larvae immunostained with anti-znp-1 antibody. The black-and-white fluorescent signals were inverted to negative film for a clear presentation. Dorsal view, anterior to the left. on, optic nerve. (e) Trunk region of WT and *kars1*^{-/-} larvae which were immunostained with anti-znp-1 antibody. ImageJ was used to measure the diameter of primary motor axons as indicated by red line in the right-down panels (enlarged from red box). Statistics are shown on the right-hand side. Black dot indicates the diameter of each motor axon. Error bars = mean ± SD. Two-tailed unpaired nonparametric Mann–Whitney test: *****p* < 0.0001. Black arrowheads indicate the reduced terminal axonal branching compared to WT. Anterior to the left and dorsal to the top. (f) The trunk region of WT and *kars1*^{-/-} larvae revealed by sagittal section. Anterior to the left and dorsal to the top. (g) The trunk region of WT and *kars1*^{-/-} larvae revealed by confocal projections of phalloidin stained muscle fiber. Anterior to the left and dorsal to the top. The lower-right panels are the higher-magnification view. (h) Representative bright-field images of WT and *kars1*^{-/-} inner ear. Anterior to the left and dorsal to the top. oto otolith, SC semicircular canal. (i) The red fluorescent conjugated phalloidin staining was performed to visualize the bundles (stereocilia) of hair cells in inner ear. Anterior to the left and dorsal to the top. ac anterior crista, am anterior macula, ce cerebellum, GCL ganglion cell layer, hb hindbrain, INL inner nuclear layer, IPL inner plexiform layer, lc lateral crista, ONL outer nuclear layer, pc posterior crista, pm posterior macula, RPE retinal pigment epithelium, TeO optic tectum.

kars1^{-/-} larvae, when compared with untreated WT controls, exhibited twofold at 3 dpf and tenfold increase at 6 dpf in *fosab* mRNA levels (Fig. S8d) suggesting seizure-like activity in homozygous animals.

Together, our morphological, behavioral, and histological analyses demonstrate that the *kars1*^{-/-} zebrafish mutant larvae exhibit visual impairment, neuromuscular dysfunction, sensorineural hearing loss, and increased expression of seizure marker, *c-fos*, thus recapitulating a number of pathologies found in individuals with *KARS1* variants.

***Kars1* loss of function triggers p53-mediated apoptosis and down-regulation of key neurodevelopmental related genes.** To determine the consequences of *Kars1* loss of function on gene expression, we performed RNA-sequencing (RNA-Seq) on WT and *kars1*^{-/-} mutants at 3 dpf and 4 dpf and compared gene expression profiles. We found 1,616 and 1,409 differentially expressed genes (DEGs) at 3 dpf and 4 dpf respectively, 563 genes overlapped between 3 dpf and 4 dpf (Fig. S9a–c, and Table S5). KEGG pathway analysis showed *kars1* loss of function dysregulated many pathways including the p53 and cell apoptosis pathway (Figs. S10–12). ARSs have been shown to regulate cell death pathways [26, 27]. To test whether the morphological defects found in *kars1*^{-/-} mutants were due to abnormal cell apoptosis, we performed a TUNEL assay and observed an increase in TUNEL-positive cells in the brain, eye, trunk, and inner ear of *kars1*^{-/-} mutants compared with sibling animals at 5 dpf (Fig. S13a, b), suggesting distinct cell types are particularly sensitive to loss of *Kars1*. Next, to determine whether increased cell apoptosis was mediated by p53 activation, we knocked down *tp53* by micro-injecting *kars1*^{-/-} mutant animals with *tp53* antisense morpholinos (MO) and subsequently performed the TUNEL assays at 3 dpf. Results showed a significant reduction in the TUNEL-positive signals in the brain, eye, ear, and trunk in the MO-injected *kars1*^{-/-} mutant (Fig. 4a–c). Strikingly, reduction in eye size (Fig. 4d) and upregulation of several apoptosis markers were restored to WT levels (Fig. 4e), therefore confirming the p53 pathway was successfully knocked down, and furthermore implicating it in reduction of eye size. To further characterize the functional rescue at the molecular level after inhibiting the p53 pathway, we examined the expression of six genes we previously found to be downregulated in *kars1*^{-/-} mutants (Fig. 4f). All six genes showed at least partially restored expression upon p53 knockdown in *kars1*^{-/-} mutants. Taken together, the loss of *Kars1* upregulated the p53 pathway thus leading to apoptosis thereby causing multiple phenotypic abnormalities.

To validate our findings, we used CRISPR/Cas9 technology to generate biallelic variants. Coinjecting WT *kars1* mRNAs with the *kars1* sgRNAs rescued these phenotypes, confirming they arise from *Kars1* loss of function (Fig. 4g). Importantly, coinjection of *tp53* sgRNAs with *kars1* sgRNAs restored the eye and head size of

the *kars1* F₀ mutants (Fig. 4g–i). Moreover, whereas 90% of *kars1* F₀ mutant animals died by 10 dpf, only 20% of animals coinjected with either *kars1* mRNAs or *tp53* sgRNAs died by 10 dpf (Fig. 4j). Histological analysis showed vacuolated spongiosus appearance in the brain was significantly restored in *kars1;tp53* F₀ mutants compared to *kars1* F₀ mutants, as was eye volume and retinal layer organization (Fig. 4k) and vision/hearing startle responses (Fig. S13c, d). At the molecular level, *kars1* F₀ mutants showed significantly reduced *kars1* expression and increased *tp53* expression compared to the uninjected control, whereas *kars1;tp53* F₀ mutants showed significantly reduced expression of both *kars1* and *tp53* (Fig. S13e). Additionally, *kars1* F₀ mutants showed increased *casp8* and decreased *mbpa*, *neurod1*, and *stxbp1a* expression compared to controls that was restored in *kars1;tp53* F₀ mutants (Fig. S13f). Together, our results showed *kars1* F₀ mutants phenocopy the *kars1*^{-/-} mutant, and p53 depletion mitigates the morphological, behavior, and molecular phenotypes due to loss of *Kars1*.

DISCUSSION

Deciphering how variants in different ARS genes cause diverse organ-specific phenotypes is crucial to inform therapeutic approaches for ARS-related disorders. We report 10 novel and 4 known variants in *KARS1* from 22 patients belonging to 16 unrelated families. Having included the clinical and neuroimaging data from our cohort and the corresponding data from the previously published 30 *KARS1* cases (25 families), we made a cumulative phenotypic characterization for 52 cases with biallelic *KARS1* variants (Fig. 1c).

Notably, our cohort expands the phenotypic spectrum of *KARS1* variants to include autism/hyperactivity. Additionally, we highlight a variety of *KARS1*-associated dysmorphic facial features, as facial dysmorphism has rarely been described in previous *KARS1* reports. It is reported in 11/52 individuals, where ten cases were identified in our cohort and one case from McLaughlin et al. [2]. We also provide further supporting evidence for skeletal myopathy, a phenotype that has previously been reported in one case [17]. Our case with hypertrophic cardiomyopathy (family 4) seems to also highlight the importance of this phenotype as in the previous few reports [17, 28]. Finally, we highlight cerebellar ataxia might be a frequent *KARS1*-associated feature that was previously reported only in 3/30 (10%) cases but present in 32% (7/22) of our cohort. Our cumulative phenotypic analysis showed that similar to other ARS, *KARS1* expresses predominant neurological and neurosensory phenotypes associated with facial dysmorphism [29].

The systematic analysis of all available neuroimaging data, including the present cases, suggests the spectrum of manifestations associated with *KARS1* variants is wide, ranging from normal brain appearance to a severe leukodystrophy with

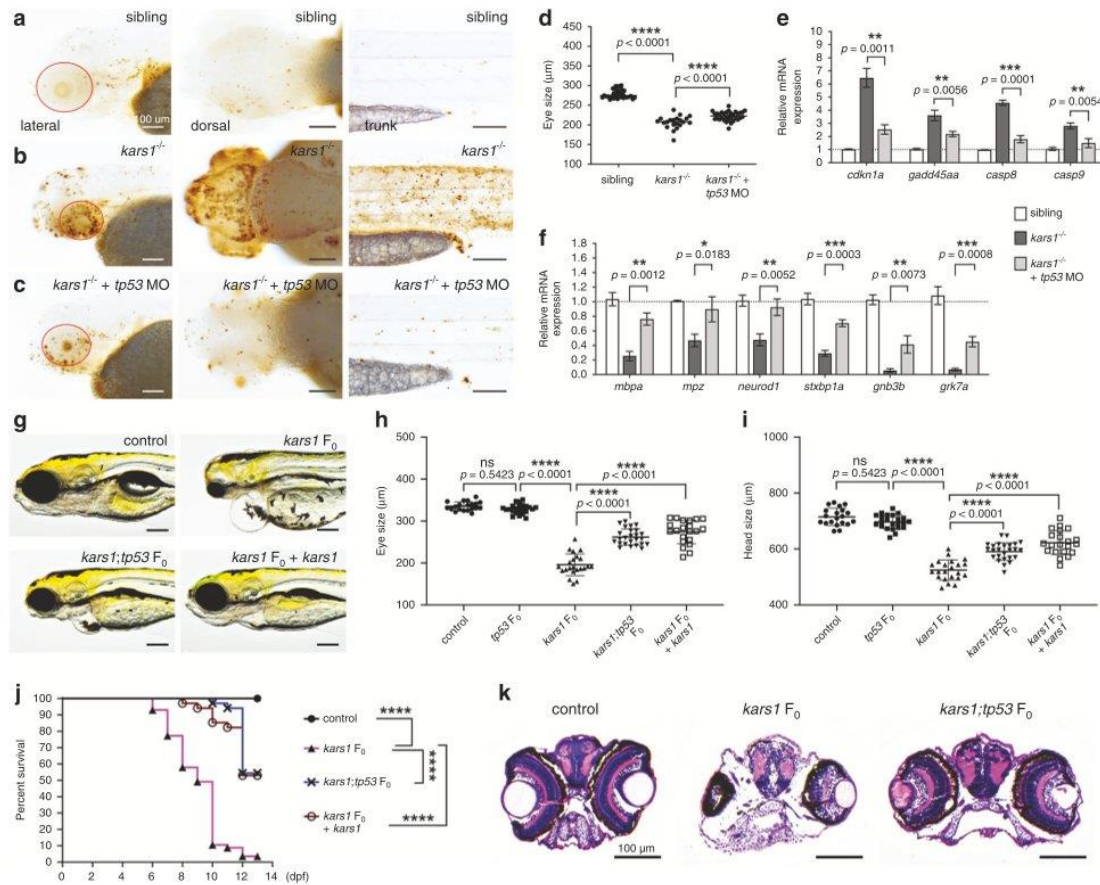


Fig. 4 Cell apoptosis was activated by *kars1* loss of function through p53 pathway. (a–c) Representative images of sibling, *kars1*^{-/-}, and *kars1*^{-/-} + *p53* MO at 3 dpf after TUNEL staining. Red circle indicates eye region. Scale bars = 100 μ m. (d) The eye size measurements of sibling, *kars1*^{-/-} and *kars1*^{-/-} + *p53* MO at 3 dpf. (e) The expression levels of p53 pathway genes were examined by reverse transcription quantitative polymerase chain reaction (RT-qPCR) after *p53* MO injection. (f) Those downregulated genes in RNA-seq data were examined by RT-qPCR after *p53* MO injection. For (e,f), the expression levels were normalized to 18 S housekeeping gene. Error bars = mean \pm SD. Two-tailed unpaired Student's *t*-test with Holm–Sidak multiple comparisons correction: ns, not significant $p \geq 0.05$, * $p < 0.05$, ** $p < 0.01$, and *** $p < 0.001$. (g) Representative images of uninjected control, *kars1* F₀ mutant, *kars1;tp53* F₀ mutant, and *kars1* F₀ mutant co-injected with *kars1* messenger RNA (mRNA) at 5 dpf. Lateral view, anterior to the left. (h,i) Measurement of eye and head size in control, *tp53* F₀ mutant, *kars1* F₀ mutant, *kars1;tp53* F₀ mutant, and *kars1* F₀ mutant co-injected with 150 picogram (pg) and 200 pg of *kars1* mRNA at 5 dpf. For (d,h,i), each symbol represents one animal. Error bars = mean \pm SD. One-way analysis of variance (ANOVA) with Tukey's multiple comparisons test: ns, not significant $p \geq 0.05$ and **** $p < 0.0001$. (j) Kaplan–Meier survival curves. Time is shown in days. Log rank test: **** $p < 0.0001$. (k) Histology analysis of uninjected control, *kars1* F₀ mutant and *kars1;tp53* F₀ mutant by cross-section.

rapid brain atrophy. Slightly more than one third (18/52, 34.6%) presented with a progressive leukodystrophy, involving the corpus callosum and sparing the U fibers, variably extending to the spinal cord and cerebellar white matter, often associated with peculiar cerebral and spinal cord calcifications [18–20]. Less specific patterns included faint diffuse (6/52, 11.5%) or multifocal periventricular (7/52, 13.4%) white matter signal alterations. Interestingly, a third of the present patients had callosal hypoplasia, a likely underestimated feature previously described in three subjects with *KARS1* variants [16, 30]. This finding is only partly related to the loss of cerebral white matter volume, as the corpus callosum in these subjects is thin but also shorter than normal. In addition, we uncovered hypoplasia of the pons in one third of subjects, and atrophy of cerebellum with prevalent vermian involvement in 20% of cases. Taken together, these neuroimaging features expand the phenotypes related to *KARS1* variants, indicating a prenatal onset of

the disease often associated with a rapid neurodegenerative course [31, 32].

Although a clear genotype–phenotype correlation in *KARS1*-related disease is lacking, we noticed some interesting associations. The *KARS1* c.379T>C (p.[Phe127Leu]) variant was present in the case from family 1 in a homozygous state, and the same variant was present in compound heterozygosity in one of the cases from the Ardisson et al. report [18]. Besides the typical developmental delay and hearing loss, both cases shared other phenotypic similarity including seizures, psychomotor regression, hypotonia, spastic tetraparesis, and brain calcifications. The *KARS1* c.683C>T (p.[Pro228Leu]) variant was present in compound heterozygosity in family 9 and a report by Scheidecker et al. [21], and both families manifested ataxia, visual impairment, and dystonia. Identifying and characterizing homozygous individuals

with these variants in the future would be of interest to further evaluate this potential association.

Biallelic *KARS1* variants have emerged as a cause of rare early-onset childhood neurodegenerative disorders presenting with a multiorgan dysfunction suggestive of mitochondrial disorders but usually with normal biochemical assays. Therefore, in addition to the initial association of biallelic *KARS1* variants with Charcot-Marie-Tooth disease and nonsyndromic hearing loss in single isolated cases (2/50), an early-onset complex neurological and syndromic phenotype should be assigned to *KARS1* in OMIM. This might yield more families with *KARS1*-related disease and improve understanding of its neurobiology and phenotypic spectrum.

The physiological relevance of several ARS genes has been assessed in vivo using zebrafish [33–35]. Here, we showed *kars1* homozygous (*kars1*^{-/-}) zebrafish larvae exhibit the phenotypic hallmarks associated with pathogenic variants reported in patients. In agreement with our study, *Kars1* knockdown in *Xenopus* caused developmental defects of head and eyes; loss of myelination and reduced expression of myelin binding protein, leading to incomplete formation of white matter; and reduced brain volume suggesting an important role of *KARS1* across the species [20].

Loss of ARS enzymes have been shown to activate the p53 signaling pathway [36]. Likewise, in zebrafish, overexpression of an editing-defective valyl-tRNA synthetase (VAR51) activates the p53 signaling pathway, and increased expression of targets such as cyclin-dependent kinase inhibitor p21 (*cdkn1a*) and *gadd45* leading to cell death [37]. *Kars1*^{-/-} mutants show upregulation of p53 signaling and apoptosis pathway genes. Interestingly, upregulation of p53 signaling has been connected to apoptosis of human oligodendrocytes (a type of myelin-forming cells) [38], and cuprizone- [39] or compressed spinal cord injury- [40] induced demyelination (one of the categories in leukodystrophy classification) in mice. Genetic or pharmacological inhibition of p53 decreased the susceptibility of cuprizone-induced demyelination and increased the survival rate of oligodendrocytes [39]. These data and our current findings emphasize that p53 pathway inhibitors might represent potential therapeutics for *KARS1* patients.

One of the limitations of this study is lack of functional variant analysis in zebrafish. However, our structural modeling data shows 27/36 variants occur in the aminoacylation domain, and therefore, likely affect enzyme activity. Since *KARS1* is a multifunctional protein, variants in this study could affect the canonical as well as noncanonical functions of the protein.

In summary, our findings underscore a conserved and unique requirement for ARS during nervous system and muscle development to prevent p53-mediated apoptosis and disease. Our disease model offers promising avenues to explore the biallelic contributions of *KARS1*, and similar approaches could be exploited to understand a number of diseases associated variants in essential genes.

DATA AVAILABILITY

Human variant data included in this study have been deposited in Leiden Open Variation Database (LOVD) and available through following accession numbers: 0000685774, 0000685798, 0000685800, 0000685801, 0000685802, 0000685803, 0000685804, 0000685805. Reagents related to zebrafish experiments described in this paper are available upon request.

Received: 11 February 2021; Revised: 20 May 2021; Accepted: 24 May 2021;

Published online: 25 June 2021

REFERENCES

- Meyer-Schuman R, Antonellis A. Emerging mechanisms of aminoacyl-tRNA synthetase mutations in recessive and dominant human disease. *Hum Mol Genet.* 2017;26(R2):R114–27.

- McLaughlin HM, Sakaguchi R, Liu C, Igarashi T, Pehlivan D, Chu K, et al. Compound heterozygosity for loss-of-function lysyl-tRNA synthetase mutations in a patient with peripheral neuropathy. *Am J Hum Genet.* 2010;87:560–6.
- Scheper GC, van der Kloot T, van Andel RJ, van Berkel CG, Sissler M, Smet J, et al. Mitochondrial aspartyl-tRNA synthetase deficiency causes leukoencephalopathy with brain stem and spinal cord involvement and lactate elevation. *Nat Genet.* 2007;39:534–9.
- Messmer M, Florentz C, Schwenzler H, Scheper GC, van der Knaap MS, Maréchal-Drouard L, et al. A human pathology-related mutation prevents import of an aminoacyl-tRNA synthetase into mitochondria. *Biochem J.* 2011;433:441–6.
- Maffezzini C, Laine I, Dallabona C, Clemente P, Calvo-Garrido J, Wibom R, et al. Mutations in the mitochondrial tryptophanyl-tRNA synthetase cause growth retardation and progressive leukoencephalopathy. *Mol Genet Genomic Med.* 2019;7:e654.
- Götz A, Tyynismaa H, Euro L, Ellonen P, Hyötyläinen T, Ojala T, et al. Exome sequencing identifies mitochondrial alanyl-tRNA synthetase mutations in infantile mitochondrial cardiomyopathy. *Am J Hum Genet.* 2011;88:635–42.
- Almalki A, Alston CL, Parker A, Simonic I, Mehta SG, He L, et al. Mutation of the human mitochondrial phenylalanine-tRNA synthetase causes infantile-onset epilepsy and cytochrome c oxidase deficiency. *Biochim Biophys Acta.* 2014; 1842:56–64.
- Latour P, Thauvin-Robinet C, Baudelet-Méry C, Soichot P, Cusin V, Favre L, et al. A major determinant for binding and aminoacylation of tRNA(Ala) in cytoplasmic Alanyl-tRNA synthetase is mutated in dominant axonal Charcot-Marie-Tooth disease. *Am J Hum Genet.* 2010;86:77–82.
- McLaughlin HM, Sakaguchi R, Giblin W, Wilson TE, Biesecker L, & NISC Comparative Sequencing Program et al. A recurrent loss-of-function alanyl-tRNA synthetase (AARS) mutation in patients with Charcot-Marie-Tooth disease type 2N (CMT2N). *Hum Mutat* 33, 244–53 (2012).
- Gonzalez M, McLaughlin H, Houlden H, Guo M, Yo-Tsen L, Hadjivassiliou M, et al. Exome sequencing identifies a significant variant in methionyl-tRNA synthetase (MARS) in a family with late-onset CMT2. *J Neurol Neurosurg Psychiatry.* 2013;84: 1247–9.
- Safka Brozkova D, Deconinck T, Griffin LB, Ferbert A, Haberova J, Mazanec R, et al. Loss of function mutations in HARS cause a spectrum of inherited peripheral neuropathies. *Brain* 2015;138(Pt 8):2161–72.
- Oprescu SN, Griffin LB, Beg AA, Antonellis A. Predicting the pathogenicity of aminoacyl-tRNA synthetase mutations. *Methods* 2017;113:139–51.
- Tolkunova E, Park H, Xia J, King MP, Davidson E. The human lysyl-tRNA synthetase gene encodes both the cytoplasmic and mitochondrial enzymes by means of an unusual alternative splicing of the primary transcript. *J Biol Chem.* 2000;275: 35063–9.
- Santos-Cortez RL, Lee K, Azeem Z, Antonellis PJ, Pollock LM, Khan S, et al. Mutations in *KARS*, encoding lysyl-tRNA synthetase, cause autosomal-recessive nonsyndromic hearing impairment DFNB89. *Am J Hum Genet.* 2013;93:132–40.
- Zhou XL, He LX, Yu LJ, Wang Y, Wang XJ, Wang ED, et al. Mutations in *KARS* cause early-onset hearing loss and leukoencephalopathy: Potential pathogenic mechanism. *Hum Mutat.* 2017;38:1740–50.
- McMillan HJ, Humphreys P, Smith A, Schwartzentruber J, Chakraborty P, Bulman DE, et al. Congenital visual impairment and progressive microcephaly due to Lysyl-transfer ribonucleic acid (RNA) synthetase (*KARS*) mutations: The expanding phenotype of aminoacyl-transfer RNA synthetase mutations in human disease. *J Child Neurol.* 2015;30:1037–43.
- Verrigni D, Diodato D, Di Nottia M, Torraco A, Bellacchio E, Rizza T, et al. Novel mutations in *KARS* cause hypertrophic cardiomyopathy and combined mitochondrial respiratory chain defect. *Clin Genet.* 2017;91:918–23.
- Ardissone A, Tonduti D, Legati A, Lamantea E, Barone R, Dorboz I, et al. *KARS*-related diseases: progressive leukoencephalopathy with brainstem and spinal cord calcifications as new phenotype and a review of literature. *Orphanet J Rare Dis.* 2018;13:45.
- Sun C, Song J, Jiang Y, Zhao C, Lu J, Li Y, et al. Loss-of-function mutations in Lysyl-tRNA synthetase cause various leukoencephalopathy phenotypes. *Neurol Genet.* 2019;5:e565.
- Itoh M, Dai H, Horike SI, Gonzalez J, Kitami Y, Meguro-Horike M, et al. Biallelic *KARS* pathogenic variants cause an early-onset progressive leukodystrophy. *Brain* 2019;142:560–73.
- Scheidecker S, Bär S, Stoetzel C, Geoffroy V, Lannes B, & Rinaldi B, et al. Mutations in *KARS* cause a severe neurological and neurosensory disease with optic neuropathy. *Hum Mutat* 2019;40:1826–40.
- Dickinson ME, Flenniken AM, Ji X, Teboul L, Wong MD, White JK, et al. High-throughput discovery of novel developmental phenotypes. *Nature* 2016;537: 508–14.
- Murray CR, Abel SN, McClure MB, Foster J, Walke MI, Jayakar P, et al. Novel causative variants in *DYRK1A*, *KARS*, and *KAT6A* associated with intellectual disability and additional phenotypic features. *J Pediatr Genet.* 2017;6:77–83.

24. Lieber DS, Calvo SE, Shanahan K, Slate NG, Liu S, Hershman SG, et al. Targeted exome sequencing of suspected mitochondrial disorders. *Neurology* 2013;80:1762–70.
25. Fay RR, Popper AN. Evolution of hearing in vertebrates: the inner ears and processing. *Hear Res.* 2000;149:1–10.
26. Park SG, Schimmel P, Kim S. Aminoacyl tRNA synthetases and their connections to disease. *Proc Natl Acad Sci USA.* 2008;105:11043–9.
27. Hyeon DY, Kim JH, Ahn TJ, Cho Y, Hwang D, Kim S. Evolution of the multi-tRNA synthetase complex and its role in cancer. *J Biol Chem.* 2019;294:5340–51.
28. Kohda M, Tokuzawa Y, Kishita Y, Nyuzuki H, Moriyama Y, Mizuno Y, et al. A comprehensive genomic analysis reveals the genetic landscape of mitochondrial respiratory chain complex deficiencies. *PLoS Genet.* 2016;12:e1005679.
29. Fuchs SA, Schene IF, Kok G, Jansen JM, Nikkels P, van Gassen K, et al. Aminoacyl-tRNA synthetase deficiencies in search of common themes. *Genet Med.* 2019;21:319–30.
30. Vargas A, Rojas J, Aivasovsky I, Vergara S, Castellanos M, Prieto C, et al. Progressive early-onset leukodystrophy related to biallelic variants in the KARS gene: The first case described in Latin America. *Genes* 2020;11:1437.
31. Edvardson S, Shaag A, Kolesnikova O, Gomori JM, Tarassov I, Einbinder T, et al. Deleterious mutation in the mitochondrial arginyl-transfer RNA synthetase gene is associated with pontocerebellar hypoplasia. *Am J Hum Genet.* 2007;81:857–62.
32. Mendes MI, Green LMC, Bertini E, Tonduti D, Aiello C, Smith D, et al. RARS1-related hypomyelinating leukodystrophy: Expanding the spectrum. *Ann Clin Transl Neurol.* 2020;7:83–93.
33. Malissovass N, Griffin LB, Antonellis A, Beis D. Dimerization is required for GARS-mediated neurotoxicity in dominant CMT disease. *Hum Mol Genet.* 2016;25:1528–42.
34. Siekierska A, Stamberger H, Deconinck T, Opreacu SN, Partoens M, Zhang Y, et al. Biallelic VARS variants cause developmental encephalopathy with microcephaly that is recapitulated in vars knockout zebrafish. *Nat Commun.* 2019;10:708.
35. Friedman J, Smith DE, Issa MY, Stanley V, Wang R, Mendes MI, et al. Biallelic mutations in valyl-tRNA synthetase gene VARS are associated with a progressive neurodevelopmental epileptic encephalopathy. *Nat Commun.* 2019;10:707.
36. Fukushima K, Motomura S, Kuraoka A, Nakano H, Nishimoto T. A single point mutation of hamster aminoacyl-tRNA synthetase causes apoptosis by deprivation of cognate amino acid residue. *Genes Cells.* 1996;1:1087–99.
37. Song Y, Shi Y, Carland TM, Lian S, Sasaki T, Schork NJ, et al. p53-Dependent DNA damage response sensitive to editing-defective tRNA synthetase in zebrafish. *Proc Natl Acad Sci USA.* 2016;113:8460–5.
38. Ladiwala U, Li H, Antel JP, Nalbantoglu J. p53 Induction by tumor necrosis factor- α and involvement of p53 in cell death of human oligodendrocytes. *J Neurochem.* 1999;73:605–11.
39. Li J, Ghiani CA, Kim JY, Liu A, Sandoval J, DeVellis J, et al. Inhibition of p53 transcriptional activity: a potential target for future development of therapeutic strategies for primary demyelination. *J Neurosci.* 2008;28:6118–27.
40. Ma L, Yu HJ, Gan SW, Gong R, Mou KJ, Xue J, et al. p53-Mediated oligodendrocyte apoptosis initiates demyelination after compressed spinal cord injury by enhancing ER-mitochondria interaction and E2F1 expression. *Neurosci Lett.* 2017;644:55–61.

ACKNOWLEDGEMENTS

This research is supported by a grant from National Institutes of Health (NIH) GM103636 (Project 3), and the Presbyterian Health Foundation (PHF) (G.K.V.); NIH grants R01NS048453, R01NS052455 (J.G.G.); Intramural Funding (fortune) at the University of Tübingen (2545-1-0 to B.V.) and the Ministry of Science, Research and Art Baden-Württemberg (to B.V.). Sequencing and analysis were provided by the

GENOMICS ENGLAND RESEARCH CONSORTIUM

J. C. Ambrose³⁶, P. Arumugam³⁶, M. Bleda³⁶, F. Boardman-Pretty^{36,37}, C. R. Boustred³⁶, H. Brittain³⁶, M. J. Caulfield^{36,37}, G. C. Chan³⁶, T. Fowler³⁶, A. Giess³⁶, A. Hamblin³⁶, S. Henderson^{36,37}, T. J. P. Hubbard³⁶, R. Jackson³⁶, L. J. Jones^{36,37}, D. Kasperaviciute^{36,37}, M. Kayikci³⁶, A. Kousathanas³⁶, L. Lahnstein³⁶, S. E. A. Leigh³⁶, I. U. S. Leong³⁶, F. J. Lopez³⁶, F. Maleady-Crowe³⁶, L. Moutsianas^{36,37}, M. Mueller^{36,37}, N. Murugaesu³⁶, A. C. Need^{36,37}, P. O'Donovan³⁶, C. A. Odhams³⁶, C. Patch^{36,37}, D. Perez-Gil³⁶, M. B. Pereira³⁶, J. Pullinger³⁶, T. Rahim³⁶, A. Rendon³⁶, T. Rogers³⁶, K. Savage³⁶, K. Sawant³⁶, R. H. Scott³⁶, A. Siddiq³⁶, A. Sieghart³⁶, S. C. Smith³⁶, A. Sosinsky^{36,37}, A. Stuckey³⁶, M. Tanguy³⁶, E. R. A. Thomas^{36,37}, S. R. Thompson³⁶, A. Tucci^{36,37}, E. Walsh³⁶, M. J. Welland³⁶, E. Williams³⁶, K. Witkowska³⁶ and S. M. Wood^{36,37}

³⁶Genomics England, London, UK. ³⁷William Harvey Research Institute, Queen Mary University of London, London, UK.

Broad Institute (UM1 HG008900, R01HG009141) and Yale Center for Mendelian Disorders (U54HG006504 to M. Gunel). This research was made possible in part through the 100,000 Genomes Project, UK.

AUTHOR CONTRIBUTIONS

Conceptualization: S.J.L., B.V., R.M., M.S.Z., V.S., F.A., J.G.G., G.K.V. Data curation: B.V., R.K., R.M., M.S., P.B., A.A., A.T.P., G.A., J.I.E.V., H.A.D.H., N.M., A.O., J.T., D.L.R., J.M., T.S., A.R., M.S.Z., G.K.V. Formal analysis: S.J.L., B.V., P.G.B., R.K., C.P., M.S., V.S., P.V., P.B., F.A.I., A.T.P., N.M., J.M., L.S.P., D.V.R., E.T., H.Z.E., S.M., T.B.P., H.Y., J.D.W., M.B., B.F., S.K.N. Funding acquisition: B.V., J.G.G., G.K.V. Investigation: A.O., J.T., D.L.R., T.S., B.T., H.G., F.A.I., F.A.S., A.S., K.S., M.G.H., M.K., J.L.M., H.H., E.G.K., F.S.A., T.H., M.S.Z., J.G.G. Project administration: G.K.V. Resources: G.E.R.C. Supervision: B.V., M.G.H., M.K., H.H., F.S.A., T.H., J.G.G., G.K.V. Validation: B.V., R.K., R.M., M.S., P.B., G.A., J.I.E.V., H.A.D.H., N.M., A.O., J.T., D.V.R., A.R., E.T., M.S.Z. Visualization S.D., M.J. Writing—original draft: S.J.L., G.V., B.V., M.S.Z., P.G.B., V.S., M.J., and M.S., Writing—review & editing: S.M.B.

ETHICS DECLARATION

Informed written consent including use of pictures and videos was obtained prior to study inclusion. This study was performed under the tenets of the Declaration of Helsinki and approved by the Ethics Commission of the University of Wuerzburg (46/15), University of Tübingen (197/2019B001), and University of California—San Diego (140028). All experimental animal care was performed in accordance with institutional and NIH guidelines and regulations. The study protocol was approved by the Institutional Animal Care and Use Committee of Oklahoma Medical Research Foundation, protocol 17-02.

DISCLAIMER

The contents of this publication are the sole responsibility of the author(s) and do not necessarily reflect the views, opinions or policies of Uniformed Services University of the Health Sciences (USUHS); The Henry M. Jackson Foundation for the Advancement of Military Medicine, Inc.; the Department of Defense (DoD); the Departments of the Army, Navy, or Air Force. Mention of trade names, commercial products, or organizations does not imply endorsement by the US Government.

COMPETING INTERESTS

H.Z.E., T.B.P., E.T., S.M., and H.Y. are employees of GeneDx, Inc. The other authors declare no competing interests.

ADDITIONAL INFORMATION

Supplementary information The online version contains supplementary material available at <https://doi.org/10.1038/s41436-021-01239-1>.

Correspondence and requests for materials should be addressed to G.K.V.

Reprints and permission information is available at <http://www.nature.com/reprints>

Publisher's note Springer Nature remains neutral with regard to jurisdictional claims in published maps and institutional affiliations.

10.9 Attachment 9

Bi-allelic variants in SPATA5L1 lead to intellectual disability, spastic-dystonic cerebral palsy, epilepsy, and hearing loss

REPORT

Bi-allelic variants in *SPATA5L1* lead to intellectual disability, spastic-dystonic cerebral palsy, epilepsy, and hearing loss

Elodie M. Richard,^{1,7,6} Somayeh Bakhtiari,^{2,3,7,6} Ashley P.L. Marsh,^{2,3,7,6} Rauan Kaiyrzhanov,^{4,7,6} Matias Wagner,^{5,6,7,6} Sheetal Shetty,^{2,3} Alex Pagnozzi,⁷ Sandra M. Nordlie,^{2,3} Brandon S. Guida,^{2,3} Patricia Cornejo,^{8,9,10} Helen Magee,^{2,3} James Liu,^{2,3} Bethany Y. Norton,^{2,3} Richard I. Webster,¹¹ Lisa Worgan,¹² Hakon Hakonarson,¹³ Jiankang Li,¹⁴ Yiran Guo,^{15,16} Mahim Jain,¹⁷ Alyssa Blesson,¹⁸ Lance H. Rodan,^{19,20} Mary-Alice Abbott,²¹ Anne Comi,^{22,23} Julie S. Cohen,^{22,23} Bader Alhaddad,⁵ Thomas Meitinger,⁵ Dominic Lenz,²⁴ Andreas Ziegler,²⁵ Urania Kotzaeridou,²⁵ Theresa Brunet,⁵ Anna Chassevent,²² Constance Smith-Hicks,^{22,23} Joseph Ekstein,²⁶ Tzvi Weiden,²⁷ Andreas Hahn,²⁸ Nazira Zharkinbekova,²⁹ Peter Turpenny,³⁰ Arianna Tucci,³¹ Melissa Yelton,³² Rita Horvath,³³ Serdal Gungor,³⁴ Semra Hiz,^{35,36} Yavuz Oktay,^{35,37} Hanns Lochmuller,³⁸ Marcella Zollino,^{39,40} Manuela Morleo,⁴¹ Giuseppe Marangi,^{39,40} Vincenzo Nigro,^{41,42} Annalaura Torella,^{41,42} Michele Pinelli,⁴¹ Simona Amenta,^{39,40} Ralf A. Husain,⁴³ Benita Grossmann,⁴⁴ Marion Rapp,⁴⁵

(Author list continued on next page)

Summary

Spermatogenesis-associated 5 like 1 (*SPATA5L1*) represents an orphan gene encoding a protein of unknown function. We report 28 bi-allelic variants in *SPATA5L1* associated with sensorineural hearing loss in 47 individuals from 28 (26 unrelated) families. In addition, 25/47 affected individuals (53%) presented with microcephaly, developmental delay/intellectual disability, cerebral palsy, and/or epilepsy. Modeling indicated damaging effect of variants on the protein, largely via destabilizing effects on protein domains. Brain imaging revealed diminished cerebral volume, thin corpus callosum, and periventricular leukomalacia, and quantitative volumetry demonstrated significantly diminished white matter volumes in several individuals. Immunofluorescent imaging in rat hippocampal neurons revealed localization of Spata5l1 in neuronal and glial cell nuclei and more prominent expression in neurons. In the rodent inner ear, Spata5l1 is expressed in the neurosensory hair cells and inner ear supporting cells. Transcriptomic analysis performed with fibroblasts from affected individuals was able to distinguish affected from controls by principal components. Analysis of differentially expressed genes and networks suggested a role for *SPATA5L1* in cell surface adhesion receptor function, intracellular focal adhesions, and DNA replication and mitosis. Collectively, our results indicate that bi-allelic *SPATA5L1* variants lead to a human disease characterized by sensorineural hearing loss (SNHL) with or without a nonprogressive mixed neurodevelopmental phenotype.

Neurodevelopmental disorders (NDDs) frequently occur because disruption of early brain morphogenesis and connectivity can affect multiple intersecting domains of development. These disorders represent a wide spectrum of clinical manifestations, ranging from single organ (e.g., brain) pathology to embryonic lethality due to failure of

¹Department of Otorhinolaryngology Head and Neck Surgery, School of Medicine, University of Maryland, Baltimore, MD 21201, USA; ²Barrow Neurological Institute, Phoenix Children's Hospital, Phoenix, AZ 85016, USA; ³Departments of Child Health, Neurology, Cellular, and Molecular Medicine and Program in Genetics, University of Arizona College of Medicine – Phoenix, Phoenix, AZ 85004, USA; ⁴Department of Neuromuscular Disorders, Institute of Neurology, University College London, Queen Square, WC1N 3BG London, UK; ⁵Institute of Human Genetics, Klinikum rechts der Isar, School of Medicine, Technical University of Munich, 81675 Munich, Germany; ⁶Institute of Neurogenomics, Helmholtz Zentrum München, 85764 Neuherberg, Germany; ⁷CSIRO Health and Biosecurity, The Australian e-Health Research Centre, Brisbane, QLD 4029, Australia; ⁸Pediatric Neuroradiology Division, Pediatric Radiology, Barrow Neurological Institute, Phoenix Children's Hospital, Phoenix, AZ 85016, USA; ⁹University of Arizona College of Medicine, Phoenix, AZ 85004, USA; ¹⁰Mayo Clinic, Scottsdale, AZ 85259, USA; ¹¹Neurology Department, The Children's Hospital at Westmead, Westmead, NSW 2145, Australia; ¹²Department of Medical Genomics, Royal Prince Alfred Hospital, Sydney, NSW 2050, Australia; ¹³Center for Applied Genomics, Children's Hospital of Philadelphia, Philadelphia, PA, USA; ¹⁴Department of Computer Science, City University of Hong Kong, Kowloon 999077, Hong Kong; ¹⁵Center for Applied Genomics, Children's Hospital of Philadelphia, Philadelphia, PA 19104, USA; ¹⁶Center for Data Driven Discovery in Biomedicine, Children's Hospital of Philadelphia, Philadelphia, PA 19146, USA; ¹⁷Department of Bone and Osteogenesis Imperfecta, Kennedy Krieger Institute, Baltimore, MD 21205, USA; ¹⁸Center for Autism and Related Disorders, Kennedy Krieger Institute, Baltimore, MD 21211, USA; ¹⁹Division of Genetics and Genomics, Boston Children's Hospital, Boston, MA 02115, USA; ²⁰Department of Neurology, Boston Children's Hospital, Boston, MA 02115, USA; ²¹University of Massachusetts Medical School – Baystate, Baystate Children's Hospital, Springfield, MA 01107, USA; ²²Department of Neurology and Developmental Medicine, Kennedy Krieger Institute, Baltimore, MD 21205, USA; ²³Department of Neurology, Johns Hopkins University School of Medicine, Baltimore, MD 21287, USA; ²⁴Centre of Child and Adolescent Medicine, Department of Pediatric Neurology and Metabolic Medicine, Heidelberg University Hospital, 69120 Heidelberg, Germany; ²⁵Department of Child Neurology and Metabolic Medicine, Center for Pediatric and Adolescent Medicine, University Hospital Heidelberg, Im Neuenheimer Feld 430, 69120 Heidelberg, Germany; ²⁶Dor Yeshorim, Committee for Prevention of Jewish Genetic Diseases, New York, NY 11211, USA;

(Affiliations continued on next page)

© 2021

2006 The American Journal of Human Genetics 108, 2006–2016, October 7, 2021



Claudia Steen,⁴⁶ Iris Marquardt,⁴⁷ Mona Grimmel,⁴⁴ Ute Grasshoff,⁴⁴ G. Christoph Korenke,⁴⁷ Marta Owczarek-Lipska,^{48,49} John Neidhardt,^{48,50} Francesca Clementina Radio,⁵¹ Cecilia Mancini,⁵¹ Dianela Judith Claps Sepulveda,⁵¹ Kirsty McWalter,⁵² Amber Begtrup,⁵² Amy Crunk,⁵² Maria J. Guillen Sacoto,⁵² Richard Person,⁵² Rhonda E. Schnur,⁵² Maria Margherita Mancardi,⁵³ Florian Kreuder,⁵⁴ Pasquale Striano,^{55,56} Federico Zara,^{56,57} Wendy K. Chung,⁵⁸ Warren A. Marks,^{59,60} Clare L. van Eyk,^{61,62} Dani L. Webber,^{61,62} Mark A. Corbett,^{61,62} Kelly Harper,^{61,62} Jesia G. Berry,^{61,62} Alastair H. MacLennan,^{61,62} Jozef Gecz,^{61,62,63} Marco Tartaglia,⁵¹ Vincenzo Salpietro,^{55,56} John Christodoulou,^{64,65} Jan Kaslin,⁵⁴ Sergio Padilla-Lopez,^{2,3} Kaya Bilguvar,^{66,67} Alexander Munchau,⁴⁵ Zubair M. Ahmed,^{1,68} Robert B. Hufnagel,⁶⁹ Michael C. Fahey,⁷⁰ Reza Maroofian,⁴ Henry Houlden,⁴ Heinrich Sticht,⁷¹ Shrikant M. Mane,^{66,67} Aboulfazel Rad,⁷² Barbara Vona,⁷² Sheng Chih Jin,⁷³ Tobias B. Haack,^{44,74} Christine Makowski,⁷⁵ Yoel Hirsch,²⁶ Saima Riazuddin,^{1,68,*} and Michael C. Kruer^{2,3,*}

vital organs, yet common, recognizable NDD phenotypes include intellectual disability, hearing loss, cerebral palsy, autism, and epilepsy. Prior work has revealed that homozygous or compound heterozygous variants in the spermatogenesis-associated 5 gene (*SPATA5* [MIM: 613940]) cause an NDD syndrome¹ that features microcephaly, cortical visual impairment, intellectual disability, spastic cerebral palsy, epilepsy, and sensorineural hearing loss (SNHL) (MIM: 616577). Neuroimaging features included hypomyelination in some individuals and a thin corpus callosum. Based on the domain structure, *SPATA5* has been grouped into the ATPase associated with diverse activities (AAA+) protein family.² Knockdown of *Spata5* in rat

cortical neurons led to abnormal mitochondrial morphology and fission/fusion ratios,³ suggesting a role in energy metabolism. In humans, *SPATA5* has a paralog, spermatogenesis-associated 5 like 1 (*SPATA5L1*), that is 35% identical and 52% similar by *Drosophila* RNAi Research Center Integrative Ortholog Prediction Tool (DI-OPT) alignment. Previous genome-wide association studies have found that *SPATA5L1* resides within a locus associated with chronic kidney disease in a combined North American and Dutch cohort,⁴ which was replicated in Japanese⁵ and Mongolian⁶ cohorts. However, no Mendelian disease-associated variants have been previously reported in *SPATA5L1*.

²⁷Dor Yeshorim, Committee for Prevention of Jewish Genetic Diseases, Jerusalem 9054020, Israel; ²⁸Department of Child Neurology, Justus-Liebig-Universität Giessen, 35392 Giessen, Germany; ²⁹Department of Neurology, South Kazakhstan Medical Academy, Shymkent 160001, Kazakhstan; ³⁰Clinical Genetics, Royal Devon & Exeter NHS Foundation Trust, EX1 2ED Exeter, UK; ³¹Clinical Pharmacology, William Harvey Research Institute, Charterhouse Square, School of Medicine and Dentistry Queen Mary University of London, London EC1M 6BQ, UK; ³²Penn State Health Children's Hospital, Hershey, PA 17033, USA; ³³Department of Clinical Neurosciences, John Van Geest Cambridge Centre for Brain Repair, University of Cambridge School of Clinical Medicine, CB2 0PY Cambridge, UK; ³⁴Inonu University, Faculty of Medicine, Turgut Ozal Research Center, Department of Paediatric Neurology, 44280 Malatya, Turkey; ³⁵Izmir Biomedicine and Genome Center, Dokuz Eylul University Health Campus, 35340 Izmir, Turkey; ³⁶Department of Pediatric Neurology, Faculty of Medicine, Dokuz Eylul University, 35340 Izmir, Turkey; ³⁷Department of Medical Biology, Faculty of Medicine, Dokuz Eylul University, 35220 Izmir, Turkey; ³⁸Children's Hospital of Eastern Ontario Research Institute; Division of Neurology, Department of Medicine, The Ottawa Hospital, and Brain and Mind Research Institute, University of Ottawa, Ottawa, ON K1H 8L1, Canada; ³⁹Università Cattolica Sacro Cuore, Facoltà di Medicina e Chirurgia, Dipartimento Scienze della Vita e Sanità Pubblica, 00168 Roma, Italy; ⁴⁰Fondazione Policlinico A. Gemelli IRCCS, Sezione di Medicina Genomica, 00168 Roma, Italy; ⁴¹Telethon Institute of Genetics and Medicine, 80078 Pozzuoli, Naples, Italy; ⁴²Department of Precision Medicine, University of Campania "Luigi Vanvitelli," 80138 Naples, Italy; ⁴³Department of Neuropediatrics, Jena University Hospital, 07747 Jena, Germany; ⁴⁴Institute of Medical Genetics and Applied Genomics, University of Tübingen, 72076 Tübingen, Germany; ⁴⁵Institute of Systems Motor Science, University of Lübeck, 23538 Lübeck, Germany; ⁴⁶Department of Paediatric and Adolescent Medicine, St Joseph Hospital, 12101 Berlin, Germany; ⁴⁷University Children's Hospital Oldenburg, Department of Neuropaediatric and Metabolic Diseases, 26133 Oldenburg, Germany; ⁴⁸Human Genetics, Faculty of Medicine and Health Sciences, University of Oldenburg, 26129 Oldenburg, Germany; ⁴⁹Junior Research Group, Genetics of Childhood Brain Malformations, Faculty VI-School of Medicine and Health Sciences, University of Oldenburg, 26129 Oldenburg, Germany; ⁵⁰Research Center Neurosensory Science, University of Oldenburg, 26129 Oldenburg, Germany; ⁵¹Genetics and Rare Diseases Research Division, Ospedale Pediatrico Bambino Gesù, IRCCS, 00146 Rome, Italy; ⁵²GeneDx, 207 Perry Parkway, Gaithersburg, MD 20877, USA; ⁵³Unit of Child Neuropsychiatry, Department of Clinical and Surgical Neurosciences and Rehabilitation, IRCCS Giannina Gaslini, Genoa 16147, Italy; ⁵⁴Australian Regenerative Medicine Institute, Monash University, Clayton, VIC 3168, Australia; ⁵⁵Pediatric Neurology and Muscular Diseases Unit, IRCCS Istituto Giannina Gaslini, 16148 Genoa, Italy; ⁵⁶Department of Neurosciences, Rehabilitation, Ophthalmology, Genetics, Maternal and Child Health, University of Genoa, 16142 Genoa, Italy; ⁵⁷Unit of Medical Genetics, IRCCS Istituto Giannina Gaslini, 16147 Genoa, Italy; ⁵⁸Departments of Pediatrics and Medicine, Columbia University, New York, NY 10032, USA; ⁵⁹Department of Neurology, Cook Children's Medical Center, Fort Worth, TX 76104, USA; ⁶⁰Department of Pediatrics, University of North Texas Health Science Center, Fort Worth, TX 76107, USA; ⁶¹Robinson Research Institute, Faculty of Health and Medical Sciences, University of Adelaide, Adelaide, SA 5006, Australia; ⁶²Adelaide Medical School, Faculty of Health and Medical Sciences, University of Adelaide, Adelaide, SA 5000, Australia; ⁶³South Australian Health and Medical Research Institute, Adelaide, SA 5000, Australia; ⁶⁴Brain and Mitochondrial Research Group, Murdoch Children's Research Institute, Melbourne Department of Paediatrics, University of Melbourne, Melbourne, VIC 3052, Australia; ⁶⁵Discipline of Child and Adolescent Health, University of Sydney, Sydney, NSW 2006, Australia; ⁶⁶Yale Center for Genome Analysis, Yale University, New Haven, CT 06520, USA; ⁶⁷Department of Genetics, Yale University School of Medicine, New Haven, CT 06510, USA; ⁶⁸Department of Biochemistry and Molecular Biology, School of Medicine, University of Maryland, Baltimore, MD 21201, USA; ⁶⁹Ophthalmic Genetics and Visual Function Branch, National Eye Institute, National Institutes of Health, Bethesda, MD 20892, USA; ⁷⁰Department of Paediatrics, Monash University, Melbourne, VIC 3168, Australia; ⁷¹Institute of Biochemistry, Friedrich-Alexander-Universität Erlangen-Nürnberg, 91054 Erlangen, Germany; ⁷²Department of Otolaryngology - Head and Neck Surgery, Tübingen Hearing Research Centre, Eberhard Karls University Tübingen, 72076 Tübingen, Germany; ⁷³Department of Genetics, Washington University School of Medicine, St. Louis, MO 63110, USA; ⁷⁴Centre for Rare Diseases, University of Tübingen, 72074 Tübingen, Germany; ⁷⁵Department of Paediatrics, Adolescent Medicine and Neonatology, Munich Clinic, Schwabing Hospital and Technical University of Munich, School of Medicine, 80804 Munich, Germany

*These authors contributed equally

*Correspondence: sriazuddin@som.umaryland.edu (S.R.), kruerm@arizona.edu (M.C.K.)
<https://doi.org/10.1016/j.ajhg.2021.08.003>

Here, as part of large-scale sequencing screens of individuals with SNHL and cerebral palsy, we detected bi-allelic, predicted deleterious variants in *SPATA5L1* (HGNC: 28762, GenBank: NM_024063.3). Using GeneMatcher⁷ services, we subsequently connected with colleagues worldwide. Together, we report 28 unique *SPATA5L1* variants in 47 affected individuals from 28 (26 unrelated) families. All human subjects' studies were performed in accordance with the ethical standards of the responsible committee on human experimentation according to institutional and national standards. Proper informed consent was obtained for all participants. Sequencing was performed at numerous centers, but all used Illumina systems and institutional pipelines based on current GATK best practices.^{8,9} Details regarding sequencing metrics and variant prioritization can be found in the [supplemental material and methods](#). Among the identified variants, 25 were present in the cohort in compound heterozygous form and three were found as homozygous variants (Figure S1). Out of these three, one missense variant, c.1199C>T (p.Thr400Ile), also segregates in a compound heterozygous fashion in two other families. Most putatively damaging variants were private except for five that were detected in multiple families: c.527G>T (p.Gly176Val), c.1398T>G (p.Ile466Met), c.606_619dup14 (p.Glu207-Glyfs*25), c.1199C>T (p.Thr400Ile), and c.2066G>T (p.Gly689Val); the former two were found in both the neurologic presentation and isolated hearing loss cases, and the latter two were found only in individuals with neurologic presentation. The pathogenicity of missense variants was predicted by³ 3 algorithms (Table S1). None of the identified variants were found in homozygous form in gnomAD.

All affected individuals with bi-allelic variants in *SPATA5L1* presented with mild, moderate, or severe hearing loss, and about half (25/47, 53%) also exhibited neurologic features, particularly global developmental delay/intellectual disability (seen in all individuals with neurologic involvement). Other prominent neurological findings included spastic-dystonic cerebral palsy in approximately two-thirds, epilepsy (16/25, 64%), and cortical visual impairment (15/25, 60%). Clinical features of our cohort are summarized in Table 1 and Figure 1A (and detailed in Tables S2 and S3). Operational definitions for presence/absence of NDDs can be found in the [supplemental material and methods](#). Case video review indicated visual impairment, impaired expressive language, intellectual disability, and mixed movement disorders with resultant orthopedic complications (Videos S1, S2, S3, S4, S5, and S6).

Most individuals exhibited a movement disorder, typically spasticity (17/25, 68%), dystonia (15/25, 60%), or a combination of these two forms of hypertonia (13/25, 52%). This usually occurred in a quadriplegic or generalized distribution. More than half (17/25, 68%) of the individuals had isolated hypotonia, although these individuals tended to be younger and may not have manifested their full motor phenotype. Some individuals were reported to exhibit ataxia, while non-epileptic myoclonus was identi-

fied in one. Stereotypies were seen in several individuals as well. The degree of cognitive impairment seen in affected individuals varied from severe to profound. For severely affected individuals, hyporesponsiveness to environmental stimuli was seen. Autistic features were absent except for in two individuals. Additional neuropsychiatric features were not reported, and behavior problems were not prominent. A combination of focal and generalized seizure types was reported. Few individuals (4/25, 16%) exhibited infantile spasms, often associated with a clinical diagnosis of West syndrome. Other forms of generalized seizures included myoclonic (7/25, 28%), absence (3/25, 12%), and generalized tonic-clonic (11/25, 44%) events. Focal epilepsy (4/25, 16%), sometimes with secondary generalization, was evident in several individuals as well, and a subset demonstrated mixed focal and generalized semiologies. One individual was reported to have evidence of electrical status epilepticus in slow wave sleep (ESES), and seizures in some were intractable or described in the context of a developmental or epileptic encephalopathy.

Microcephaly was present in about half of the affected individuals (13/25, 52%). Facial dysmorphism, assessed locally and confirmed by a trained dysmorphologist (M.C.E.) whenever possible, was noted in one-third (9/25) of affected individuals. Facial features included down-slanting palpebral fissures, widow's peak, low frontal hairline, large ears, tooth malformation, high palate, bitemporal narrowing, sparse eyebrows, depressed nasal bridge, and micrognathia as well as prominent upper lip, small chin, and mild telecanthus, evident in individual facial photographs (Figure 1B). A gestalt representation of "SPATA5L1 facies" was also constructed with the Face2Gene RESEARCH application (FDNA, Boston, MA, USA). However, this facial gestalt did not highlight any consistent dysmorphism, evidenced by the lack of a significant difference between the case and the age-, sex-, and ethnicity-matched control cohort ($p = 0.223$, Figure S2).

Neuroimaging findings were assessed by a board-certified neuroradiologist (P.C.). Some individuals' brains were morphologically normal, but relatively consistent features included diminished cortical volume, periventricular leukomalacia, widened Sylvian fissures, anterior temporal hypoplasia, and hypoplastic corpus callosum (Figure 2A). More variable features included delayed myelination in toddlers, an "ears of the lynx"-like appearance, incomplete hippocampal rotation, optic nerve hypoplasia, and small pons. To further characterize the structural neuroanatomic findings, we performed a quantitative volumetric analysis with DICOM data from clinical magnetic resonance images by using a previously described method.¹⁰ This analysis revealed a significance decrease in white matter volume in *SPATA5L1* cases compared to controls (Figure 2B).

Intriguingly, a subset of individuals (DY1–DY11) with bi-allelic *SPATA5L1* variants presented with isolated, non-syndromic hearing loss without neurological features (22/47, 47%, Figure S1, Table S2). These individuals were all of Ashkenazi Jewish descent, and in all, the missense variant

Table 1. Bi-allelic variants in SPATASL1 cause a neurodevelopmental disorder featuring intellectual disability, cerebral palsy, epilepsy, and hearing loss

Family	Family 1	Family 2	Family 3	Family 4	Family 5	Family 6	Family 7	Family 8	Family 9
Patient	1 (proband)	3 (proband)	5	6	7	8	9	10 (proband)	13
cDNA (GenBank: NM_024063.3)	c.1304_1305del (pat.); c.121G>C (mat.)	c.734T>A (pat.); c.1398T>G (mat.)	c.1A>T (pat.); c.2066G>T (mat.)	c.515C>A (pat.); c.196G>T (mat.)	c.1973G>A (pat.); c.2176_2177del (mat.)	c.76A>G (pat.); c.1079T>C (mat.)	c.1556C>A (hom.)	c.1199C>T (hom.)	c.1676delC (pat.); c.1682T>C (mat.)
Protein (GenBank: NP_076968.2)	p.Ile435Argfs*4 (pat.); p.Ala41Pro (mat.)	p.Val245Glu (pat.); p.Ile466Met (mat.)	p.Met1? (pat.); p.Gly689Val (mat.)	p.Pro172His (pat.); p.Asp66Tyr (mat.)	p.Arg658Lys (pat.); p.Val726Lysfs*13 (mat.)	p.Thr26Ala (pat.); p.Phe360Ser (mat.)	p.Ala519Asp (hom.)	p.Thr400Ile (hom.)	p.Ala559Glufs*33 (pat.); p.Leu561Ser (mat.)
Ancestry	Iraqi	European, with Ashkenazi Jewish ancestry	American; mat. ethnicity, Italian and Afro-American	mixed European	Spanish	African American	Turkish	Kazakh	mixed, Eastern European, and Scandinavian
Sex	male	male	female	male	male	female	female	female	male
Age at diagnosis	first year of life	32 months	27 months	23 years	4 months	9–12 months	5 years	7 months	1 month
Hearing impairment	+	+	+	+	+	+	+	+	+
Spasticity	+	–	+	–	–	–	+	+	+
Dystonia / hypotonia	+ / –	+ / +	– / +	– / N/A	– / +	N/A / –	+ / –	+ / +	– / +
Pattern	spastic quadriplegia	N/A	spastic quadriplegia	N/A	N/A	N/A	spastic-dystonic tetraparesis	spastic quadriplegia	spastic quadriplegia
Microcephaly (HC)	+ (acq., 47 cm at 6 years)	–	+ (acq., 46 cm at 3 years)	–	+ (acq., 45 cm at 1 year)	–	+ (27 cm at birth)	+ (45 cm at 6 years)	–
DD / ID	+ profound DD	+ global DD	+ global DD	+ severe DD	+ profound DD	+	+ severe DD	+ profound DD / ID	+ profound DD
Epilepsy	+	–	–	+	–	+	+	+	+
Dysmorphic features	–	+	–	–	–	–	–	+	+
Visual impairment	cortical visual blindness	–	cortical visual impairment	–	–	N/A	severe cortical visual impairment	probable cortical blindness	severe impairment
MRI findings	progressive CO and CB volume loss; thin CC; periventricular T2 hyperintensities; subtle GP hyperintensity bilaterally	concern for delayed myelination	delayed myelination; thin CC	CC lipoma, otherwise normal	normal	thin CC; enlarged 4 th ventricle; mega cisterna magna; possible brainstem hypoplasia; possible delayed myelination	profound cortical atrophy with predominant reduction of the white matter; cerebellum and brainstem normal	paucity of periventricular WM bilaterally with patchy confluent T2 hyperintensity; thin CC; generalized CO atrophy	normal (age 14 months); repeat MRI showed diminished cortical volume
Family	Family 10	Family 11	Family 12	Family 13	Family 14	Family 15	Family 16	Family 17	Family 18
Patient	14	15	16 (proband)	18	19	20	21	22 (proband)	25

(Continued on next page)

Table 1. Continued

Family	Family 10	Family 11	Family 12	Family 13	Family 14	Family 15	Family 16	Family 17	Family 18
cDNA (GenBank: NM_024063.3)	c.190C>T; c.1826C>G	c.85T>G (hom.)	c.1199C>T (pat.); c.1090-2A>G (mat.)	c.2066G>T (pat.); c.527G>T (mat.)	c.527G>T (pat.); c.2006T>G (mat.)	c.527G>T; c.1199C>T	c.213T>G; c.1313T>C (hom.)	c.1091T>A (pat.); c.1918C>T (mat.)	c.1648_1649insC; c.2066G>T
Protein (GenBank: NP_076968.2)	p.Arg64Trp; p.Ser609*	p.Cys29Gly (hom.)	p.Thr400Ile (pat.); p.? (mat.)	p.Gly689Val (pat.); p.Gly176Val (mat.)	p.Gly176Val (pat.); p.Met669Arg (mat.)	p.Gly176Val; p.Thr400Ile	p.Phe711Leu (hom.); p.Leu438Pro (hom.)	p.Val364Glu (pat.); p.Arg640* (mat.)	p.Phe550Serfs*16; p.Gly689Val
Ancestry	African American	Turkish	European (German)	Italian	European (German)	German	Arabian	German	Italian
Sex	male	male	male	male	female	male	male	male	male
Age at diagnosis	3 months	14 months	5 years	5 years, 6 months	2–3 months	15 years, 6 months	8 weeks	14 years, 9 months	5 months
Hearing impairment	+	+	+	+	+	+	+	+	+
Spasticity	+	–	+	+	+	+	+	+	+
Dystonia / hypotonia	+ / +	+ / –	+ / +	+ / +	+ / +	+ / +	+ / +	+ / +	+ / +
Pattern	spastic quadriplegia	quadripareisis	spastic quadriplegia	spastic quadriplegia	spastic quadriplegia	hypotonic dystonic spastic quadriplegia	hypotonic dystonic spastic quadriplegia	hypotonic dystonic spastic quadriplegia	hypotonic dystonic spastic quadriplegia
Microcephaly (HC)	+	+ (34 cm at birth)	–	+ (acq.)	+ (cong.)	+ (–2 SD at 1 year)	+ (32 cm at birth)	–	+ (48 cm at 6 years)
DD / ID	+ profound global DD	+	+ profound global DD	+ severe ID	+ severe ID	+ profound global DD	+ profound global DD	+ profound global DD	+ profound global DD
Epilepsy	+	+	–	+	–	+	+	+	+
Dysmorphic features	–	–	–	+	–	N/A	+	–	+
Visual impairment	–	–	mild myopia	N/A	severe impairment	–	severe impairment	severe impairment	central visual impairment
MRI findings	diffusely diminished CO volumes; ex vacuo dilatation LV; delayed myelination; thin CC	bilateral peritrigonal hyperintensity	diminished CO volume; periventricular WM hyperintensity	ventricle enlargement (slight); WM hyperintensity	diffuse slightly diminished CO volume; thin CC; lactate peak visualized on MRS (2 years)	mildly diminished CO volume; mildly atrophic BG; delayed myelination of the CC	mega cisterna magna; embryonic variant posterior cerebral artery	normal (11 months); slightly enlarged ventricles (19 months); no progression of ventricular enlargement (25 months); delayed myelination, thin CC (4.5 years)	brain hypomyelination; diffuse slight brain atrophy

Abbreviations: CO, cortical; CB, cerebellar; CC, corpus callosum; DD, developmental delay; ID, intellectual disability; GP, globus pallidus; WM, white matter; BG, basal ganglia; MRS, magnetic resonance spectroscopy; mat., maternal; pat., paternal; hom., homozygous; +, clinical feature detected; –, clinical feature not observed; N/A, no information provided for clinical feature; SD, standard deviation; p, percentile; acq., acquired postnatally; cong., congenital; HC, head circumference. T2 is an MRI signal acquisition parameter.

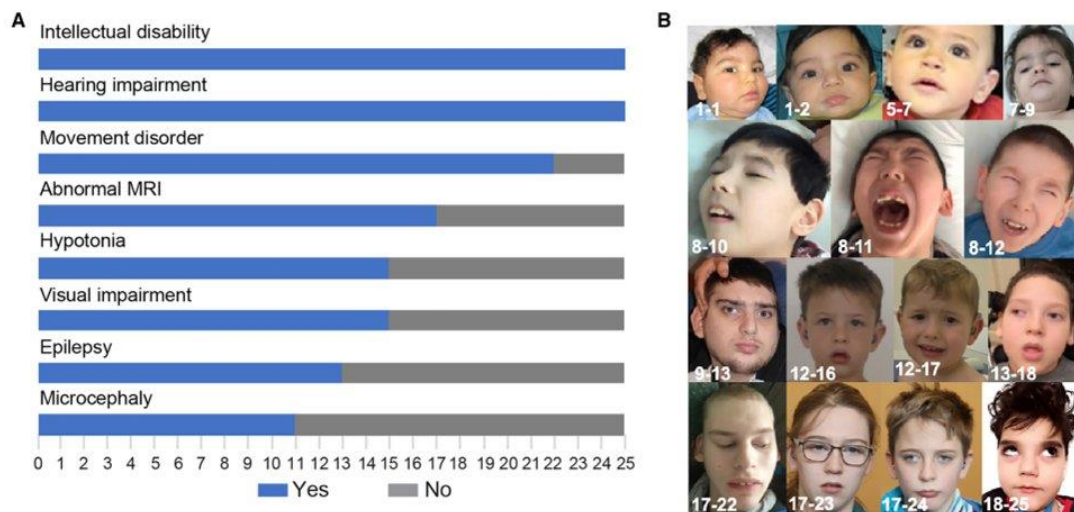


Figure 1. Prevalent clinical features of individuals with bi-allelic variants in *SPATASL1*

(A) Bar graph illustrating the prevalence of the most relevant clinical features from the 25 individuals for whom full datasets were available from 18 families with the neurodevelopmental phenotype. Blue: individuals with the clinical feature. Gray: individuals without the clinical feature.

(B) Representative clinical features of individuals carrying bi-allelic *SPATASL1* variants with the severe neurodevelopmental phenotype, showing subtle and non-specific dysmorphic features, including downsloping palpebral fissures, bitemporal narrowing, and depressed nasal bridge.

c.1398T>G was identified in compound heterozygosity with various other pathogenic alleles, suggesting a hypomorphic founder allele, resulting in a partial rather than complete loss-of-protein function. According to gnomAD, the allele frequency of this variant is 0.0029 in individuals of Ashkenazi Jewish background, indicating a frequency of homozygotes of 0.8/100,000. The fact that no individuals with SNHL hearing loss and homozygosity for the c.1398T>G allele were identified further raises the question whether the variant would not lead to a clinical phenotype in homozygous form. Like the cases with neurologic involvement, the bilateral SNHL associated with isolated cases was mild to profound. There appeared to be some benefit to cochlear implants among individuals who received this intervention.

SPATASL1 belongs to the AAA+ ATPases protein superfamily, a functionally diverse group of enzymes that hydrolyze ATP to induce changes in target substrates. Variants identified in our cohort are spread throughout the gene and protein (Figure 3A, visualized with Geneious Prime 2021.0.1). Structural effects of a subset of missense variants detected in our cohort were assessed by VIPUR¹¹ and Missense3D¹² based on a three-dimensional model of *SPATASL1*. Of the 13 variants investigated, 11 variants were predicted to have a deleterious effect on protein structure (Figure 3B) via a combination of destabilizing effects, including steric clashes, loss of hydrophobic packing, loss of polar interactions, and the emergence of buried charged residues (Figure S3). All variants predicted to be deleterious are expected to destabilize domains within *SPATASL1*,

except for the p.Gly689Val variant, which is predicted to create steric clashes with the ATP ligand, affecting ATP-binding properties.

We next sought to define the typical protein localization of *SPATASL1*. *SPATASL1* mRNA has been detected (albeit at low levels) in both neurons and glia, both during embryonic and adult stages of human brain development (Figure 4A). We confirmed this at the protein level in rat dissociated hippocampal cultures, identifying Spata511 immunoreactivity within neurons, astrocytes, oligodendrocytes, and microglia; the most prominent staining was in neurons (Figure 4B). *Spata511* localized primarily to the nucleus. Within the ear, both inner and outer hair cells exhibit detectable levels of *Spata511* transcript (Figure 4C). Rat whole mounts stained with a commercial antibody against Spata511 demonstrated that Spata511 is present in hair cells and pillar cells of the organ of Corti (Figure 4D), suggesting that loss of wild-type protein may lead to sensorineural hearing loss by disrupting normal function within these structures.

The precise function of *SPATASL1* in brain, inner ear, and other tissues is currently unknown. However, the sequence similarity and overlapping clinical manifestations in individuals harboring putatively loss-of-function or protein-damaging variants in *SPATA5* and *SPATASL1* led us to speculate as to a potential redundancy between the two proteins. Given the proposed role of *SPATA5* in mitochondrial function,¹ we assessed oxidative phosphorylation (OXPHOS) in primary fibroblasts from affected individuals 2-3, 2-4, 7-9 (i.e., individuals 3 and 4 from family

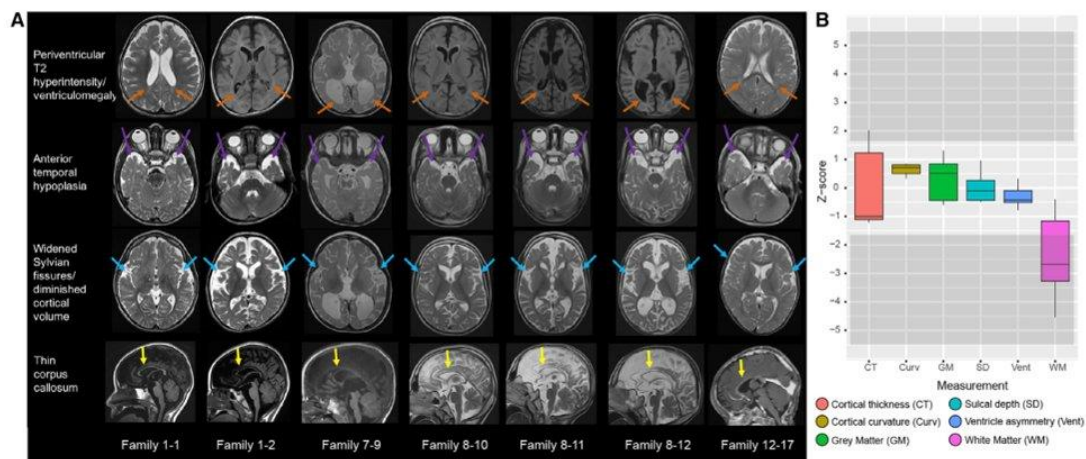


Figure 2. Neuroimaging features in individuals harboring bi-allelic predicted-deleterious variants in *SPATA5L1*

(A) T1 and T2/FLAIR MRI images were assessed for the presence of periventricular leukomalacia (defined as T2 hyperintensity and/or diminished white matter volume/ex vacuo ventriculomegaly evident adjacent to the ventricles); anterior temporal lobe hypoplasia; widened Sylvian fissures (characterized as diminished coverage of the insular cortex), diminished cortical volume; and thin/dysplastic corpus callosum. Ages were 4 years old (1-1, 1-2), 21 years old (7-9), 10 years old (8-10), 7 years old (8-11), 6 years old (8-12), and 1 year old (12-16).

(B) Boxplot of six structural measures quantified from brain MRI volumes, represented as Z scores, in comparison to an age-matched control cohort of typically developing children.

2 and individual 9 from family 7) in comparison to passage and age-matched controls by using the Seahorse XF96 assay. These assays indicated no impairment of OXPHOS in affected fibroblasts (Figure S4), suggesting that despite the degree of clinical overlap seen in affected individuals, the two proteins may have divergent functions. Indeed, a mitochondrial localization for *SPATA5L1* is not predicted via MitoMiner¹³ and it is absent from the MitoCarta3.0 human and mouse inventory.¹⁴ However, alterations to mitochondrial biogenesis remain possible, and we cannot exclude disruption to mitochondrial morphology and dynamics (as observed in *SPATA5*-deficient neurons).³

Next, we turned to an unbiased transcriptome approach to try to distinguish *SPATA5L1* fibroblast cell lines from controls. The analysis was performed in the same affected (plus 1-1 and 4-6, i.e., individual 1 from family 1 and individual 6 from family 4) cell lines utilized for the Seahorse study and in passage and age-matched controls. Principal-component analysis from RNA sequencing (RNA-seq) data indicated that individuals harboring bi-allelic *SPATA5L1* variants could be distinguished from controls on the basis of their differentially expressed genes (Figure 5A). This provided proof of principle data supporting the p.Ala41Pro, p.Val245Glu, p.Ile435fs, p.Ile466Met, and p.Ala519Asn variants as bona fide disease-associated variants. These findings allowed us to pool these data for subsequent analyses. Significantly upregulated networks were not identified. However, several significantly downregulated genes were identified (Figures 5B and 5C). These genes converged on several hubs (Figures 5D–5F), pointing to a role for *SPATA5L1* in mitosis (mitotic nuclear division, sister chromatid

segregation, mitotic spindle organization, kinetochores) and DNA replication (DNA conformation change, single-stranded DNA binding, DNA helicase activity). Adhesion receptors, which connect cell-substrate junctions (Figure 5E) and include fibronectin-binding (Figure 5F) integrins (i.e., *ITGA8*; Figure 5B), cadherins (Figure 5F), and immunoglobulin superfamily members (i.e., *L1CAM*; Figure 5B), were significantly downregulated. Members of the AAA+ ATPases protein superfamily have known roles in mitosis, DNA replication, metabolism, and repair processes.¹⁵ For example, cytoplasmic dynein plays a role in mammalian mitotic spindle formation,¹⁶ while WRNIP1 protects stalled replication forks from degradation.¹⁷ Our transcriptome analyses posit a potential role for *SPATA5L1* in mitosis and DNA replication, however additional studies are required for assessment of this possibility.

Our clinical, radiologic, genomic, and transcriptomic evidence support the existence of a mixed neurodevelopmental syndrome with hearing loss due to bi-allelic variants in *SPATA5L1*. The pathogenicity of the variants we identified is supported by their rarity (many private variants), predicted deleteriousness by multiple algorithms, consistent phenotype in affected individuals, and RNA-seq validation of several variants. Although we did identify individual loss-of-function (premature stop, frameshift, start-loss, stop-loss, or canonical splice site) alleles, we did not identify bi-allelic loss-of-function variants, suggesting that perhaps human knockout genotypes might show reduced viability. We were not able to clearly identify any firm genotype-phenotype correlations. Our morphologic neuroimaging analyses revealed thin corpus callosum,

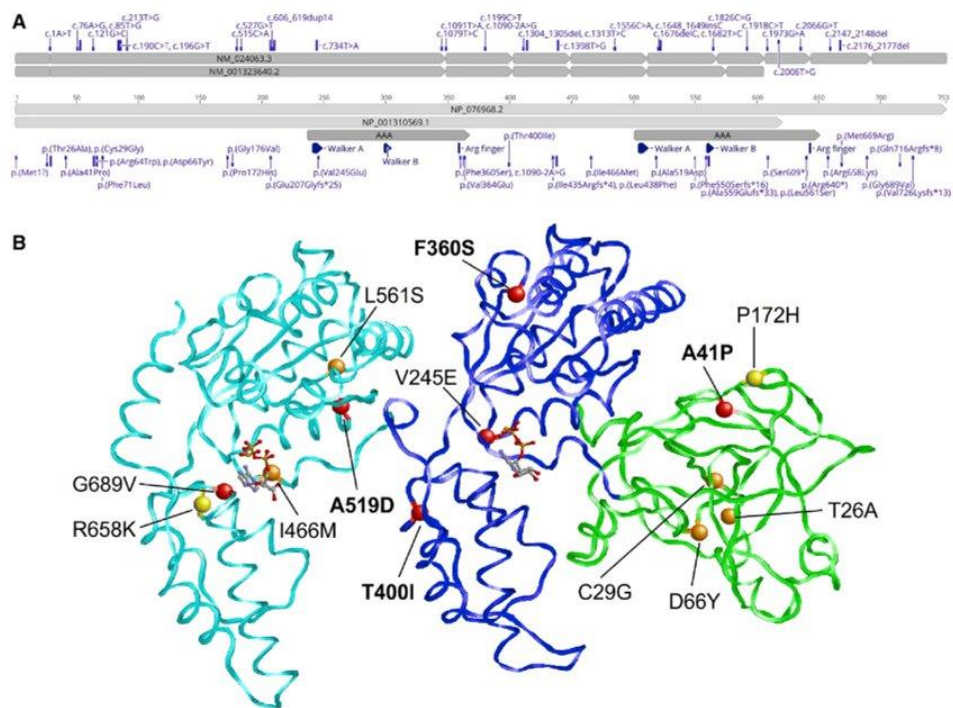


Figure 3. Distribution and predicted structural effects of *SPATASL1* variants
 (A) Alternative splicing leads to two distinct *SPATASL1* transcripts (top), resulting in a full-length and short isoform (bottom). The variant numbering is based on the full-length transcript and isoform, GenBank: NM_024063.3 and GenBank: NP_076968.2. Non-coding and coding regions of exons are denoted by flat-edged and pointed-edged rectangles, respectively.
 (B) Structural effects of a subset of variants identified in this study were evaluated with a three-dimensional model of *SPATASL1* based on the structure of the homologous ATPase p97 (PDB: 5FTN). The *SPATASL1* structure is shown in ribbon presentation, depicting the N-terminal domain (green) and two conserved ATPase domains (AAA, blue and cyan). ATP ligands are shown in stick presentation. Altered residues are highlighted as balls and labeled. Red and orange balls indicate variants that were classified as deleterious by two or one methods, respectively. Yellow balls indicate variants that were predicted to have little effect on protein structure. The variants depicted in more detail in [Figure S3](#) are labeled in bold letters.

diminished cortical volume, open opercula, and anterior temporal hypoplasia in several individuals, while quantitative morphometry indicated that white matter volume was significantly diminished in multiple members of the cohort. When observed, microcephaly correlated with reduced white matter volume (as observed in affected individuals 10-2, 12-1, 13-1).

Although *SPATASL1* is an orphan gene, our transcriptomic studies provide some clues as to its function. Adhesion receptors collectively play a major role in the control of cell-extracellular matrix (fibronectin-integrin and immunoglobulin superfamily members) and cell-cell interactions (cadherin family members). These interactions in turn integrate cell growth/migration and proliferation on the basis of environmental cues such as contact inhibition. Fibronectin-integrin binding is known to be mediated through focal adhesions, intracellular cytoskeleton/signaling hubs that transmit extracellular cues through phosphorylation events (i.e., protein serine-threonine kinase activator activity) and ultimately control DNA replica-

tion and mitosis. Although neuroimaging in our affected individuals did not indicate malformations of cortical development that would suggest abnormalities of neuronal migration, the diminished cortical volumes and microcephaly seen may reflect impairment of neuronal cell division during brain development.

In conclusion, we present evidence that rare coding variants and loss-of-function alleles in *SPATASL1* lead to hearing loss and a mixed neurodevelopmental disorder that features microcephaly, global developmental delay/intellectual disability, spastic-dystonic cerebral palsy (some children presented with hypotonia), and focal or generalized epilepsy. Although our studies support a role for *SPATASL1* in DNA replication, further experimental studies will be required to support or refute this hypothesis.

Data and code availability

Variants identified in this study have been submitted to ClinVar (accession numbers pending). Original data are available from the authors upon reasonable request.

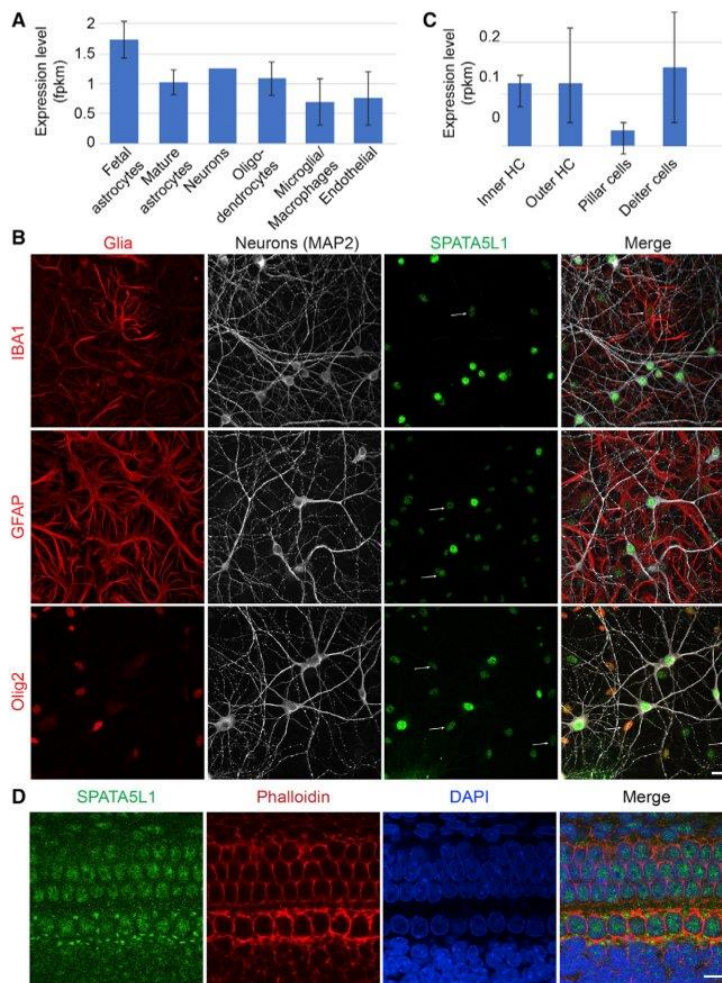


Figure 4. *Spata5l1* is expressed in the inner ear and the brain of rodents/humans (A) *SPATA5L1* is expressed in all cellular subtypes of the human brain (Brain RNA-Seq database).

(B) Representative immunofluorescent labeling of endogenous *SPATA5L1* (green) in rat hippocampal neurons in culture highlight the co-localization of the protein within the nuclei of neurons (MAP2), as well as the nuclei of glial cells (red): microglia (IBA1), astrocytes (GFAP), and oligodendrocytes (Olig2). Signal intensity of *SPATA5L1* immunolabeling suggests protein expression is higher in neurons compared to glial cells. Arrows indicate the localization of *SPATA5L1* in the nuclei of glial cells. All images are projections of confocal optical section stacks. Scale bar: 25 μ m.

(C) *Spata5l1* is expressed at low levels in hair cells (inner and outer) as well as supporting cells (pillar and Deiter cells) in adult mice (adapted from gEAR portal). HC, hair cells.

(D) Representative immunofluorescent labeling of endogenous *SPATA5L1* (green) in Sprague Dawley rat organ of Corti at E20. Immunolabeling shows *SPATA5L1* is present in the hair and pillar cells of the organ of Corti. DAPI (blue) and Rhodamine Phalloidin (red) were used for counterstaining the nuclei and the cytoskeleton, respectively. All images are projections of confocal optical section stacks. Scale bar: 10 μ m.

Health Research (Foundation Grant FDN-167281), the Canadian Institutes of Health Research and Muscular Dystrophy Canada (Network Catalyst Grant for NMD4C), the Canada Foundation for Innovation (CFI-JELF 38412), and the Canada Research Chairs Program (Canada Research Chair in Neuromuscular Genomics and Health,

Supplemental information

Supplemental information can be found online at <https://doi.org/10.1016/j.ajhg.2021.08.003>.

Acknowledgments

The authors are grateful to the participants and their families, without whose support this work would not have been possible. K.Mc., A.B., A.C., M.J.G.S., R.E.P., and R.E.S. are employees of GenDx. We thank Minerva Contreras and Thomas Blanpied for assisting with neuronal culture and the CIBR platform (UMSOM, Baltimore, MD, USA). This work was supported in part by R01NS107428 (S.R.), 1R01NS106298 (M.C.K.), and Cerebral Palsy Alliance Research Foundation PG07217 award to W.M. and M.C.K. Portions of this work were also funded by the Fondazione Bambino Gesù (Vite Coraggiose), the Italian Ministry of Health (Ricerca 5 \times 1000) to M.T.A., and in part by Telethon Undiagnosed Diseases Program (TUDP, GSP15001). H.L. receives support from the Canadian Institutes of

950-232279). B.V. is funded by intramural funding (fortune) at the University of Tübingen (2545-1-0) and the Ministry of Science, Research, and Art Baden-Württemberg. R.H. is supported by NEI intramural funds. W.K.C. receives support from the JPB Foundation and SFARI. S.C.J. is supported by a K99/R00 Pathway to Independence Award (K99HL143036 and R00HL143036-02) and the Clinical and Translational Research Funding Program award (CTSA1405). This project was funded in part by The Foundation for Barnes-Jewish Hospital and their generous donors and by the NIH/National Center for Advancing Translational Sciences grant UL1TR002345. Several families were enrolled as part of the SYNAPS Study Group collaboration funded by The Wellcome Trust and strategic award (Synaptopathies) funding (WT093205 MA and WT104033AIA). This research was conducted as part of the Queen Square Genomics group at University College London, supported by the National Institute for Health Research University College London Hospitals Biomedical Research Centre. A.P.L.M. was supported by a NHMRC Early Career Research Fellowship (GNT1156820). S.B.'s contributions were funded by a Cerebral Palsy Alliance Research Foundation Career

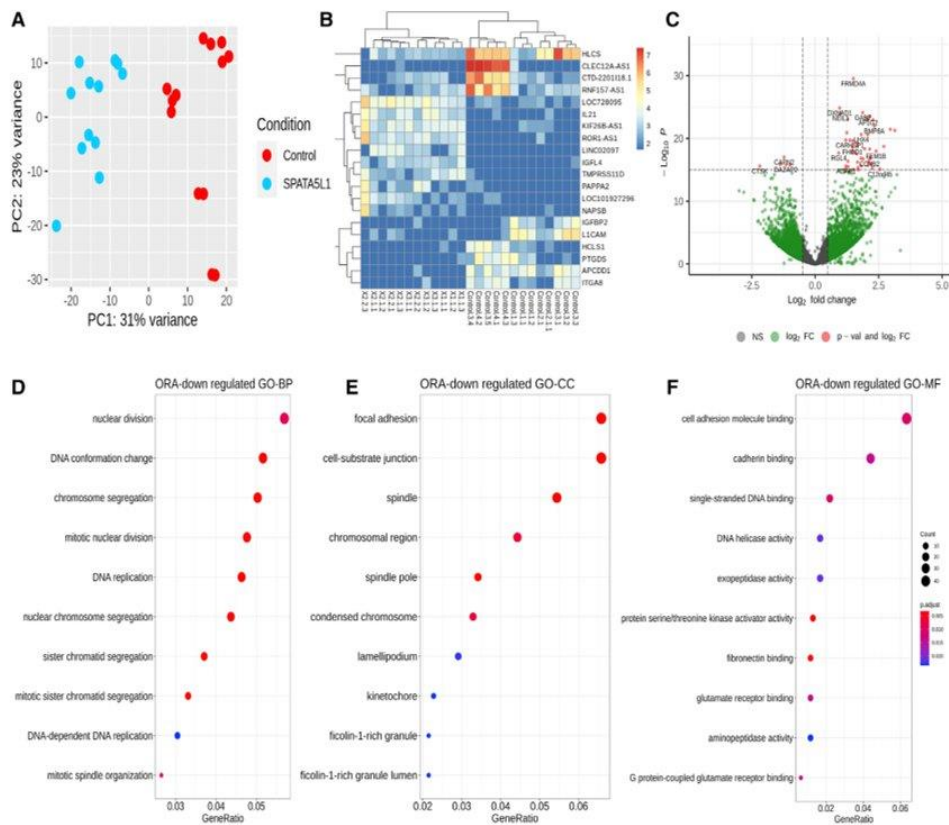


Figure 5. Analysis of gene expression patterns in *SPATASL1* fibroblasts by RNA-seq reveals differential expression of DNA replication and mitosis-related genes

(A) Principal-component analysis plot shows a differential clustering of *SPATASL1* samples ($n = 4$) from control samples ($n = 4$). (B) Transcriptomic heatmap of the top 20 differentially expressed genes (top ten with fold change > 1.5 and $p < 0.05$ and bottom 10 with fold change < 0.5 and $p < 0.05$). Red/yellow colors represent highly expressed genes and blue colors represent under-expressed genes for these 20 genes in the respective case and control samples. The legend corresponds to expression values. (C) Volcano plot highlighting genes with large fold changes that are either significantly upregulated or downregulated between *SPATASL1* and control samples. \log_2 fold change of normalized counts (red dots indicate genes with $p < 10^{-16}$). (D) Over-representation analysis (ORA) for downregulated genes (\log_2 fold change < -1 , $p < 0.05$) for GO-BP (Gene Ontology Biological Processes). (E) Over-representation analysis (ORA) for downregulated genes (\log_2 fold change < -1 , $p < 0.05$) for GO-CC (Gene Ontology Cellular Components). (F) Over-representation analysis (ORA) for downregulated genes (\log_2 fold change < -1 , $p < 0.05$) for GO-CC and GO-MF (Gene Ontology Molecular Functions).

Development Award. C.v.E., M.A.C., and A.H.M. were supported by Australian National Health and Medical Research Council Project Grant (1099163). J.G. was supported by Australian National Health and Medical Research Council Fellowship (1041920) and Channel 7 CRF Chair for the Prevention of Childhood Disability. C.v.E. was supported by The Hospital Research Foundation Mid-Career Fellowship. C.v.E., M.A.C., A.H.M., and J.G. were supported by infrastructure funding from the Tenix Foundation. The content is solely the responsibility of the authors and does not necessarily represent the official views of the National Institutes of Health.

Declaration of interests

The authors declare no competing interests.

Received: May 28, 2021
 Accepted: August 4, 2021
 Published: October 7, 2021

Web resources

Brain RNA-Seq, <http://www.brainrnaseq.org/>
 BrainSpan Atlas of the Developing Human Brain, <https://www.brainspan.org/>
 CADD, <https://cadd.gs.washington.edu/>
 DIOPT, https://www.flymai.org/cgi-bin/DRSC_prot_align.pl
 gEAR portal, <https://umgear.org/>
 gnomAD, <https://gnomad.broadinstitute.org/>
 MARRVEL, <http://marrvel.org/>

MutationTaster, <http://mutationtaster.org/>
OMIM, <https://omim.org/>
PolyPhen-2, <http://genetics.bwh.harvard.edu/pph2/>
Provean, <http://provean.jcvi.org>
SIFT, <https://sift.bii.a-star.edu.sg/>

References

1. Tanaka, A.J., Cho, M.T., Millan, F., Juusola, J., Retterer, K., Joshi, C., Niyazov, D., Garnica, A., Gratz, E., Deardorff, M., et al. (2015). Mutations in SPATA5 Are Associated with Microcephaly, Intellectual Disability, Seizures, and Hearing Loss. *Am. J. Hum. Genet.* *97*, 457–464.
2. Liu, Y., Black, J., Kisiel, N., and Kulesz-Martin, M.F. (2000). SPAF, a new AAA-protein specific to early spermatogenesis and malignant conversion. *Oncogene* *19*, 1579–1588.
3. Puusepp, S., Kovacs-Nagy, R., Alhaddad, B., Braunsch, M., Hoffmann, G.F., Kotzaeridou, U., Lichvarova, L., Liiv, M., Makowski, C., Mandel, M., et al. (2018). Compound heterozygous SPATA5 variants in four families and functional studies of SPATA5 deficiency. *Eur. J. Hum. Genet.* *26*, 407–419.
4. Köttgen, A., Glazer, N.L., Dehghan, A., Hwang, S.J., Katz, R., Li, M., Yang, Q., Gudnason, V., Launer, L.J., Harris, T.B., et al. (2009). Multiple loci associated with indices of renal function and chronic kidney disease. *Nat. Genet.* *41*, 712–717.
5. Kubo, Y., Imaizumi, T., Ando, M., Nakatochi, M., Yasuda, Y., Honda, H., Kuwatsuka, Y., Kato, S., Kikuchi, K., Kondo, T., et al. (2017). Association between kidney function and genetic polymorphisms in atherosclerotic and chronic kidney diseases: A cross-sectional study in Japanese male workers. *PLoS ONE* *12*, e0185476.
6. Park, H., Kim, H.J., Lee, S., Yoo, Y.J., Ju, Y.S., Lee, J.E., Cho, S.I., Sung, J., Kim, J.I., and Seo, J.S. (2013). A family-based association study after genome-wide linkage analysis identified two genetic loci for renal function in a Mongolian population. *Kidney Int.* *83*, 285–292.
7. Sobreira, N., Schiettecatte, F., Valle, D., and Hamosh, A. (2015). GeneMatcher: a matching tool for connecting investigators with an interest in the same gene. *Hum. Mutat.* *36*, 928–930.
8. McKenna, A., Hanna, M., Banks, E., Sivachenko, A., Cibulskis, K., Kernytshy, A., Garimella, K., Altshuler, D., Gabriel, S., Daly, M., and DePristo, M.A. (2010). The Genome Analysis Toolkit: a MapReduce framework for analyzing next-generation DNA sequencing data. *Genome Res.* *20*, 1297–1303.
9. Van der Auwera, G.A., Carneiro, M.O., Hartl, C., Poplin, R., Del Angel, G., Levy-Moonshine, A., Jordan, T., Shakir, K., Roazen, D., Thibault, J., et al. (2013). From FastQ data to high confidence variant calls: the Genome Analysis Toolkit best practices pipeline. *Curr. Protoc. Bioinformatics* *43*, 11.10.1–11.10.33.
10. Pagnozzi, A.M., Dowson, N., Doecke, J., Fiori, S., Bradley, A.P., Boyd, R.N., and Rose, S. (2017). Identifying relevant biomarkers of brain injury from structural MRI: Validation using automated approaches in children with unilateral cerebral palsy. *PLoS ONE* *12*, e0181605.
11. Baugh, E.H., Simmons-Edler, R., Müller, C.L., Alford, R.F., Volfovsky, N., Lash, A.E., and Bonneau, R. (2016). Robust classification of protein variation using structural modelling and large-scale data integration. *Nucleic Acids Res.* *44*, 2501–2513.
12. Ittisoponpisan, S., Islam, S.A., Khanna, T., Alhuzimi, E., David, A., and Sternberg, M.J.E. (2019). Can Predicted Protein 3D Structures Provide Reliable Insights into whether Missense Variants Are Disease Associated? *J. Mol. Biol.* *431*, 2197–2212.
13. Smith, A.C., and Robinson, A.J. (2016). MitoMiner v3.1, an update on the mitochondrial proteomics database. *Nucleic Acids Res.* *44* (D1), D1258–D1261.
14. Rath, S., Sharma, R., Gupta, R., Ast, T., Chan, C., Durham, T.J., Goodman, R.P., Grabarek, Z., Haas, M.E., Hung, W.H.W., et al. (2021). MitoCarta3.0: an updated mitochondrial proteome now with sub-organelle localization and pathway annotations. *Nucleic Acids Res.* *48*, D1541–D1547.
15. Snider, J., Thibault, G., and Houry, W.A. (2008). The AAA+ superfamily of functionally diverse proteins. *Genome Biol.* *9*, 216.
16. Vaisberg, E.A., Koonce, M.P., and McIntosh, J.R. (1993). Cytoplasmic dynein plays a role in mammalian mitotic spindle formation. *J. Cell Biol.* *123*, 849–858.
17. Leuzzi, G., Marabitti, V., Pichierri, P., and Franchitto, A. (2016). WRNIP1 protects stalled forks from degradation and promotes fork restart after replication stress. *EMBO J.* *35*, 1437–1451.

10.10 Attachment 10

Identification of three novel homozygous variants in *COL9A3* causing autosomal recessive Stickler syndrome

RESEARCH

Open Access

Identification of three novel homozygous variants in *COL9A3* causing autosomal recessive Stickler syndrome



Aboufazel Rad¹, Maryam Najafi^{2,3}, Fatemeh Suri⁴, Soheila Abedini^{5,6}, Stephen Loum¹, Ehsan Ghayoor Karimiani⁶, Narsis Daftarian⁷, David Murphy⁵, Mohammad Doosti³, Afroz Moghaddasi⁴, Hamid Ahmadi⁴, Hamideh Sabbaghi⁸, Mohsen Rajati⁹, Narges Hashemi¹⁰, Barbara Vona^{1,11,12} and Miriam Schmidts^{2,3,13*}

Abstract

Background: Stickler syndrome (STL) is a rare, clinically and molecularly heterogeneous connective tissue disorder. Pathogenic variants occurring in a variety of genes cause STL, mainly inherited in an autosomal dominant fashion. Autosomal recessive STL is ultra-rare with only four families with biallelic *COL9A3* variants reported to date.

Results: Here, we report three unrelated families clinically diagnosed with STL carrying different novel biallelic loss of function variants in *COL9A3*. Further, we have collected *COL9A3* genotype–phenotype associations from the literature.

Conclusion: Our report substantially expands the molecular genetics and clinical basis of autosomal recessive STL and provides an overview about allelic *COL9A3* disorders.

Keywords: Autosomal recessive Stickler syndrome, *COL9A3*, Collagen, Hearing loss, Retinal detachment

Background

Stickler syndrome (STL) is a rare, clinically and genetically heterogeneous connective tissue disorder divided into six clinical subtypes with overlapping features, including ocular pathologies (myopia, retinal detachment, vitreoretinal degeneration, cataract), hearing impairment (sensorineural, mixed, and/or conductive), craniofacial abnormalities (midface hypoplasia, anteverted nares, depressed nasal bridge and either Pierre Robin sequence or cleft palate and micrognathia) and joint problems (mild spondyloepiphyseal dysplasia, and precocious osteoarthritis) [1]. These features exhibit substantial variable expressivity according to clinical subtype [1]. STL is molecularly diagnosed by the presence

of pathogenic variants in six collagen-type genes including *COL2A1*, *COL11A1*, *COL11A2*, *COL9A1*, *COL9A2*, *COL9A3*, and two non-collagen genes consisting of *LRP2* and *LOXL3* [1–3], following a predominantly autosomal dominant inheritance pattern.

The heteropolymer collagen XI/IX/II are critical in the extracellular matrix of joints, bones, ligaments and connective tissues throughout the body [4]. *COL2A1* encodes collagen type II alpha 1 chain. Heterozygous variants that cause functional haploinsufficiency are responsible for autosomal dominant STL type I (OMIM #108300), representing the most common subtype, accounting for roughly 80–90% of STL [5, 6]. Pathogenic variants in *COL11A1* cause the second most common STL subtype, type II (OMIM #604841) (10–20%). Variants in this gene likewise typically follow a dominant inheritance pattern [7], although five families have been described with STL and biallelic *COL11A1* mutations [8–10]. *COL11A2* pathogenic variants are very rare and cause

*Correspondence: miriam.schmidts@uniklinik-freiburg.de

³ Pediatric Genetics Division, Center for Pediatrics and Adolescent Medicine, University Hospital Freiburg, Freiburg University Faculty of Medicine, Mathildenstrasse 1, 79106 Freiburg, Germany
Full list of author information is available at the end of the article



© The Author(s) 2022. **Open Access** This article is licensed under a Creative Commons Attribution 4.0 International License, which permits use, sharing, adaptation, distribution and reproduction in any medium or format, as long as you give appropriate credit to the original author(s) and the source, provide a link to the Creative Commons licence, and indicate if changes were made. The images or other third party material in this article are included in the article's Creative Commons licence, unless indicated otherwise in a credit line to the material. If material is not included in the article's Creative Commons licence and your intended use is not permitted by statutory regulation or exceeds the permitted use, you will need to obtain permission directly from the copyright holder. To view a copy of this licence, visit <http://creativecommons.org/licenses/by/4.0/>. The Creative Commons Public Domain Dedication waiver (<http://creativecommons.org/publicdomain/zero/1.0/>) applies to the data made available in this article, unless otherwise stated in a credit line to the data.

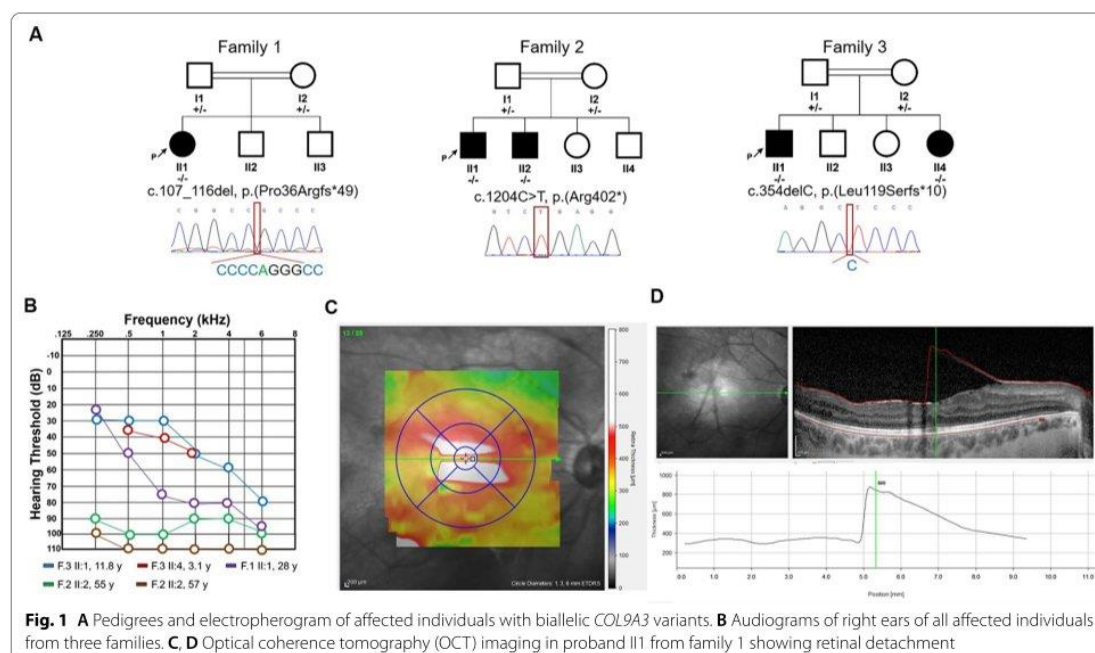


Fig. 1 **A** Pedigrees and electropherogram of affected individuals with biallelic *COL9A3* variants. **B** Audiograms of right ears of all affected individuals from three families. **C, D** Optical coherence tomography (OCT) imaging in proband II1 from family 1 showing retinal detachment

autosomal dominant non-ocular Stickler syndrome (type III, OMIM#184840), also known as otospondyloomegachondroplasia (OSMEDA, OMIM# 120290), as well as Weissenbacher-Zweymüller syndrome (WZS) (OMIM #184840) [11]. Biallelic variants in *LOXL3*, a member of the lysyl oxidase family of genes, have recently been causally associated with STL in two unrelated families [2, 12]. A biallelic missense variant in *LRP2* has likewise been suggested to cause STL [3].

Collagen IX proteins are encoded by *COL9A1*, *COL9A2* and *COL9A3* that together form fibril heterotrimer associated collagens and have been recently linked to autosomal recessive STL [13]. Very recently, heterozygous *COL9A3* variants have been identified as causing peripheral vitreoretinal degeneration and retinal detachment [14]. *COL9A1* and *COL9A2* are causally associated with autosomal recessive STL type IV (OMIM #614134) and V (OMIM #61484), respectively. The main clinical characteristics of individuals affected with biallelic *COL9A1* variants include moderate-to-severe sensorineural hearing loss, moderate-to-high myopia with vitreoretinopathy, and epiphyseal dysplasia, whereas *COL9A2* variants are associated with high myopia, vitreoretinal degeneration, retinal detachment, hearing loss, and short stature. Only very recently, biallelic mutations in *COL9A3* have been described to cause autosomal recessive STL in four unrelated families with seven patients. The main

phenotypes that are common in all these patients consisted of high myopia, moderate to severe sensorineural hearing loss, and spondylo/epiphyseal dysplasia. Here, we report three additional unrelated consanguineous STL families with five affected individuals in total who each present three novel biallelic *COL9A3* variants.

Results

Clinical assessments

Three unrelated consanguineous families of Iranian descent were referred for genetic testing due to hearing and vision impairment (Fig. 1), as well as skeletal dysplasia that resulted in a clinical diagnosis of STL (Fig. 2).

The female proband (II1) from Family 1 is the oldest and only affected individual out of three children from first cousin parents. She had a normal delivery and birth, with a birth weight of 3.2 kg (-0.43 SD). She was 28 years old at last examination with a weight of 64 kg ($+0.41$ SD), height of 157 cm (-0.8 SD) and occipitofrontal circumference (OFC) of 55 cm ($+0.62$ SD). She suffers from high myopia in both eyes, in addition to vitreoretinal degeneration with empty vitreous, multiple lattice degenerations and retinal pigmentary changes. There was unilateral absence of the frontal sinus in her skull X-ray. She has severe and progressive sensorineural hearing loss. X-ray and detailed examination of her joints and bones, including mobility testing

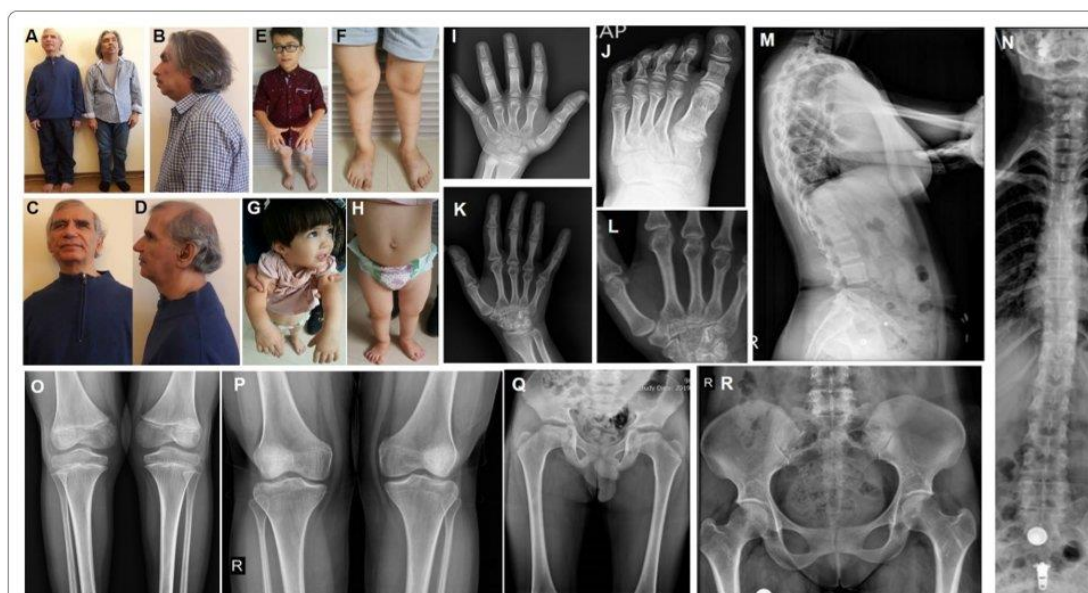


Fig. 2 Pictures of four affected individuals and standard radiographs of the spine, pelvis and limbs of two patients. **A–D** Pictures of two affected individuals from family 2 who both have herniated cervical discs. **E, F** Pictures of affected individual III1 from family 3 showing short stature, pes planus, bowed tibia, genu valga and rotated distal femora distal femur. **G, H** Clinical appearance of proband III1 from family 1 showing pes planus, mild midface hypoplasia, upturned nose and low set ears. **I, J** Hand and foot radiographs showing short metacarpalia and a broad big toe for individual III1 from family 3 at the age of 10 years. **K, L** Radiograph images of the right hand and wrist joint of individual III1 from family 1 at the age of 28 years, showing short metacarpalia with widened epiphyses and an irregular radius epiphysis. **M, N** Radiographs of the spine of III1 from family 1, showing mild platyspondyly of the thoracic spine as well as signs of ankylosing spondylitis. **O** Knee radiograph of proband III1 from family 3 showing genua valga and irregular femur epiphyses. **P** Knee radiograph of proband III1 from family 1 demonstrating genua valga and widened femur epiphyses. **Q** Pelvis radiograph individual III1 of from family 3 showing a flat acetabular roof with irregularities and flattened capiti femori, as well as broadened and shortened necks. **R** Radiograph of the pelvis of individual III1 from family 1 showing a relatively narrow intraarticular space but well developed capiti femori and no flattening of the acetabular roof

and examination for signs of osteoarthritis were normal, however she complained of pain in her knee joints. Typical STL craniofacial features such as midface hypoplasia, cleft palate, micrognathia, depressed nasal bridge and anteverted nares are absent.

Family 2 presented with two affected individuals out of four children who were born from a first cousin marriage. The proband (III1) and his affected sibling (II2) both had a normal delivery around term, measurements at birth could not be obtained. Weight, height and OFC at last clinical assessment (at 65 and 57 years-old) were 68 kg (−0.16 SD) and 66 kg (−0.39 SD), 166 cm (−1.4 SD) and 163 cm (−1.8 SD), 56 cm (+0.62 SD) and 57 cm (+1.32 SD), respectively. Both had a history of multiple vitreoretinal surgeries due to recurrent rhegmatogenous retinal detachments resulting from advanced vitreoretinal degeneration. Despite vitreoretinal surgeries, the older patient is considered blind without light perception (NLP) in either eye while his sibling has counting finger vision for one eye while NLP was noted for the other eye.

Both suffer from severe and progressive sensorineural hearing loss. Likewise, both show a herniated cervical disc and muscular atrophy was noted in the older sibling. No radiologic documentation was available for review.

Family 3 presented with two affected and two healthy children from first cousin parents. Both affected individuals had normal delivery with a birth weight of 3.4 kg (−0.26 SD) and 3.75 kg (+0.71 SD), length of 49 cm (−0.6 SD) and 49.5 cm (0.1 SD), and OFC of 35 cm (−0.40 SD) and 36 cm (+0.62 SD). The most current weight, height and OFC measurements for the proband (III1) at age 11.8 years and his sister (II4) at age 3.1 years are 32 kg (−1.43 SD), 137 cm (0.9 SD), and 53 cm (−0.53 SD) and 12 kg (−0.05 SD), 84 cm (−0.6 SD), and 48 cm (+0.39 SD), respectively. Both affected individuals have myopia and congenital moderate to severe progressive sensorineural hearing impairment. The affected male complains of knee joint pain, especially when he runs. X-ray and detailed examination demonstrated spondyloepiphyseal dysplasia in both children. Both individuals

Table 1 Summary of genetic and clinical findings in probands with biallelic *COL9A3* variants

	p.(Pro36Argfs*49) Family 1	p.(Arg402*) Family 2, Patient 1	p.(Arg402*) Family 2, Patient 2	p. (Leu119Serfs*10) Family 3, Patient 1	p. (Leu119Serfs*10) Family 3, Patient 2	p.(Gln393Cysfs*25) Faletra et al. [15] Patient 1
Ethnicity	Iranian	Iranian	Iranian	Iranian	Iranian	Moroccan
Consanguinity	First cousin	First cousin	First cousin	First cousin	First cousin	First cousin
Sex	Female	Male	Male	Male	Female	Female
Age in years	28	65	57	11 years, 8 months	3 years, 1 month	4
Birth	Uncomplicated (normal delivery)	Uncomplicated (normal delivery)	Uncomplicated (normal delivery)	Uncomplicated	Uncomplicated	NA
<i>Measurements</i>						
OFC at last examination	55 cm (+0.62 SD)	56 cm (+0.62 SD)	57 cm (+1.32 SD)	53 cm (−0.53 SD)	48 cm (+0.39 SD)	NA
Weight at last evaluation	64 kg (+0.41 SD)	68 kg (−0.16 SD)	66 kg (−0.39 SD)	32 kg (−1.43 SD)	12 kg (−0.05 SD)	16 kg
Height at last examination	157 cm (−0.8 SD)	166 cm (−1.4 SD)	163 cm (−1.8 SD)	137 cm (0.9 SD)	84 cm (−0.6 SD)	107 cm
Myopia	Moderate-to-high	High	High	High	High	Moderate-to-high
Vitreoretinal degeneration	No	Yes	Yes	No	No	No
Cataract	No	Yes	Yes	No	No	No
Retinal detachment	No	Yes	Yes	No	No	No
<i>Auditory system</i>						
Hearing loss	Yes	Yes	Yes	Yes	Yes	Yes
Age at onset	NA	NA	NA	Early onset	Early onset	Early onset
Type	Sensorineural	Sensorineural	Sensorineural	Sensorineural	Sensorineural	Sensorineural
Degree of hearing loss	Severe	Profound	Profound	Moderate-to-severe	Moderate-to-severe	Moderate-to-severe
Progressive/stable	Progressive	Progressive	Progressive	Progressive	Progressive	Progressive
<i>Joints</i>						
Short stature	No	No	No	No	No	No
Spondyloepiphyseal dysplasia	No	No	No	Yes	Yes	No
Epiphyseal dysplasia	No	No	No	Yes	Yes	Yes
<i>Craniofacial structures</i>						
Midface hypoplasia	No	No	No	No	Yes	Yes
Cleft palate	No	No	No	No	No	No
	p. (Gln393Cysfs*25) Faletra et al. [15] Patient 2	p. (Gln393Cysfs*25) Faletra et al. [15] Patient 3	p. (Pro218Alafs*49) Hanson-Kahn et al. [16]	p.(Arg471Ter) Nixon et al. [13] Patient 1	p.(Arg471Ter) Nixon et al. [13] Patient 2	p.(Arg90Ter) and p.(Arg577Ter) Markova et al. [19]
Ethnicity	Moroccan	Moroccan	Indian	NA	NA	Russian
Consanguinity	First cousin	First cousin	Third cousin	NA	NA	No
Sex	Male	Male	NA	NA	NA	Male
Age in years	11	16	12	18	20	
Birth	NA	NA	Uncomplicated (Caesarean section)	NA	NA	At term
<i>Measurements</i>						
OFC at last examination	NA	NA	NA	NA	NA	NA
Weight at last evaluation	38 kg	60 kg	NA	NA	NA	13 kg (50th %ile)

Table 1 (continued)

	p. (Gln393Cysfs*25) Faletra et al. [15] Patient 2	p. (Gln393Cysfs*25) Faletra et al. [15] Patient 3	p. (Pro218Alafs*49) Hanson-Kahn et al. [16]	p.(Arg471Ter) Nixon et al. [13] Patient 1	p.(Arg471Ter) Nixon et al. [13] Patient 2	p.(Arg90Ter) and p.(Arg577Ter) Markova et al. [19]
Height at last examination	144 cm	170 cm	NA	NA	NA	88 cm (25–50th %ile)
Myopia	Moderate-to-high	Moderate-to-high	High	High	High	High
Vitreoretinal degeneration	No	No	No	No	No	Yes
Cataract	No	No	No	No	No	No
Retinal detachment	No	No	No	No	No	No
<i>Auditory system</i>						
Hearing loss	Yes	Yes	Yes	Yes	Yes	Yes
Age at onset	NA	NA	Early onset	NA	NA	Yes
Type	Sensorineural	Sensorineural	Sensorineural	Sensorineural	Sensorineural	Senorineural
Degree of hearing loss	Moderate-to-severe	Moderate-to-severe	Moderate-to-severe	Severe	Severe	Severe
Progressive/stable	Progressive	Progressive	Stable	Progressive	Progressive	NA
<i>Joints</i>						
Short stature	No	No	No	No	No	No
Spondyloepiphyseal dysplasia	No	No	No	No	No	Yes
Epiphyseal dysplasia	Yes	Yes	Yes	NA	NA	Yes
<i>Craniofacial structures</i>						
Midface hypoplasia	Yes	Yes	Yes	No	No	Yes
Cleft palate	No	No	No	No	No	No

NA not ascertained, OFC occipitofrontal circumference, SD standard deviation

III and II4 have pes planus, depressed nasal bridge and anteverted nares, with midface hypoplasia and downslanting palpebral fissures more pronounced in II4. Detailed clinical features of all affected individuals are described in Table 1 and Additional file 1: Table S1. None of the individuals showed signs of intellectual disability.

Genetic analysis

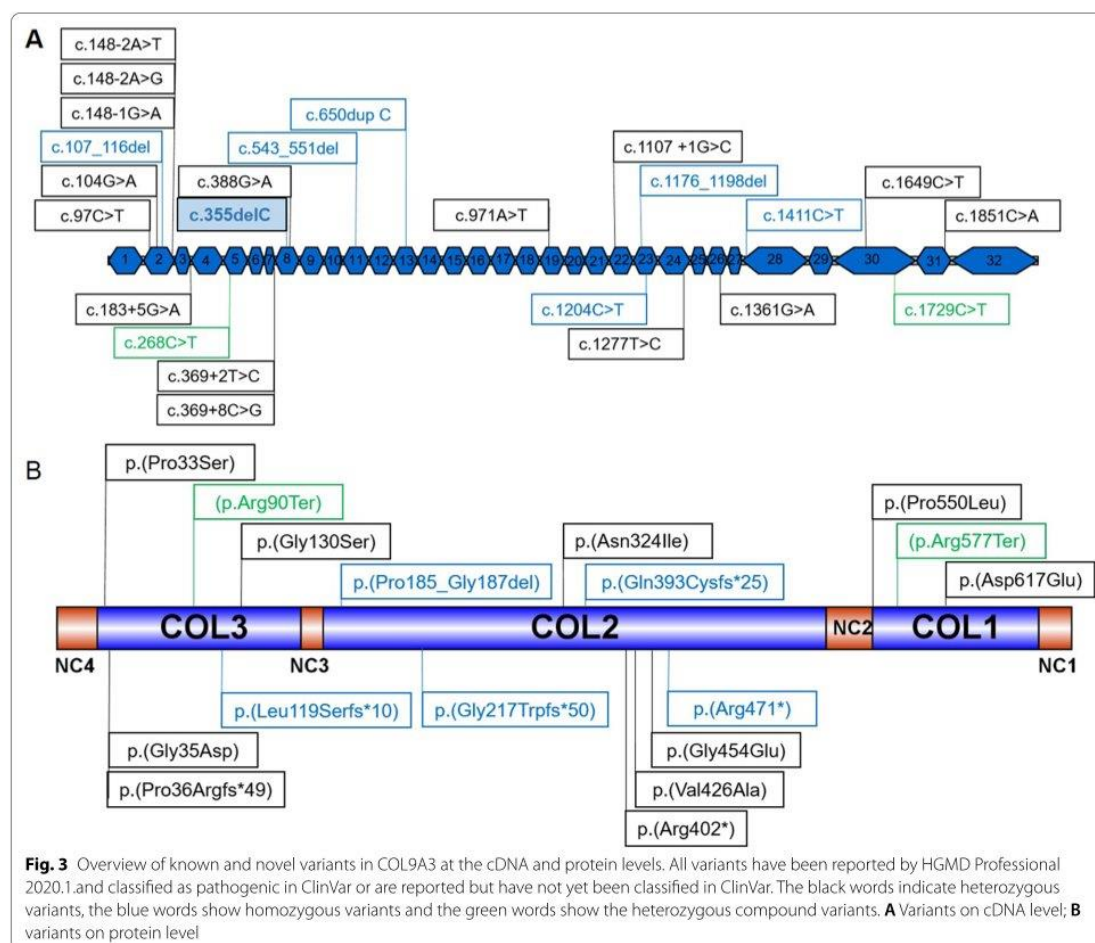
The DNA of probands from the three unrelated families (family 1 Proband II1, family 2 proband III1, family 3 proband II1) was subjected to Exome Sequencing (ES), revealing three different novel, homozygous loss of function (LOF) variants in *COL9A3*, NM_001853.3. The proband in Family 1 was found to have a *COL9A3* deletion (c.107_116del, p.(Pro36Argfs*49), rs1470627424), causing a frameshift in exon 2. The allele frequency in gnomAD is 0.00001390 with two carriers, while other public genomic databases such as Iranome and GME, and 1000 genomes have not reported this variant. The proband in family 2 disclosed a *COL9A3* nonsense variant (c.1204C>T, p.(Arg402*), rs989413835) in exon 23, while the proband in Family 3 showed a one base pair deletion in *COL9A3* [c.355delC, p.(Leu119Serfs*9)] in

exon 7. Both variants have not been reported in public databases.

Discussion

Here, we report three families with five affected individuals clinically diagnosed with autosomal recessive STL due to biallelic LOF variants in *COL9A3*. Our report reaffirms previous studies that have described four families with biallelic LOF causing autosomal recessive STL, increasing the total number of families reported to date to seven [13, 15, 16]. These *COL9A3* variants as well as other disease causing *COL9A3* variants submitted to HGMD are visualized in Fig. 3 for localization on cDNA as well as on protein level.

COL9A3, along with two other heterodimers (*COL9A1* and *COL9A2*), belongs to the collagen IX complex, forming a fibril-associated collagen with interrupted triple (FACIT) helices and connecting with collagen II and XI fibrils. A *Col9a1* knockout mouse study previously demonstrated that absence of this protein in mice results in the loss of the entire collagen IX heterotrimer complex [17]. Recent reports on the clinical phenotype of STL and MED syndromes that are caused by variants affecting



different members of collagen IX have supported the hypothesis that each of the three proteins is essential for collagen IX function [13, 18].

While a variety of disorders have been described to result from heterozygous pathogenic variants in *COL9A3*, only four unrelated STL families and one family with nonsyndromic hearing loss have been reported to date carrying biallelic variants (Table 2). Allelic disorders resulting from *COL9A3* variants include nonsyndromic hearing loss, MED, pseudoachondroplasia, cerebral palsy, and lumbar disc disease and severe peripheral vitreoretinal degeneration and retinal detachment (Table 2).

Consistent clinical features among STL patients with biallelic *COL9A3* LOF alleles comprise moderate-to-profound progressive sensorineural hearing loss and moderate high myopia with vitreoretinal degeneration. Retinal detachment and cataract occur occasionally. In

contrast, skeletal involvement seems to be more variable. For instance, Nixon et al. [13] reported a family with two affected siblings where the oldest affected sibling had severe arthropathy in the shoulders and hip, requiring a wheelchair. The X-ray of this patient showed spinal scoliosis and narrowing of the articular space in both knees, while the younger affected sibling did not show any of these signs. In line with this report, we also observed that the affected individuals in family 2, at the ages of 65 and 57 years-old, suffer only from myopia, hearing loss and each have a herniated cervical disc while the two much younger affected individuals in family 3, at ages 3 and 11 years-old, have more prominent skeletal findings that include radiological signs of spondyloepiphyseal dysplasia as well as craniofacial abnormalities including depressed nasal bridge and anteverted nares (Table 1). Moreover, Nixon et al. [13] observed that carrier parents

Table 2 Pathogenic *COL9A3* variants reported in HGMD and associated clinical phenotypes

c.DNA position	Protein position	Exon/intron	Description	Zygoty	dbSNP	ClinVar	Reported phenotype	References
–	–		99 bp duplication (CNV)	Het	NA	NA	Sensorineural hearing loss	Ji (2014) BMC Ear Nose Throat Disord 14,9
c.97C>T	p.(Pro33Ser)	2	Missense	Het	rs745914662	NA	Cerebral palsy	Pingel (2019) Am J Med Genet B Neuropsychiatr Genet 180,12
c.104G>A	p.(Gly35Asp)	2	Missense	Het	rs1390736361	NA	Multiple epiphyseal dysplasia	Jeong (2014) BMC Musculoskelet Disord 15,371
c.148-1G>A	p.?	2	Splicing	Het	rs606231367	NA	Multiple epiphyseal dysplasia	Lohiniva (2000) Am J Med Genet 90,216
c.148-2A>G	p.?	2	Splicing	Het	NA	NA	Multiple epiphyseal dysplasia	Jackson (2012) Hum Mutat 33,144
c.148-2A>T	p.?	2	Splicing	Het	NA	P	Multiple epiphyseal dysplasia	Paasilta (1999) Am J Hum Genet 64,1036
c.183+5G>A	p.?	3	Splicing	Het	NA	P	Multiple epiphyseal dysplasia	Nakashima (2005) Am J Med Genet 132A,181
c.268C>T	p.(Arg90Ter)	5	Nonsense	Comp het	rs763259234	NA	Stickler syndrome	Markova (2021) Mol Genet Genomic Med
c.369+2T>C	p.?	7	Splicing	Het	rs1057518693	P	Multiple epiphyseal dysplasia	Posey (2017) N Engl J Med 376,21
c.369+8C>G	p.?	7	Splicing	Het	NA	NA	Multiple epiphyseal dysplasia	Lord (2019) Genome Res 29,159
c.388G>A	p.(Gly130Ser)	8	Missense	Het	rs139401633	VUS	Severe peripheral vitreoretinal degeneration and retinal detachment	M. Nash (2021) European Journal of Human Genetics
c.543_551del	p.(Pro185_Gly187del)	11	In frame	Hom	rs765392378	NA	Nonsyndromic hearing loss	Asamura (2005) Auris Nasus Larynx 32,113
c.650dup C	p.(Gly217Trp-fster50)	13	Frameshift	Hom	NA	NA	Stickler syndrome	Hanson-Kahn (2018) Am J Med Genet A 176,2887
c.971A>T	p.(Asn324Ile)	19	Missense	Het	NA	NA	Pseudoachondroplasia	Jung (2010) Int J Mol Med 26,885
c.1107+1G>C	p.?	21	Splicing	Het			Severe peripheral vitreoretinal degeneration and retinal detachment	M. Nash (2021) European Journal of Human Genetics
c.1176_1198del	p.(Gln393Cyste*25)	23	Frameshift	Hom	rs606231470	VUS	Stickler syndrome	Faletta (2014) Am J Med Genet A 164,42
c.1277T>C	p.(Val426Ala)	24	Missense	Het	NA	NA	Pseudoachondroplasia	Jung (2010) Int J Mol Med 26,885
c.1361G>A	p.(Gly454Glu)	26	Missense	Het	NA	NA	Nonsyndromic hearing loss	Miyagawa (2013) PLoS One 8,e71381
c.1411C>T	p.(Arg471ter)	28	Nonsense	Hom	rs747896279	P	Stickler syndrome	Nixon (2019) Am J Med Genet A 179,1498
c.1649C>T	p.(Pro550Leu)	30	Missense	Het	rs535230112	NA	Nonsyndromic hearing loss	Miyagawa (2013) PLoS One 8, e71381
c.1729C>T	p.(Arg577Ter)	30	Nonsense	Comp het	rs1201247953	NA	Stickler syndrome	Markova (2021) Mol Genet Genomic Med
c.1851C>A	p.(Asp617Glu)	31	Missense	Het	rs199577452	NA	Nonsyndromic hearing loss	Asamura N Auris Nasus Larynx 32,113

All variants are reported using the NM_001853.3 transcript

Comp het compound heterozygous, Het heterozygous, Hom homozygous, P pathogenic, VUS variant of uncertain significance, NA not ascertained

can manifest mild STL phenotypes, while our report and others [15, 16, 19] have not observed mild phenotypes in heterozygous individuals. Besides Nixon's report, Markova et al. [19] introduced a more severe case with compound heterozygous variants with vitreoretinal degeneration, early onset osteoarthritis, midface hypoplasia, hip dysplasia, speech developmental delay, spina bifida, kyphosis, and eye pigment rearrangement.

Conclusion

In summary, our report consolidates that homozygous loss of function variants in *COL9A3* cause STL (type VI). We find high myopia and moderate-severe hearing loss to be consistent features amongst all cases while skeletal findings seem more variable.

Material and methods

Subjects

Three unrelated Iranian families with syndromic phenotypes including hearing loss, vision impairment and skeletal dysplasia were referred for clinical genetic diagnostics. Blood samples were collected after obtaining informed consent from patients or their parents. Molecular genetic diagnostic testing was performed in Nijmegen via the Radboud innovative diagnostics programme and at the University of Tuebingen (197/2019BO01). Informed consent from the parents or legal guardians of the patients/participants was obtained for the publication of their data.

Exome and Sanger sequencing

After extraction of DNAs from whole blood by standard protocol, proband DNA samples were subjected to exome capture using the Agilent SureSelect Human All Exon V6 Kit and exome sequencing (ES) was performed on an Illumina HiSeq 2500 sequencer for an average 50 × sequencing depth, resulting in sequences of greater than 100 bases from each end of the fragments [Cambridge (Novogene UK)]. Exome data were processed for analysis using a GATK-based pipeline [20] that uses Burrows-Wheeler alignment [21] to the GRCh37/UCSC hg19 (Families 1 and 2) and GRCh38/UCSC hg38 (Family 3). VarScan version 2.2.5, MuTec and GATK Somatic Indel Detector were used to detect SNV and InDels, respectively. The protocol to interpret potential pathogenic variants was previously described [22]. For population-specific filtering, gnomAD [23], Iranome [24] and Greater Middle East (GME) Variome Project [25] databases were used.

Segregation analysis using Sanger sequencing was performed in available family members to confirm variant segregation after PCR amplification. Primers are available upon request.

Web resources

ClinVar, <https://www.ncbi.nlm.nih.gov/clinvar/>.

Exome Aggregation Consortium (ExAC), <http://exac.broadinstitute.org>.

Genome Aggregation Database (*gnomAD*), <http://gnomad.broadinstitute.org/>.

Abbreviations

DNA: Deoxyribonucleic acid; ES: Exome sequencing; FACIT: Fibril-associated collagen with interrupted triple helices; GATK: Genome Analysis Toolkit; GME: Greater Middle East; LOF: Loss of function; MED: Multiple Epiphyseal Dysplasia; OFC: Occipitofrontal circumference; PCR: Polymerase Chain Reaction; SD: Standard deviation; SNV: Single Nucleotide Variant; STL: Stickler syndrome.

Supplementary Information

The online version contains supplementary material available at <https://doi.org/10.1186/s13023-022-02244-6>.

Additional file 1. Table S1: Clinical features of probands affected by *COL9A3* variants.

Acknowledgements

The authors thank the families for their participation in this study.

Authors' contributions

FS, RM, EGK, ND, MD, AM, HA, HS, MR and NH recruited the probands and/or were involved in their clinical care. AR, MN, SL and DM conducted genetic data analysis. AR, MN, BV and MS conceived the study. AR, MN, BV and MS drafted the manuscript. BV and MS supervised the study. All authors read and approved the final version of the manuscript.

Funding

Open Access funding enabled and organized by Projekt DEAL. This research was supported by Intramural Funding (*fortune*) at the University of Tübingen (2545-1-0 to B.V.) and the Ministry of Science, Research and Art Baden-Württemberg (to B.V.). MS acknowledges funding from the European Research Council (ERC): ERC starting grant TREATCilia (Grant Agreement No. 716344) and funding from the Deutsche Forschungsgemeinschaft (DFG, German Research Foundation)—Project-ID 431984000—SFB 1453 (CRC Nephgen).

Availability of data and materials

Data can be made available on personal request. Variants reported in this study have been deposited in the Leiden Open Variation Database (LOVD) and are available through the following variant accession numbers: 0000364418, 0000364419 and 0000364420.

Declarations

Ethics approval and consent to participate

Molecular genetic diagnostic testing was performed in Nijmegen via the Radboud innovative diagnostics programme and at the University of Tuebingen (197/2019BO01).

Consent for publication

Informed consent from the parents or legal guardians of the patients/participants was obtained for the publication of their data.

Competing interests

The authors declare no competing interests.

Author details

¹Department of Otolaryngology, Head and Neck Surgery, Tübingen Hearing Research Centre, Eberhard Karls University, 72076 Tübingen, Germany. ²Genome Research Division, Human Genetics Department, Radboud University Medical Center, Geert Grooteplein Zuid 10, Nijmegen, The Netherlands. ³Pediatric Genetics Division, Center for Pediatrics and Adolescent Medicine, University Hospital Freiburg, Freiburg University Faculty of Medicine, Mathildenstrasse 1, 79106 Freiburg, Germany. ⁴Ophthalmic Research Center, Research Institute for Ophthalmology and Vision Science, Shahid Beheshti University of Medical Sciences, Tehran, Iran. ⁵Department of Medical Genetics and Molecular Medicine, School of Medicine, Mashhad University of Medical Science, Mashhad, Iran. ⁶Department of Molecular Genetics, Next Generation Genetic Polyclinic, Mashhad, Iran. ⁷Ocular Tissue Engineering Research Center, Research Institute for Ophthalmology and Vision Science, Shahid Beheshti University of Medical Sciences, Tehran, Iran. ⁸Ophthalmic Epidemiology Research Center, Research Institute for Ophthalmology and Vision Science, Shahid Beheshti University of Medical Sciences, Tehran, Iran. ⁹Department of Otorhinolaryngology, School of Medicine, Ghaem Hospital, Sinus and Surgical Endoscopic Research Center, Mashhad University of Medical Sciences, Mashhad, Iran. ¹⁰Department of Pediatric Neurology, Faculty of Medicine, Mashhad University of Medical Sciences, Mashhad, Iran. ¹¹Present Address: Institute of Human Genetics, University Medical Center Göttingen, Göttingen, Germany. ¹²Present Address: Institute for Auditory Neuroscience and InnerEar Lab, University Medical Center Göttingen, Göttingen, Germany. ¹³CIBSS - Centre for Integrative Biological Signalling Studies, University of Freiburg, 79104 Freiburg, Germany.

Received: 15 May 2021 Accepted: 10 February 2022

Published online: 03 March 2022

References

- Robin NH, Moran RT, Ala-Kokko L. Stickler syndrome. *GeneReviews* [Internet]. University of Washington, Seattle; 2021.
- Alzahrani F, Al Hazzaa SA, Tayeb H, Alkuraya FS. LOXL3, encoding lysyl oxidase-like 3, is mutated in a family with autosomal recessive Stickler syndrome. *Hum Genet.* 2015;134(4):451–3.
- Schrauwen I, Sommen M, Claes C, Pinner J, Flaherty M, Collins F, et al. Broadening the phenotype of LRP2 mutations: a new mutation in LRP2 causes a predominantly ocular phenotype suggestive of Stickler syndrome. *Clin Genet.* 2014;86(3):282–6.
- Kadler KE, Hill A, Canty-Laird EG. Collagen fibrillogenesis: fibronectin, integrins, and minor collagens as organizers and nucleators. *Curr Opin Cell Biol.* 2008;20(5):495–501.
- Liberfarb RM, Levy HP, Rose PS, Wilkin DJ, Davis J, Balog JZ, et al. The Stickler syndrome: genotype/phenotype correlation in 10 families with Stickler syndrome resulting from seven mutations in the type II collagen gene locus COL2A1. *Genet Med.* 2003;5(1):21–7.
- Hoornaert KP, Vereecke I, Dewinter C, Rosenberg T, Beemer FA, Leroy JG, et al. Stickler syndrome caused by COL2A1 mutations: genotype–phenotype correlation in a series of 100 patients. *Eur J Hum Genet.* 2010;18(8):872–80.
- Majava M, Hoornaert KP, Bartholdi D, Bouma MC, Bouman K, Carrera M, et al. A report on 10 new patients with heterozygous mutations in the COL11A1 gene and a review of genotype–phenotype correlations in type XI collagenopathies. *Am J Med Genet A.* 2007;143(3):258–64.
- Alzahrani F, Alshammari MJ, Alkuraya FS. Molecular pathogenesis of fibrochondrogenesis: is it really simple COL11A1 deficiency? *Gene.* 2012;511(2):480.
- Richards AJ, Fincham GS, McNinch A, Hill D, Poulson AV, Castle B, et al. Alternative splicing modifies the effect of mutations in COL11A1 and results in recessive type 2 Stickler syndrome with profound hearing loss. *J Med Genet.* 2013;50(11):765–71.
- Nixon T, Richards AJ, Lomas A, Abbs S, Vasudevan P, McNinch A, et al. Inherited and de novo biallelic pathogenic variants in COL11A1 result in type 2 Stickler syndrome with severe hearing loss. *Mol Genet Genom Med.* 2020;8:e1354.
- Vuoristo MM, Pappas JG, Jansen V, Ala-Kokko L. A stop codon mutation in COL11A2 induces exon skipping and leads to non-ocular Stickler syndrome. *Am J Med Genet A.* 2004;130(2):160–4.
- Chan TK, Alkaabi MK, ElBarky AM, El-Hattab AW. LOXL3 novel mutation causing a rare form of autosomal recessive Stickler syndrome. *Clin Genet.* 2019;95(2):325–8.
- Nixon TR, Alexander P, Richards A, McNinch A, Bearcroft PW, Cobben J, et al. Homozygous Type IX collagen variants (COL9A1, COL9A2, and COL9A3) causing recessive Stickler syndrome—expanding the phenotype. *Am J Med Genet A.* 2019;179(8):1498–506.
- Nash BM, Watson CJG, Hughes E, Hou AL, Loi TH, Bennetts B, et al. Heterozygous COL9A3 variants cause severe peripheral vitreoretinal degeneration and retinal detachment. *Eur J Hum Genet.* 2021;29(5):881–6.
- Faletta F, D'Adamo AP, Bruno I, Athanasakis E, Biskup S, Esposito L, et al. Autosomal recessive Stickler syndrome due to a loss of function mutation in the COL9A3 gene. *Am J Med Genet A.* 2014;164(1):42–7.
- Hanson-Kahn A, Li B, Cohn DH, Nickerson DA, Bamshad MJ, Genomics UoWCFM, et al. Autosomal recessive Stickler syndrome resulting from a COL9A3 mutation. *Am J Med Genet Part A.* 2018;176(12):2887–91.
- Hagg R, Hedborn E, Möllers U, Aszódi A, Fässler R, Bruckner P. Absence of the $\alpha 1$ (IX) chain leads to a functional knock-out of the entire collagen IX protein in mice. *J Biol Chem.* 1997;272(33):20650–4.
- Jackson GC, Marcus-Soekarman D, Stolte-Dijkstra I, Verrips A, Taylor JA, Briggs MD. Type IX collagen gene mutations can result in multiple epiphyseal dysplasia that is associated with osteochondritis dissecans and a mild myopathy. *Am J Med Genet A.* 2010;152(4):863–9.
- Markova T, Sparber P, Borovikov A, Nagornova T, Dadali E. Clinical and genetic characterization of autosomal recessive stickler syndrome caused by novel compound heterozygous mutations in the COL9A3 gene. *Mol Genet Genom Med.* 2021;9:e1620.
- McKenna A, Hanna M, Banks E, Sivachenko A, Cibulskis K, Kernytzky A, et al. The genome analysis toolkit: a MapReduce framework for analyzing next-generation DNA sequencing data. *Genome Res.* 2010;20(9):1297–303.
- Li H, Durbin R. Fast and accurate long-read alignment with Burrows-Wheeler transform. *Bioinformatics.* 2010;26(5):589–95.
- Rad A, Altunoglu U, Miller R, Maroofian R, James KN, Çağlayan AO, et al. MAB21L1 loss of function causes a syndromic neurodevelopmental disorder with distinctive cerebellar, ocular, craniofacial and genital features (COFG syndrome). *J Med Genet.* 2019;56(5):332–9.
- Karczewski KJ, Francioli LC, Tiao G, Cummings BB, Alföldi J, Wang Q, et al. The mutational constraint spectrum quantified from variation in 141,456 humans. *Nature.* 2020;581(7809):434–43.
- Fattahi Z, Beheshtian M, Mohseni M, Poustchi H, Sellars E, Nezhadi SH, et al. Iranome: a catalog of genomic variations in the Iranian population. *Hum Mutat.* 2019;40(11):1968–84.
- Scott EM, Halees A, Itan Y, Spencer EG, He Y, Azab MA, et al. Characterization of Greater Middle Eastern genetic variation for enhanced disease gene discovery. *Nat Genet.* 2016;48(9):1071–6.

Publisher's Note

Springer Nature remains neutral with regard to jurisdictional claims in published maps and institutional affiliations.

Ready to submit your research? Choose BMC and benefit from:

- fast, convenient online submission
- thorough peer review by experienced researchers in your field
- rapid publication on acceptance
- support for research data, including large and complex data types
- gold Open Access which fosters wider collaboration and increased citations
- maximum visibility for your research: over 100M website views per year

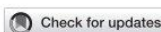
At BMC, research is always in progress.

Learn more biomedcentral.com/submissions



10.11 Attachment 11

Unraveling haplotype errors in the DFNA33 locus



OPEN ACCESS

EDITED BY

Trevor Lucas,
Medical University of Vienna, Austria

REVIEWED BY

Ammar Husami,
Cincinnati Children's Hospital Medical
Center, United States
Eliane Chouery,
Lebanese American University, Lebanon

*CORRESPONDENCE

Barbara Vona,
✉ barbara.vona@med.uni-goettingen.de
Katrin Neumann,
✉ katrin.neumann@uni-muenster.de

RECEIVED 02 May 2023

ACCEPTED 04 August 2023

PUBLISHED 21 August 2023

CITATION

Vona B, Regele S, Rad A, Strenzke N,
Pater JA, Neumann K, Sturm M, Haack TB
and Am Zehnhoff-Dinnesen AG (2023),
Unraveling haplotype errors in
the DFNA33 locus.
Front. Genet. 14:1214736.
doi: 10.3389/fgene.2023.1214736

COPYRIGHT

© 2023 Vona, Regele, Rad, Strenzke,
Pater, Neumann, Sturm, Haack and Am
Zehnhoff-Dinnesen. This is an open-
access article distributed under the terms
of the Creative Commons Attribution
License (CC BY). The use, distribution or
reproduction in other forums is
permitted, provided the original author(s)
and the copyright owner(s) are credited
and that the original publication in this
journal is cited, in accordance with
accepted academic practice. No use,
distribution or reproduction is permitted
which does not comply with these terms.

Unraveling haplotype errors in the DFNA33 locus

Barbara Vona^{1,2,3*}, Sabrina Regele⁴, Aboufazel Rad¹,
Nicola Strenzke⁵, Justin A. Pater^{6,7}, Katrin Neumann^{4*},
Marc Sturm⁸, Tobias B. Haack^{8,9} and
Antoinette G. Am Zehnhoff-Dinnesen⁴

¹Tübingen Hearing Research Centre, Department of Otolaryngology, Head and Neck Surgery, Eberhard Karls University Tübingen, Tübingen, Germany, ²Institute of Human Genetics, University Medical Center Göttingen, Göttingen, Germany, ³Institute for Auditory Neuroscience and InnerEarLab, University Medical Center Göttingen, Göttingen, Germany, ⁴Department of Phoniatrics and Pedaudiology, University Hospital Münster, University of Münster, Münster, Germany, ⁵Auditory Systems Physiology Group, Department of Otolaryngology and Institute for Auditory Neuroscience, University Medical Center Göttingen, Göttingen, Germany, ⁶Dana-Farber Cancer Institute, Harvard Medical School, Boston, MA, United States, ⁷Health Sciences Centre, Faculty of Medicine, Memorial University, St. John's, NL, Canada, ⁸Institute of Medical Genetics and Applied Genomics, University of Tübingen, Tübingen, Germany, ⁹Centre for Rare Diseases, University of Tübingen, Tübingen, Germany

Genetic heterogeneity makes it difficult to identify the causal genes for hearing loss. Studies from previous decades have mapped numerous genetic loci, providing critical supporting evidence for gene discovery studies. Despite widespread sequencing accessibility, many historically mapped loci remain without a causal gene. The DFNA33 locus was mapped in 2009 and coincidentally contains *ATP11A*, a gene recently associated with autosomal dominant hearing loss and auditory neuropathy type 2. In a rare opportunity, we genome-sequenced a member of the original family to determine whether the DFNA33 locus may also be assigned to *ATP11A*. We identified a deep intronic variant in *ATP11A* that showed evidence of functionally normal splicing. Furthermore, we re-assessed haplotypes from the originally published DFNA33 family and identified two double recombination events and one triple recombination event in the pedigree, a highly unlikely occurrence, especially at this scale. This brief research report also serves as a call to the community to revisit families who have previously been involved in gene mapping studies, provide closure, and resolve these historical loci.

KEYWORDS

ATP11A, DFNA33, genome sequencing, haplotype analysis, hereditary hearing loss, unresolved deafness loci

1 Introduction

Meiotic recombination (also called crossing over) underlies genomic diversity and maintains fidelity during chromosome segregation. Although each chromosome generally presents at least one crossover (Sun et al., 2005), the recombination rate is not fixed but rather influenced by intrinsic (for example, genetic background (Koehler et al., 2002)) and extrinsic (such as age and environment (Williamson et al., 1970; Rose and Baillie, 1979; Tanzi et al., 1992)) factors and has a non-uniform distribution, with evidence of recombination “hot” and “cold spots” (Kong et al., 2002). Furthermore, the recombination rate and chromosome size are strongly correlated, with smaller chromosomes having higher recombination rates (Sun et al., 2005; Farré et al., 2013). Recombination frequencies are a

measure of the genetic linkage and are essential for constructing linkage maps. Genes that are closer together have a greater chance of being inherited together due to a lower likelihood of undergoing fewer recombination events. Double crossovers are regarded as rare events, with the vast majority of double recombinations being the result of genotyping errors (Housworth and Stahl, 2003).

By definition, linkage is an occurrence in which adjacent genes tend to be inherited together (Wang et al., 2017). Linkage analysis requires genome-wide genotyping of families and is used to investigate how traits are segregated. Specifically, it can estimate whether phenotypes have a tendency to be inherited together, indicating the closeness of genes responsible for those traits in the genome. Linkage analysis of families segregating a Mendelian condition, such as autosomal dominant hearing impairment, aims to uncover few statistically significant linkage intervals, significantly reducing the number of candidate regions that are investigated in targeted sequencing. These studies have proven enormously successful for gene identification and have been re-defined and transformed in several ways, following the widespread emergence and application of disruptive high-throughput sequencing technologies (Teare and Santibañez Koref, 2014; Bamshad et al., 2019).

Hereditary hearing impairment is among the most genetically heterogeneous disorders observed in humans, making gene mapping and identification a comparatively enormous task (Wright et al., 2018). Family participation has been paramount to advancing the field. These families have been valuable for historical gene mapping efforts, following the uninformative screening of select known genes. The Hereditary Hearing Loss Homepage (<https://hereditaryhearingloss.org/>) has diligently documented mapped loci and regularly updates content with new genes as they are discovered. Despite the advent of widely accessible sequencing technologies, many of these families have been lost to follow up for a variety of reasons. As a result, it is a reasonable assumption that many of these loci will remain without a causal gene assigned. Furthermore, in spite of the success of mapping deafness loci and cost-effective genome sequencing technologies, the identification of causal genes is not always straightforward, even in families that are large and, therefore, informative by providing more information about meiotic recombination events. This is additionally reflected in the large number of families who have participated in historical linkage studies but remain without a causal gene identified. At least 20 autosomal dominant (DFNA) loci have been mapped (Hereditary Hearing Loss Homepage) that remain without a causal gene assigned. The majority of them were mapped before the widespread use of high-throughput sequencing. There are also several examples of independent investigators discovering the same gene under a pre-assigned DFN locus. For example, the DFNA20 and DFNA26 loci merged as DFNA20/26 when two teams discovered *ACTG1* as a gene responsible for autosomal dominant hearing loss for these asynchronously mapped loci (van Wijk et al., 2003; Zhu et al., 2003). Among the remaining loci with an unknown causal gene is DFNA33 that was published in 2009 through the ascertainment of a large, multi-generational German family, segregating progressive sensorineural non-syndromic hearing loss with a variable post-lingual onset (Bönsch et al., 2009). This brief research report describes follow-up genome sequencing analysis in light of the recent discovery of

ATP11A, a gene that is responsible for autosomal dominant non-syndromic hearing loss (DFNA84) (Pater et al., 2022) and auditory neuropathy (AUNA2) (Chepurwar et al., 2022), which coincidentally also overlaps with the DFNA33 genomic coordinates at chr13q34.

2 Methods

2.1 Participant recruitment and audiometry

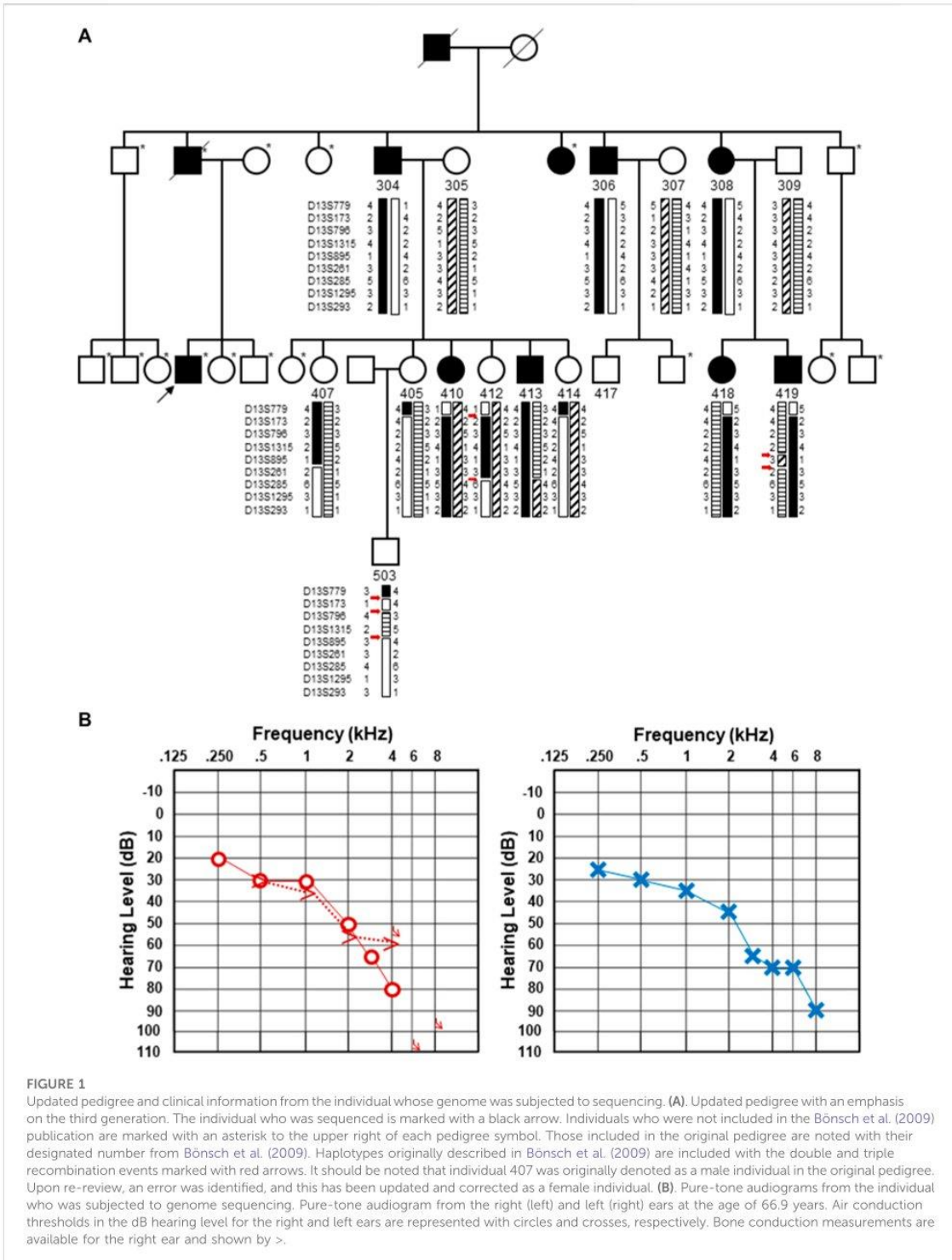
Through extensive re-recruitment efforts, an affected individual from the originally published DFNA33 family (Bönsch et al., 2009) was re-ascertained as part of a large diverse-population rare disease study (ethics commission approval number 197/2019BO1). The pedigree was re-evaluated and re-drawn.

The affected individual underwent a complete ear, nose, and throat examination that included binocular ear microscopy and external ear inspection. Pure-tone audiometry was performed according to current standards to determine hearing thresholds at routinely measured frequencies (0.25, 0.5, 1, 2, 4, 6, and 8 kHz). Both air and bone conduction thresholds were measured. Tympanometry was performed to measure tympanic membrane compliance and middle ear pressure.

2.2 Whole-genome sequencing, bioinformatics filtering, and variant classification

Whole genome sequencing was performed on genomic DNA extracted from peripheral blood using standard protocols, as previously described (Weisschuh et al., 2020). The sequencing library was prepared with the TruSeq DNA PCR-free protocol (Illumina, San Diego, USA) for subsequent sequencing as 2×150 bp paired-end reads on a NovaSeq 6000 platform (Illumina, San Diego, USA). Bioinformatic processing of raw read data, annotation, and variant calling was performed using the megSAP pipeline (<https://github.com/imgag/megSAP>) developed at the Institute of Medical Genetics and Applied Genomics, University Hospital Tübingen, Germany, and includes an in-house genome database called the NGS Database (NGSD), which consists data on more than 3,000 individuals to ascertain sequencing artifacts and variant frequencies. Visualization was performed using the Integrative Genomics Viewer.

Bioinformatics filters were used to support the analysis of variants, following autosomal dominant and recessive modes of inheritance, as described previously (Falb et al., 2023). This included analysis of sequence variants and copy number variations in 298 known hearing loss-associated genes (Supplementary Table S1). Allele-based filters selecting variants with an allele frequency (including sub-populations) $\leq 1\%$, variants present in ≤ 20 other individuals in NGSD, and those previously annotated as pathogenic/likely pathogenic in HGMD and ClinVar yielded a short list of heterozygous variants in these hearing loss-associated genes. Minor allele frequencies were derived from gnomAD, 1000 Genomes Project, ExAC, dbSNP, and NGSD. The Alamut Visual (Interactive Biosoftware, SOPHiA GENETICS, Rouen, France)



splice window that includes splice predictions from SpliceSiteFinder-like, MaxEntScan, NNSPLICE, GeneSplicer, and ESEfinder, as well as RESCUE-ESE predictors, was used to assess the effect of variants on splicing.

Variant classification applied the American College of Medical Genetics and Genomics (ACMG) guidelines that are adapted for hereditary hearing loss (Oza et al., 2018) and referenced the Deafness Variation Database (Azaiez et al., 2018). The classification was assisted through the use of the public version of Varsome (Kopanov et al., 2019).

2.3 *In vitro* splicing analysis

A region spanning *ATP11A* exons 8 to 10 was PCR-amplified from the genomic DNA of the patient and a healthy control using gene-specific primers with a *XhoI* restriction site (*ATP11A* Ex8-10 forward: 5'-aattctcgagAAAATCACCGAAGCCATGAG-3') and a *Bam*HI restriction site (*ATP11A* Ex8-10 reverse: 5'-attggatccATGGTGAGAGGAGCTGTTGG-3'). The 5,014-bp amplicon was ligated into a multiple cloning site between native exons A and B in a linearized pSPL3 exon-trapping vector. The vector was transformed into DH5 α competent cells (NEB 5-alpha, New England Biolabs) and plated overnight. The wild-type and mutant-containing vector sequences were confirmed by Sanger sequencing and transfected into HEK 293T cells using the FuGENE Transfection Reagent (Promega). Total RNA was prepared from 24-h post-transfected cells using an miRNeasy Mini Kit (QIAGEN), and reverse transcription was carried out using a High-Capacity RNA-to-cDNA Kit (Applied Biosystems). Amplified fragments were visualized on 1.5% agarose gel and, subsequently, Sanger sequenced.

3 Results

3.1 Audiological characterization

The affected individual, who was not in the original DFNA33 report, is a direct descendent of a hearing-impaired father who had four affected siblings, three of whom were previously described (Bönsch et al., 2009) (Figure 1A). The individual reported progressive, high-frequency sensorineural hearing impairment without subjective vertigo and tinnitus. The individual's thresholds mirror the average thresholds of individuals previously described in their family (Bönsch et al., 2009) up to 2 kHz, where the individual shows steeply increasing thresholds to severe-to-profound hearing loss at 8 kHz in the left ear and no thresholds at 6 and 8 kHz in the right ear. An audiogram at the age of 66.9 years is shown in Figure 1B. A tympanogram showed normal bilateral results with regular tympanic membrane compliance. Upon comparison of the audiogram with the hearing of men in the same age group (ISO, 2017), the hearing thresholds at all measured frequencies were found to be significantly lower than the expected hearing threshold for this age group.

3.2 Genome sequencing, bioinformatics analysis, and the *in vitro* splicing assay of a deep intronic variant

Whole-genome sequencing resulted in an average 51.7 \times coverage of the genome. An analysis of sequence variants and copy number variations in 289 known hearing loss-associated genes (Supplementary Table S1) excluded a putative pathogenic genetic aberration. These variants, shown in Supplementary Table S2, were excluded based on criteria such as their presence in a homozygous state in other presumably normal hearing individuals in NGSD, low *in silico* pathogenicity prediction scores, no predicted effect on splicing, or an obvious clinical mismatch.

Following the initial hypothesis that *ATP11A* may be the gene for the DFNA33 locus and the growing clinical and functional evidence asserting *ATP11A* is an essential protein for a normal functioning auditory system, our analysis then focused on the previously mapped DFNA33 locus coordinates (GRCh37: 110,300,001-115,169,878), as well as *ATP11A* (Supplementary Table S3), and uncovered variants that were either identified in other in-house patients with presumed normal hearing or were likely benign based on bioinformatics assessment. Only one deep intronic variant in *ATP11A* intron 8 (chr13:113421269C>G (GRCh37), ENST00000375630:c.725 + 737C>T) was predicted via *in silico* tools to activate exonic splice enhancers. This variant was tested with an *in vitro* splicing assay using established protocols (Rad et al., 2021; Vona et al., 2021) and yielded a functionally normal result (Figure 2). Taken together, the variant is classified as likely benign (PM2_Supporting, BP4_Supporting, and BS3_Strong; -4 points (likely benign point range: -6 to -1)). On this basis, we conclude that following short-read genome sequencing, a method employed for the identification of the first described *ATP11A* variant (Pater et al., 2022), we present evidence that does not support *ATP11A* as being the gene for the DFNA33 locus and acknowledge that we have been extremely fortunate to re-recruit an individual from the DFNA33 family.

3.3 Haplotype review

Upon close inspection, we noted that the haplotypes that were used to define the DFNA33 boundaries of the disease interval in the original Bönsch et al. paper show several unlikely events (Bönsch et al., 2009, shown in Figure 1A for clarity). These include three recombination events in a small chromosomal interval in individual 503 and two recombination events in a relatively short interval in individuals 412 and 419. The fine mapping and recapitulation of haplotypes seem improbable and may be due to genotyping or other errors. Due to this observation, the DFNA33 disease interval may be inaccurate. Therefore, we performed genome-wide analysis of variants that did not yield an obvious candidate and informative result for follow-up and thus required additional family members in order to significantly narrow variants.

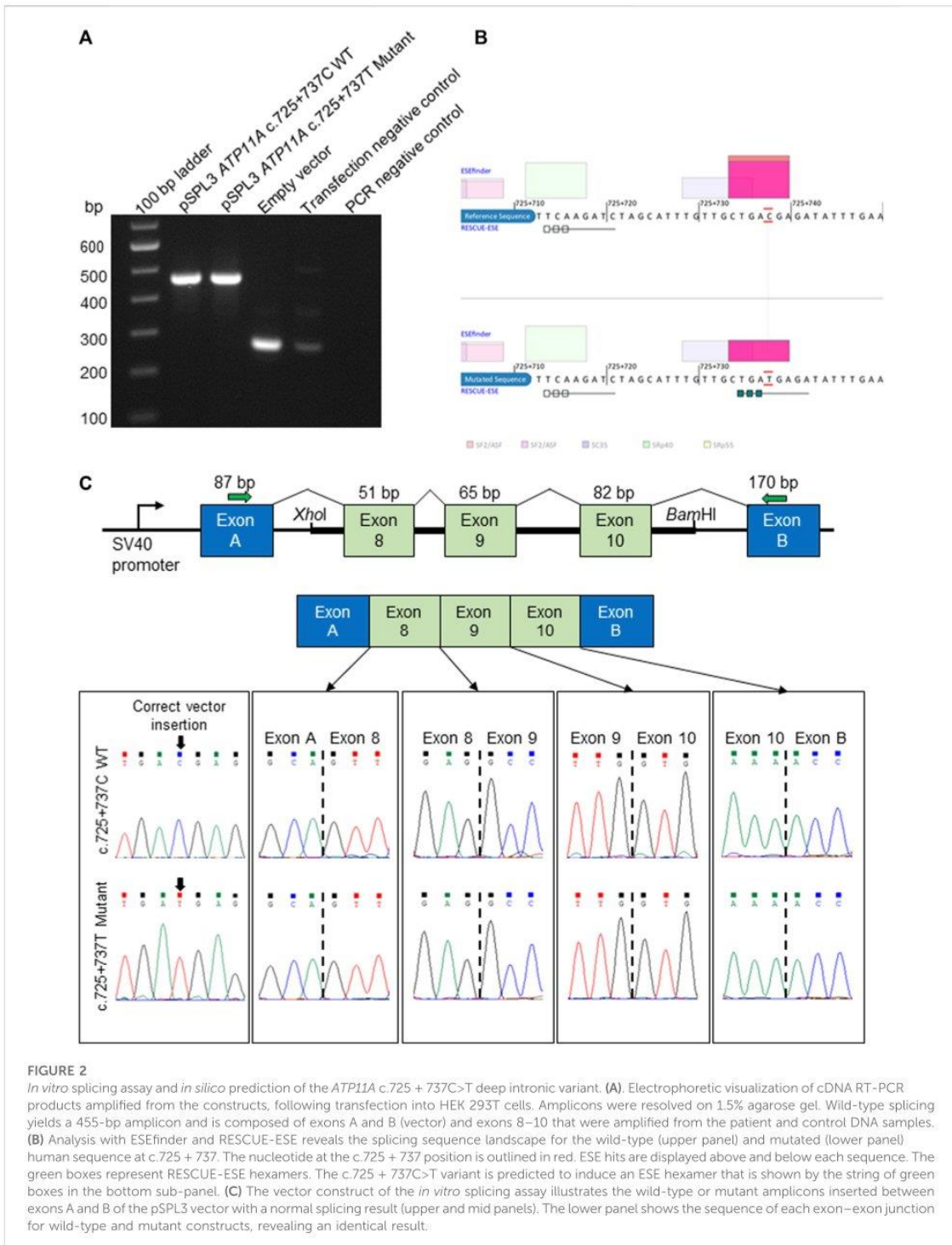


FIGURE 2

In vitro splicing assay and *in silico* prediction of the *ATP11A* c.725 + 737C>T deep intronic variant. (A) Electrophoretic visualization of cDNA RT-PCR products amplified from the constructs, following transfection into HEK 293T cells. Amplicons were resolved on 1.5% agarose gel. Wild-type splicing yields a 455-bp amplicon and is composed of exons A and B (vector) and exons 8–10 that were amplified from the patient and control DNA samples. (B) Analysis with ESEfinder and RESCUE-ESE reveals the splicing sequence landscape for the wild-type (upper panel) and mutated (lower panel) human sequence at c.725 + 737. The nucleotide at the c.725 + 737 position is outlined in red. ESE hits are displayed above and below each sequence. The green boxes represent RESCUE-ESE hexamers. The c.725 + 737C>T variant is predicted to induce an ESE hexamer that is shown by the string of green boxes in the bottom sub-panel. (C) The vector construct of the *in vitro* splicing assay illustrates the wild-type or mutant amplicons inserted between exons A and B of the pSPL3 vector with a normal splicing result (upper and mid panels). The lower panel shows the sequence of each exon–exon junction for wild-type and mutant constructs, revealing an identical result.

4 Discussion

Although a conventional understanding of recombination rates approximates about one crossover per homologous pair of chromosomes, it varies dramatically on a number of different scales and shows non-uniform distribution. However, mapping recombination patterns have uncovered chromosomal regions enriched for hotspots that are separated from regions that do not appear to recombine. The deCODE genetic map created chromosomal genetic maps that also included sex-averaged recombination rates (Kong et al., 2002). Analysis of the chr13q34 region with these data does not suggest the DFNA33 locus is a recombination hotspot (data not shown).

Closely adjacent double or triple recombination events involving phasing errors are suggestive of genotyping errors (Housworth and Stahl, 2003). Although crossing over may appear random, it is tightly regulated and occurs at a low frequency due to factors that prevent excessive recombination and the disruption of favorable genetic combinations (Séguéla-Arnaud et al., 2015). Although we should have noted the unlikely double and triple recombination events in individuals 412, 419, and 503 previously, performing genome sequencing and functional analysis of a candidate splice variant was important for excluding a newly associated disease gene in the previously mapped significant interval.

With increased access to advanced sequencing technologies, the continuous follow-up of undiagnosed families with historical linkage is essential for the discernment of correct DFN-locus assignment. Our study highlights the necessity and potential to refine understanding of the number of total unresolved loci through a simple review of historical loci for such unlikely events. A problematic bottleneck will be re-contacting and re-establishing contact with the original families as maintaining connections to families over decades can be challenging. Considering the size of this unresolved family, although unlikely, we cannot exclude multi-locus heterogeneity or the presence of phenocopies. Furthermore, it was unfortunate that we could not recruit the entire family for repeat linkage analysis and genome sequencing of additional affected individuals to increase the chances of uncovering the causal genetic variant. The most convincing case for excluding DFNA33 altogether would be through the identification of a causal variant, either within the DFNA33 locus or elsewhere in the genome, which is a limiting factor of our work. Using a short-read genome-sequencing approach, we cannot exclude epigenetic modifications or short-inverted duplications. Nonetheless, re-assessment of haplotypes combined with new genome sequencing data can provide some value in better understanding unsolved DFNA loci.

Data availability statement

The datasets presented in this study can be found in online repositories. The names of the repository/repositories and accession number(s) can be found at: <https://databases.lovd.nl/shared/individuals/00435034>, #00435034.

Ethics statement

The studies involving humans were approved by the Faculty of Medicine Ethics Committee at the University of Tübingen. The studies were conducted in accordance with the local legislation and institutional requirements. The participants provided their written informed consent to participate in this study.

Author contributions

SR, KN, and AA recruited the patient and ascertained clinical data. BV, MS, and TH contributed to genome sequence analysis. NS and JP analyzed and aided interpretation of results. AR and BV carried out the splicing assay. BV, SR, JP, and AA drafted the manuscript. All authors contributed to the article and approved the submitted version.

Funding

This work was supported by the Centers for Rare Diseases Tübingen, intramural funding (fortune) at the University of Tübingen (2545-1-0 to BV), and the German Research Foundation (DFG) VO 2138/7-1 (BV, #469177153). Additional support from the DFG was provided via SFB 889 (Project A06 to NS) via the Heisenberg program (NS, #406266759) and the Multiscale Bioimaging Cluster of Excellence (MBExC).

Acknowledgments

The authors thank the participating individual for making this analysis possible.

Conflict of interest

The authors declare that the research was conducted in the absence of any commercial or financial relationships that could be construed as a potential conflict of interest.

Publisher's note

All claims expressed in this article are solely those of the authors and do not necessarily represent those of their affiliated organizations, or those of the publisher, the editors, and the reviewers. Any product that may be evaluated in this article, or claim that may be made by its manufacturer, is not guaranteed or endorsed by the publisher.

Supplementary material

The Supplementary Material for this article can be found online at: <https://www.frontiersin.org/articles/10.3389/fgene.2023.1214736/full#supplementary-material>

References

- Azaiez, H., Booth, K. T., Ephraim, S. S., Crone, B., Black-Ziegelbein, E. A., Marini, R. J., et al. (2018). Genomic landscape and mutational signatures of deafness-associated genes. *Am. J. Hum. Genet.* 103 (4), 484–497. doi:10.1016/j.ajhg.2018.08.006
- Bamshad, M. J., Nickerson, D. A., and Chong, J. X. (2019). Mendelian gene discovery: fast and furious with No end in sight. *Am. J. Hum. Genet.* 105 (3), 448–455. doi:10.1016/j.ajhg.2019.07.011
- Bönsch, D., Schmidt, C.-M., Scheer, P., Bohlender, J., Neumann, C., Am Zehnhoff-Dinnesen, A., et al. (2009). A new gene locus for an autosomal-dominant non-syndromic hearing impairment (DFNA 33) is situated on chromosome 13q34-qter. *HNO* 57 (4), 371–376. doi:10.1007/s00106-008-1832-9
- Chepurwar, S., von Loh, S. M., Wigger, D. C., Neef, J., Frommolt, P., Beutner, D., et al. (2022). A mutation in ATP11A causes autosomal-dominant auditory neuropathy type 2. *Hum. Mol. Genet.* 32, 1083–1089. doi:10.1093/hmg/ddac267
- Falb, R. J., Müller, A. J., Klein, W., Grimm, M., Grasshoff, U., Spranger, S., et al. (2023). Bi-allelic loss-of-function variants in KIF21A cause severe fetal akinesia with arthrogyria multiplex. *J. Med. Genet.* 60 (1), 48–56. doi:10.1136/jmedgenet-2021-108064
- Farré, M., Micheletti, D., and Ruiz-Herrera, A. (2013). Recombination rates and genomic shuffling in human and chimpanzee—a new twist in the chromosomal speciation theory. *Mol. Biol. Evol.* 30 (4), 853–864. doi:10.1093/molbev/mss272
- Housworth, E. A., and Stahl, F. W. (2003). Crossover interference in humans. *Am. J. Hum. Genet.* 73 (1), 188–197. doi:10.1086/376610
- ISO (2017). *7029 Acoustics-statistical distribution of hearing thresholds related to age and gender*. 3rd ed. Switzerland: Geneva.
- Koehler, K. E., Cherry, J. P., Lynn, A., Hunt, P. A., and Hassold, T. J. (2002). Genetic control of mammalian meiotic recombination. I. Variation in exchange frequencies among males from inbred mouse strains. *Genetics* 162 (1), 297–306. doi:10.1093/genetics/162.1.297
- Kong, A., Gudbjartsson, D. F., Sainz, J., Jonsson, G. M., Gudjonsson, S. A., Richardson, B., et al. (2002). A high-resolution recombination map of the human genome. *Nat. Genet.* 31 (3), 241–247. doi:10.1038/ng917
- Kopanos, C., Tsiolkas, V., Kouris, A., Chapple, C. E., Albarca Aguilera, M., Meyer, R., et al. (2019). VarSome: the human genomic variant search engine. *Bioinform. Oxf. Engl.* 35 (11), 1978–1980. doi:10.1093/bioinformatics/bty897
- Oza, A. M., DiStefano, M. T., Hemphill, S. E., Cushman, B. J., Grant, A. R., Siegert, R. K., et al. (2018). Expert specification of the ACMG/AMP variant interpretation guidelines for genetic hearing loss. *Hum. Mutat.* 39 (11), 1593–1613. doi:10.1002/humu.23630
- Pater, J. A., Penney, C., O’Rielly, D. D., Griffin, A., Kamal, L., Brownstein, Z., et al. (2022). Autosomal dominant non-syndromic hearing loss maps to DFNA33 (13q34) and co-segregates with splice and frameshift variants in ATP11A, a phospholipid flippase gene. *Hum. Genet.* 141, 431–444. doi:10.1007/s00439-022-02444-x
- Rad, A., Schade-Mann, T., Gamberdinger, P., Yanus, G. A., Schulte, B., Müller, M., et al. (2021). Aberrant COL11A1 splicing causes prelingual autosomal dominant nonsyndromic hearing loss in the DFNA37 locus. *Hum. Mutat.* 42 (1), 25–30. doi:10.1002/humu.24136
- Rose, A. M., and Baillie, D. L. (1979). The effect of temperature and parental age on recombination and nondisjunction in *CAENORHABDITIS ELEGANS*. *Genetics* 92 (2), 409–418. doi:10.1093/genetics/92.2.409
- Séguéla-Arnaud, M., Crismani, W., Larchevêque, C., Mazel, J., Froger, N., Choinard, S., et al. (2015). Multiple mechanisms limit meiotic crossovers: TOP3a and two BLM homologs antagonize crossovers in parallel to FANCM. *Proc. Natl. Acad. Sci. U. S. A.* 112 (15), 4713–4718. doi:10.1073/pnas.1423107112
- Sun, F., Trpkov, K., Rademaker, A., Ko, E., and Martin, R. H. (2005). Variation in meiotic recombination frequencies among human males. *Hum. Genet.* 116 (3), 172–178. doi:10.1007/s00439-004-1215-6
- Tanzi, R. E., Watkins, P. C., Stewart, G. D., Wexler, N. S., Gusella, J. F., and Haines, J. L. (1992). A genetic linkage map of human chromosome 21: analysis of recombination as a function of sex and age. *Am. J. Hum. Genet.* 50 (3), 551–558.
- Teare, M. D., and Santibañez Koref, M. F. (2014). Linkage analysis and the study of Mendelian disease in the era of whole exome and genome sequencing. *Briefings Funct. Genomics* 13 (5), 378–383. doi:10.1093/bfpg/elu024
- van Wijk, E., Krieger, E., Kemperman, M. H., De Leenheer, E. M. R., Huygen, P. L. M., Cremers, C. W. R. J., et al. (2003). A mutation in the gamma actin 1 (ACTG1) gene causes autosomal dominant hearing loss (DFNA20/26). *J. Med. Genet.* 40 (12), 879–884. doi:10.1136/jmg.40.12.879
- Vona, B., Mazaheri, N., Lin, S.-J., Dunbar, L. A., Maroofian, R., Azaiez, H., et al. (2021). A biallelic variant in CLRN2 causes non-syndromic hearing loss in humans. *Hum. Genet.* 140 (6), 915–931. doi:10.1007/s00439-020-02254-z
- Wang, J., Sun, L., Jiang, L., Sang, M., Ye, M., Cheng, T., et al. (2017). A high-dimensional linkage analysis model for characterizing crossover interference. *Briefings Bioinforma.* 18 (3), 382–393. doi:10.1093/bib/bbw033
- Weisschuh, N., Mazzola, P., Heinrich, T., Haack, T., Wissinger, B., Tonagel, F., et al. (2020). First submicroscopic inversion of the OPA1 gene identified in dominant optic atrophy - a case report. *BMC Med. Genet.* 21 (1), 236. doi:10.1186/s12881-020-01166-z
- Williamson, J. H., Parker, D. R., and Manchester, W. G. (1970). X-ray-induced recombination in the fourth chromosome of *Drosophila melanogaster* females. I. Kinetics and brood patterns. *Mutat. Res.* 9 (3), 287–297. doi:10.1016/0027-5107(70)90130-2
- Wright, C. F., FitzPatrick, D. R., and Firth, H. V. (2018). Paediatric genomics: diagnosing rare disease in children. *Nat. Rev. Genet.* 19 (5), 325–268. doi:10.1038/nrg.2018.12
- Zhu, M., Yang, T., Wei, S., DeWan, A. T., Morell, R. J., Efenbein, J. L., et al. (2003). Mutations in the gamma-actin gene (ACTG1) are associated with dominant progressive deafness (DFNA20/26). *Am. J. Hum. Genet.* 73 (5), 1082–1091. doi:10.1086/379286

10.12 Attachment 12

Expanding the spectrum of phenotypes for *MPDZ*: report of four unrelated families and review of the literature

Expanding the spectrum of phenotypes for *MPDZ*: Report of four unrelated families and review of the literature

Aboufazi Rad¹ | Oliver Bartsch² | Somayeh Bakhtiari^{3,4} | Changlian Zhu^{5,6} |
Yiran Xu⁶ | Fabíola P. Monteiro⁷ | Fernando Kok^{7,8} |
Anneke T. Vulto-van Silfhout^{9,10} | Michael C. Kruer^{3,4} | Michael R. Bowl¹¹ |
Barbara Vona^{1,12,13}

¹Department of Otolaryngology – Head and Neck Surgery, Tübingen Hearing Research Centre, Eberhard Karls University Tübingen, Tübingen, Germany

²Medical Care Centre Section Human Genetics and Institute of Human Genetics, University Medical Centre of the Johannes Gutenberg University Mainz, Mainz, Germany

³Barrow Neurological Institute, Phoenix Children's Hospital, Phoenix, Arizona, USA

⁴Department of Child Health, Cellular and Molecular Medicine, Genetics, and Neurology, University of Arizona College of Medicine-Phoenix, Phoenix, Arizona, USA

⁵Center for Brain Repair and Rehabilitation, Institute of Neuroscience and Physiology, University of Gothenburg, Göteborg, Sweden

⁶Henan Key Laboratory of Child Brain Injury and Henan Pediatric Clinical Research Center, Institute of Neuroscience and Third Affiliated Hospital of Zhengzhou University, Zhengzhou, China

⁷Medical Department, Mendelics Genomic Analysis, Sao Paulo, Brazil

⁸Neurogenetics, Neurology Department, Hospital das Clínicas da Universidade de São Paulo, São Paulo, Brazil

⁹Department of Human Genetics, Radboud University Medical Centre, Nijmegen, the Netherlands

¹⁰Department of Clinical Genetics, Maastricht University Medical Center, Maastricht, the Netherlands

¹¹UCL Ear Institute, University College London, London, UK

¹²Institute of Human Genetics, University Medical Center Göttingen, Göttingen, Germany

¹³Institute for Auditory Neuroscience and InnerEarLab, University Medical Center Göttingen, Göttingen, Germany

Correspondence

Barbara Vona, Institute of Human Genetics, Institute for Auditory Neuroscience and InnerEarLab, University Medical Center Göttingen, Göttingen, Germany.
Email: barbara.vona@med.uni-goettingen.de

Funding information

Medizinischen Fakultät, Eberhard Karls Universität Tübingen, Grant/Award Number: 2545-1-0; Ministerium für Wissenschaft, Forschung und Kunst Baden-Württemberg; Deutsche Forschungsgemeinschaft VO 2138/7-1, Grant/Award Number: 469177153; National Natural Science Foundation of China, Grant/Award Number: U21A20347

Abstract

MPDZ, a gene with diverse functions mediating cell–cell junction interactions, receptor signaling, and binding multivalent scaffold proteins, is associated with a spectrum of clinically heterogeneous phenotypes with biallelic perturbation. Despite its clinical relevance, the mechanistic underpinnings of these variants remain elusive, underscoring the need for extensive case series and functional investigations. In this study, we conducted a systematic review of cases in the literature through two electronic databases following the PRISMA guidelines. We selected nine studies, including 18 patients, with homozygous or compound heterozygous variants in *MPDZ* and added five patients from four unrelated families with novel *MPDZ* variants. To evaluate the role of *Mpdz* on hearing, we analyzed available auditory electrophysiology data from a knockout murine model (*Mpdz^{em1(IMPC)}/em1(IMPC)*) generated by the International Mouse Phenotyping Consortium. Using exome and genome sequencing, we identified three families with compound heterozygous variants, and one family with a

This is an open access article under the terms of the [Creative Commons Attribution License](https://creativecommons.org/licenses/by/4.0/), which permits use, distribution and reproduction in any medium, provided the original work is properly cited.

© 2024 The Author(s). *Clinical Genetics* published by John Wiley & Sons Ltd.

homozygous frameshift variant. *MPDZ*-related disease is clinically heterogeneous with hydrocephaly, vision impairment, hearing impairment and cardiovascular disease occurring most frequently. Additionally, we describe two unrelated patients with spasticity, expanding the phenotypic spectrum. Our murine analysis of the *Mpdz^{em1}* (*IMPC*)/*em1(IMPC)* allele showed severe hearing impairment. Overall, we expand understanding of *MPDZ*-related phenotypes and highlight hearing impairment and spasticity among the heterogeneous phenotypes.

KEYWORDS

hearing loss, hydrocephaly, *MPDZ*, phenotypic heterogeneity, spasticity

1 | INTRODUCTION

MPDZ, also known as *MUPP1* (OMIM: 603785), encodes the multiple PDZ domain crumbs cell polarity complex component. This protein stands as the largest among PDZ (PSD95/DLG1/ZO1) domain-containing proteins, with 13 PDZ domains. Its initial discovery originated from interaction with the HTR2C serotonin receptor from a yeast 2-hybrid screen using human fetal brain cDNA.^{1,2} PDZ domain proteins represent a diverse and abundant family of interaction domain scaffolding proteins, and they fulfill crucial roles across various cellular contexts, orchestrating intricate networks of interactions. This expansive network involves interactions with more than 15 proteins, encompassing members of the tight junctions protein family, G protein-coupled receptors (GPCRs), SynGAP, and CaMKII at synapses,^{3,4} as well as delta like protein 1 and 4 (DLL1/4) and NECTIN2 at epithelial apical junctions.⁵

The *MPDZ* gene-disease relationship with biallelic variants currently extends to congenital hydrocephalus type 2 with or without brain or eye abnormalities (OMIM: 615219); however, the literature presents a continuously evolving and complex phenotypic landscape. Functional studies have contributed to our understanding of the phenotypic manifestations linked to *MPDZ*. For instance, Feldner et al. used a mouse model (*Mpdz^{-/-}*) revealing that *Mpdz* depletion impairs multiple endoplasmic functions, potentially leading to perinatal-onset hydrocephalus.⁶ Yang et al. identified a crucial role of *Mpdz* in the choroid plexus, where choroid plexus hyperpermeability, attributed to *Mpdz* deficiency, precipitated hydrocephalus in a *Mpdz^{-/-}* murine model.⁷ Jarysta and Tarchini⁸ uncovered a novel functional importance of *MPDZ* in cochlear hair cell development. Interestingly, *MPDZ* expression was not localized to the apical cell junctions in the epithelium but rather at the hair cell apical membrane. *Mpdz* mutants exhibited misaligned stereocilia placement and dysmorphic hair bundles.⁸

Due to the manifold and expanding clinical and genetic data described, we sought to address this complexity by presenting a case-series comprising four unrelated families with biallelic *MPDZ* variants. Additionally, we reviewed the existing literature to compile a detailed report on the wide array of phenotypes associated with *MPDZ* variants. We also analyzed auditory phenotyping data from a murine model. Our results reaffirm the role of *MPDZ* in hearing impairment

and spasticity while contributing new information about the clinical landscape resulting from biallelic *MPDZ* variants.

2 | METHODS

2.1 | Patient recruitment

This study was approved by the University of Tübingen Ethics Commission, No. 197/2019BO1 and the University Medical Center Göttingen, local institutional ethics board, No. 3/2/16. Four unrelated families presenting a variety of clinical indications were aggregated from four different centers by direct communication or via GeneMatcher.⁹ Blood samples were collected after obtaining informed consent from patients or their parents. Informed consent from the parents or legal guardians of the patients/participants was obtained for the publication of their data.

2.2 | Literature search strategy and selection criteria

Electronic bibliographic databases including PubMed (<https://pubmed.ncbi.nlm.nih.gov/> accessed on 11 February 2024) and Web of Science (<https://www.webofscience.com/> accessed on February 11, 2024) were used for the literature search. The search strategy used the keyword “*MPDZ*” for each database. We used EndNote 21 (<https://endnote.com/> accessed on January 9, 2024) to collect all the results in a single library.

Our inclusion criteria encompassed publications that reported patients with suspected deleterious homozygous, and compound heterozygous variants in *MPDZ*. The exclusion criteria were: (i) duplicate publications; (ii) studies unrelated to the scope of this paper; (iii) reports in the form of abstracts, reviews, theses, and conference papers; and (iv) studies describing patients with heterozygous or homozygous variants in *MPDZ* classified as likely benign based on ACMG/ClinGen criteria.

The full text of all the potentially eligible articles and their supplementary information were obtained by two authors (AR and BV) working independently.

2.3 | Sequencing, bioinformatics analysis, and variant classification

Following extraction of DNAs from whole blood by standard protocol, proband DNA samples were subjected to exome capture using either the Agilent SureSelect Human All Exon V6 Kit (Families 1 and 3), or the Nextera Exome Capture (Family 2), or genome enrichment with the Illumina DNA PCR free Prep Kit (Family 4). Exome sequencing (ES) was performed on an Illumina HiSeq 2500 sequencer for an average 50× sequencing depth, resulting in sequences of greater than 100 bases from each end of the fragments. The proband of Family 1 was sequenced at the Institute of Human Genetics, University Medical Centre of the Johannes Gutenberg University Mainz, Family 2 at Mendelics Genomic Analysis, and Family 3 at Zhengzhou University. For Family 4, the genome sequencing was performed on the Illumina NovaSeq 6000 at the Radboud University Medical Centre, Nijmegen, the Netherlands. Read alignment and variant calling were performed using DRAGEN Bio-IT Platform (Illumina). Exome data were processed for analysis using a GATK-based pipeline¹⁰ that used Burrows-Wheeler alignment¹¹ to the GRCh37/UCSC hg19 human genome assembly. Single nucleotide variant and InDel detection utilized VarScan version 2.2.5, MuTec and GATK Somatic Indel Detector. A previously described protocol aided interpretation of potentially pathogenic variants.¹² gnomAD v4.0.0¹³ was used for population-specific filtering. The prediction of two in silico tools including REVEL¹⁴ and CADD¹⁵ were used to assess the pathogenicity of variants. All variants were classified based on ACMG and ClinGen Sequence Interpretation (SVI) Working Group guidelines.

Segregation analysis using Sanger sequencing was performed in available family members of Families 1, 2, and 3 to confirm variant segregation after polymerase chain reaction (PCR) amplification. Primers are available upon request.

2.4 | Splice variant prediction and in vitro splicing assay

Prediction of aberrant splicing used Alamut Genova v.1.4, employing SpliceSiteFinder-like, MaxEntScan, NNSPLICE and GeneSplicer. A mini-gene splice assay was done as previously described^{16,17} to assay splice effects of the c.5231+1G>A variant. Briefly, PCR amplicons were generated from the genomic DNAs of an affected (Family 1, II-2) and wild-type individual (mother, I-2) using a forward primer with a *Xho*I restriction site (MPDZ Ex3 *Xho*I F: 5'-aattctcgag-TAATTTTGGCCCACTACCC-3') and a reverse primer with a *Bam*HI restriction site (MPDZ Ex3 *Bam*HI R: 5'-attggatccCCTTCGTTGCA-TAAGGATGAC-3'). The 1176 bp amplicon included the entire genomic region spanning exons 37 and 38, as well as additional flanking 320 bp (5') and 306 bp (3') sequence that was ligated into a multiple cloning site between native exons A and B in the linearized pSPL3 exon-trapping vector. The vector was transformed into DH5α competent cells and plated overnight. All mutant mini-genes were Sanger sequence confirmed.

Homozygous and wild-type mini-genes were transfected in triplicate into HEK 293T cells cultured in FBS-free medium in 12 well culture plates with a density of 1×10^5 cells per mL. The mini-genes in the pSPL3 vector were transiently transfected using 3 μL of FuGENE 6 Transfection Reagent (Roche) with 1 μg of vector. An empty vector and HEK 293T cells were included as controls. The transfected cells were harvested 24 h post-transfection. Total RNA was prepared using the miRNAeasy Mini Kit (Qiagen). Approximately 500 ng of RNA was reverse transcribed using a High-Capacity RNA-to-cDNA Kit (Applied Biosystems) following manufacturer's protocols. The cDNA was used for PCR amplification using a vector specific SD6 forward (5'-TCTGAGTCACCTGGACAACC-3') and a terminal *MPDZ* exon 3 reverse cDNA primer (5'-CAAGATATCCTCAGCTGTGACC-3'). The resulting amplified fragments were visualized on a 1.5% agarose gel. cDNA amplicons were Sanger sequenced. Individual cDNA amplicons from the c.5231+1G>A variant were TA-cloned following standard protocols (dual promoter with pCRII, Invitrogen).

3 | RESULTS

3.1 | Review of the literature

The systematic review of literature considered 162 abstracts. Following adherence to inclusion and exclusion criteria, nine studies remained that reported patients with biallelic *MPDZ* variants who were analyzed in detail for clinical information. The PRISMA flowchart summarizes the process of identification and selection of nine publications describing 18 patients (Figure 1). Additionally, we incorporated data from five patients from four unrelated families, resulting in 23 patients (10 [43.5%] male, 6 [26.1%] female, 5 [21.7%] fetuses, and 2 [8.7%] no information available).

The analysis revealed the presence of 25 distinct homozygous or heterozygous variants distributed across 15 exons and 3 introns of *MPDZ*. Sixteen out of 25 were located within the 13 PDZ domains of *MPDZ*. Notably, in individuals with severe phenotypes, at least one variant was located within the PDZ domain (Table S1).

3.2 | Clinical spectrum of phenotypes associated with biallelic *MPDZ* variants

Patients with *MPDZ* variants exhibited a wide range of clinical phenotypes (Table 1). The literature reports 23 patients with ages ranging from fetal stage to 43 years old. Among these patients, 12 (52.2%) presented hydrocephalus, ranging from lethal to mild, with three patients characterized as mild. Al-Dosari et al.²⁷ initially described two patients with severe hydrocephalus, labeling the condition as non-syndromic hydrocephalus. However, a broader phenotypic constellation was subsequently identified in patients with *MPDZ*-related disorders. Nine patients (39.1%) exhibited various forms of vision impairment. Recently, two separate reports described vision impairment as including macular coloboma as well as bilateral macular

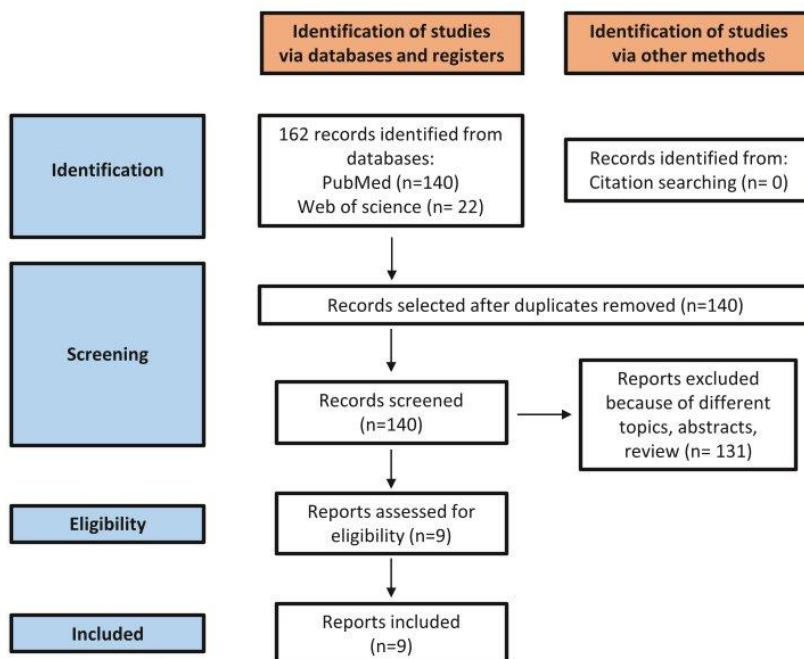


FIGURE 1 PRISMA flowchart of the literature review. [Colour figure can be viewed at wileyonlinelibrary.com]

colobomas with symmetric patches of chorioretinal atrophy in the temporal periphery, respectively. Six patients (26.1%) were described as having congenital hearing impairment, varying from mild to profound. Interestingly, two Pakistani siblings had hearing loss due to a biallelic variant in *MPDZ*. Another patient with the same variant (c.2324C>T, p.Pro775Leu) and non-syndromic hearing loss was also reported in ClinVar (variation ID: 995976). Cardiovascular abnormalities were observed in four (17.4%) patients with various phenotypes, including congenital heart defects, aberrant subclavian artery, and portal vein thrombosis. Seven (30.4%) patients had macrocephaly, and three (13.0%) had frontal bossing. Skeletal anomalies, such as persistent fetal pads and striking creases over the knee, as well as joint hypermobility, were seen in two patients (8.7%) each. Two patients each (8.7%) exhibited hypotonia and spasticity. Three patients (13.0%) had intellectual disability, and three patients (13.0%) experienced seizures. In a study by Shaheen et al., one patient was identified with intrahepatic cholestasis and multicystic dysplastic kidney; however, this patient had a variant in *TJP2* (classified likely pathogenic based on ACMG guidelines) explaining these phenotypes.²⁵

3.3 | Clinical assessment

We studied four unrelated families originating from various global regions (Europe, South America, and Asia), each displaying a variety of phenotypes including hydrocephaly, seizure, spastic paraparesis, hearing loss, cardiac abnormalities and vision impairment.

3.4 | Family 1

The female proband (II-2) in Family 1, patient 1 in Table 1, is one of two living affected children out of three children, delivered at term to non-consanguineous parents (Figure 2A). Hydrocephalus was first noted prenatally in the 27th week of gestation. She was born at 34 gestational weeks with marked primary hydrocephalus and occipital frontal circumference (OFC) 42 cm (>99th percentile + 6z). She exhibited delayed speech development, virtually not speaking at all until age 5 years and was initially suspected to have congenital hearing loss that was clinically diagnosed as mild to moderate sensorineural hearing loss. At age 5 years, she received hearing aids, which significantly improved her speech. At age 6 years and 3 months, height was 117 cm (31st percentile), weight was 16.5 kg (2nd percentile -2.1z) and OFC was 53 cm (92nd percentile +1.4z). She had a developmental delay of approximately 30% of her age, suggesting learning disability or mild intellectual disability. The youngest daughter (II-3) in this family was delivered at term and similarly had prenatal hydrocephalus detected in week 22+2 of gestation. She failed universal newborn hearing screening. An older female sibling had died at age 8 months but evidence is too sparse to include or exclude as a same disease in this family.

3.5 | Family 2

The proband in Family 2 is a 43-year-old female, the youngest of four siblings born to non-consanguineous parents (Figure 2A). Family

TABLE 1 Description of phenotype and genotype of 24 selected patients.

	Number/ sex/ ethnicity	Variant	Age of last examination	Hydrocephalus	Vision impairment	Hearing loss	Cardiovascular	Macrocephaly/ frontal bossing/ skeletal anomalies	Seizure/ Intellectual disability/MRI	Spasticity/ hypotonia	Detailed clinical information
Current study (Family 1, II.2)	1/F/ German	c.3508C>T, p.Arg1170* (mat), c.5231+1G>A p.? (pat)	6 years	Yes	No	Yes	No	Yes/Yes/No	No/No/NA	No/No	Primary hydrocephaly, congenital mild to moderate sensorineural hearing loss
Current study (Family 1, II.3)	2/F/ German	c.3508C>T, p.Arg1170* (mat), c.5231+1G>A p.? (pat)	1 year	Yes	No	Yes	No	Yes/No/No	No/No/NA	No/No	Primary hydrocephaly, congenital mild to moderate sensorineural hearing loss
Current study (Family 2, II.4)	3/F/ Brazilian	c.1026dup p.Ala343Serfs*22 (pat), c.4993G>A p.Ala1665Thr (mat)	43 years	No, but mild ex- vacuum ventricle enlargement	Yes	No	No	No/No/No	No/No/ Remarkable	Yes/No	Bilaterally increased P100 wave latency with normal amplitude on VEP, ABR disclosing widened I-V interpeak interval on the left ear. No abnormalities on the right ear. Sinus arrhythmia; MRI—bilateral tenuous T2 and Flair white matter hyperintensities in the cerebral hemispheres and anterior portion of the corpus callosum, and mild “ex-vacuum” lateral ventricle enlargement
Current study (Family 3, II.1)	4/M/Han Chinese	c.5362G>C p.Val1788Leu (mat), c.5701G>C p.Val1901Leu (pat)	3 years	No	No	No	No	No/No/No	No/No/NA	Yes/No	NA
Current study (Family 4, II.1)	5/M/NA	c.4282_4288del p.Ile1428Serfs*7	4 years	Yes	Yes	No	No	Yes/Yes/No	Yes/Yes/ Remarkable	No/No	Septo-optic dysplasia, antenatal hydrocephalus, bilateral macular colobomas
Iyengar et al. (2022) ¹⁸	6/M/NA	c.3100C>T p.Arg1034* (mat), c.747+2T>G, p.? (pat)	4 years	No	Yes	No	No	No/No/No	No/No/NA	No/No	Bilateral macular colobomas with symmetric patches of chororetinal atrophy in the temporal periphery; another sister died at 1 month of age secondary to an unknown cardiovascular issue, but records are unavailable
Iyengar et al. (2022) ¹⁸	7/M/NA	c.3100C>T p.Arg1034* (mat), c.747+2T>G, p.? (pat)	9 years	No	Yes	No	No	No/No/No	No/No/NA	No/No	Subtle thinning of the temporal fovea in both eyes

(Continues)

TABLE 1 (Continued)

Number/ sex/ ethnicity	Variant	Age of last examination	Hydrocephalus	Vision impairment	Hearing loss	Cardiovascular	Macrocephaly/ frontal bossing/ skeletal anomalies	Seizure/ Intellectual disability/MRI	Spasticity/ hypotonia	Detailed clinical information
Zhang et al. (2022) ¹⁹	8/M/ Chinese c.4301delA p.Asp1434fs*3 (mat), c.5255C>G p.Ser1752* (pat)	26 years	No	Yes	No	No	No/No/No	No/No/NA	No/No	Macular coloboma: One deceased sibling with unknown reason of death
Bharadwaj et al. (2022) ²⁰	9/ F/Pakistani c.2324C>T p.Pro775Leu	NA	No	No	Yes	No	No/No/No	No/No/NA	No/No	Congenital profound sensorineural hearing loss
Bharadwaj et al. (2022) ²⁰	10/ M/Pakistani c.2324C>T p.Pro775Leu	NA	No	No	Yes	No	No/No/No	No/No/NA	No/No	Congenital profound sensorineural hearing loss
Bertolli et al. (2021) ²¹	11/NA/NA c.3253A>T p.Lys1085*	NA	NA	NA	NA	Yes	NA/NA/NA	NA/NA/NA	NA/NA	Ventricular septal defect, atrial septal defect, secundum atrial septal defect, ventriculomegaly, abnormality of the septum pellucidum, antenatal onset
Moazzeni et al. (2020) ²²	12/ F/Iranian c.409G>T p.Val137Phe	NA	No	Yes	Yes	No	No/No/No	No/No/NA	No/No	Congenital hereditary endothelial dystrophy, congenital mild sensorineural hearing loss
Al-Jezawi et al. (2018) ²³	13/M/ Emirati c.394G>A p.Gly132Ser (mat), c.1744C>G p.Leu582Val (pat)	9 months	Yes	No	No	No	Yes/Yes/No	No/No/ Remarkable	No/No	The brother of the mother has a daughter with hydrocephalus and VP shunt. MRI: widened CSF spaces in the frontoparietal region bilaterally and mild dilation of lateral and third ventricles
Harripaul et al. (2018) ²⁴	14/M/NA c.5898_5901del, p.Phe1967Leufs*3	NA	No	No	No	No	No/No/No	No/Yes/NA	No/No	NA
Shaheen et al. (2017) ²⁵	15/M/ Saudi c.628C>T p.Gln210*	NA	Yes	No	No	No	Yes/No/No	No/Yes/NA	No/No	One affected brother with severe hydrocephalus died 1 day after delivery, no more information is available for this sibling
Shaheen et al. (2017) ²⁵	16/F/ Palestinian c.4469del p.Gln1490Argfs*19	2.5 years	Yes	No	No	Yes	No/Yes/Yes	No/No/ Remarkable	No/No	Aberrant subclavian artery, moderate ASD; MRI: dilation of the lateral ventricles and the third ventricle; asymmetric face and bulbous nose, delayed motor development, congenital diaphragmatic hernia

TABLE 1 (Continued)

	Number/ sex/ ethnicity	Variant	Age of last examination	Hydrocephalus	Vision impairment	Hearing loss	Cardiovascular	Macrocephaly/ frontal bossing/ skeletal anomalies	Seizure/ Intellectual disability/MRI	Spasticity/ hypotonia	Detailed clinical information
Shaheen et al. (2017) ²⁵	17/M/Scott- Irish-Dutch	c.2230C>T p.Arg744* (NA), c.3211C>T p.Arg1071* (NA)	8 years	Yes	Yes	Yes	Yes	No/No/Yes	No/No/ Remarkable	No/No	Foveal dysplasia, thin inner retina, bilateral lacrimal ducts stenosis; sensorineural hearing loss; aberrant subclavian artery, portal vein thrombosis; MRI: small olfactory bulbs, minimal dilatation of the lateral brain ventricles, multiple bilateral foci of subependymal nodular gray matter heterotopia and enlarged massa intermedia; lung hypoplasia; small teeth, two posterior hair whorls, lung hypoplasia, malrotation of gut, downslanting palpebral fissures, posteriorly rotated ears
Shaheen et al. (2017) ²⁵	18/ M/Kuwait	c.5278G>A p.Ala1760Thr	15 months	Yes	Yes	No	No	Yes/No/No	No/No/ Remarkable	No/Yes	Iris coloboma, Prominent optic nerve; MRI: enlarged third and lateral ventricles and extra- axial spaces, and increased signal intensity within the central tegmental tracts and frontal horns; progressive familial intrahepatic cholestasis (this was because of TJP2), multicystic dysplastic kidney
Saugier- Veber et al. (2017) ²⁶	19/Fetus/ Senegalese	c.1291_1294del p.Val431Metfs*14	Terminate at 30 WG.	NA	NA	NA	NA	Yes/No/No	NA/NA/ Remarkable	NA/NA	MRI: at 28 weeks gestation confirmed massive hydrocephalus
Saugier- Veber et al (2017) ²⁶	20/Fetus/ NA	c.533+1G>T p.?	Terminated at 29 and 25 WG	Yes	NA	NA	NA	NA/NA/NA	NA/NA/NA	NA/NA	Affected sibling was delivered 35 weeks gestation with 2920 g weight, 41.5 cm (95 percentile), soon after birth underwent ventricular shunting, but died a few weeks later from meningoencephalitis
Saugier- Veber et al. (2017) ²⁶	21/Fetus/ NA	c.2248C>T p.Arg750*	Terminated at 29 and 25 WG	Yes	NA	NA	NA	NA/NA/NA	NA/NA/NA	NA/NA	All three terminations were done because of severe isolated recurrent hydrocephalus

(Continues)

TABLE 1 (Continued)

	Number/ sex/ ethnicity	Variant	Age of last examination	Hydrocephalus	Vision impairment	Hearing loss	Cardiovascular	Macrocephaly/ frontal bossing/ skeletal anomalies	Seizure/ Intellectual disability/MRI	Spasticity/ hypotonia	Detailed clinical information
Al-Dosari et al. (2013) ²⁷	22/Fetus/ Saudi	c.628C>T p.Gln210*	10 months	Yes	Yes	NA	Yes	NA/NA/NA	Yes/No/ Remarkable	No/Yes	Chorioretinal coloboma involving maculae bilaterally; small to moderate atrial septal defect with left to right shunt; MRI: extreme dilatation of the supratentorial ventricular system. The cerebral aqueduct was not significantly dilated. The corpus callosum could not be identified but the falx was present; Mother has a brother with CH, 24 y, with a ventriculoperitoneal shunt, at age 1 year, his IQ is estimated about 60. Her sister is now 12 years with CH who was operated on at the age of 1 month.
Al-Dosari et al. (2013) ²⁷	23/Fetus/ Saudi	c.628C>T p.Gln210*	NA	Yes	NA	NA	NA	NA/NA/NA	NA/NA/NA	NA/NA	Family has two abortions possibly affected by history

Abbreviations: ASD, atrial septal defect; CH, congenital hydrocephalus; CSF, cerebrospinal fluid; F, female; M, male; mat, maternal; NA, not information available; pat, paternal; VEP, visual evoked potential; VP, ventriculoperitoneal.

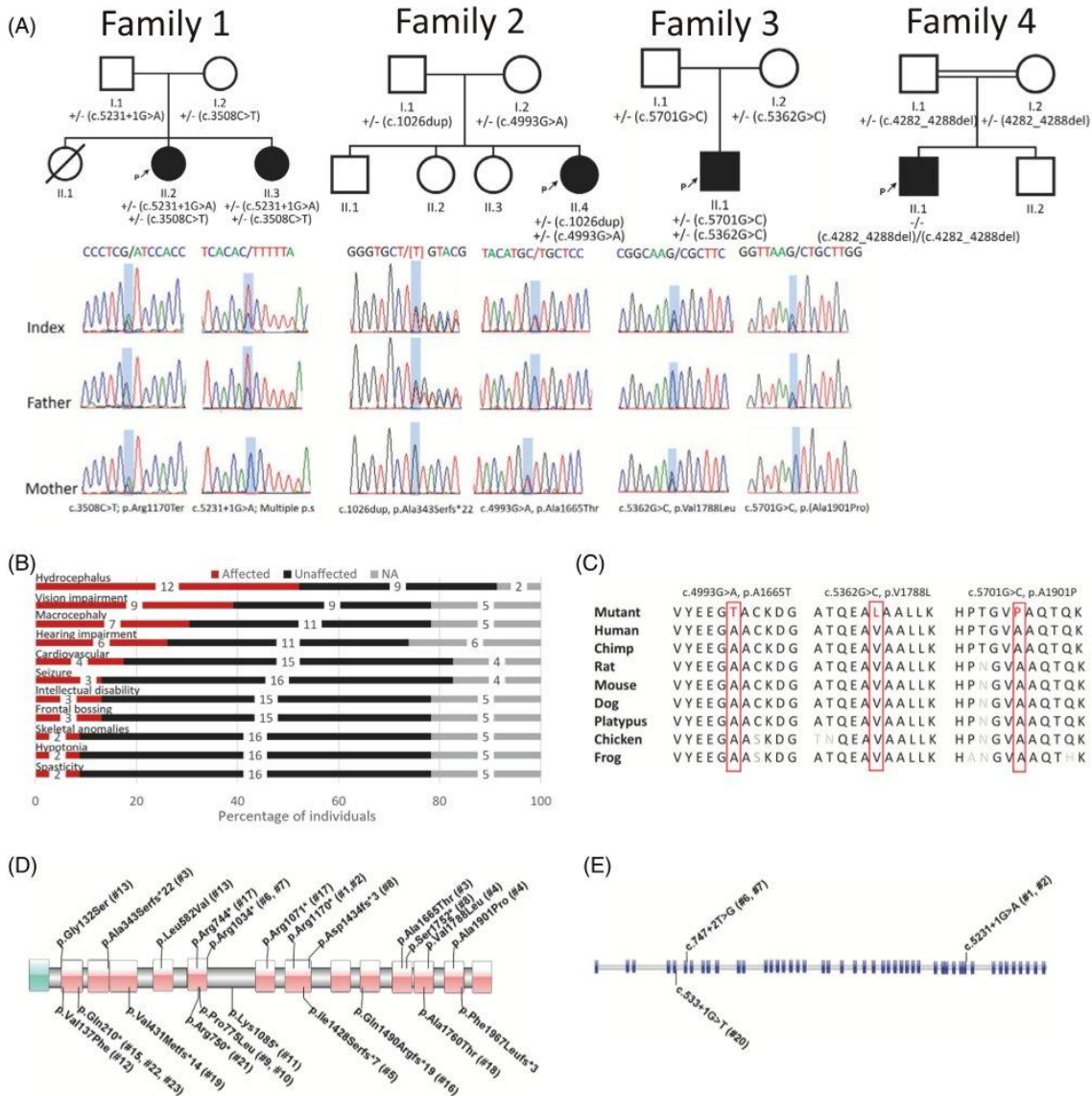


FIGURE 2 (A) Pedigrees and electropherograms of affected individuals. (B) Bar graph summarizing proportions of various clinical findings in patients with biallelic *MPDZ* variants. Red—affected, black—unaffected, gray—no information available. The X axis shows the percentage of patients and the number inside the bars shows the number of patients included in each of the categories. (C) Interspecies alignment was evaluated by Alamut Visual Plus v.1.6.1 and indicates the complete conservation down to invertebrates of the amino acid residues affected by the substitutions. (D) Overview of known and novel variants in *MPDZ* at the protein level (three variants are splicing which are shown in the cDNA schematic, see (E)). All variants were extracted from published papers or the current study. The pink region belongs to the PDZ domains (1–13) and the turquoise region is L27 domain. For each variant, the ID of patients are labeled after # and these IDs are based on Table 1. The variants in the upper part of the figure were detected in compound heterozygosity and those in the lower part of the figure were identified as homozygous variants. (E) Overview of known and novel variants in *MPDZ* that affect splicing. The blue regions represent exons. The variants in the upper part of the figure were detecting in compound heterozygosity while the variant at the lower part of the figure was homozygous. [Colour figure can be viewed at wileyonlinelibrary.com]

history is only remarkable for the proband's mother, apparently having a tendency towards walking on her toes (toe walking) since childhood but is otherwise unremarkable.

The proband was born at term by cesarean section (C-section) due to multiple previous maternal C-sections, without any complications and after an uneventful pregnancy. At birth, her weight was

3500 g and length was 52 cm. She was discharged from the maternity ward with her mother 72 h after birth. She subsequently presented normal psychomotor development, in both language and motor skills, having walked without support at 9 months of age. During her childhood and until the beginning of adolescence the only noticeable feature was toe-walking. At 12 years of age, gait abnormalities were initially noted by her mother, not being perceived by the proband herself, and appeared to remain stable until 25 years of age when her walking difficulty began to progress and lower limb spasticity was noticed. Her gait difficulties worsened progressively and by 32 years of age, she needed a walking aid in the form of crutches. She presently uses a wheelchair for long distances and two-point crutches for short distances. She also complains of urinary urgency and occasional urinary incontinence. She has no previous medical history of seizures, hospital admissions or surgeries. Her neurological examination disclosed bilateral lower limb spasticity, with hyperreflexia and positive bilateral Babinsky sign, characterizing a spastic paraparesis. She has no upper limb compromise and cognition is normal.

Previous examinations included normal fundoscopy and visual campimetry; a visual evoked potential test disclosing bilaterally increased P100 wave latency with normal amplitude; an ABR with widened I–V interpeak interval on the left and normal values on the right; an electromyography demonstrating mildly decreased right and left fibular nerves and left median nerve amplitudes; normal serological and biochemistry cerebrospinal fluid tests; a normal echocardiogram, as well as abdominal, kidney and urinary tract ultrasounds; and a cystography showing an overactive neurogenic bladder. Brain MRI with spectroscopy disclosed bilateral tenuous T2 and Flair white matter hyperintensities in the cerebral hemispheres and anterior portion of the corpus callosum, with reduced values of fractional anisotropy associated with increased myo-inositol levels in spectroscopy, suggestive of myelin sheath lesion, and mild “ex-vacuum” lateral ventricle enlargement.

3.6 | Family 3

The proband in Family 3 is a male child evaluated at 3 years of age due to concerns of abnormal walking positions (Figure 2A). Neurological examination revealed the presence of spastic quadriplegia of cerebral palsy. CT and EEG performed during 3 years of age revealed no abnormalities. He is the only affected child in the family and was born full-term via vaginal delivery with no complications.

3.7 | Family 4

The proband in Family 4 is a 4-year-old boy with an unremarkable family history except parental consanguinity (Figure 2A). He was diagnosed with hydrocephalus prenatally. There was no history of maternal illness or substance use during pregnancy. He was born at 37 weeks and 4 days of gestation with a birth weight of 3695 g by C-section because of cephalo-pelvic disproportion. A postnatal MRI showed ventriculomegaly with absent septum pellucidum, broad

interthalamic connection and hypoplastic optic nerve and chiasm and a diagnosis of septo-optic dysplasia was made. Epileptic seizures started at the age of 1 year. He was treated with lacosamide and lamotrigine. At the age of 4 years, bilateral macular coloboma were noted. He has a vision of 2/7.5 bilateral. He visited a medical day care because of developmental delay. Physical examination showed a height of 114.1 cm (+0.2 SD), weight of 21.0 kg (+0.7 SD) and head circumference of 54 cm (+1.9 SD). He has a triangular face with a high, broad, and prominent forehead and a pointed chin, hypertelorism with a broad nasal bridge and a narrow mouth. No other abnormalities were noted.

3.8 | Genetic analysis

The DNAs of probands from the four unrelated families (Family 1 II-2, Family 2 II-4, Family 3 II-1, Family 4 II-1) revealed variants in *MPDZ* (NM_001378778.1). The proband in Family 1 was identified with compound heterozygous variants including a maternally inherited c.3508C>T, p.Arg1170* nonsense variant in exon 25 with a minor allele frequency (MAF) of 0.00002567 in gnomAD (with 39 carriers) and a paternally inherited c.5231+1G>A, p.? canonical splice variant in intron 38, absent in gnomAD. The proband in Family 2 also presented compound heterozygous variants including a paternally inherited c.1026dupA, p.Ala343Serfs*22 frameshift variant in exon 8, absent in gnomAD, and a maternally inherited c.4993G>A, p.-Ala1665Thr missense variant in exon 37 with a MAF of 0.00001611 in gnomAD (with 26 carriers). The proband in Family 3 was identified with compound heterozygous missense variants including a maternally inherited c.5362G>C, p.Val1788Leu variant in exon 39 with a MAF of 0.000001371 in gnomAD (with two carriers) and a paternally inherited c.5701G>C, p.Ala1901Pro variant in exon 43 with a MAF of 0.000001592 in gnomAD (with one carrier). The proband in Family 4 presented a homozygous frameshift variant c.4282_4288del, p.-Ile1428Serfs*7 located in exon 30 that is absent in gnomAD. Previous genetic testing in this family was performed analyzing *HESX1* and *SOX2*, which revealed no abnormalities. Array analysis revealed a 12q12 deletion (chr12:40,562,013-40,774,520, GRCh37) that was inherited from the unaffected mother.

3.9 | Mini-gene assay

In vitro RNA studies of the c.5231+1G>A variant impacting a highly conserved donor splice site in intron 38 identified aberrant splicing in this region. The wild-type control showed evidence of alternative splicing (four different splice products) between exons 37 and 38. This result is consistent with the splicing model predicted by the Genotype-Tissue Expression (GTEx) portal (<https://gtexportal.org/home/gene/MPDZ>). Based on this portal, 13 different transcripts use these two exons, with one of these transcripts (ENST00000438511.5) skipping exon 37. Figure 3 shows four different splicing outcomes in this region, with all of them using the donor site in intron 38. Four

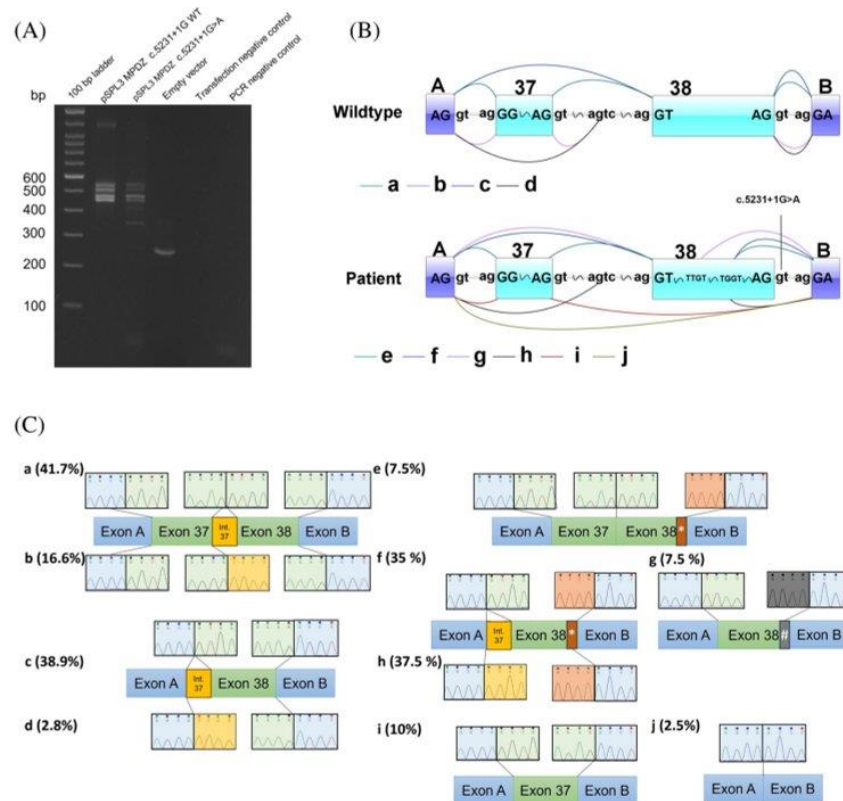


FIGURE 3 (A) Gel electrophoresis of the RT-PCR from the wild-type control, the c.5231+1G>A variant, and empty pSPL3 vector amplicons, as well as transfection negative and PCR negative controls. (B, C) The vector construct of the *in vitro* splice assay illustrates the wild-type or mutant amplicons inserted between exons A and B of the pSPL3 vector with a splicing schematic of the wild-type allele (upper B) and c.5231+1G>A variant (lower B). The wild-type construct shows four alternative splicing isoforms (a–d). The c.5231+1G>A variant activates two cryptic donor splice sites in exon 38 (e, f, g, and h). The variant showed evidence of skipping exon 38 following the variant (i) and skipping of both exons 37 and 38 (j). The empty vector control, with result summarized as equivalent to (j) and skipping of exons 37 and 38, performed as expected. The “*” in e and f indicates TGGT cryptic splice site and “#” in g shows the TTGT cryptic splice site in exon 38. The int. 37 refers to intron 37. [Colour figure can be viewed at wileyonlinelibrary.com]

alternative splicing amplicons were identified including amplicons showing evidence of: inclusion of both exons 37 and 38 (a), inclusion of both exons 37 and 38 but with a cryptic acceptor site activation in intron 37 (b), skipping of exon 37 (c), as well as skipping of exon 37 and usage of a cryptic acceptor site in intron 37 (d) (Figure 3B,C). However, the c.5231+1G>A variant indicates that the donor splice site in intron 38 is skipped and instead, either usage of two cryptic splice sites (e–h) or skipping of exon 38 occurred (i and j). The first cryptic splice site (TGGT) in exon 38 causes a frameshift variant: g.13121740_13121746del, r.5227_5231+2del, p.Asn1745Tyrfs*36. The second cryptic splice site in this exon, TTGT, causes an inframe deletion: g.13121739_13121749del, c.5223_5231+2del, p.Gly1742_Arg1744del. The skipping of exon 38 causes another frameshift variant: g.13121741_13121934del, c.5041_5231+3del, p.Asn1681Lysfs*38. TA cloning of the amplicon pool approximated the proportion of alternatively spliced amplicons in this region. The percentage of four different splicing

outcomes from 36 clones for the wild-type are 41.7%, 16.6%, 38.9% and 2.8% for a–d, respectively (Figure 3C). The percentage of the six different amplicons from 43 clones for the c.5231+1G>A variant are: 7.5%, 35%, 7.5%, 37.5%, 10%, and 2.5%, for e, f, g, h, i, and j, respectively.

3.10 | ABR analysis in a murine model

As part of the International Mouse Phenotyping Consortium (IMPC) programme (<https://www.mousephenotype.org/>), a *Mpdz* knockout mouse model (*Mpdz*^{em1(IMPC)}) was generated at the Jackson Laboratory employing CRISPR/Cas9-mediated genome editing.^{28,29} This resulted in a non-homologous end joining event involving exon 6 of the *Mpdz* gene, leading to a 136 bp deletion coupled with a 29 bp insertion, which is predicted to cause a frameshift and early truncation (Figure 4A). Mice homozygous for this allele are viable and so were

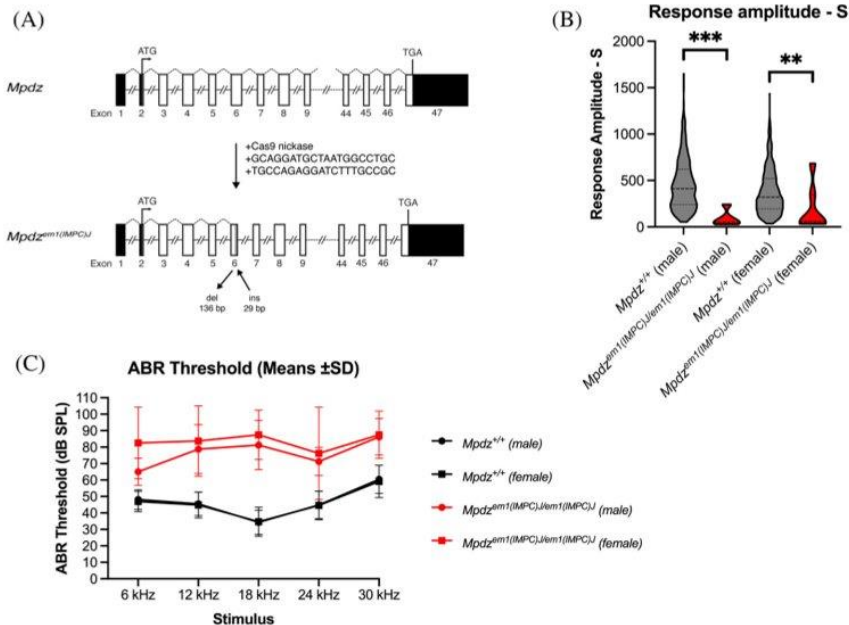


FIGURE 4 *Mpdz* knockout mice exhibit phenotypes consistent with hearing loss. (A) Schematic of the *Mpdz*^{em1(IMPC/J)} allele. (B) Chart showing the IMPC-derived data from an acoustic startle phenotyping assay measuring the Response amplitude-S in 7 female and 5 male *Mpdz* mutant mice compared to 489 female and 476 male wild-type controls. (C) Chart showing the IMPC-derived ABR threshold data in response to frequency specific acoustic stimuli in 4 female and 4 male *Mpdz* mutant mice compared to 606 female and 591 male wild-type controls. ***p* < 0.01; ****p* < 0.001. [Colour figure can be viewed at wileyonlinelibrary.com]

subject to the IMPC adult mouse phenotyping pipeline that includes an acoustic startle (Response amplitude-S) test at 10-weeks of age and an auditory brainstem response (ABR) test at 14-weeks of age. As part of the programme, phenotyping data generated from knockout mice can be compared with a running wild-type baseline of “normal” values for each test. At 10-weeks of age, in response to a 110 dB sound stimulus both male and female homozygous *Mpdz* knockout mice exhibit a significantly reduced startle reflex compared to wild-type mice (Figure 4B). At 14-weeks of age, both male and female homozygous *Mpdz* knockout mice exhibit elevated ABR hearing thresholds at all frequencies tested compared to wild-type mice (Figure 4C). Together these data indicate that *Mpdz* is critical for hearing in mice, and indicate that this model could be a valuable tool to investigate the pleiotropic and mechanistic effects of this gene.

4 | DISCUSSION

Biallelic variants in *MPDZ* have been implicated in a spectrum of phenotypes, but few functional studies have been performed to elucidate the disease mechanisms particularly for hydrocephalus and hearing impairment.^{6–8} Here, we studied four unrelated families exhibiting a spectrum of phenotypes and identified novel variants in *MPDZ*. Initially, *MPDZ* was primarily associated with congenital hydrocephalus, encompassing a broad range of severities from stillbirth to severe congenital hydrocephalus.²⁷ However, subsequent identification of disease-causing variants in *MPDZ* revealed additional features, including vision impairment, hearing impairment, cardiac abnormalities, controllable seizure, mild intellectual disability,²⁴ lung hypoplasia, malrotation of the gut, and multicystic dysplastic kidney (Figure 2B).

Eleven out of 25 variants aggregated from the literature and current study were previously deposited in ClinVar (Figure 2D,E). In total, ClinVar submissions currently report 84 pathogenic/likely pathogenic *MPDZ* variants, including 35 frameshift, 28 nonsense, and 21 splicing variants, albeit with zygosity not provided (accessed February 2024). Remarkably, only 20 variants are explicitly associated with non-syndromic hydrocephalus, while the remainder are described as not provided/Inborn genetic diseases. Furthermore, there are 799 missense variants that are all classified as variants of uncertain significance (VUS). While this “VUS-explosion” is not exclusively unique to *MPDZ*, this suggests that the existing gaps of knowledge from both the mechanistic and clinical sides are in dire need of expansion in order to identify potential patients from this VUS-pool. Additionally, the under-characterized gene-phenotype description in key databases such as OMIM may further serve as a hurdle to the full appreciation of *MPDZ*-spectrum phenotypes. In our systematic review of the literature, we aimed to increase awareness of the current state of knowledge pertaining to a vast array of possible phenotypes.

Understanding the mechanisms of tissue specificity in heritable diseases remains a significant challenge. For instance, *RB1* is a well-known cell cycle gene but perturbations only cause retinoblastoma despite its broader cellular functions.³⁰ Although initial reports have suggested that severe hydrocephalus was caused by nonsense variants in *MPDZ*,²⁷ our study and very recent publications reveal that a variety of variants distributed from exons 5 to 45 may cause a wide range of phenotypes including a milder presentation. In our study, a homozygous LOF variant was identified in a patient with a severe phenotype involving hydrocephalus, vision impairment, macrocephaly and seizures. Another family presented with affected individuals with two LOF variants (nonsense and splicing variants, located in exon

25 and intron 38, respectively) that were associated with mild hydrocephalus, hearing loss and cardiac issues. In contrast, other compound heterozygous variants (frameshift [exon 7] and missense variants [exon 12]) in Family 2 and two missense variants (exons 12 and 14) in Family 3 were associated with spasticity. We analyzed the variant region and observed an evolutionary conserved region (Figure 2C). In the literature, compound heterozygous variants (splicing [exon 5] and missense variants [exon 14]) demonstrated external hydrocephalus with mild dilatation of lateral and third ventricles without other abnormal features (including vision and hearing impairment).²³ Recently, Zhang et al. has demonstrated that two LOF variants (nonsense [exon 39] and frameshift [exon 31]) only caused bilateral macular coloboma.¹⁹ Additionally, Iyengar et al.¹⁸ reported two affected siblings with variable structural abnormalities of the retina caused by compound heterozygous variants (nonsense [exon 22] and splicing [intron 6]).¹⁸ One study described 10 heterozygous variants associated with retinitis pigmentosa and Leber congenital amaurosis, but this study had a methodological limitation, and it was not fully supporting the diagnosis.³¹

Based on the literature, two missense variants with a mild phenotype have been described: a homozygous missense variant p.Pro775Leu causing only hearing loss in a Pakistani family,²⁰ as well as a different missense variant p.Val137Phe causing hearing loss and congenital hereditary endothelial dystrophy in an Iranian family.²² Additionally, Al-Jezawi et al.²³ identified two compound heterozygous novel variants (c.394G>A and c.1744C>G) in a patient with macrocephaly and communicating hydrocephalus. The *in vitro* functional study of the c.394G>A genetic variant revealed exon 5 skipping. Notably, this variant has a ClinVar entry (variation ID: 992337) with conflicting classifications of pathogenicity, being reported both as a VUS and likely pathogenic. Interestingly, the general population (gnomAD v.4) shows an entry with a homozygous status for this variant. To address this discrepancy, it is possible that this variant may only cause disease when combined with another pathogenic variant. Therefore, we recommend further *in vivo* functional studies to elucidate the role of both variants detected in this study. In our current study, we have identified two missense variants *in trans* (c.5362G>C and c.5701G>C) in a patient (F3, II-1) primarily affected by spasticity. Utilizing *in silico* tools, we predict that both variants are damaging, and interestingly, they are ultra-rare in the general population (gnomAD v.4). As, we detected another patient (F2, II-4) with spasticity caused by a compound heterozygous combination of variants (a frameshift and a missense), based on this finding, we hypothesize that the compound heterozygosity involving two missense variants may lead to a similar phenotype in patient F3, II-1. However, since this is the initial description of this phenotype for this specific gene, we recommend further functional studies to confirm the pathogenic impact of these missense variants in this patient. The variability in *MPDZ*-related phenotypes, ranging from mild to severe, may be attributed to several factors, including the presence of multiple transcripts (18 isoforms with 10 protein coding isoforms based on Ensembl) and/or regulation by NMD, which generally targets stop codons in both mutated and normal transcripts that adhere to the 50-nucleotide rule.³² For instance, based on GTEx, six transcripts in *MPDZ* do not use a common last

exon that is used in the MANE transcript. However, this hypothesis remains to be clarified via functional studies.

MPDZ functions as a scaffold protein for tight-junction-related proteins, adherens junction proteins, and transmembrane receptors. It comprises 13 PDZ domains that interact with the ion channel subunit C-terminal tail sequences and G-protein coupled receptors. Functional studies in *Mpdz*^{-/-} mice implicate its role in ependymal and/or choroid plexus dysfunction, potentially explaining the brain abnormalities associated with *MPDZ* variants.⁷ Furthermore, it has been demonstrated that *Mpdz* plays a role at the hair cell apical membrane where it colocalizes with MAGUK p55 subfamily member 5 (MPP5) and Crumbs protein CRB3, offering insight into its potential function in the inner ear.⁸ Family 1 in this study supports the role of *MPDZ* in hearing. Nevertheless, the function of missense/inframe variants and the role of specific domains remains poorly understood.

In conclusion, our review summarized the various genotypes and phenotypes related to *MPDZ*. This review also reports novel variants in *MPDZ* with detailed phenotypic information. To the best of our knowledge, we highlight that biallelic variants in *MPDZ* can primarily cause spasticity in 8% of patients. Current evidence suggests that the spectrum of phenotypes may be influenced by location within the gene. Continued evaluation of new cases and functional studies on missense variants are essential for elucidating the precise roles of different domains and variant type on *MPDZ*-related phenotypes.

AUTHOR CONTRIBUTIONS

BV and AR conceptualized the study and designed the experiments. OB collected clinical information and conducted WES and segregation studies in Family 1. FPM and FK collected clinical information and conducted WES and segregation studies in Family 2. SB, CZ, YX, and MCK collected clinical information, and conducted WES and segregation studies in Family 3. AVS collected clinical information and conducted WGS in Family 4. MRB performed the analysis of data from the knockout murine model. BV and AR performed the systematic literature review. BV and AR prepared the complete first draft of the manuscript. The manuscript was reviewed and approved by all authors.

ACKNOWLEDGEMENTS

The authors thank the families for their participation in this study. This study was supported by Intramural Funding (fortune) at the University of Tübingen (2545-1-0), the Ministry of Science, Research and Art Baden-Württemberg and the German Research Foundation DFG VO 2138/7-1 grant 469177153 (BV) and the National Nature Science Foundation of China (U21A20347). BV is a member of the European Reference Network on Rare Congenital Malformations and Rare Intellectual Disability (ERN-ITHACA) (EU Framework Partnership Agreement ID: 3HP-HP-FPA ERN-01-2016/739516). We acknowledge support by the Open Access Publication Funds of the University of Göttingen. Open Access funding enabled and organized by Projekt DEAL.

CONFLICT OF INTEREST STATEMENT

The authors declare no conflict of interest.

DATA AVAILABILITY STATEMENT

The data that support the findings of this study are openly available in Leiden Open Variation Database (LOVD), variant IDs #0000960145-#0000960151.

ORCID

Changlian Zhu  <https://orcid.org/0000-0002-5029-6730>

Barbara Vona  <https://orcid.org/0000-0002-6719-3447>

REFERENCES

- Ullmer C, Schmuck K, Figge A, Lübbert H. Cloning and characterization of MUPP1, a novel PDZ domain protein. *FEBS Lett.* 1998; 424(1-2):63-68.
- Simpson EH, Suffolk R, Jackson IJ. Identification, sequence, and mapping of the mouse multiple PDZ domain protein gene, *Mpdz*. *Genomics.* 1999;59(1):102-104.
- Guillaume JL, Daulat AM, Maurice P, et al. The PDZ protein mupp1 promotes Gi coupling and signaling of the Mt1 melatonin receptor. *J Biol Chem.* 2008;283(24):16762-16771.
- Krapivinsky G, Medina I, Krapivinsky L, Gapon S, Clapham DE. Syn-GAP-MUPP1-CaMKII synaptic complexes regulate p38 MAP kinase activity and NMDA receptor-dependent synaptic AMPA receptor potentiation. *Neuron.* 2004;43(4):563-574.
- Tetzlaff F, Adam MG, Feldner A, et al. MPDZ promotes DLL4-induced notch signaling during angiogenesis. *Elife.* 2018;7:7.
- Feldner A, Adam MG, Tetzlaff F, et al. Loss of *Mpdz* impairs ependymal cell integrity leading to perinatal-onset hydrocephalus in mice. *EMBO Mol Med.* 2017;9(7):890-905.
- Yang J, Simonneau C, Kilker R, et al. Murine MPDZ-linked hydrocephalus is caused by hyperpermeability of the choroid plexus. *EMBO Mol Med.* 2019;11(1):1-19.
- Jarysta A, Tarchini B. Multiple PDZ domain protein maintains patterning of the apical cytoskeleton in sensory hair cells. *Development.* 2021;148(14):1-14.
- Sobreira N, Schiettecatte F, Valle D, Hamosh A. GeneMatcher: a matching tool for connecting investigators with an interest in the same gene. *Hum Mutat.* 2015;36(10):928-930.
- McKenna A, Hanna M, Banks E, et al. The genome analysis toolkit: a MapReduce framework for analyzing next-generation DNA sequencing data. *Genome Res.* 2010;20(9):1297-1303.
- Li H, Durbin R. Fast and accurate long-read alignment with Burrows-Wheeler transform. *Bioinformatics.* 2010;26(5):589-595.
- Rad A, Altunoglu U, Miller R, et al. MAB21L1 loss of function causes a syndromic neurodevelopmental disorder with distinctive cerebellar, ocular, craniofacial and genital features (COFG syndrome). *J Med Genet.* 2019;56(5):332-339.
- Karczewski KJ, Francioli LC, Tiao G, et al. The mutational constraint spectrum quantified from variation in 141,456 humans. *Nature.* 2020; 581(7809):434-443.
- Ioannidis NM, Rothstein JH, Pejaver V, et al. REVEL: an ensemble method for predicting the pathogenicity of rare missense variants. *Am J Hum Genet.* 2016;99(4):877-885.
- Schubach M, Maass T, Nazaretyan L, Röner S, Kircher M. CADD v1.7: using protein language models, regulatory CNNs and other nucleotide-level scores to improve genome-wide variant predictions. *Nucleic Acids Res.* 2024;52(D1):D1143-D1154.
- Rad A, Schade-Mann T, Gamerding P, et al. Aberrant COL11A1 splicing causes prelingual autosomal dominant nonsyndromic hearing loss in the DFNA37 locus. *Hum Mutat.* 2021;42(1):25-30.
- Tompson SW, Young TL. Assaying the effects of splice site variants by exon trapping in a mammalian cell line. *Bio Protoc.* 2017;7(10):1-18.
- Iyengar R, Dearthoff M, Schmidt R, Nagiel A. Retinal manifestations in autosomal recessive MPDZ maculopathy: report of two cases and literature review. *Ophthalmic Genet.* 2023;44(6):572-576.
- Zhang S, Zhang F, Wang J, et al. Novel compound heterozygous variations in MPDZ gene caused isolated bilateral macular Coloboma in a Chinese family. *Cells.* 2022;11(22):3602.
- Bharadwaj T, Schrauwen I, Rehman S, et al. ADAMTS1, MPDZ, MVD, and SEZ6: candidate genes for autosomal recessive nonsyndromic hearing impairment. *Eur J Hum Genet.* 2022;30(1):22-33.
- Bertoli-Avella A M, Beetz C, Ameziane N, et al. Successful application of genome sequencing in a diagnostic setting: 1007 index cases from a clinically heterogeneous cohort. *Eur J Hum Genet.* 2020;29(1):141-153.
- Moazzini H, Javadi MA, Asgari D, et al. Observation of nine previously reported and 10 non-reported SLC4A11 mutations among 20 Iranian CHED probands and identification of an MPDZ mutation as possible cause of CHED and FECD in one family. *Br J Ophthalmol.* 2020;104(11):1621-1628.
- Al-Jezawi NK, Al-Shamsi AM, Suleiman J, et al. Compound heterozygous variants in the multiple PDZ domain protein (MPDZ) cause a case of mild non-progressive communicating hydrocephalus. *BMC Med Genet.* 2018;19(1):34.
- Harripaul R, Vasli N, Mikhailov A, et al. Mapping autosomal recessive intellectual disability: combined microarray and exome sequencing identifies 26 novel candidate genes in 192 consanguineous families. *Mol Psychiatry.* 2018;23(4):973-984.
- Shaheen R, Sebail MA, Patel N, et al. The genetic landscape of familial congenital hydrocephalus. *Ann Neurol.* 2017;81(6):890-897.
- Saugier-Verber P, Marguet F, Lecoquiere F, et al. Hydrocephalus due to multiple ependymal malformations is caused by mutations in the MPDZ gene. *Acta Neuropathol Commun.* 2017;5(1):36.
- Al-Dosari MS, Al-Owain M, Tulbah M, et al. Mutation in MPDZ causes severe congenital hydrocephalus. *J Med Genet.* 2013;50(1):54-58.
- Groza T, Gomez FL, Mashhadi HH, et al. The International Mouse Phenotyping Consortium: comprehensive knockout phenotyping underpinning the study of human disease. *Nucleic Acids Res.* 2023; 51(D1):D1038-D1045.
- Bowl MR, Simon MM, Ingham NJ, et al. A large scale hearing loss screen reveals an extensive unexplored genetic landscape for auditory dysfunction. *Nat Commun.* 2017;8(1):886.
- Hekselman I, Yeger-Lotem E. Mechanisms of tissue and cell-type specificity in heritable traits and diseases. *Nat Rev Genet.* 2020;21(3):137-150.
- Ali M, Hocking PM, McKibbin M, et al. *Mpdz* null allele in an avian model of retinal degeneration and mutations in human leber congenital amaurosis and retinitis pigmentosa. *Invest Ophthalmol Vis Sci.* 2011;52(10):7432-7440.
- Maquat LE. Nonsense-mediated mRNA decay: splicing, translation and mRNP dynamics. *Nat Rev Mol Cell Biol.* 2004;5(2):89-99.

SUPPORTING INFORMATION

Additional supporting information can be found online in the Supporting Information section at the end of this article.

How to cite this article: Rad A, Bartsch O, Bakhtiari S, et al. Expanding the spectrum of phenotypes for MPDZ: Report of four unrelated families and review of the literature. *Clinical Genetics.* 2024;1-14. doi:10.1111/cge.14563